



Anatoli Unitsky

Scientist and inventor, author of more than 200 scientific papers, 20 monographs and over 150 inventions in the field of construction, transport, mechanical engineering, electronics and chemical industry.

Creator of SkyWay and geocosmic transport systems, as well as a number of transport and infrastructure projects based on the string technology. Head of two UN projects (1998, 2002), member of the USSR Cosmonautics Federation.

President of SkyWay Group of Companies.
General Designer of SkyWay Technologies Co.

ISBN 978-985-90498-2-8



9 789859 049828

Minsk, 2019

A. Unitsky

STRING TRANSPORT SYSTEMS:
on Earth and in Space

A. Unitsky

STRING TRANSPORT SYSTEMS: on Earth and in Space



A. Unitsky

STRING TRANSPORT SYSTEMS: on Earth and in Space

Minsk, 2019

Table of contents

Preface	08
<hr/>	
Preface to Edition 2019	10
Preface to Edition 2017	14
TIPS-based (Theory of Inventive Problem Solving) history of Unitsky's String Technologies	22
<hr/>	
History of SkyWay in pictures	34
<hr/>	
Optimization of Transportation System	92
<hr/>	
Innovative SkyWay transport and infrastructure technologies	104
<hr/>	

MONOGRAPH

PART 1

String Transport System

158

PREFACE	160
<hr/>	
CHAPTER 1	
General concept of STS as an alternative to the existing kinds of transport	166
<hr/>	
CHAPTER 2	
Design features of String Transport System	179
2.1. STS basic diagram	179
2.2. String track structure	184
2.3. Supports	193
2.4. Transport module	199
2.5. STS construction technology	203
2.6. Technical and economical comparison of transport systems	207
<hr/>	
CHAPTER 3	
Mechanics problems of high-speed transport	219
3.1. Dynamic motion of transport modules on string guide track	219
3.2. Strength of transport modules and string rail guide	223
3.3. Tribology of wheel – string contact	225
<hr/>	
CHAPTER 4	
Dynamic model and estimated parameters of transport modules motion on the string transport line	231
4.1. Derivation of motion equation for the String Transport System	231
4.2. Vibration analysis of flexible string. STL first approximation	246

4.3. Oscillations of a String Transport System with elastic body	266
4.4. Numerical study of STL span dynamic deflection	290
Conventional symbols	306
Bibliography	308

History of United Planetary Transport in pictures

312

Intellectual Property Rights to geocosmic transport and infrastructure complex “United Planetary Transport”

336

1. Essence of valuation object	338
2. Prerequisites for creating a valuation object	339
3. Planet – for life, space – for industrial technologies	339
4. Quantitative and qualitative characteristics of the valuation object	342
4.1. General characteristics of UPT	342
4.2. Construction of UPT	345
4.3. Conditions for UPT to enter into the near-Earth orbit	346
4.4. Conditions necessary for the creation of SIT “Orbita”	353
4.5. UPT geocosmic carrier cost	360
4.6. Economic effect of using UPT	364
5. Information about the author of the appraised intellectual property	366

MONOGRAPH PART 2

United Planetary Transport

368

INTRODUCTION	370
1. Need for space industrialization	370
2. Selection of criteria for space industrialization	374
3. Conservation laws in relation to geocosmic transport	379
3.1. Energy conservation law	379
3.2. Laws of impulse conservation and conservation of angular momentum	380
3.3. Conservation law of center-of-mass motion	381
3.4. Analysis of conservation laws in relation to GCT	381
4. United Planetary Transport	389

CHAPTER 1

Dynamics of the UPT exit into space in Earth’s equatorial plane	395
1.1. Problem setting	396
1.2. Differential equations of motion for the component of the rotor – capsule system in the atmosphere	397
1.3. Analysis of motion equations of the system in the atmosphere	399
1.4. Dynamics of the rotor – capsule system when moving in the atmosphere	401
1.5. Rotor dynamics at the elastic extension section in outer space	404
1.6. Dynamics of rotor oscillatory motion	406
1.7. Rotor motion equations at the friction extension section	410
1.8. Choice of sections of elastic and friction extension. Dynamics of the controlled radial rotor motion	414
1.9. Rotor motion at the final stage	418
1.10. Problem of the UPT rotor placement into orbit. Example	421

CHAPTER 2

Dynamics of the UPT placement into orbit with energy dissipation by means of capsule ejection 426

- 2.1. Motion control of the rotor – capsule element in the atmosphere with regard to capsule rotation 427
- 2.2. Dynamics of the system radial motion in atmosphere 430
- 2.3. Radial system motion with stop in position $x = x'$ 432
- 2.4. Rotor and capsule movement at later stages 435
- 2.5. System motion at the last stage 439
- 2.6. Dependence between system parameters at the initial and final motion stages 442
- 2.7. System dynamics when entering the permanent orbit 447
- 2.8. Problem of system placement into the intermediate orbit 452
- 2.9. Variation of radial system acceleration 454

CHAPTER 3

Rotor maneuvering in order to avoid objects moving in equatorial plane 457

- 3.1. Setting a problem on the UPT rotor maneuvering 459
- 3.2. Differential equations of the UPT rotor motion outside the equatorial plane 461
- 3.3. Method of problem solving 465
- 3.4. Dynamics of rotor free motion. Problem solution on rotor removal from the planet attraction zone 467
- 3.5. Rotor dynamics at the stage of angular motion damping 472
- 3.6. Rotor motion at the stage of radial motion damping 475
- 3.7. Problems on rotor maneuvering in Uranus and Saturn conditions 477

CHAPTER 4

Problems of creating an accelerator for the UPT rotor 483

- 4.1. System of rotor lift to the capsule center 483
- 4.2. Problems of creating a linear electric motor for rotor acceleration to cosmic velocity 486
- 4.3. Project of the combined rotor acceleration and levitation system 489
- 4.4. Problem on the UPT rotor acceleration 493

- 4.5. Dynamics of rotor disturbed motion upon violations of the acceleration system operation 495
- 4.6. Other possible disturbances of rotor motion when accelerating 500

CHAPTER 5

Parameter estimation of the aerodynamic heating process for the UPT rotor in the absence of protective capsule 505

- 5.1. Investigation results on aerodynamic machinery heating. Review 505
- 5.2. Problem setting 507
- 5.3. Approximate calculation of air flow parameters in the rotor surface vicinity 510
- 5.4. Approximate calculation of temperature field in the rotor surface vicinity in the absence of the protective cover sublimation process 513
- 5.5. Quasi-stationary calculation of rotor surface temperature in the absence of sublimation process 518
- 5.6. Quasi-stationary calculation of evaporation dynamics of sublimated coating for the rotor thermal protection 520
- 5.7. Certain conclusions 523

SUMMARY 1995 525

- Conventional symbols 532
- Bibliography 536
- Scientific and technical reports 539

SUMMARY 2019

Optimal transport systems as a platform for the transition to a new stage of civilization

540

Preface

Preface to Edition 2019

10

Preface to Edition 2017

14

08



Preface to Edition 2019

The most of this monograph “String Transport Systems: on Earth and in Space” was written between 1977 and 1995, when its first edition was published. Industrial designs of the string transport system were certified in 2017, when the monograph was issued for the second time. It has been more than 40 years from the birth of a breakthrough transport and infrastructure project to its practical implementation. All this time the idea of SkyWay has been improved, not changing in its engineering essence.

The re-edition 2017 was published unchanged since 1995, despite the fact that the inland transport systems have already been implemented and the practices made their own adjustments. However, everything remained stable and unchanged – the time just confirmed the initial studies and calculations. This re-edition required only minor clarifications, and also allowed adding some information regarding the assessment of the mar-

ket value of intellectual property on the United Planetary Transport, as well as adding a section on optimization of the transport systems and a new visual material.

The invariable relevance of this book from the moment it was written to the present day proves the validity of the fundamental principles, which are behind the string transport systems. Today these systems have already been implemented based on the research collected in the first part of this monograph. In the near future, they should be delivered to master the Space on the basis of the studies gathered in the second part hereof.

The point of establishing and mainstreaming the string transport systems both on the Earth and in the Space is described in the preface to the first part of the book and in the introduction to the second, which, like the most, has been left unchanged. Everything that I have been talking about and writing since 1977 has become more relevant today.



*The string transport
on Earth is a fact.*

*The string transport
in the Space is a task
of tomorrow,
managing which will
result in whether
our civilization
will have a future.*



*A. Unitsky
General Designer,
SkyWay Technologies Co.*

The number of cars in the world is approaching the critical maximum level, as well as the share of environmentally destructive facilities. At the same time, the planet resources are being depleted, and their production causes more and more harm to the wildlife, i.e. the Earth's biosphere. Using the string transport on Earth and relocating the harmful production by means of the string transport to near-Earth space is still the most balanced, justified and elaborated plan for the infrastructural development of our terrestrial technocratic civilization. Its survival depends on the humanity being capable to follow this program. Otherwise, in two or three generations, there will be a point of no return – we will doom



not only ourselves and our children, but also our common home. I am confident that it is for this reason that the preface to the first part of the book and the introduction to the second will be understandable and important for the widest audience, and not just for transport specialists.

The preface to Edition 2017 details this idea and describes the major milestones that have been made on the way to implementing the string transport systems since the first edition of the monograph. In addition, having read it and correlating the predictions herein with the status of the string transport, the reader will once again be able to find that these forecasts of the author are real. The string transport on Earth is a fact.

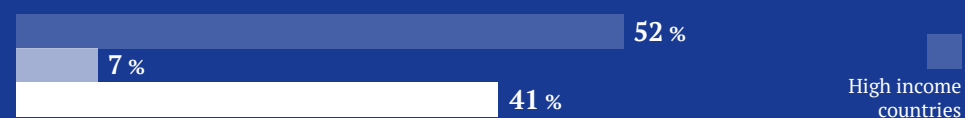
The string transport in the Space is a task of tomorrow, managing which will result in whether our civilization will have a future. In this book, I set out the reasons why this task is such essential and describe how it can be solved.

*Best Regards,
Eng. Anatoli Unitsky*

World population



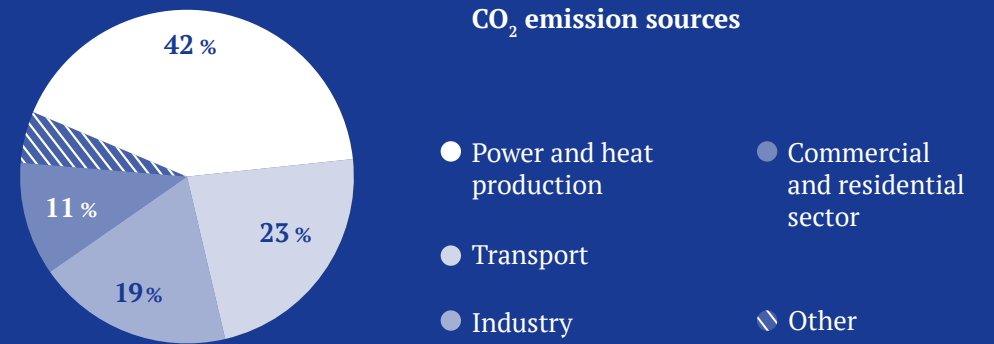
Vehicles



> **7.6** bln people
world population

> **1** bln vehicles
global market

CO₂ emission sources



≈ **32.5** Gt of CO₂
released into the atmosphere worldwide per year

Source:
Netherlands environmental
assessment agency

Preface to Edition 2017

The first edition of the scientific monograph “String Transport Systems: on Earth and in Space” offered to your attention was published in 1995. The string transport systems were predominantly a theory at that time, and practical implementation of this transport and infrastructure technology was limited to merely an acting model in 1 : 10 scale. However, fully functional engineering and scientific schools on this direction had already been formed by then. The work of those schools prepared the conditions for the creation of full-scale test sections of elevated string transport systems demonstrated to a wide international scientific and engineering community in the Republic of Belarus in 2017. It became possible only because the author of this monograph established another school – a design and engineering one – under OJSC Yunitskiy Scientific and Production Company in Moscow in 2000.

At present, SkyWay Technologies Co. alone, which is a part of the international SkyWay Holding, in Minsk



***String transport
is not a system,
but a comprehensive
complex that comprises
dozens of systems
and even more
subsystems.***

has 15 design bureaus with more than 300 scientists, engineers, constructors, architects and designers employed.

Their area of focus includes:

- rail-string transport overpasses;
- rolling stock (cargo, urban and high-speed intercity electromobility on steel wheels – passenger unibuses, unicars and unibikes, as well as cargo unitrucks and unitranses);
- “second level” infrastructure – stations, railway and freight terminals, depots, etc., as well as automated systems of safety, control, power supply and communications.

Therefore, the string transport is not a system, but a comprehensive complex that comprises dozens of systems and even more subsystems.

The industrial prototypes of urban, touring passenger and cargo rail-string complexes are showcased on the territory of the SkyWay demonstration and certification center (in previous terminology – string tracks) in the town of Maryina Gorka, 60 km from Minsk.

The speed over 100 km/h has already been achieved at the section of the lightweight string complex with an overpass 800 m long. All basic engineering calculations on the overground rail-string track structures of an overpass type presented in the first part of this monograph have been confirmed. There is no doubt that by the time this book is issued, the speed of 150 km/h will have been reached. In the very near future, we will conquer the stated milestone of

500 km/h – the speed sufficient to bring the ground transport to a qualitatively new level.

I hope you will be able to appreciate the enormous work accomplished by the author of this publication, as well as by the scientific, engineering and design schools established and headed by him. The current development stage of string transport complexes inspires and proves in practice the feasibility of the original hypothesis. Therefore, we confidently look to the future and believe that the string transport is the most promising line of development for the global transport and infrastructure sector.

The existing infrastructure solutions have exhausted themselves, ceased to meet the imperatives of our time and do not open any new opportunities. The existing transport is in fact not a solution to many problems, but their source. About 1.5 mln people die in traffic-related accidents worldwide annually, and over 10 mln people get injured and become disabled. Rolled up in asphalt and buried under railway sleepers is fertile soil, the area of which is equal to five areas of Great Britain. Soils are degraded and contaminated with carcinogens on the territory ten times larger. We all have forgotten that we did not inherit the Earth from our ancestors – we borrowed it from our children.

Transport – cars, aircraft, railway, helicopters, ships and rockets, industrial conveyors, oil and gas pipelines, as well as industry and infrastructure associated with the same is one of the

main sources of environmental contamination and poses the greatest environmental hazard. The existing transport corridors are overloaded, the actual speed of passenger and cargo transportation is obviously inadequate, whereas the construction of new communications is unaffordable for the whole range of countries and regions due to their skyrocketing prices.

All this impedes the progressive development of the world economy and causes uneven distribution of social and infrastructure benefits among the population of the planet. The string transport will provide a comprehensive solution to address the global challenges, particularly through its transport and infrastructure part, which will be realized in the 21st century as a global network – Transnet. Its total length will cover dozens of millions of kilometres and will be similar to its “elder brother” the

Internet. Transnet will be able to meet the whole range of communications requirements (not only transportation, but also energy and information requirements) being at the same time much more cost-efficient and effective compared to all the existing alternatives. In addition, it is characterized by a high level of safety, durability and sustainability.

Unibuses and unicars will be able to move at a speed of up to 150 km/h in the city – they will unclog the existing highways, reduce noise pollution as well as hazardous emissions into the atmosphere. High-speed unibuses and unilyots for intercity connection can reach the speed up to 500–600 km/h; with special design, in a forevacuum tunnel – up to 1,250 km/h. However, the construction cost for all kinds of elevated string transport (urban, cargo, high-speed and hyper-speed) is by several times lower

compared to other transport systems of the second level comparable in terms of speed and volume of transportation.

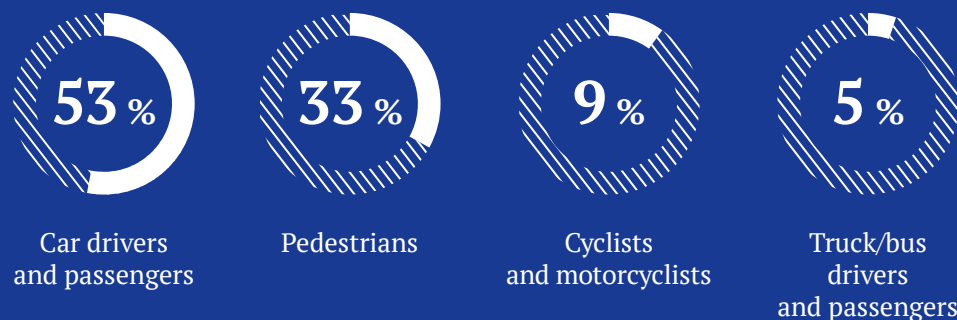
A possibility of construction on territories with a challenging terrain and adverse climatic conditions, small footprint, preservation of natural landscapes, versatility and integrability with communications lines, power transmission lines – these are just a few of many advantages that the string technology provides. Taking all this into consideration, it is safe to say that the universal application of such systems can contribute to a vigorous and large-scale growth in the social and economic life of any country worldwide.

The string transport can become a framework and a technical basis to consolidate the society. This is also confirmed in practice. The project managed to gather around a million participants from 237 countries and

FF
The string transport can become a framework and a technical basis to consolidate the society.

territories all over the world (it is actually more than in the UN) for the period of 2014–2017 – just in three years from the moment the author of the monograph announced a crowdfunding program for the construction of the string transport test sections. All these people encourage the technology development in one way or another; over 300,000 of them have already become investors. This happened without any large advertising campaigns or government support. Therefore, one can only imagine those tremendous

Car accident groups



62 % of all traffic fatalities occur in 10 countries



Source: World Health Organization

“The UPT implementation will open up for the humanity unlimited prospects for space colonization.”

opportunities for the consolidation of the society that the string transport technologies, which are not limited to only SkyWay, represent, if their widespread introduction is offered at

the level of the national or international program.

The very essence of transport implies uniting people. The string transport can fulfill this purpose both at the local and general planetary levels. The description of the corresponding transport system for the industrial exploration and space colonization – also a string one – is given in the second part of this scientific monograph.

United Planetary Transport (UPT) is a reusable geocosmic transport and infrastructure complex for the non-rocket exploration of near space. In the future, it will allow to take about 10 mln tons of cargo and 1 mln

“Science has no period of limitation. It is not worth adjusting or rebuilding it to fit the current market trends.”

people involved in the creation and operation of the circumterrestrial space industry to the orbit in one trip. The modern world rocket and space industry that has already got investment in the amount of trillions of dollars by now would require about a million years to accomplish what the UPT can do in just one year. The UPT will be able to go out into space up to 100 times per year. Along with that, the cost of shipping each tonne of payload to the intended orbit will be thousands of times lower than by the existing carrier rockets.

The UPT implementation will open up for the humanity unlimited

prospects for space colonization. It will be possible to transfer all harmful production from our homeworld to space to avoid the contamination of the terrestrial biosphere. Nowadays similar ideas gain in popularity since space is a virtually inexhaustible source of energy, raw materials, spatial resources and fundamentally new technological opportunities (zero gravity, deep vacuum, etc.) that can be used for industrial purposes. This allows producing better quality products compared to those produced on the Earth, at a lower cost, without doing damage to our common home – the biosphere. At the same time, it will give an opportunity to ultimately solve the ecological issues and provide a comfortable living environment for new generations.

The UPT project was developed by the author of the monograph nearly 40 years ago and has been repeatedly examined and verified by computational methods during this time. All engineering solutions employed in the





project are widely known, tried and tested, and implemented in industry now. The project budget will amount to about 2 tln USD, with the implementation period of about 25 years.

At present, there is practically no place left on the planet free from transport-related problems. My engineering school offers the technologies to address these issues, transform the life for the better and set the vector for the civilization development for many centuries ahead!

We have already achieved substantial results and have passed on from pure science to production and commercial realization of string transport systems. We continue to work, develop ourselves, grow and are ready to come to any place and any cou-

ntry, which is not devoid of the sense of responsibility for the future – its future and the future of the whole planet.

The author deliberately refused to edit his previous scientific work written by him about 30 years ago and published in 1995. Therefore, the first publication of the monograph including its preface has not been changed. Only new illustrations and photos have been added to show how this theoretical scientific research has made headway to the practical implementation in metal, concrete and composites.

Science has no period of limitation. It is not worth adjusting or rebuilding it to fit the current market trends – to enable jet flights to the Moon to

get helium-3 or to the Mars to build a colony there and die in a spacesuit not only from suffocation in human waste but also because of the absence of our Earth’s air and our Earth’s healthy food.

*Affectionately yours,
Anatoli Unitsky*

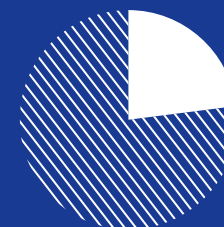
Air pollution sources



Soil pollution sources



Water pollution sources



23%
of deaths worldwide are related to environmental pollution

Source:
World Health Organization

**TIPS-based
(Theory of Inventive
Problem Solving)
history of Unitsky's
String Technologies**



22

TIPS-based (Theory of Inventive Problem Solving) history of Unitsky's String Technologies

A boy from an obscure village of Kryuki in the center of the marshes of the Belarusian Polesie in the Gomel region was fascinated by the space since he was six. He did not know anything about Konstantin Tsiolkovsky, the pioneer of the astronautic theory; he did not read anything about aerospace engineers Wernher von Braun and Sergei Korolev; and the first cosmonaut Yuri Gagarin did not yet make his historic flight... But the boy began to draw and design rockets with no reason.

Not only to design, but also to launch them "into space". As "fuel", he used combs that burned no worse than gunpowder, scraps of Soviet films that

the projectionist threw out while rewinding the tapes, preparing to show the film in a rural club. But the most suitable for this purpose was German smokeless gunpowder, that looked like long macaroni. The young inventor



*He had no doubts
and believed
that the future
of the humankind
is in the space.*

1949

1951

1953

1955

1957

1959

1961

1963

searched a site of the German weapons warehouse blown up by the partisans near Posudovo railway station (just 8 km from his native village) for it.

This was unsafe. The site of the former weapons warehouse was marked with warning signs for those inquisitive boys who died trying to disassemble shells and mines found there. However, this did not stop the young enthusiast, although he knew that it was a minefield. He tried to be very careful.

It was in the mid-1950s and that boy was Anatoli Unitsky.

In 1962, the family moved to Kazakhstan, to the city of Jezkazgan, in search of a better life: it was hard to make living for a mother with two children in their village. There was the Baikonur cosmodrome not far from the place where they settled. Observing how real rockets take off into the sky, Anatoli's interest became even stronger. He had already constructed more sophisticated devices than before: developed the technology of making the bodies of rocket mock-ups and stabilizers from paper and office glue – the only materials available for a pupil of those years. He made solid-fuel engines, the temperature in which reached thousands of degrees, from multilayer composites that he invented – blotter sodden with a special glue, wounded



on the very same invented driftpin. Experimentally, he picked up a composition of black smoke powder from components that were sold in pharmacies and hardware stores. When young Anatoli was in the eighth grade, his multi-stage rockets were already able to climb a few kilometers. He also had "astronauts" – gray mice, which then descended on parachutes made of tissue paper.

Anatoli Unitsky quickly realized the imperfection and drawbacks of the rockets. Not only in his mock-ups. He once noted that it was possible to learn about the next launch (Baikonur cosmodrome was 200 km away) not only from tomorrow's newspapers,

EE
Anatoli revealed and understood the environmental problems of the rocket way of space exploration: climate change and destruction, magnetic storms, sharp cooling or heating.



but also due to a sharp change in weather – not for the better. In those days, the successful launch was highlighted in the press, and when something went wrong, they kept it secret.

Having gained the basic knowledge in physics and mathematics, participating in numerous math competitions, having thoroughly studied the works of Tsiolkovsky, Anatoli Unitsky began his independent analysis of the rocket way of space exploration. He was fascinated by science fiction, began to study the scientific papers of foreign scientists and inventors. He had no doubts and believed that the future of the humankind is in the space.

But, unfortunately, it was a big disappointment.

It turned out that the energy efficiency of a launch vehicle, considering the extra energy costs for fuel components and expendable elements, is less than 1 %. Even the modern steam locomotive efficiency was 15 %. The efficiency of a photon spacecraft, using which the science fiction writers explored the universe, was significantly less than one thousandth of a percent. This discovery (he did all the necessary calculations himself) stunned the young scientist.

Such space technological solutions as excessive jet engine power of launch vehicles (about 100 mln HP), high jet flow rates (many times higher



than the speed of the fastest bullet), high temperatures of the combustion products (twice the temperature in the open-hearth furnace) did not inspire the inventor and made him upset. All this rocket power was thrown out not just in the terrestrial atmosphere in which we all live, but in the most vulnerable upper layers – the ozone layer and the ionosphere.

Anatoli revealed and understood the environmental problems of the rocket way of space exploration: climate change and destruction, magnetic storms, sharp cooling or heating. It was aggravated by the extremely

high toxicity of rocket fuel and its combustion products: some fuels turned out to be so poisonous that only 2 mg is enough to kill a man.

Anatoli Unitsky was even more surprised when he realized what transport job the launch vehicle could do. After all, a rocket is just a vehicle, and nothing more. A vehicle!

Being calculated using elementary mathematics, it turns out that in just a few decades only about 10 thousand tons of useful cargoes have been sent to the near-Earth orbit at altitudes of about 300 km. On Earth the same volume of cargo over the same years

1965

1967

1969

1971

1973

1975

1977

1979

“Going beyond the everyman, Anatoli Unitsky asked himself what would happen if the transport system rises to space, and its center of mass remains in place, that is, on the Earth?”



and at the same 300-kilometer distance can be moved just by one horse, harnessed into a single wagon.

Therefore, a paradoxical and disappointing conclusion arises: all the achievements of modern cosmonautics are secured by a single (insanely expensive) “space wagon”. It is a wagon, which pulls the same posh “space horse”, efficiency of which is much lower than that of a locomotive, and more dangerous than the most venomous snake.

In such a way, Anatoli destroyed his youthful dreams of a bright future – space cities, orbital factories and power plants. They cannot be serviced with only one “wagon”. So, his illusions continued to collapse. When in 15 years Unitsky published his findings and reasoning in Soviet popular

science magazines, he became a person of interest for the KGB. Reasons? There were two. First, he dared to doubt the great achievements of Soviet space science and technology. The second – he proposed a pseudoscientific way of non-rocket exploration of the outer space.

Anatoli further deepened his knowledge. He entered Tyumen industrial Institute, specializing in the railway (roads and facilities) engineering.

In the future, he needed the knowledge gained in the Institute on the strength of materials, theory of elasticity, theoretical mechanics, construction mechanics, physics, higher mathematics, design of suspension and cable-stayed bridges, theory of mechanisms and machines and other sciences.

Student Unitsky discovered the greatest opportunities for research. He understood that the most environmentally friendly way to escape to the outer space is to use the so-called Baron Munchhausen principle as an engine for the space transportation system. Everyone knows that the famous Baron raised himself and his horse over the swamp pulling himself by his own hair bunch.

It would seem like a fantasy, a fairy tale, and impracticable. But Anatoli saw the main advantage in this principle that was good because the Munchhausen’s transport system, climbing up, was not supported by the external environment and it was absolutely ecofriendly.

However, there was one thing. The Baron did not study in a Soviet

school and therefore could not know that he violated one of the conservation laws: you cannot move the center of mass of the system in space at the expense of its internal forces. We know that the Baron could

“Then the answer came: then there would no limits using the internal forces of the system, and after that, it would be possible to create the most environmentally friendly space transport.”

1981

1983

1985

1987

1989

1991

1993

1995

This structure can become stable only in one case: if it is stretched, that is, if it is a string.

only tear off his hair bunch or break his arm, but could not raise (pull out of the swamp) himself and the horse.

Going beyond the everyman, Anatoli Unitsky asked himself what would happen if the transport system rises to space, and its center of mass remains in place, that is, on the Earth? Then the answer came: then there would be no limits using the internal forces of the system, and after that, it would be possible to create the most environmentally friendly space transport.

At first glance, it seems that this task does not have a solution. But, according to Unitsky, it is very simple. A spacecraft must be made not in the form of a rocket, but in the form of a ring. The ring is worn on the globe equatorially. It can increase in diameter and reach an altitude of 300 km or more, for which it is necessary to stretch it by about 5 %, because the initial diameter of the ring is equal to the diameter of the planet – 12,756 km.

In both cases, whether the ring lies on the surface of the planet or the ring is in orbit, the center of mass of the transport system will remain in the same place, since it will always match the center of mass of the planet.

How to increase the diameter of the ring? For example, it can be inflated like a balloon. However, it is clear that the gas pressure in this case should be equal to billions of atmospheres, and it is known that no material of the ring walls will withstand such pressure.



Such a structure also cannot be self-supporting (like in one of Nikola Tesla's ideas, where he proposed to build an unsupported bridge around the equator), because it is equivalent to building an arch bridge with a span equal to the Earth's diameter, that is more than 12 thousand km. There are no such strong materials, and the structure, compressed by such huge loads, will lose its stability, since its transverse dimensions are infinitesimal compared to its length. Even if it is assumed that this torus is 10 m across, the ratio of this transverse dimension

to the ring length (40 thousand km) will be 1 : 4,000,000.

This structure can become stable only in one case: if it is stretched, that is, if it is a string. This structure must be stretched by internal, rather than external forces. Technically, it is permissible to do this using centrifugal force, if there is a circular vacuum tunnel inside the torus covering the planet. Inside the tunnel there should be an infinite (also circular, encompassing the planet) rotor suspended by a magnetic field without touching the walls.

When using a linear electric motor the rotor is accelerated inside the vacuum tunnel, that is, around the Earth, to the first cosmic velocity, it will become weightless. If it continues to spin further, then there will be an excessive centrifugal force, which will tend to increase the diameter of the ring. If this force exceeds the weight of the structure, then each linear meter will begin to rise vertically upwards. The ring, increasing in diameter silently, and correspondingly, stretching, for a couple of hours will take a circular orbit, for example, at an altitude of 300 km, lifting millions of tons of cargo into space and, if necessary, millions of passengers per one trip.

Having found the principal solution, Anatoli Unitsky continued to develop the design of the United Planetary





Transport (UPT) at the engineering and design levels.

In 1986, he became a member of the USSR Cosmonautics Federation, and in 1988 he conducted the First International Scientific and Technical Conference “Non-rocket Space Industrialization: Problems, Ideas, Projects” in Gomel, where UPT became the main project for the future space industrialization. He created its own school of sciences and published the first scientific monograph “String Transport Systems: on Earth and in Space” in 1995.

“The inventor made the next step: why not to put a rail car on this string overpass and to simplify the overpass to a string rail.”

2013

2015

2017

2019

2021

2023

2025

2027

He obsessively worked on the project. At the same time, he faced a barrage of criticism; foes tried to lead him astray. Their main reason for the impracticability of the project was that for its implementation (construction of an overpass around the Earth, with which UPT should be started) there was not enough building materials.

To dispose these dubious arguments, Unitsky had to deal with the optimization of the overpass. It delivered its benefits. The optimization led to a lightweight string structure, for the construction of which it would be enough to use the concrete, used in the dam of just one Sayano-Shushenskaya HPP, and the metal, spent just for every twentieth car manufactured on the Earth.

The inventor made the next step: why not to put a rail car on this string overpass and to simplify the overpass to a string rail.

Step by step, the Unitsky String Transport (UST) was created. It provides two variants: mounted (a rail car stands on two string rails) and suspended (a rail car is suspended from below a string track structure consisting of one or two string rails), as well as five classes: ultra-light, light, medium, heavy and ultra-heavy for the speed range from 40 to 500 km/h.

The development of the load-bearing string structures subsequently led to the creation of string bridges and

“The entire world and universe come to a single Design: made of the smallest quantum strings.”

overpasses, string runways, string high-rise buildings, string vacuum glass and other various string technologies. It is well-known that the string design is widely used in the nature. For example, the bones of our skeleton are so strong because they are made of strings: some fibers are stretched (pre-stressed) in them; others are compressed. Indeed, the entire world and universe come to a single Design: made of the smallest quantum strings.

One of the chapters of the documentary novel by Anatoli Borovsky “Unitsky’s Sky Ways” / 2nd ed., Ext. – Gomel: JSC Polespechat, 2014. – Pp. 300–306.

**History
of SkyWay
in pictures**



34



Eduard and Yulia Unitsky together with their nine-month old son Anatoli. 1950



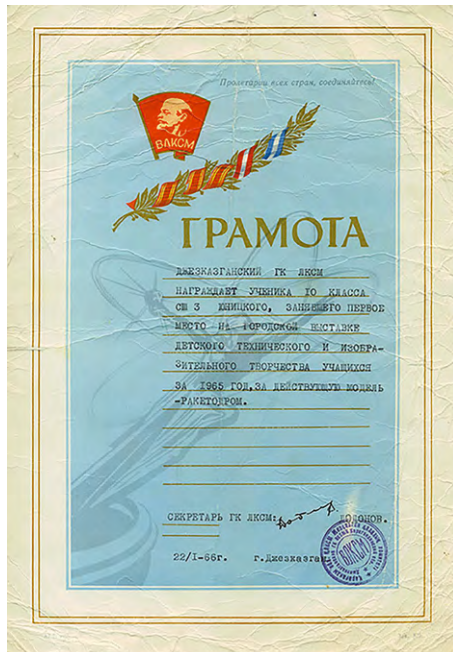
The 3rd grade of the Kryukov school. In the center – teacher Polina Aleksandrovna and her favorite pupil little Anatoli Unitsky. May 1959



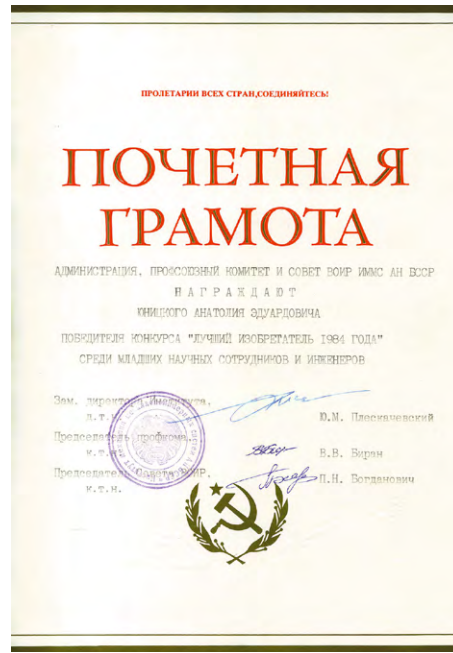
Little Anatoli with his sister Tamara. 1954



Little Anatoli Unitsky. 1963



The first award of Anatoli Unitsky: Diploma for the acting model of a rocketdrome. January 1966



Diploma of Honor granted to Anatoli Unitsky, the winner of the Contest "The Best Inventor of 1984"



Anatoli Unitsky's Copyright Certificate



Mass media about the string transport and UPT projects, developed by Eng. Anatoli Unitsky



From an article in “Belarus” magazine. March 1987



Scene from documentary film “To the Sky by Wheel”, Belarusfilm Film Studio. 1989



Institute of Mechanics of Metal-Polymer Systems of the Academy of Sciences of the BSSR. 1987



Conference “Non-rocket Industrialization of Space: Problems, Ideas, Projects”. Gomel, April 1988



Monograph “String Transport Systems: on Earth and in Space” by Anatoli Unitsky. 1995



Fair "Innovations". Leipzig, March 1995



Wind-tunnel test of a high-speed unibus model (scale 1 : 5).
St. Petersburg, February 1996



United Nations Grant FS-RUS-98-S01 for the project
"Sustainable Development of Human Settlements and Improvement
of Their Communication Infrastructure with the String Transport System". 1998



UST at the Exhibition organized by the Moscow Administration. May 1999



Wind-tunnel test of a double-body unibus model (scale 1 : 5).
St. Petersburg, October 2000



Exhibition Special Transport-99. Moscow, May 1999



First test of a double-rail track and a double-body unibus model (scale 1 : 5).
Tushino airfield, December 2000



Presentation of UST acting models (scales 1 : 5 and 1 : 10)
to Moscow Region Governor Mr. Boris Gromov. Ozyory, December 2000



Demonstration of UST acting model (scale 1 : 5)
to the Administration and residents of Ozyorsky district.
Ozyory, Moscow Region, January 2001



Ambassador Extraordinary and Plenipotentiary
of Malaysia Datuk Yahya bin Baba got acquainted with UST.
Kolomenskoye Museum-Reserve, Moscow, January 2001



Presentation of UST acting model (scale 1 : 5).
Kolomenskoye Museum-Reserve, Moscow, January 2001



Work on high-speed unibus design (scale 1 : 1). Moscow, March 2001



Presentation of UST acting model (scale 1 : 5) to the officials of the Ministry of Transport of the Russian Federation. Moscow, May 2001



Presentation of UST acting model (scale 1 : 5) to the Ambassador of Philippines to the Russian Federation. Moscow, April 2001



UST acting model at the 6th national exhibition "Technologies from Russia - 2001". Moscow, May 2001



Anatoli Unitsky and Nadezhda Kosareva at the Track Structure stand under construction at the UST test site. Ozyory, Moscow Region, June 2001



Installation of assemblies for the second anchor support at the UST Track Structure stand under construction. Ozyory, Moscow Region, August 2001



Wind-tunnel test of a high-speed unibus model. St. Petersburg, August 2001



Solemn reception at the Embassy of Malaysia on the occasion of Malaysia's Independence Day. Moscow, August 2001



Solemn reception at the Embassy of Malaysia on the occasion of Malaysia's Independence Day. Moscow, August 2001



Demonstration of trial tests of UST track structure to Moscow Region Governor Mr. Boris Gromov. Ozyory, Moscow Region, October 2001



Presentation of UST Track Structure stand under construction to First Deputy Minister of Transport of the Moscow Region Mr. Andrey Kokurin. Ozyory, Moscow Region, October 2001



Moscow Region Governor Mr. Boris Gromov visited the trial tests of UST track structure. Ozyory, Moscow Region, October 2001



Trial tests of UST track structure. Ozyory, Moscow region, October 2001



Krasnoyarsk Krai Governor Mr. Alexander Lebed visited the official presentation of UST Track Structure test stand. Ozyory, Moscow Region, October 2001

UN HABITAT
FOR A BETTER URBAN FUTURE

Центр ООН по населённым пунктам (Хабитат)
Правительство Российской Федерации
Государственный комитет Российской Федерации
по строительству и жилищно-коммунальному комплексу

**ОБЕСПЕЧЕНИЕ УСТОЙЧИВОГО РАЗВИТИЯ НАСЕЛЁННЫХ ПУНКТОВ
И ЗАЩИТА ГОРОДСКОЙ ОКРУЖАЮЩЕЙ СРЕДЫ
С ИСПОЛЬЗОВАНИЕМ СТРУННОЙ ТРАНСПОРТНОЙ СИСТЕМЫ**

Номер проекта:
FS-RUS-02-S03
Январь 2002 г.

Подписано:
от Центра ООН
по населённым пунктам (Хабитат)

А. ТИБАЙДЖУКА
Исполнительный директор программы ООН
по населённым пунктам (Хабитат)

Подписано:
от Правительства
Российской Федерации

А.Ш. ШАМУЗАФАРОВ
Председатель Госстроя России

United Nations Grant FS-RUS-02-S03 for the project “Sustainable Development of Human Settlements and Protection of Urban Environment with the String Transport System”. 2002



UST at the international exhibition of urban transport CityTransExpo. Moscow, February 2002



Demonstration of UST to First Deputy Minister of Transport of the Russian Federation Mr. Anatoly Nasonov at the CityTransExpo international specialized exhibition of urban transport. Moscow, February 2002



Working visit of First Deputy Minister of Transport of the Russian Federation Mr. Anatoly Nasonov to the UST test site. Ozyory, Moscow Region, March 2002



Presentation of UST project and acting model at a meeting in the State Committee for Construction of Russia. Moscow, December 2004



Presentation of UST to General Director of Dubai Municipality. Dubai, April 2005



Presentation of suspended UST acting model to Deputy Mayor of Khabarovsk Mr. Victor Novitskiy and Director of UN-Habitat Center in Moscow Mr. Vladimir Storchevus. Khabarovsk, April 2006



Demonstration of UST acting model to Mayor of Bishkek Mr. Arstanbek Nogoiev. Bishkek, February 2006



Negotiations with partners from China. Sharjah, July 2006



Presentation of the widespread application of UST in the conditions of the Far North of Russia to Khanty-Mansi Autonomous Okrug – Yugra Governor Alexander Filipenko. Khanty-Mansiysk, July 2006



Presentation of Nizhny Novgorod – Moscow high-speed UST project to Nizhny Novgorod Region Governor Valery Shantsev. Nizhny Novgorod, June 2007



UST LLC at the exhibition of investment projects “Yugra Invest – 2007”. Khanty-Mansiysk, October 2007



High-speed SkyWay (visualization). 2008



Moscow – St. Petersburg high-speed track (*visualization*). 2009



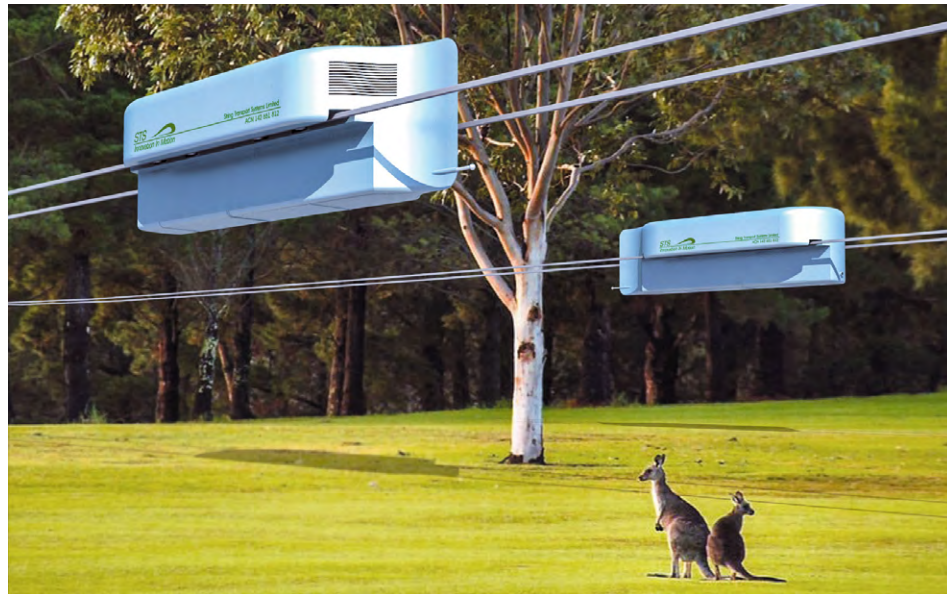
SkyWay passenger station for suspended unibuses (*visualization*). 2009



Demonstration of UST test stand to businessman Mr. Ahmad from Iran.
Ozyory, Moscow region, July 2009



SkyWay cargo cableway in Australia (*visualization*). 2010



SkyWay cargo track in Australia for mounted unitrucks with a low center of gravity (visualization). 2010



High-speed SkyWay (visualization). 2011



SkyWay large-capacity urban mounted unibus (visualization). 2011



SkyWay urban mounted unibus (visualization). 2011



SkyWay cargo mounted train on a double-track string truss-type overpass (visualization). 2011



Transfer station from high-speed interurban to urban SkyWay (visualization). 2012



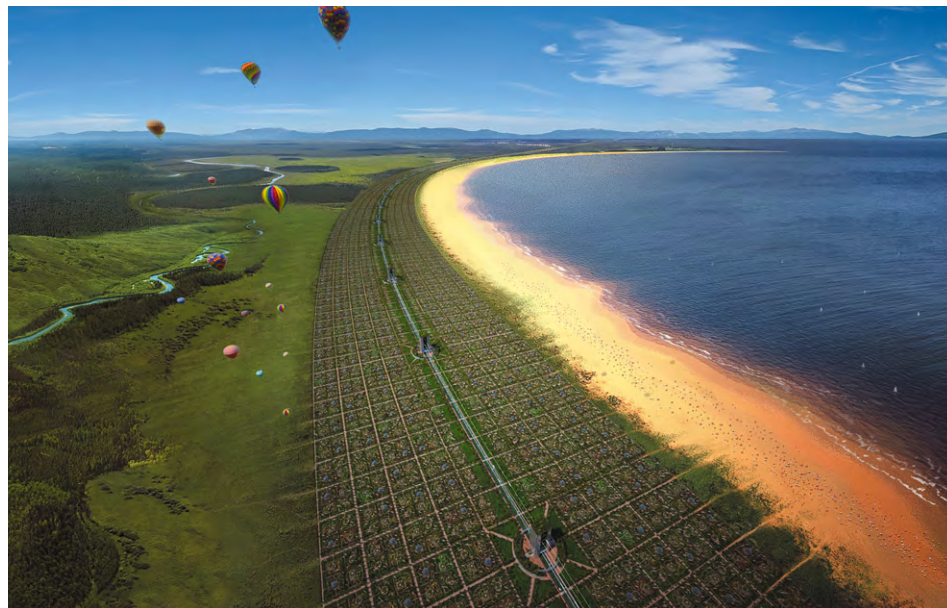
At TV show "Brainstorm: New Transport". Moscow, February 2013



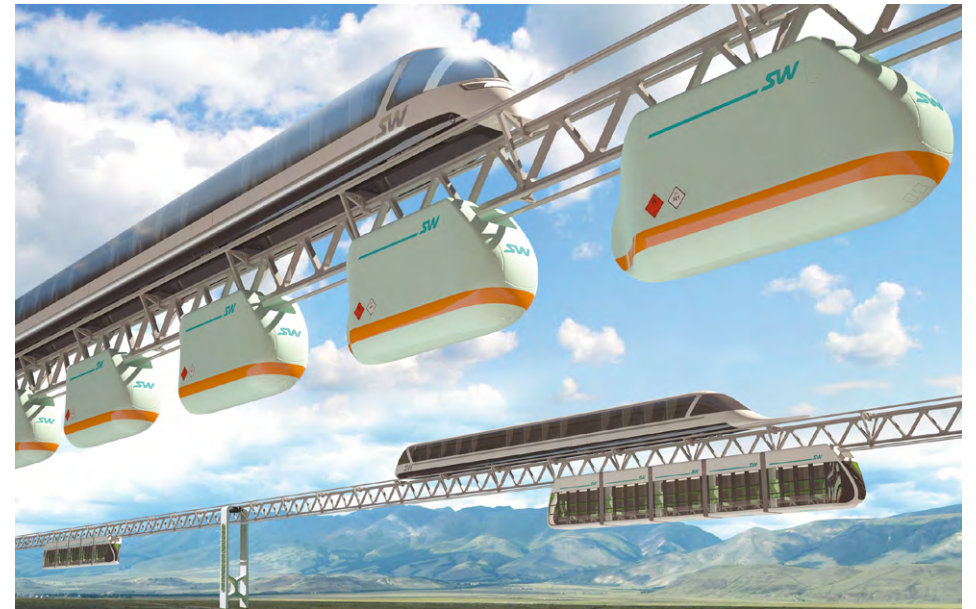
International scientific and technical conference "SkyWay technology – the core of the Eurasian development". Minsk, June 2014



Urban mounted SkyWay in the linear city on sea shelf (visualization). 2014



SkyWay linear city on seashore (visualization). 2014



SkyWay rolling stock (visualization). 2015



SkyWay offshore track with a sagging track structure (visualization). 2015



Excavation for the anchor support in EcoTechnoPark. Maryina Gorka, August 2015



"Plant a Tree" Campaign in EcoTechnoPark. Maryina Gorka, October 2015



SkyWay Kilometer Zero. EcoTechnoPark, Maryina Gorka, October 2015



Grand opening of SkyWay Kilometer Zero. EcoTechnoPark, Maryina Gorka, October 2015



Participants of the Conference dedicated to the Grand opening of SkyWay Kilometer Zero. Minsk, October 2015



SkyWay EcoFest. EcoTechnoPark, Maryina Gorka, April 2016



Construction of the pylons of the first high-speed anchor support SkyWay. EcoTechnoPark, Maryina Gorka, November 2015



SkyWay EcoTechnoPark visit by the former Head of Department of Planning, Transport and Infrastructure of South Australia Mr. Rod Hook. Maryina Gorka, June 2016



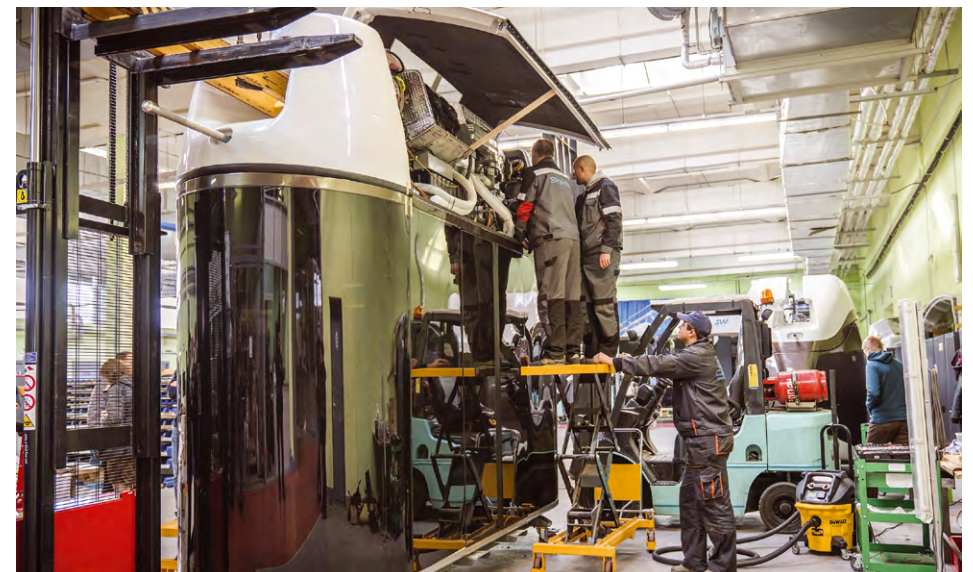
SkyWay Technologies Co. team. Minsk, 2016



Installation of the trusses of the urban track structure.
EcoTechnoPark, Maryina Gorka, February 2017



SkyWay General Designer Anatoli Unitsky became Honorary Vice-President
of the Arab-Slovak Chamber of Commerce and Industry.
Minsk, February 2017.



SkyWay pilot production workshop. Minsk, February 2017



SkyWay General Designer Anatoli Unitsky with the spiritual leader of Tibet Dalai Lama XIV during a business trip to India. Dharmsala, May 2017



SkyWay EcoFest. EcoTechnoPark, Maryina Gorka, July 2017



SkyWay General Designer Anatoli Unitsky presents a three-section unicar at the XI International Exhibition "Transport of Russia". Moscow, December 2017.



Agreement on integrated cooperation of SkyWay Technologies Co. with the Russian University of Transport. Moscow, December 2017



Nadezhda Kosareva, General Director, SkyWay Technologies Co. 2018



Serving the certificates confirming the compliance of the quality management system applied in the Company with the requirements of the international standard ISO 9001: 2015, and the national standard of the Republic of Belarus STB ISO 9001-2015, to Nadezhda Kosareva, General Director, SkyWay Technologies Co. Minsk, March 2018



Testing of unitruck. EcoTechnoPark, Maryina Gorka, 2018



Unibike and unibus. EcoTechnoPark, Maryina Gorka, 2018



Testing of a double-rail unibus. EcoTechnoPark, Maryina Gorka, 2018



New model of SkyWay rolling stock – uniwind.
EcoTechnoPark, Maryina Gorka, 2018



SkyWay cargo complex, the overpass of which has two structures:
a conveyor belt (unitrans) and cargo modules (unitruck).
EcoTechnoPark, Maryina Gorka, 2018.



Testing of traction modules of a double-rail unibus UR-220.
EcoTechnoPark, Maryina Gorka, 2018



International Exhibition Railway Tech Indonesia 2018.
Jakarta, March 2018



Testing of unibus in EcoTechnoPark. Maryina Gorka, May 2018



International Exhibition Future Cities Show 2018.
Dubai, April 2018



Testing of unicar in EcoTechnoPark. Maryina Gorka, May 2018



EcoFest 2018: SkyWay General Designer Anatoli Unitsky speaks to thousands of investors from dozens of countries across the world. EcoTechnoPark, Maryina Gorka, August 2018



SkyWay EcoFest. EcoTechnoPark, Maryina Gorka, August 2018



Testing of new types of SkyWay rolling stock. EcoTechnoPark, Maryina Gorka, September 2018



Presentation of SkyWay project "Unimobile" at the specialized exhibition "InvaExpo. Society for Everyone". Moscow, September 2018



Design of SkyWay Innovation Center (SWIC) in Sharjah (visualization).
UAE, November 2018



Grand opening of the construction site of SkyWay Innovation Center in Sharjah.
UAE, November 2018

PASSENGER	
	UNIWIIND U4-651 PASSENGER CAPACITY: 2 MAXIMUM SPEED: 150 km/h
	UNIBIKE U4-621 PASSENGER CAPACITY: 2 MAXIMUM SPEED: 150 km/h
	UNICAR U4-430 PASSENGER CAPACITY: 6 MAXIMUM SPEED: 150 km/h
	UNICAR U4-430-T3 PASSENGER CAPACITY: 18 MAXIMUM SPEED: 150 km/h
	UNIBUS U4-210 PASSENGER CAPACITY: 14 MAXIMUM SPEED: 150 km/h
	UNIBUS U4-210-T2 PASSENGER CAPACITY: 28 MAXIMUM SPEED: 150 km/h
	UNIBUS U4-210-T3 PASSENGER CAPACITY: 42 MAXIMUM SPEED: 150 km/h
	UNIBUS U4-220 PASSENGER CAPACITY: 24 MAXIMUM SPEED: 150 km/h
	UNIBUS U4-220-T2 PASSENGER CAPACITY: 48 MAXIMUM SPEED: 150 km/h
	UNIBUS U4-220-T3 PASSENGER CAPACITY: 72 MAXIMUM SPEED: 150 km/h
	HIGH-SPEED UNIBUS U4-365 PASSENGER CAPACITY: 6 MAXIMUM SPEED: 500 km/h
FREIGHT	
	UNITRUCK U4-131 LOAD CAPACITY: 1700 kg MAXIMUM SPEED: 150 km/h
	UNITRANS U4-100 LOAD CAPACITY: 65 kg/1 lin. m MAXIMUM SPEED: 36 km/h
	UNICONT U4-192-01 LOAD CAPACITY: 32,000 kg MAXIMUM SPEED: 120 km/h

SkyWay vehicle range. 2018



SkyWay high-speed unibus was demonstrated to a wide audience at the specialized transport exhibition InnoTrans for the first time. Berlin, September 2018



SkyWay General Designer Anatoli Unitsky and SkyWay flagship – high-speed unibus. Berlin, September 2018



Transport Exhibition InnoTrans. Berlin, September 2018



SkyWay General Designer Anatoli Unitsky is awarded with the International Peace Prize from Slovakia. Bratislava, December 2018.



SkyWay linear city (visualization). 2018



SkyWay linear city (visualization). 2018



SkyWay sea port (visualization). 2018



United Planetary Transport (UPT) (visualization). 2018

Optimization of Transportation System



92

Optimization of Transportation System*

Over 300 types and design variants of transportation systems are known at present. However, which of them is near-perfect? What is an ideal transportation system?

If the cargo is loaded at point A – for example, in London – and delivered to point B – for example, to Vladivostok – the energy state of the cargo does not change, it has the same height above sea level and the same zero speed relative to the Earth’s surface at point B. In this case, the effective transportation work in the Earth’s gravitational field equals zero from the physics point of view; ideally, the energy consumption required to move the load should equal zero as well. Since the energy is consumed anyway, the efficiency factor of any real ground transport system will always be zero from the standpoint of mechanics as zero divided by any number results in zero. Any ground vehicle consumes energy not for efficient transportation but for overcoming environmental resistance and destruction of this environment. Therefore, improvements in transportation should be aimed not at increasing engine power, payload, passenger capacity or speed, as is the case now, but at reducing the resistance to movement – primarily in high-speed transportation (over 300 km/h) since many types of resistance increase in proportion to the velocity squared and cubed.

Table 1 shows an analysis of the main types of resistance to movement of an average high-speed transport module moving at a speed of 100 m/s (360 km/h), having a mass of 10 tons (module – 50 passengers) and a cross-sectional area (mid-section) of 5 m². The main resistance to the movement of such a vehicle is aerodynamic resistance, which depends not only on the shape of the vehicle body and the quality of its surface but also on its placement relative to the track structure.

The monorail suspension pattern used in the Transrapid Maglev train, Germany (table 1 – leftmost pattern), has the highest value of the aerodynamic

* Based on the article by Anatoli Unitsky “Optimization of Elevated Transport System” published in the Engineering and Automation Problems International Scientific Journal (Moscow). – 2005. – No. 4. – Pp. 45–50.

Table 1 – Resistance to movement of an average high-speed transport module

Value	Aerodynamic resistance**			Wheel			Air suspension (air cushion) (efficiency factor 30%)	Magnetic levitation + linear electric motor (efficiency factor 40%)
	Diagram	C_x^{min}	$C_x^{min} = 0.1$	Pneumatic tire ($k_{tr} = 0.05$)	Steel with conic wheels ($k_{tr} = 0.001$)	Steel with independent suspension without a cone ($k_{tr} = 0.0005$)		
Resistance power, kW		1,120	310	500	10	5	2,600	1,700
Fuel consumption, t/year		1,220	620	550	11	5.5	2,800	1,800
Cost of fuel, thous. USD/year****		610	340	275	5.5	2.75	1,400	900
Resistance power, mln kW		11,200	6,200	5,000	100	50	26,000	17,000
Fuel consumption, mln t/year		12,200	6,800	5,500	110	55	28,000	18,000
Cost of fuel, bln USD/year		6,100	3,400	2,750	55	27.5	14,000	9,000
Fleet of modules on the planet (10 mln pcs)								

* Average transport module: motion speed – 10 m/s (360 km/h); weight – 10 t; capacity – 50 passengers (6 t of cargo); utilization factor – 0.5 (12 h/day); fuel consumption – 0.25 kg/kWh; compartment mid-section – $f_m = 5 \text{ m}^2$.

** Aerodynamic resistance power: $P_{ar} = \frac{1}{2} \rho v^3 C_x f_m$ (where ρ – air density, v – motion speed, C_x – aerodynamic drag coefficient, f_m – compartment mid-section).

*** k_{tr} – wheel rolling resistance.

**** Worldwide average fuel cost – 0.5 USD/kg.

drag coefficient C_x . Its value at a speed of 100 m/s cannot be lower than 0.3 due to the skirt covering the carrier beam and the velocity gradient in the air gap between the skirt moving at a speed of 100 m/s and a fixed beam. The minimal possible value C_x for the vehicle placed close to the roadbed (as is the case with the car) is 0.2 due to the aerofoil effect created by a fixed roadbed (table 1 – pattern in the middle). A wingless vehicle flying at an altitude of 10 m or more has the lowest value $C_x = 0.1$ (table 1 – rightmost pattern). In the first case, the aerodynamic drag power will be 1,120 kW (power of two tank engines), in the second case – 620 kW (power of a diesel-locomotive shunter), in the third – 310 kW (engine power of a modern high-speed car)

The difference in aerodynamic drag power is especially significant considering the scale factor. Suppose that 10 mln high-speed modules will operate on 10 mln km of roads in the future, considering that the length of the road network in the world exceeds 30 mln km today. That makes one module per 1 km of tracks or one module per 600–800 inhabitants, which is about 50 times less than cars. Then, the annual fuel consumption to overcome aerodynamic drag will amount to 12.2 bln tons for modules with a skirt and 6.8 bln tons for modules of a car type. This exceeds the anticipated oil production – according to the World Energy Council, the global oil consumption will reach 5.3 bln tons in 2020. The cost of annual fuel consumption by high-speed transport will be as follows: in the first case – 6.1 tln USD, whereas in the second case – 3.4 tln USD (based on the worldwide average fuel price of 0.5 USD/kg as of 2005).

Only a wingless aircraft named “unibus” by the author features appropriate values. Such transport will consume 3.4 bln tons of fuel per year worth 1.7 tln USD. Today this is roughly equal to the global fuel consumption by transport, including electrified roads – railways, trams, trolleybuses, metro, maglev trains, cable and monorail roads, conveyors and pipelines.

The difference in the annual fuel consumption as per the first and third patterns will reach 8.8 bln tons, which makes 4.4 tln USD in value terms. Moreover, the skirt alone, which increases the midsection of high-speed vehicles by at least 1 m², will cause excessive fuel consumption of 2 bln tons/year for the amount of 1 tln USD.

Vehicles using an air cushion and magnetic suspension with a linear electric motor feature low performance as well. Not only do they have poor aerodynamics, but their suspension system is rather sensitive to the gap between the roadbed and the skirt. The gap in Transrapid, for example, should not exceed 10 mm. A gap increase leads to a sharp drop in drive efficiency which does not exceed 40 %. In addition, this suspension is sensitive to impurities in the gap including those in the form of snow or ice. Taking into account the efficiency of power plants, where primary generation of electricity takes place, its losses

in power lines, numerous transformer substations, converters, cable facilities, electric motors, the total energy efficiency of such a system makes about 10 %, while the modern steam locomotive efficiency reaches 15 %. If we talk about fuel consumption, its total annual consumption in the latter case would be 18 bln tons at a cost of 9 tln USD. The cost of fuel consumption required for aerodynamics must be added to these fuel costs as well.

The wheel features better performance compared to other suspension systems of a high-speed vehicle relative to the track structure. However, a rubber (pneumatic) wheel is not suitable for high speeds since its rolling resistance at a speed of 100 m/s increases and is nearly equal to 0.05 (i.e. its efficiency is 95 %). Therefore, additional engine power for an average module of 500 kW will be required in order to overcome this resistance (in addition to aerodynamic resistance). This will lead to the additional fuel consumption of 5.5 bln tons/year (2.75 tln USD per year) for the specified global fleet of high-speed vehicles.

A steel wheel with an independent (automobile) suspension and a cylindrical support is characterized by the best performance. A railway wheel pair where the left and right wheels always have differences in diameters, as well as their conical bearing surface result in the wheel pair slipping relative to the rail, which increases the rolling resistance coefficient from 0.001 to 0.002. The cost of this difference of 0.001 for the above-mentioned fleet of vehicles will amount to 110 mln tons of fuel per year worth 55 bln USD. This slight difference will make 11 bln tons of fuel worth 5.5 tln USD for 100 years, although the point at issue seems to be a trifle: to use a wheel with an efficiency of 99.9 % or 99.8 %?

It is unlikely that a propulsion unit having efficiency higher than 99.9 % will be invented for a high-speed vehicle in the 21st century. Therefore, a steel rigid wheel will most probably continue to dominate in high-speed transportation as the most economically viable solution.

Increased economic efficiency inherent in a SkyWay unibus is especially clearly visible at low speed of 100 km/h typical of road transport. The engine power for a 50-passenger unibus with the weight of 10 tons required to maintain a speed of 100 km/h on a horizontal track section at established traffic makes 9 kW (of which 6.6 kW – aerodynamic resistance, 1.5 kW – rolling resistance of a steel cylindrical wheel on a steel rail, 0.9 kW – transmission losses). In this

**It is unlikely
that a propulsion unit
having efficiency
higher than 99.9 %
will be invented
for a high-speed vehicle
in the 21st century.**

case, fuel consumption per 100 km of the track will be 2 litres, or 0.04 l/100 passengers-km, or 0.4 l/1,000 passengers-km. This is by 20–30 times more cost-effective compared to a car – top cars consume 1–1.5 litres of fuel per 100 passengers-km at worse indexes of comfort, safety and sustainability; by 200–300 times more cost-effective compared to an aircraft – a 50-seat plane consumes 500–700 litres of fuel per 100 km.

A considerable amount of resources will be required for creating the global network of high-speed roads in the 21st century. In Russia alone, it is necessary to build at least 5 mln km of new roads just to catch up with the USA in the 20th century. Meanwhile, 3/4 of the Russian territory is covered with marshes, permafrost, taiga and mountains, whereas its area by 1.8 times exceeds the area of the USA

The main resources required to establish a 10 mln km network of express roads are shown in table 2.

The most significant resource is alienated land. In the case of ground track laying, it will be required about 50 mln hectares (500 thous. km²) of alienated land, which is equal to the total area of such countries as Austria, Hungary, Greece, Denmark, Israel, Switzerland and Cuba. Considering an understated average value of this land of 200 thous. USD/hectars, the cost of this resource will amount to 10 tln USD. Therefore, the tracks should be laid above the ground on supports, at the second level.

There are two ways to create a superstructure between the supports: 1) using a rigid beam; 2) using a highly stretched flexible thread. Since absolutely rigid systems do not exist, the design relative rigidity for spans of bridges and overpasses equal to 1/400–1/800 was adopted worldwide as a compromise between the requirements for reduced material consumption for superstructures and the requirements for obtaining the highest possible value of the track structure rigidity under the impact of calculated moving load.

Figure 1 shows a beam span of a single-way monorail-type track. The relative deflection of this beam is proportional to the square of its length and inversely proportional to the height in the third degree, to the elasticity modulus of the material and to the coefficient taking into account the shape of the beam cross-section. Therefore, when designing a beam span, attempts are made to reduce the span, to increase the beam height and to use a material with a high elasticity modulus.

The figure 1c shows the optimal cross-section of a steel beam of a maximum lightweight box type, having relative rigidity of 1/400 at a 50 m span when exposed to the load of 10 tf. The steel consumption for this beam will make 750 kg/m (total beam weight at a span $G = 37.5$ tons), the cross-sectional area – 960 cm². With sharp variations in temperature of 100 °C ranging from –50 °C in winter to +50 °C in summer in the sun, the thermal forces in such a beam can

Table 2 – Main resources required for building a network of high-speed multilane roads, length – 10 mln km

Resource	Unit of measurement	Ground track				Above-ground track			
		Roadbed		Rail track structure	For wheeled transport		Beam spans (steel)		String Spans
		asphalt concrete	reinforced concrete		roadbed (overpass)	monorail	Magnetic (air) cushion		
1. Allocated land plot (including infrastructure) (200,000 USD/ha)	mln ha bln USD	50 10,000	50 10,000	50 10,000	30 6,000	5 1,000	5 1,000	2 400	
2. Earthworks (5 USD/m ³)	bln m ³ bln USD	200 1,000	200 1,000	200 1,000	20 100	10 50	10 50	5 25	
3. Reinforced concrete structures (500 USD/m ³)	bln m ³ bln USD	2 1,000	50 25,000	10 5,000	100 50,000	5 2,500	10 5,000	2 1,000	
4. Steel structures (2,000 USD/t)	bln t bln USD	0.1 200	4 8,000	5 10,000	20 40,000	20 40,000	40 80,000	3 6,000	
5. Granular sub-base (20 USD/m ³)	bln m ³ bln USD	50 1,000	10 200	30 600	-	-	-	-	
6. Sand cushion (10 USD/m ³)	bln m ³ bln USD	50 500	50 500	20 200	-	-	-	-	
7. Asphalt concrete surface (100 USD/t)	bln t bln USD	100 10,000	-	-	3 300	-	-	-	
Total (for a network of roads)	tln USD	23.7	44.7	26.8	96.4	43.6	86.1	7.4	
Total (for 1 km of track)	mln USD/km	2.4	4.5	2.7	9.6	4.4	8.6	0.7	
Average motion speed	km/h	120	120	200	150	150	350	350	

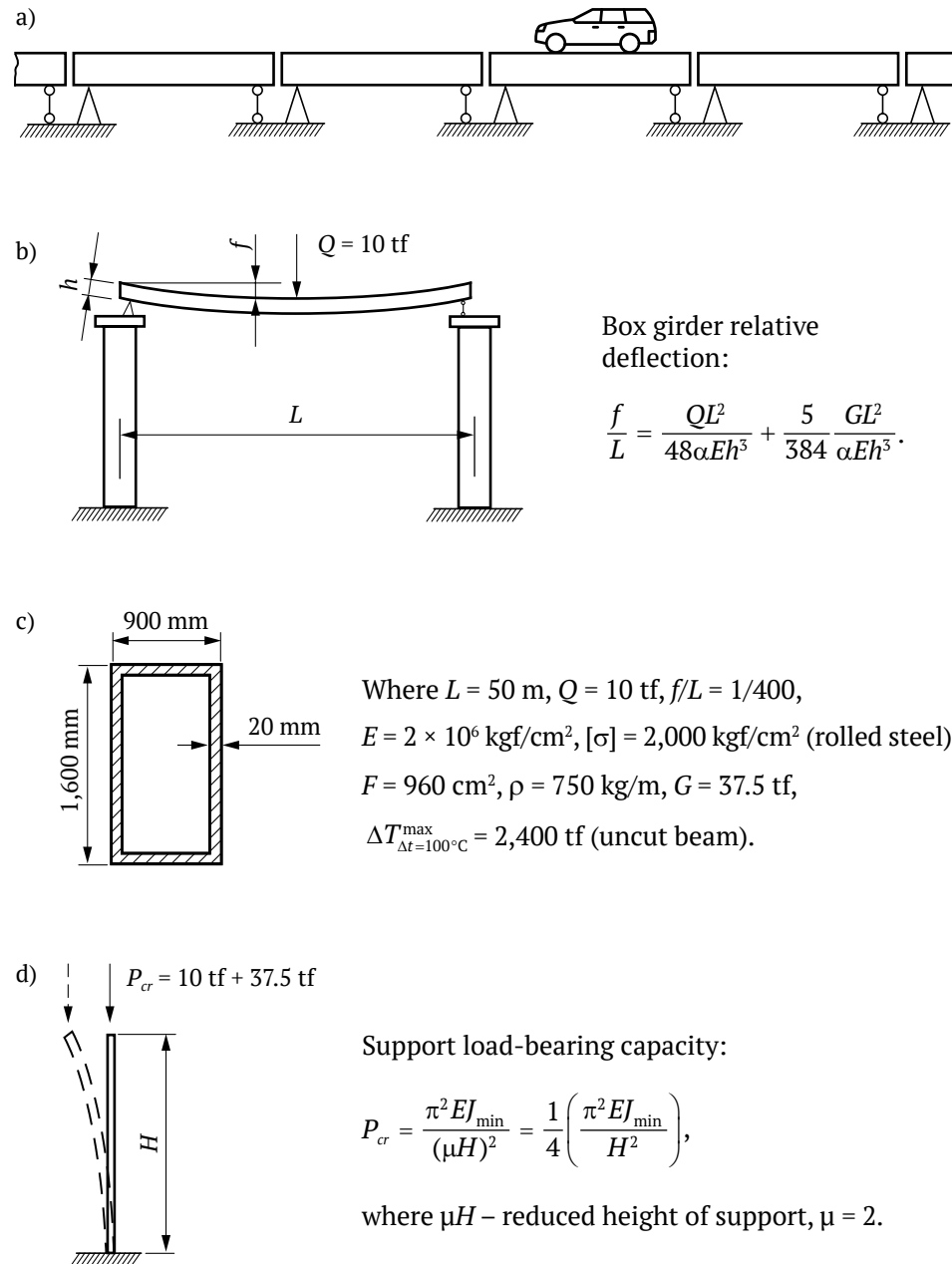


Figure 1 – Beam span:
 a) beam trestle diagram; b) beam span;
 c) optimal box girder cross-section;
 d) operation scheme for a beam span cross-section support

reach 2,400 tf. This is the reason why the beam has an expansion joint leaning its ends on the support crossbar. Since the top of the support is not fixed, the μ coefficient, which determines the reduced height of the support when determining its bearing capacity, equals to 2.

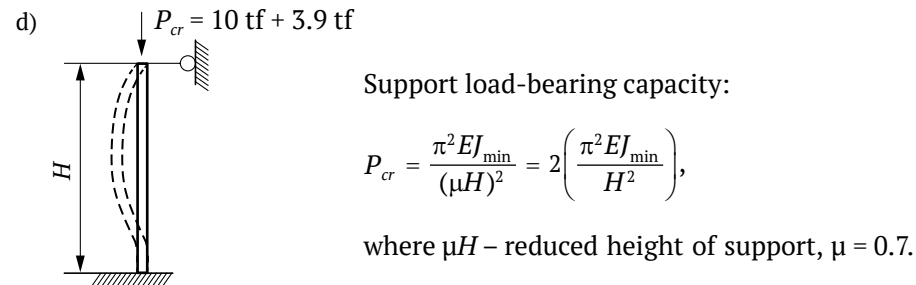
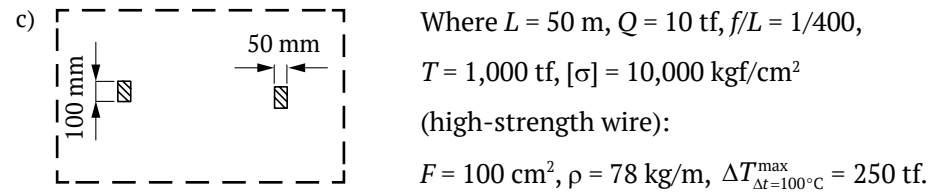
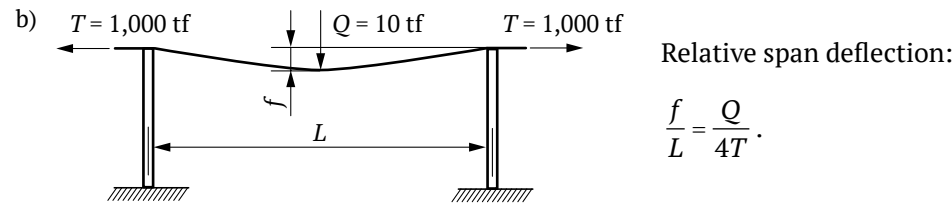
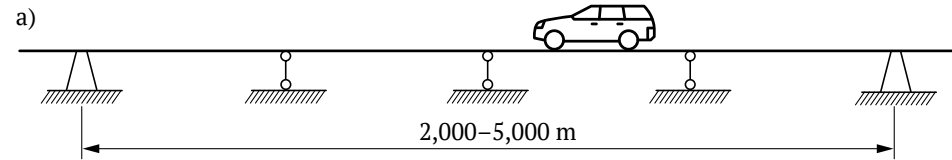
Let us consider the string superstructure (figure 2). The relative deflection of such a span is proportional to the Q load and inversely proportional to the T tension of the string. It should be noted that the relative deflection of the string span does not depend on the string material, its shape or transverse dimensions, as well as on the span length. In order to achieve relative rigidity of 1/400 under the load of 10 tf, the string tension must be equal to 1,000 tf. Since the span rigidity does not depend on the shape of the string cross-section, it can be made, for example, from high-strength wire having the design tensile stress of about 10 thous. kgf/cm² (SNiP construction rules and regulations for bridges 2.05.03-84 allow characteristic resistance to tensile stress in prestressing strands K-7 of 13,200–14,000 kgf/cm²). Then, the cross-sectional area of a steel string will make 100 cm², whereas its weight – 78 kg/m (total weight at the span – 3.9 tons).

Since the top of the support is fixed to the string (attached to the track structure), the μ coefficient, which determines the reduced height of the support, is 0.7. Therefore, at the same height of the support as for the beam span, the support of the string span will have 8 times greater bearing capacity (see bearing capacity of supports in figures 1 and 2). Since the beam span 50 m long weighs 37.5 tf and the string span only 3.9 tf, the calculated material intensity of supports and string-type spans will be about 10 times lower. The cost of string tracks will also be lower by the same amount as the cost of high-strength steel wire is approximately equal to the cost of rolled steel and makes 1,000–1,500 USD/t (with VAT) in Russia.

In order to enhance string protection from any adverse external effects (mechanical, climatic, etc.) and increase track rigidity under a vehicle wheel, the string must be placed inside a special rail concreting them with each other using a high-strength composite.

The cost of the main resources required to build 1 km of an average double-way high-speed rail-string track will amount to about 700 thous. USD. This will yield the following savings for the road network 10 mln km long: 16.3 tln USD compared to highways with asphalt surface; 37.3 tln USD compared to highways with reinforced concrete surface; 19.4 tln USD compared to railways; 89 tln USD compared to automobile trestles; 36.2 tln USD compared to a monorail-type trestle; 78.7 tln USD compared to an overpass for maglev trains (table 2).

Based on the above analysis, the conclusion can be drawn that it is more feasible to build a high-speed road network in the 21st century on supports using a stretched track structure without forming a solid roadbed. It is most



e) Relative string elongation under load ($f/L = 1/400$)

$$\delta L = \frac{\sqrt{(L/2)^2 + f^2} - L/2}{L/2} = 0.0000124.$$

String stress increase under load ($f/L = 1/400$)

$$\sigma_Q - [\sigma] = \delta L \times E = 24.8 \text{ kgf/cm}^2.$$

Figure 2 – String span:

a) string overpass diagram; b) string span;

c) string track structure cross-section; d) operation scheme for a string span support;

e) dependencies affecting the string stress-strain behavior

reasonable to use a cylindrical steel wheel with an independent suspension as a propulsion unit. Fuel energy is best converted into mechanical work directly on board the vehicle, for example by means of an internal combustion engine. Such an elevated transport system is optimal from the standpoint of exact sciences – physics, mechanics, building mechanics, material resistance, aerodynamics, economic analysis – and is called Unitsky's String Transport (UST)*. No other prospective elevated transport system, including those described in science fiction (anti-gravity ships, gravitolyots, flying saucers, etc.) will have a higher technical, economic or environmental performance than UST.

* Today, Unitsky's String Transport is developing under the SkyWay brand.

**Innovative
SkyWay transport
and infrastructure
technologies**

104



SKYWAY PHILOSOPHY

**Transport should be a solution to problems, not their source.
The SkyWay system provides passenger and cargo transportation
in a separate space – on the “second level” above the ground.**

The fact that SkyWay vehicles move above the ground on a specially designed rail-string overpass ensures a number of advantages: optimized aerodynamics, increased speed, unprecedented safety, rational use of land and resources, minimized environmental damage caused by transport. In addition, the cost of construction and operation is significantly lower compared to the existing transport solutions.



SKYWAY

MANUFACTURING FACILITY

Special design and technological bureau with “Unibus” pilot production carries out the whole range of works for SkyWay rolling stock manufacture:

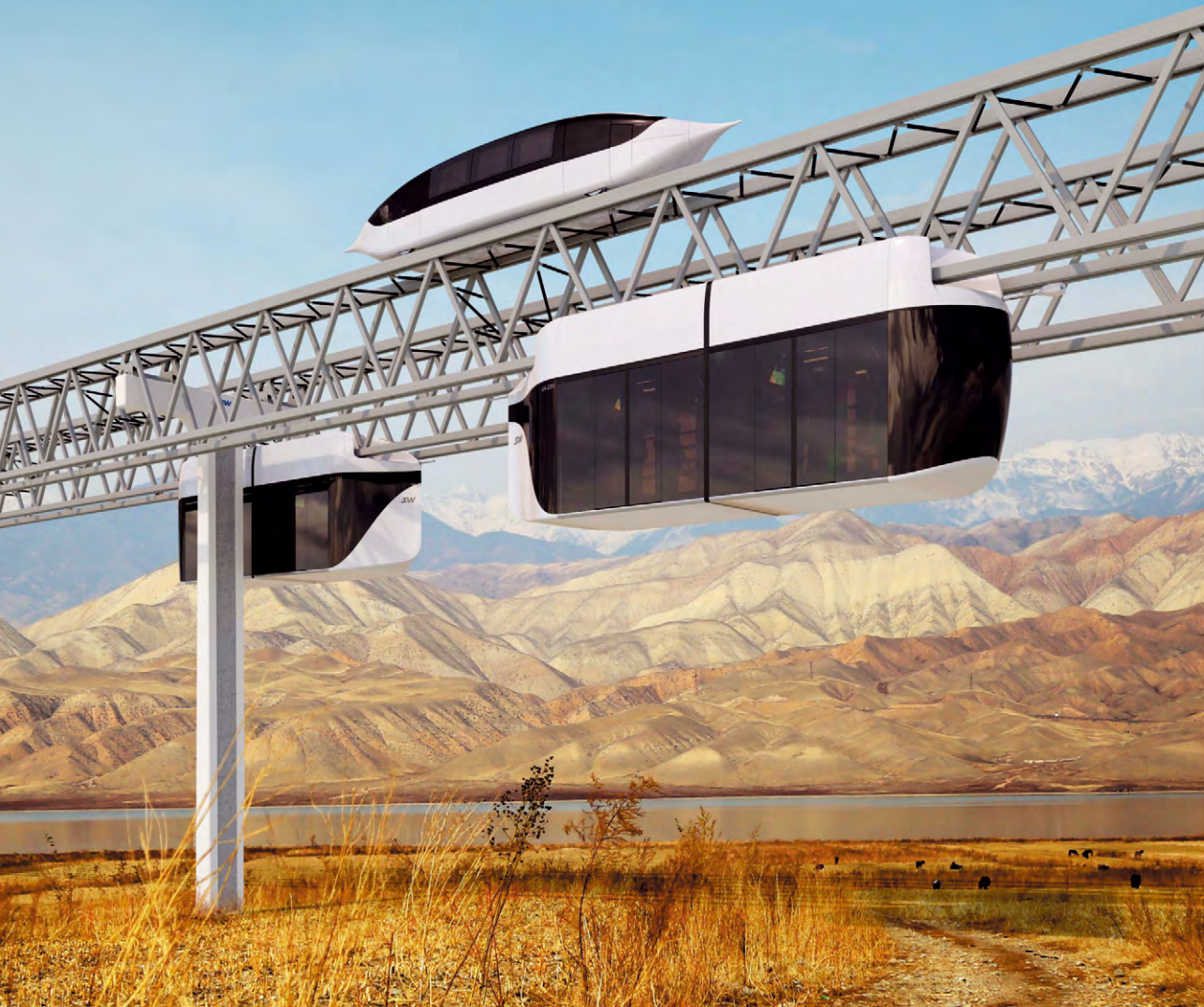
- production of accessories, devices and components;
- testing of mechanical units and electronics;
- industrial prototypes testing.

The manufacturing facility serves to work out the most responsible and important technological solutions, the main SkyWay know-how.



MAIN TRANSPORT SOLUTIONS

The SkyWay systems can meet a wide range of transportation demands offering a possibility of highly efficient passenger and cargo transportation for any distances under any natural and climatic conditions.



SkyWay – speed, safety, comfort, affordability, cost effectiveness, sustainability.

SkyWay – increased social activities for people.

SkyWay – the basis for the information, power, transport and communications network of a new generation.



All types of SkyWay systems are distinguished by energy efficiency, minimal adverse environmental impact and a high safety level of passenger and cargo transportation.

UNIBUS AND UNICAR

MODEL RANGE:

- large class double-rail unibus (passenger capacity: 7–60 people; in articulated vehicles – up to 84–600)



- middle class monorail unibus (passenger capacity: 3–14 people; in articulated vehicles – up to 84)



Certificate of compliance
No. ДСАТ RU.MT.770C050

- small class monorail unicar (passenger capacity: 2–6 people; in articulated vehicles – up to 6–60)



Maximum speed: 150 km/h.

Performance: up to 50,000 passengers/hour and more.

Maximum longitudinal slope of the track (at special design): 30 %.



URBAN TRANSPORT

It fits harmoniously into the existing infrastructure of any megalopolis.



UNIBIKE

Certificate of compliance
No. ДСАТ RU.MT.77OC051

A light and compact vehicle on steel wheels. It combines the features of a high-performance electric vehicle of the transport system and a sports and recreational facility.

In addition to the built-in (and external) power sources, the unibike is equipped with a bicycle generator so that it can be driven by the muscular force of passengers.

In the future – an alternative to a car, bicycle and motorcycle.

The model range includes single-, double-, three-, four- and five-seat unibikes.

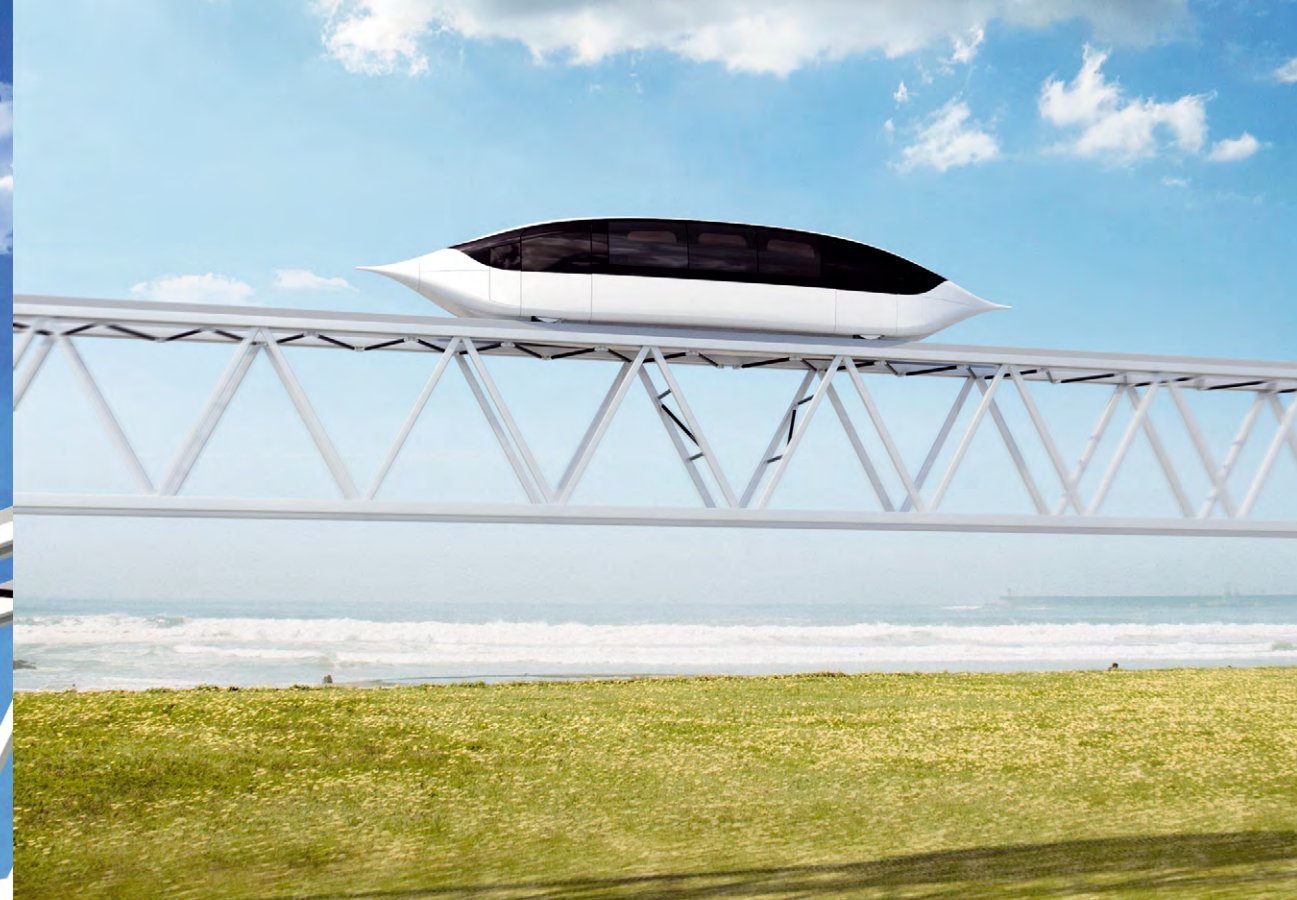
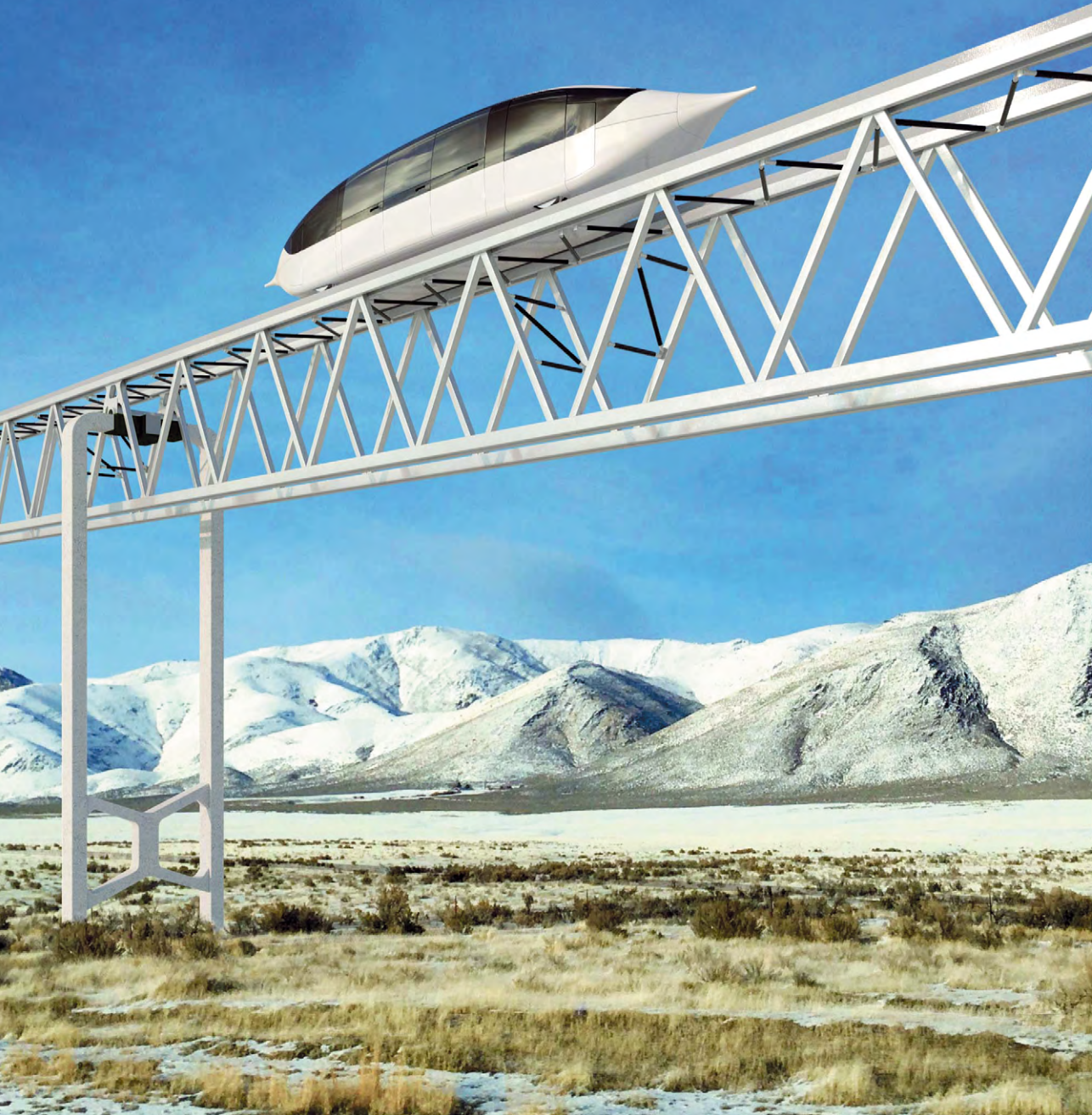


Maximum speed: 150 km/h.

Performance: up to 20,000 passengers/hour and more.

Maximum longitudinal slope of the track (at special design): 30 %.

HIGH-SPEED UNIBUS



HIGH-SPEED TRANSPORT

A mounted vehicle on steel wheels, designed for intercity passenger and cargo transportation for distances up to 10,000 km.

High speed is provided by the specially designed string-rail overpass and high aerodynamic efficiency of the vehicle.

Maximum speed: up to 500 km/h (in prospect – 600 km/h).

Passenger capacity: 4–40 people.

Performance: up to 500,000 passengers/day and more.

Maximum longitudinal slope of the track: up to 20 %.

CARGO

TRANSPORT



Transport system designed for cargo transportation over distances of up to 500 km and more.

UNITRUCK



The cargo rolling stock is based on suspended urban passenger minibuses.

A special range of containers was developed to allow docking with maritime, railway and automobile containers for liquid, bulk, break-bulk and special cargo. Containers for perishable goods are equipped with a thermal control system (in winter) and air conditioning (in summer); containers for environmentally hazardous goods have a multi-layer high-strength body, etc.

Cargo SkyWay application:

- bulk cargo transportation (ore, coal, construction materials, overburden, etc.);
- general cargo transportation (containers, wood, metal, etc.);
- liquid cargo transportation (oil and petroleum products, liquefied gas, potable water, etc.);
- special cargo transportation (cryogenic liquids, radioactive and explosive substances, weapons, etc.).

Speed of cargo transportation: up to 150 km/h.

Performance: up to 200 mln tonnes/year and more.

Maximum longitudinal slope of the track: up to 30 %.

UNITRANS



The efficiency of the product pipeline is provided by 24/7 year-round continuous operation, which allows to transport large volumes of cargo.

Belt-type product pipeline on steel wheels includes special loading and unloading terminals with continuous cargo loading/unloading. It allows fast and cheap transportation of bulk cargo.

The system is indispensable in remote and hard-to-reach places, particularly when developing mineral deposits.

Unitrans application:

- bulk cargo transportation (ore, coal, construction materials, overburden, etc.).

Speed of cargo transportation: up to 36 km/h.

Performance: up to 200 mln tonnes/year and more.

Maximum longitudinal slope of the track (at special design): up to 45 %.

CARGO

TRANSPORT

SKYWAY SYSTEM

SEA PORT

The advantages of using the SkyWay cargo transport system in a sea port:

- delivery of cargo (bulk, liquid and general) offshore to 15–20 km or more without a significant cost increase;
- no need to create quay walls, dredge and fix shore for mooring of large vessels;
- it is possible to deliver cargo to a seaport at original depth (up to 50 m);
- SkyWay transport system and a port form a unified logistics complex, operating in automatic mode;
- cargo transportation: up to 200 mln tons/year and more;
- type of bulk cargo transportation: from a mining enterprise to a bulk carrier without intermediate storage.



ECOHOUSE:

HOUSE OF THE FUTURE TODAY

The time of faceless identical buildings has passed. A man needs eco-friendly architecture being a source of daily spiritual joy. The society has come to the conclusion that people should not conquer the nature, but live with it in full harmony and mutual understanding.



ECO-FRIENDLY

An ecohouse is built using “green” technologies, as well as environmentally friendly materials that do not harm the nature.

A project considers cardinal points, wind rose, landscape, human-friendly zoning of internal premises and overall geometry of building construction.

COST-EFFECTIVE

An ecohouse is provided with heat, electricity and hot water using renewable energy sources – sun, ground, wind.

An integrated approach when designing a building naturally uses renewable energy systems as constructive design elements.

AESTHETIC

An original step towards the reproduction of natural balance – roof gardening – is not only a good view of the roof, but also a sky-high part of the terrestrial ecosystem.

The development of “green” technologies gives the opportunity to create beautiful, multifunctional, environmentally friendly admirable ecohouses.

LINEAR CITY:

IN UNITY WITH NATURE



SkyWay tracks contribute to the development of linear cities – cluster-type urban settlements harmoniously integrated into the environment.

The ground surface is intended for pedestrians to walk and plants to grow, whereas transport, power and information communication lines are located above the ground at the “second level”. The construction of linear cities will not require cutting down forests, building motor roads and railways, or disturbing biogeocenosis in the construction zone in any similar way.

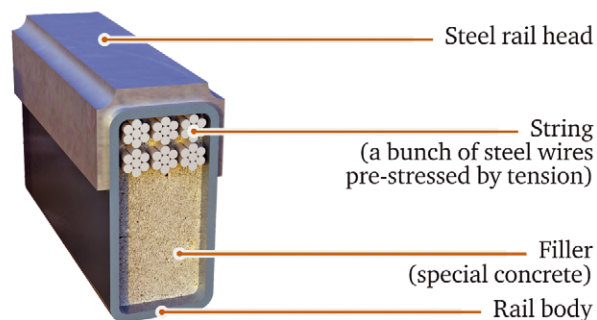
The SkyWay horizontal lifts will connect neighbouring high-rise buildings, settlements, as well as residential, commercial, entertainment, production and multifunctional clusters. The SkyWay high-speed transport arteries will take you to any point of the Earth.

SkyWay linear cities can be built in mountains, in desert and flooded areas, including complex terrain, in taiga and jungle, as well as on sea shelf.

BASIC ENGINEERING ELEMENTS

The basis of SkyWay technology – an innovative string rail

Design variant of a semi-rigid string rail



A string rail is an ordinary uncut (along its length) steel, reinforced concrete or steel-reinforced concrete beam or truss equipped with a rail head and additionally reinforced with pre-stressed (stretched) strings.

A string rail combines the features of a flexible thread (at a large span between supports) and a rigid beam (at a small span – under a rail automobile wheel and above the support).

A flat rail head and a cylindrical steel wheel provide minimal energy consumption for movement.

The power of wheel rolling resistance for a unibus of 5,000 kg at the speed of 450 km/h:

$$P_{rr} = m \cdot g \cdot c_{rr} \cdot v = 5,000 \text{ kg} \cdot 9.81 \text{ m/s}^2 \cdot 0.0015 \cdot 125 \text{ m/s} \approx 9.2 \text{ kW.}$$

Compare:

when using pneumatic tires with $c_{rr} = 0.18$ (for $v = 450 \text{ km/h}$)

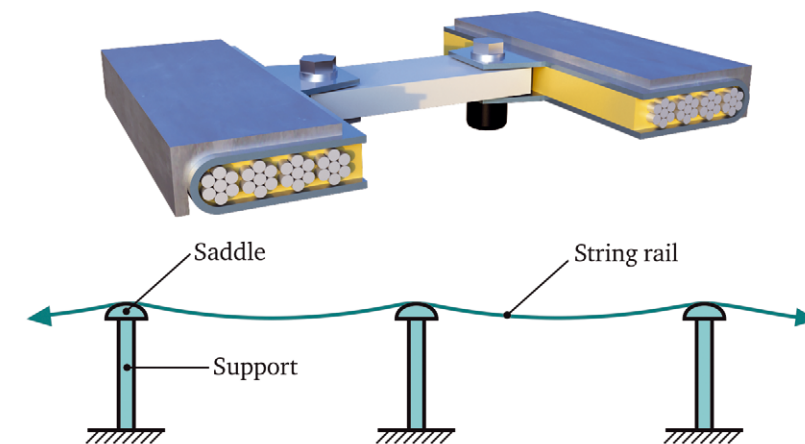
$$P_{rr} \approx 1,100 \text{ kW.}$$

TYPES OF STRING RAILS

AND THE CORRESPONDING DESIGNS OF TRACK STRUCTURE

Flexible rail

Flexible uncut track structure (variant)



It is not an analogue to cableway:

- use of rail (less rolling resistance of steel wheel);
- lower energy consumption for movement (3–5 times lower);
- possible to use a gravitation engine on a span when moving down and a gravitational brake when moving up (energy cost reduction by 3–5 times);
- high durability (5–7 times higher).

Motion speed: from 30–60 (on support) up to 120–150 km/h.

Relative structural rigidity: 1/100–1/500.

Track structure curve radius:

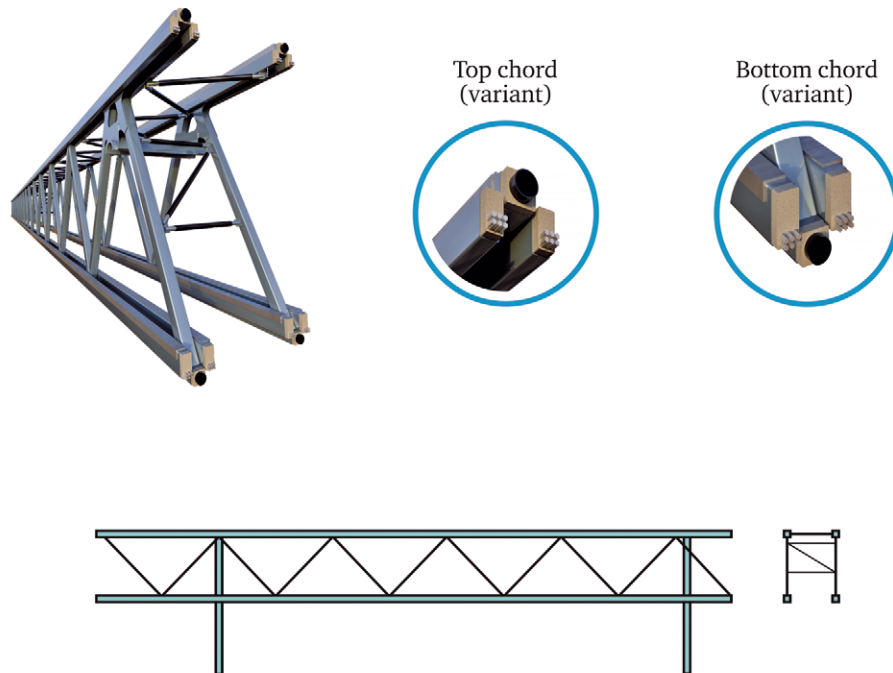
$r = 100$ (on support)... 2,000 m.

TYPES OF STRING RAILS

AND THE CORRESPONDING DESIGNS OF TRACK STRUCTURE

Rigid rail (truss)

Rigid uncut track structure



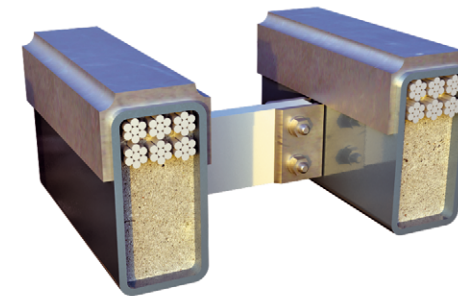
Motion speed: from 100 to 600 km/h.

Relative structural rigidity: 1/1,000–1/10,000.

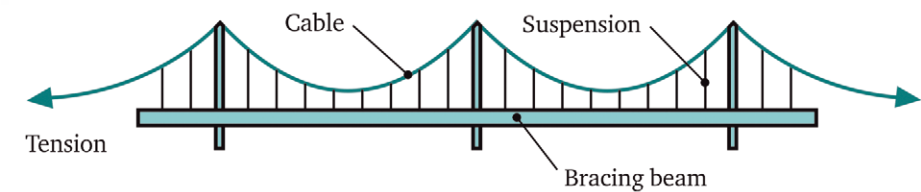
Track structure curve radius:
 $r = 5,000 \dots 50,000$ m.

Semi-rigid rail

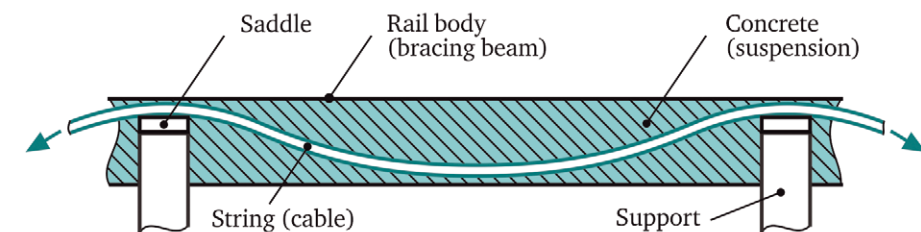
Semi-rigid uncut track structure



Hanging bridge



The SkyWay track structure design follows the design of a hanging bridge combining all its main elements.



Motion speed: from 50 up to 250 km/h.

Relative structural rigidity: 1/500–1/2,000.

Track structure curve radius:
 $r = 500 \dots 5,000$ m.

SKYWAY TECHNOLOGY

VS CONVENTIONAL BEAM OVERPASS

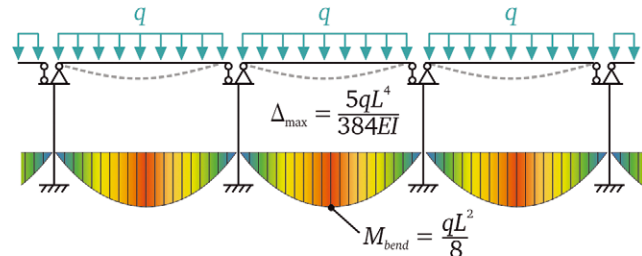


Split overpass (conventional bridge)

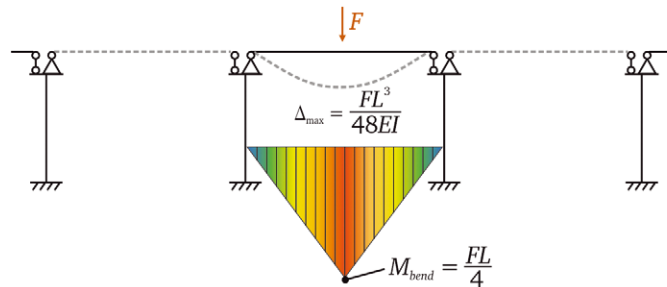


A solid roadbed gives additional load on support and has a high cost.

Bending moment diagram with distributed load



Bending moment diagram with concentrated force

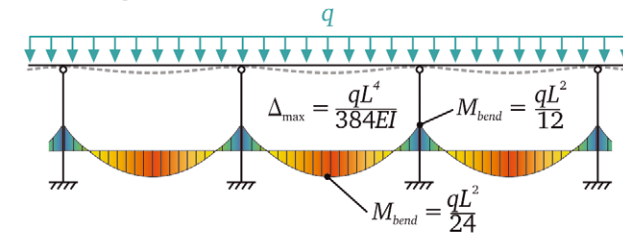


90 % of load in a conventional overpass – its own weight. The overpass carries itself, not the useful load.

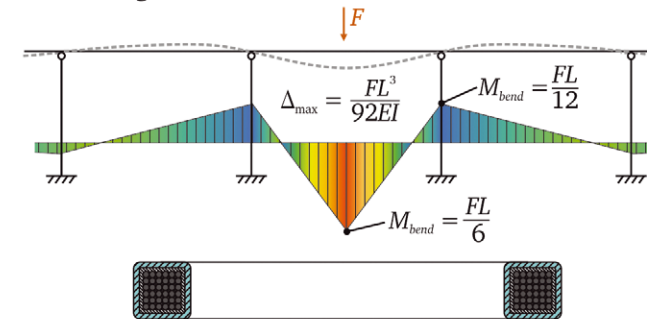


Innovative uncut pre-stressed rail-string overpass (SkyWay technology)

Bending moment diagram with distributed load



Bending moment diagram with concentrated force



With equally distributed load, SkyWay overpass is 5 times stiffer (smoother) and 3 times stronger than a conventional girder bridge.

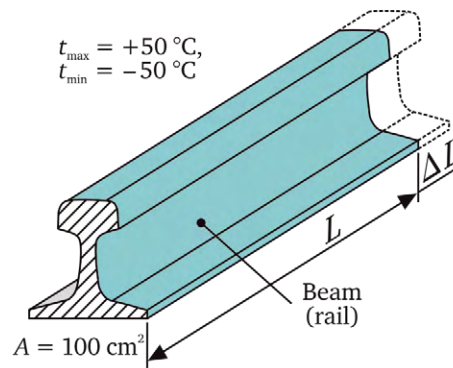
With equally concentrated force, the SkyWay overpass is 1.9 times more rigid (smoother) and 1.5 times stronger than a conventional girder bridge.

The SkyWay overpass decreases the amount of building materials required for its construction compared to a conventional overpass. As a result, the construction cost is significantly reduced.

10 % of load in a SkyWay overpass – its own weight. The overpass carries the useful load, not itself in contrast to conventional bridges.

PRE-STRESSED SKYWAY STRING TRACK –

AN OPTIMAL SOLUTION TO COMPENSATE THERMAL DISTORTION



Under thermal effects:

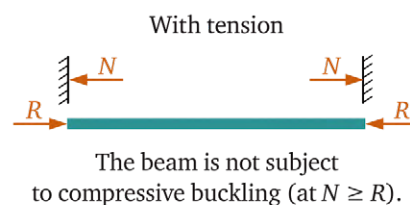
– absolute deformation
 $\Delta L = a \cdot L \cdot \Delta t$;

– relative deformation
 $\epsilon = \frac{\Delta L}{L} = a \cdot \Delta t$.

For steel,

the thermal coefficient of linear expansion (per 1 °C)
 $a = 0.000012$; with $\Delta t = 100\text{ }^{\circ}\text{C}$, $\epsilon = 0.0012 = 1/833$
(the extension will be 1.2 m per 1 km).

Test of a rigidly restrained beam for strength and stability under thermal effect ($\Delta t = 100\text{ }^{\circ}\text{C}$)



Test for strength:

– compression strain of longitudinal fibres:

$$\sigma = E \cdot \epsilon = E \cdot a \cdot \Delta t \leq \sigma_{02}$$

For steel,

with $E = 2 \cdot 10^5\text{ MPa}$ and $\Delta t = 100\text{ }^{\circ}\text{C}$:

$$\sigma = 2 \cdot 10^5 \cdot 0.0012 = 240\text{ MPa (ca. } 2.4\text{ t/cm}^2\text{)}.$$

Test for stability:

– longitudinal compression force arising in a restrained beam at temperature differences:

$$N_{\text{comp}} = \sigma \cdot A = E \cdot a \cdot \Delta t \cdot A \leq P_{cr} = \frac{4\pi^2 EI}{L^2}$$

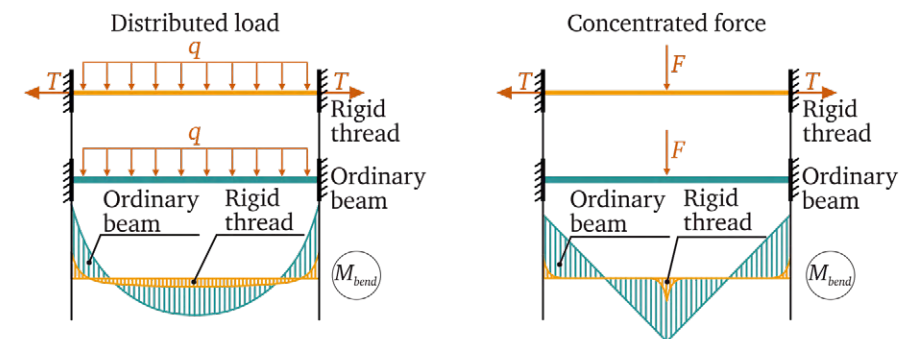
For steel,

with $\sigma = 240\text{ MPa}$ and $A = 100\text{ cm}^2$:

$$N_{\text{comp}} = 240 \cdot 0.01 = 2.4\text{ MN (ca. } 240\text{ t)}.$$

With the pre-stressing force more than 2.4 MN, there will be no compression forces in the structure and it will not lose its stability.

Bending moment diagrams in a restrained beam (conventional design) and in a pre-stressed rigid thread (SkyWay design)



Bending moments in a rigid thread are by 10 times lower than in a conventional beam.

Conclusion

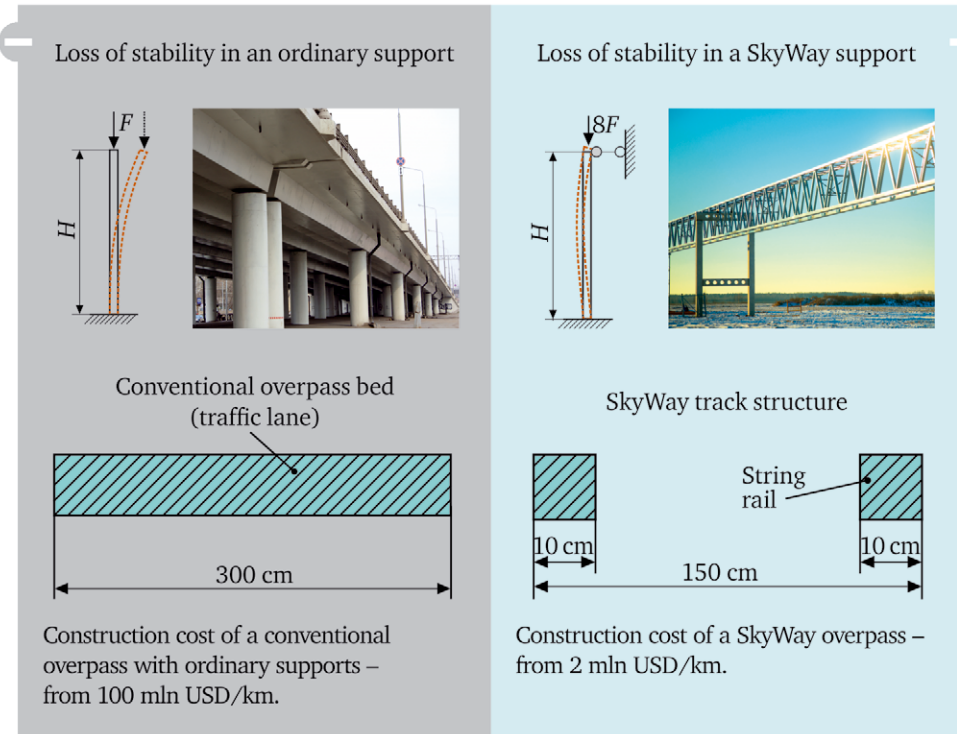
The most dangerous phenomenon when heating a rigidly restrained beam is the loss of its stability.

Solution

A pre-stressed beam with the rated force of $T \geq N_{\text{comp}}$ ensures that even temperature difference of $\Delta t = 100\text{ }^{\circ}\text{C}$ will not cause compression forces in longitudinal fibers of the beam.

HIGH EVENNESS OF THE TRACK

IS ACHIEVED DUE TO USING AN UNCUT STRING RAIL BETWEEN ANCHOR SUPPORTS

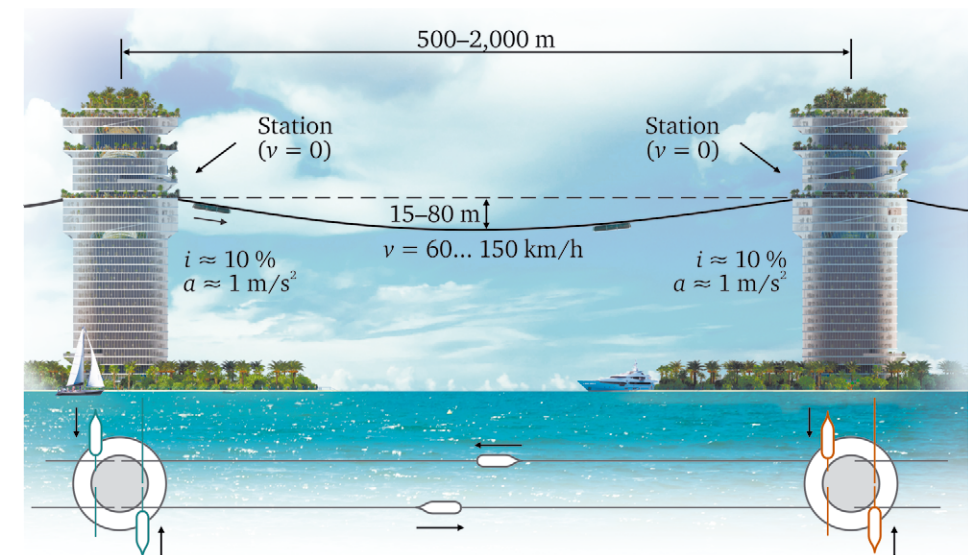


- Intermediate supports installed at a span from 25 up to 100 metres (to ensure rigidity of the uncut track structure) allow to use light structures.
- Fixing of the support top to the track structure additionally increases its load-bearing capacity by 8 times.
- The amount of materials required for installation of supports can be reduced by 8 times, resulting in cost reduction by the same figure.

An uncut structure of the string rail in its overpass design reduces the amount of building materials and their cost by 15 times and more compared to a conventional beam overpass.

APPLICATION OF ENERGY CONSERVATION LAW IN INNOVATIVE SKYWAY TRANSPORT

In terms of energy consumption, an overpass with a sagging track structure is by times more efficient than a road with a straight track structure.



The drive in the SkyWay transport system with a sagging track structure is only required to compensate for aerodynamic losses and to overcome steel wheels rolling resistance on a steel rail (about 10 kW for a 50-seat vehicle). It is explained by the fact that an engine is not used at a downhill section of the track – a vehicle is accelerated by gravity (“gravity” engine).

The unibus does not need brakes at an uphill section – it is slowed down by gravity (“gravity” brakes).

Energy recovery at the scheme “potential energy at station → kinetic energy of motion on overpass → potential energy at next station” occurs without using a recovery unit according to the laws of physics. The efficiency of such recovery is 100 %.

SMOOTH MOVEMENT

Split overpass (conventional bridge)

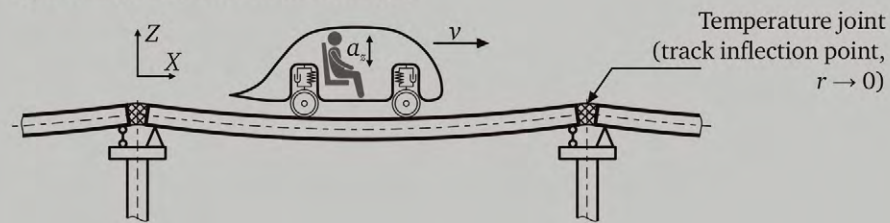


Diagram of vertical acceleration felt by passengers during movement

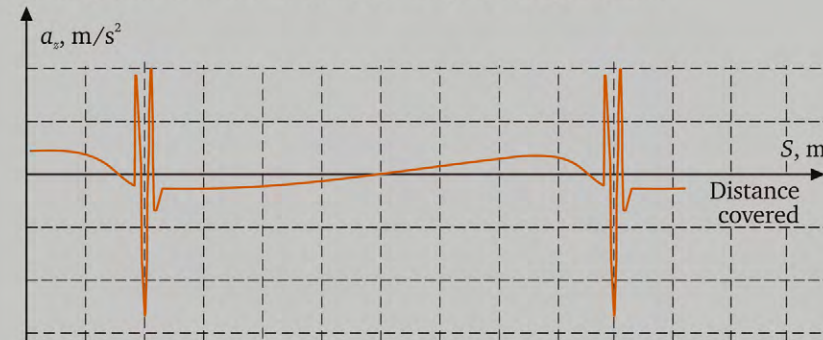
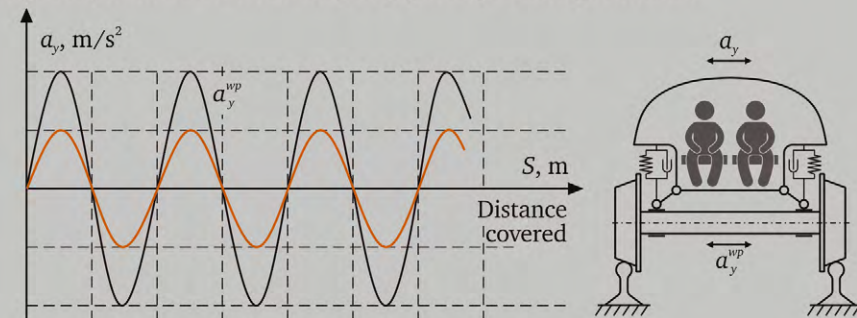


Diagram of transverse acceleration felt by passengers during movement



Disadvantages:

- peak acceleration values when moving through supports;
- more complicated design of the supporting node with a temperature joint.

Uncut pre-stressed overpass (SkyWay technology)

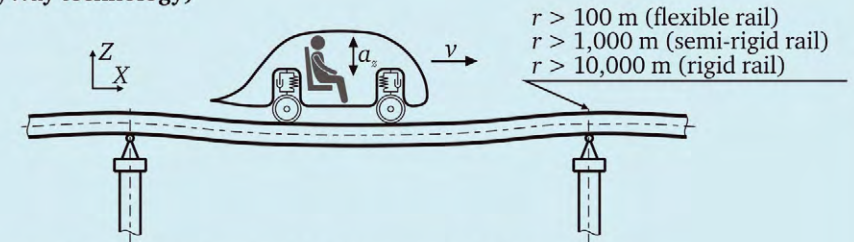


Diagram of vertical acceleration felt by passengers during movement

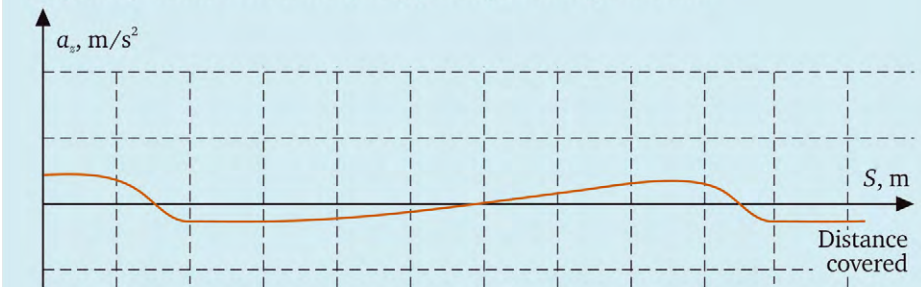
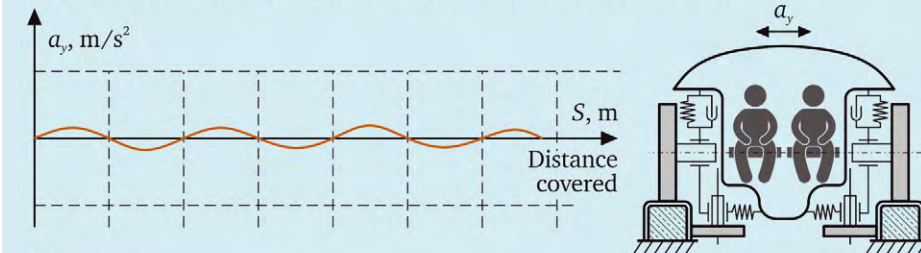


Diagram of transverse acceleration felt by passengers during movement



Advantages:

- smooth change of acceleration when moving through supports;
- more simple design of the supporting node.

Evaluation	Index of smooth movement, W
Very good	Less than 2
Good	2-2.5
Satisfactory for passengers	2.5-3
Impermissible for passengers	3-3.25
Permissible for cargo	3.6-4.25

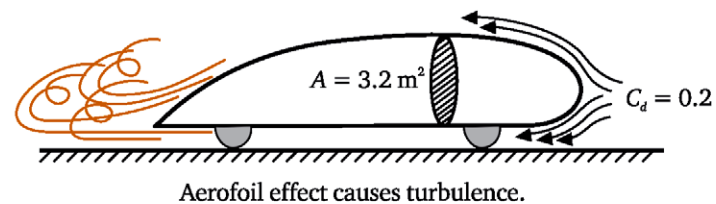
Unsafe for passengers from the physiological perspective: 4.5.

— SkyWay — Highway and railway

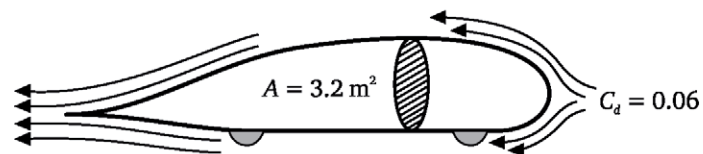
AERODYNAMICS OF A WHEEL VEHICLE

Wind tunnel tests of the innovative SkyWay rolling stock (unibus) in 1994–2009 gave the result $C_d = 0.075$.

This provides saving of drive power in one SkyWay vehicle of about 600 kW compared to the most advanced of alternative ground vehicles ($C_d = 0.2$).



As a result of wind tunnel tests carried out in 2017, C_d of the SkyWay rolling stock was improved to 0.06: $\Delta C_d = 0.2 - 0.06 = 0.14$.



Power saving of aerodynamic resistance (at a speed of 450 km/h):

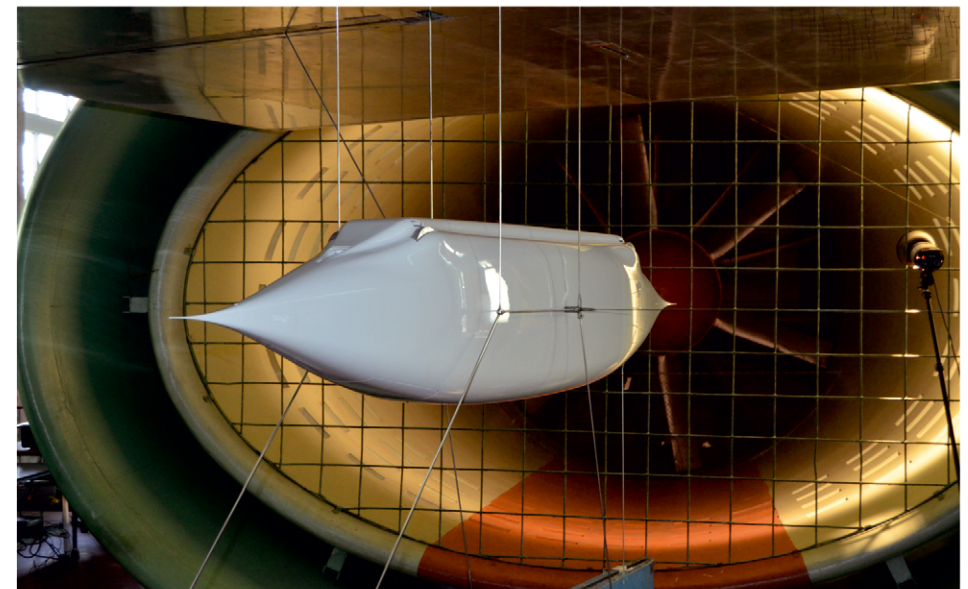
$$\Delta P_{ar} = \frac{1}{2} \rho \cdot v^3 \cdot \Delta C_d \cdot A \cdot k = \frac{1}{2} \cdot 1.25 \text{ kg/m}^3 \cdot (125 \text{ m/s})^3 \cdot 0.14 \cdot 3.2 \text{ m}^2 \cdot 1.1 \approx 600 \text{ kW}.$$

Energy (fuel) saving by one high-speed unibus for 25 years of operation will be about 22,000 tonnes, at the cost of about 20 mln USD.

Thus, a thousand unbuses with unique aerodynamic properties can save over 20 mln tonnes of fuel, at the cost of more than 20 bln USD. Along with this, 70 mln tonnes of atmospheric oxygen will be saved from burning out and more than 100 mln tonnes of polluting substances will not be generated.



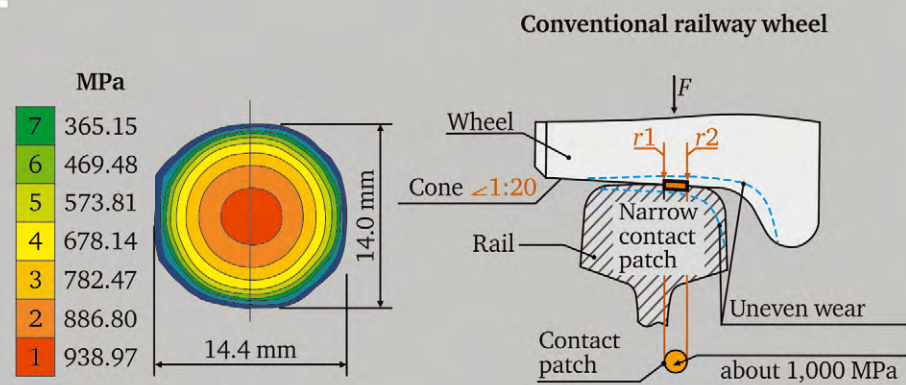
The location of the track structure above the ground and the absence of a solid roadbed eliminates the main problem of high-speed transport – aerofoil effect. This alone allows to improve vehicle aerodynamics twofold.



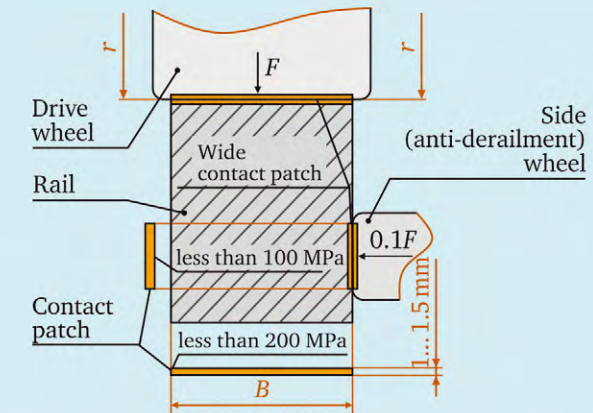
Testing a high-speed unibus (scale 1 : 5) in a wind tunnel, 2017

ADVANTAGES OF SKYWAY

STEEL WHEELS

**Increased wheel wear and noise due to:**

- big contact stresses (1,000 MPa and more) caused by a small size of contact patch;
- slipping in the contact patch caused by a difference of seating diameters in the conical wheel surface;
- operation of brake mechanisms (brake shoes cause additional wheel tread wear);
- big static and dynamic wheel loads combined with inevitable track irregularities;
- rigid wheel pair prone to self oscillations, which increase wear and noise;
- asymmetrical load application onto the rail head.

Innovative unibus wheel

Calculation of contact stress for a high-speed unibus with gross weight of 5 tonnes:

$$\sigma_c = 0.418 \cdot \sqrt{\frac{F \cdot E}{B \cdot q \cdot r}} = 0.418 \cdot \sqrt{\frac{0.0125 \text{ MN} \cdot 2.1 \cdot 10^5 \text{ MPa}}{0.08 \text{ m} \cdot 0.8 \cdot 0.26 \text{ m}}} = 163 \text{ MPa (ca. } 1.7 \text{ t/cm}^2\text{)},$$

where F – wheel load;

E – effective elastic modulus;

B – width of wheel supporting part;

r – wheel radius;

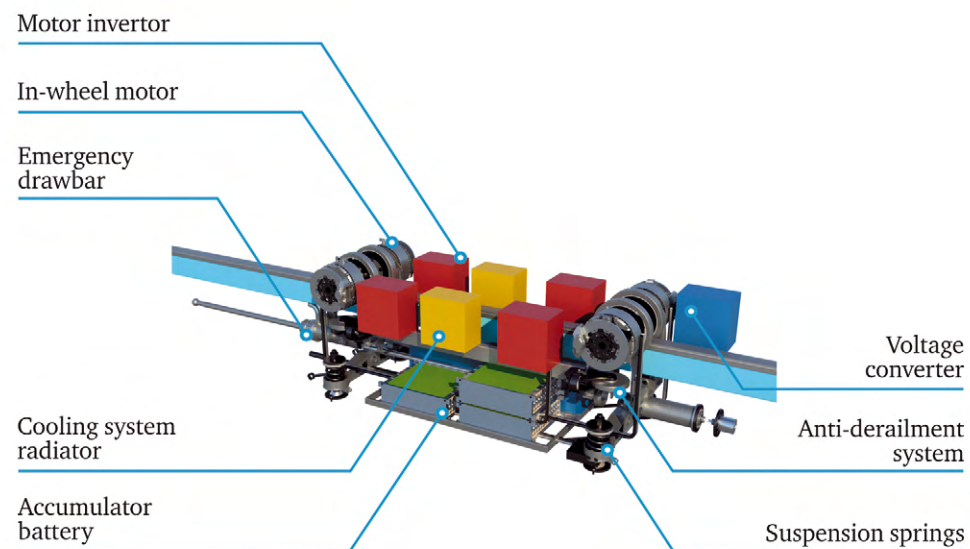
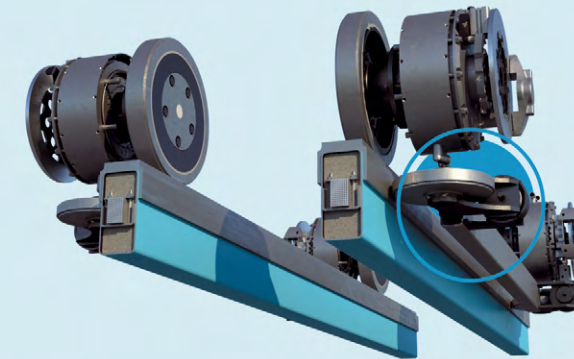
q – coefficient of contact irregularity by length.

Advantages of SkyWay transport wheels:

- insignificant contact stress (less than 200 MPa) due to a wide contact patch (by rail head width);
- no slipping in the contact patch (cylinder rolling along the plane);
- disk brake mechanisms and ABS preventing wheels locking;
- small wheel load and absence of joints on the track;
- symmetrical rail head wear (vertically and horizontally);
- minor wheel rolling resistance due to a narrow contact patch (in the direction of wheel rolling).

CHASSIS

LAYOUT

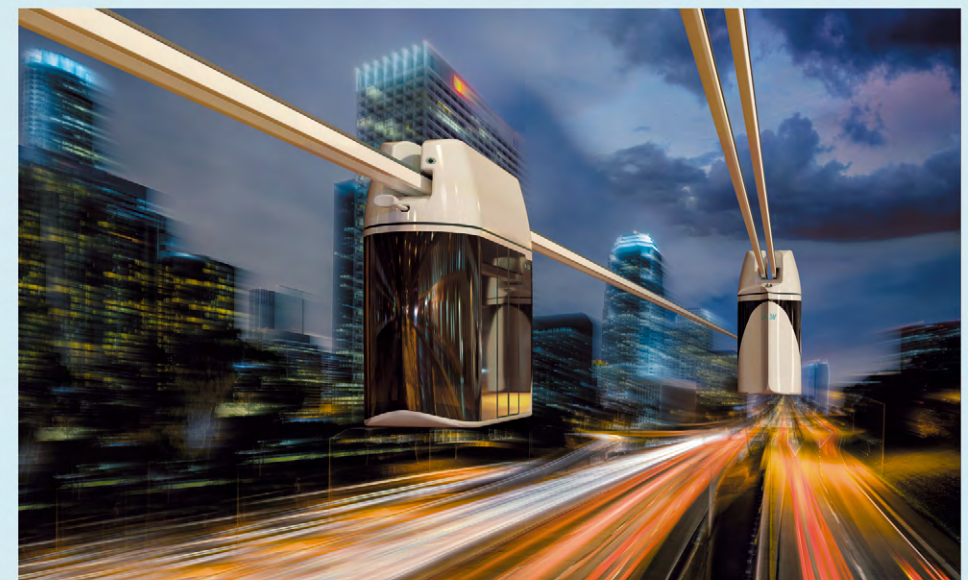


SAFETY OF TRANSPORT SYSTEMS

High resistance to vandalism and acts of terrorism.

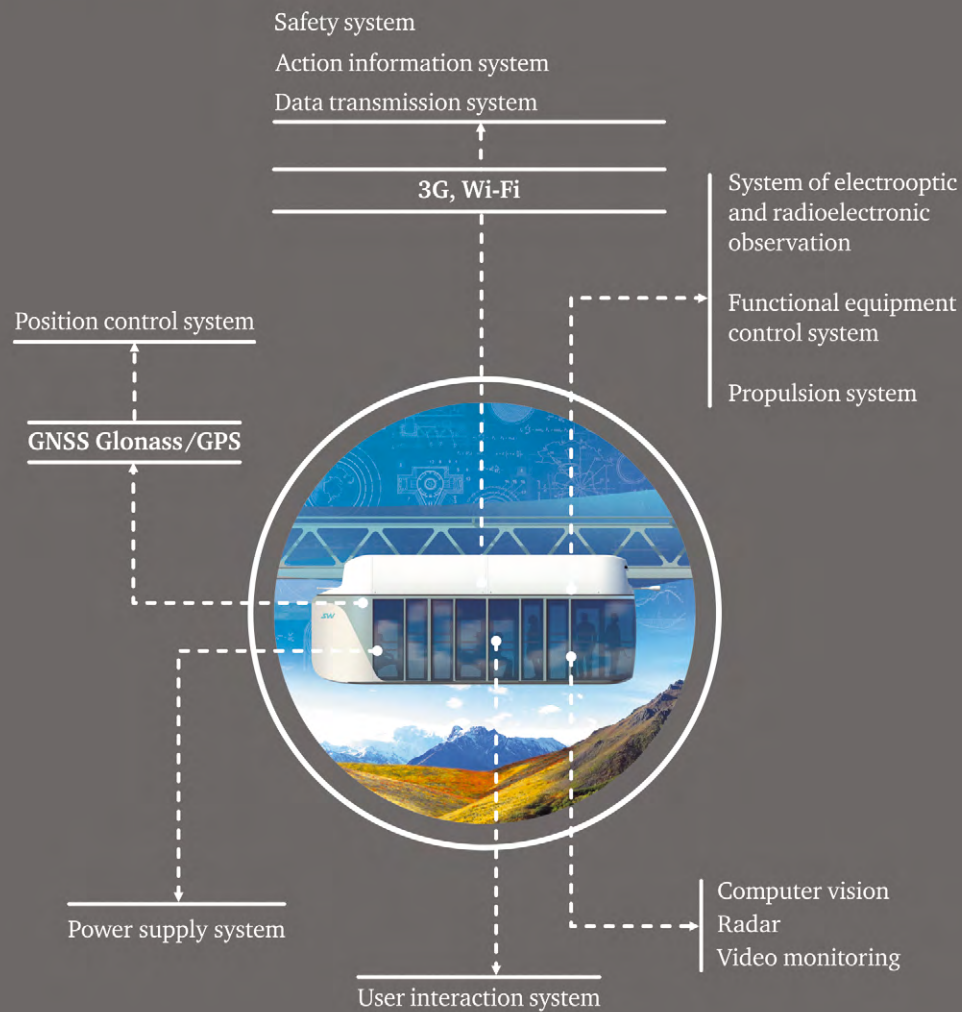
Location of the track structure above the ground enhances traffic safety by appr. 100 times.

Anti-derailment system increases traffic safety by another 10 times.



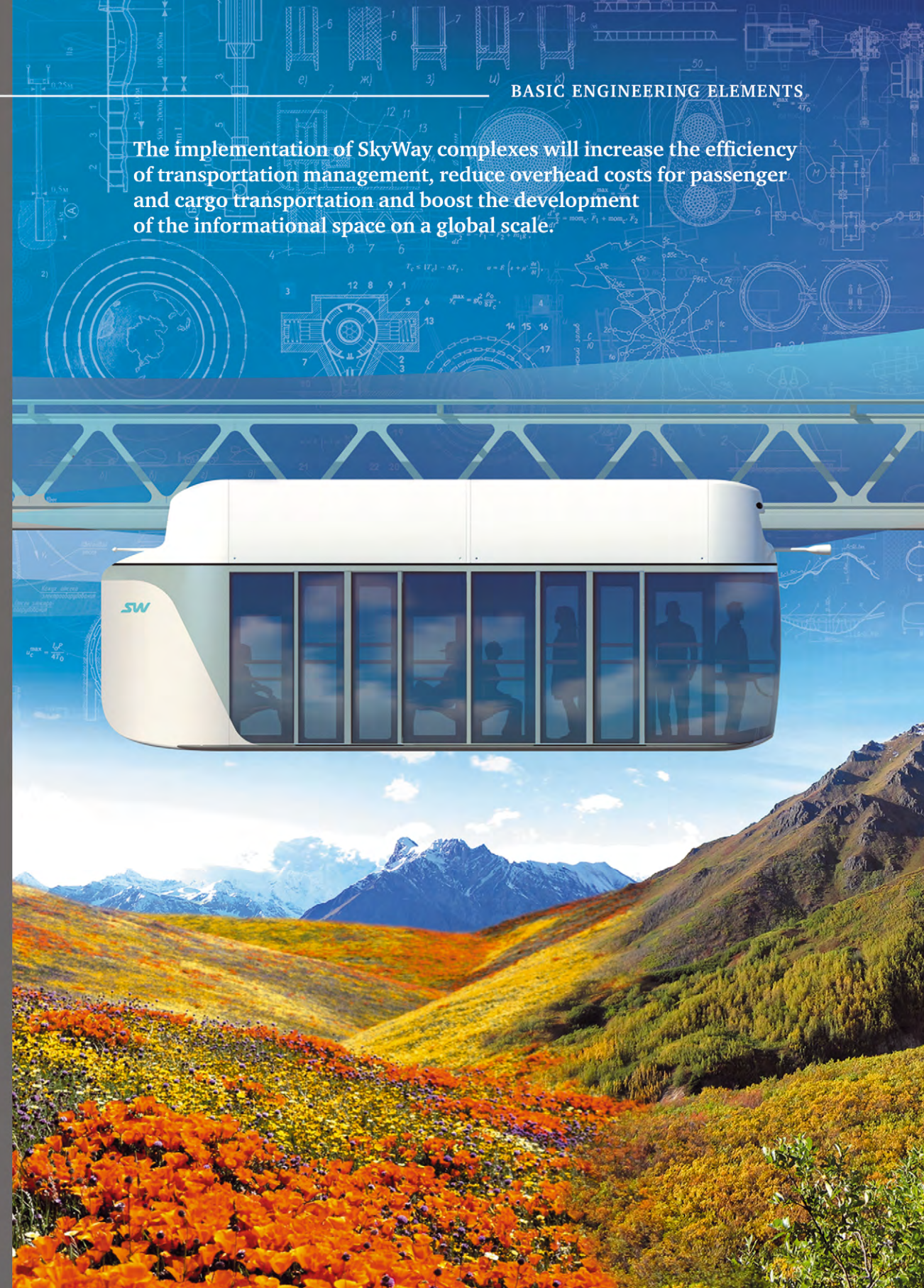
INTELLECTUAL CONTROL SYSTEMS OF SKYWAY TRANSPORT COMPLEX

The control system of SkyWay transport complex comprises a wide range of wireless and wired communications based on conventional information and electronic technologies.

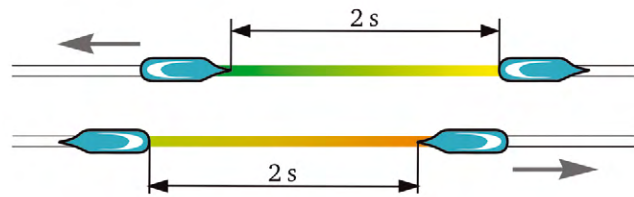


BASIC ENGINEERING ELEMENTS

The implementation of SkyWay complexes will increase the efficiency of transportation management, reduce overhead costs for passenger and cargo transportation and boost the development of the informational space on a global scale.



TRANSPORTATION CAPACITY OF INNOVATIVE SKYWAY TRANSPORT SYSTEM



A safe time interval between unibuses for real-time control systems is 2 s.

The indicated requirements are recommended by the Automated People Mover (APM) Standards Committee.

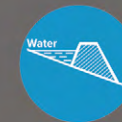
The peak traffic capacity of the SkyWay transport system at 20-hour operation – 360,000 passengers per day in one direction (considering the permitted interval of 2 s and the basic capacity for a single unibus of 10 seats).

The peak traffic capacity for a bidirectional system – 720,000 passengers per day.

SkyWay performance can be additionally increased by raising modules capacity and uniting them in trains.



SKYWAY AND ECOLOGY



No earth embankment (low-pressure dam)



Preservation of natural ecosystems and geobiocenosis



Minimal local land acquisition (reduced by 20 times)



Reduced amount of hazardous emissions into the atmosphere (by times) due to less power consumption



Increased electrical, vibro- and noise safety (by 10 times)



Reduced resource consumption – saving of raw materials, land, power, labour and finances

SKYWAY COMPARED

TO THE EXISTING AND ADVANCED ANALOGUES



As estimated by the Russian Academy of Sciences, the innovative SkyWay transport technology is the most cost-efficient, sustainable and safe of all existing and advanced transport systems.



Maglev



Monorail



Motor transport

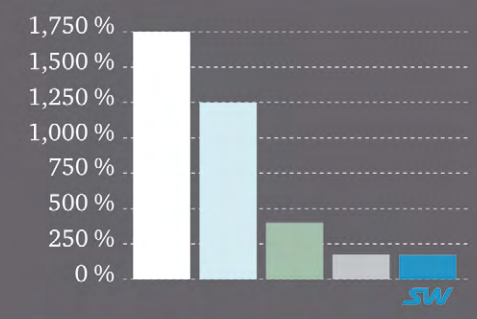


Railway

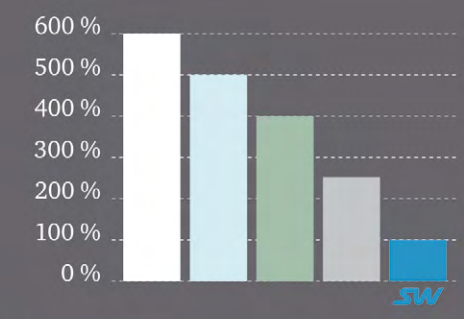


SkyWay string transport

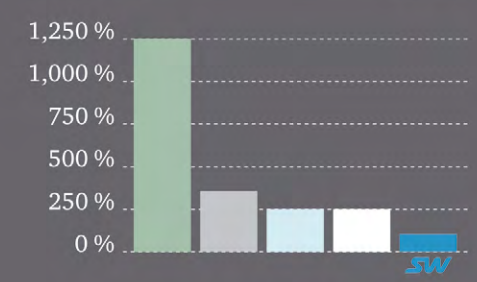
CAPEX



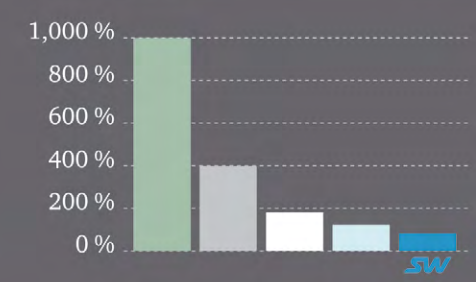
OPEX



Environmental pollution

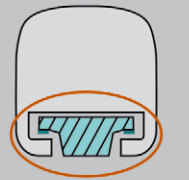


Traffic accident rate

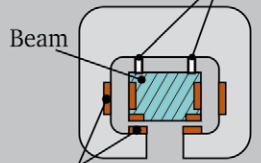


ADVANTAGES OF HIGH-SPEED SKYWAY

Maglev



Wheels



Beam

Magnets

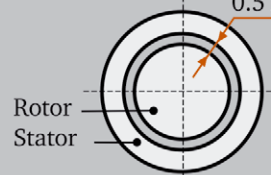


The track structure operation is more labour intensive due to its complicated configuration and technical components (electric coils, switching devices, etc.), which require constant maintenance and machinery for cleaning the track from snow and icing.

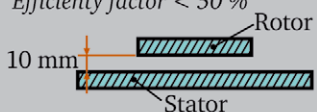
The track structure is expensive as it has a massive roadbed. The installation of electric coils and a complicated anti-derailment system is required.

Ordinary electric motor
Efficiency factor > 90 %

0.5 mm



Linear electric motor
Efficiency factor < 50 %



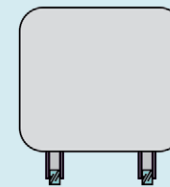
Rotor

Stator

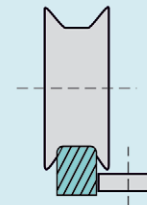
Overpass cost – from 50 mln USD/km.

The use of a linear electric motor gives the efficiency factor not more than 50 % as the clearance between a rotor and a stator (e.g., in Transrapid) cannot be less than 10 mm. However, the clearance should not exceed 0.5 mm for the effective electric motor operation.

High-speed SkyWay



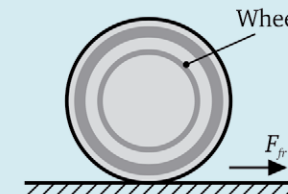
The track structure operation does not require any additional machinery as it is capable of self-cleaning (e.g., from snow and icing) and has no complicated technical elements (electric coils, etc.).



The SkyWay track structure is lighter and cheaper due to its elegant design. It does not require the installation of electric coils and provides a simple anti-derailment system.



Overpass cost – from 2 mln USD/km.



The use of a steel wheel gives the efficiency factor over 99.8 %.

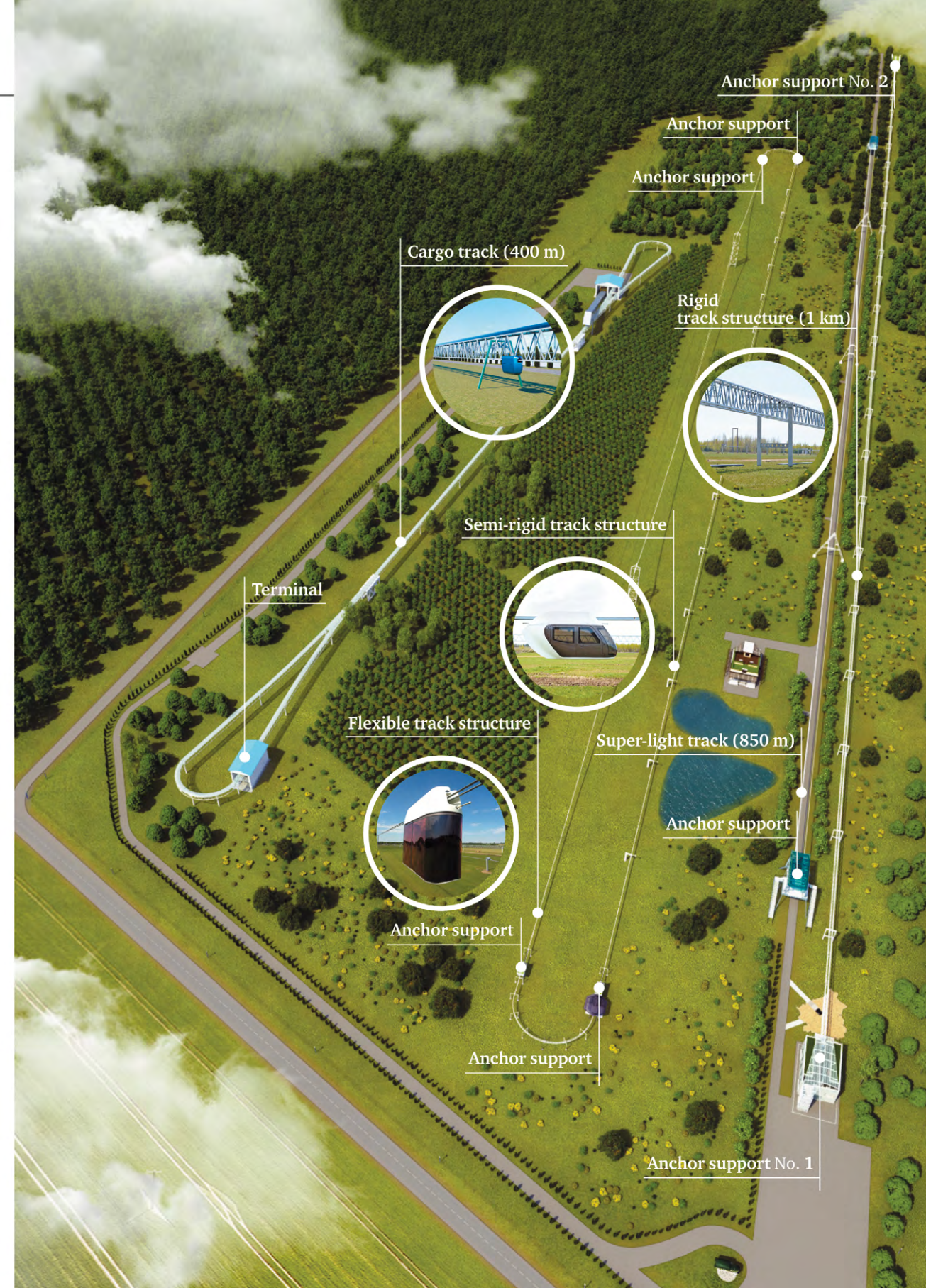
SKYWAY TECHNOLOGIES CO. PROJECT – ECOTECHNOPARK

EcoTechnoPark is a centre for practical implementation of state-of-the-art SkyWay technologies, their international expert evaluation and certification.

The construction of EcoTechnoPark (area – 35.9 ha) is carried out near the town of Maryina Gorka (Republic of Belarus).

EcoTechnoPark aims to:

- demonstrate the working industrial prototypes of SkyWay transport and infrastructure complexes: cargo, urban and intercity high-speed;
- facilitate the certification process for every complex and their components – a transport overpass, rolling stock, infrastructure, etc.;
- contribute to the constant development and improvement of the SkyWay technology;
- demonstrate the ecological potential of the SkyWay technology – minimal footprint for the track, reduced material and power (fuel) consumption in the course of construction and operation, etc.;
- showcase the related communications infrastructure, including ecogenic, bio- and agrotechnologies.



PROSPECTS

FOR SKYWAY TECHNOLOGY APPLICATION

- Exploration and development of underdeveloped and hard-to-reach territories, creation of a single network of cargo, urban and high-speed intercity tracks.
- Maximal reduction of capital and operating expenses for transport and infrastructure construction.
- Qualitative change in the economic structure of countries and increased GDP.
- Integration of countries into international transport corridors, creation of a fundamentally new logistics of the 21st century.
- Development of related branches for track structure and rolling stock manufacture (metallurgy, chemical, petrochemical and radio-electronic industries, machine building, construction, etc.).

All innovative SkyWay components can be manufactured at the places of project implementation using the existing technological base.



Track structure



Rolling stock



Automated control system



Infrastructure

MONOGRAPH

PART 1

String Transport System

PREFACE	160
CHAPTER 1 General concept of STS as an alternative to the existing kinds of transport	166
CHAPTER 2 Design features of String Transport System	179
CHAPTER 3 Mechanics problems of high-speed transport	219
CHAPTER 4 Dynamic model and estimated parameters of transport modules motion on the string transport line	231
Conventional symbols	306
Bibliography	308

158



MONOGRAPH PART 1

String Transport System

Preface

The task of creating a fundamentally new kind of high-speed ground transport is highly relevant at present. This transport should on the one hand combine the advantages of the existing kinds of transport, such as high speed of a plane and a maglev train, low net cost of railway transportation, high capacity of traffic arteries and ecological safety of electromobiles. On the other hand, it should be free from their disadvantages, such as environmental hazard and a high accident rate of motor transport, large areas of land acquisition for the construction of motor roads and railways, airports remoteness from cities, high cost and complicated solutions to scientific and technical problems when creating and operating electromobiles



***When solving
new questions
in science
and technology,
making the first step
is always most difficult.***

Mstislav V. Keldysh

and maglev trains. Apart from that, increasing communication of the world community puts forward additional demands: transport should be individual; it should provide rapid, safe and comfortable connection regardless of the distance and be available to a non-professional user.

The leading countries of the world offer national programs to promising high-speed kinds of ground transport, with independent developments carried out by many large companies. This includes wheeled transport, electromobiles, high-speed railway and maglev trains. Some rather exotic projects are also under development. For example, one of the Japanese companies offers a concept of an underground airline, which envisages a plane with short wings flying in an underground tunnel.

Starting from 1960s, scientists and engineers of different countries worldwide in the field of creating new kinds of high-speed ground transport have concentrated their efforts on the search of contactless (wheel-free) systems to achieve the speed of 500 km/h. Developers of magnetic levitation transport, transport with a linear traction electric drive and a magnetic stabilization system have faced serious challenges. This is evidenced by the fact that back in the USSR, a total of over 10 bln USD was spent on research in that field. However, not a single acting track has been built so far.

The above said implies an inevitably high cost of overpasses and maglev transport rolling stock and, consequently, high travel cost.

However, the latest developments in technology testify that the wheel has not exhausted its possibilities yet. The speed record of a car registered in the Guinness World Records is 1,190 km/h; of a platform speeded up on a rail track with an engine – 9,851 km/h. Such are the records. The speed of 500–60 km/h is sufficient for the purposes of ground transport; it is only 5,000–6,000 revolutions per minute for a medium-size wheel. The emerging problems at high motion speed of wheeled transport are not due to a wheel as such, but due to the necessity to provide high evenness of the roadbed. In order to achieve record speeds, a very smooth bottom surface of a dried-up salt lake is used nowadays. But what can be smoother than a highly tensed string? A string has actually been used for transport purposes for a long time – although not as a guide, but rather as a drive mechanism providing the high speed of an arrow shot from a bow. A bowstring has a short length. Then, if a string is stretched between supports spaced from each other at a great distance, there will inevitably appear a parabolic sag due to the action of gravity.

The first part of the book is specifically dedicated to the method, which allows making an ideally even and very rigid track for the movement of electric wheeled transport using a string. It considers a basic diagram of a string transport system (STS) providing the description of separate units, assemblies and design elements. The dynamic motion of the rolling stock and oscillations of the string track structure are thoroughly analyzed, and the project feasibility study is given.

The latest developments in technology testify that the wheel has not exhausted its possibilities yet.

The highest speed listed in the Guinness Book of World Records

Car speed

1,190 km/h

Platform accelerated on a rail track by an engine

9,851 km/h

This work offers for the first time the general concept of the STS (**Chapter 1**), elaborates its design (**Chapter 2**) and carries out an analysis of the main scientific and technical problems arising in the course of the project implementation (**Chapter 3**). They particularly include the following: calculation and control of transport modules dynamic motion on a string transport overpass (STO), research of modules and load-bearing structure strength, tribology of the wheel-string contact at super-high speeds and other questions.

Chapter 4 gives the results of developing a dynamic model and the estimated parameters for transport modules motion on a string transport overpass.

Based on a number of common assumptions, the equations were obtained to describe motion in the vertical plane of the track structure – modules system. In order to solve the equations with a few restrictions to the design parameters of the system, a method of successive approximation is offered, and the task on track structure oscillations under the action of moving loads is formulated.

The STO oscillations were investigated for the case where the elasticity modulus of an STO string rail body is small and the filler material is incompressible.

Formulae for a maximal span deflection for the single load and line load movement were obtained. Line oscillations with regard to the elastic and dissipative properties of the body and the filler were studied. An analysis of the decay time for long and short waves after removing the load from the span was

carried out. The resonance conditions with the line load moving on the overpass having a solid and a split body were obtained.

The results of the calculations of the dynamic span deflection with various modes of loads movement and different values of design parameters are shown in the form of diagrams. A detailed analysis of the obtained diagrams has been made; the generalizations and conclusions have been formulated.

The idea of string transport originated when the author was working on a grand project – the program of non-rocket space exploration. He managed to find the only possible solution not contradictory to the laws of physics based on the principle of Baron Munchausen, who as is known

What can be smoother than a highly tensed string?

The idea of string transport originated when the author was working on a grand project – the program of non-rocket space exploration.

pulled himself and the horse out of a swamp by his own hair. The implementation of this idea is possible if the center of masses of the space transportation system coincides with the Earth's center. In order to achieve this, it should cover the planet in the form of a ring. In this case, magnetic levitation will be used instead of hair, and it will be possible to go into space using the centrifugal forces created by the rotor moving along the structure.

This is the basic diagram of the United Planetary Transport (UPT).

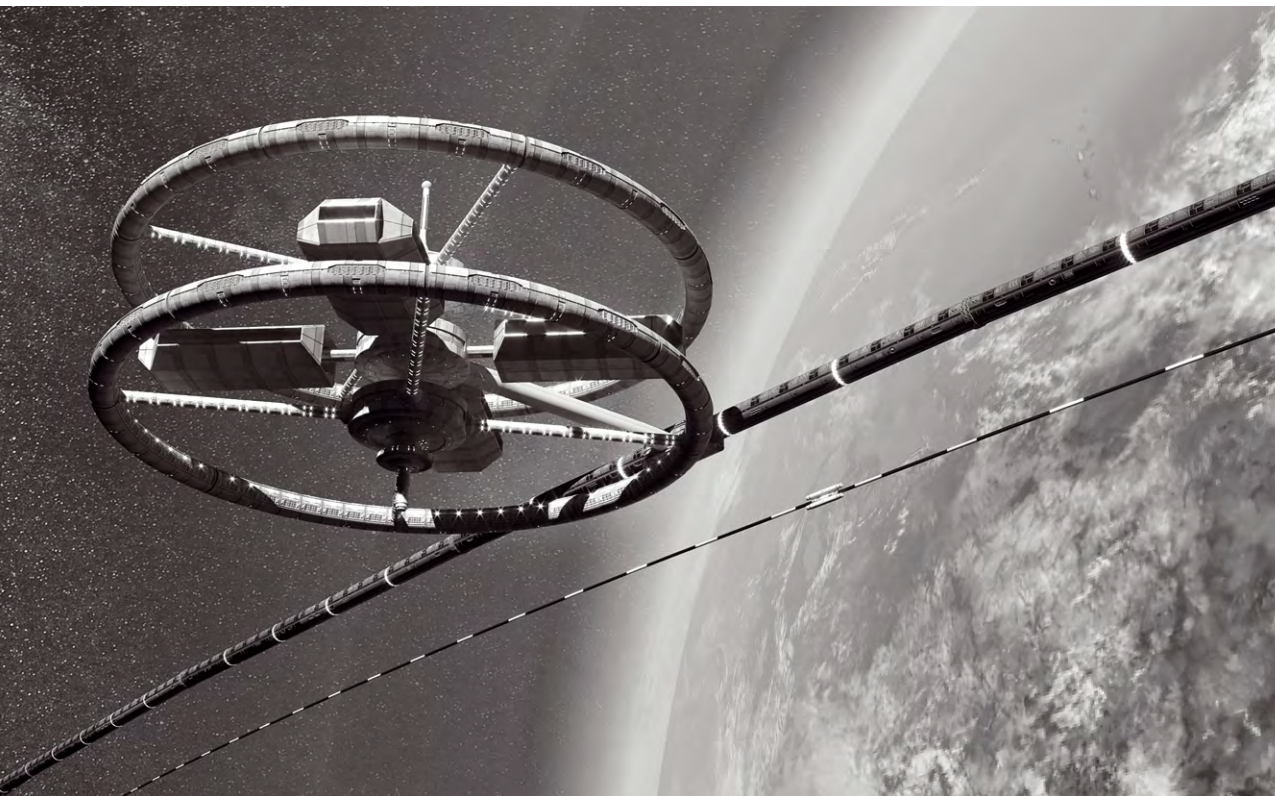
The second part of the book is dedicated to the UPT and the substantiation of the inevitable industrial space exploration in the future using non-rocket systems. It describes the UPT design, the systems of rotor acceleration to the second cosmic velocity, dynamic motion inside the atmosphere and in outer space. It also analyzes the structure of the Uranus and Saturn rings that could be built with the help of similar technical systems. It considers other questions discussed at the first All-Union scientific and technical conference Non-Rocket Space Industrialization: Problems, Ideas, Projects organized

by the author and held on April 26–28, 1988 in Gomel.

Both parts of the book are united not only by the same authorship, but also by the fact that both the STS and the UPT are string transport systems since their transverse dimensions are infinitely small compared to the length and they are stretched in a longitudinal direction to the significant efforts. The STS project appeared as a result of work on the UPT overpass. The creation of this overpass is the most labor consuming part of the project as the overpass will be thousands of kilometers long and should encircle the Earth in one of the latitudes. For this reason, the UPT basic diagram faced criticism on the part of numerous opponents. The desire to simplify and cheapen the overpass design has led to the creation of a linear string system, which is proposed to be used as a track structure for high-speed ground transport.

There is no rigorous research on the projects described in this monograph anywhere in the world. This is evidenced by the results of the patent search as to the novelty on international applications for string transport systems and by the analysis of scientific publications.

The STS project appeared as a result of work on the UPT overpass.



The author considers it is his duty to express sincere gratitude to the:

Candidate of Physical and Mathematical Sciences, **Vyarvilskaya O.N.**,

Candidate of Physical and Mathematical Sciences, **Savenkov V.A.**,

Candidate of Physical and Mathematical Sciences, **Savchuk V.P.**,

Candidate of Physical and Mathematical Sciences, **Kozlovskiy N.I.**

(Belarusian State University) for the assistance in preparation of Chapter 4 (Part 1);

Candidate of Technical Sciences, **Shilko S.V.**,

Candidate of Technical Sciences, **Chizhik S.A.** (Institute of Mechanics of Metal-Polymer Systems under the Academy of Sciences of Belarus)

for the assistance in preparation of Chapter 3 and 4 (Part 1);

Candidate of Physical and Mathematical Sciences, **Kazban A.M.**

(Voronezh Polytechnic Institute),

Candidate of Technical Sciences, **Lizarev A.D.**

for the assistance in preparation of Chapters 1–5 (Part 2);

to the Doctor of Engineering,

Petrokovets M.I. – for the review of Part 2 of the monograph.

Chapter 1

General concept of STS as an alternative to the existing kinds of transport

A traffic artery for the movement of transport modules is the basis of any transport system. As a rule, it is extremely material intensive (a roadbed, a rail track, bridges, tunnels, earthwork, etc.); therefore, its costs determine the main cost of the whole system. In this regard, the efficient use of physical and mechanical properties of materials in the structure of transport communications is very important.

In terms of the maximal use of physical and mechanical properties of materials, tension is the most favorable state of materials out of four types of stress strain behavior: tension, compression, bending and torsion. It can be illustrated with the following example. The Ostankino Tower in compression, a highway bridge with a 500-metre span, which experiences bending, and a 500 m long cable in tension with cargo of 100 tons suspended to it have approximately the same length and are designed for approximately the same payload. However, material consumption of the last structure is by a thousand times less since the cable diameter will be less than 10 cm; whereas both the tower and the bridge with a similar span have over 10 m in diameter.

A calculation model with unique properties, the elements of which work in tension, is known from mechanics: loaded up to the materials tensile strength, it can carry even bigger additional load without collapsing.

If a string is taken, put through two blocks and loaded up to the tensile strength with effort T (figure 1.1a), it will not collapse even with additional load in the middle of the span $P < 2T$ due to deflection y_s (figure 1.1b).

This structure can be transformed into a long linear circuit (figure 1.2a), where blocks act as movable supports 3, and instead of cargo with weight T a string is stretched with effort T and fixed in rigid supports 4.

The analysis of the given diagrams shows that with $P < 0.1T$ the tension in a string with restraint (figure 1.2b) exceeds the same tension in a string with blocks (figure 1.1b) by only 1 % even if every span (in the first case) has the same load P . With a less loaded string, this difference will be even less. This difference can be neglected in engineering calculations. Thus, if $P < 0.01T$ the difference becomes small to negligible – less than 0.1 %.

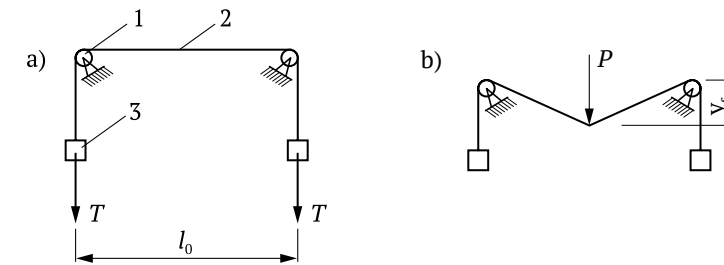


Figure 1.1 – String block system:
a – without external load; b – with load; 1 – block; 2 – string; 3 – load

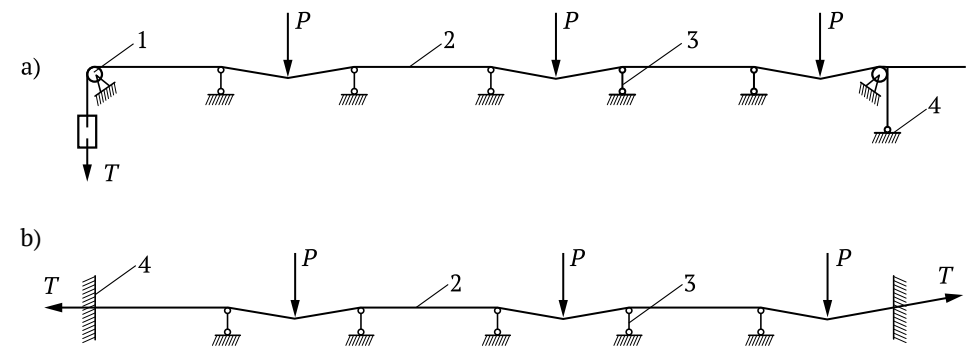


Figure 1.2 – String linear system:
a – with a block at a string end; b – with restraint of string ends;
1 – block; 2 – string; 3 – hinged support; 4 – restraint (anchor)

The diagram can be used as a basis for the creation of new transport lines [39, 40, 41, 42, 43] (NLT transport) and modernization of conventional bridges and viaducts (string motor and railway bridges).

The NTL transport moves on a track structure, which is based on two string rails designed in a special way (figure 1.3). Strings 2 and 4 are made of separate wires or stripes of high-strength material (for example, of steel) stretched with a tension of several hundred tons and mounted on light supports 5–50 m and more high, spaced from each other at the distance of 40–100 m and more (figure 1.4–1.15). Transport modules are powered with electric energy via wheels in contact with string rails. The NTL track structure is designed so that the working surface (rail head) used for the movement of a transport wheel is a smooth surface without any joints (“a velvet way”). It is important that evenness of a rail does not depend on string sag y_s under the action of module weight between the supports. Despite low material consumption, the track structure

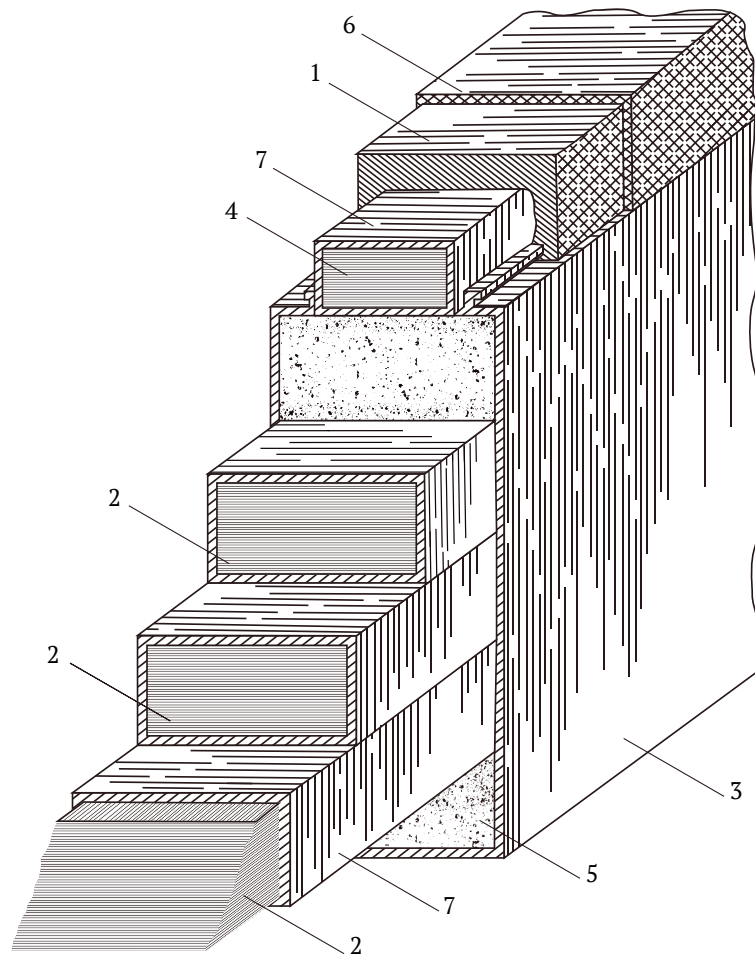


Figure 1.3 – String rail design:
1 – head; 2 – main string; 3 – body; 4 – additional string;
5 – filler; 6 – wear-resistant coating; 7 – protective cover of a string

will be not less rigid than massive conventional beam road and railway bridges, as stated in Chapters 2 and 4. In fact, its deflection under the action of working load (moving transport modules) will be 1/1,000 and less of the span length.

If the speed is over 200 m/s (720 km/h), the transport system should be placed in a special tube with a diameter of 2–3 m, with the air pumped out. The tube can be located above or under the ground, or under water at the depth of 10–100 m and more not to hinder navigation and not to be exposed to the destructive effect of natural disasters.

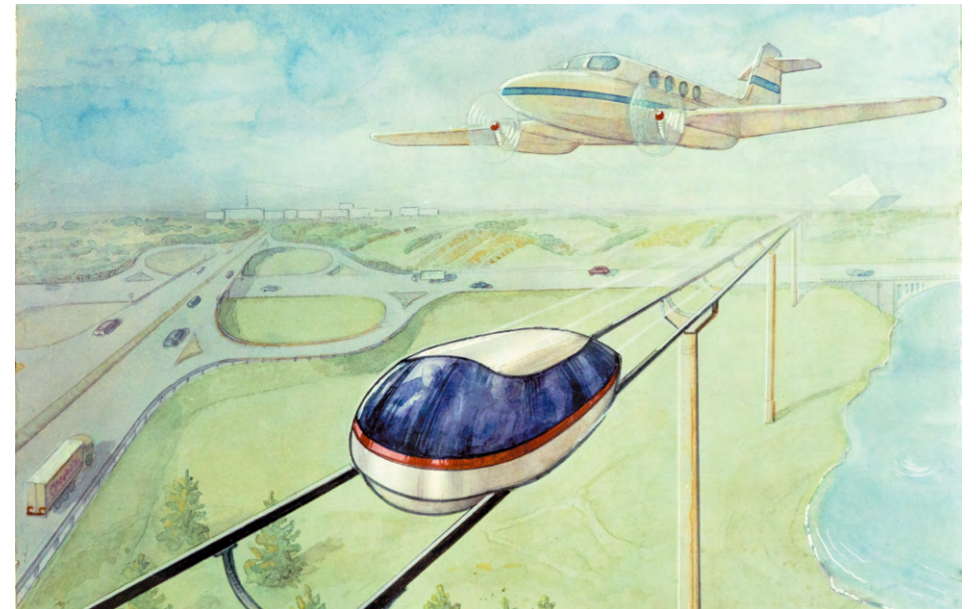


Figure 1.4 – NTL speed comparable to that of a plane



Figure 1.5 – NTL track on tower supports (about 100 m)

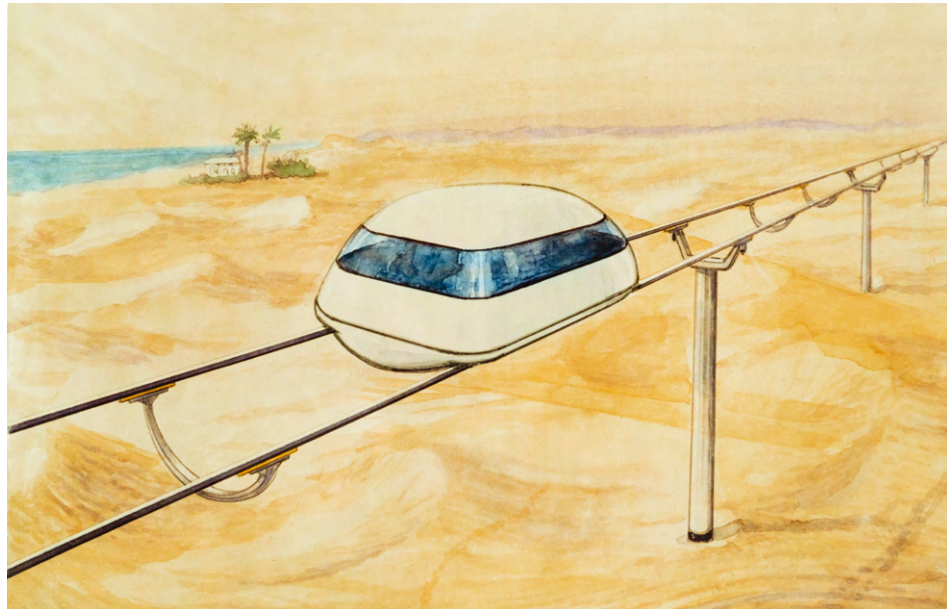


Figure 1.6 – NTL track in a desert

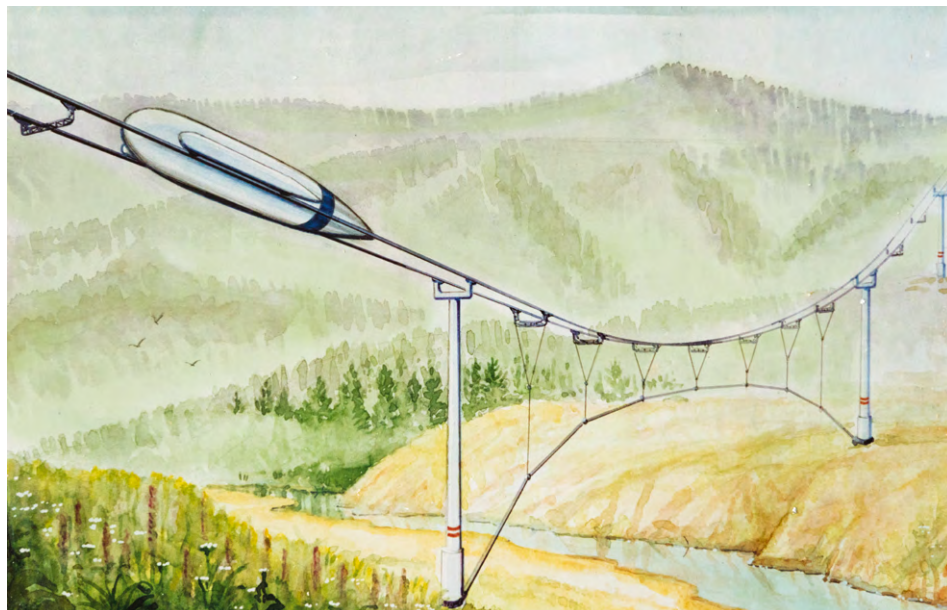


Figure 1.7 – NTL track in the mountains

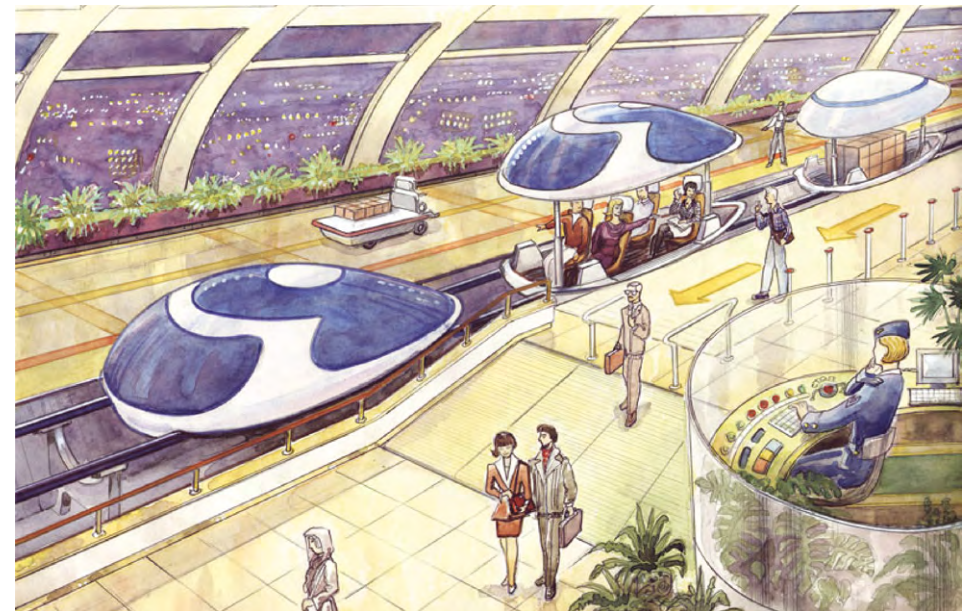


Figure 1.8 – Station

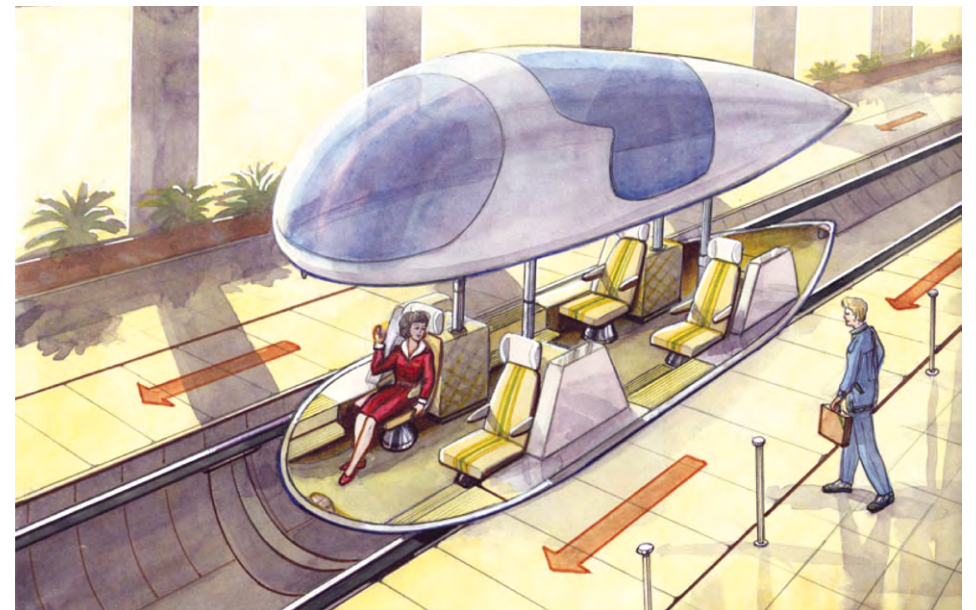


Figure 1.9 – Boarding a transport module



Figure 1.10 – NTL track in the city

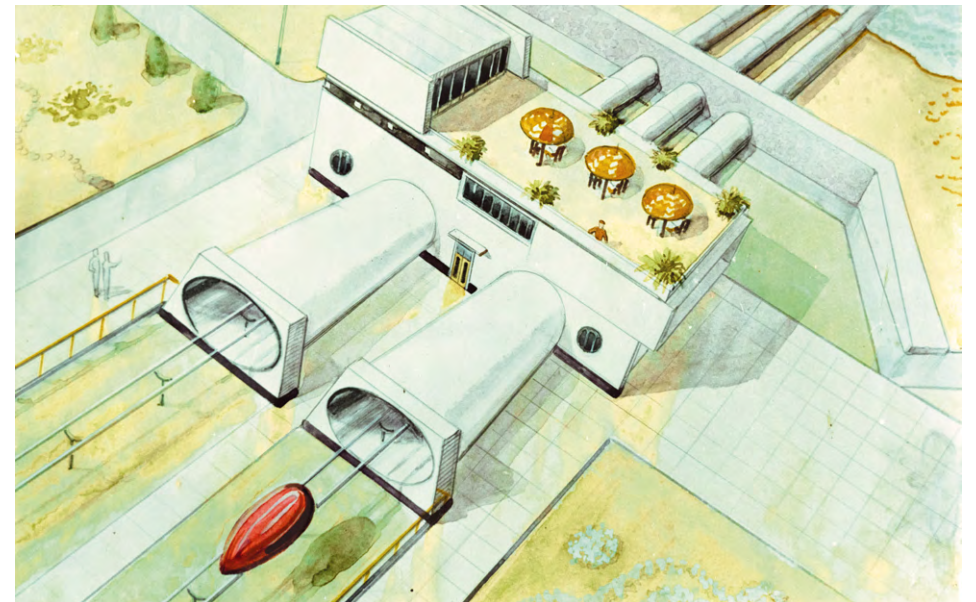


Figure 1.12 – NTL track enters the sea section

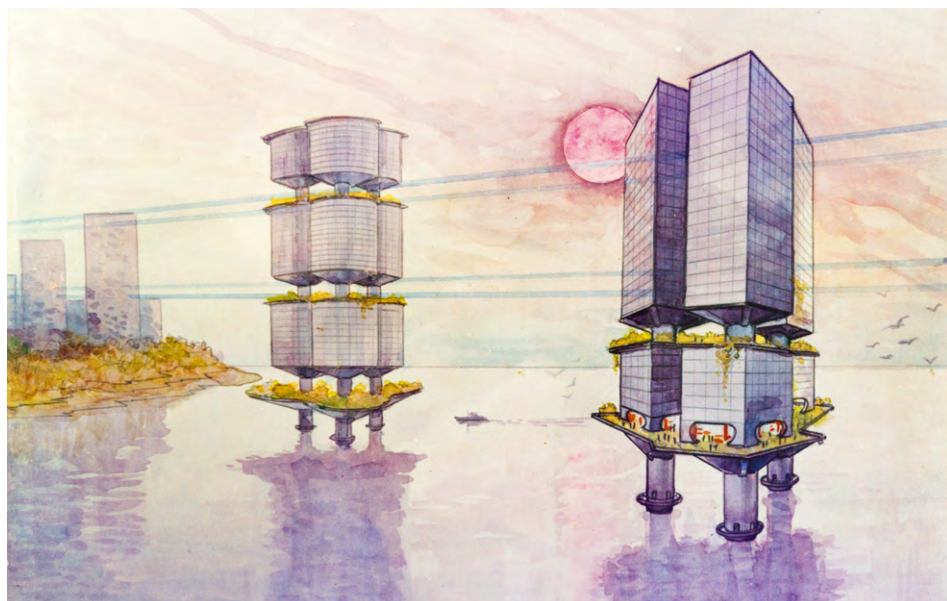


Figure 1.11 – NTL track on a shelf sea (skyscrapers act as supports)

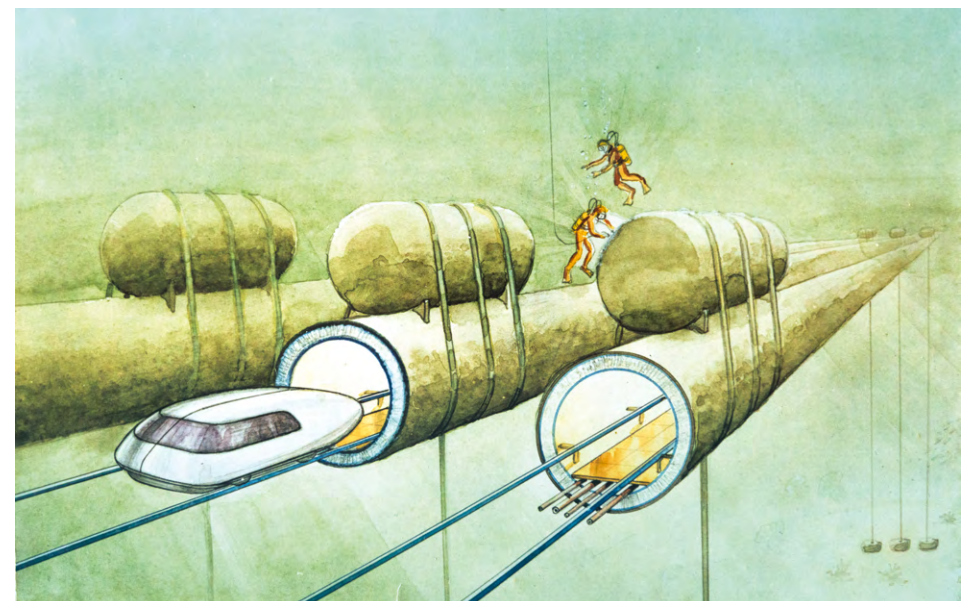


Figure 1.13 – Sea section of NTL track
(forevacuum tube tunnel of zero buoyancy at the depth of 50 m)

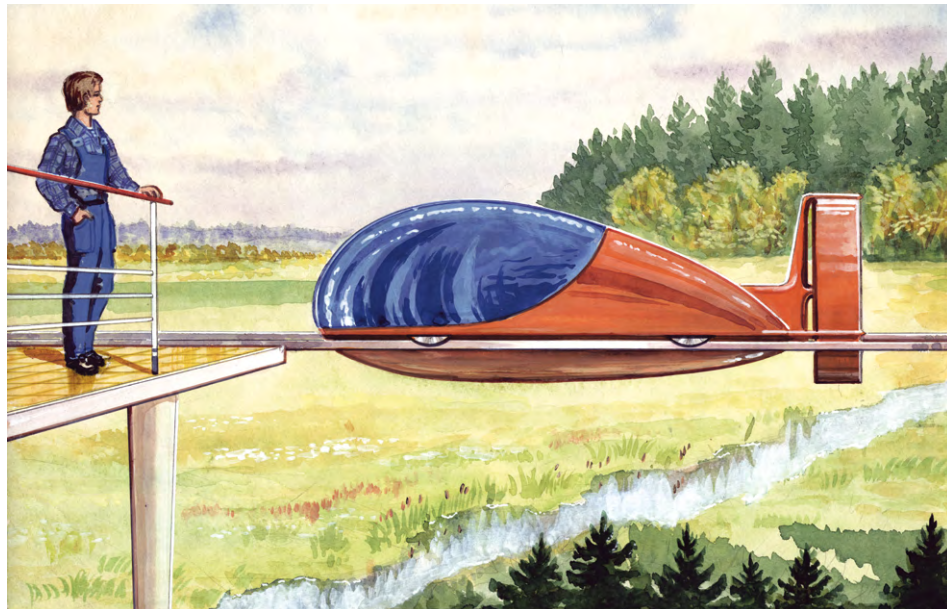


Figure 1.14 – Utran with a pushing propeller

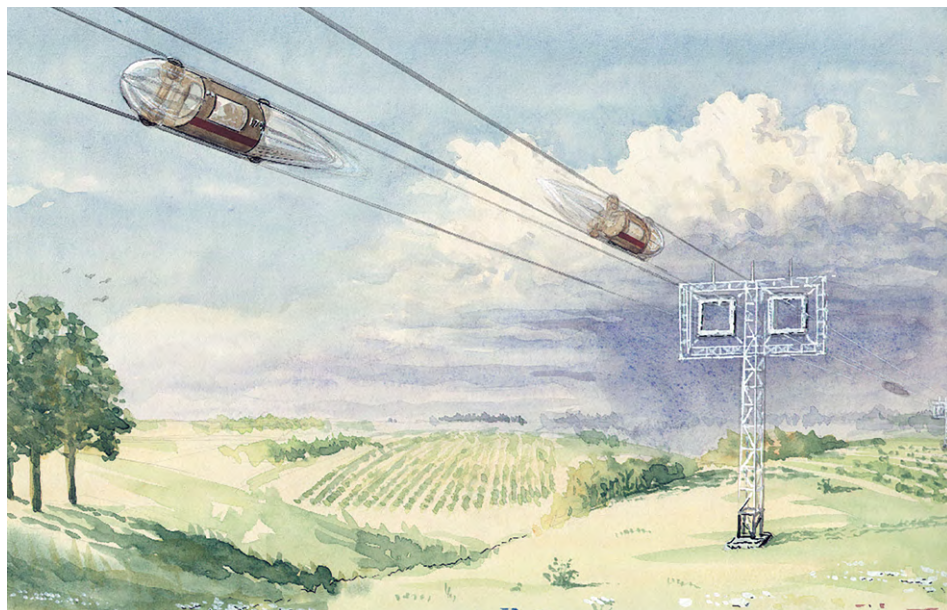


Figure 1.15 – Design variant of intermediate support

The NTL transport will compare favorably with the existing kinds of ground transport almost by all criteria*:

- it is ecologically clean as it consumes electric energy (power supply from the existing electricity mains), practically noiseless and has a small footprint since it does not require large areas of land acquisition for construction and operation, which is especially important both in industrially developed regions (the existing network of transport, energy and other communications or the existing development are not disturbed), and on undeveloped and hard-to-reach territories where the existing biogeocenosis will not be disturbed, either, preserving hills and mountains, taiga and jungles, waterlogged lands and shelf sea;
- it has a high carrying capacity (one line – up to 1 mln passengers and up to 500,000 tons of cargo per day), although it will be profitable even with the low traffic volume (about 1,000 passengers per day), which is explained by low cost of tracks and transport modules, and low operating expenses;
- it does not require a lot of resources for construction (for example, for a similar capacity, basic materials – steel and concrete – are required significantly less compared to those for the construction of roads and railways; as for the amount of digging work, the NTL are by hundred times more cost-efficient);
- it is the most economical transport since energy losses when in operation are determined only by aerodynamics (the NTL electric drive energy efficiency reaches 90 %), and the NTL aerodynamic properties can be close to ideal as the transport module practically has no protruding parts and is not affected by aerofoil effect worsening the efficiency thanks to the absence of a solid roadbed;
- it is easy in operation and control (adjustable parameters – motion speed and distance between neighboring transport modules – allow easy automation of motion control and abandoning a driver);
- it has a significantly smaller unit cost of construction (related to carrying capacity) in contrast to highways and railways;
- it is based on the already existing scientific and technical solutions and its implementation does not require an extremely high scientific, technical or production potential;
- it allows reaching the speed of 1,000 km/h in the future due to its location in a vacuum tunnel of a small diameter (about 2.5 m) when using the magnetic levitation and linear electric motor systems;

* A more detailed substantiation of the advantages of the NTL transport system is given in Chapter 2 below.

- it has a high level of comfort when in motion thanks to the absence of vibration, noise, overloading and other factors, as well as the elimination of such undesirable automobile associates as exhaust fumes and the fumes of combustible and lubricating materials when moving on the track structure similar to a “velvet way”;

- it is all-weather transport as adverse weather conditions (rain, snow, hurricane, dust storms, etc.) will have no negative impact on its operation;

- it provides high safety of movement since the transport system retains its durability even in extreme conditions (earthquake, landslide, hurricane, flood, etc.) as the fall of one or several neighboring supports will only cause an increased span, but will not disturb the track structure integrity, and the operatorless vehicle control allows reducing accident rate to zero;

- it is a versatile kind of transport due to the possibility of its use both at ground and sea sections of transport lines;

- it is more durable than railways and motor roads. The NTL track elements exposed to dynamic impact are stronger and more durable than conventional material for motor roads – concrete and asphalt-concrete, and have far more favorable operating conditions than rails and sleepers – both due to the absence of joints and higher evenness of rail strings, and significantly smaller contact stresses in a wheel – rail pair. Moreover, the NTL have no factor of track contamination or longstanding storage of irreversible deformation in earth embankments;

- NTL tracks easily overcome deep gorges, straits and other similar obstacles up to 5–10 km wide without intermediate supports and can go up and down the hills at the declivity angle of up to 45–60 degrees due to the special design of transport modules;

- material consumption and, consequently, the cost of NTL tracks depends little on the terrain and its peculiarities, therefore the development of desert lands, marshy land, permafrost regions, taiga, tundra, ocean shelf, mountains, etc. is greatly facilitated using the new transport system.

The list of advantages of the NTL transport also includes the fact that the transport module will be cheaper than a car by 2–3 times, whereas its comfort level will be higher. It should be noted that even an inexperienced operator will be able to use it by means of entering a destination code into the automated control system (for example, voice activated navigation).

Technical, operating, economic and other features of the NTL system compared to the basic kinds of transport are shown in table 1 below.

Table 1 – Comparative data of the NTL system and other transport systems (for bidirectional transportation of 10,000 passengers per hour)

Parameter	Transport system (average data per 1 km of the track)					
	NTL	Highway			Railway	Civil aviation
		asphalt concrete surface	reinforced concrete surface	overpass		
1	2	3	4	5	6	7
1. Resource consumption						
1.1. Volume of earthwork, thousand m ³	0.1	75	75	2	50	1
1.2. Steel consumption, thousand tons	0.1	0.01	0.1	0.5	0.4	0.01
1.3. Concrete and reinforced concrete consumption, thousand m ³	0.1	0.1	4	8	0.5	0.5
1.4. Crushed stone consumption, thousand m ³	–	5	5	–	5	0.5
1.5. Asphalt concrete consumption, thousand m ³	–	4	–	1.5	–	0.1
1.6. Footprint for track construction, ha	0.02	5	5	2	5	1
2. Performance characteristics						
2.1. Operating speed*, km/h	250**–500	80–100	80–100	80–100	100–150	200–500
2.2. Cost of the track, relative units	1	3	4	10	4	1
2.3. Vehicle engine hp, kW/passenger	5	20	20	20	15	100

* The operating speed is taken at the distance of 1,000 km based on passenger transportation from the departure city center to the destination city center (considering the time spent to purchase tickets, arrive at the airport, wait for the departure, fueling, driver's rest, etc.).

** The costs for the NTL system are given for the operating speed of 500 km/h.

Table 1 finished

1	2	3	4	5	6	7
2.4. Energy costs for transportation, kWh/passenger/1,000 km	55	220	220	220	120	250
2.5. Type of energy used	Electricity	Chemical	Chemical	Chemical	Electricity	Chemical
2.6. Energy cost, relative units	1	5	5	5	1.2	6
2.7. Rolling stock cost for the distance of 1,000 km, relative units	1	5	5	5	2	10
2.8. Operating personnel salary, relative units	1	10	10	10	2	5
2.9. Cost of terminals, stations and related services, relative units	2	1	1	1	2	5
2.10. Factors that hinder traffic safety	None. All-weather	Fog, rain, ice slick, snow drifts	Fog, rain, ice slick, snow drifts	Fog, rain, ice slick, snow drifts	Snow drifts	Fog, snow, thunderstorm, birds
2.11. Adverse impact	None	Chemical pollution, pollution of soil waters, noise, disturbs natural migration of animals	Chemical pollution, pollution of soil waters, noise, disturbs natural migration of animals	Chemical pollution, noise	Noise, soil vibration, disturbs natural migration of animals, pollution of soil waters	Chemical pollution, noise, contrail
2.12. Average speed of continuous track construction, km/day	1	0.5	0.5	0.05	0.5	–

Chapter 2

Design features of String Transport System

The STS developer is the NTL (New Transport Lines) company created for these purposes in Minsk in 1994, whereas the patent holder and author is STS General Designer Anatoli Unitsky and NTL Neue Transportlinien GmbH (Berlin) established in Germany in 1994 for the legal protection of the project. An international application for the Linear Transport System invention (Geneva, Switzerland) No. PCT/IB 94/00065 dd 08/04/94 was filed for the STS basic diagram and its design features, and the first patent (Russian Federation, patent No. 94026782/11 dd 26/09/94) was obtained.

The entry into the national phase for patenting in 40 countries of the world will be carried out in 1996. Therefore, the STS design features can be revealed in this work only within the international application, although the degree of STS elaboration is significantly higher at present.

2.1. STS basic diagram

The string transport system is a structure of great length reaching thousands of kilometers. The characteristics of this system – reliability, durability, speed limit, cost of construction and operation, etc. – will depend not only on the design of its separate components, but also on their linear arrangement. The arrangement for the most typical track sections (a plain, a mountainous area and a sea section) is shown in figure 2.1.

The string track structure 1 is placed on supports, which are divided into three characteristic types: intermediate (backup) support 2, anchor support 3 and brake support 4. The supports are installed, correspondingly, at intervals of $l_0 = 10\text{--}200$ m and more, $l_a = 1\text{--}100$ km, $l_b = 0.1\text{--}10$ km. The distance between the supports is subject to the construction technology, local terrain, the material used for the load-bearing structural members, particularly for the string, operating conditions, the weight and design speed of a transport module, the string tension force and other factors.

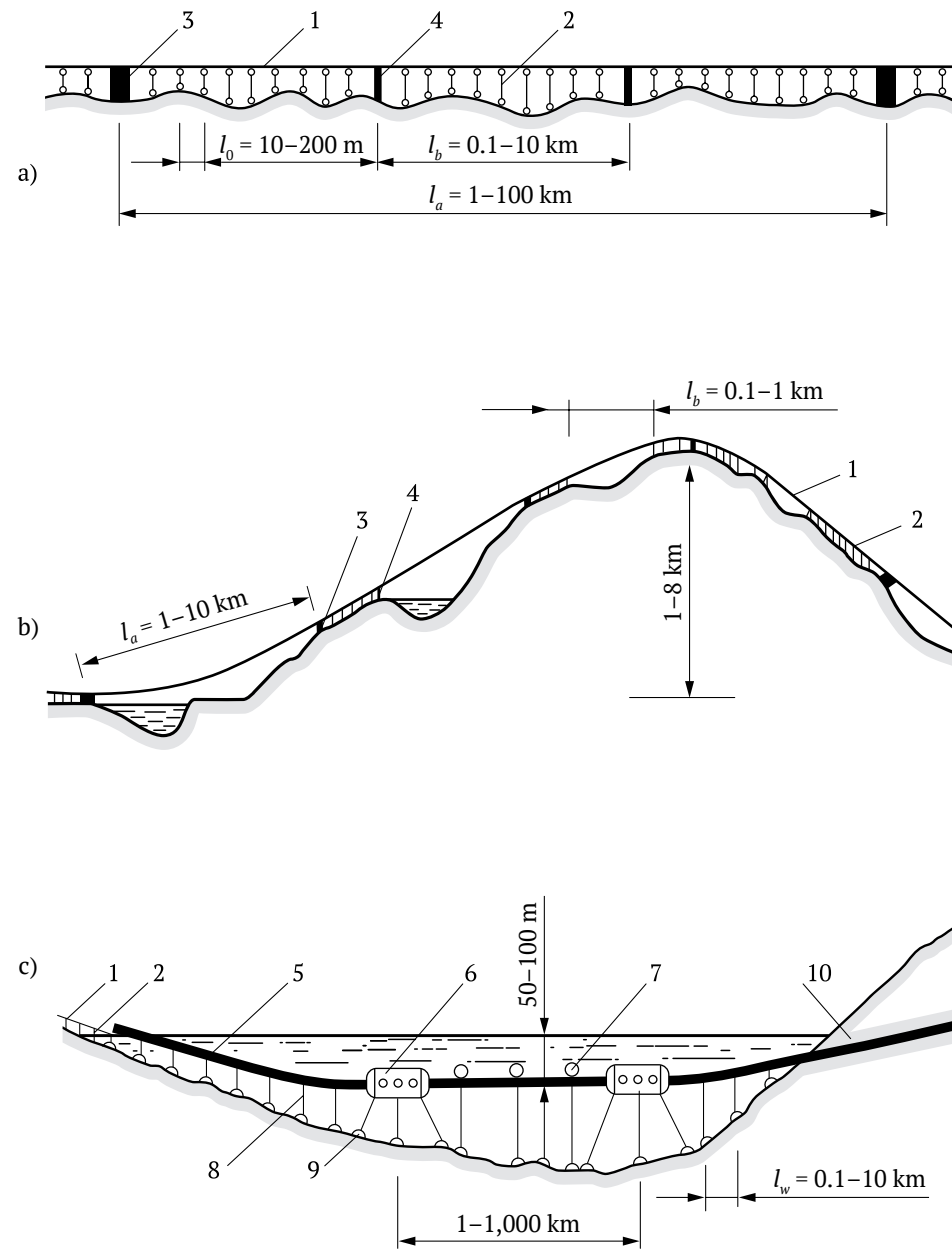


Figure 2.1 – STS linear circuit (variants):

a – plain; b – mountainous area; c – sea section;

1 – string track structure; 2 – intermediate (backup) support; 3 – anchor support;

4 – brake support; 5 – tube tunnel; 6 – underwater floating station;

7 – supporting float; 8 – anchor pull; 9 – anchor; 10 – underground tunnel

The track can cover distance l_b between the neighbouring brake supports in one span 0.1–1 km and more long (without intermediate supports) at the sections with challenging terrain. In this case, the parabolic deflection of the sagging string track structure under the action of gravity force can be $(0.001–0.01)l_b$ and can be smoothly integrated into the longitudinal track profile (figure 2.1b).

In similar situations, the STS can cover distance l_a between the neighboring anchor supports in one span up to 10 km long. In this way, it will be possible to overcome deep gorges, straits, distances between an island and a continent or between the tops of neighboring mountains, and other obstacles. In this case, a parabolic deflection of the track structure under the action of gravity force will not exceed $0.05l_a$, which also allows to smoothly integrate it into the longitudinal track profile.

The STS track at the sea section is placed in an underwater tube tunnel 5 with zero buoyancy at the depth of 50–100 m and more. The location at such depth excludes the impact of destructive storms or the possibility of being affected by a submarine or a deep-draft ship.

The tunnel can run at a greater depth in order to bypass powerful sea currents. Floats 7 anchored at the bottom of the sea serve to provide excessive buoyancy, to avoid tube flooding under the impact of moving load. Considering low material consumption of anchor pulls and their sparse location (every 0.1–10 km), the sea depth has no significance for the STS cost. Underwater floating stations 6 designed with high excessive buoyancy act as anchor supports. STS intermediate and brake supports of small dimensions are located inside the tunnel. A tube tunnel made of steel or pre-stressed reinforced concrete has the inside diameter of 2.5–3 m and is stretched in longitudinal direction up to the effort of about 1,000 tf and more. Therefore, it will also act in the STS as a string with a span l_w .

The track structure has no sags (figure 2.2a) at the main STS sections, i.e., at the sections with the length l_0 (between backup supports 2), since the static deflection y_s of string 3 is placed (hidden) inside its structure. The load of the track structure and transport module weight is transferred to the string via gasket 4, the height of which varies along the span from zero (above the support) to the maximal value y_s (in the middle of the span). Therefore, rail head 5 used for the movement of transport module wheels has an even surface under static conditions, without any joints or sags.

It is possible to design the STS with the rail head working surface as a wavy line (figure 2.2b). Its form is a mirror reflection in relation to the direct line 8 of the track structure dynamic deflection u_d at the time of transport module movement.

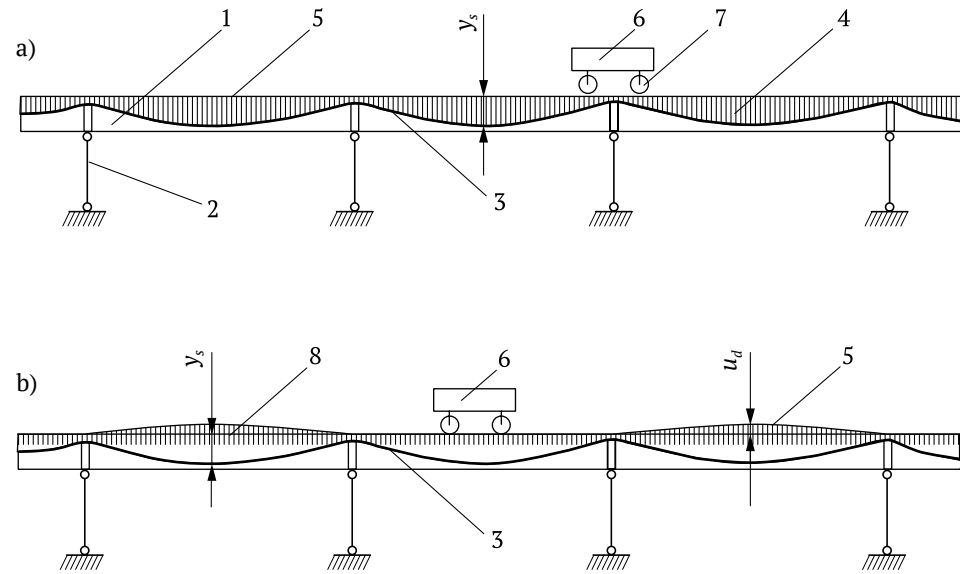


Figure 2.2 – Diagram of longitudinal section for the string track structure:
 a – track structure without a sag; b – with a bulge (contracurvature);
 1 – track structure; 2 – intermediate support; 3 – string;
 4 – gasket (retainer) of variable height; 5 – rail head;
 6 – transport module; 7 – wheel; 8 – direct line

As a result, the superstructure goes down to line 8 and the motion trajectory of the module at any time is a straight line.

Figure 2.3 shows the dependences of the maximal static deflections of a string on the mass per unit length ρ_1 (linear mass) of the track structure (y_s^{\max}). Figure 2.4 shows maximal sags of the track structure (u_s^{\max}) under the impact of single load P (load and sag – in the middle of the span) for different values of T_s tension force of a string with a parabolic deflection, and T_0 tension force of the track structure (apart from the strings, it can also have a stretched rail head, body and other structural components). The calculations were carried out based on the formulae presented in Chapter 4.

The diagrams in figure 2.3 evidence that the values $y_s^{\max} \leq 10$ cm can be reached with $l_0 = 40-100$ m and more, $T_s = 100-1,000$ tf and more and $\rho_1 = 10-100$ kg/m and more. Such a parabolic deflection can be easily placed (hidden) inside the track structure if the height of the rail section is within 10–25 cm.

The analysis of dependence in figure 2.4 shows that the values $u_s^{\max} \leq 5$ cm can be reached for $P = 1-5$ tf with $l_0 = 25-100$ m and $T_0 = 100-1,000$ tf.

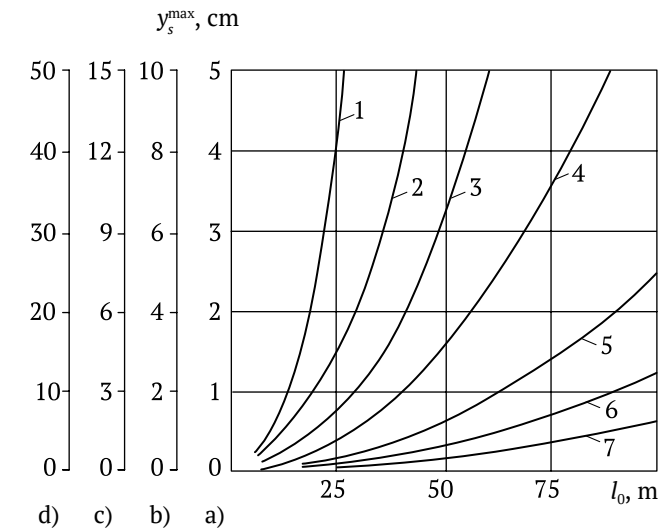


Figure 2.3 – Maximal parabolic deflection of a string under the action of the track structure weight:
 a – for $\rho_1 = 50$ kg/m; b – 100 kg/m; c – 150 kg/m; d – 500 kg/m;
 1–7, correspondingly, with $T_s = 100, 250, 500, 1,000, 2,500, 5,000$ and $10,000$ tf

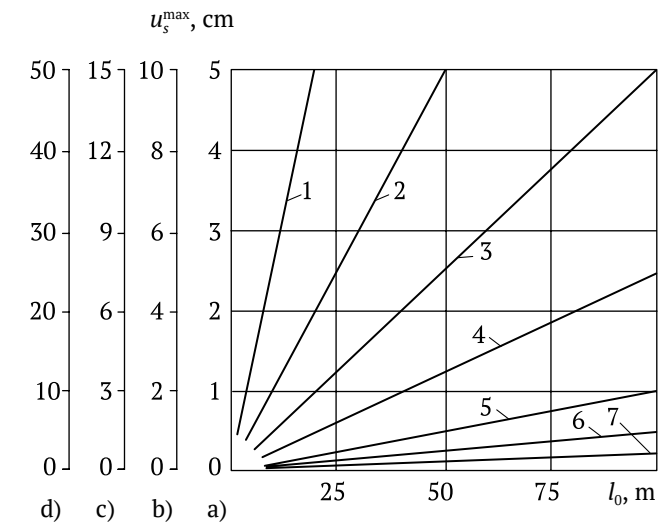


Figure 2.4 – Maximal track structure deflection under the action of single load:
 a – for $P = 1$ tf; b – 2 tf; c – 3 tf; d – 10 tf;
 1–7, correspondingly, with $T_0 = 100, 250, 500, 1,000, 2,500, 5,000$ and $10,000$ tf

In this case, the relative amount of deflection (referred to the span length) will be $u_s^{\max}/l_0 < 0.002$. Therefore, under the action of payload, the STS will have higher relative rigidity than the existing road bridges and viaducts. In fact, the relative deflection of superstructures of road bridges and viaducts at rated loads will be higher.

When operating the STS, there will be possible such motion modes of transport modules when each of them moves on an undisturbed track structure leaving its dynamic deflections and oscillations behind, as will be shown below (in Chapter 4).

Oscillations will extinguish in a fraction of a second, therefore the time headway between the neighboring transport modules can be 0.5–1 s. This will provide the ultimate capacity of the STS double-line track of 100,000–300,000 trips per day. If the rolling stock capacity is ten passengers and more and 5 tons and more, it will serve 1 mln passengers per day and more and 1 mln tons of cargo per day and more.

2.2. String track structure

The string track structure can be assembled with a various number of string rails (figure 2.5): from one to four and more. The rails can be arranged vertically or horizontally, or form a triangle or a quadrangle in cross section. Each of these diagrams has its advantages and disadvantages.

Figure 2.6 shows the STS design variant with two rails arranged vertically, whereas figure 2.7 shows the variant with three rails arranged horizontally.

Table 2.1 provides a comparison of different layout diagrams for rails in a double-rail track structure: a) horizontally (figure 2.5, diagrams 4–8), b) vertically (figure 2.5, diagrams 9–10).

The dimension stability of the track along the entire length is provided by cross bars (bridges) that act as railway sleepers.

In contrast to sleepers, the bars do not transfer load from the moving rolling stock to the base; therefore, they can be more widely spaced, every 5–50 m. The span will depend on the tension force of the strings, rails rigidity, weight of the transport module, cross-wind force and other factors, and must maintain the track with the accuracy of about 1 mm. It is high tension force of strings and not the cross bars that act as the main tool for maintaining stability of the track width.

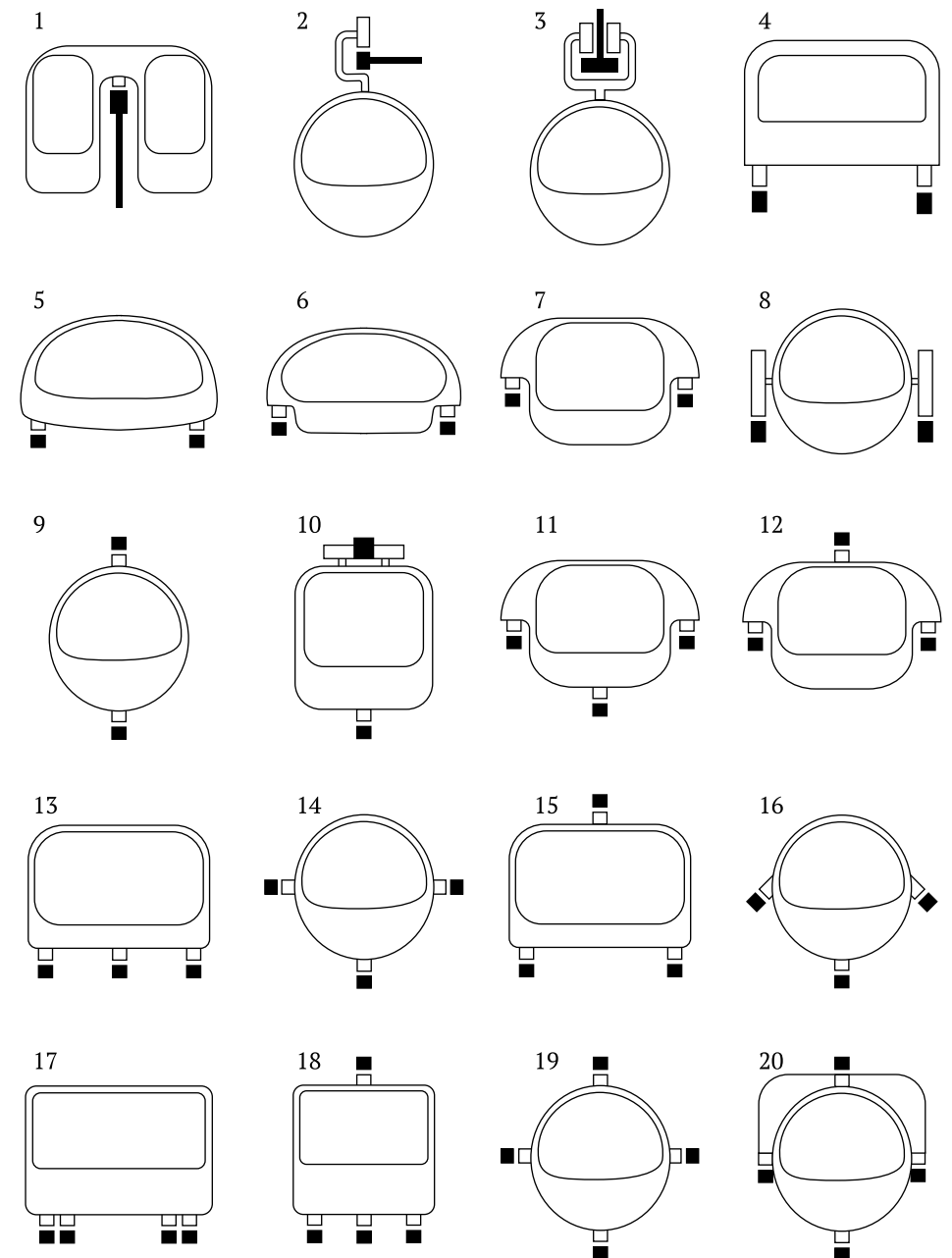


Figure 2.5 – Rails layout diagram (variants):
1, 2, 3 – STS with one rail; 4, 5, 6, 7, 8 – with two rails horizontally arranged;
9, 10 – with two rails vertically arranged; 11, 12, 13, 14, 15, 16 – with three rails;
17, 18, 19, 20 – with four rails



Figure 2.6 – STS with two rails located in a vertical plane

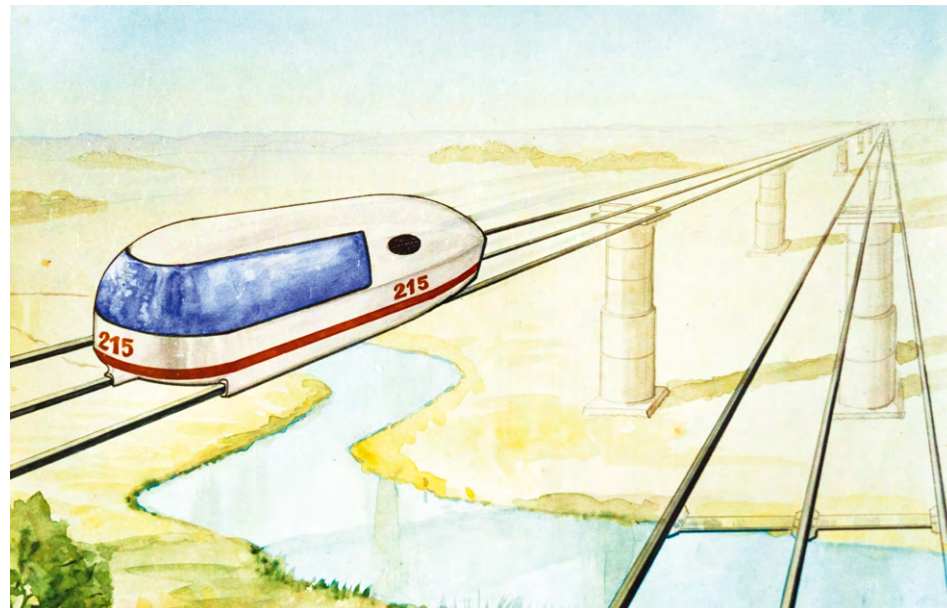


Figure 2.7– STS with three rails located in a horizontal plane

Table 2.1 – Advantages and disadvantages of different layout diagrams for two rails in a track structure

DIAGRAM A (strings are arranged horizontally)	DIAGRAM B (strings are arranged vertically)
1	2
1. Advantages	
<p>1.1. It is possible to use transport modules with a different cab height, up to 2–3 m (and, consequently, different comfort level), with the track width unchanged.</p> <p>1.2. More comfortable passenger boarding/alighting (the upper string does not prevent, unlike in diagram B); emergency evacuation of a transport module is possible from any place on the track, for example, by helicopter.</p> <p>1.3. Larger passenger capacity with the same dimensions of a transport module as, in contrast to diagram B, one row of the compartment can have two and more seats (diagram B is critical to asymmetrical load, therefore every row should have one seat on center) and, consequently, less power consumption for motion based on one passenger and lower material consumption.</p> <p>1.4. Several times lower weight of cross bars that determine the track width (shorter by 2–3 times and less loaded than in diagram B as there is no need to transfer load from the lower string to the upper one).</p> <p>1.5. Good overview of the area (no structural members at passengers' eye level or above heads).</p> <p>1.6. Symmetrical track structure (left and right rails are identical).</p> <p>1.7. Traditional layout arrangement (familiar design similar to that of a car, train – with wheels below).</p> <p>1.8. No chance of derailment in case of failure of one or several wheels ("wings" of a transport module will operate in case of wheel failure similar to skis).</p>	<p>1.1. Improved aerodynamics (no wheel fair-ings, unlike in diagram A; three wheels are possible – two below and one above, where-as the min number of wheels in diagram A – four), consequently, the speed is higher and noise level is lower (it is important when moving in the air, though in a vacuum tube, it does not make much difference).</p> <p>1.2. Lower weight of a transport module with the same length as for diagram A (no "wings" and a more favorable stress strain behavior of the load-bearing structure of the module body).</p> <p>1.3. Impossibility of aerodynamic "take-off" (derailment) of a transport module at high speed, for example, as a result of a sudden side gust of wind or a whirlwind.</p> <p>1.4. Motion is possible at any angle, up to 90°, i.e., vertically upward or down, for example, in the mountains (by means of wheel alignment).</p> <p>1.5. A transport module fits into a tube (including into a vacuum tube) of a smaller diameter (with the equal track width), which makes the construction cheaper.</p> <p>1.6. Stability against the track structure overturning at spans over 100 m (for example, when running through a gorge) is provided without any additional measures, by means of prestressing the upper string to have higher tension than the lower one.</p> <p>1.7. A bicycle (motorcycle) motion plan (two lower bearing wheels), which will provide steady motion at high speed by means of electronics, without upper bearing wheels.</p>

Table 2.1 continued

1	2
<p>1.9. It is possible to go through a turnout switch at a greater speed than in diagram B (turnout switch by the scheme: “up” or “down”) as passengers and a transport module adapt to vertical load more easily than to side load; this will speed up the transfer to another track and will not require braking of other modules when doing such maneuvers.</p>	<p>1.8. The track structure and a transport module have no skew arising because of irregular string tensioning in different rails (for example, as a result of breakage of some stretched elements – strips, cables or wires – in one of the rails).</p> <p>1.9. The turnout switch is simpler and has a traditional design (rolling stock moving to the side), less time for switching into another position (it is sufficient to move the rail aside by 0.1 m for switching, whereas such movement up or down will exceed 1 m in diagram A).</p>
2. Disadvantages	
<p>2.1. The aerodynamics is worse (since the rolling stock body cannot have a perfectly round shape in cross section because of the wheels), which causes increased power consumption for motion in the air (with the equal length of transport modules).</p> <p>2.2. There is a possibility of transport module derailment at high speed (aerodynamic take-off); therefore, additional measures are required to increase the weight although they worsen the rolling stock aerodynamic properties (spoiler or the suitable aerodynamic shape of the body to exclude aerodynamic take-off at any wind gusts or transport speed).</p> <p>2.3. Higher weight with the same rolling stock length (due to the “wings”, their fairings and a more massive bearing structure because of the worse stress strain behavior of the body).</p> <p>2.4. Possibility to move without special measures only at the angle of 10–15° (which cannot be reached by the existing railways and maglev trains though); when equipping transport modules with side wheels (they can replace flanges), it is possible to move at the angle up to 60° due to their alignment.</p>	<p>2.1. It will be impossible to increase the cab height in the future, i.e., improve its comfort level, without changing the track height (as it is impossible to change the railway gauge today).</p> <p>2.2. Increased wear of side working surfaces of the upper string rail and upper wheels flanges due to side loads (this disadvantage can be eliminated: a) by introducing the system of the rolling stock active alignment; b) by introducing two side wheels for each upper wheel replacing flanges).</p> <p>2.3. Other conditions being equal, higher supports are required; consequently, the supports cost will increase by 10–20 %.</p> <p>2.4. Poor overview of the area when moving in the air (the rail is above, flickering of cross bars and supports superstructures, which will not be notable at high speed though, except for the upper string, as blades in the rotating plane or helicopter propeller are not notable either).</p> <p>2.5. Several times higher mass of cross bars and higher loads on them (due to their larger length and the necessity to transfer load – about half of the rolling stock weight – from the lower rail to the upper one to include it into operation and unload the lower rail).</p>

Table 2.1 finished

1	2
<p>2.5. It is required to adopt additional measures to ensure stability against the track structure (pair of rails) overturning at spans over 100 m, for example when going through a gorge (by providing ballast below, or stay ropes above, or a parabolic rope supporting structure).</p> <p>2.6. A skew of the track structure and the rolling stock is possible because of irregular string tensioning in left and right rails (for example, due to breakage of some prestressed elements in one of the strings).</p>	<p>2.6. Asymmetrical track structure – a lower rail being a more loaded one differs from the upper rail (this increases, although insignificantly, the amount of the track structure design elements).</p> <p>2.7. Unconventional (uncommon) layout design (wheels below and above, which is not typical of the existing kinds of transport).</p> <p>2.8. Higher possibility of electrical breakdown between rails through cross bars, since bars in diagram B connect the rails with each other from both sides, and in diagram A – from one side, from below.</p>

The layout diagrams for cross bars in the STS track structure are shown in figure 2.8 (along the track) and figure 2.9 (in STS cross section).

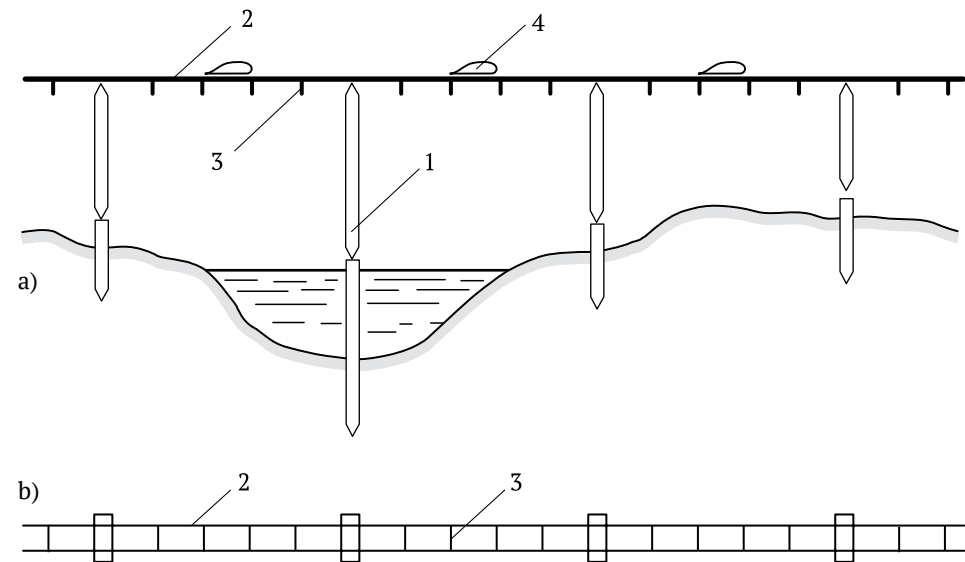


Figure 2.8 – Layout diagram for cross bars along the track:
 a – STS side view; b – top view; 1 – backup support;
 2 – rail; 3 – cross bar; 4 – transport module

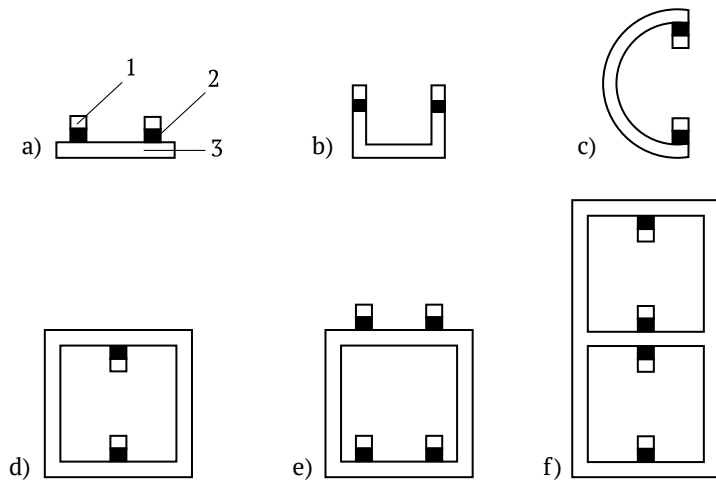


Figure 2.9 – Layout diagrams for cross bars in the STS track structure (variants):
a, b, c, d – single-deck STS; e, f – double-deck;
1 – rail; 2 – electrical insulator; 3 – cross bar

The main element of the STS track structure is a string rail; its design variants are shown in figure 2.10.

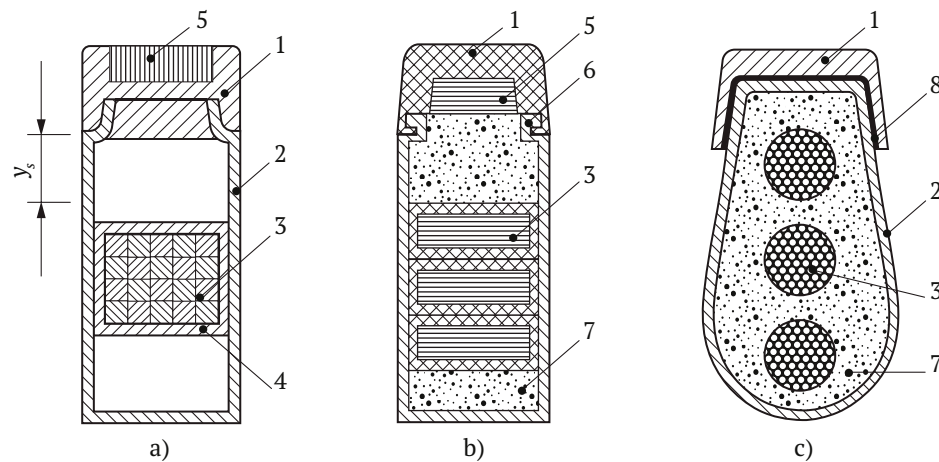


Figure 2.10 – String rail design (variants):
a – with a string of wires; b – with a string of strips, c – with a string-cable;
1 – rail head; 2 – body; 3 – string; 4 – protective cover of a string;
5 – additional string; 6 – latch bolt; 7 – filler; 8 – glue

String 3 consists of separate pre-stressed elements (wires, rods, cables or strips) located in parallel to each other along the string. They have in cross section a round, rectangular, hexangular or another shape determined by the technological and design features of the specific STS design variant. The string elements can be placed in protective cover 4, which can be made of metal, polymer or composite material. The protective cover, similar to body 2, can perform functions of electrical insulation, heat insulation and damping to suppress oscillations transferred to the string when a transport module in motion. String 3 (figure 2.10a) can be rigidly connected (fixed) to the rail body wall with a protective cover, for example, by means of welding, glue, rivets or in any other known mechanical method. In this case, the upper unfilled part of the rail body with the height y_s , acts as a gasket of variable height in the track structure.

The string can be assembled out of separate strips located either horizontally (figure 2.10b) or vertically, or in a combined way, and put in several insulated enclosures that can be rigidly connected to each other and a side rail body wall or separated using a lubricant.

String wires, cables or strips can be made of any material, the tensile strength of which is over 5,000 kgf/cm²: high-strength steel, aluminum or titanium alloys, glass fiber, carbon-filled plastic, fiber: boron, silicon carbide, aluminum oxide, carbon fiber, aramid and other high-strength polymer, ceramic or composite material.

Stretched elements in the string can be separated using a liquid, consistent or solid lubricant. Availability of grease environment will increase string durability and its corrosion resistance; in case of breakage of separate wires in the string (for example, due to manufacturing deficiency) this will allow them to shrink in length without violating the stress-strain state of the other rail elements. The string can be pre-stressed almost to its ultimate tensile strength T_s , due to this feature and to the fact that tension in the string is virtually the same in the presence and absence of moving load (see Chapter 1):

$$T_s = [T_s] - \Delta T_t,$$

where ΔT_t – the change of tension force in the string due to its thermal distortion.

With the ultimate tensile strength of string material $[\sigma_s] > 10,000$ kgf/cm², the maximal values of ΔT_t for high-strength steel, even in a harsh continental climate, will be less than $0.2[T_s]$. Therefore, the prestressing force of the STS string can range within $0.7[T_s] < [T_s] < 0.9[T_s]$. The string pre-stressing force can increase up to $0.9[T_s] < T_s < 0.95[T_s]$ in the STS operated at constant temperature regimes, for example, in underground or underwater tunnels, on track

sections with thermal regulation of the string. This will allow maximal use of the strength potential of string material.

The described STS feature eliminates the need for temperature expansion joints along the track structure length; however, it will cause seasonal tension variation in its stretched elements – to its increase in winter and decrease in summer. Therefore, the maximal values of the string parabolic deflection y_s (in the middle of the span) will range within 10–20 % of the original value (from –5...–10 % to +5...+10 % of the design position – see figure 2.2) throughout a year due to the variation in value T_s . The values y_s will range within 1 % of the design value throughout a year in a more moderate climate and when using higher-strength and less rigid materials. This will not affect the STS operation (evenness of a rail head vertically) since an additional track structure bulge (in winter) and a sag (in summer) will be about $(10^{-3}-10^{-5})l_0$.

In order to increase the track structure stability under the action of temperature stresses, all rigid rail elements – a rail head and its body – can be prestressed up to 1,000 kgf/cm². Then, all rail elements will experience only tensile stress, regardless of the ambient temperature, which eliminates the loss of longitudinal stability. Although the strings in the rail structure stretched to the force of hundreds of tons assume the appearance of compression stress in some elements, without causing the loss of rail longitudinal stability.

A rail can be equipped with an additional string 5 (figure 2.10a, 2.10b) placed along the head in parallel to it (without a sag in the middle of the span). This will increase lateral rigidity of a rail head under the action of lateral wind load caused by wheels of moving modules, etc.

A rail head can be made of metal, ceramics (metal ceramics), polymer (metal polymer), composite and other high-strength, wear resistant and conductive material – homogeneous or multilayer material, for example, with a special wear resistant renewable coating. In this case, the requirements to the STS rail head material can be many times reduced compared to the material for a conventional rail. Unlike the latter, the values of the following parameters in the STS will be by times lower: wheel load (approximately with the same diameter and the width of a contact part); the mass of a spring-loaded part (with higher evenness of the track), which determines dynamic bearing pressures at high speeds; density of electric current going through a rail – wheel contact, and other factors.

A gasket of variable height for aligning the string parabolic deflection y_s can be made in the rail as a special filler 7 in the open space of a hollow body (figure 2.10b, 2.10c) or mechanically fixed with, for example, rivet. The filler will also perform a few additional functions: a) heat insulator (for heat insulation of the most stressed element – the string); b) electrical insulator (to insulate the string from a current carrying head and body, if necessary); c) damper

(to damp mutual vibrations of a rail head, body and string); d) protection from mechanical damage of a string from outside (for example, it must be able to withstand a gunshot). The following can be used as filler material: monolithic or porous (expanded) polymeric materials, metal, ceramic and composite material, various concretes or polymer concretes, as well as various fiber material – with closed or communicating pores, filled with special liquid, consistent or solid fillers.

2.3. Supports

The STS supports are divided into three characteristic types, which differ in the amount of horizontal (longitudinal) load, acting in the process of track construction and operation: a) intermediate (backup) support; b) brake support; c) anchor support.

A backup support is installed at a span $l_0 = 25-200$ m and more and designed mainly for vertical load of the track structure and traffic weight. For a single-track line with a linear track structure mass of about $\rho_{ts} = 100$ kg/m, $l_0 = 50$ m and the transport module mass $m_{tm} = 5,000$ kg, the vertical load on a support will range within 15 tf with regard to dynamic loading. Therefore, the supports can be made relatively light and elegant (figure 2.11–2.13). In terms of height, the supports are divided into four types: a) low-height (up to 10 m); b) average height (10–25 m); c) tower supports (25–50 m); d) super high (50–100 m and higher). As for the structure, the backup supports can be single-track, double-track, single-deck or multi-deck (figure 2.14). A backup support is the main type of supports in the STS and sets the length of the design span l_0 , vibration dynamics of the string transport system, the amount of payload and the main cost of the transport line bearing part. The support must also carry horizontal transverse load, acting on the STS structural members and traffic.

Brake supports are designed for longitudinal load arising in the process of STS operation at transport modules acceleration and braking, for a longitudinal component of the structure weight arising at sloping track sections, as well as for the difference in temperature stresses arising in track structure elements at the neighboring sections (except for the stresses in the string). The supports are spaced at intervals of $l_b = 0.1-10$ km, which are determined by local terrain, traffic density and design features for each specific STS variant: a) a brake support combined with a backup support; b) supports not combined with each other. In the first case, $l_b = l_0$ and the maximal brake forces for one support will be insignificant – within 1 tf. Therefore, all types of backup supports shown in figure 2.11–2.13 will be brake supports, as well. It should be noted that local brake forces will be redistributed to a higher number of supports, including

to anchor supports, via stretched strings. Certain yielding of supports in the direction of transport movement will contribute to it, as well.

Anchor supports in the STS (figure 2.15) are spaced at intervals of $l_a = 1-100$ km, which are determined by the construction technology of the string track structure, terrain and rated force of strings tensioning.

These supports are used to anchor the stretched strings; therefore, they are designed for a unilateral effect of horizontal forces (100–1,000 tf and more) arising in the process of STS operation, and also – in case of breakage of all strings in the track (for example, as a result of a plane falling to the track structure).

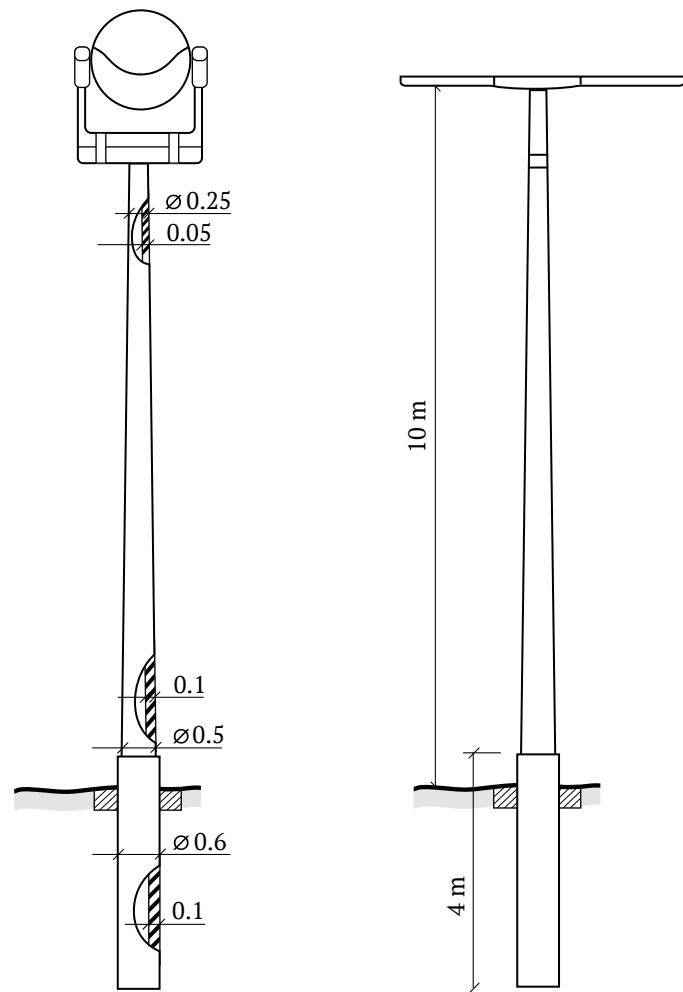


Figure 2.11 – Intermediate low-height support of the single-track STS (variant)

In case all strings are broken, a section of the track structure between the neighboring anchor supports is subject to repair. From this perspective, the distance between them should be minimal, although this will cause track appreciation. The supports also carry additional stresses arising in the string as a result of its thermal distortion, which can reach 20 % of the rated force of strings tensioning in climatic zones with a harsh continental climate. Such additional loads can arise only in the course of track construction (at its terminal points if left uncompleted for the winter), and on the first and last anchor support of the track.

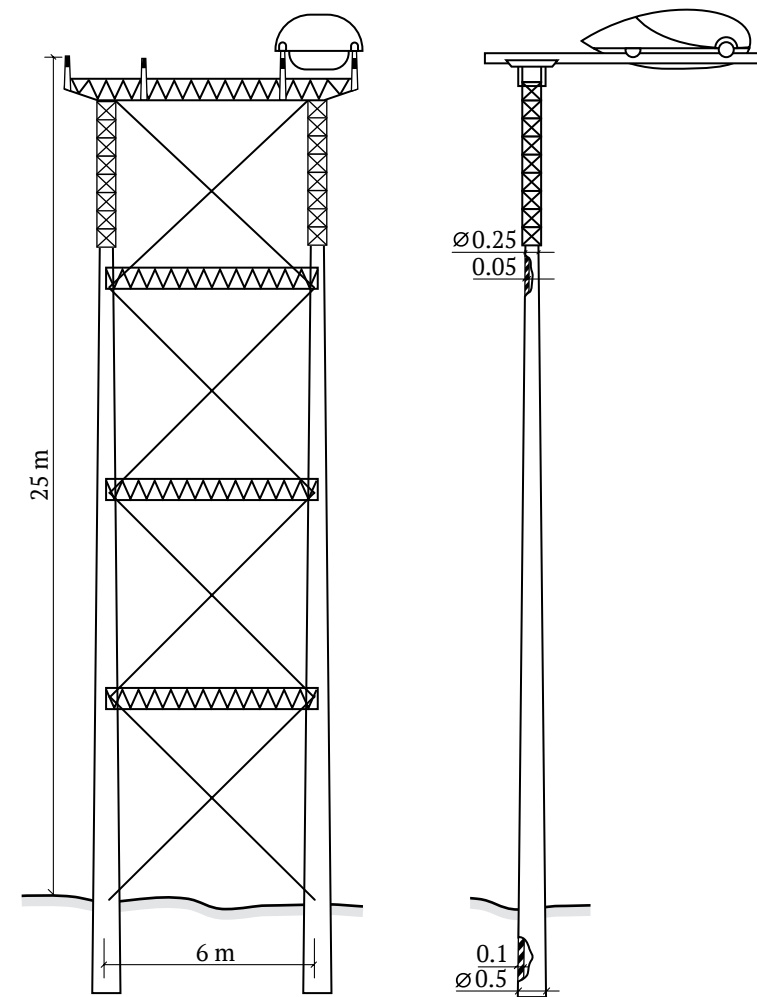


Figure 2.12 – Intermediate support of average height for the double-track STS (variant)

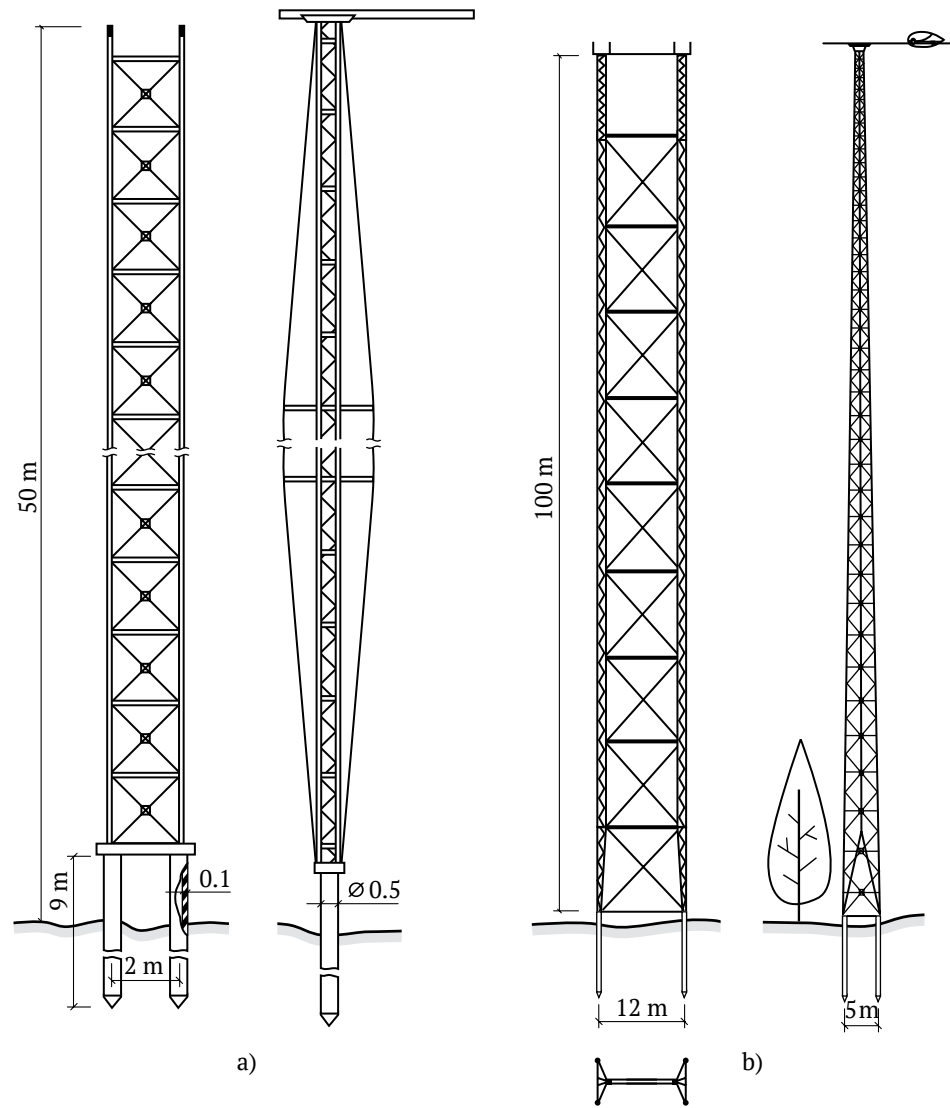


Figure 2.13 – STS intermediate supports (variants):
a – tower (single-track STS); b – super high (double-track STS)

Temperature loads on intermediate anchor supports will be associated not with the temperature difference of the structure in summer and in winter, but with the temperature difference of the neighboring track sections (for example, when one of them is located in the sun, and the other – in the shade).

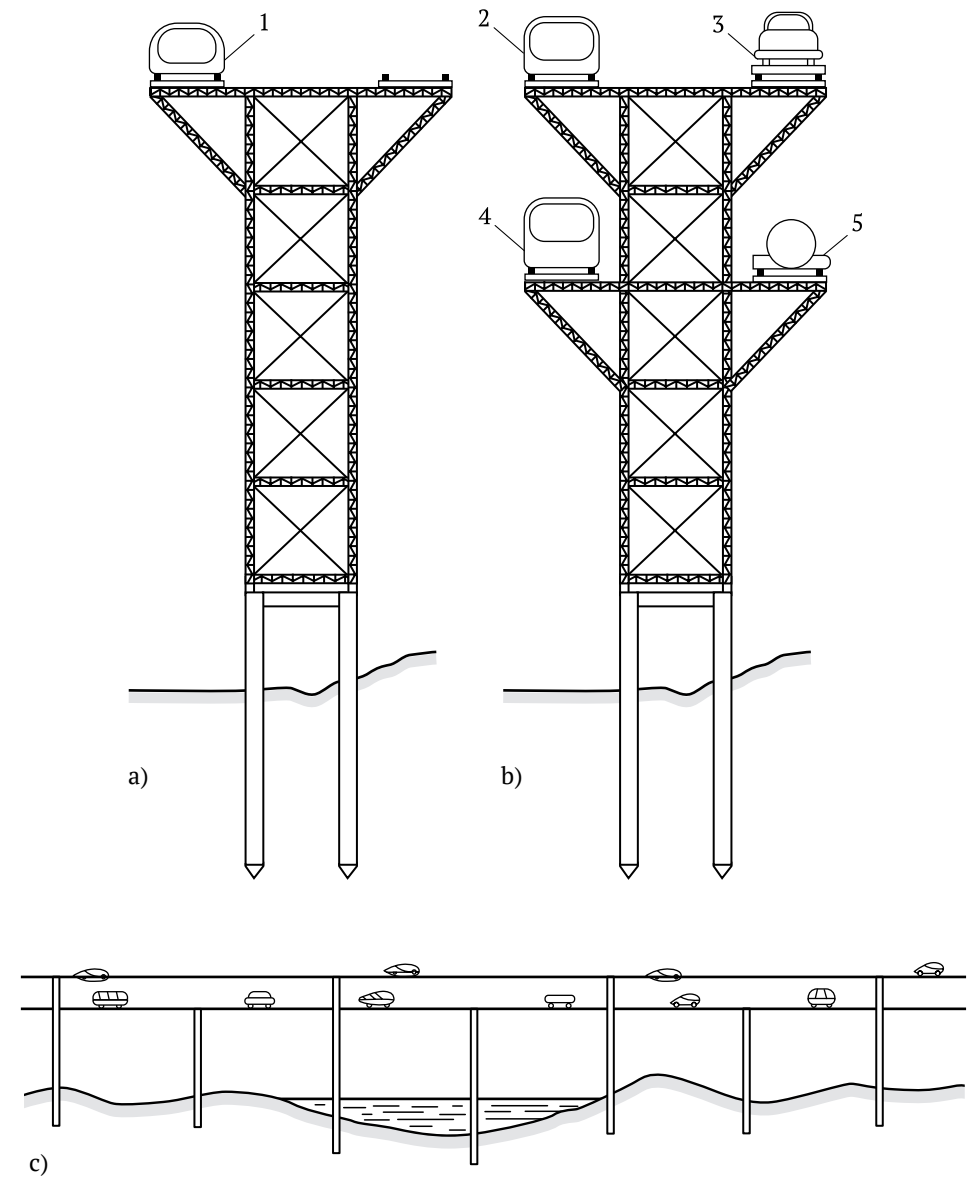


Figure 2.14 – Multi-deck intermediate support:
a – 1st stage of construction (single-deck support for high-speed passenger transport);
b – 2nd stage (the second deck is added for cargo transport and passenger public transport);
c – side view of a double-deck support;
1–5 – transport modules, correspondingly: for individual use; sort of a minibus;
a platform to transport cargo within loading gauge, for example, cars; sort of a bus;
a platform for containerized transportation (bulk, liquid and break bulk cargo)

The existing or specially built buildings and structures can be used as anchor supports, as well. A part of anchor supports can be combined with terminals (figure 2.16).

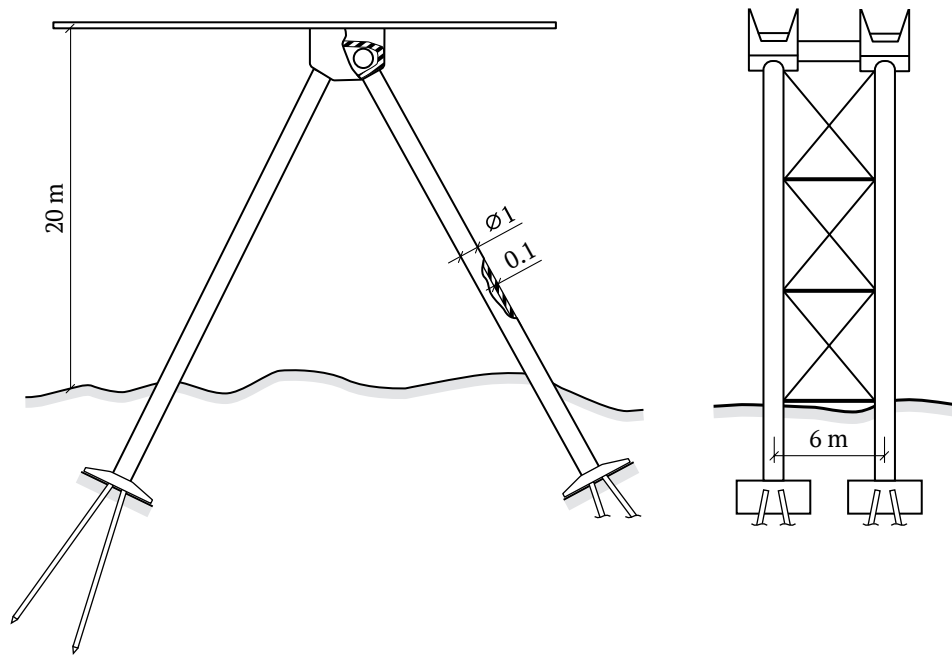


Figure 2.15 – Anchor support (variant)

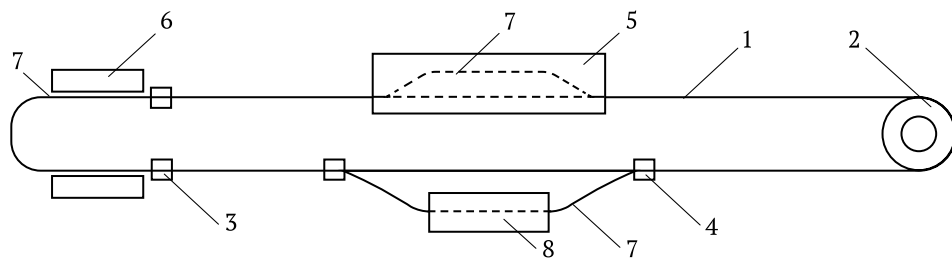


Figure 2.16 – Layout diagram for specialized anchor supports:
1 – STS track; 2, 3, 4, 5 – anchor supports, correspondingly:
ring terminal support in the form of a station; ordinary terminal support;
intermediate support with a turnout switch;
intermediate support in the form of a building (terminal); 6 – platform;
7 – section of the track structure made of ordinary rails; 8 – intermediate station

2.4. Transport module

The rolling stock movement on the STS track structure is carried out by means of wheels used to collect current and supply electric power to the drive (as a variant). The rolling stock driving unit can be made in the following form (figure 2.17): a) rotation motor (rotor electric motor, internal combustion

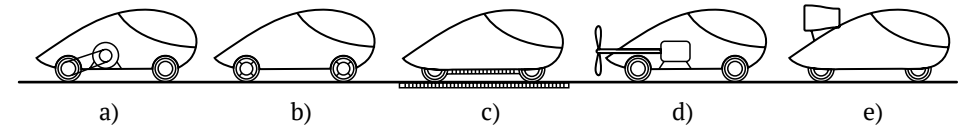


Figure 2.17 – Transport module with different types of driving unit:
a, d – rotation motor with wheel drive and air propeller, correspondingly;
b – in-wheel motor; c – linear electric motor; e – gas turbine

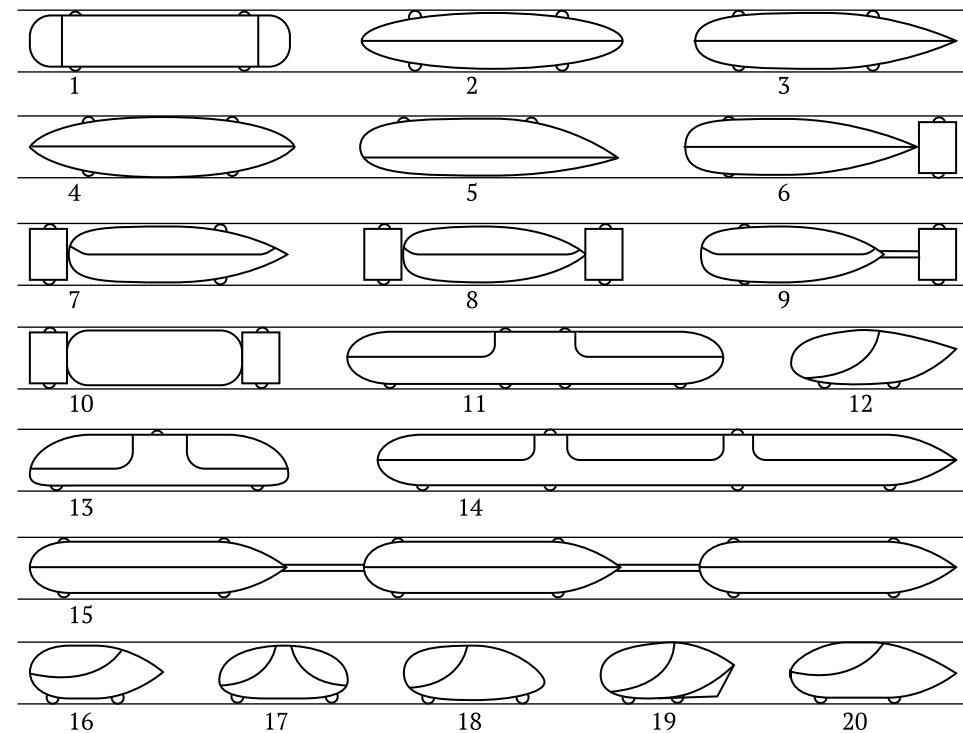


Figure 2.18 – Design variants of the rolling stock body and wheels arrangement for STS with two vertically located rails: 1, 2, 4, 11, 13, 17 – with a symmetrical body; 3, 5, 12, 16, 18, 20 – with an asymmetrical body; 6, 7, 8, 9, 10, 19 – with wheels outside the body; 14 – train; 15 – train of separate units connected by mechanical coupling

engine, diesel, etc.) transmitting rotation to at least one wheel; b) in-wheel motor (electric or another); c) linear electric motor; d) air propeller that receives rotation from an electric or another motor; e) gas turbine. The specified classification suggests that only one type of a driving unit can be an electric one – a linear electric motor. All other variants allow a non-electric drive, the use of which will be determined based on ecological, economic and other considerations. In case of undeveloped regions (deserts, tundra, taiga, permafrost regions, mountain groups, etc.), it will be more economically feasible to use transport modules with an internal combustion engine or diesel operating on eco-friendly fuel (e.g. hydrogen) instead of constructing new electric lines to power the STS.

The wheel arrangement in transport modules with different design variants of the body – symmetrical (for two-way movement) and asymmetrical (for one-way movement) – for the STS with two vertically located rails is shown in figure 2.18. The layout arrangement of a four-seat long distance rolling stock is shown in figure 2.19. The main energy losses in the STS at high speeds (over 300 km/h) will depend on aerodynamics, i.e., on aerodynamic efficiency of the streamlining of the transport module body shape. It can be easily achieved since the body has no protruding parts, except for narrow wheels protruding for 5–10 cm. For the same reason, it is more feasible to make all joints and openings in the body in a longitudinal direction, towards airflow, in order to avoid air swirls. Therefore, in case of high-speed transport modules, preference should be given to the design where a body opens on the principle of a shell (figure 2.20).

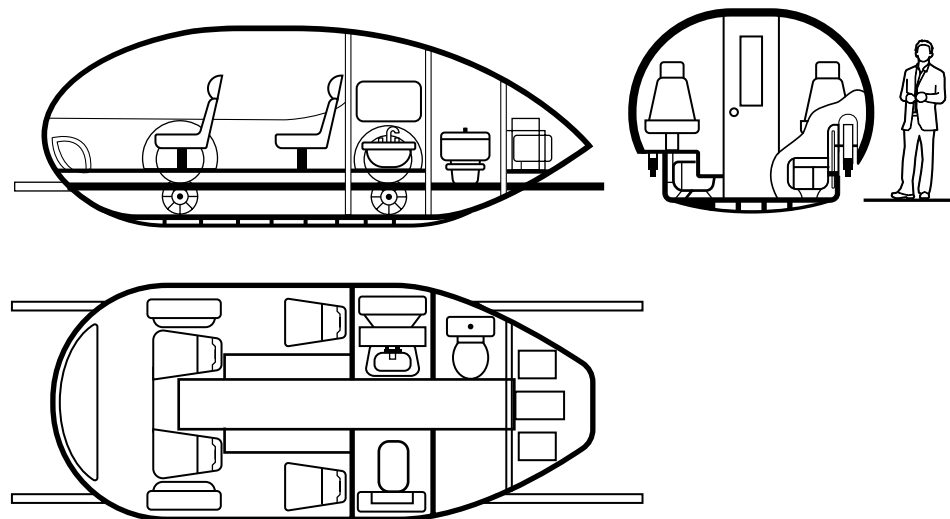


Figure 2.19 – Four-seat long distance rolling stock (Family electric vehicle)

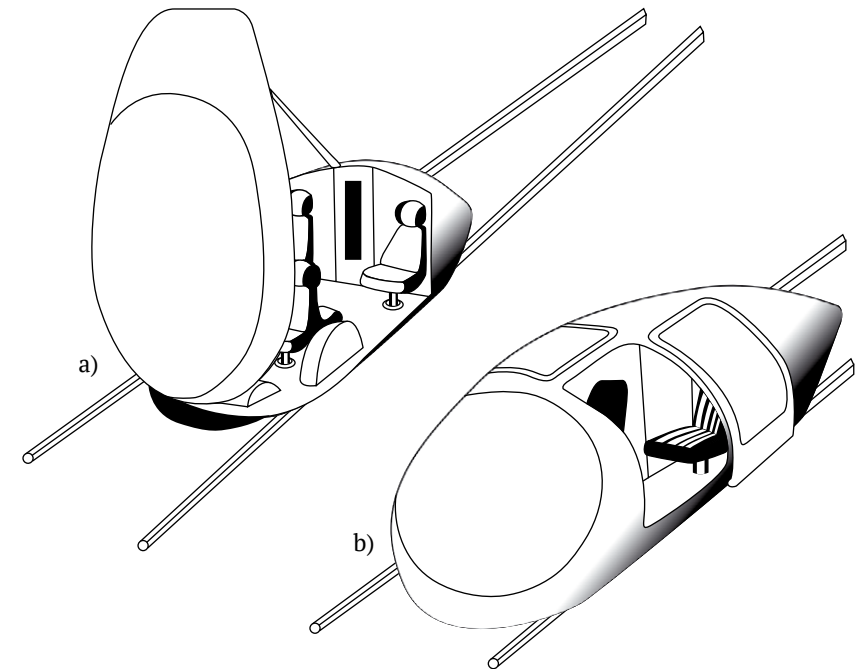


Figure 2.20 – Layout diagram for openings in the rolling stock body: a – in a longitudinal direction (a shell body); b – with transverse openings (a door in the body)

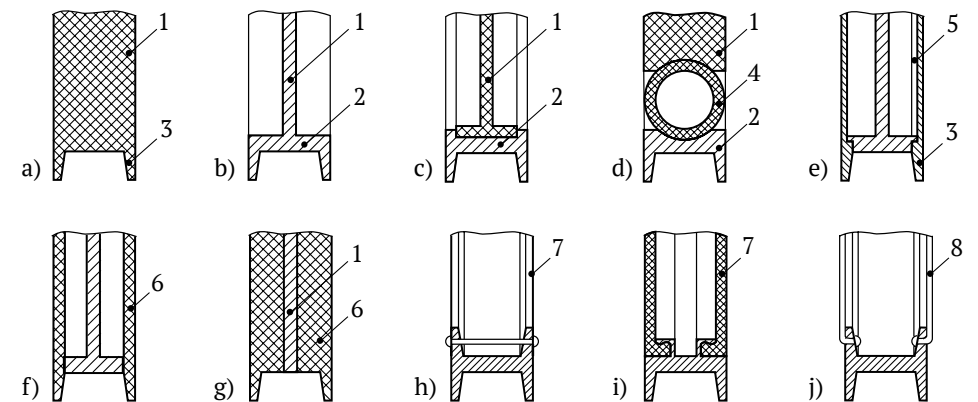


Figure 2.21 – Wheel design (variants):
a, b – solid (monolithic) wheel; c, d, h, i, j – compound wheel with a mobile rim;
e, f, g – combined wheel with mobile flanges;
1 – wheel body; 2 – rim; 3 – flange; 4 – elastic toroidal element;
5 – elastic plate; 6 – cushion disk; 7 – membrane; 8 – spoke

Every wheel has an independent suspension and two flanges fixing the wheel position on the rail in order to decrease the wheel mass and eliminate passing a wheel set axle through a cab. At high travel speed, it is essential to reduce dynamic loads arising due to fine irregularities of the rail track and its oscillations.

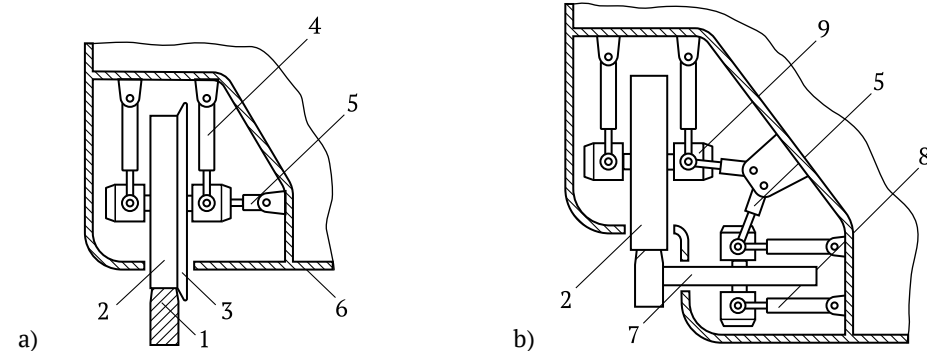


Figure 2.22 – Design of wheel suspension (variants): a – wheel with one flange; b – wheel without flanges; 1 – rail; 2 – main wheel; 3 – flange; 4 – suspension; 5 – damper; 6 – transport module body; 7 – additional (side) wheel; 8 – additional wheel suspension; 9 – bearing unit – current collection

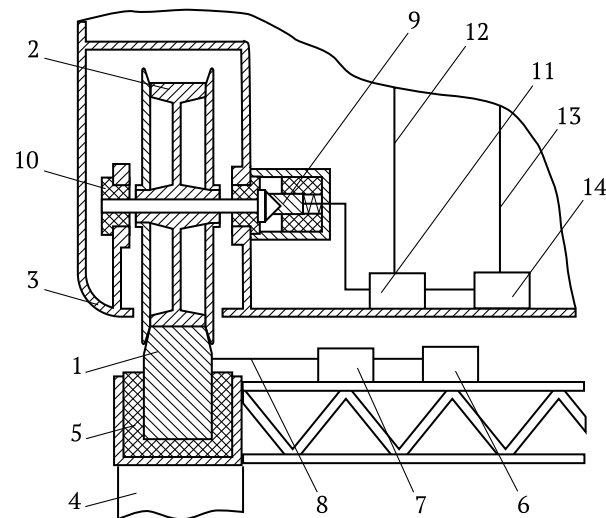


Figure 2.23 – Power supply diagram for transport module: 1 – rail; 2 – wheel; 3 – module body; 4 – STS support; 5 – electrical rail insulator; 6 – electric power source; 7 – converter; 8 – electricity mains for rail power supply; 9 – current collection from a wheel axle; 10 – bearing unit; 11 – switchgear; 12 – high-voltage network; 13 – low-voltage network; 14 – low-voltage power source (accumulator)

Therefore, a wheel can be made as compound (figure 2.21) and its rim or flanges enable transverse motion (in relation to the rail). It is also possible to make a wheel with one flange or without flanges (figure 2.22).

The transport module power supply is carried out via a wheel – rail contact (figure 2.23). It will be efficient even at high speeds since this contact is not sliding, and the contact patch will have rather high forces clamping a wheel to the rail.

2.5. STS construction technology

A prefabricated string should be stretched to the design value using technological equipment (tension force or tensile extension of the string is used as a reference parameter). Then, its ends are rigidly secured to anchor supports by any known method, for example, by welding. If the distance between anchor supports exceeds the length of wires in the string, they should be successively joined with each other to the butt end, for example, by welding using a joint plate. The specified joints are spaced along the string length so that its arbitrary cross-section has maximum one joint – this is done to ensure a defect-free string.

Brake and intermediate (backup) supports are installed beforehand or in the process of string tensioning, or after it. Figure 2.24 shows a variant of construction stages for the STS track. Figure 2.25–2.28 show a double-line track and its main construction stages. A string is stretched either together with an insulated enclosure or successively by one or several string components (wires or strips). After the installation of intermediate supports and string tensioning, a technological platform is launched on them. It can move independently and rigidly fix its position in relation to the supports. Using a platform, a hollow rail body is mounted successively, span after span, secured in a design position and filled with a filler; then a rail head and cross bars are mounted and other works required for the track structure assembly are carried out. All these works are easily mechanized and automated and can be performed 24/7 in any weather. This will ensure high speed of continuous construction of the STS track, its low labor intensity and net cost. In order to eliminate fine irregularities and microwaviness of working surfaces of the assembled rail head and its transverse backlash-free joints, it is possible to grind them off along the transport system length.

The STS construction can also be conducted with the help of a special building combined machine, when a string and other tensioned rail elements are stretched not to the anchor support but to a combined machine. Moving along the track by means of legs-supports, a combined machine will leave

behind assembled intermediate supports with a ready rail track – when reaching anchor supports, it will firmly connect them with intermediate supports.

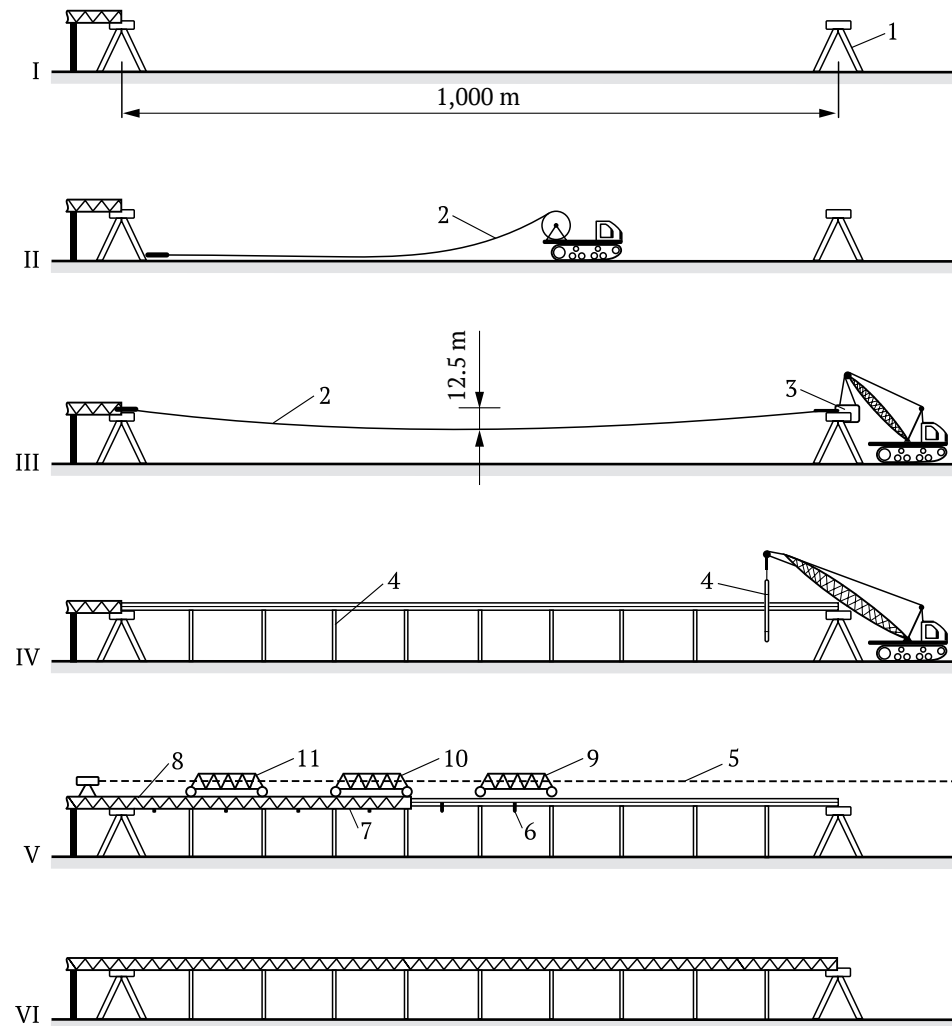


Figure 2.24 – Construction technology for the STS track:

- 1 – anchor support; 2 – cable (string component); 3 – cable tensioning device;
- 4 – intermediate support; 5 – hair line; 6 – cross bar; 7 – rail body; 8 – rail head;
- 9, 10, 11 – technological platforms to install, correspondingly:
cross bars, rail body and rail head; I – construction of anchor support;
- II – spacing of string cables along the track; III – string tensioning and anchoring;
- IV – installation of intermediate supports;
- V – assembly of rail components and track structure; VI – ready track section



Figure 2.25 – Double-line track

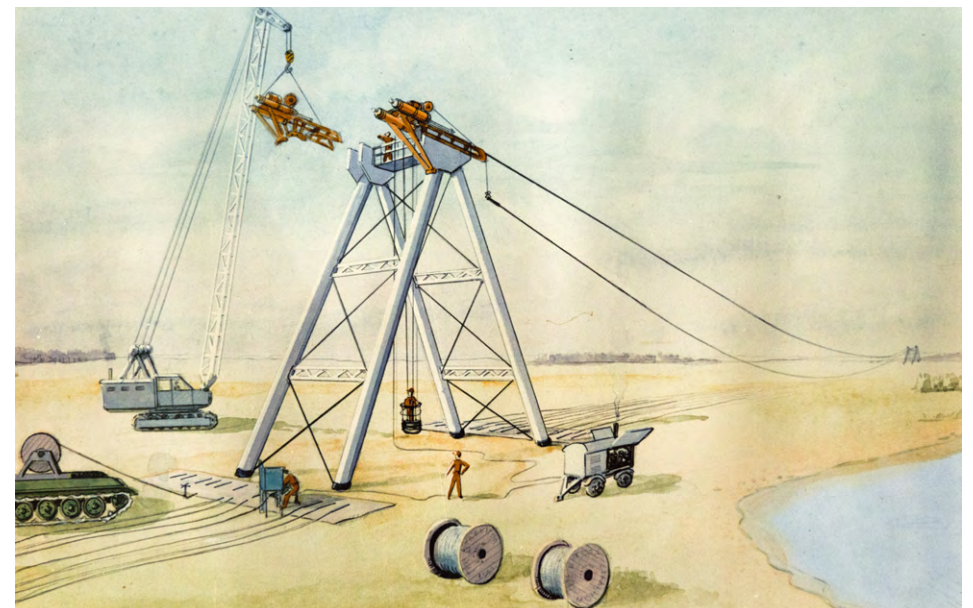


Figure 2.26 – String tensioning to anchor support

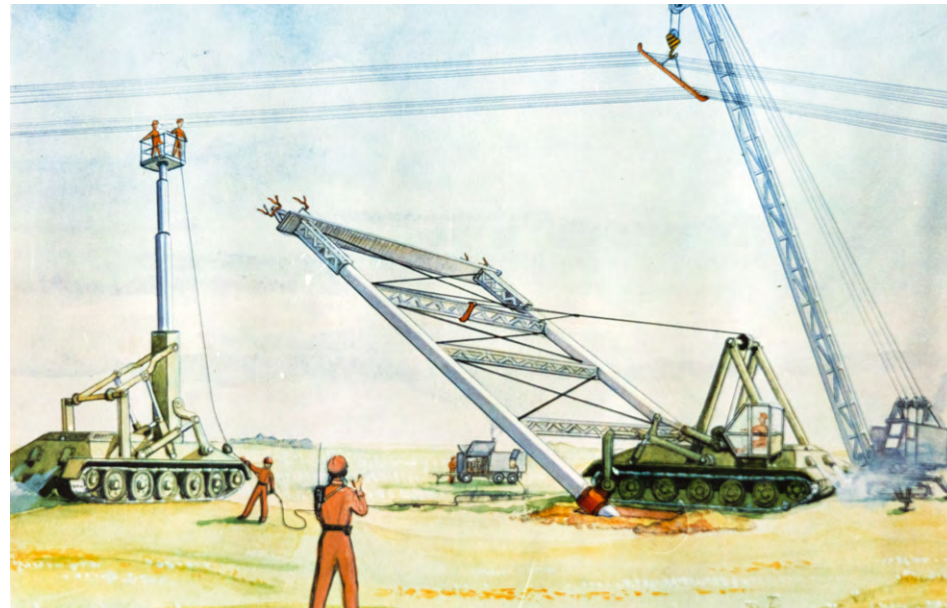


Figure 2.27 – Installation of intermediate support

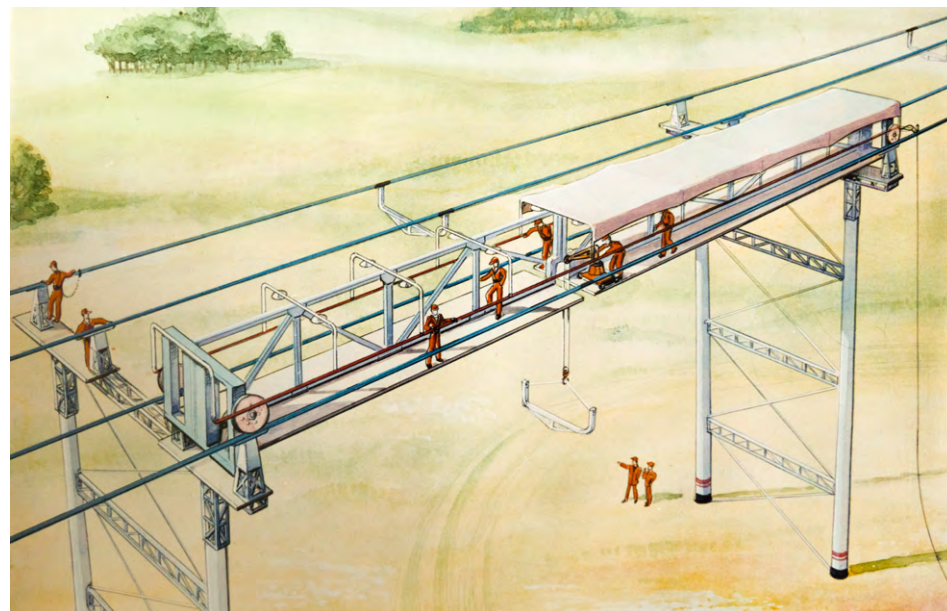


Figure 2.28 – Technological platform for string track structure assembly

2.6. Technical and economical comparison of transport systems

It is feasible to make the STS technical and economical comparison with railway, automobile, air transport and maglev trains. The main STS competitors are automobile and conventional high-speed railway transport.

In all cases of technical and economical comparison, great importance should be attached to the specific power consumption for transportation. STS transport modules have comparatively low power consumption. This is related to a number of reasons, the main of which are given in table 2.2. High engine efficiency and low energy losses for movement (high aerodynamic properties and low mechanical losses due to the movement of a rigid wheel on a smooth rigid track) make the STS transport the most cost-efficient compared to the existing kinds of high-speed transport proposing a similar travel speed.

Special attention should be placed on the change of aerodynamic drag with the increased vehicle speed. It reaches 50 % at the speed of 200 km/h, and exceeds 90 % of total running resistance at 500 km/h; whereas at the speed of 50 km/h, it is about 5 % and the rest 95 % – mechanical resistance. Full power consumption by the STS rolling stock in the open atmospheric environment will make 0.05–0.12 kWh/passenger-km, as, for example, the engine of 50 kW in five-seat rolling stock with dimensions of 4×2×1.5 m will provide the speed of 200 km/h; the engine of 100 kW will provide the speed of 300 km/h, and the engine of 300 kW – the speed of 500 km/h. This will decrease power consumption by 2.5 times compared to high-speed railway, by 2 times compared to maglev and by 11 times compared to jet planes [2]. This figure can be significantly improved in rarefied atmosphere (when moving in a tube with the air pumped out) – up to 0.005–0.01 kWh/passenger-km, i.e., by about 100 times compared to planes.

However, despite the importance of saving energy costs, the relative energy cost reaches only 7.5 % among other costs for the existing kinds of high-speed transport, for example, a maglev train. The main part of costs consists in the construction of a track structure together with stations and can reach dozens or even hundreds of millions USD per one km. Since the STS line is 10 times cheaper than high-speed railways and the maglev track structure, the rate of electricity cost in total costs will dominate compared to other costs.

Material consumption and the cost of an STS double-line track are shown in table 2.3. The data are given for a track with the following parameters: an average height of supports – 20 m; the distance between intermediate supports – 50 m; the distance between anchor supports – 2 km; tension force of one string rail track structure (two rails) – 320 tf; the track gauge – 2 m; the distance between the track structure axes – 6 m; location of stations and sites for emergency stops: at the cost of 100,000 USD – every 10 km; at the cost of 1 mln USD – every 100 km; at the cost of 50 mln USD – every 1,000 km.

Table 2.2 – Comparative analysis of aerodynamic and other energy properties of various high-speed vehicles

Vehicle	Reasons causing aerodynamic penalty	Other reasons causing energy losses
1	2	3
STS transport module	Wheels protruding from the body (wheel width up to 10 cm, protruding from the body for 5–10 cm – the other part of the wheel is in an enclosed space). The specific area of the outer module* surface in contact with the air: 2–3 m ² /passenger, 3–5 m ² /(1 t of cargo).	Distortion of a string rail track structure under the effect of moving load (maximal relative track deflection is 10 ⁻³ –10 ⁻⁴). Energy losses in a wheel suspension (due to high evenness of a rail track, the suspension amplitude of oscillation will be within 1 cm). The specific weight of module structure**: 0.2–0.3 t/passenger; 0.3–0.5 t/(1 t of cargo). Drive efficiency: up to 80–90 %.
Plane	A lot of protruding structural members: wings, flaps, vertical and horizontal rudders, engines, etc. A lot of cross joints on the outer surface due to availability of access holes, portholes, doors, joints of individual sheets in the casing, rivets, etc. The specific area of the outer plane surface: 5–10 m ² /passenger, 20–50 m ² /(1 t of cargo).	A need to have carrying capacity, the creation of which requires a lot of energy. In order to create an impulse, a necessity to throw back air or fuel combustion products at high speed and in large quantity, which leads to significant energy losses (and provokes serious ecological problems, especially when moving in rarefied layers of atmosphere and ozone layer, where most air routes go). A necessity to carry fuel during the whole route (fuel mass exceeds the weight of transported passengers and comparable to the weight of transported cargo), which requires a significant part of this fuel. A necessity to rise to the altitude of 10 km, which requires additional power consumption. The specific weight of plane structure (fueled): 0.3–0.5 t/passenger, 2–5 t/(1 t of cargo). Drive efficiency: up to 30–40 %.

* It characterizes rates of energy loss required to overcome aerodynamic drag.

** It characterizes rates of energy loss required to accelerate, brake, uplift, etc. the rolling stock.

Table 2.2 finished

1	2	3
Automobile	A lot of protruding structural elements: wide wheels, completely open for incoming air streams, suspension, wheel drive, side and rear-view mirror, elements of cooling radiator used for incoming air, windscreen wipers*, etc. A lot of cross joints on the outer surface due to availability of a hood, doors, trunk, headlights, front, rear and side windows, etc. The specific area of the outer automobile surface: 3–5 m ² /passenger, 10–20 m ² /(1 t of cargo).	Tire distortion (relative distortion reaches 10 ⁻¹). Roadbed distortion under a wheel (relative deflection under a truck is 10 ⁻³ –10 ⁻⁴). Energy loss in a wheel suspension (oscillations of the suspension reach 5–10 cm even on a smooth road). The roadbed surface is close to the automobile bottom, which at high speed causes aerofoil effect and energy losses. The specific weight of automobile structure: 0.2–0.5 t/passenger, 1–2 t/(1 t of cargo). Drive efficiency: up to 40–50 %.
Maglev train	A need for large size magnetic levitation systems to suspend the rolling stock to the overpass, with an extended surface and small gaps with the roadbed that suck in air at high speed. A lot of cross joints on the outer surface due to magnetic levitation systems and a linear electric motor, windows, doors, etc. The specific area of the outer rolling stock surface: 4–8 m ² /passenger, 10–20 m ² /(1 t of cargo).	A need to have electric magnetic levitation, the creation of which requires a lot of energy. Large energy losses in the maglev system due to the change of air gaps when moving (the suspension system efficiency is critical to air gaps). The specific weight of the rolling stock structure: 0.5–1 t/passenger, 2–5 t/(1 t of cargo). Appearance of reactive electromagnetic motion resistance forces, significantly reducing drive efficiency (up to 40–50 % or less).**
High-speed train	A lot of large size protruding elements: wheel pairs, their suspension, completely open for incoming air streams, etc. Quite a number of cross joints on the outer surface due to gaps between carriages, windows, doors, etc. The specific area of the outer train surface: 3–6 m ² /passenger, 5–10 m ² /(1 t of cargo).	Distortion of rails and railway track under the effect of moving load (relative deflection is 10 ⁻³ –10 ⁻⁴). Significant energy losses in a wheel set suspension due to large weight of a spring-loaded part. The specific weight of train structure: 1–2 t/passenger, 0.5–1 t/(1 t of cargo). Electric train drive efficiency: up to 70–80 %.

* Windscreen wipers will take up to 10 kW of engine power, a protruding mirror – up to 20 kW at the speed of 500–600 km/h due to aerodynamic drag. The impact of cross joints, offsets, holes and gaps on the outer body surface is equally great due to the incoming air flow imbalance and thus arising whirlwinds.

** Power losses for the rolling stock with a 40 tons capacity reach 2,400 kW [2]. This power is enough for 20 STS transport modules capable to transport 200 passengers.

Table 2.3 – Material consumption and cost of land plot for an STS double-line track 1 km long

STS structural component	Material	Material consumption per 1 km of the track		Estimated cost*, thous. USD/km
		mass, t	volume, m ³	
1	2	3	4	5
1. String rails, in total	–	–	–	160
Including:				
1.1. Head	Rolled steel	24	–	36
1.2. Body	Aluminum sheet 1 mm thick	4	–	18
1.3. String	Steel, wire 1 mm in diameter	47	–	70
1.4. Filler	Composite material	–	32	16
1.5. Mastic glue	Mastic	1	–	2
1.6. Protective cover of a string	Polymer	2	–	8
1.7. String waterproofing	Polymer	1	–	6
1.8. Other	–	–	–	4
2. Cross bars, in total	–	–	–	10
3. Intermediate supports, in total	–	–	–	90
Including:				
3.1. Piles	Reinforced concrete	–	160	32
3.2. Lintels, braces	Rolled steel	24	–	24
3.3. Supports superstructure	Rolled steel	30	–	30
3.4. Other	–	–	–	4
4. Anchor supports, in total	–	–	–	25
Including:				
4.1. Support body	Reinforced concrete	–	45	9

* An average cost estimate is based on the cost of materials, manufacture and assembly of structure elements, and transport costs in the Republic of Belarus (at 1995 values).

Table 2.3 finished

	1	2	3	4	5
4.2. Pile foundation		Reinforced concrete	–	16	4
4.3. Metal structures		Rolled steel	2	–	2
4.4. Components of anchor clamping		Steel	1	–	2
4.5. Other		–	–	–	8
5. Excavation works		–	–	–	5
6. Rail electrical feeding system		–	–	–	50
7. Monitoring system for supports and track structure		–	–	–	10
8. Traffic monitoring system		–	–	–	20
9. Emergency power supply system		–	–	–	10
10. Traffic motion control system (turnout switches, etc)		–	–	–	20
11. Intermediate supports and sites for emergency stops		–	–	–	70
12. Design and survey work		–	–	–	5
13. Cost of land acquisition and its preparation for construction		–	–	–	10
14. Other costs		–	–	–	15
Total					500

The data analysis given in table 2.3 allows the following conclusion.

The STS track has low material consumption. For example, it requires about 150 kg/m of steel for a double-line track and 75 kg/m – for a single-line track, considering auxiliary systems. It is an approximate weight of one running meter of a rail in the existing railways. Thus, just using one rail 1,000 km long (its weight will be 75,000 tons), it is possible to build the entire STS single-line track of the same length.

A small amount of reinforced concrete is required for the construction of a STS load-bearing part – 220 m³/km. Taking into account its consumption to build stations and auxiliary systems, the amount of reinforced concrete will be about 500 m³/km. Compare: the reinforced concrete consumption to build the fencing for high-speed railways and maglev tracks reaches 750 m³/km [2].

Instead of such fencing 1 km long, a three-kilometer section of a load-bearing part for the STS double-line track could be built, or 1.5 km of a fully equipped track.

The excavation expenses and consequently their scope are not large, either. The STS track can run without any embankments and digging on any terrain. Excavation works will be local (boring of planting pits for supports), and their scope will be within 100–200 m³/km. Compare: the volume of the dug soil when building one kilometer of a modern highway and railway, particularly on rough terrain, equals to the volume of excavation works when building an STS track 100–1,000 km long.

The consumption of other construction materials for the STS track structure and supports is just as small; such construction materials include inexpensive and widely available industrially manufactured materials.

The STS rolling stock cost can be compared to that of passenger cars, which are similar on dimensions and in terms of design.

Series-produced electric motors of 100 kW are by 1.5–2 times cheaper than internal combustion engines of the same capacity; they are also more reliable, durable and easier in operation and maintenance.

The body of an STS transport module will be cheaper than that of an automobile of the same size due to more simple design (absence of a radiator, doors, trunk, hood, headlights, parking, braking and other lights, windscreen wiper, window-lift mechanism, etc.).

The STS rolling stock chassis and suspension will be also simpler and cheaper compared to those of a car due to the absence of unreliable and expensive rubber tires and wheel turning mechanisms, as well as due to simplified supply of a running torque to non-rotating wheels, absence of requirements to passability of rough terrain, etc.

The control systems for engine rpm and wheel torque in both vehicles are roughly equal in terms of cost and complexity (in the STS – it is an engine rpm control unit, whereas in a car – it is a transmission, coupling, engine fuel control system, etc.).

The rolling stock motion control system will be significantly simpler and cheaper than that of a car since it will have few controlled parameters: motion speed, distance to the neighboring rolling stock and rolling stock location on the line (GPS coordinates). Driving a car is rather complicated – the very fact that despite the blossom of computer technology, only driver's brain has managed to cope with this task so far attests to it. Therefore, a driver factor should

be taken into consideration in the system of car control and when determining its cost: hundreds of millions of people all over the world today spend several hours a day on driving – even despite the constant lack of time. In this regard, an inexpensive controller with the wired-in control program controlled and monitored by linear computers united in the network will cope with the task of STS rolling stock control. In contrast, the car control system includes, apart from actuation mechanisms (a steering wheel, a steering column, a wheel turning mechanism, gas pedals, brake pedals, clutch pedals, gear-change mechanism, etc.), the whole system of information visualization required for control, which is not applicable in the STS: a windscreen wiper with mechanisms of setting into motion and washing fluid supply (provide cleanliness of windscreen glass and consequently visibility of the track), headlights, fender lamps, parking lights, an instrument board, mirrors, audible beep, etc.

The cab interior and exterior of the STS rolling stock and an automobile will be similar and will range widely depending on customers' taste.

Moreover, the STS rolling stock and the transport system itself have no such components as a fuel tank (consequently, the whole chain of related elements is not required: filling stations along the track, oil-processing plants for petrol and diesel, oil wells); diverter system, jamming system and reburn system. For example, the recent strengthening of ecological requirements to an automobile has caused its significant value appreciation.

With regard to the above arguments, it is possible to predict that the STS rolling stock in series production will be 1.5–2 times cheaper compared to a car of the same capacity, with the middle class interior will cost about 10 thous. USD. Compare: a pair of seats in the Airbus A-340 first class cabin made in small-scale production costs 25 thous. USD. Thus, 100 five-seat rolling stock worth a total of 1 mln USD is required to transport 500 passengers – this is an approximate capacity of advanced airbuses and high-speed trains. Compare: the airbus cost – about 100 mln USD, a modern railway passenger carriage (capacity of 50–100 people) – about 1 mln USD, one maglev train carriage (capacity of 50–100 people) – 4 mln USD.

The expenses related to the STS track operation can be analyzed compared to high-speed railways, and transport modules – compared to an automobile. The annual operating expenses will depend on carrying capacity of the track and on design speed. The technical and economic performance of a double-line STS track is given in table 2.4, and the total costs of passenger and cargo transportation – in tables 2.5 and 2.6, correspondingly. The expenses are given with regard to the characteristics of the transport line and rolling stock shown in table 2.4.

The data given in table 2.5 and 2.6 should be regarded as a special case since rigid requirements for the transport line and rolling stock payback period

were used (5 years), high electricity cost (0.02 USD/kWh) was taken, etc. Their optimization will allow decreasing the total costs by 1.5–2 times. However, with the traffic of 50 thous. and 100 thous. passengers per day, the travel cost per one passenger (13.23 and 7.95 USD, correspondingly) for the distance of 1,000 km will be cheaper compared to that of a train by 2–3 times.

With the increase in traffic, the share of electricity cost in the total costs increases, as well. For example, with the transportation volume of 5,000 passengers per day, the electricity share is only 4 %; with the transportation volume of 100 thous. passengers per day – 27.7 %. The share of electricity cost is even higher in cargo transportation – with the transportation volume of 10 thous. and 250 thous. tons per day it is 21.1 % and 71.4 %, correspondingly. Therefore, it is more feasible to carry out cargo transportation in a low speed range (100–250 km/h), which allows lower energy losses for aerodynamics. It is also reasonable to build cheaper special cargo tracks for these purposes.

Table 2.7 gives the transportation costs at a reduced speed: 300 km/h for passenger and 200 km/h for cargo transport modules. In order to determine the impact of other factors, the following STS parameters were used: a) for a transport line: coefficient of line development – 1.02, annual OPEX – 5 % of the line cost (25 thous. USD/km), rate of profit – 10 %; b) for the rolling stock: use coefficient – 0.7; rolling stock fleet reserve – 15 %; annual mileage – 1.6 mln km for passenger and 1.07 mln km for cargo rolling stock; average speed – 300 km/h and 200 km/h, correspondingly; rate of profit – 10 %; specific energy consumption – 0.067 kWh/passenger-km and 0.17 kWh/(t·km), correspondingly; electricity cost – 0.01 USD/kWh. Other STS parameters comply with the data specified in table 2.4.

Table 2.7 suggests that the costs for passenger and cargo transportation for the specified data can be reduced by 2.1–2.7 times, i.e., to the values of 3.87 USD/(1,000 passenger-km) and 3.81 USD/(1,000 t·km), correspondingly. Such low costs will allow to increase the transportation tariff by 1.5–2 times and raise the rate of profit from the track up to 30 %, from the rolling stock – up to 50 %. This will make the STS project very attractive for investors, construction and machine building companies engaged in the project development and implementation.

Table 2.4 – Technical and economic performance of a double-line STS track

Indicator	Value
1. Transport line characteristics	
1.1. Total cost, thousand USD/km	500
1.2. Depreciation costs, %	5
1.3. Coefficient of line development	1.1
1.4. Annual OPEX and costs for maintenance and repair of track structure and supports, % of cost (thousand USD/km)	10 (50)
1.5. Rate of profit, %	20
2. Rolling stock characteristics	
2.1. Cost, thousand USD/unit	
• passenger:	
business class	10
first class	15
luxury class	20
• cargo	5
2.2. Capacity, people:	
business class	5
first class	2
luxury class (sleeping carriage).	1
2.3. Capacity, kg:	
• passenger	500
• cargo	1,500
2.4. Total mass, kg:	
• passenger	1,500
• cargo	1,000
2.5. Coefficient of line use	0.5
2.6. Rolling stock fleet reserve, %	20
2.7. Average speed, km/h	500
2.8. Annual mileage of one rolling stock, mln km	1.825
2.9. Annual transportation volume of one transport module:	
• thousand passengers/1,000 km	8.29
• thousand tons cargo/1,000 km	2.49
2.10. Specific energy consumption for traction:	
• passenger, kWh/passenger-km	0.1
• cargo, kWh/(t·km)	0.33
2.11. Depreciation costs, %	10
2.12. Annual OPEX, % of rolling stock cost	10
2.13. Rate of profit, %	20

Table 2.5 – Costs of passenger transportation on an STS line 1,000 km long

Indicator	Volume of passenger transportation, thous. passeng./day (mln passeng./year)					
	Single-line track			Double-line track		
	1 (0.365)	2.5 (0.913)	5 (1.825)	10 (3.65)	50 (18.25)	100 (36.5)
1. Total costs for STS, USD per 1,000 passenger-km	266.37	108.16	55.42	55.42	13.23	7.95
Including:						
1.1. Transport line expenses, in total	263.69	105.48	52.49	52.74	10.55	5.27
Including:						
• depreciation costs	37.67	15.07	7.53	7.53	1.51	0.75
• OPEX	75.34	30.14	15.07	15.07	3.01	1.51
• deductions for profit	150.68	60.27	30.14	30.14	6.03	3.01
1.2. Rolling stock expenses, in total	2.68	2.68	2.68	2.68	2.68	2.68
Including:						
• depreciation costs – 0.12 USD/ passenger,						
• OPEX – 0.12 USD/passenger,						
• deductions for profit – 0.24 USD/passenger,						
• electricity cost – 2.2 USD/passenger (based on cost of energy 0.02 USD/kWh)						
2. Amount of rolling stock on the line, units	44	110	220	440	2,200	4,400
3. Rolling stock cost, mln USD	0.44	1.1	2.2	4.4	22	44
4. Average headway between neighboring rolling stock in a transport flow (on one line):						
• time, s	432	173	86.4	86.4	17.3	8.64
• distance, km	60	24	12	12	2.4	1.2

Table 2.6 – Costs of cargo transportation on an STS line 1,000 km long

Indicator	Volume of cargo transportation, thous. t/day (mln t/year)					
	Single-line track			Double-line track		
	5 (1.825)	10 (3.65)	25 (9.125)	50 (18.25)	100 (36.5)	250 (91.25)
1. Total costs for STS, USD per 1,000 tons-km	60.80	34.43	18.60	18.60	13.33	10.17
Including:						
1.1. Transport line expenses, in total	52.74	26.37	10.54	10.54	5.27	2.11
Including:						
• depreciation costs	7.53	3.77	1.51	1.51	0.75	0.30
• OPEX	15.07	7.53	3.01	3.01	1.51	0.60
• deductions for profit	30.14	15.07	6.02	6.02	3.01	1.21
1.2. Rolling stock expenses, in total	8.06	8.06	8.06	8.06	8.06	8.06
Including:						
• depreciation costs – 0.20 USD/t,						
• OPEX – 0.20 USD/t,						
• deductions for profit – 0.40 USD/t,						
• electricity cost – 7.26 USD/t						
2. Amount of transport modules on the line, thousand units	0.73	1.47	3.66	7.33	14.7	36.6
3. Rolling stock cost, mln USD	3.67	7.35	18.3	36.7	73.5	183
4. Average headway between neighboring modules in a transport flow (on one line):						
• time, s	25.9	13.0	5.18	5.18	2.59	1.04
• distance, km	3.6	1.8	0.72	0.72	0.36	0.14

Table 2.7 – Transportation costs for an STS line at a reduced speed:
300 km/h for passenger and 200 km/h for cargo transport modules
(track length – 1,000 km)

Indicator	Transportation volume			
	Passenger, thous. passeng./day (mln passeng./year)		Cargo, thous. t/day (mln t/year)	
	5* (1.825)	100** (36.5)	10* (3.65)	250** (91.25)
1. Total costs for STS, USD per 1,000 passenger-km USD per 1,000 tons·km	29.02 –	3.87 –	– 16.66	– 3.81
Including:				
1.1. Transport line expenses, in total	27.95	2.80	13.97	1.12
Including:				
• depreciation costs	6.99	0.70	3.49	0.28
• OPEX	6.99	0.70	3.49	0.28
• deductions for profit	13.97	1.40	6.99	0.56
1.2. Rolling stock expenses, in total	1.07	1.07	2.69	2.69
Including: for passenger (cargo) transportation:				
• Including: for passenger (cargo) transportation: depreciation costs – 0.13 USD/passenger (0.32 USD/t),				
• OPEX – 0.13 USD/passenger (0.32 USD/t),				
• deductions for profit – 0.13 USD/passenger (0.32 USD/t),				
• electricity cost – 0.68 USD/passenger (1.73 USD/t)				
2. Amount of transport modules on the line, thousand units	0.23	4.65	2.33	58.2
3. Rolling stock cost, mln USD	2.3	46.5	11.6	291
4. Average headway between neighboring modules in a transport flow (on one line):				
• time, s	86.4	8.64	13.0	1.04
• distance, km	7.2	0.72	0.72	0.057

* Single-line track.

** Double-line track.

Chapter 3

Mechanics problems of high-speed transport

3.1. Dynamic motion of transport modules on string guide track

Rather high standards to strength parameters of the STS high-speed transport require solving a complex of theoretical and application tasks. One of the most challenging tasks is the assessment of the limits of permissible motion modes, which provide the required static and dynamic characteristics (distortion, tension, movement, acceleration, natural frequencies, smooth motion, etc.) for the proper functioning of the transport system in operation. The dynamic and stability problems of that kind are discussed in the monographs [12, 13, 17, 25, 35].

The analysis should be made in a probabilistic formulation; however, a deterministic approach is possible at early stages. The main tasks of the dynamic analysis are as follows:

- determination of frequencies and forms of natural oscillation;
- computation of the amplitude frequency response;
- research of the forced oscillations regime.

The aim of the computation of vehicle dynamic performance is in most cases to determine the accelerations and movements in target points of the structure and to compare the obtained values with the norms and technical specifications. When designing with regard to accidental exposure, the requirements to these parameters should be considered in a probabilistic formulation.

As structural design practice shows, even simple models that allow applying easy numerical solutions produce good results for the rationally engineered systems (the scope of computation is proportional to the dynamic imperfect design). The structural design efficiency relies heavily on the range of its natural frequencies. Consequently, it is highly important to ensure the preset dynamic properties at the initial design stage.

The mechanical impact on the STS module from the track is expressed as kinematic vibrational loading (deterministic or accidental) of vehicle compo-

nents. The dynamics of this impact is determined by the track state, travel speed, and elastic and dissipative properties of the transport module suspension. The STS guide track is exposed to cyclic loading from moving modules with further spreading of excitation energy in the form of different waves.

Module. The STS allows realizing extremely high speeds (over 500 km/h). The requirements to the transport module chassis are rather high considering that the dynamic impact intensity of the track on the transport modules increases at a higher speed. The need of optimizing the parameters of the rolling stock chassis is due to the fact that the creation of shock absorbers with limited dimensions and weight capable of providing traffic safety is a rather complicated technical problem. In the field of railway transport mechanics, various questions on oscillations of the suspension system components have been studied by now, numerical solutions to multidimensional nonlinear dynamic problems have been obtained. When creating the rolling stock chassis, the theory of vibration protection for vehicles and operators is used, as outlined in the work by R.I. Furunzhiev [36].

In my opinion a range of assumptions made in the monograph by Kamaev V.A. [13] related to the problem of optimizing the rolling stock chassis in the existing railway locomotives and carriages is true for the new type of transport – the string transport system. Let us look at them in more detail.

The peculiarity of transport units as dynamic objects is related to the fact that the vibration source is not only kinematic excitation arising at wheel rolling along the guide track, but also inertial excitation arising at units operation. It has been established that in certain cases self-oscillations arise at wheels rolling fixed rigidly to make wheel sets. The research of an oscillating process is complicated due to a high order of the mathematical model of the system with the availability of non-linear elements. A certain simplification of the model with regard to the string transport system is related to the fact that a locomotive is exposed to additional impact from neighboring carriages or a locomotive, whereas a module of the transport system under consideration is a functionally complete transport object.

From the point of view of system analysis, it is required to simultaneously consider the following main interrelated oscillations: bolster structure in the longitudinal vertical plane; unsprung mass in the vertical plane; lateral oscillations; oscillations in traction drive, etc. [13] points out a significant complexity of the task on optimization of vibration protection and a limited number of works dedicated to this question. Particularly, the work is cited dedicated to the optimization of parameters for a two-phase spring suspension of carriages and electric trains as a dynamic system with non-correlational input actions [12].

It has to be admitted that the dynamic analysis of vehicles becomes more difficult due to the absence of reliable data on the parameters of separate calculation models components. There are practically no characteristics of dissipation in certain body components; quantitative and qualitative evaluation of track excitation are contradictory. In this regard, the questions on identification of elastic dissipative properties of the rolling stock suspension components based on experimental information are quite relevant.

It is also important to take into consideration the interaction of vertical and lateral oscillations due to the following reasons: technological errors when making elastic dissipative components and locating the centers of masses of basic equipment; presence of significantly non-linear elements in the suspension (for example, joints with Coulomb friction); peculiarities of tractive force transfer. The forces in the wheel – rail contact are crucial for lateral oscillations and, in their turn, depend on vertical oscillations.

Vibration exciters of the transport module include geometric irregularities of the guide and wheels, instability of elastic dissipative properties of the string transport line; impact of air environment; random changes in suspension characteristics; control action. The impact of air environment grows rapidly with the increase in travel speed. At present, it is difficult to make a feasible choice of the law of interaction for the oscillating rolling stock and the air environment due to the absence of experimental data and great complexity of the task related to the body movement in the boundary layer of the air. When calculating the dynamics of the existing trains, whose speed usually does not exceed 200 km/h, this factor is neglected. It is clear that such an assumption in the motion analysis of the STS is incorrect.

The actions caused by the operation of main units have a polyharmonic view and rely on the characteristics of the equipment installed.

Normally a task of decreasing vibration caused by load-bearing units can be solved independently of the problem of chassis design [13]. It is explained by a perceptible difference in exciting frequencies of the equipment and natural frequencies of the rolling stock as a system of solid bodies with elastic bonds at a small weight of the equipment in relation to the rolling stock weight. In respect to the STS, this assumption needs justification. In fact, the module mass is comparable to the equipment mass; the difference (compared to conventional trains) consists in the ratio of frequencies of exciting oscillations and natural frequencies of the transport module oscillations.

A range of mechanics problems is related to the transport module aerodynamics. Absence of the calculating theory for the aerodynamic drag coefficient C_x at present leaves experimental methods of determining the specified parameter as the priority ones. [6] states in respect to line-haul trains that there exists a stable correlation field, which allows finding a connection between the results

of model and full-scale tests. In order to calculate the aerodynamic drag coefficient for a full-scale body, the following formula is proposed:

$$C_x = C_{x0} + K_\beta \beta,$$

where $C_{x0} = C_{x0}^{\text{mod}} \lambda$, λ – correlation coefficient from the model to the full-scale body; K_β – coefficient of air flow contact angle; β – air flow contact angle; C_{x0}^{mod} – aerodynamic drag coefficient of a scaled model at a zero flow contact angle ($\beta = 0$).

As the first approximation, the given dependence can be used for aerodynamic design of advanced vehicles. More detailed data can be obtained in the course of wind-tunnel tests using transport module models of different configuration.

String. Chapter 4 outlines the results of vibration analysis of the string transport line on the assumption of its uniformity, which allows applying d’Alambert’s principle.

The direction for the improvement of the developed dynamic model is determined by the fact that the STS being an elastic mechanical system is most probably quasi-homogeneous, since it is formed by periodic alternation of sections with the same parameters (sections of the string line between neighboring supports). Such systems not being fully homogeneous act like homogeneous systems under certain conditions, causing a form of oscillations similar to a sinusoidal one and allowing the existence of running and standing waves [32]. Particularly, long axles with numerous circular grooves or similar disks attached at equal distances have the specified properties. The parametric force is transferred via a quasi-homogeneous dynamic system in the form of running waves at a phase speed found on the formula [17]:

$$v = \sqrt{c/J},$$

where c – rigidity of the section; J – inertia moment of the typical section (the typical section is measured by a number of sections (or masses) travelled per second).

Thus, action at distance will be felt in some time required for a wave to pass the entire system losing energy as a result of damping. The experimental research of oscillations spreading [32] has shown that conventional computation methods for dynamic systems (d’Alambert’s principle, second sort Lagrange’s equations) based on Newton’s laws determine accurately only standing waves, i.e., natural frequencies and their corresponding forms of oscillations.

System loading at forced resonance oscillations is determined both by standing and running waves. Since different sections in the running wave, which

exists due to the dissipative properties of the line, oscillate in different time phases, and the standing wave is characterized by equal time phases, there exists a phase shift found through experimental research between the forces determined by the running wave and the displacements determined by the standing wave. For a more detailed identification of power factors acting at the sections when the excitation energy spreads throughout the system, it is necessary to take into consideration phase shifts determined by phase speeds of running waves [32].

The evaluation of dynamic impact of a guide track on a transport module caused by irregularities of a head surface at different speeds is of interest, too. This factor will primarily affect the fatigue strength of transport module parts and contact stability of a wheel – guide pair.

As the cross section of a string transport line is small compared to the existing track structures (bridges, flyovers, etc.), it appears that critical conditions causing loss of guide strength and stability under the impact of wind load are unlikely (this question was discussed in respect to bridge structures in the work [45]). However, guide oscillations of aerodynamic nature [44] require additional research from the perspective of smooth movement at high speed.

3.2. Strength of transport modules and string rail guide

Safe operation of the STS relies on the strength of the string rail overpass and transport module components. Let us consider the features of strength assessment based on the existing computation methods.

Guide. The guide of the string transport system has a composite structure (figure 1.3, 2.10). The strings, being the components carrying the tension force, comprise separate wires, cables or strips and look like an untwisted cable. String integrity is provided by a protective envelope. The strings are interconnected by means of a filler. A filler made of material with high damping properties and the strings are enclosed into a component – a body, which is a protective shell of a rectangular or curvilinear section. Bearing pressures are carried by the head with wear-resistant coating.

Thus, components with different functional properties (high-strength wires, damping filler, protective body, a head with high contact rigidity and antifriction coating) ensure the required characteristics of a guide on the whole.

At present, there is considerable experience in research of the stress condition of separate components of the above composite structure. For example, there exist computation methods for cable strips with regard to arbitrary damage to cables [3], stress strain behavior of shell structures with a filler [9]

and multi-layer parts [27]. There was established experimentally a dependence of bending vibrations parameters on static tension [21]. However, for a strength analysis of the STS guide, it is required to build a model that would comprehensively consider mechanical properties of all constituents, adhesive contact in the head – body conjunction, contact loading of a head and string pre-stressing. It is possible to use a connection model described in [48] as initial approximation. The analysis of strength and stability of STS supports presents no significant difficulties and is based on known computation methods for framed structures like frames and trusses with regard to the characteristics of loading on each type of support (see the table 3).

Table 3

Type of support	Loading source	Type of load
Intermediate	Weight of the track structure and transport module	Vertical static about 15 tf
	Load component caused by transport module motion	Vertical dynamic
	Wind load	Transverse transient
Brake	Transport module acceleration and braking	Longitudinal dynamic
	Structure weight at track slopes; different thermal distortion at neighboring track sections	Longitudinal static
Anchor	String tensioning in the process of construction or at breakage	Longitudinal one-time about 100–1,000 tf
	String tensioning on the first and last anchor supports	Longitudinal static about 100–1,000 tf
	Thermal distortion of strings	Longitudinal static reaching 20 % of tension force

Modern matrix computation methods for elastic systems [18, 25] can be applied for a more detailed research. The strength assessment of supports at crash impact [10] as well as the study of loading flexible (cable) components used when fixing the supports at water track sections [29] have certain specific features.

Transport module. When designing an STS module, a modern approach is required capable of eliminating distinctions between design, strength

and technological aspects, which is widespread when creating high-speed transport (for example, in aviation) [15]. A method, when optimal results are achieved by means of local variation of material properties in the zones of stress concentration, involves the use of composites and allows reducing structure weight, expenses for manufacture and operation, and increase safety, life cycle and comfort level.

However, the calculation of composite structures is rather complicated, which is explained by anisotropy of elasticity and strength, non-uniformity and relatively small (compared to metals) admissible deformation, as well as by residual stresses and composites degradation (aging). In fact, there are a lot of variants of destruction: due to stretching, compression, in-plane shear, interlaminar shear, flat stretching, etc. Therefore, it is required to have performance characteristics at stretching, compression and shear of an anisotropic monolayer in the form of a series of diagrams illustrating the change in strength and elasticity depending on fiber orientation in the matrix

With the availability of information on external loading on a transport module (inertia and aerodynamic forces, oscillations of a propulsion installation, etc.) and criteria of material damage, it becomes possible to analyze and optimize stress condition of the entire module. It can be done by means of a computer-aided analysis using modern discrete methods to simulate loading of a total of components (rods, panels, membranes).

3.3. Tribology of wheel – string contact

A tribological aspect is one of the most important aspects of STS functioning. Friction interaction at wheels rolling on a string transport line has a range of peculiarities.

Thus, modules move at a speed, which significantly surpasses the speed of conventional types of railway transport. Apart from its direct purpose – movement in the right direction and traction transfer – the rolling contact is structurally current carrying. At first thought, this makes it rather stressed.

However, with a sufficiently developed contact area, along with a small weight of a transport module, specific pressures will be many times less than in a railway wheel – rail junction. Besides, a large contact area will provide reduction of current density to the acceptable value.

The realization of traction and braking forces is substantially facilitated if provide adjoining of a significant part of wheel surface and the head of a string transport line. Thus, a high degree of adjoining structurally tends to be efficient in terms of the transfer of tangential stresses in the conditions of small weight of a transport module, and the reduction of normal contact stresses and current

density. Along with that, there arises additional sliding due to the geometry of the conformal rolling contact [7].

It is essential to choose the profile of a wheel work surface and the STS guide head from the perspective of increased wear resistance. Thus, similar to the methodology set forth in the work [38], it is feasible to calculate an optimized profile close to the form of natural wear and tear for this type of junction. Particularly, according to [38], the design longevity of the profile that coincides with the worn-out one is increased by 12 % compared to a standard railway wheel profile. Apart from increased wear resistance, it is possible to expect that traction capacity will grow as a result of profile optimization due to a more uniform distribution of friction forces in the contact zone. It is convenient to implement this in the STS structure, which is not yet subject to the standard for guide profile and wheels.

From a methodological point of view, the research of friction interaction between a wheel and a guide results in the formulation of a range of contact problems, whose complexity depends on a number of accepted assumptions and simplifying hypotheses. Let us consider a possible sequence of development of the corresponding formulations.

1. For the approximate calculation of contact stresses when evaluating the strength of a string line head, it is possible to neglect the impact of friction forces and to use simple analytical dependence obtained on the assumption that the contact area is small compared to the sizes of a wheel and head [5].

2. A more complicated model is required to take into account the process of circumferential load transfer and description of the effect of forming contact sliding and adhesion zones as a result of traction and braking forces. The difficulty when solving such problems is related to a different type of boundary conditions that should be met in sliding and adhesion zones. The configuration of these zones is unknown in advance. In this case, computational models offered by various authors and discussed in a famous general monograph on contact mechanics by Johnson K. [7] are of interest. Kalker J. offered a partial slip model for a case of interaction of an elastic wheel with an elastic foundation according to a non-linear sliding theory [46].

3. Slipping in the wheel – rail junction, which always accompanies the propulsive thrust, is at the same time a reason of energy dissipation due to external friction and surface wear and tear. Consequently, the development of the above models is related to the necessity of describing the kinetics of transition processes with regard to the change in contact parameters over time, for example, wear and tear of the transport system parts during its operation. In this case, models within the variation methods of mechanics based on energy principles are useful, as well.

Slipping, wear and tear. A variational approach described in [37] has potential for the mathematical description of a transition process at rolling with regard to wear and tear caused by slipping. When making a numerical study of stress fields and displacement fields in the contact area divided into an adhesion zone and a sliding zone, a load program was set. Under the program, the relation of a tangential force T_T to the normal force N changed from zero to the ultimate value equal to the friction force fN and corresponding to the beginning of sliding. With the purpose of modelling the dependence of friction coefficient on slip velocity \dot{u} , approximation $f(\dot{u})$ was set at a local contact section when transferring from the state of rest to sliding.

The calculation of life prediction for a wheel and a guide head based on the maximally admissible wear $[I_v]$ can be made on the assumption that the intensity of linear wear depends on the pressure in the degree $\gamma > 1$:

$$i(x, t) = K_1 p^\gamma(x, t).$$

At boundary element contact discretization, the slip distance for j section of h surface is determined by the difference of displacements at neighboring loading steps r and $r + 1$:

$$\Delta u_j^r = u_j^r - u_j^{r-1}; \quad r = 1, \dots, n; \quad j = 1, \dots, m.$$

If slipping is rather small compared to a discretization interval, it is possible to neglect the difference in contact pressure at a local surface section at the elementary wear step. As a result, at a total number of wear steps q , the volume wear can be found by summing:

$$I_v = \sum_{r=1}^q \sum_{j=1}^n \sum_{j=1}^m K_1 p^\gamma(x_j, t^r) (u_j^r - u_j^{r-1}) h.$$

It is important to achieve good adhesion of drive wheels to the guide track at small weight of a transport module (compared to a conventional locomotive) in order to ensure the effective STS operation at modules acceleration and braking. As noted above, facilitation of an STS operating mode is provided by conformity (adjoining) of contact surfaces. The research of contact interaction with conformal surfaces at body rolling was carried out in [24]. In addition, it is possible to optimize kinetic dependence of an adhesion coefficient. In contrast to a popular opinion stating that an adhesion coefficient is reduced at wheels spinning, the recent experimental research has shown that spinning is permissible to increase the potential adhesion coefficient [30]. In this respect, it is of interest to detect a slippage level, which provides maximal traction

force T_T with minimal energy losses A_f and surface wear I_v . The formulation of an optimization problem with regard to the mutual effect of parameters appear as follows:

$$\begin{aligned} \max T_T; \quad T_T &= \int_0^{S_s} \tau ds; \\ \min I_v; \quad I_v &= I_v(A_f); \quad A_f = A_f(\dot{u}, \tau, S_s); \\ \dot{u} &= \dot{u}(f); \quad \tau = \tau(f); \quad S_s = S_s(f), \end{aligned}$$

where $f = f(\dot{u})$.

Using numerical modelling [37], there were obtained estimated changes in volumetric wear I_v depending on T_T/N at a different ratio of static friction coefficient f_0 and coefficient of sliding friction $f_s = f_0 + \Delta f$. It has been established that the wear depends nonlinearly on the adhesion coefficient T_T/N . With $\Delta f < 0$, two sections can be identified at the dependence $I(T_T/N)$ – a flat one corresponding to small values T_T/N , and a section of sharp increase in wear with ratio of T_T/N close to the ultimate value. The specified result complies with the experimental findings on the measurement of energy loss at oscillating circumferential load.

A sharper increase in critical force and wear rate $I_v(f)$ with the increased traction force T_T typical of the case $\Delta f > 0$ is due to the simultaneous increase in the length of sliding zone and tangential contact stresses in it, which lacks at $\Delta f \leq 0$. This is evidenced by the phenomenon of self-terminating slippage [30] observed within the range of locomotive speed from 0 to 70 km/h (a recorded value of $\Delta f = 0.8f_0$). This kinetic dependence is apparently related to the increased adhesive contact of surfaces as a result of elimination of antifricition films (dust, oxides, moisture, lubrication) and formation of layers of wear particles. It is possible to predict that this useful effect will manifest itself at STS module wheels slipping in the corresponding speed range when contact parameters are properly used. In order to choose friction parameters f_0 and Δf in real operating conditions, it is required to find a functional connection between the specified characteristics and surface condition before and after slipping.

The peculiarities of friction effect in thrust transfer units in cableways, elevators, etc. using a flexible guide are under consideration in [49]. The ratios obtained by the authors describe limiting cases of elastic slipping in a cable sheave for different pairs of contact surfaces.

Electrical conductivity. As specified in [14], in order to increase the working capacity of high-current sliding contacts, it is required to apply metal contacts with lubrication filled with dispersion electroconductive fillers or composite metal-containing materials. The optimization of contact properties achieved by using metallized solid lubrications being a part of the composite allows operating such current collectors at slip velocity up to 100 m/s.

The current collector in the rolling contact for feeding the STS module electric drive (similar to an electromotive wheel) tends to be less stressed. Continuous renewal of the contact zone at rolling improves heat dissipation conditions, which creates the preconditions for speed increase. Along with that, it is required on the one hand to conduct research of the stress strain behavior of the contact of bodies having a surface layer with a complex composite structure and operating in the conditions of elastohydrodynamic lubrication with regard to electric current passing (strength aspect). On the other hand, it is essential to study the role of the contact stress state at electric current passing and heat generation (electric and thermal aspects).

Temperature. The feature of friction interaction between a wheel and a guide track in the string transport line consists in high slipping speed, for example, at module emergency braking. At present, such speeds are created when accelerating special sleds at rocket tracks. The tracks allow reproducing subsonic and supersonic speeds (up to 2,500 m/s) where the temperature of friction surface can reach the melting temperature of rubbing bodies [1, 19].

However, for the specified type of tests, there is a sliding mode of rocket sled runners along the guide, and it is significantly more stressed compared to wheel rolling of an STS module. Nevertheless, the information analysis of this kind is useful when selecting the materials and evaluating the resource of the system under consideration.

In order to study thermal dynamics of friction in the wheel – rail junction of the string transport system, obviously, the methods of physical simulation of external friction using similarity criteria can be useful – for example, those that were successfully applied to work out new structures of electromotive traction gears [4]. It is possible to use a roller pair as a model, where a wheel – guide is simulated at mutual rollers rolling-off with some slipping. It is possible to obtain the current values of friction coefficients successively setting for a roller pair working parameters connected to the parameters of the model contact points with scaling parameters.

The method of generalized variables is also applicable when selecting an optimal material composition for a current collector. Wheel wear-resistance, as well as current collector parts, depends on many factors acting together and simultaneously. First of all, it is necessary to name the operating mode

parameters (speed, load, amount of moisture affecting the contact, temperature); physical and mechanical contact parameters (temperature conductivity, arc resistance, rigidity, hardness of parts material), as well as mass and geometric characteristics of contacting bodies.

It is well known that the area of actual contact takes an insignificant portion of a nominal area determined by the geometry of bodies. Consequently, between interacting parts, there are microcavities filled with air or other environment and being a reason of thermal resistance. In this regard, of special value are the results of solving the problem on contacting [8], which implies that thermal resistance is inversely proportional to contact pressure. This allows us to study the impact of loading, thermophysical and mechanical parameters of contacting bodies on contact pressure, heat flow and size of a contact area.

Chapter 4

Dynamic model and estimated parameters of transport modules motion on the string transport line*

4.1. Derivation of motion equation for the String Transport System

This section serves for the derivation of an equation system, which describes joint movement of transport modules (TM) on the elevated string transport line (STL) based on common assumptions towards the STS structure. Awareness of the characteristic features of the problem allowed building a procedure of successive approximations to solving this system; in this case, the first approximation is the solution to the problem on the movement of non-inertia loads on the STL. As special cases, the results of the chapter formulate, for example, the statement of the problem on oscillations of flexible beams (rigid wires) under the impact of moving loads [35].

Let us consider a horizontal STS with a number of spans N_0 . The length of each span is l_0 . It is assumed that the system comprises two equal parallel STL used for TM movement. The key components that form a part of a STL are as follows (figure 4.1):

- a) thin-walled metal casing 1 of box section (in the general case of variable area due to the variation in outside dimensions; internal dimensions of the casing are constant);
- b) pre-stressed (stretched) elements 2 and 3 weakly resistant to bending, further called the upper and lower strings, correspondingly;
- c) filler 4 – continuous medium occupying the volume inside the casing.

Elements 2 and 3 are called strings since each of them consists of a large number of thin and flexible pre-stressed layers (wires) not connected to each

* Chapter 4 is based on the materials of scientific reports “Research of transport motion on a flexible bridge” and “Some questions on dynamics of the string transport system” made in 1994 in Minsk on the order of the General Designer of STS Anatoli Unitsky by an authoring team composed of: Vyarvilskaya O.N., Kozlovskiy N.I., Savenkov V.A., Savchuk V.P. and Unitsky A.E.

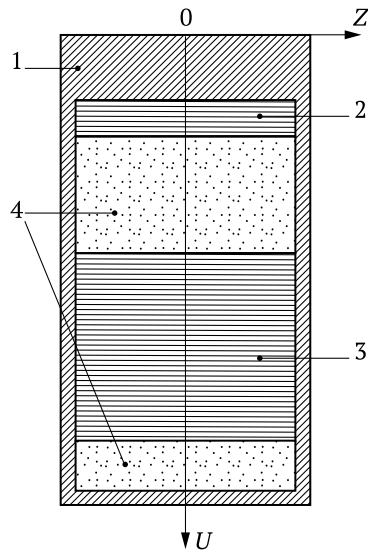


Figure 4.1

other and enclosed in the common flexible casing (there is no friction between the layers thanks to lubrication dividing them). The filler will be considered a medium that has elastic and dissipative properties, low density compared to the density of strings and STL body. On that ground, attributing the filler mass to the casing mass, let us consider the filler to be a weightless connection between line components. Let us assume that each line has a longitudinal vertical medium plane and is subject to the impact of only vertical loads lying in this plane. The dynamic conditions, where the lines are located, are assumed to be equal. With these assumptions, it is possible to limit itself only to the consideration of heave oscillations of STL cross-section in the medium plane under the impact of moving loads. Please note that this conclusion is also fair in the case when the lines are symmetrical in relation to the vertical plane axis and connected to each other so that the line points move only vertically. Let us further imply heave oscillations of the specified cross-section in plane ZOU (figure 4.2) when analyzing oscillations of the line or span.

Let us assume that a transport module is a bogie having a platform with a mass of $2m_1$, and four motionless uniformly loaded wheels with a mass of m_2 each. A shock-absorber (wheel suspension) is modelled with a spring having rigidity c and a damper connected in parallel, whose operating force is proportional to the change speed coefficient v_a of spring length. Let us denote the distance between the axes of front and rear bogie wheels in a horizontal position l_1 .

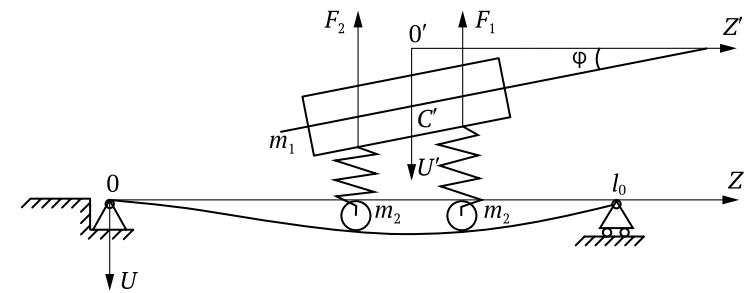


Figure 4.2

The time marking starts from the moment $t = 0$, when the front wheel of the first TM moves from a speedup section to the first span of a motionless STL.

4.1.1. Derivation of equations for STL oscillations

In order to derive an equation system describing STL oscillations, it is required to write down motion equations for line components with regard to the connections between them.

1. Oscillation equation of an STL body. We get an equation of bending heave oscillations of an STL body with a filler. Let us consider that for the body material and the filler, the dependence of normal stress σ on relative deformation ε is given by the formula:

$$\sigma = E \left(\varepsilon + \mu' \frac{\partial \varepsilon}{\partial t} \right), \quad (4.1)$$

where constants E – a Young's modulus and μ' – a coefficient characterizing internal friction of the material. Let us make an assumption that when studying heave oscillations, an STL body with a filler is a uniform beam with average values of E and μ' in (4.1). Then, the equation of the body lateral oscillations can be taken in the form [35]:

$$E \frac{\partial^2}{\partial z^2} \left[I \frac{\partial^2}{\partial z^2} \left(u + \mu' \frac{\partial u}{\partial t} \right) \right] + \rho_0 \frac{\partial^2 u}{\partial t^2} = f(z, t) + R_1 + R_2 + \rho_0 g, \quad (4.2)$$

here $u(z, t)$ – a deflection; $I(z)$ – moment of inertia of cross section; $\rho(z)$ – linear density of the body with a filler; $f(z, t)$ – intensity of external load

on the body without regard to gravity force; $R_1(z, t)$, $R_2(z, t)$ – degree of the upper and lower strings impact on the body, correspondingly, g – free fall acceleration.

By virtue of the introduced assumptions, the motion equations of upper and lower strings will be written as follows:

$$\rho_1 \frac{\partial^2 y_1}{\partial t^2} - T_1 \frac{\partial^2 y_2}{\partial z^2} = f_1(z, t) - R_1 + R_{21} + \rho_1 g; \quad (4.3)$$

$$\rho_2 \frac{\partial^2 y_2}{\partial t^2} - T_2 \frac{\partial^2 y_2}{\partial z^2} = f_2(z, t) - R_2 - R_{21} + \rho_2 g, \quad (4.4)$$

here y_1 , y_2 – spans of the corresponding strings; ρ_1 , ρ_2 – linear densities; T_1 , T_2 – tensions; f_1 , f_2 – intensity of external load related to the upper and lower strings, correspondingly; R_{21} – degree of the lower string impact on the upper string.

In order to derive the STL oscillation equations in the general case, let us assume the upper string casing connected to the line body

$$y_1(z, t) = u(z, t). \quad (4.5)$$

Then, we can assume that:

$$f_1(z, t) = 0; \quad R_{21}(z, t) = 0 \quad (4.6)$$

and after adding equations (4.2), (4.3) get the motion equation for the line body with the upper string:

$$E \frac{\partial^2}{\partial z^2} \left[I \frac{\partial^2}{\partial z^2} \left(u + \mu' \frac{\partial u}{\partial t} \right) \right] + \rho_s \frac{\partial^2 u}{\partial t^2} - T_1 \frac{\partial^2 u}{\partial z^2} = f(z, t) + R_2 + \rho_s g, \quad (4.7)$$

where $\rho_s = \rho_1 + \rho_0$.

Let us assume that the lower string can move vertically in relation to the STL body interacting with it by means of a filler; in a balanced state it carries not only the dead load but also the load caused by the body weight with a filler and the upper string, i.e.,

$$R_2 = R_2^{\text{din}} - \rho_s g, \quad (4.8)$$

where $R_2^{\text{din}}(x, t)$ – a dynamic component of the lower string impact on the body.

Figure 4.3 shows the STL without transport modules in a balanced state, $y_{20}(z)$ – a static deflection of the lower string.

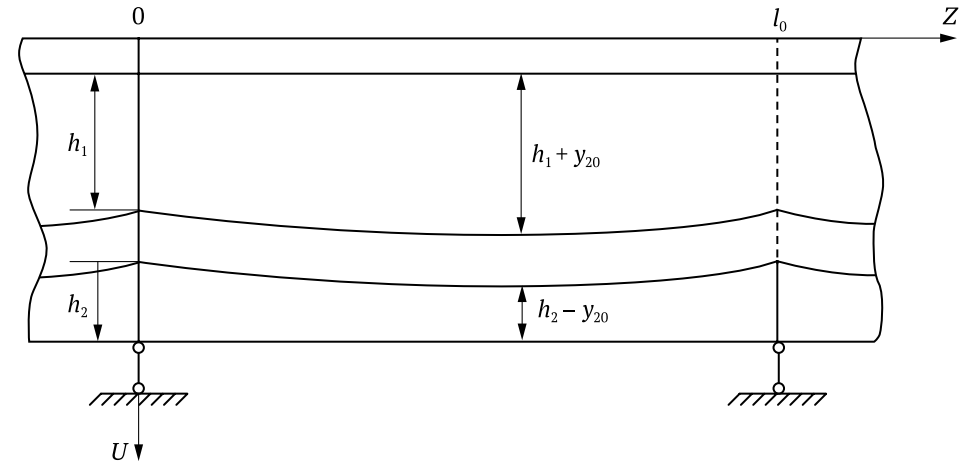


Figure 4.3

Since the filler tensions and distortions towards axis $0U$ satisfy the equality (4.1), R_2^{din} will be written as follows:

$$R_2^{\text{din}} = E_w a \left(1 + \mu_w \frac{\partial}{\partial t} \right) \frac{y_2 - u - y_{20}}{h_1 + y_{20}} + E_n a \left(1 + \mu_n \frac{\partial}{\partial t} \right) \frac{y_2 - u - y_{20}}{h_2 + y_{20}}, \quad (4.9)$$

where E_w , μ_w , E_n , μ_n – constants characterizing the filler above and under the string, correspondingly; a – filler width.

In practically important cases, the maximal value of static deflection y_{20}^{max} does not exceed a few centimeters. Therefore, taking into consideration a small change of static deflection along the span, let us replace y_{20} in the equation denominator (4.9) with its average value $0.5y_{20}^{\text{max}}$ and introduce the function:

$$u_2(z, t) = y_2(z, t) - y_{20}(z, t). \quad (4.10)$$

The function $u_2(x, t)$ describes the lower string deflection in relation to its balanced position. Then, equation (4.9) can be written as follows:

$$R_2^{\text{din}} = E_2 \left(1 + \mu_2 \frac{\partial}{\partial t} \right) (u_2 - u). \quad (4.11)$$

Here

$$E_2 = \frac{aE_w}{h_1 + 0.5y_{20}^{\text{max}}} + \frac{aE_n}{h_1 - 0.5y_{20}^{\text{max}}}; \quad (4.12)$$

$$\mu_2 = \frac{1}{E_2} \left[\frac{a\mu_w E_w}{h_1 + 0.5y_{20}^{\max}} + \frac{a\mu_n E_n}{h_2 - 0.5y_{20}^{\max}} \right].$$

Taking into consideration equalities (4.10), (4.11) equations (4.4), (4.7) take on the form:

$$\begin{aligned} & E \frac{\partial^2}{\partial z^2} \left[I(z) \frac{\partial^2}{\partial z^2} \left(u + \mu' \frac{\partial u}{\partial t} \right) \right] + \rho_s(z) \frac{\partial^2 u}{\partial t^2} - \\ & - T_1(z) \frac{\partial^2 u}{\partial z^2} + E_2 \left(1 + \mu_2 \frac{\partial}{\partial t} \right) (u - u_2) = f(z, t); \quad (4.13) \\ & \rho_2 \frac{\partial^2 u_2}{\partial t^2} - T_2 \frac{\partial^2 u_2}{\partial z^2} + E_2 \left(1 + \mu_2 \frac{\partial}{\partial t} \right) (u_2 - u) = f_2(z, t). \end{aligned}$$

Equations (4.13) represent a system of equations describing motion of the line with a variable cross-section area of the body in relation to the equilibrium position.

The obtained dependences allow us to consider several practically important particular cases.

Case 1. If the body cross-section area does not change along the beam, then I, ρ_s – constants; and equations (4.13) take on the form:

$$\begin{aligned} & EI \frac{\partial^4 u}{\partial z^4} + \mu' EI \frac{\partial^5 u}{\partial t \partial z^4} + \rho_s(z) \frac{\partial^2 u}{\partial t^2} - T_1 \frac{\partial^2 u}{\partial z^2} + \\ & + E_2 \left(1 + \mu_2 \frac{\partial}{\partial t} \right) (u - u_2) = f(z, t); \quad (4.14) \\ & \rho_2 \frac{\partial^2 u_2}{\partial t^2} - T_2 \frac{\partial^2 u_2}{\partial z^2} + E_2 \left(1 + \mu_2 \frac{\partial}{\partial t} \right) (u_2 - u) = f_2(z, t). \end{aligned}$$

Case 2. It corresponds to high rigidity of the filler or to the situation when the lower string touches a rigid body at maximal deflection.

Let us sum up equations (4.14) and pass to the limit at $E_2 \rightarrow \infty$. Then, based on the second equation we get $u_2 = u$, and the system (4.14) will be reduced to one equation:

$$EI \frac{\partial^4 u}{\partial z^4} + \mu' EI \frac{\partial^5 u}{\partial t \partial z^4} + \rho_s \frac{\partial^2 u}{\partial t^2} - (T_1 + T_2) \frac{\partial^2 u}{\partial z^2} = f(z, t), \quad (4.15)$$

describing motion of the STL with the uniform cross section of the body and two strings fastened with it.

Case 3. If we can neglect rigidity of the line body and its density, we get the following equation based on (4.15):

$$\rho' \frac{\partial^2 u}{\partial t^2} = T' \frac{\partial^2 u}{\partial z^2} + f(z, t), \quad (4.16)$$

where $\rho' = \rho_1 + \rho_2$, $T' = T_1 + T_2$.

Equation (4.16) describes oscillations of a flexible STL, the strings of which are connected so that the vertically measured distances between them are constant in the process of movement.

4.1.2. Motion equation for a transport module on STL

Let us consider the TM motion in relation to the system $O'Z'U'$ (figure 4.2) moving at a constant speed v towards axis $O'Z'$. The distance between axes OZ and $O'Z'$ is equal to the height of the module platform mass center above the basic horizontal plane.

Let us derive motion equations for a single transport module driving up to an STL at the time $t = 0$. Let us consider that the TM wheels do not lose contact with the line surface. Then, the TM motion equations will be presented as plane-parallel motion equations of its platform and will be written as follows:

$$m_1 \frac{d^2 U}{dt^2} = -F_1 - F_2 + m_1 g; \quad (4.17)$$

$$I_c \frac{d^2 \varphi}{dt^2} = \text{mom}_c \bar{F}_1 + \text{mom}_c \bar{F}_2.$$

Here $U = O'C'$; φ – a slope angle of the platform axis; I_c – platform inertia moment in relation to the mass center C' ; \bar{F}_1, \bar{F}_2 – reaction forces of shock-absorbers acting on the platform. Let us suppose that the mass center is located in the platform center. Forces \bar{F}_1, \bar{F}_2 can be expressed through dynamic compression of springs:

$$F_1 = \left(c + v_a \frac{d}{dt} \right) \left[U - 0.5l_1\varphi - u(vt, t) \sigma \left(0, N_0 \frac{l_0}{v} \right) \right] + 0.5m_1g; \quad (4.18)$$

$$F_2 = \left(c + v_a \frac{d}{dt} \right) \left[U - 0.5l_1\varphi - u(vt - l_1, t) \sigma \left(\frac{l_1}{v}, \frac{N_0l_0 + l_1}{v} \right) \right] + 0.5m_1g.$$

Equations (4.18) take into consideration that angle φ will be small at platform motion and a time function will be introduced

$$\sigma(t_1, t_2) = \begin{cases} 1, & t \in [t_1, t_2]; \\ 0, & t \notin [t_1, t_2]. \end{cases} \quad (4.19)$$

Considering equalities (4.18) let us write equations (4.17) as follows:

$$\begin{aligned} m_1 \frac{d^2U}{dt^2} + 2v \frac{dv}{dt} + 2cU &= \left(c + v \frac{d}{dt} \right) \times \\ &\times \left[u(vt, t) \sigma \left(0, N_0 \frac{l_0}{v} \right) + u(vt - l_1, t) \sigma \left(\frac{l_1}{v}, \frac{N_0l_0 + l_1}{v} \right) \right]; \\ I_c \frac{d^2\varphi}{dt^2} + 0.5vl_1^2 \frac{d\varphi}{dt} + 0.5cl_1^2\varphi &= 0.5l_1 \left(c + v \frac{d}{dt} \right) \times \\ &\times \left[u(vt - l_1, t) \sigma \left(\frac{l_1}{v}, \frac{N_0l_0 + l_1}{v} \right) + u(vt - l_1, t) \sigma \left(0, N_0 \frac{l_0}{v} \right) \right]. \end{aligned} \quad (4.20)$$

Thus, the received system of equations describes the motion of a single transport module along a N_0 – span STL.

Motion equations (4.20) for a single module can be easily generalized to get motion equations for a module with number $i = 1, 2, 3, \dots$ in a traffic of modules. Let us assume for simplicity that all modules are equal, mechanically not connected with one another and follow each other at the same distance l_2 at constant speed v . Then, for functions $U_i(t)$ and $\varphi_i(t)$ determining the module position, we get the following system:

$$m_1 \frac{d^2U_i}{dt^2} + 2v \frac{dU_i}{dt} + 2cU_i = \left(c + v \frac{d}{dt} \right) \left[u(vt - z_{1i}, t) \sigma_{1i} + u(vt - z_{2i}, t) \sigma_{2i} \right];$$

$$I_c \frac{d^2\varphi_i}{dt^2} + 0.5vl_1^2 \frac{d\varphi_i}{dt} + 0.5cl_1^2\varphi_i = \quad (4.21)$$

$$= 0.5l_1 \left(c + v \frac{d}{dt} \right) \left[u(vt - z_{2i}, t) \sigma_{2i} + u(vt - z_{1i}, t) \sigma_{1i} \right],$$

where

$$z_{1i} = (l_1 + l_2)(i - 1); \quad \sigma_{1i} = \sigma \left(\frac{z_{1i}}{v}, \frac{N_0l_0 + z_{1i}}{v} \right); \quad (4.22)$$

$$z_{2i} = z_{1i} + l_1; \quad \sigma_{2i} = \sigma \left(\frac{z_{2i}}{v}, \frac{N_0l_0 + z_{2i}}{v} \right).$$

4.1.3. Derivation of cooperative motion equations for transport modules and STL

Let us consider an STL – single module system. The STL and module force interaction takes place in contact points of the wheels and the line work surface. In order to determine the interaction forces, let us add gravity force and inertia force of wheels mass to forces \bar{F}_1, \bar{F}_2 determined by equalities (4.18). Thus, the function $f(z, t)$ in equations (4.13)–(4.16) at a single module motion will take on the form:

$$\begin{aligned} f(z, t) &= \left[F_1 + m_2g - m_2 \frac{d^2u(vt, t)}{dt^2} \right] \delta(z - vt) + \\ &+ \left[F_2 + m_2g - m_2 \frac{d^2u(vt - l_1, t)}{dt^2} \right] \delta(z - vt + l_1) + \tilde{f}(z, t), \end{aligned} \quad (4.23)$$

where $\tilde{f}(z, t)$ – density of outer forces in relation to the STL, unrelated to the module, $\delta(z)$ – Dirac δ -function [16]. Since each module wheel affects the line during time nl_0/v , (4.23) will take on the form:

$$f(z, t) = \left[(m_1 + 2m_2) \frac{g}{2} + \left(c + v \frac{d}{dt} \right) (U - 0.5l_1\varphi - u(vt, t)) \right] -$$

$$\begin{aligned}
& -m_2 \frac{d^2 u(vt, t)}{dt^2} \Big] \delta(z - vt) \sigma \left(0, \frac{Nl_0}{v} \right) + \left[(m_1 + 2m_2) \frac{g}{2} + \right. \\
& \left. + \left(c + v \frac{d}{dt} \right) (U + 0.5l_1 \varphi - u(vt - l_1, t)) - \right. \\
& \left. - m_2 \frac{d^2 u(vt - l_1, t)}{dt^2} \right] \delta(z - vt + l_1) \sigma \left(\frac{l_1}{v}, \frac{Nl_0}{v} \right). \quad (4.24)
\end{aligned}$$

We will get a system of cooperative motion equations for the STL and a single module by combining equations (4.13) and equations (4.20). This equation system is a generalization of a beam oscillation equation under the impact of moving mass [35]. Particular cases of motion equations for the STL – single module system are derived by combining equations (4.20) and equations (4.14) (STL with a uniform body along the length), (4.15) (STL, whose strings are fastened to the body) or (4.16) (flexible STL with fastened strings).

Assuming that a module drives up to a motionless STL from an acceleration horizontal area, the initial conditions will be zero:

$$\begin{aligned}
U(0) = \frac{dU(0)}{dt} = 0; \quad \varphi(0) = \frac{d\varphi(0)}{dt} = 0; \\
u(z, 0) = \frac{\partial u(z, 0)}{\partial t} = 0; \quad u_2(z, 0) = \frac{\partial u_2(z, 0)}{\partial t} = 0. \quad (4.25)
\end{aligned}$$

The boundary conditions for functions u , u_2 are determined by means of securing the STL on supports.

Let us move on to consider an STL – traffic of modules system. In order to determine the force impact of the modules traffic on the line, it is enough to sum up the forces affecting the STL on the part of individual modules. Consequently, with regard to equality (4.24), function $f(z, t)$ in equations (4.13)–(4.16) can be presented as follows:

$$\begin{aligned}
f(z, t) = \sum_{i=1}^{i_0} \left[(m_1 + 2m_2) \frac{g}{2} + \left(c + v \frac{d}{dt} \right) (U_i - 0.5l_1 \varphi_i - u(vt - z_{1i}, t)) - \right. \\
\left. - m_2 \frac{d^2 u(vt - z_{1i}, t)}{dt^2} \right] \delta_{1i} \sigma_{1i} + \sum_{i=1}^{i_0} \left[(m_1 + 2m_2) \frac{g}{2} + \left(c + v \frac{d}{dt} \right) \times \right.
\end{aligned}$$

$$\times \left(U_i - 0.5l_1 \varphi_i - u(vt - z_{2i}, t) \right) - m_2 \frac{d^2 u(vt - z_{2i}, t)}{dt^2} \Big] \delta_{2i} \sigma_{2i} + \tilde{f}(z, t). \quad (4.26)$$

Here z_{1i} , z_{2i} , δ_{1i} , δ_{2i} are given by equalities (4.22); i_0 – a number of modules, whose wheels contacted with the line before the considered moment of time,

$$\delta_{1i} = \delta(z - vt, z_{1i}); \quad \delta_{2i} = \delta(z - vt, z_{2i}). \quad (4.27)$$

Combining the STL motion equations (one of the systems (4.13)–(4.16) where $f(z, t)$ is written as (4.26)) with modules motion equations (4.21), we will derive a system of cooperative motion equations for the STL and modules. Notice that a number of equations of this system depends on the time interval value where the motion is considered.

4.1.4. Analysis of motion equations choice of solution method

Let us consider the system of motion equations for a single module and STL (4.13), (4.20). These equations are connected to each other by means of right parts, which contain the required functions. An analytical solution of equations (4.13), (4.20) presents considerable difficulties in the general case, despite their linearity. The solution of the problem on the motion of module traffic on the STL is even more difficult. Therefore, it is more feasible to detect the characteristic features of the problem in order to facilitate its solution.

Let us introduce non-dimensional variables on the formulae

$$z = l_0 \bar{z}; \quad t = t_0 \bar{t}; \quad U = U_0 \bar{U}; \quad u = u_0 \bar{u}; \quad \varphi = 2 \frac{u_0}{l_1} \bar{\varphi}, \quad (4.28)$$

where $t_0 = \left(\frac{\rho_s + \rho_2}{T_1 + T_2 + EI/l_0^2} \right)^{1/2}$; u_0 – a typical size on OU , axis; a maximal deflection of an STL span, for example, can be taken to represent it.

Then, the part of expression (4.24) marked by the first pair of square brackets will take on the form:

$$\begin{aligned}
& (m_1 + 2m_2) \frac{g}{2} + \left(c + v \frac{d}{dt} \right) \left(U - 0.5l_1 \varphi - u(vt, t) - m_2 \frac{d^2 u(vt, t)}{dt^2} \right) = \\
& = (m_1 + m_2) \frac{g}{2} \left[1 + \frac{2u_0}{(m_1 + m_2)g} \left(c + \frac{v}{t_0} \frac{d}{d\bar{t}} \right) \right] (U - \bar{\varphi} - \bar{u}(vt, t)) -
\end{aligned}$$

$$- \frac{2u_0 m_2}{(m_1 + 2m_2)g} \left[\frac{1}{t^2} \frac{\partial^2 \bar{u}(vt, t)}{\partial t^2} + \frac{2v}{t_0 l_0} \frac{\partial^2 \bar{u}(vt, t)}{\partial t \partial \bar{z}} + \frac{v^2}{l_0^2} \frac{\partial^2 \bar{u}(vt, t)}{\partial \bar{z}^2} \right]. \quad (4.29)$$

The order of variables in the square brackets of equality (4.29) is determined by the following expressions:

$$\varepsilon c; \quad \frac{\varepsilon v}{t_0}; \quad \varepsilon \frac{m_2}{t_0^2}; \quad 2\varepsilon \frac{m_2 v}{t_0 l_0}; \quad 2\varepsilon m_2 \frac{v^2}{l_0^2}, \quad (4.30)$$

where

$$\varepsilon = \frac{2u_0}{(m_1 + 2m_2)g}.$$

Let us find the values of these expressions for parameters values typical of the transport module – STL system. Let us assume that

$$m_1 = 10^5 \text{ kg}; \quad m_2 \ll m_1; \quad l_0 = 50 \text{ m}; \quad T_1 + T_2 + EI/L_0^2 = 10^7 \text{ H};$$

$$\rho_s + \rho_2 = 100 \text{ kg/m}; \quad v = 100 \text{ m/s}. \quad (4.31)$$

Suppose that $u_0 = 0.1 \text{ m}$, which exceeds the maximal deflection in case (4.31), as will be shown further. Then, we will get the values of expressions (4.30) (the sizes are omitted):

$$2 \times 10^{-5} c; \quad 6 \times 10^{-4} v; \quad 2 \times 10^{-2} m_2; \quad 2.5 \times 10^{-3} m_2; \quad 8 \times 10^{-5} m_2. \quad (4.32)$$

The first two expressions (4.32) are obviously significantly less than unity for real values c and v ; the rest depend on m_2 , and more specifically – on the relation m_2/m_1 . With a typical value of $m_2/m_1 < 10^2$, all parameters (4.32) are small compared to unity. The problem parameters are interrelated: an increase in tensions T_1, T_2 , for example, causes a decrease in the value, and vice versa. As a result, values (4.30) remain to be small under any real values of all problem parameters, if the following conditions are met

$$\frac{m_2}{m_1} < 10^{-2}; \quad \varepsilon c \ll 1; \quad \frac{\varepsilon v}{t_0} \ll 1. \quad (4.33)$$

The above said in relation to the expression in the first square bracket of function (4.24) is obviously fair for the part marked by the second pair of square brackets and for similar expressions of function (4.26).

Let us assume that interrelations (4.33) are realized. Then, the solution of motion equations for modules and STL can be found by expanding small parameters (4.33) in powers, proceeding to non-dimensional values first. It is also possible to build recurrent equations in order to determine successive approximations of the required functions, taking into account that the summands in square brackets of functions (4.24), (4.26) prevail over the others. Both these procedures are equivalent and provide the solutions similar in form. Let us dwell on the second solution method and write down the equations for successive approximations of the required functions at the TM traffic motion. Using for this purpose equations (4.13), (4.21) and function (4.26), we will get:

$$\begin{aligned} & E \frac{\partial^2}{\partial z^2} \left[I(z) \frac{\partial^2}{\partial z^2} \left(u^{(k+1)} + \mu' \frac{\partial u^{(k+1)}}{\partial t} \right) \right] + \rho_s(z) \frac{\partial^2 u^{(k+1)}}{\partial t^2} - T_1 \frac{\partial^2 u^{(k+1)}}{\partial z^2} + \\ & + E_2 \left(1 + \mu_2 \frac{\partial}{\partial t} \right) \left(u^{(k+1)} - u_2^{(k+1)} \right) = \sum_{i=1}^{i_0} \left[(m_1 + 2m_2) \frac{g}{2} + \right. \\ & \left. + \left(c + v_a \frac{d}{dt} \right) \left(U_i^{(k)} - 0.5l_1 \varphi_i^{(k)} - u^{(k)}(vt - z_{1i}, t) \right) - m_2 \frac{d^2 u^{(k)}(vt - z_{1i}, t)}{dt^2} \right] \delta_{1i} \sigma_{1i} + \\ & + \sum_{i=1}^{i_0} \left[(m_1 + 2m_2) \frac{g}{2} + \left(c + v \frac{\partial}{\partial t} \right) \left(U_i^{(k)} + 0.5l_1 \varphi_i^{(k)}(vt - z_{2i}, t) \right) - \right. \\ & \left. - m_2 \frac{d^2 u^{(k)}(vt - z_{2i}, t)}{dt^2} \right] \delta_{2i} \sigma_{2i} + \tilde{f}(z, t); \\ & \rho_2(z) \frac{\partial^2 u^{(k+1)}}{\partial t^2} - T_2(z) \frac{\partial^2 u^{(k+1)}}{\partial z^2} + E_2 \left(1 + \mu_2 \frac{\partial}{\partial t} \right) \left(u_2^{(k+1)} - u^{(k+1)} \right) = f_2(z, t); \end{aligned} \quad (4.34)$$

$$\begin{aligned} & m_1 \frac{d^2 U_i^{(k+1)}}{dt^2} + 2v \frac{dU_i^{(k+1)}}{dt} + 2cU_i^{(k+1)} = \\ & = \left(c + v \frac{d}{dt} \right) u^{(k)}(vt - z_{1i}, t) \sigma_{1i} + \left(c + v \frac{d}{dt} \right) u^{(k)}(vt - z_{2i}, t) \sigma_{2i}; \end{aligned}$$

$$I_c \frac{d^2 \varphi_i^{(k+1)}}{dt^2} + 0.5v l_1^2 \frac{d\varphi_i^{(k+1)}}{dt} + 0.5c l_1^2 \varphi_i^{(k+1)} =$$

$$= 0.5l_1 \left[\left(c + v \frac{d}{dt} \right) u^{(k)}(vt - z_{2i}, t) \sigma_{2i} - \left(c + v \frac{d}{dt} \right) u^{(k)}(vt - z_{1i}, t) \sigma_{1i} \right],$$

$$k = 0, 1, 2, \dots; \quad i = \overline{1, i_0}; \quad U_i^{(0)} = \varphi_i^{(0)} = u^{(0)} = 0.$$

We derive therefrom the following differential equations for the first approximation of the required functions:

$$E \frac{\partial^2}{\partial z^2} \left[I \frac{\partial^2}{\partial z^2} \left(u^1 + \mu' \frac{\partial u^1}{\partial t} \right) \right] + \rho_s \frac{\partial^2 u^1}{\partial t^2} - T_1 \frac{\partial^2 u^1}{\partial z^2} +$$

$$+ E_2 \left(1 + \mu_2 \frac{\partial}{\partial t} \right) (u^1 - u_2^1) = P \sum_{i=1}^{i_0} (\delta_{1i} \sigma_{1i} + \delta_{2i} \sigma_{2i}) + \tilde{f}_2; \quad (4.35)$$

$$\rho_2 \frac{\partial^2 u_2^1}{\partial t^2} - T_2 \frac{\partial^2 u_2^1}{\partial z^2} + E_2 \left(1 + \mu_2 \frac{\partial}{\partial t} \right) (u_2^{(1)} - u^{(1)}) = f_2;$$

$$m_1 \frac{\partial^2 U_i^1}{\partial t^2} + 2v \frac{dU_i^1}{dt} + 2cU_i^1 = 0; \quad (4.36)$$

$$I_c \frac{d^2 \varphi_i^1}{\partial t^2} + 0.5v l_1^2 \frac{d\varphi_i^1}{dt} + 0.5c l_1^2 \varphi_i^1 = 0, \quad i = \overline{1, i_0}.$$

Here power $P = 0.5(m_1 + 2m_2)g$.

Equations (4.35) describe the STL oscillations under the impact of moving non-inertia loads (forces). Under zero initial conditions, equations (4.36) have a zero solution:

$$U_i^{(1)}(t) = 0; \quad \varphi_i^{(1)}(t) = 0.$$

Consequently, in the first approximation, the points of modules platforms make a straight-line motion.

Let us consider the structure of the solution to the first approximation equations for a one-span STL. Let us assume that $N_0 = 1$, $f = 0$ and $f_2 = 0$. This means that a one-span STL oscillates only under the impact of moving loads

of value P . Let us consider the solution of equations (4.35) at zero initial conditions and suppose first that $i_0 = 1$. Then, the right part of the first equation (4.35) is written as:

$$P \left[\delta(z - vt) \sigma \left(0, \frac{l_0}{v} \right) + \delta(z - vt + l_1) \sigma \left(\frac{l_1}{v}, \frac{l_0 + l_1}{v} \right) \right]. \quad (4.37)$$

It is easily seen that the second summand of expression (4.37) is derived from the first one by time offset for the value l_1/v . Then, the solution to equations (4.35) due to their linearity can be presented as a sum of two components:

$$u^{(1)}(z, t) = u(z, t) \sigma(0, \infty) + u \left(z, t - \frac{l_1}{v} \right) \sigma \left(\frac{l_1}{v}, \infty \right); \quad (4.38)$$

$$u_2^{(1)}(z, t) = u_2(z, t) \sigma(0, \infty) + u_2 \left(z, t - \frac{l_1}{v} \right) \sigma \left(\frac{l_1}{v}, \infty \right),$$

where functions $u(z, t)$, $u_2(z, t)$ are the solutions to the equation system:

$$E \frac{\partial^2}{\partial z^2} \left[I \frac{\partial^2}{\partial z^2} \left(u + \mu' \frac{\partial u}{\partial t} \right) \right] + \rho_s \frac{\partial^2 u}{\partial t^2} - T_1 \frac{\partial^2 u}{\partial z^2} +$$

$$+ E_2 \left(1 + \mu_2 \frac{\partial}{\partial t} \right) (u - u_2) = P \delta(z - vt) \sigma \left(0, \frac{l_0}{v} \right); \quad (4.39)$$

$$\rho_2 \frac{\partial^2 u_2}{\partial t^2} - T_2 \frac{\partial^2 u_2}{\partial z^2} + E_2 \left(1 + \mu_2 \frac{\partial}{\partial t} \right) (u - u_2) = 0,$$

describing the STL oscillations at single load motion of value P . In the general case, with arbitrary i_0 , we get the following instead of equalities (4.38):

$$u^{(1)}(z, t) = \sum_{i=1}^{i_0} \left[u \left(z, t - \frac{z_{1i}}{v} \right) \sigma \left(\frac{z_{1i}}{v}, \infty \right) + u \left(z, t - \frac{z_{2i}}{v} \right) \sigma \left(\frac{z_{2i}}{v}, \infty \right) \right]; \quad (4.40)$$

$$u_2^{(1)}(z, t) = \sum_{i=1}^{i_0} \left[u_2 \left(z, t - \frac{z_{1i}}{v} \right) \sigma \left(\frac{z_{1i}}{v}, \infty \right) + u_2 \left(z, t - \frac{z_{2i}}{v} \right) \sigma \left(\frac{z_{2i}}{v}, \infty \right) \right].$$

Functions (4.40) allow us to interpret the solution of equations (4.35) as a result of impact on the STL caused by a system $2i_0$ of single loads, the distances between which (l_1 and $l_1 + l_2$) are interleaved, or two systems of single equally spaced loads (number of loads i_0).

Thus, the problem on oscillations of a single-span STL with transport modules moving on it in a first approximation consists in solving the problem of span oscillations under the impact of single load.

4.2. Vibration analysis of flexible string. STL first approximation

This section considers loading of a string transport line with the body, whose rigidity can be neglected. There has been studied the span balance under the impact of one or two equal loads; there have been obtained formulae for a maximal static deflection. A detailed analysis has been given for span oscillations at single load and line load movement for different speeds; maximal dynamic deflections have been determined and non-resonant motion modes have been detected. There has been built a trajectory of a single load, and found a maximal span deflection under the load.

4.2.1. Problem setting. Static analysis

Let us consider a N_0 -span STL, whose body rigidity and mass can be neglected. Let us assume that STL strings are connected to each other with weightless bonds so that the distances between their vertical points are constant. Let us assume line supports as rigid bilateral constraints.

From the assumptions made, it follows that the neighboring spans do not have reciprocal effect on each other at motion and, consequently, spans oscillations at a first approximation will be equal to the accuracy of time offset for the value l_0/v . It means that the problem consists in the research of one-span STL oscillations under the effect of moving loads. From equations (4.16), (4.35), (4.39) it can be inferred that the span oscillations at single load movement can be described by equation

$$\frac{\partial^2 u}{\partial t^2} - a^2 \frac{\partial^2 u}{\partial z^2} = \frac{P}{\rho'} \delta(z - vt) \sigma \left(0, \frac{l_0}{v} \right), \quad (4.41)$$

$$\text{where } a = (T'/\rho')^{1/2} = \left(\frac{T_1 + T_2}{\rho_1 + \rho_2} \right)^{1/2}.$$

Boundary and initial conditions of the problem:

$$u(0, t) = u(l_0, t) = 0; \quad (4.42)$$

$$u(z, 0) = \frac{\partial u(z, 0)}{\partial t} = 0. \quad (4.43)$$

If concentrated load does not affect the span, the balance equation of the span lower string, which ensures horizontal position of the upper string, takes on the form:

$$T_2 \frac{d^2 y_{20}}{dz^2} + (\rho_1 + \rho_2) g = 0.$$

Therefrom, with regard to zero boundary conditions, we will get a displacement function

$$y_{20}(x) = g \frac{\rho_1 + \rho_2}{2T_2} (l_0 - z)z,$$

which was used to derive equations (4.13). It is obvious that

$$y_{20}^{\max} = gl_0^2 \frac{\rho_1 + \rho_2}{8T_2}.$$

Assuming, for example, that the span length $l_0 = 50$ m, the total weight per unit length of strings $\rho_1 + \rho_2 = 100$ kg/m and string tensioning $T_2 = 10^7$ N, the maximal displacement $y_{20}^{\max} = 3.125$ cm. A small displacement value y_{20}^{\max} allows to replace function $y_{20}(z)$ in formulae (4.9) with its average value at the span.

Let us assume that two equal loads of P value affect the span in points $z = b$, $z = b + l_1$. As a result, the span is divided into three sections, whose balance is described by an equation

$$\frac{d^2 u_i}{dz^2} = 0, \quad i = \overline{1, 3}.$$

Therefrom, subject to the following conditions

$$u^1(0) = u^3(l_0) = 0; \quad u^1(b) = u^2(b); \quad u^2(b + l_1) = u^3(b + l_1);$$

$$T' \frac{d}{dz} (u^2 - u^1)_{z=b} = -P; \quad T' \frac{d}{dz} (u^3 - u^2)_{z=b+l_1} = -P$$

let us find:

$$u^i(z) = \frac{P}{T'} (C^i z + D^i), \quad i = \overline{1, 3};$$

$$C^1 = 2 - \frac{2b + l_1}{l_0}; \quad C^2 = C^1 - 1; \quad C^3 = -\frac{2b + l_1}{l_0};$$

$$D^1 = 0; \quad D^2 = b; \quad D^3 = 2b + l_1.$$

Simple reasoning suggest that the maximal span deflection

$$u^{\max} = \frac{P}{T'} \left[-\frac{2}{l_0} b^2 + b \left(2 - \frac{3l_1}{l_0} \right) - \frac{l_1^2}{l_0} + l_1 \right].$$

Assuming l_1 to be a constant, let us find:

$$u_s^{\max} = \max u_{\max}(b).$$

After simple calculations, we get:

$$u_s^{\max} = \begin{cases} \frac{l_0 P}{2T'} \left(1 - \frac{l_1}{2l_0} \right)^2, & 0 \leq l_1 \leq \frac{2}{3} l_0; \\ \frac{l_1 P}{2T'} \left(1 - \frac{l_1}{l_0} \right), & \frac{2}{3} \leq l_1 \leq l_0. \end{cases} \quad (4.44)$$

Assuming in (4.44) that $l_1 = 0$ and dividing the received result by half, we will get the maximal span deflection under the impact of one load P :

$$u_s^{1\max} = \frac{l_0 P}{4T'}. \quad (4.45)$$

4.2.2. Span oscillations at single load motion

In order to determine span oscillations under the impact of single load, it is required to solve equation (4.41) subject to conditions (4.42), (4.43).

Dynamic deflection. General case. Let us introduce a new variable z' for convenience of further transformations

$$z = \frac{l_0 z'}{\pi}.$$

Equation (4.41) and conditions (4.42), (4.43) will be written as:

$$\frac{\partial^2 u}{\partial t^2} - a^2 \frac{\pi^2}{l_0^2} \frac{\partial^2 u}{\partial z'^2} = \frac{P}{\rho' l_0} \delta \left(\frac{l_0}{\pi} z' - vt \right) \sigma \left(0, \frac{l_0}{v} \right); \quad (4.46)$$

$$u(0, t) = u(\pi, t) = 0; \quad (4.47)$$

$$u(z', 0) = \frac{\partial u(z', 0)}{\partial t} = 0. \quad (4.48)$$

In order to solve the received problem, let us apply Fourier sine integral transform in finite limits [33] for equation (4.46). As a result, we get the following equation

$$\frac{\partial^2 \tilde{u}}{\partial t^2} - a^2 \frac{\pi^2}{l_0^2} n^2 \tilde{u} = \frac{\pi P}{\rho' l_0} \sin \frac{\pi v n}{l_0} t \sigma \left(0, \frac{l_0}{v} \right) \quad (4.49)$$

with the conditions

$$\tilde{u}(n, 0) = \frac{d\tilde{u}(n, 0)}{dt} = 0 \quad (4.50)$$

for a transformant

$$\tilde{u}(n, t) = \int_0^\pi u(z', t) \sin(nz') dz'.$$

Solving equation (4.49) under conditions (4.50), we get as follows:

$$\tilde{u}(n, t) = \frac{\pi A}{2n^2} \begin{cases} v \sin \frac{a\pi n}{l_0} t - a \sin \frac{v\pi n}{l_0} t, & 0 \leq t \leq \frac{l_0}{v}; \\ v \left[\sin \frac{a\pi n}{l_0} t + \sin \pi n \left(1 + \frac{a}{v} - \frac{at}{l_0} \right) \right], & t > \frac{l_0}{v}. \end{cases} \quad (4.51)$$

Here

$$A = \frac{2Pl}{\rho' a \pi^2 (v^2 - a^2)}.$$

The solution of the initial problem is presented in expanded form

$$u(z', t) = \frac{2}{\pi} \sum_{n=1}^{\infty} \tilde{u}(n, t) \sin nz'. \quad (4.52)$$

Returning to the previous variable z in equality (4.52), we get:

$$u(z, t) = \sum_{n=1}^{\infty} \frac{1}{n^2} \sin \frac{n\pi}{l_0} z \begin{cases} v \sin \frac{a\pi n}{l_0} t - a \sin \frac{v\pi n}{l_0} t, & 0 \leq t \leq \frac{l_0}{v}; \\ v \left[\sin \frac{a\pi n}{l_0} t + \sin \pi n \left(1 + \frac{a}{v} - \frac{at}{l_0} \right) \right], & t > \frac{l_0}{v}. \end{cases} \quad (4.53)$$

Expression (4.53) allows us to calculate a dynamic span deflection in the general case, i.e., for any speeds $v \neq a$ and time moment t . Calculating the limit of function $u(z, t)$ at $v \rightarrow a$ we get as follows:

$$u(z, t) = \frac{gl_0(m_1 + 2m_2)}{2\rho' \pi^2 a^2} \sum_{n=1}^{\infty} \sin \frac{n\pi}{l_0} z \times \begin{cases} \frac{1}{n^2} \left(\sin \frac{a\pi n}{l_0} t - \frac{a\pi n t}{l_0} \cos \frac{a\pi n}{l_0} t, & 0 \leq t \leq \frac{l_0}{a}; \\ -\frac{\pi}{n} \cos \frac{a\pi n}{l_0} t, & t > \frac{l_0}{a}. \end{cases}$$

Due to a good convergence of the trigonometric series used, function (4.53) is convenient for numerical analysis. A qualitative analysis of this function is only possible after its simplification by means of summing up the series included into equality (4.53). Let us use a famous series [6] for this purpose:

$$\sum_{n=1}^{\infty} \frac{1}{n^2} \sin nz \sin ny = \begin{cases} z \frac{\pi - y}{2}, & -y \leq z \leq y; \\ y \frac{\pi - z}{2}, & y \leq z \leq 2\pi - y, \quad 0 < y < \pi. \end{cases} \quad (4.54)$$

After expanding (4.54) for summing up the series in expression (4.53), there arise qualitatively different situations depending on the correlation of load motion speed v and disturbance velocity along the string $a = (T/\rho)^{1/2}$. Therefore, let us consider some particular cases.

1. Case $v > a = (T/\rho)^{1/2}$ (load motion speed exceeds the deformation wave propagation speed along the string). Maximal dynamic deflection.

The series of equality (4.53) based on expansion (4.54) will be written as follows:

$$I_1 = v \sum_{n=1}^{\infty} \frac{1}{n^2} \sin n \frac{a\pi t}{l_0} \sin n \frac{\pi z}{l_0} = \frac{v\pi^2}{2l_0} \begin{cases} z \left(1 - \frac{vt}{l_0} \right), & 0 < z < at, \quad \left[0 < t < \frac{l_0}{a} \right]; \\ at \left(1 - \frac{z}{l_0} \right), & at \leq z \leq 2l_0 - at; \end{cases}$$

$$I_2 = a \sum_{n=1}^{\infty} \frac{1}{n^2} \sin n \frac{v\pi t}{l_0} \sin n \frac{\pi z}{l_0} = \frac{a\pi^2}{2l_0} \begin{cases} z \left(1 - \frac{vt}{l_0} \right), & 0 < z < vt, \quad \left[0 < t < \frac{l_0}{v} \right]; \\ vt \left(1 - \frac{z}{l_0} \right), & vt \leq z \leq 2l_0 - vt; \end{cases}$$

$$I_3 = v \sum_{n=1}^{\infty} \frac{1}{n^2} \sin n\pi \left(1 + \frac{a}{v} - \frac{at}{l_0} \right) \sin n \frac{\pi z}{l_0} =$$

$$= v\pi^2 \begin{cases} \frac{z}{2l_0} \left(\frac{at}{l_0} - \frac{a}{v} \right), & 0 < z < l_0 + l_0 \frac{a}{v} - at, \quad \left[\frac{l_0}{v} < t < \frac{l_0}{a} + \frac{l_0}{v} \right]; \\ \left(1 + \frac{a}{v} - \frac{at}{l_0} \right), & l_0 + l_0 \frac{a}{v} - at \leq z \leq l_0 - l_0 \frac{a}{v} + at; \end{cases}$$

$$I_4 = -v \sum_{n=1}^{\infty} \frac{1}{n^2} \sin n \frac{a\pi t}{l_0} \sin n \frac{\pi z}{l_0} = -v \sum_{n=1}^{\infty} \frac{1}{n^2} \sin n \frac{a\pi}{l_0} \left(t - \frac{l_0}{a} \right) \sin n \frac{\pi}{l_0} (l_0 - z) =$$

$$= \frac{v\pi^2}{2l_0} \begin{cases} (l_0 - z)(2l_0 - at), & z \geq 2l_0 - at, \quad \left[\frac{l_0}{a} < t < 2\frac{l_0}{a} \right]; \\ vt \left(1 - \frac{z}{l_0} \right), & z \leq 2l_0 - at. \end{cases}$$

Let us omit intermediate calculations and write down the dynamic deflection u at time intervals transformed by crossing ranges of definitions of the corresponding series I_k and function (4.53).

Where $0 \leq t \leq \frac{l_0}{v} : u = A(I_1 - I_2)$,

$$I_1 - I_2 = \frac{\pi^2}{2l_0} \begin{cases} z(v-a), & 0 \leq z < at; \\ a(vt-z), & at \leq z < vt; \\ 0, & vt \leq z \leq l_0. \end{cases}$$

Where $\frac{l_0}{v} < t \leq \frac{l_0}{2a} \left(1 + \frac{a}{v}\right) : u = A(I_1 + I_3)$,

$$I_1 + I_3 = \frac{\pi^2}{2l_0} \begin{cases} z(v-a), & z < at; \\ a(vt-z), & at \leq z < l_0 + l_0 \frac{a}{v} - at; \\ (v+a)(l_0-z), & l_0 + l_0 \frac{a}{v} - at \leq z \leq l_0. \end{cases}$$

Where $\frac{l_0}{2a} \left(1 + \frac{a}{v}\right) < t \leq \frac{l_0}{a} : u = A(I_1 + I_3)$,

$$I_1 + I_3 = \frac{\pi^2}{2l_0} \begin{cases} z(v-a), & 0 \leq z < l_0 + l_0 \frac{a}{v} - at; \\ a \left(l_0 + l_0 \frac{v}{a} - z - vt \right), & l_0 + l_0 \frac{a}{v} - at < z \leq at; \\ (v+a)(l_0-z), & at < z \leq l_0. \end{cases}$$

Where $\frac{l_0}{a} \left(1 + \frac{a}{v}\right) < t < \frac{l_0}{a} + \frac{l_0}{v} : u = A(I_3 - I_4)$,

$$I_3 - I_4 = \frac{\pi^2}{2l_0} \begin{cases} z(v-a), & 0 \leq z < l_0 + l_0 \frac{a}{v} - at; \\ a \left(l_0 + l_0 \frac{v}{a} - z - vt \right), & l_0 + l_0 \frac{a}{v} - at < z \leq 2l_0 - at; \\ (l_0-z)(a-v), & 2l_0 - at < z \leq l_0. \end{cases}$$

Figure 4.4 shows the forms of spans at the considered time intervals.

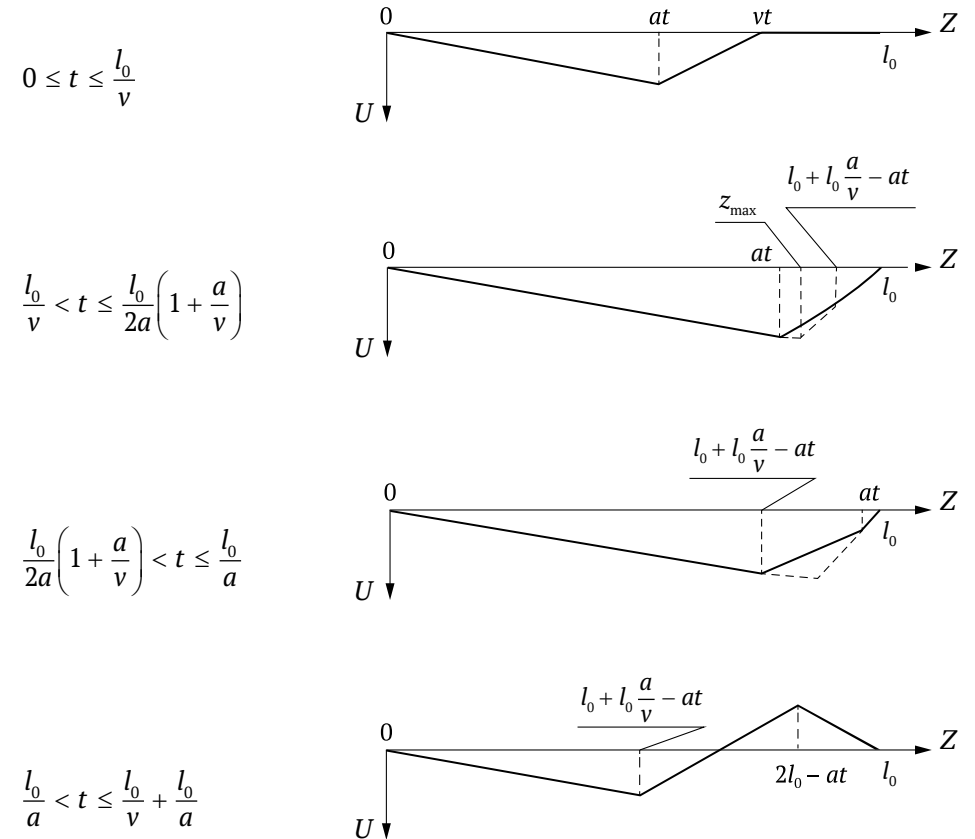


Figure 4.4

The load trajectory is a straight line, i.e., the load moves on an undisturbed part of the span. Taking into account the periodicity of function I_3, I_4 in time, it is possible to continue them for new time intervals and get function $u(z, t)$ at these intervals. However, there is no need for doing so since after the load leaves the span at time moment l_0/v , the span motion can be considered a result of the development of perturbations of its form and speed taken place at any one time $t > l_0/v$. As it follows from figure 4.4 and the corresponding formula for u , at the moment

$$t = \frac{l_0}{2a} \left(1 + \frac{a}{v}\right)$$

the speeds of span points are zero. Consequently, starting from this moment, the span form, as a form of a vibrating string, can be built using a geometric method described, for example, in [7].

Let us use figure 4.4 to determine the maximal dynamic span deflection $u_d^{1\max}$. It is easy to see that the maximal deflection is achieved at the time moment

$$t^{1\max} = \frac{l_0}{2a} \left(1 + \frac{a}{v} \right)$$

at the point

$$z^{1\max} = at^{1\max} = l_0 \frac{v+a}{2v}$$

of the span. Consequently,

$$u_d^{1\max} = A \frac{\pi^2}{2l_0} (v-a) z^{1\max} = \frac{Pl_0}{2\rho'av} = \frac{Pl_0}{2(T'\rho'v)^{1/2}} = 2u_s^{1\max} \frac{a}{v}. \quad (4.55)$$

Based on (4.55), it follows that with an increased v the maximal dynamic span deflection decreases, whereas at speed v close to speed a , it exceeds the maximal static deflection twofold.

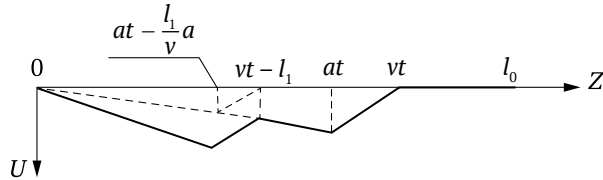


Figure 4.5

Using Figure 4.4, it is possible to get a span form with a TM moving on it, i.e., two loads with value P at distance l_1 from each other. For this purpose, it is enough to sum up the span form for the chosen time moment from Figure 4.4 and the form corresponding to this moment and shifted in time for value l_1/v . Figure 4.5 shows the span form at $l_1/v < t < l_0/v$, as an example.

The conducted geometry analysis of the span form at the movement of two loads allows us to conclude that the maximal dynamic deflection $u_d^{2\max}$ is achieved at the time moment

$$t^{2\max} = t^{1\max} + \frac{l_1}{2v}$$

at the point of the string

$$z^{2\max} = z^{1\max} + \frac{l_1}{2} \frac{a}{v}.$$

Then

$$\begin{aligned} u_d^{2\max} &= 2u(z^{2\max}, t^{2\max}) = \frac{Pl_0}{\rho'av} \left(1 - \frac{l_1}{l_0} \frac{a}{a+v} \right) = \\ &= 2u_d^{1\max} \left(1 - \frac{l_1}{l_0} \frac{a}{a+v} \right) = 2u_s^{1\max} \left(1 - \frac{l_1}{l_0} \frac{a}{a+v} \right) \frac{a}{v}. \end{aligned} \quad (4.56)$$

2. Case $a/2 \leq v < a$ (load motion speed is less than the deformation wave propagation speed along the string). Maximal deflection.

In contrast to the previous case, for summing up the series in equality (4.53) at $v < a$, only this limit is not enough for the load motion speed; therefore, it is required to introduce additional limits for v when making calculations. This is a sign that at $v < a$, span oscillations will be qualitatively different depending on which of the intervals

$$\left[\frac{a}{i+1}, \frac{a}{i} \right], \quad i = 1, 2, \dots$$

v belongs to. Let us consider the first of these intervals, i.e., let us assume that

$$v \in \left[\frac{a}{2}, a \right).$$

In order to get a finite expression for function $u(z, t)$, apart from functions I_1-I_4 let us apply the function

$$\begin{aligned} I_5 &= -v \sum_{n=1}^{\infty} \frac{1}{n^2} \sin n \frac{a\pi t}{l_0} \sin n \frac{\pi z}{l_0} = v \sum_{n=1}^{\infty} \frac{1}{n^2} \sin n \frac{a\pi}{l_0} \left(t - \frac{2l_0}{a} \right) \sin n \frac{\pi z}{l_0} = \\ &= -\frac{v\pi^2}{2l_0} \begin{cases} z \left(3v - \frac{at}{l_0} \right), & 0 < z < at - 2l_0, \quad \left[\frac{2l_0}{a} < t < \frac{3l_0}{a} \right]; \\ (at - 2l_0) \left(1 - \frac{z}{l_0} \right), & at - 2l_0 \leq z \leq 4l_0 - at. \end{cases} \end{aligned}$$

Let us omit some intermediate calculations and write down the displacement function $u(z, t)$ at several successive time intervals.

Where $0 \leq t \leq \frac{l_0}{a} : u = A(I_1 - I_2)$,

$$I_1 - I_2 = \frac{\pi^2}{2l_0} \begin{cases} z(v - a), & 0 \leq z < vt; \\ v(z - at), & vt \leq z < at; \\ 0, & at \leq z \leq l_0. \end{cases}$$

Where $\frac{l_0}{a} < t \leq \frac{2l_0}{a+v} : u = -A(I_2 + I_4)$,

$$I_2 + I_4 = \frac{\pi^2}{2l_0} \begin{cases} z(a - v), & 0 \leq z < vt; \\ z(at - z), & vt \leq z < \frac{2l_0}{a+v}; \\ 2v(l_0 - z), & \frac{2l_0}{a+v} \leq z \leq l_0. \end{cases}$$

Where $\frac{2l_0}{a+v} \leq t < \frac{l_0}{v} : u = -A(I_2 + I_4)$,

$$I_2 + I_4 = \frac{\pi^2}{2l_0} \begin{cases} z(a - v), & 0 \leq z < 2l_0 - at; \\ z(a - 2v) + v(2l_0 - at), & 2l_0 - at < z < vt; \\ 2v(l_0 - z), & vt \leq z \leq l_0. \end{cases}$$

Where $\frac{l_0}{v} \leq t < \frac{2l_0}{a} : u = A(I_3 - I_4)$,

$$I_3 - I_4 = \frac{\pi^2}{2l_0} \begin{cases} z(v - a), & 0 \leq z < 2l_0 - at; \\ z(2v - a) + v(at - 2l_0), & 2l_0 - at \leq z < l_0 + \frac{l_0 a}{v} - at; \\ (a - v)(l_0 - z), & l_0 + \frac{l_0 a}{v} - at < z \leq l_0. \end{cases}$$

Where $\frac{2l_0}{a} \leq t < \frac{l_0}{2a} \left(3 + \frac{a}{v}\right) : u = A(I_3 - I_5)$,

$$I_3 - I_5 = \frac{\pi^2}{2l_0} \begin{cases} 3z(v - a), & 0 \leq z < at - 2l_0; \\ z(2v - a) + v(at - 2l_0), & at - 2l_0 \leq z < l_0 + \frac{l_0 a}{v} - at; \\ (a - v)(l_0 - z), & l_0 + \frac{l_0 a}{v} - at \leq z \leq l_0. \end{cases}$$

The span forms corresponding to the considered time intervals are shown in figure 4.6. Where

$$t = \frac{l_0}{2a} \left(3 + \frac{a}{v}\right)$$

the speed of span points becomes zero as is seen from the figure and, consequently, its form can be obtained at any later time by means of any geometric construction described in [31].

The coordinate $z^{1\max}$ of maximal dynamic deflection $u_d^{1\max}$ and time moment $t^{1\max}$, when this deflection is reached, are easily determined from figure 4.6:

$$t^{1\max} = \frac{2l_0}{a+v}; \quad z^{1\max} = \frac{2vl_0}{a+v}.$$

Then,

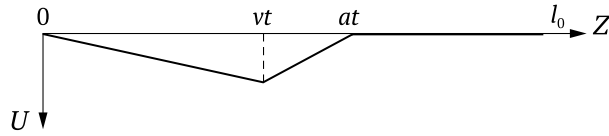
$$u_d^{1\max} = A \frac{\pi^2}{2l_0} x^{1\max} = \frac{2Pl_0}{\rho' av} \frac{1}{\left(1 + \frac{a}{v}\right)^2} = 8u_s^{1\max} \frac{av}{(v+a)^2}. \quad (4.57)$$

From this equality, it follows in particular that at a decreased speed v from a to $a/2$, deflection $u_d^{1\max}$ is decreased by 9/8 times.

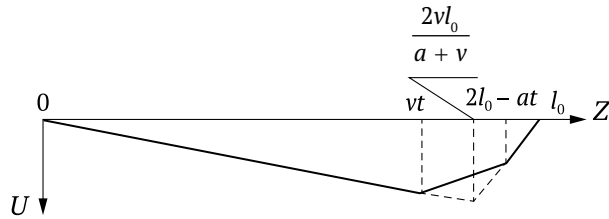
Similarly, the span deflection can be found where

$$\frac{a}{i+1} \leq v \leq \frac{a}{i} \text{ for any } i.$$

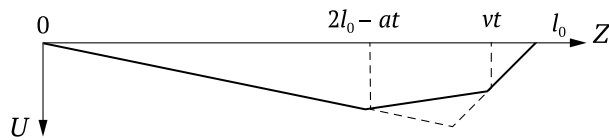
$$0 \leq t \leq \frac{l_0}{a}$$



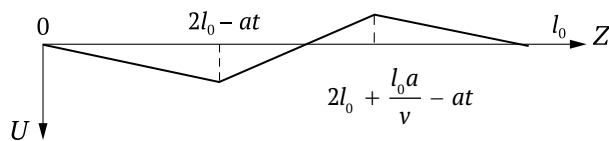
$$\frac{l_0}{a} < t < \frac{2l_0}{a+v}$$



$$\frac{2l_0}{a+v} \leq t < \frac{l_0}{v}$$



$$\frac{l_0}{v} \leq t < \frac{2l_0}{a}$$



$$\frac{2l_0}{a} \leq t < \frac{l_0}{2a} \left(3 + \frac{a}{v} \right)$$

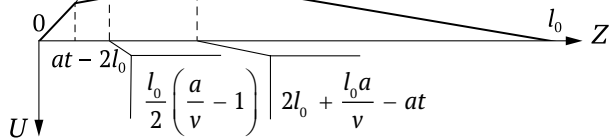


Figure 4.6

4.2.3. Dynamic span deflection at load flow movement

Let us suppose that at the time moment $t = 0$, the motionless span gets the first load out of load flow i_0 of value P moving at a constant speed v at distance l' from each other. From a practical perspective, it is essential to know the value of a dynamic span deflection after load i_0 has passed, depending on the values of constants l' , v and i_0 . Particularly, in order to arrange a continuous load movement, it is required to find such values l' and v , i.e., such motion modes, where the maximal dynamic span deflection remains limited for a large number of loads ($i_0 \rightarrow \infty$). No less important is to find resonant motion modes, i.e., those values of parameters l' and v , where the maximal dynamic deflection increases without limit with an increased amount of loads having passed on the span.

In order to consider the tasks set, let us use the results received in clauses 4.1.4 and 4.2.2, wherefrom it follows that the dynamic span deflection u_d is given by the equality:

$$u_d(z, t) = \sum_{i=1}^{i_0} u \left(z, t - (i-1) \frac{l'}{v} \right) \sigma \left((i-1) \frac{l'}{v}, \infty \right), \quad (4.58)$$

where the function $u(z, t)$ is determined by the formula (4.53). From the equality (4.53), it follows that the function $u(z, t)$ at $t > i_0/v$ is recurrent on t with the period $t_0 = 2l_0/a$. Then, the function $u(z, t - (i-1)l'/v)$ has the same period at $t > l_0/v + (i-1)l'/v$, whereas $u_d(z, t)$ - at $t > l_0/v + (i_0-1)l'/v$. Consequently, deflection u_d for small numbers i_0 at a fixed moment in the interval

$$l_0/v + (i_0-1)l'/v < t^* < l_0/v + (i-1)l'/v + t_0$$

can be determined in a geometric way. For doing so, it is obviously required as follows:

- 1) build a function graph $u(z, t^* - (i_0-1)l'/v)$ at the interval $0 \leq z \leq l_0$;
- 2) extend the graph periodically for the values $z > l_0$;
- 3) sum up i_0 of function graphs $u(z, t^* - (i_0-1)l'/v)$ at the interval $0 \leq z \leq l_0$ by shifting every successive one in the negative direction of OZ axis by l' in relation to the preceding one.

Some conclusions from the equality (4.53) can be made at certain l' and v values without geometric constructions.

1. Case $v = \frac{a}{2k+1}$; $k = 1, 2, 3, \dots, l' - \text{any.}$

From the equality (4.53), we have:

$$\begin{aligned}
u(z, t) &= Av \sum_{n=1}^{\infty} \frac{1}{n^2} \left[\sin \frac{n\pi a}{l_0} t + \sin n\pi \left(1 + \frac{a}{l_0} \right) \right] \sin \frac{n\pi z}{l_0} = \\
&= Av \sum_{n=1}^{\infty} \frac{1}{n^2} \left[\sin \frac{n\pi a}{l_0} t + \sin n\pi \left(2(k+1) - \frac{at}{l_0} \right) \right] \sin \frac{n\pi z}{l_0} = 0, \quad (4.59) \\
& \quad t > \frac{l_0}{v}; \quad 0 \leq z \leq l_0.
\end{aligned}$$

This identical equation means that the excitation, created by single load moving on the span, fully disappears after it leaves the span. It also follows that at flow movement, the loads leaving the span do not cause any impact to its deformation, and span deflection is determined only by the loads moving on it. Consequently, the maximal span deflection is limited and can be found if we set distances between the loads.

The analysis of the span deformation behavior allows us to make a conclusion that at $l' \geq 2kl_0/(2k+1)$, each load drives into an undisturbed span section, i.e., all loads are in equal motion conditions. Thus, span oscillations in the considered motion mode disappear due to mutual suppression of deformation waves. In addition, a positive feature of this motion mode is a necessity to accurately maintain only the speed neglecting the intervals between the loads, which can be any.

2. Case $v = \frac{a}{2k}$; $l = \frac{j-0.5}{k}$; $k, j = 1, 2, 3, \dots$

Equality (4.53) in this case will be written as follows:

$$u(z, t) = 2Av \sum_{n=1}^{\infty} \frac{1}{n^2} \sin \frac{n\pi a}{l_0} t \sin \frac{n\pi z}{l_0}, \quad t > \frac{l_0}{v}.$$

It follows from here:

$$\begin{aligned}
u\left(z, t - (i-1)\frac{l'}{v}\right) &= u\left(z, t - (i-1)(2j-1)\frac{l_0}{f}\right) = \\
&= u\left(z, t + (i-1)\frac{l_0}{f}\right) = (-1)^{i-1} u(z, t), \quad t > \frac{l_0}{v} + (i-1)\frac{l'}{v}.
\end{aligned}$$

Then, from the equality (4.58), we get:

$$\begin{aligned}
u_d(z, t) &= u(z, t) \sum_{i=1}^{i_0} (-1)^{i-1} = \begin{cases} u(z, t), & i_0 - \text{odd-numbered;} \\ 0, & i_0 - \text{even-numbered,} \end{cases} \\
& \quad t > \frac{l_0}{v} + (i_0 - 1)\frac{l'}{v}.
\end{aligned}$$

This means that in the considered motion mode, the span deflection after load i_0 has passed is equal to the deflection after one load has passed, if i_0 is odd-numbered; and it is equal to zero, if i_0 is even-numbered, i.e., the deflection is limited at any i_0 .

The maximal motion speed $v = 0.5a$, whereas the minimal distance between the loads $l' = 0.5l_0$ (two loads can move on the span simultaneously). A detailed analysis carried out for the specified values v and l' allows us to come to the conclusion that the maximal span deflection u_d^{\max} is equal to the maximal dynamic deflection at single load movement with this speed, i.e.,

$$u_d^{\max} = u_d^{1\max} = 4/9 Pl_0/T'.$$

Since due to the equalities (4.44), (4.45)

$$u_s^{2\max} = \frac{9Pl_0}{32T'}; \quad u_s^{1\max} = \frac{Pl_0}{4T'},$$

then

$$u_d^{\max} = \frac{128}{81} u_s^{2\max} = 1.58 u_s^{2\max};$$

$$u_d^{\max} = \frac{16}{9} u_s^{1\max} = 1.78 u_s^{1\max}.$$

3. Case $\frac{l'}{v} = jt_0$; $v \neq \frac{a}{2k+1}$; $j, k = 1, 2, 3, \dots$

Based on equalities (4.53), (4.58), it follows that

$$u_d(z, t) = i_0 u(z, t); \quad t > \frac{l_0}{v} + (i_0 - 1)\frac{l_0}{v}.$$

Thus, for the time period l'/v divisible by period t_0 , the dynamic span deflection (and particularly the maximal dynamic deflection) increases proportionally to the number of loads having passed the span. From the practical perspective, it is the most unfavourable motion mode of loads, which causes resonant swaying of the span. In order to neutralize it, reliable oscillation damping is required.

$$4. \text{ Case } \frac{l'}{v} = \left(j - \frac{1}{2}\right)t_0; v \neq \frac{a}{2k+1}; j, k = 1, 2, 3, \dots$$

For this motion mode based on formulae (4.53), (4.58), we get as follows

$$\begin{aligned} u_d(z, t) = & Av \left[\frac{i_0}{2} \right] \sum_{n=1}^{\infty} (1 + (-1)^n) \frac{1}{n^2} \left[\sin \frac{na\pi t}{l_0} t + \right. \\ & \left. + \sin n\pi \left(1 + \frac{a}{v} - \frac{at}{l_0} \right) \right] \sin \frac{n\pi z}{l_0} + \\ & + Av \left(i_0 - 2 \left[\frac{i_0}{2} \right] \right) \sum_{n=1}^{\infty} \frac{1}{n^2} \left[\sin \frac{na\pi t}{l_0} + \sin n\pi \left(1 + \frac{a}{v} - \frac{at}{l_0} \right) \right] \sin \frac{n\pi z}{l_0}, \\ & t > \frac{l_0}{v} + (i_0 - 1) \frac{l'}{v}. \end{aligned}$$

Here, $\left[\frac{i_0}{2} \right]$ means the integral part of number $\frac{i_0}{2}$.

By analyzing this equality, the conclusion can be drawn that the span deflection grows with an increased amount of loads having passed on the span slower than in the previous case. However, this motion mode leads to resonant swaying of the span, as well.

As already pointed out earlier, the modules traffic in first approximation is equivalent to two loads traffic, if loads of the second flow lag behind the corresponding loads of the first flow at distance l_1 , and the distance between loads in the flows $l' = l_1 = l_2$. Since $l_1 \leq l_0$, the conclusions related to the load flows are fair for the modules flow, as well, as it is easy to make sure.

4.2.4. Calculation of single load trajectory.

Maximal span deflection under load

The span deflection at single load movement is given by formula (4.53):

$$u(z, t) = A \sum_{n=1}^{\infty} \frac{1}{n^2} \left(v \sin \frac{na\pi t}{l_0} - a \sin \frac{nv\pi t}{l_0} \right) \sin \frac{n\pi z}{l_0},$$

$$0 \leq t \leq \frac{l_0}{v}. \quad (4.60)$$

The equation of single load trajectory will be obviously written as follows:

$$u = W(z), \quad (4.61)$$

where

$$W(z) = u \left(z, \frac{z}{v} \right) = A \sum_{n=1}^{\infty} \frac{1}{n^2} \left(v \sin \frac{na\pi z}{vl_0} - a \sin \frac{n\pi z}{l_0} \right) \sin \frac{n\pi z}{l_0}. \quad (4.62)$$

Going in equality (4.62) to the limit at $v \rightarrow 0$, we get:

$$W(x) \Big|_{v=0} = \frac{2Pl_0}{\rho' \pi^2 a^2} \sum_{n=1}^{\infty} \frac{1}{n^2} \sin^2 \frac{n\pi z}{l_0}. \quad (4.63)$$

This series is summed up with the help of formula (4.54)

$$\sum_{n=1}^{\infty} \frac{1}{n^2} \sin^2 \frac{n\pi z}{l_0} = -\frac{\pi^2}{2l_0^2} z(l_0 - z). \quad (4.64)$$

Since z is a load coordinate, the maximal span deflection at $v = 0$ will be at the point of maximum function (4.64), i.e., for $z = l_0/2$. Substituting this value into (4.63) and (4.64), we get:

$$W^{\max} \Big|_{v=0} = \frac{Pl_0}{4\rho' a^2} = u_s^{1\max}.$$

Let us now assume that $0 < v < a$ and write down the function (4.62) as follows:

$$W(l_0 y) = B \left[\alpha y(1 - y) - \frac{2}{\pi^2} J_1(y) \right] = W_1(y), \quad 0 \leq y \leq 1. \quad (4.65)$$

Here

$$\alpha = \frac{a}{v}; \quad y = \frac{z}{l_0}; \quad B = \frac{Pl_0\alpha}{\rho'a^2(\alpha^2 - 1)};$$

$$J_1(y) = \sum_{n=1}^{\infty} \frac{1}{n^2} \sin n\alpha\pi y \sin n\pi y.$$

Taking into account that

$$J_1(y) = \sum_{n=1}^{\infty} \frac{1}{n^2} \sin n(\alpha\pi y - 2\pi k) \sin n\pi y, \quad k = 0, 1, 2, \dots,$$

let us sum up this series using formula (4.54) for all $0 \leq y \leq 1$.

$$J_1(y) = \frac{\pi^2}{2} \begin{cases} f_2(0, y), & 0 \leq y \leq \frac{2}{\alpha+1}; \\ f_1(1, y), & \frac{2}{\alpha+1} \leq y \leq \frac{2}{\alpha-1}; \\ f_2(1, y), & \frac{2}{\alpha-1} \leq y \leq \frac{2}{\alpha+1}; \\ \dots \\ f_1(n, y), & \frac{2n}{\alpha+1} \leq y \leq \frac{2n}{\alpha-1}; \\ f_2(n, y), & \frac{2n}{\alpha-1} \leq y \leq \frac{2n}{\alpha+1}; \\ \dots \end{cases} \quad (4.66)$$

Here

$$f_1(n, y) = (\alpha y - 2n)(1 - y); \quad f_2(n, y) = y(1 + 2n - \alpha y).$$

To make value y take all values from the open interval $[0, 1]$, n should reach the value n_0 , where n_0 is the lowest natural number complying with the inequality

$$n_0 \geq (\alpha - 1)/2.$$

After substituting (4.66) into (4.65), we get:

$$W_1(y) = B \begin{cases} \varphi_2(0, y), & 0 \leq y \leq \frac{2}{\alpha+1}; \\ \varphi_1(n, y), & \frac{2n}{\alpha-1} \leq y \leq \frac{2(n+1)}{\alpha-1}; \\ \varphi_2(n, y), & \frac{2n}{\alpha-1} \leq y \leq \frac{2(n+1)}{\alpha+1}, \end{cases} \quad (4.67)$$

where

$$\varphi_1(n, y) = 2n(1 - y); \quad \varphi_2(n, y) = y(\alpha - 1 - 2n); \quad n = \overline{1, n_0}.$$

It follows from (4.67) that the load trajectory consists of linear segments, the starting and final segments of which are those determined by functions $\varphi_2(0, y)$ and $\varphi_1(n_0, y)$, correspondingly.

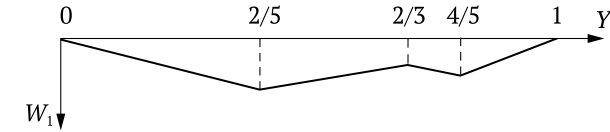


Figure 4.7

Figure 4.7 shows the load trajectory at $\alpha = 4$. It is easy to see that at segments φ_2 the function $W_1(y)$ increases, and at φ_1 it decreases. Therefore, it is clear that:

$$W_1^{\max} = \max_{0 \leq y \leq 1} W_1(y) = B \max_{n=0, n_0-1} \varphi_2 \left(n, \frac{2(n+1)}{\alpha+1} \right).$$

Let us find, for example, the value W_1^{\max} with ratio of the deformation wave propagation velocity to the load motion speed $\alpha = \frac{a}{v} = 7$. In this case, $n = 3$; consequently:

$$\begin{aligned} W_1^{\max} &= B \max \left(\frac{2}{\alpha+1}(\alpha-1), \frac{4}{\alpha+1}(\alpha-3), \frac{6}{\alpha+1}(\alpha-5) \right) = \\ &= \frac{B}{8} \max(12, 16, 12) = 2B \frac{7}{24} \frac{Pl_0}{\rho'a^2} = \frac{7}{6} u_s^{1\max}. \end{aligned}$$

4.3. Oscillations of a String Transport System with elastic body

In a properly designed dynamic system of vibration amplitude, the efforts in elastic elements and the loads carried by supports should have lower values in the working area than those received at static load equal to the maximal amplitude of variable force.

However, outside the working area, a transient resonant state is possible when the vibration amplitude and dynamic forces are significant. Resonant amplitudes are determined by damping in the system and the passage speed through a resonant area in a transient mode. In relation to the operation of a string transport line, transport module rolling up and back the spans is such a transient mode.

If damping typical of a dynamic system is insufficient to keep the amplitude of transient resonant oscillations within tolerable limits, it is required to introduce additional damping. The damping element in the STL structure is the body filler.

This section is dedicated to the research of STL oscillations with regard to elastic and dissipative properties of the body and filler. There have been solved the problems on the movement of single load and load flow on the STL with a split body above the supports and on the movement of load flow on an unsplit solid STL. There has been conducted an analysis of the damping time for long and short waves after the load leaves the span; as well as obtained the resonance conditions at load flow movement on the STL with a solid and a split body.

4.3.1. Single load at STL with a split body

Let us consider a multi-span STL with a freely supported body, which has cuts above the supports. The line is united into a single unity by means of stretched strings. It is obvious that every span in this case will oscillate regardless of the others, and the task consists in solving the system (4.39) within the interval $0 \leq z \leq l_0$ under the corresponding boundary and initial conditions. Let us assume the supports to be rigid, and a lower string attached to the STL body in the initial and finite span points. The following boundary and initial conditions result from the above:

$$\text{where } z = 0, l_0 : u = \frac{\partial^2 u}{\partial z^2} = 0; \quad u_2 = 0; \quad (4.68)$$

$$\text{where } t = 0, l_0 : u_1 = \frac{\partial u_1}{\partial t} = 0; \quad u_2 = \frac{\partial u_2}{\partial t} = 0. \quad (4.69)$$

Let us assume that the STL body cross-section area does not depend on z coordinate. Then, motion equations (4.39) will be written as follows:

$$\begin{aligned} EI \frac{\partial^4 u}{\partial z^4} + EI \mu' \frac{\partial^5 u}{\partial t \partial z^4} + \rho_s \frac{\partial^2 u}{\partial t^2} - T_1 \frac{\partial^2 u}{\partial z^2} + \\ + E_2 \left(1 + \mu' \frac{\partial}{\partial t} \right) (u - u_2) = P \delta(z - vt) \sigma \left(0, \frac{l_0}{v} \right); \\ \rho_2 \frac{\partial^2 u_2}{\partial t^2} - T_2 \frac{\partial^2 u_2}{\partial z^2} + E_2 \left(1 + \mu_2 \frac{\partial}{\partial t} \right) (u - u_2) = 0. \end{aligned} \quad (4.70)$$

Let us find the solution to the system (4.70) in the form of trigonometric series

$$\begin{aligned} u(z, t) &= \sum_{n=1}^{\infty} q_n(t) \sin \frac{n\pi z}{l_0}; \\ u_2(z, t) &= \sum_{n=1}^{\infty} q_{2n}(t) \sin \frac{n\pi z}{l_0}. \end{aligned} \quad (4.71)$$

Taking into account that

$$\delta(z - vt) = \frac{2}{l_0} \sum_{n=1}^{\infty} q_n(t) \sin \frac{n\pi vt}{l_0} \sin \frac{n\pi z}{l_0},$$

we will get the equation system to determine the unknown coefficients $q_n(t)$, $q_{2n}(t)$ (the prime mark implies a time derivative):

$$q_n'' + (n_1^4 E_{11} \mu') q_n' - E_{21} \mu_2 q_{2n}' + (n_1^4 E_{11} + n_1^2 T_{11} + E_{21}) q_n - E_{21} q_{2n} = \varphi_n(t); \quad (4.72)$$

$$q_{2n}'' + E_{22} \mu_2' q_{2n}' + E_{22} \mu_2 q_{2n}' + (n_1^2 T_{22} + E_{22}) q_{2n} - E_{22} q_n = 0.$$

Here

$$\varphi_n(t) = A \sin \frac{n\pi vt}{l_0} \sigma \left(0, \frac{l_0}{v} \right); \quad A = \frac{2P}{\rho_s l_0}; \quad n_1 = \frac{n\pi}{l_0};$$

$$E_{11} = \frac{EI}{\rho_s}; \quad E_{21} = \frac{E_2}{\rho_s}; \quad E_{22} = \frac{E_2}{\rho_2}; \quad T_{11} = \frac{T_1}{\rho_s}; \quad T_{22} = \frac{T_2}{\rho_2}.$$

In order to solve equations (4.72) with zero initial conditions, let us apply the integral Laplace transformation [33]. As a result, we will get the following equation system for the transformant of the required functions:

$$\begin{aligned} \tilde{q}_n(\lambda) & \left[\lambda^2 + \lambda(n_1^4 E_{11} \mu_1' + E_{21} \mu_2) + n_1^4 E_{11} + n_1^2 T_{11} + E_{21} \right] - \\ & - \tilde{q}_{2n}(\lambda) \left[\lambda E_{21} \mu_2 + E_{21} \right] = \tilde{\varphi}_n(\lambda); \\ -\tilde{q}_n(\lambda) & \left[\lambda E_{22} \mu_2 + E_{22} \right] + \tilde{q}_{2n}(\lambda) \left[\lambda^2 + \lambda E_{22} \mu_{22} + n_1^2 T_{22} + E_{22} \right] = 0, \end{aligned}$$

whose solution has the view:

$$\tilde{q}_n(\lambda) = \tilde{\varphi}_n \tilde{q}_n(\lambda); \quad \tilde{q}_{2n}(\lambda) = \tilde{\varphi}_n \tilde{q}_{2n}(\lambda), \quad (4.73)$$

where

$$\tilde{\varphi}_n(\lambda) = \int_0^{\infty} \varphi_n(t) \exp(-\lambda t) dt; \quad (4.74)$$

$$\tilde{q}_n(\lambda) = \frac{\lambda^2 + n_1^2 T_{22} + E_{22}(\lambda \mu_2 + 1)}{\Delta(\lambda)}; \quad \tilde{q}_{2n}(\lambda) = \frac{E_{22}(\lambda \mu_2 + 1)}{\Delta(\lambda)};$$

$$\Delta(\lambda) = \lambda^4 + a_3 \lambda^3 + a_2 \lambda^2 + a_1 \lambda + a_0, \quad (4.75)$$

where

$$a_3 = n_1^4 E_{11} \mu_1' + (E_{21} + E_{22}) \mu_2;$$

$$a_2 = n_1^4 E_{11} + n_1^2 (T_{11} + T_{22}) + E_{21} + E_{22} + n_1^4 E_{11} E_{22} \mu_1' \mu_2 = a_{20} + n_1^4 E_{11} E_{22} \mu_1' \mu_2;$$

$$a_1 = (n_1^6 T_{22} + n_1^4 E_{22}) E_{11} \mu_1' + (n_1^4 E_{11} E_{22} + n_1^2 (T_{22} E_{21} + T_{11} E_{22})) \mu_2;$$

$$a_0 = n_1^6 E_{11} T_{22} + n_1^4 (E_{11} E_{22} + T_{11} E_{22}) + n_1^2 (T_{11} E_{22} + T_{22} E_{21}).$$

Now applying the inverse Laplace transformation to equalities (4.73), we get as follows:

$$q_n(t) = \int_0^t \varphi_n(\tau) g_n(t - \tau) d\tau; \quad q_{2n}(t) = \int_0^t \varphi_n(\tau) g_{2n}(t - \tau) d\tau; \quad (4.76)$$

$$g_n(t) = \sum_{k=1}^4 \operatorname{Res}_{\lambda_k} (\tilde{g}_n(\lambda) \exp(\lambda t)); \quad (4.77)$$

$$g_{2n}(t) = \sum_{k=1}^4 \operatorname{Res}_{\lambda_k} (\tilde{g}_{2n}(\lambda) \exp(\lambda t)),$$

where λ_k – the roots of equation

$$\Delta(\lambda) = 0. \quad (4.78)$$

In practically important cases μ_1' , μ_2 are small and the roots of equation (4.78) will be complex and pair-conjugate. Let us introduce designations for them

$$\lambda_1 = \alpha_1 + i\beta_1; \quad \lambda_2 = \alpha_2 + i\beta_2; \quad \lambda_3 = \bar{\lambda}_1; \quad \lambda_4 = \bar{\lambda}_2$$

(a bar symbol marks conjugate values).

Applying a residue theory and omitting intermediate transformations, we will get the following expressions for $q_n(t)$

$$\begin{aligned} q_n(t) & = A \sum_{k=1}^2 \left[g_{5k} \sin \gamma_n t + g_{6k} \cos \gamma_n t + \right. \\ & \left. + \exp(\alpha_k t) (g_{7k} \sin \beta_k t + g_{8k} \cos \beta_k t) \right], \quad 0 \leq t \leq \frac{l_0}{v}; \\ q_n(t) & = A \sum_{k=1}^2 \left\{ \exp \left(\alpha_k \left(t - \frac{l_0}{v} \right) \right) \left[G_{1k} \sin(\delta_{1k} + \beta_k t) + \right. \right. \\ & \left. \left. + G_{2k} \cos(\delta_{1k} - \beta_k t) + G_{3k} \sin(\delta_{2k} - \beta_k t) + G_{4k} \cos(\delta_{2k} - \beta_k t) \right] + \right. \\ & \left. + \exp(\alpha_k t) (g_{7k} \sin \beta_k t + g_{8k} \cos \beta_k t) \right\}, \quad t > \frac{l_0}{v}. \quad (4.79) \end{aligned}$$

Here

$$g_{5k} = -g_{5k}\alpha_k b_{1k} - g_{4k}(\beta_k b_{1k} - \gamma_n b_{2k});$$

$$g_{6k} = g_{5k}(\beta_k b_{2k} - \gamma_n b_{1k}) - g_{4k}\alpha_k b_{2k};$$

$$g_{7k} = g_{3k}\alpha_k b_{2k} + g_{4k}(\beta_k b_{2k} - \gamma_n b_{1k});$$

$$g_{8k} = g_{4k}\alpha_k b_{2k} - g_{3k}(\beta_k b_{2k} - \gamma_n b_{1k});$$

$$G_{1k} = -g_{5k}a_{1k} - g_{4k}d_{1k}; \quad G_{2k} = -g_{4k}a_{1k} - g_{5k}d_{1k};$$

$$G_{3k} = -g_{5k}a_{2k} - g_{4k}d_{2k}; \quad G_{4k} = -g_{4k}a_{2k} - g_{3k}d_{2k};$$

$$b_{1k} = \frac{1}{b_{3k}} + \frac{1}{b_{4k}}; \quad b_{2k} = \frac{1}{b_{4k}} + \frac{1}{b_{3k}};$$

$$b_{3k} = \alpha_k^2 + (\beta_k + \gamma_n)^2; \quad b_{4k} = \alpha_k^2 + (\beta_k - \gamma_n)^2;$$

$$a_{1k} = \frac{\alpha_k}{b_{3k}}; \quad a_{2k} = \frac{\alpha_k}{b_{4k}}; \quad d_{1k} = \frac{\beta_k + \gamma_n}{b_{3k}}; \quad d_{2k} = \frac{\beta_k - \gamma_n}{b_{4k}};$$

$$\delta_{1k} = \pi n + \beta_k \frac{l_0}{v}; \quad \delta_{2k} = -\pi n + \beta_k \frac{l_0}{v}.$$

Then, going back to (4.71), we will get a calculated expression for displacement $u(z, t)$:

$$u(z, t) = \sum_{n=1}^{\infty} q_n(t) \sin \frac{n\pi z}{l_0}. \quad (4.80)$$

If necessary, function $u_2(z, t)$ can be derived in a similar way.

Let us find now the roots λ_k , $k = 1, 2$ of equation (4.78), taking into consideration that for real materials μ' , $\mu_2 \ll 1$. Thus, for example, μ' for steel has the order 10^{-4} , for rubber $\mu_2 - 10^{-5}$. Based on this, the roots λ_k as a function of μ' , μ_2 can be found by an expansion in series in powers of μ' , μ_2 :

$$\lambda_k(\mu, \mu_2) = \lambda_k(0, 0) + \frac{\partial \lambda_k(0, 0)}{\partial \mu} \mu' + \frac{\partial \lambda_k(0, 0)}{\partial \mu_2} \mu_2 + \dots, \quad (4.81)$$

in this case, $\lambda_k(0, 0)$ is a root of equation

$$\lambda^4 + a_{20}\lambda^2 + a_0 = 0, \quad (4.82)$$

wherefrom

$$\lambda_k^2(0, 0) = 0.5 \left(-a_{20} + (-1)^k D^{1/2} \right); \quad (4.83)$$

$$D = \left[n_1^4 E_{11} + n_1^2 (T_{11} - T_{22}) + E_{21} - E_{22} \right]^2 + 4E_{21}E_{22} = D_1^2 + 4E_{21}E_{22};$$

$$D_1 = n_1^4 E_{11} + n_1^2 (T_{11} - T_{22}) + E_{21} - E_{22}.$$

Since parameters a_{20} and a_0 are positive under any values of constant D , then

$$\lambda_k^2(0, 0) < 0, \quad k = 1, 2,$$

then

$$\lambda_k^2(0, 0) < \frac{i}{\sqrt{2}} \left[a_{20} - (-1)^k D^{1/2} \right]^{1/2}. \quad (4.84)$$

Differentiating equation (4.78) successively in μ' and μ_2 , let us find:

$$\frac{\partial \lambda_k(0, 0)}{\partial \mu'} = \frac{1}{4} n_1^4 E_{11} \left[-1 + \frac{(-1)^k D_1}{D^{1/2}} \right]; \quad (4.85)$$

$$\frac{\partial \lambda_k(0, 0)}{\partial \mu_2} = -\frac{1}{4} (E_{21} + E_{22}) - \frac{D_1 (E_{22} - E_{21}) - 4E_{21}E_{22}}{4(-1)^k D^{1/2}}. \quad (4.86)$$

If we restrict to three terms of a series, then substituting (4.84)–(4.86) into the expansion (4.81) we will get the approximate values of roots λ_k . It is clear that

$$\beta_k = \left[0.5 \left(a_{20} - (-1)^k D^{1/2} \right) \right]^{1/2}; \quad (4.87)$$

$$\alpha_k = \frac{\partial \lambda_k(0, 0)}{\partial \mu} \mu' + \frac{\partial \lambda_k(0, 0)}{\partial \mu_2} \mu_2, \quad k = 1, 2.$$

It is of interest to evaluate the time span during which the vibration amplitude decreases to some specified value. Coefficients α_k depend on n and characterize the standing wave rate of decay, whose length is l_0/n . In fact, the i -fold decrease in the amplitude of such a wave will happen in the time span

$$t_i(n) = \max_{k=1,2} \frac{\ln l/i}{\alpha_k(n)} = \frac{\ln i}{\min_{k=1,2}(-\alpha_k(n))}. \quad (4.88)$$

Let us first find t_1 for long-length waves, i.e., let us assume that $n = 1, 2, \dots, n_2$ and, apart from that, the following correlation is fair

$$|\eta(n)(\eta(n) + 2E_0)| < 1, \quad (4.89)$$

where

$$\eta(n) = \frac{n_1^4 E_{11} + n_1^2 (T_{11} - T_{22})}{E_{21} + E_{22}}; \quad E_0 = \frac{E_{21} - E_{22}}{E_{21} + E_{22}}.$$

The inequality (4.89) is realized, for example, with the initial data

$$n_2 = 1; \quad l_0 = 50 \text{ m}; \quad T_{11}, T_{22} \leq 10^7 \text{ N}; \quad E_{21}, E_{22} \geq 10^5 \text{ Pa}; \quad E_{11} < 10^9 \text{ Pa}.$$

Transforming the values (4.85)–(4.86), we will get:

$$\frac{\partial \lambda_k(0, 0)}{\partial \mu'} = \frac{1}{4} n_1^4 E_{11} \left[-1 + (-1)^k \frac{\eta(n) + E_0}{[1 + 2E_0\eta(n) + \eta^2(n)]^{1/2}} \right]; \quad (4.90)$$

$$\frac{\partial \lambda_k(0, 0)}{\partial \mu_2} = -\frac{E_{21} + E_{22}}{4} \left[1 - \frac{E_0\eta(n) + 1}{(-1)^k [1 + 2E_0\eta(n) + \eta^2(n)]^{1/2}} \right]. \quad (4.91)$$

Expanding the right parts of equalities (4.90), (4.91) as series in powers of η and keeping the second-order terms inclusive, we get as follows:

$$\begin{aligned} \frac{\partial \lambda_k(0, 0)}{\partial \mu'} &= \frac{1}{4} n_1^4 E_{11} \left[-1 + (-1)^k (E_0 + \eta(n)(1 - E_0^2)\eta^2(n)) \right]; \\ \frac{\partial \lambda_k(0, 0)}{\partial \mu_2} &= \frac{E_{11} + E_{22}}{4} \left[-1 + (-1)^k \left(1 - \frac{1}{2}(1 - E_0^2)\eta^2(n) \right) \right]. \end{aligned} \quad (4.92)$$

The minimal value $-\alpha_k$ will be obviously at $k = 2$, i.e.,

$$\begin{aligned} \min_{k=1,2}(-\alpha_k) &= \frac{n_1^4 E_{11}}{4} (1 - E_0) [(1 + E_0)\eta(n) + \\ &+ (1 + E_0)E_0\eta^2(n) + 1] \mu' + \mu_2 \frac{E_{21} + E_{22}}{8} (1 - E_0)^2 \eta^2(n). \end{aligned} \quad (4.93)$$

Calculation example. Let us assume $E_{11} = 10^4 \text{ Pa}$, $E_{21} = 10^6 \text{ Pa}$, $E_{22} = 0.5 \times 10^6 \text{ Pa}$, $T_{11} = 10^6 \text{ N}$, $T_{22} = 0.5 \times 10^7 \text{ N}$, $l_0 = 50 \text{ m}$. Based on analysis $\eta(n)$, it follows that it is possible to take $n_2 = 10$ and $\eta(n) \approx -10^{-3}n^2$ for such parameter values. Then, the equality (4.81) will be simplified as follows

$$\begin{aligned} \min_{k=1,2}(-\alpha_k) &= 0.025n^4 (1 + 1.33 \times 10^{-3}n^2 + 0.66 \times 10^{-6}n^4) \mu' + \\ &+ 0.43n^4 \mu_2 \approx n^4 (0.025\mu' + 0.43\mu_2), \quad n \leq 10, \end{aligned}$$

and from (4.88), we will get the time of, for example, a ten-fold decrease in wave amplitude

$$t_{10}(n) = \frac{\ln 10}{\min_{k=1,2}(-\alpha_k)} = \frac{5.34}{n^4 (0.058\mu' + \mu_2)}, \quad n \leq 10. \quad (4.94)$$

It follows therefrom that if coefficients μ' , μ_2 have the order 10^{-3} , then the order $t_{10}(1)$ is equal to 10^3 s (17 min), and $t_{10}(10)$ has the order of 0.1 s. Consequently, after the load leaves the span, the span deflection decreases unevenly along the wave length: the shorter the wave is, the faster it fades. A quick fading of the longest waves, as follows from formula (4.94), cannot result only from the dissipative properties of the STL materials. Let us remind that these conclusions are only fair for those wave lengths (values n), where the inequality (4.89) is fair.

Let us now find $t_1(n)$ for large n , i.e., for very short waves. Let us assume that $n > n_3$ and the following inequality is realized

$$\frac{1 + 2E_0\eta(n_3)}{\eta^2(n_3)} < 1. \quad (4.95)$$

(For the data of the considered example, $n_3 = 112$).

Let us expand the right parts of equalities (4.90), (4.91) as series in powers of $\frac{1}{\eta(n)}$ and limit ourselves with the terms $\frac{1}{\eta^2}$.

$$\frac{\partial \lambda_k(0, 0)}{\partial \mu'} = \frac{1}{4} n^4 E_{11} \left[-1 + (-1)^k \left(1 - \frac{1}{2} (1 - E_0)^2 \frac{1}{\eta^2} \right) \right];$$

$$\frac{\partial \lambda_k(0, 0)}{\partial \mu_2} = \frac{E_{21} + E_{22}}{4} \left[1 + (-1)^k \left(E_0 + \frac{1}{\eta} (1 - E_0)^2 + \frac{3}{2} E_0 (E_0^2 - 1) \frac{1}{\eta^2} \right) \right],$$

$$n \geq 112.$$

It follows therefrom:

$$\begin{aligned} \min_{k=1,2}(-\alpha_k) &\approx \frac{E_{22}}{2} \left(\frac{l_0 E_{21}}{\pi_4 E_{11} n^4} \mu' + \mu_2 \right) = \\ &= 0.25 \times 10^6 \left(\frac{6.43 \times 10^6}{n^4} \mu' + \mu_2 \right), \quad n \geq 112. \end{aligned} \quad (4.96)$$

Particularly, for $n = 112$

$$\min_{k=1,2}(-\alpha_k) = 0.25 \times 10^6 (4.1 \times 10^{-2} \mu' + \mu_2). \quad (4.97)$$

Substituting (4.96), (4.97) into equality (4.88), we will get:

$$\begin{aligned} t_{10}(n) &= \frac{0.92 \times 10^{-5}}{\frac{6.43 \times 10^6}{n^4} \mu' + \mu_2}; \quad t_{10}(112) = \frac{0.92 \times 10^{-5}}{4.1 \times 10^{-2} \mu' + \mu_2}, \\ &n \geq 112. \end{aligned} \quad (4.98)$$

It follows therefrom that the time of a ten-fold decrease in wave amplitude with length l_0/n , $n \geq 112$ has the order 0.01 s, if the order of coefficients μ' , μ_2 is 10^{-5} . Based on equalities (3.31) and (3.27) it also follows that with identical values μ' , μ_2 , the contribution to damping of waves of the STL body material is by 17 times less for a large length and by $24 \times \left(\frac{112}{n}\right)^{-4}$ times less for the length l_0/n , $n \geq 112$, compared to the filler working in compression-tensioning between the strings. Consequently, supposing that $\mu_2 = 0$, and $\mu' \neq 0$ (the filler does

not dissipate energy at compression-tensioning), short waves (n is large) will subside rather slowly, that is the STL will sound for a long time. In this regard, it is crucial to choose a filler with good damping properties.

4.3.2. Load flow at STL with a split body

Setting up and solving a problem. Assuming that equal concentrated loads P move at a constant speed v at equidistance l' from each other on the string transport line, considered in clause 4.3.1. The STL was in a balanced state before the load started to move. If damping coefficients μ' and μ_2 differ from zero, then the STL natural oscillations are damped and, consequently, the line movement will be stationary in some time. Let us describe a stationary mode of the STL forced oscillations.

The span motion equations are written as follows:

$$EI \frac{\partial^4 u}{\partial z^4} + \mu' EI \frac{\partial^5 u}{\partial t \partial z^4} + \rho_s \frac{\partial^2 u}{\partial t^2} - T_1 \frac{\partial^2 u}{\partial z^2} + E_2 \left(1 + \mu_2 \frac{\partial}{\partial t} \right) (u - u_2) = f(z, t); \quad (4.99)$$

$$\rho_2 \frac{\partial^2 u_2}{\partial t^2} - T_1 \frac{\partial^2 u_2}{\partial z^2} + E_2 \left(1 + \mu' \frac{\partial}{\partial t} \right) (u_2 - u) = 0.$$

Since $l' \geq l_0$, the length of load movement on the span $t_1 = l_0/v$ is less than time interval $t_2 = l'/v$ between the neighbouring loads. Consequently, within the time period $2t_3$ ($t_3 = 0.5(t_2 - t_1)$), there is no load on the span. For the convenience of further calculations, let us assume that the first load appears on the span at time moment $t = t_3$. Then, its impact is described by the function

$$f(z, t) = P\delta(z - v(t - t_3))\sigma(t_3, t_1 + t_3). \quad (4.100)$$

In a time moment $2t_3$ after the first load leaves the span, the second load appears on the span, i.e., the load impact on the span is repeated with the period t_2 . Consequently, in order to describe the impact of load flow on the span, it is required to write down the expression below for the function $f(z, t)$ instead of the formula (4.100)

$$f(z, t) = \begin{cases} P\delta(z - v(t - t_3))\sigma(t_3, t_1 + t_3), & 0 \leq t \leq t_2; \\ f(z, t + t_2) = f(z, t). \end{cases} \quad (4.101)$$

By analogy with the previous section, let us find the solution to the system (4.99) in the form (4.71). Then, the functions $q_n(t)$, $q_{2n}(t)$ will be found based on the following equations

$$q_n'' + (n_1^4 E_{11} \mu_1' + E_{21} \mu_2) q_n' - E_{21} \mu_2 q_{2n}' + (n_1^4 E_{11} + n_1^2 T_{11} + E_{21}) q_n - E_{21} q_{2n} = A \varphi_n(t); \quad (4.102)$$

$$q_{2n}'' + E_{22} \mu_2 q_{2n}' - E_{22} \mu_2 q_n' + (n_1^2 T_{22} + E_{22}) q_{2n} - E_{22} q_n = 0,$$

where

$$\varphi_n(t) = \begin{cases} \sin \frac{n\pi v}{l_0} (t - t_3) \sigma(t_3, t_1 + t_3), & 0 \leq t \leq t_2; \\ \varphi_n(t + t_2) = \varphi_n(t + t_2) = \varphi_n(t). \end{cases} \quad (4.103)$$

With n being odd-numbered $\varphi_n(t)$ (4.103) is an even function, and with an even-numbered n – it is odd-numbered. Then, $\varphi_n(t)$ can be approximated in series

$$\varphi_n(t) = \frac{1}{2} A_{n0} + \sum_{k=1}^{\infty} A_{nk} \cos \varepsilon_k t, \quad t \geq 0, n - \text{odd-numbered}; \quad (4.104)$$

$$\varphi_n(t) = \sum_{k=1}^{\infty} S_{nk} \cos \varepsilon_k t, \quad t \geq 0, n - \text{even-numbered}, \quad (4.105)$$

where

$$A_{nk} = \frac{2}{t^2} \int_{t^3}^{t_1+t_3} \sin \gamma_n (t - t_3) \cos \varepsilon_k t dt, \quad n - \text{odd-numbered}, k = 0, 1, \dots; \quad (4.106)$$

$$S_{nk} = \frac{2}{t^2} \int_{t^3}^{t_1+t_3} \sin \gamma_n (t - t_3) \sin \varepsilon_k t dt, \quad n - \text{even-numbered}, k = 1, 2, \dots; \quad (4.107)$$

$$\gamma_n = \frac{n\pi v}{l_0}; \quad \varepsilon_k = \frac{k\pi}{t^2} = \alpha \gamma_k; \quad \alpha = \frac{l_0}{l}.$$

Evaluating the integrals (4.106), (4.107), we will find the coefficients of series $A_{n0} = \frac{4\alpha}{\pi n}$:

$$A_{nk} = \begin{cases} 0, & k - \text{odd-numbered}; \\ \frac{4\alpha}{\pi} n (-1)^{k/2} \cos \frac{k\pi\alpha}{2}, & k - \text{even-numbered}, n - \text{odd-numbered}; \\ \frac{4\alpha}{\pi} n (-1)^{k/2+1} \sin \frac{k\pi\alpha}{2}, & k, n - \text{even-numbered}. \end{cases}$$

$$S_{nk} = \begin{cases} 0, & k - \text{odd-numbered}; \\ \frac{4\alpha}{\pi} n (-1)^{k/2+1} \sin \frac{k\pi\alpha}{2}, & k, n - \text{even-numbered}. \end{cases}$$

Let us point out that at $\alpha = 1$ we have:

$$A_{nk} = \frac{4n}{n^2 - k^2}; \quad S_{nk} = \begin{cases} 0, & n \neq k; \\ 1, & n = k. \end{cases}$$

The system (4.103) can be solved using the Laplace transformation. Taking into consideration zero initial conditions, we will get:

$$\tilde{q}(\lambda) = A \tilde{\varphi}_n(\lambda) D_n(\lambda), \quad (4.108)$$

where

$$D_n(\lambda) = \frac{\lambda^2 + n_1^2 T_{22} + E_{22} (1 + \mu_2 \lambda)}{\Delta_n(\lambda)}; \quad (4.109)$$

$$\tilde{\varphi}_n(\lambda) = \begin{cases} \frac{A_{n0}}{2\lambda} + \sum_{k=2}^{\infty} A_{nk} \frac{\lambda}{\lambda^2 + \varepsilon_k^2}, & n - \text{odd-numbered}, k - \text{even-numbered}; \\ \sum_{k=2}^{\infty} S_{nk} \frac{\varepsilon_k}{\lambda^2 + \varepsilon_k^2}, & k, n - \text{even-numbered}. \end{cases} \quad (4.110)$$

Since we are interested in the steady state motion of the span, when finding $q_n(t)$ based on equality (4.108), it is necessary to take into account only the poles of function $\varphi_n(\lambda)$. Applying the inverse Laplace transformation to equality (4.108), let us find:

$$q_n(t) = \begin{cases} \frac{A_{n0} D_n(0)}{\eta} + \sum_{k=2}^{\infty} A_{nk} [\operatorname{Re} D_n(i\varepsilon_k) \cos \varepsilon_k t + \operatorname{Im} D_n(i\varepsilon_k) \sin \varepsilon_k t], & n - \text{odd-numbered}, k - \text{even-numbered}; \\ \sum_{k=2}^{\infty} S_{nk} [\operatorname{Re} D_n(i\varepsilon_k) \sin \varepsilon_k t + \operatorname{Im} D_n(i\varepsilon_k) \cos \varepsilon_k t] A_{nk}, & k, n - \text{even-numbered}. \end{cases} \quad (4.111)$$

Here

$$\operatorname{Re} D_n(i\varepsilon_k) = \frac{R_{1n} R_n - J_{1n} J_n}{R_n^2 + J_n^2}; \quad \operatorname{Im} D_n(i\varepsilon_k) = \frac{J_{1n} R_n + J_n R_{1n}}{R_n^2 + J_n^2};$$

$$R_{1n} = n_1^2 T_{22} + E_{22} - \varepsilon_k^2; \quad J_{1n} = E_{22} \mu_2;$$

$$R_n = \varepsilon_k^4 - a_2 \varepsilon_k^2 + a_0; \quad J_n = (a_1 - a_5 \varepsilon_k^2) \varepsilon_k.$$

Substituting the function (4.111) into the expansion (4.71), we will get the span deflection under the impact of load flow.

Let us present the dynamic deflection $u(z, t)$ in the form of a sum

$$u(z, t) = u_0(z) + u_{osc}(z, t), \quad (4.112)$$

where a stationary component of the deflection is written as follows:

$$u_0(z) = \frac{4P}{\pi l \rho_s} \sum_{n=1}^{\infty} \frac{D_n(0)}{n} \sin \frac{n\pi z}{l_0}, \quad n - \text{odd-numbered}. \quad (4.113)$$

Thus, function $u_0(z)$ assumes a span form invariable with time; its oscillations under the impact of load flow movement happen in relation to this form. The oscillations are described by an oscillating term $u_{osc}(z, t)$.

Based on equality (4.113), it follows that the value of the stationary component of deflection at any point of the span is proportional to the relation P/l (average load density on the STL) and does not depend on the value of load movement speed. It is easy to see that the function graph $u_0(z)$ is symmetrical in relation to the vertical straight line passing through the midspan. This means that $u_0(z)$ does not depend on the direction of load movement, either.

The maximal value of the span $u_0^{\max}(z)$ is reached in the midspan:

$$u_0^{\max} = \frac{4P}{\pi l \rho_s} \sum_{n=1}^{\infty} \frac{D_n(0)}{n} (-1)^{[n/2]}, \quad n - \text{odd-numbered}. \quad (4.114)$$

In order to simplify further analysis, let us assume that the lower string is secured with the STL body, which is equal to very high rigidity of the filler. After a passage to the limit in equality (4.113) at $E_2 \rightarrow \infty$, we get:

$$u_0(z) = \frac{4P}{\pi l} \sum_{n=1}^{\infty} \frac{\sin \frac{n\pi z}{l_0}}{n \left(\frac{n\pi}{l_0} \right)^{1/2} \left[EI \left(\frac{n\pi}{l_0} \right)^2 + T \right]}, \quad n - \text{odd-numbered}, \quad (4.115)$$

where

$$T = T_1 + T_2.$$

The function (4.115) can be understood as a static deflection of the span under the impact of distributed load with density $f_0(z)$. Since $u_0(z)$ satisfies the equation

$$EI \frac{d^4 u_0}{dz^4} - T \frac{d^2 u_0}{dz^2} = f_0 \quad (4.116)$$

with the conditions

$$u(0) = \frac{d^2 u(0)}{dz^2} = u(l_0) = \frac{d^2 u(l_0)}{dz^2}, \quad (4.117)$$

then

$$f_0(z) = \frac{4P}{\pi l} = \sum_{n=1}^{\infty} \frac{1}{n} \sin \frac{n\pi z}{l_0}, \quad n - \text{odd-numbered}. \quad (4.118)$$

The expression (4.118) will be simplified, if it is taken into consideration that the expansion of the identity in series in sine at the interval $[0, l_0]$ is as follows:

$$1 = \frac{4}{\pi} \sum_{n=1}^{\infty} \frac{1}{n} \sin \frac{n\pi z}{l_0}, \quad n - \text{odd-numbered}.$$

Then $f_0(z) = P/l$, i.e., $u_0(z)$ – a static deflection of the span caused by an evenly distributed load with density P/l . Now that we know f_0 , it is possible to solve a problem (4.116), (4.117), find $u_0(z)$ and sum up the series (4.115).

Let us find approximately u_0^{\max} based on (4.115) limiting ourselves to only the first term due to a rapid convergence of this series.

$$u_0^{\max} = \frac{4P}{\pi l \left(\frac{\pi}{l_0}\right)^2 \left[EI \left(\frac{\pi}{l_0}\right)^2 + T \right]}. \quad (4.119)$$

For example, if we take $l' = l_0$, $l_0 = 100$ m, $P = 10^4$ N, $T = 10^7$ N, $EI = 10^5$ N · m², then $u_0^{\max} \sim 0.13$ m. The main feature of oscillating systems is resonant parameters. In order to determine resonant motion modes, it is sufficient to find the conditions where the vibration amplitude of the function $q_n(t)$ reaches the maximal value at μ' , μ_2 and becomes infinite for μ' , $\mu_2 = 0$.

It is known that resonant frequencies at low damping differ insignificantly from resonant frequencies at zero damping; therefore, let us assume that $\mu' = \mu_2 = 0$ to simplify the calculations. Then,

$$\text{Im } D_n(i\varepsilon_k) = 0; \quad \text{Re } D_n(i\varepsilon_k) = \frac{n_1^2 T_{22} + E_{22} - \varepsilon_k^2}{\varepsilon_k^4 - a_{20} \varepsilon_k^2 + a_0}$$

and the necessary resonance condition will be the following

$$\varepsilon_k^4 - a_{20} \varepsilon_k^2 + a_0 = 0. \quad (4.120)$$

Therefrom we get:

$$\varepsilon_k^2 = \frac{1}{2} \left(a_{20} + (a_{20}^2 - 4a_0)^{1/2} \right),$$

or

$$\left(\frac{v}{l} \right)^2 = \frac{1}{2k^2 \pi^2} (a_{20} + D^{1/2}). \quad (4.121)$$

Here the indices k, n take on values where $A_{nk} \neq 0$, $S_{nk} \neq 0$.

Let us study the condition (4.121) in more detail for the case

$$\frac{n_1^4 E_{11} + n_1^2 (T_{11} + T_{22})}{E_{21} + E_{22}} < 1. \quad (4.122)$$

Since $n_1 = \frac{n\pi}{l_0}$, the condition (4.122) will be realized for $n = 1, n_4$, when E_2 is big enough, i.e., the filler rigidity prevails above the body rigidity and the total tension of strings for long-length waves. Then, instead of (4.121) we will approximately get:

$$\frac{v}{l_2} = \frac{(E_{21} + E_{22})^{1/2}}{k\pi}, \quad (4.123)$$

or

$$\left(\frac{v}{l_2} \right)^2 = \frac{1}{2k^2 \pi^2} [n_1^4 E_{11} + n_1^2 (T_{11} + T_{22})]. \quad (4.124)$$

The correlation (4.124) gives a resonant oscillating mode of the span with strings as a whole, without regard to the filler compression – tension, and (4.123) – a resonance condition of the body with an upper string and of a lower string in counter oscillations due to filler deformation. Since the amplitude of counter oscillations cannot increase without limit (a lower string cannot go beyond the body limit), the condition (4.123) can be excluded from consideration.

Thus, the resonance condition for waves length l_0/n ($n \leq n_4$), when meeting the inequality (4.122), is the equality (4.124), which can be written as follows:

$$v = \frac{nl'}{kl_0} = \left(\frac{n^2 \pi^2 E_1 / l_0 + T_1 + T_2}{\rho_1 + \rho_2} \right)^{1/2}. \quad (4.125)$$

Let us assume now that the following inequality is satisfied

$$\frac{E_{11} + E_{22}}{n_1^4 E_{11} + n_1^2 (T_{11} + T_{22})} < 1, \quad n \geq n_5, \quad (4.126)$$

when the rigidity of the STL body and string tensioning prevail above the filler rigidity for waves length l_0/n , $n \geq n_5$. Then, based on equality (4.121) we will approximately get

$$v = \frac{nl'}{kl_0} T_{22}^{1/2}, \quad (4.127)$$

or

$$v = \frac{nl}{kl_0} \left[\left(\frac{n\pi}{l_0} \right)^2 E_{11} + T_{11} \right]^{1/2}, \quad n \geq n_5. \quad (4.128)$$

It is easy to make sure that (4.127) is a resonance condition in case of deviations of the body and lower string of the same sign. Consequently, both conditions (4.127) and (4.128) give resonance modes for short waves when realizing the inequality (4.126). Let us remind that in the conditions (4.121), (4.127), (4.128), the values k, n take on the values where A_{nk}, S_{nk} differ from zero.

Let us point out that we get particular cases of resonance for a flexible STL considered in clause 4.2.3 based on the obtained resonance conditions at the corresponding assumptions.

4.3.3. Load flow at the STL with a split body at l_0 divisible by l

Since the span length l_0 is divisible by the distance between loads l'

$$l_0 = sl',$$

where s – the amount of simultaneous loads on the span. Providing that one of the loads is above the support at the initial time, the impact of the loads flow on the span is determined by the following function

$$f(z, t) = P \sum_{i=1}^s \delta[z - v(t + (i-1)t_2)], \quad t \in [0; t_2];$$

$$f(z, t + t_2) = f(z, t). \quad (4.129)$$

Here

$$t_1 = \frac{l_0}{v}; \quad t_2 = \frac{l}{v} = \frac{t_1}{s}.$$

By analogy with clause 4.3.2, let us present the solution to the system (4.99) in the form of (4.71) deriving the system (4.102), where

$$\varphi_n(t) = \sum_{i=1}^s \sin \gamma_n [t + (i-1)t_2], \quad t \in [0; t_2]. \quad (4.130)$$

It is easy to make sure that $\varphi_n(t)$ at odd-numbered n is an even-numbered function, whereas at even-numbered n – it is odd-numbered for any $s = 1, 2, \dots$. In addition, at even-numbered n $\varphi_n(t) = 0$ for even-numbered s .

Then, at $t \geq 0$

$$\varphi_n(t) = \frac{1}{2} A_{n0}(s) + \sum_{k=1}^{\infty} A_{nk}(s) \cos \varepsilon_k t, \quad n - \text{odd-numbered};$$

$$\varphi_n(t) = \begin{cases} \sum_{k=1}^{\infty} S_{nk}(s) \sin \varepsilon_k t, & n - \text{even-numbered}, s - \text{odd-numbered}; \\ 0, & n, s - \text{even-numbered}. \end{cases} \quad (4.131)$$

Here

$$A_{nk}(s) = \frac{2}{t_2} \sum_{i=1}^s \int_0^{t_2} \sin \gamma_n (t + (i-1)t_2) \cos \varepsilon_k t dt, \quad n - \text{odd-numbered},$$

$$k = 0, 1, 2, \dots; \quad (4.132)$$

$$S_{nk}(s) = \frac{2}{t_2} \sum_{i=1}^s \int_0^{t_2} \sin \gamma_n (t + (i-1)t_2) \cos \varepsilon_k t dt, \quad n - \text{even-numbered},$$

$$k = 0, 1, 2, \dots$$

Evaluating the integrals (4.132), we will get as follows:

$$A_{nk}(s) = \begin{cases} 0, & k - \text{odd-numbered}; \\ \frac{4sn}{\pi(n^2 - s^2k^2)}, & k - \text{even-numbered}, n - \text{odd-numbered}; \end{cases} \quad (4.133)$$

$$S_{nk}(s) = \begin{cases} 0, & k - \text{odd-numbered}; \\ 0, & k - \text{even-numbered}, ks \neq n; \\ s, & k - \text{even-numbered}, ks = n. \end{cases}$$

Thus, in order to get a steady state motion mode, it is enough to substitute the values (4.133) into the formulae (4.111) and (4.71). The resonance conditions for the case under consideration coincide with the conditions (4.121), (4.125), (4.127), (4.128), where α should be replaced with s and n should be considered odd-numbered or equal to ks .

4.3.4. Load flow at an infinite unsplit STL at l_0 divisible by l'

Setting up and solving a problem in the general case. Let us suppose that the load flow moves on an infinite STL with a solid unsplit body freely supported on non-deformable columns. Let us assume the casing of a lower string to be rigidly secured to the STL body above the supports, and the distance between loads $l' = l_0/s$, where s is a whole number.

Let us consider the STL sustained forced vibrations under the impact of moving loads. The period of vibration is obviously determined by the relation of motion speed and span length

$$t_2 = \frac{l'}{v} = \frac{l_0}{sv} = \frac{t_1}{s}.$$

Let us divide the line into the sections with the length l_0 . It is easy to see that these sections are in equal dynamic conditions. Consequently, the STL dynamic deflection is a z -periodic function with the period l_0 . Based on this, the functions $u(z, t)$, $u_2(z, t)$ can be written as an infinite exponential series:

$$u(z, t) = \sum_{k, n=-\infty}^{\infty} U_{nk} \exp\left[2\pi i \left(k \frac{t}{t_k} + n \frac{z}{l_0}\right)\right]; \quad (4.134)$$

$$u_2(z, t) = \sum_{k, n=-\infty}^{\infty} S_{nk} \exp\left[2\pi i \left(k \frac{t}{t_k} + n \frac{z}{l_0}\right)\right]. \quad (4.135)$$

Then, the load impact on and the reaction of support to the STL body and a lower string at the specified section are determined by the following functions

$$f(z, t) = R(t)\delta(z) + P \sum_{j=1}^s \delta\left[z - v\left(t - \frac{t_1 + t_2}{2} + jt_2\right)\right]; \quad (4.136)$$

$$f_2(z, t) = R_2(t)\delta(z), \quad z \in \left[-\frac{l_0}{2}; \frac{l_0}{2}\right], \quad t \in \left[-\frac{t_2}{2}; \frac{t_2}{2}\right], \quad (4.137)$$

where $R(t)$, $R_2(t)$ is a reaction of support to the STL body and a lower string, correspondingly.

Since $f(z, t)$, $f_2(z, t)$ are periodic functions, the series expansion will be similar to the expressions for the deflection (4.134) and (4.135)

$$f(z, t) = \sum_{k, n=-\infty}^{\infty} f_{nk} \exp\left[2\pi i \left(k \frac{t}{t_2} + n \frac{z}{l_0}\right)\right]; \quad (4.138)$$

$$f_2(z, t) = \sum_{k, n=-\infty}^{\infty} C_{nk} \exp\left[2\pi i \left(k \frac{t}{t_2} + n \frac{z}{l_0}\right)\right], \quad (4.139)$$

where

$$f_{nk} = \frac{1}{l_0 t_2} \int_{-t_2/2}^{t_2/2} \exp\left(-2\pi i k \frac{t}{t_2}\right) dt \int_{-l_0/2}^{l_0/2} f(z, t) \exp\left(-2\pi i n \frac{z}{l_0}\right) dz; \quad (4.140)$$

$$C_{nk} = \frac{1}{l_0 t_2} \int_{-t_2/2}^{t_2/2} \exp\left(-2\pi i k \frac{t}{t_2}\right) dt \int_{-l_0/2}^{l_0/2} f_2(z, t) \exp\left(-2\pi i n \frac{z}{l_0}\right) dz. \quad (4.141)$$

The functions $u(z, t)$, $u_2(z, t)$ shall satisfy the equations

$$\begin{aligned} E_{11} \frac{\partial^4 u}{\partial z^4} + \mu' E_{11} \frac{\partial^5 u}{\partial t \partial z^4} + \frac{\partial^2 u}{\partial t^2} - T_{11} \frac{\partial^2 u}{\partial z^2} + \\ + E_{21} \left(1 + \mu_2 \frac{\partial}{\partial t}\right) (u - u_2) = \frac{1}{\rho} f(z, t); \end{aligned} \quad (4.142)$$

$$\frac{\partial^2 u_2}{\partial t^2} - T_{22} \frac{\partial^2 u_2}{\partial z^2} + E_{22} \left(1 + \mu_2 \frac{\partial}{\partial t}\right) (u_2 - u) = \frac{1}{\rho_2} f_2(z, t).$$

Substituting approximations (4.134), (4.135) and (4.138), (4.139) into motion equations of the body and lower string (4.142) with regard to boundary conditions on rigid supports

$$u(0, t) = 0; \quad u_2(0, t) = 0 \quad (4.143)$$

unknown coefficients v_{nk} , S_{nk} и f_{nk} , C_{nk} are determined (let us omit the summary of transformations due to cumbersome intermediate expressions).

In order to determine a dynamic deflection of the STL section, we only need to single out a real part of the function $u(z, t)$, which is the end of problem solving. The formulae giving $\text{Re}u(z, t)$ are cumbersome; therefore, we do not write them here.

Let us note that the problem for an infinite STL on elastic supports where a load flow moves at $l' > l_0$ can be solved in the specified way.

In order to receive some qualitative results, let us simplify the problem and assume that the material for the STL filler is non-deformable (E_2 is infinitely large) or (which is the same) that a lower string is fixed to the STL body. The solution to this problem can be derived from the provided solution via a passage to the limit at $E_2 \rightarrow \infty$. However, a successive solution to the simplified problem is more obvious.

The STL motion in this case is described by the equation

$$EI \frac{\partial^4}{\partial z^4} \left(1 + \mu' \frac{\partial}{\partial t}\right) u + \rho_s \frac{\partial^2 u}{\partial t^2} - T \frac{\partial^2 u}{\partial z^2} = f(z, t), \quad (4.144)$$

where the functions $u(z, t)$, $f(z, t)$ take the form (4.134) and (4.138). After substituting these functions into the equation (4.144), we will get:

$$\begin{aligned} R_0 + Ps &= 0; \\ l_0 U_{nk} \Delta_{nk} &= R_k + P\varphi_{nk}; \quad |n| + |k| \neq 0, \end{aligned} \quad (4.145)$$

where

$$\begin{aligned} \Delta_{nk} &= \operatorname{Re} \Delta_{nk} + i \operatorname{Im} \Delta_{nk}; \\ \operatorname{Re} \Delta_{nk} &= EIn_6^4 - \rho_s k_6^2 + Tn_6^2; \\ \mu' EIn_6^4 k_6 &= \operatorname{Im} \Delta_{nk}. \end{aligned}$$

Based on the condition of equality to zero of the STL deflection above the support, we get the following:

$$\sum_{n=-\infty}^{\infty} U_{nk} = 0, \quad k = 0, \pm 1, \pm 2, \dots \quad (4.146)$$

Based on equations (4.145), (4.146), let us define the coefficients U_{nk} , R_k and single out a real part of the function $u(z, t)$. Omitting intermediate calculations, let us write down an STL dynamic deflection as follows:

$$\begin{aligned} u(z, t) &= U_{00} + \frac{1}{l_0} \sum_{k=-\infty}^{\infty} \left[\operatorname{Re} R_k \sum_{n=-\infty}^{\infty} (A_{nk} \cos \beta_{nk} + B_{nk} \sin \beta_{nk}) \right] = \\ &= \operatorname{Im} R_k \sum_{k=-\infty}^{\infty} (B_{nk} \cos \beta_{nk} - A_{nk} \sin \beta_{nk}) + \\ &+ P \sum_{k=-\infty}^{\infty} \varphi_{nk} (A_{nk} \cos \beta_{nk} + B_{nk} \sin \beta_{nk}), \quad |n| + |k| \neq 0. \end{aligned} \quad (4.147)$$

Here

$$A_{nk} = \frac{\operatorname{Re} \Delta_{nk}}{|\Delta_{nk}|^2}; \quad B_{nk} = \frac{\operatorname{Im} \Delta_{nk}}{|\Delta_{nk}|^2}; \quad \beta_{nk} = n_6 z + k_6 t;$$

$$|\Delta_{nk}|^2 = (\operatorname{Re} \Delta_{nk})^2 + (\operatorname{Im} \Delta_{nk})^2;$$

$$\operatorname{Re} R_k = -P \frac{A_k C_k + B_k D_k}{A_k^2 + B_k^2}; \quad \operatorname{Im} R_k = -P \frac{A_k D_k - B_k C_k}{A_k^2 + B_k^2};$$

$$A_k = \sum_{j=-\infty}^{\infty} A_{jk}; \quad B_k = \sum_{j=-\infty}^{\infty} B_{jk};$$

$$C_k = \frac{s(-1)^{(1-s)k} \operatorname{Re} \Delta_{-ks, k}}{|\Delta_{-ks, k}|^2}; \quad D_k = \frac{s(-1)^{(1-s)k} \operatorname{Im} \Delta_{-ks, k}}{|\Delta_{-ks, k}|^2};$$

$$\operatorname{Re} R_0 = -Ps; \quad \operatorname{Im} R_0 = 0; \quad U_{00} = \frac{P}{l} A_0; \quad A_0 = \sum_{j=-\infty}^{\infty} \frac{1}{\operatorname{Re} \Delta_{j0}};$$

$$\varphi_{nk} = \begin{cases} s(-1)^{(1-s)k}, & n = -ks; \\ 0, & n \neq -ks. \end{cases}$$

A dynamic deflection (4.147) can be written as a sum of stationary and oscillating components

$$u(z, t) = u_0(z) + u_{osc}(z, t),$$

where

$$u_0(z) = \frac{Ps}{l_0} \sum_{n=-\infty}^{\infty} \frac{1 - \cos \beta_{n0}}{\operatorname{Re} \Delta_{n0}} = \frac{2P}{l} \sum_{n=1}^{\infty} \frac{1 - \cos n_6 z}{EIn_6^4 + Tn_6^2}. \quad (4.148)$$

Based on this presentation, it follows that oscillations of the STL span take place in relation to some stationary deflection $u(z, t)$ other than a horizontal one. In virtue of equation (4.148), the value of this deflection in each point of the span is proportional to the amount of simultaneous loads on the span per unit length of the span. Let us conduct a more detailed analysis of the function $u_0(z)$.

It is easy to make sure that the deflection $u_0(z)$ is symmetrical in relation to the vertical straight line passing through the midspan. This follows from the fact that the graph of each term of series (4.148) possesses the specified feature.

Consequently, a stationary component of the dynamic deflection does not depend on the direction and the load motion speed.

The function $u_0(z)$ can be interpreted as a static deflection of the span caused by distributed load with some density $f_0(z)$. Let us find now this density at $z \in [0; l_0/2]$, i.e., for a half-span. Since

$$f_0(z) = EI \frac{d^4 u_0}{dz^4} - T \frac{d^2 u_0}{dz^2},$$

then

$$f_0(z) = -\frac{2Ps}{l_0} \sum_{n=1}^{\infty} \cos \frac{2\pi n z}{l_0}. \quad (4.149)$$

Taking into consideration that the series expansion of function $\delta(z)$ in cosine on the $[0; l_0/2]$ interval takes the form

$$\delta(z) = \frac{2}{l_0} + \frac{4}{l_0} \sum_{n=1}^{\infty} \cos \frac{2\pi n z}{l_0},$$

we will get:

$$\sum_{n=1}^{\infty} \cos \frac{2\pi n z}{l_0} = \frac{l_0}{4} \delta(z) - \frac{1}{2}.$$

Substituting this series in the equality (4.149), we will derive

$$f_0(z) = \frac{Ps}{l_0} - \frac{Ps}{2} \delta(z), \quad z \in [0; l_0/2].$$

It is easy to see that when considering the $[-l_0/2; 0]$ interval, we will get the same result. Consequently,

$$f_0(z) = \frac{Ps}{l_0} - Ps \delta(z), \quad z \in [-l_0/2; l_0/2]. \quad (4.150)$$

Since $-Ps\delta(z) = R_0\delta(z)$ is a reaction of support in point $z = 0$, it follows from the equality (4.150) that the function $u_0(z)$ gives a static deflection of the span caused by evenly distributed load, which is equal to the total amount of simultaneous concentrated loads on the span.

It can be concluded from the above that $u_0(z)$ on the $[0; l_0]$ interval is the solution to the equation

$$EI \frac{d^4 u_0}{dz^4} - T \frac{d^2 u_0}{dz^2} = \frac{Ps}{l_0} \quad (4.151)$$

under the conditions

$$u_0(0) = \frac{du_0(0)}{dz} = \frac{u_0(l_0)}{dz} = 0, \quad (4.152)$$

and this solution is the sum of the series (4.148).

Let us find the maximal value of a stationary component for the deflection u_0^{\max} . Since

$$u_0^{\max} = u_0\left(\frac{l_0}{2}\right),$$

then

$$u_0^{\max} = \frac{2Ps}{l_0} \sum_{n=1}^{\infty} \frac{1 - (-1)^n}{EI n^4 + T n^2}. \quad (4.153)$$

Since (4.153) only has terms with odd-numbered values n and the series converges quickly, then it is possible to limit ourselves to only the first term of the series in order to find the approximate value u_0^{\max} . Then

$$u_0^{\max} = \frac{Pl_0^2}{\pi^2 l' \left[EI \left(\frac{2\pi}{l_0} \right)^2 + T \right]}. \quad (4.154)$$

The exact value u_0^{\max} can be found upon solving the problem (4.151), (4.152).

Let us compare the values u_0^{\max} determined by the equalities (4.154) and (4.119), in two particular cases: 1) rigidity parameter EI is very small and string tensioning T prevails above the STL body rigidity; 2) effort T is very small, i.e., the body rigidity prevails above string tensioning. It is easy to see that in the first case u_0^{\max} for an unsplit STL is by $\frac{4}{\pi}$ times and in the second case – by $\frac{16}{\pi}$ times less than u_0^{\max} for an STL with a split body.

4.4. Numerical study of STL span dynamic deflection

The main results of the research carried out in the previous section consists in deriving the formulae to determine a dynamic deflection of the STL span. However, these formulae are rather cumbersome and it is rather problematic to carry out their analysis without simplifying assumptions. Therefore, there were made ECM numerical calculations and built the graphs to determine the span form at different time moments and the movement of separate points of the span under different loading conditions and STL design parameters. The following formulae were used for calculations: (4.80) (single load at STL with a split body), (4.71), (4.111) (load flow at STL with a split body) and (4.161) (load flow at an unsplit STL). Due to a fast series convergence, the first 20 terms were taken into consideration when summing up in the formulae (4.80), (4.111); and in the formula (4.147) – the first 40 terms, which appeared to be enough to provide the required accuracy of calculation. The following parameters remained unchanged in all calculations:

$$P = 10^4 \text{ N}; \quad E_2 = 10^8 \text{ N/m}^2; \quad \mu' = 1.2 \times 10^{-5} \text{ s}; \quad \mu_2 = 10^{-5} \text{ s};$$

$$\rho_s = 20 \text{ kg/m}; \quad \rho_2 = 21 \text{ kg/m}; \quad T_1 = 10^6 \text{ N}; \quad T_2 = 5 \times 10^6 \text{ N}.$$

When studying a load flow, it was assumed that the distance between the neighboring loads is equal to the span length, i.e., $l' = l_0$. Besides, the strings of an unsplit STL were assumed to be fixed to the body, which is the same as an assumption concerning the filler non-deformity. Parameter values prone to variation when carrying out the calculations are pointed out in every specific case.

4.4.1. Dependence of a dynamic deflection on span length

Figures 4.8–4.16 show the STL span shape at the successive time moments with the rigidity parameter $EI = 10^6 \text{ N}\cdot\text{m}^2$, speed $v = 50 \text{ m/s}$ and span length $l_0 = 25, 35, 50 \text{ m}$:

$$t_k = \frac{l_0}{4v} k, \quad k = \overline{1, 5}.$$

The scale dimension 0Z for these and further figures is 1 cm per one division.

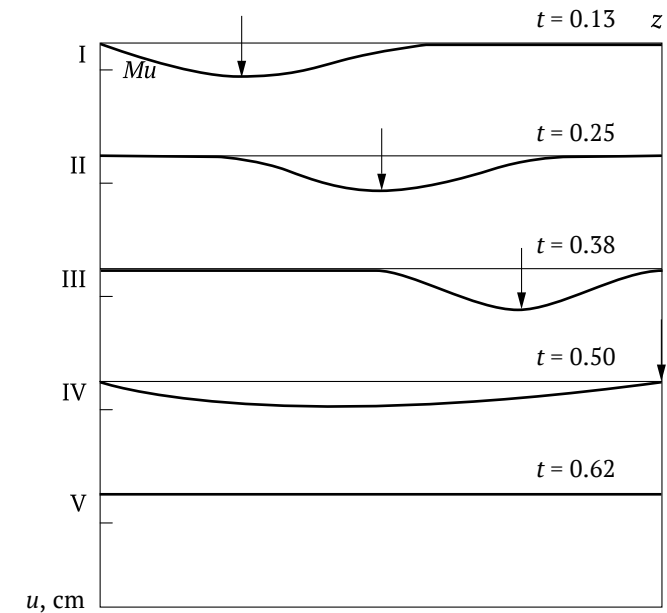


Figure 4.8

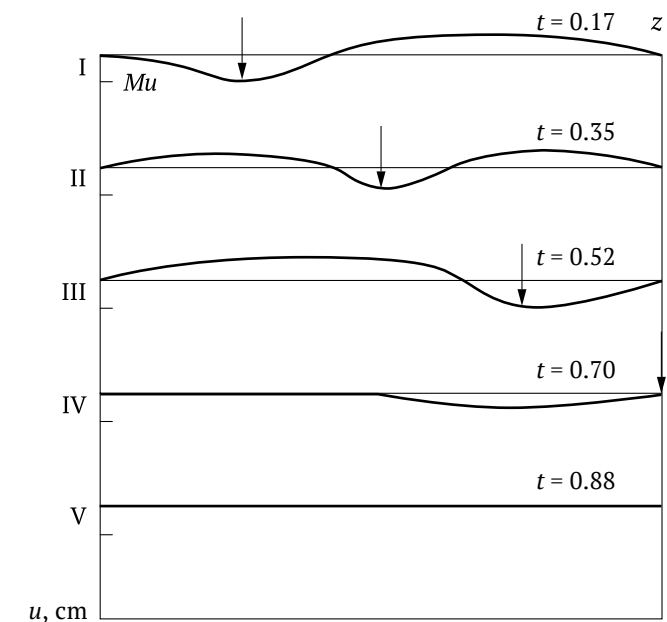


Figure 4.9

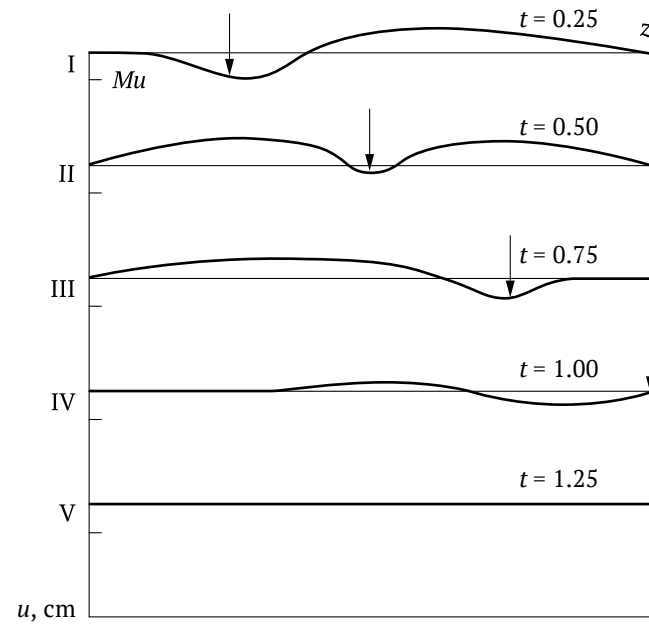


Figure 4.10

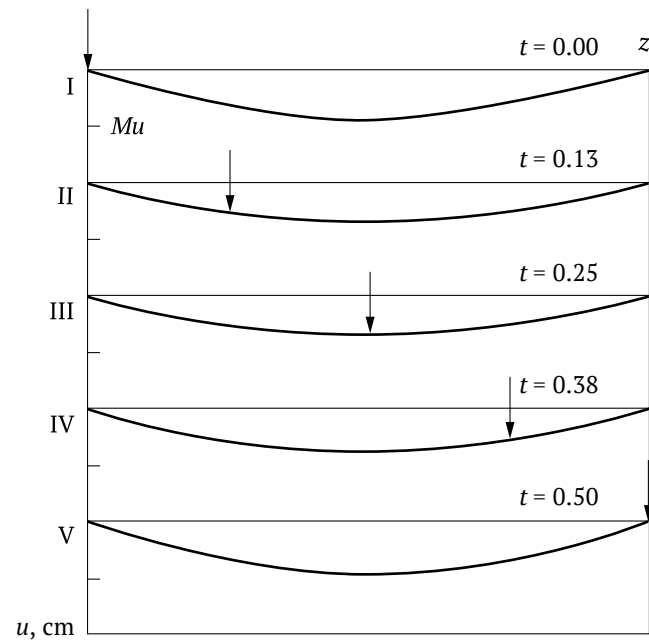


Figure 4.11

The analysis of the obtained graphs allows us to make the following conclusions.

1. Single load at STL with a split body (figures 4.8–4.10):

- span oscillations fade quickly even at low values of damping coefficients μ' , μ^2 and practically disappear after the load leaves the span;
- the load position and its motion direction are clearly seen in the span form;
- there is some impact of reflected deflection waves in the span form;
- the maximal dynamic deflection for the taken initial data does not exceed 1.5 cm.

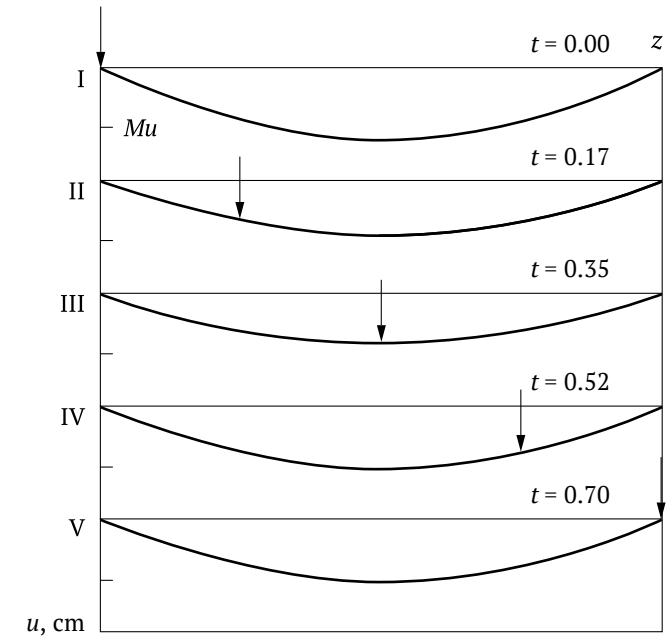


Figure 4.12

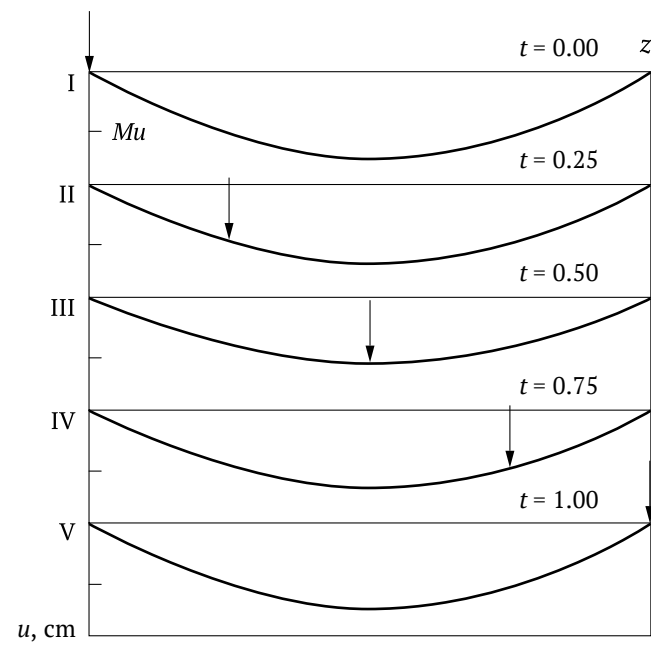


Figure 4.13

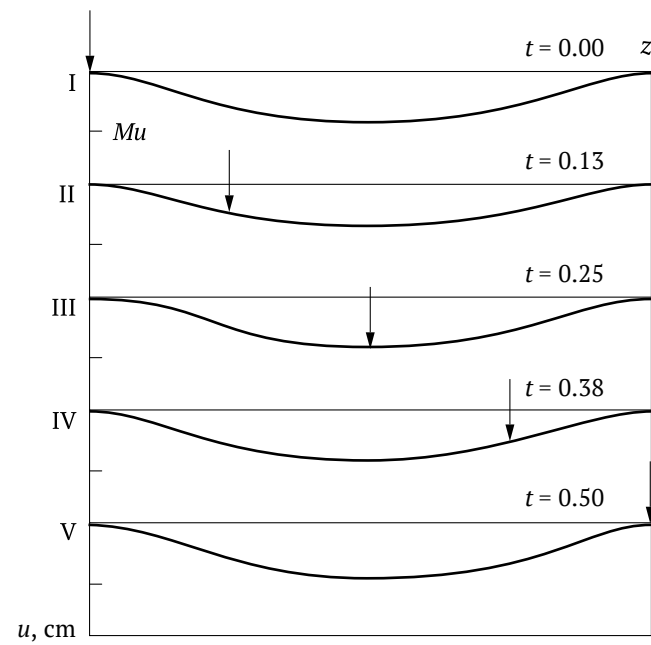


Figure 4.14

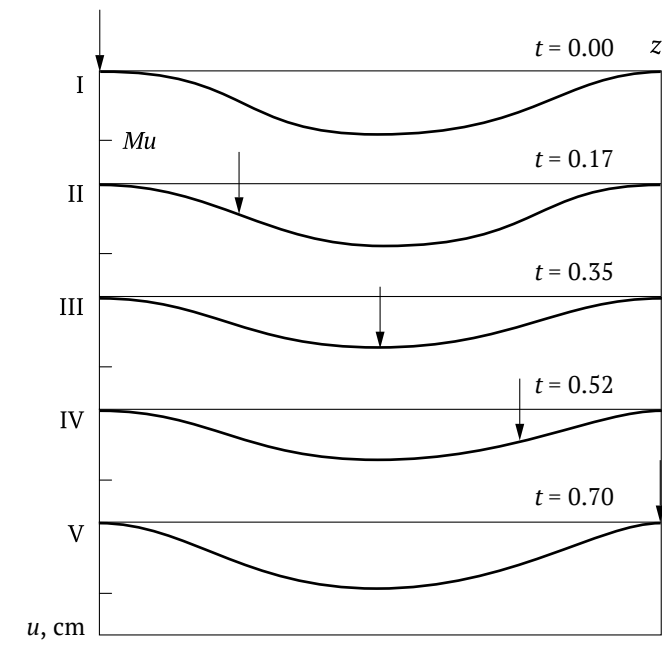


Figure 4.15

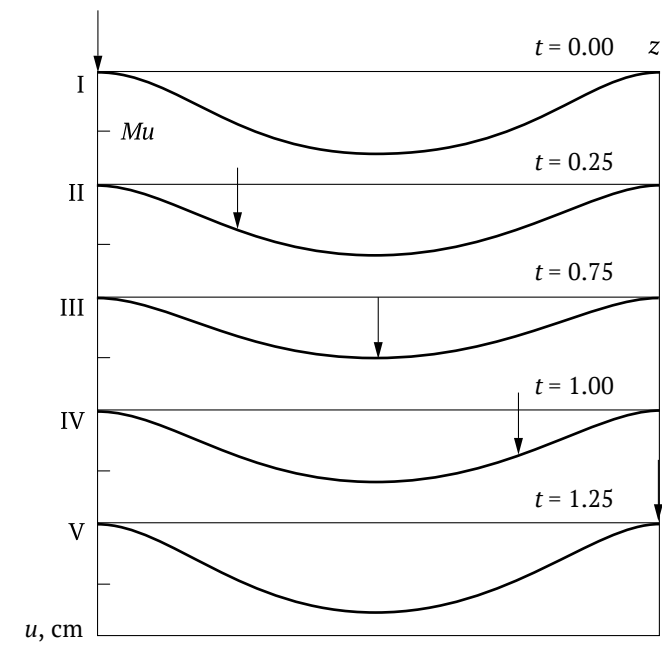


Figure 4.16

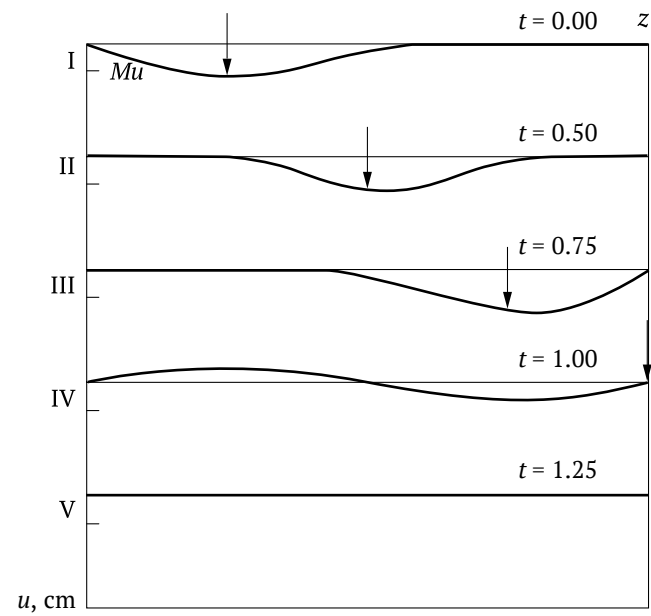


Figure 4.17

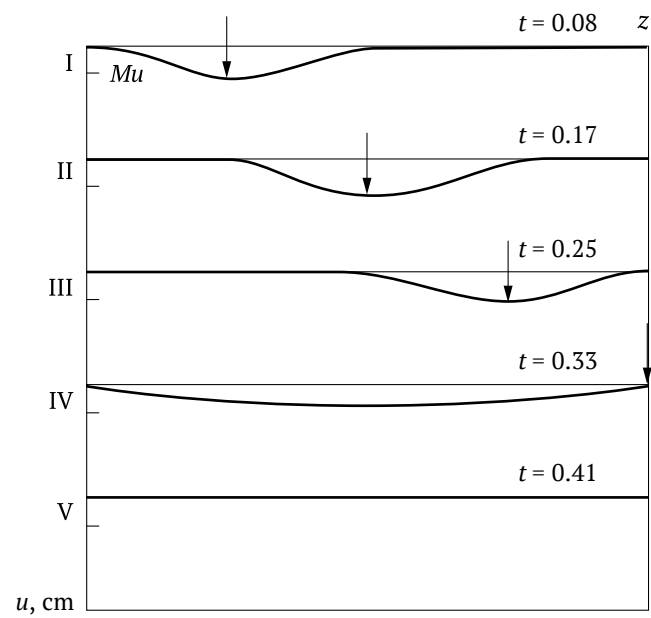


Figure 4.18

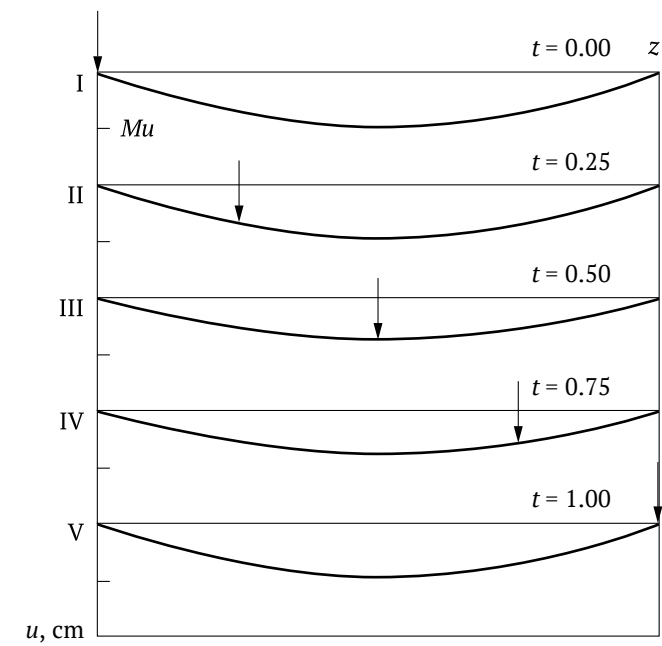


Figure 4.19

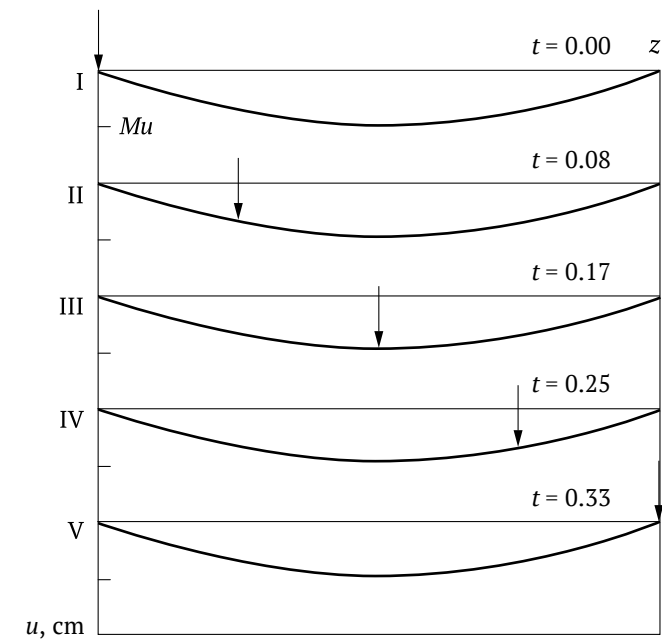


Figure 4.20

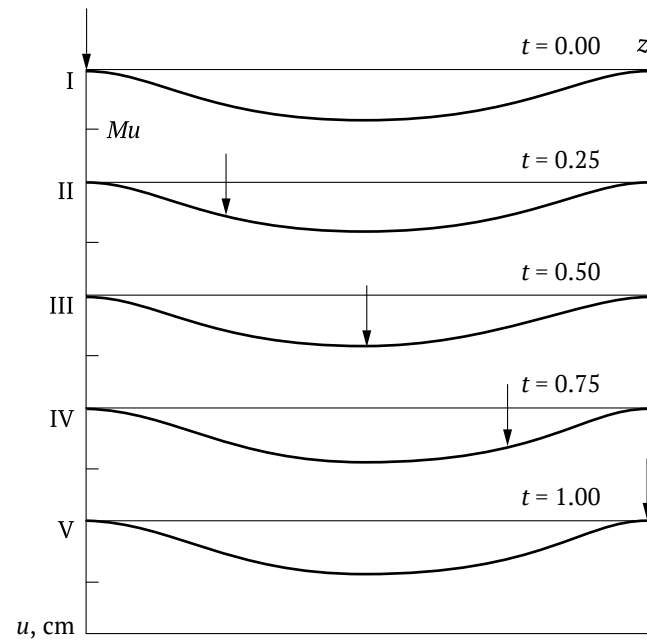


Figure 4.21

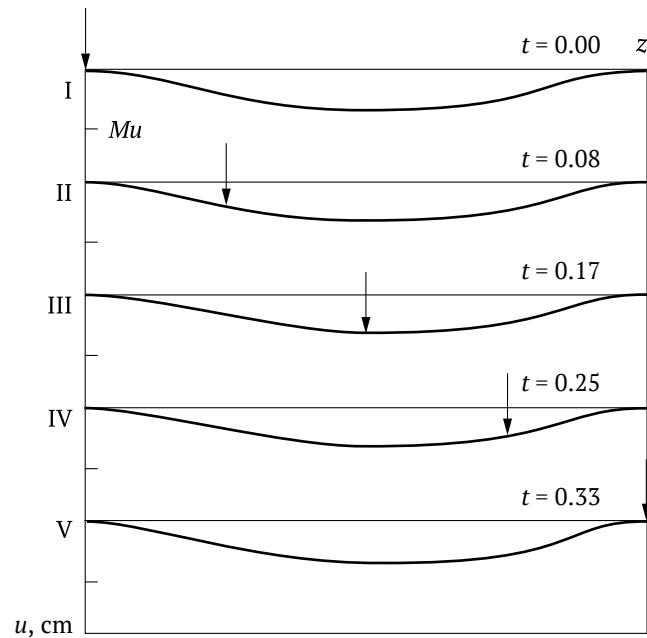


Figure 4.22

2. Load flow at STL with a split body (figures 4.11–4.13) and an unsplit STL (figures 4.14–4.16):

- a stationary component makes the main contribution to the deflection value at any point of the span ($\approx 90\%$ at $l_0 = 25$ m, $\approx 80\%$ at $l_0 = 35$ m, $\approx 70\%$ at $l_0 = 50$ m); its value can be found by solving a problem on the span balance under the impact of evenly distributed load (see clauses 4.3.2, 4.3.4);
- an oscillating component of deflection with any span length l_0 is mainly presented by a component part, which is symmetrical in relation to the midspan, i.e., a dynamic deflection depends weakly on the direction of load flow movement;
- the maximal deflection increases with the span length l_0 increased, and is small versus l_0 (table 4.1).

Table 4.1 – Maximal deflection at load flow movement

Span length l_0 , m	u_0^{\max} , cm	
	split body	unsplit body
25	0.8	0.7
35	1.0	0.8
50	1.3	1.1

4.4.2. Dependence of a dynamic span deflection on load motion speed

The conclusions on the dependence of span deflection on load speed can be made based on the analysis of span forms shown in figures 4.8, 4.11, 4.14, 4.17–4.22 at $EI = 10^6 \text{ N}\cdot\text{m}^2$, $l_0 = 25$ m, $v = 25, 50, 75$ m/s for five time moments

$$t_k = \frac{l_0}{4v} k, \quad k = \overline{1, 5}$$

1. Single load at STL with a split body (figures 4.8, 4.17, 4.18):

- the span form clearly reflects its position and motion direction at the load motion speed specified above;
- some reflected deflection waves are visible in the span form;
- the maximal dynamic deflection does not exceed 2 mm, which is significantly less than a stationary component (table 4.1);
- there are practically no span oscillations upon expiration of $l_0/4v$ s after the load leaves the span.

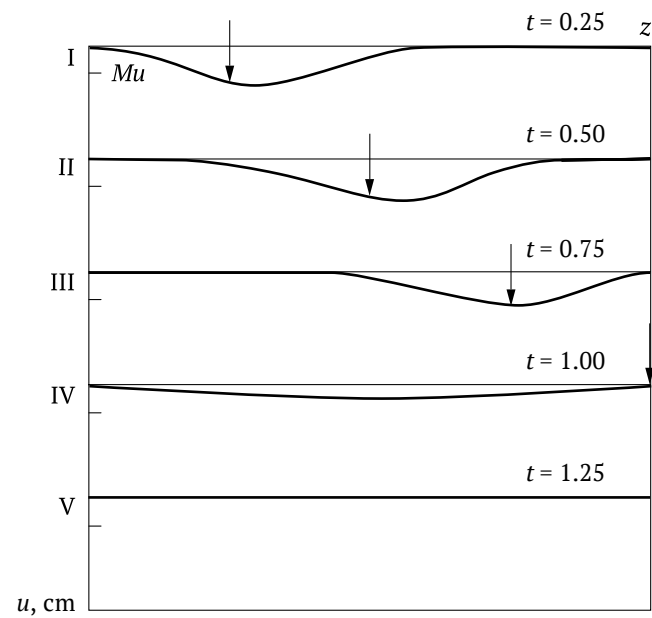


Figure 4.23

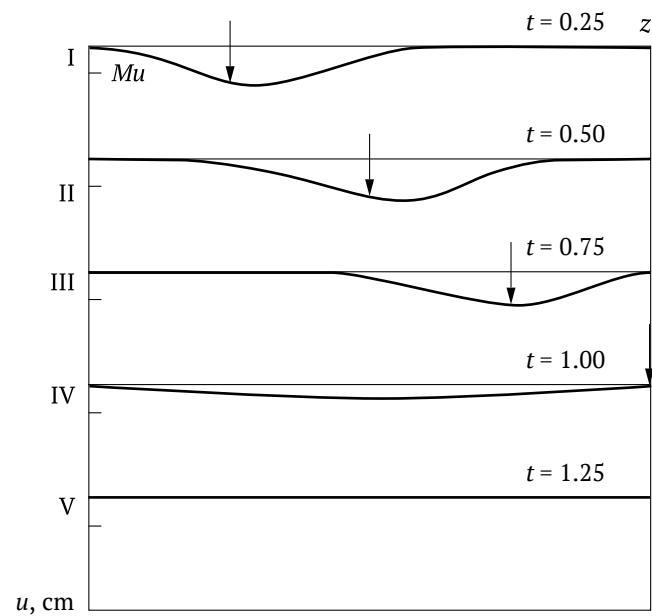


Figure 4.24

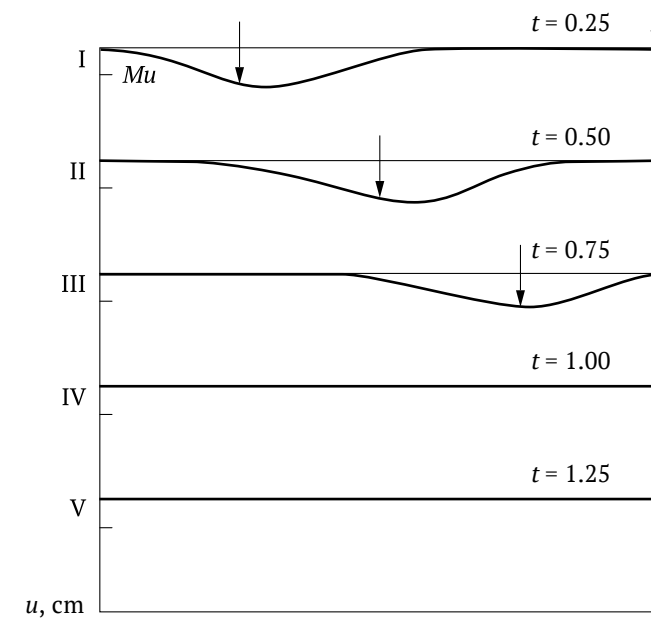
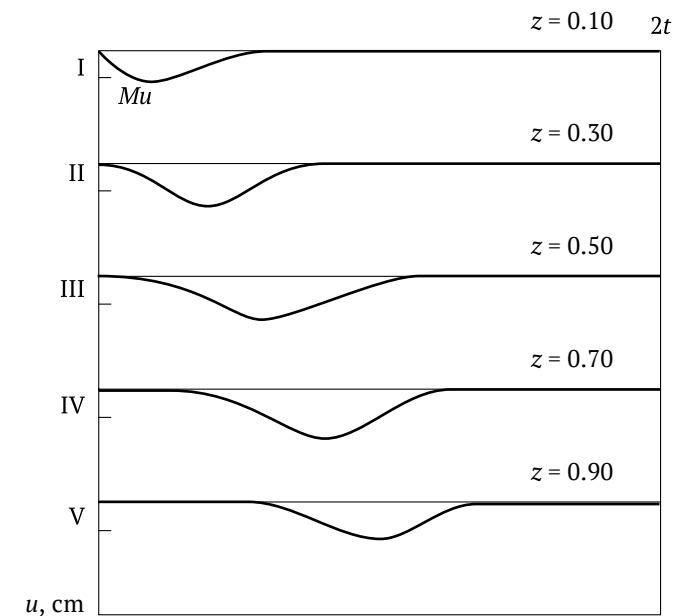
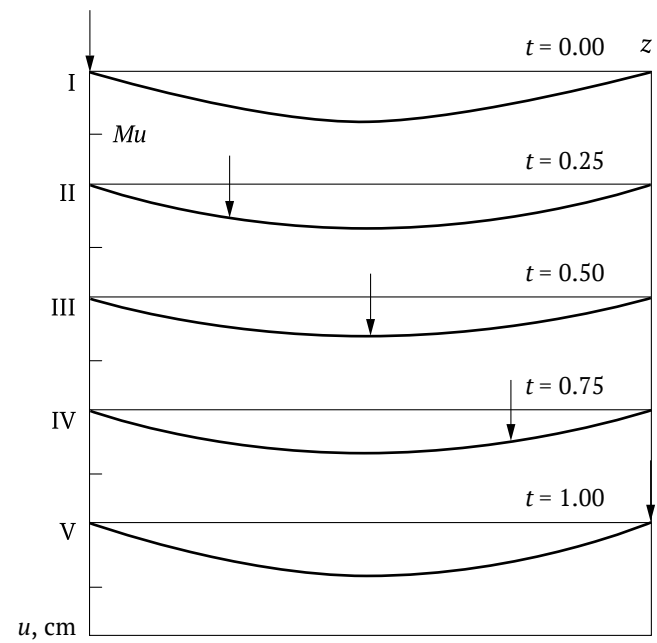


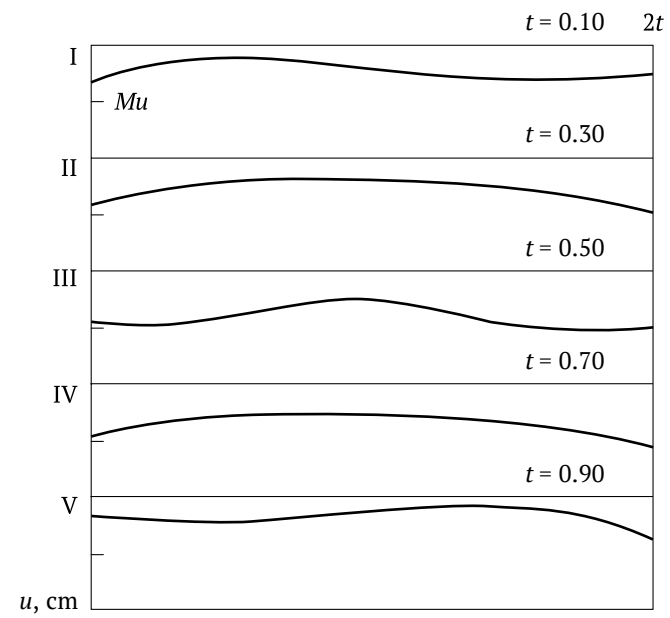
Figure 4.25



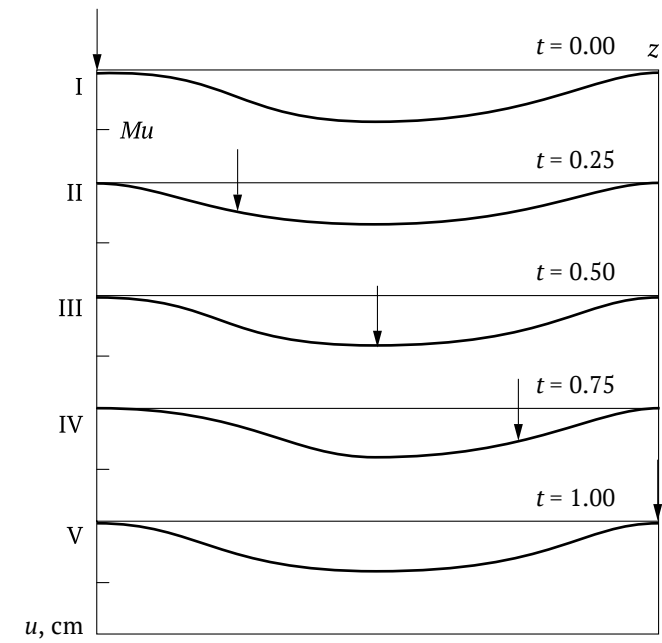
Figures 4.26-4.27



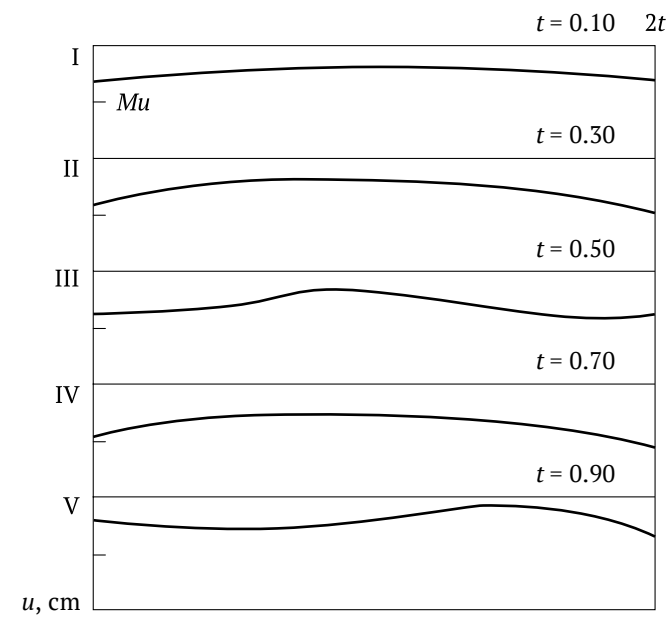
Figures 4.28–4.30



Figures 4.31–4.32



Figures 4.33–4.35



Figures 4.36–4.37

2. Load flow at STL with a split body (figures 4.11, 4.19, 4.20) and an unsplit STL (figures 4.11, 4.21, 4.22):

- a fraction of the span dynamic component $\approx 15\%$;
- the span dynamic deflection remains symmetrical in relation to its middle $z = l_0/2$ at any time, with the speed v changed;
- the maximal dynamic deflection increases insignificantly and does not exceed 0.8 cm if the load speed is increased.

4.4.3. Impact of STL rigidity on the dynamic span deflection

The span form calculated at $v = 25$ m/s, $l_0 = 25$ m with the rigidity parameter varied $EI = 10^4, 10^6, 10^7$ N·m² is shown in figures 4.17, 4.19, 4.21, 4.23–4.37 at time moments

$$t_k = \frac{l_0}{4v} k, \quad k = \overline{1, 5}.$$

It shows here the change in the dynamic deflection in time at five points of the span $x_k = 0, 1, l_0(2k - 1), k = \overline{1, 5}$. The analysis of this graphic information allows us to make the following conclusions.

1. Single load at STL with a split body (figures 4.17, 4.23–4.27):

- the maximal dynamic deflection slightly decreases and does not exceed 2 mm if the rigidity parameter EI is increased;
- there are practically no span oscillations 0.25 s after the load leaves the span;
- the span form clearly reflects the load position on the span and its motion direction at the given rigidity values;
- some impact of reflected deflection waves is visible in the span form.

2. Load flow at STL with a split body (figures 4.19, 4.28–4.32) and an unsplit STL (figures 4.21, 4.33–4.37):

- a stationary component makes the main contribution to the dynamic deflection ($\approx 80\%$);
- an oscillating component of the dynamic deflection remains symmetrical in relation to the midspan $z = l_0/2$ if the parameter EI is changed;
- the maximal dynamic span deflection does not exceed 0.7 cm and slightly decreases with EI increased.

4.4.4. General conclusions

The analysis of graphic information shown in figures 4.8–4.37 allows us to make the following conclusions:

- the span profile camber in the process of single load movement varies considerably;
- the span profile at load flow movement looks like a line with a smooth variable camber;
- there is one noticeable standing wave of length l_0 and small amplitude compared to a stationary deflection, in span oscillations in relation to a stationary form at load flow movement;
- in case of a load flow, the conditions of dynamic span loading are more favorable than those at single load movement;
- a string transport line of a continuous structure is preferable to an STL with a body split above the supports, since the maximal span deflection of an unsplit STL is less and its form has no corner points.

Conventional symbols

STS – String Transport System;
 STL – string transport line;
 TM – transport module;
 $2m_1$ – mass of TM platform;
 m_2 – mass of TM wheel;
 c, v_a – coefficients characterizing spring stiffness and damper force in TM shock-absorber;
 t – time;
 z – coordinate of STL span point;
 $u(z, t), u_2(z, t)$ – vertical deviation from balance position of work surface points of STL and lower string, correspondingly;
 $u_s^{1\max}, u_s^{2\max}$ – maximal static deflection of STL span under the impact of one or two concentrated loads, correspondingly;
 $u_d^{1\max}, u_d^{2\max}$ – maximal dynamic deflection of STL span under the impact of one or two moving loads, correspondingly;
 l' – distance between loads in the flow;
 l_0 – length of STL spans;
 l_1 – distance between the axles of front and rear TM wheels;
 l_2 – distance between TM in the flow;
 g – free fall acceleration;
 N_0 – number of STL spans;
 T_1, T_2 – tension of upper and lower strings, correspondingly;
 μ', E – STL body damping coefficient and elasticity modulus;
 μ_2, E_2 – filler damping coefficient and elasticity modulus;
 ρ_s – total mass of unit length for the body, upper string and STL filler;
 ρ_2 – mass of lower string unit length;
 $\delta(z)$ – Dirac function;
 $U(t)$ – deviation of TM platform mass center from balance position;
 $\varphi(t)$ – slope angle to the horizontal of TM platform longitudinal axis;
 I – cross section inertia moment of STL body;
 I_c – inertia moment of TM platform in relation to horizontal axis passing through the mass center and perpendicular to motion direction;

J – inertia moment of the section;
 C_x – aerodynamic drag coefficient of a full-scale body;
 β – air flow contact angle;
 C_{x0}^{mod} – aerodynamic drag coefficient of a scaled model at zero air flow contact angle ($\beta = 0$);
 K_β – coefficient of air flow contact angle;
 λ – model to prototype correlation coefficient;
 v – phase speed of running wave;
 N – normal force;
 T_T – tangential force;
 τ – tangential stress;
 $p(x, t)$ – contact pressure;
 \dot{u} – slippage velocity;
 $i(x, t)$ – linear wear intensity;
 K_T – coefficient of proportionality;
 γ – index of power;
 h – length of surface section;
 j – number of surface section;
 n – quantity of loading steps;
 r – number of loading step;
 u – surface displacement;
 m – quantity of sampling elements in a contact zone;
 I_v – volume wear;
 $[I_v]$ – wear limit;
 q – number of wear cycles;
 S_c – contact zone;
 S_s – sliding zone;
 A_f – friction work under sliding;
 f – friction coefficient;
 f_0 – static friction coefficient;
 f_s – coefficient of sliding friction.

Bibliography

1. **Balakin, V.A.** Problems of friction and wear at rocket tracks / V.A. Balakin, O.V. Pereverzeva // Friction and wear. – 1991. – No. 5 (12). – P. 896–903.
2. **Bakhvalov, Yu.A.** Transport with magnet suspension / Yu.A. Bakhvalov, V.I. Bocharov, V.A. Vinokurov [et al.]; edited by V.I. Bocharov, V.D. Nagorskiy. – M.: Mashinostroenie [Machine-building], 1991.
3. **Belmas, I.V.** The stress state of rubber-rope belts under arbitrary breakage of ropes / I.V. Belmas // Problems of machine building and reliability of vehicles. – 1993. – No. 6. – P. 45–48.
4. **Brown, E.D.** Modeling of friction and wear in machines / E.D. Brown, Yu.A. Evdokimov, A.V. Chichinadze. – M.: Mashinostroenie [Machine-building], 1982.
5. **Virabov, R.V.** Traction properties of friction gear / R.V. Virabov. – M.: Mashinostroenie [Machine-building], 1982.
6. **Vysotskiy, M.S.** Determination of aerodynamic drag coefficient C_x for a road train based on results of model tests / M.S. Vysotskiy, A.N. Evgrafov, K.A. Gostev // Proceedings of the National Academy of Sciences of Belarus, Physico-technical series. – 1995. – No. 2. – P. 46–47.
7. **Johnson, K.** Contact Mechanics / K. Johnson. – M.: Mir, 1989.
8. **Evtushenko, A.A.** Influence of thermal resistance on the main contact characteristics under conditions of plane stress problem / A.A. Evtushenko, E.V. Kovalenko // Mechanics of Solids. – 1995. – No. 4. – P. 56–62.
9. **Eltyshev, V.A.** The stress-strain state of shell structures with a filler / V.A. Eltyshev. – M.: Nauka [Science], 1981.
10. **Zabegaev, A.V.** Design of reinforced concrete structures subjected to emergency impact actions / A.V. Zabegaev // Sbornik nauchnykh trudov [Collection of scientific papers]. MIIT. – 1992. – No. 870. – P. 37–45.
11. **Zelkin, G.G.** Flying Trains / G.G. Zelkin. – Minsk: Vysheyschaya Shkola, 1984.
12. Research of dynamics and strength of passenger carriages; edited by S.I. Sokolov. – M.: Mashinostroenie [Machine-building], 1976.
13. **Kamaev, V.A.** Optimization of running parts parameters of railway rolling stock / V.A. Kamaev. – M.: Mashinostroenie [Machine-building], 1980.

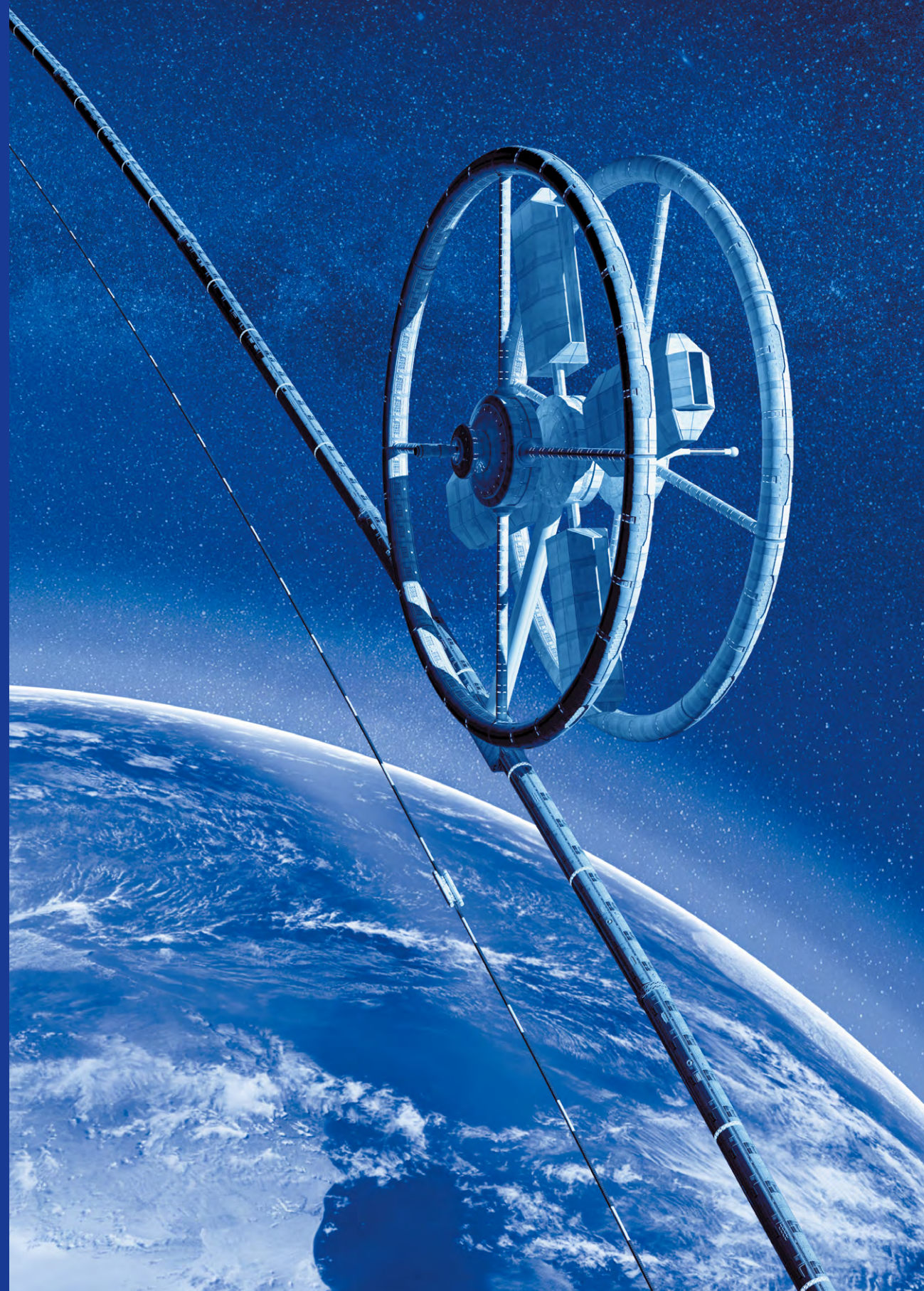
14. **Konchits, V.V.** Triboengineering of Electrical Contacts / V.V. Konchits, V.V. Meshkov, N.K. Myshkin. – Minsk: Nauka i tekhnika [Science and technology], 1986.
15. Composite materials; edited by L. Browtman, R. Krock. – M.: Mashinostroenie [Machine-building], 1978, Vol. 3. Engineering application of composites; edited by B. Noton.
16. **Korn, G.** Mathematical Handbook for Scientists and Engineers / G. Korn, T. Korn. – M.: Nauka [Science], 1970.
17. **Crawford, F.** Waves / F. Crawford – M.: Nauka [Science], 1976.
18. **Laschenikov, B.Ya.** Computer-based computational methods for buildingstructures / B.Ya. Laschenikov, Ya.B. Dmitriev, M.N. Smirnov. – M.: Stroyizdat, 1993.
19. **Lyamin, V.I.** Dynamics of rocket sleds / V.I. Lyamin. – M., 1962.
20. **Maiboroda, V.P.** Dynamic deformation of structural materials / V.P. Maiboroda, A.S. Kravchuk, N.N. Kholin. – M.: Mashinostroenie [Machine-building], 1986.
21. **Matveev, V.V.** A direct experimental estimation of static tension impact on damping properties of materials at flexural vibrations / V.V. Matveev, A.P. Bovsunovskiy // Problemy prochnosti [Problems of strength]. – 1995. – No. 4. – P. 83–93.
22. **Matsudaira, T.** Speed increase limit for trains / T. Matsudaira // Monthly bulletin of the International Railway Congress Association. – 1967. – No. 12. – P. 19–24.
23. **Moore, D.** Principles and Applications of Tribology / D. Moore. – M.: Mir, 1978.
24. **Pinegin, S.V.** Rolling Friction in Machines and Instruments / S.V. Pinegin. – M.: Mashinostroenie [Machine-building], 1976.
25. **Panovko, Ya.G.** Stability and oscillations of elastic systems / Ya.G. Panovko, I.I. Gubanova. – M.: Nauka [Science], 1987.
26. **Polyakov, V.Yu.** Modeling of fluctuations in the system “bridge – track – vehicle” / V.Yu. Polyakov, K.A. Zhukov // Sbornik nauchnykh trudov [Collection of scientific papers]. MIIT. – 1992. – No. 870. – P. 57–64.
27. **Popov, B.G.** Calculation of multilayer structures by variation-matrix methods / B.G. Popov. – M.: MGTU im. N.E. Bauman Publ., 1993.

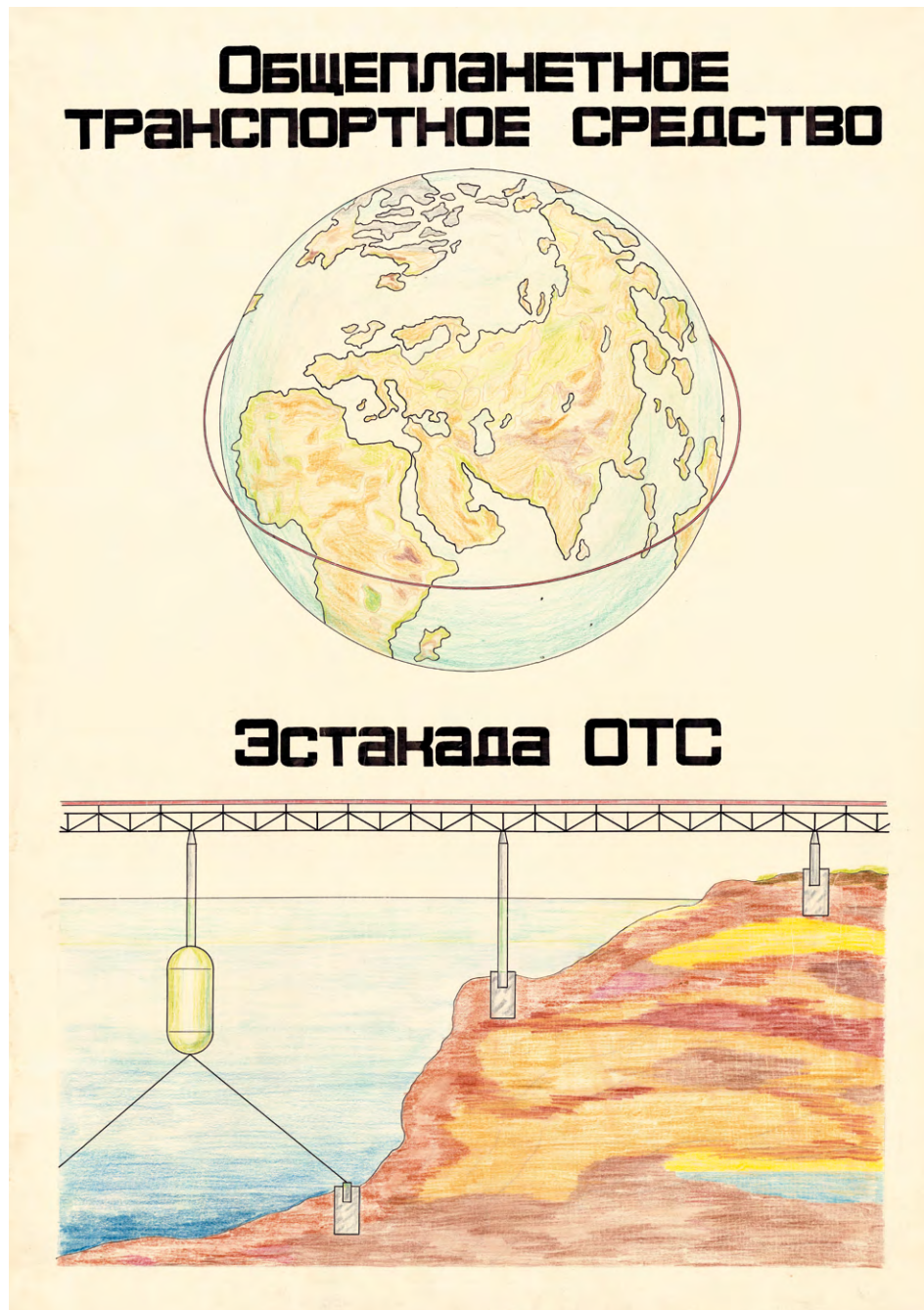
- 28. Prudnikov, A.P.** Integrals and Series / A.P. Prudnikov, Ya.A. Brychkov, O.I. Marichev. – M.: Nauka [Science], 1981.
- 29. Saltanov, N.V.** Flexible lines in flows / N.V. Saltanov. – Kiev: Naukova dumka Publ., 1974.
- 30. Samme, G.V.** Dependence of friction force on sliding speed of a locomotive wheelpair / G.V. Samme. – Friction and wear. – 1995. – No. 1 (16). – P. 55–60.
- 31. Smirnov, V.I.** A Course of Higher Mathematics / V.I. Smirnov. – M.: Fizmatgiz, 1962.
- 32. Smirnov, V.F.** Peculiarities of the behavior of dynamic systems with wave propagation of vibrational energy / V.F. Smirnov, V.F. Zyablikov // Vestnik mashinostroeniya [Bulletin of mechanical engineering]. – 1994. – No. 10. – P. 7–11.
- 33. Sneddon, I.** Fourier transforms / I. Sneddon. – M.: IL, 1955.
- 34. Tikhonov, V.S.** Analysis of the stress-strain state of a deep-water drill column in running waters / V.S. Tikhonov, V.I. Safronov // Problemy prochnosti [Problems of strength]. – 1995. – No. 8. – P. 60–67.
- 35. Filippov, A.P.** Vibrations of deformable systems / A.P. Filippov. – M.: Mashinostroenie [Machine-building], 1970.
- 36. Furunzhiev, R.I.** Design of optimal vibration protection systems / R.I. Furunzhiev. – Minsk: Vysheyshaya Shkola, 1971.
- 37. Shil'ko, S.V.** Choice of slippage coefficient when optimizing locomotive traction / S.V. Shil'ko // Theses of the reports at the International scientific and practical conference. Resource and energy saving technologies in a transport and construction complex. – Gomel, 1995. – P. 81–82.
- 38. Shultz, V.V.** Form of natural wear of machine parts and tool / V.V. Shultz. – Leningrad: Mashinostroenie [Machine-building], 1990.
- 39. Unitsky, A.E.** Linear Transport System. International invention application PCT/IB94/00065 dd 26/09/1994. Applicant “NTL Neue Transportlinien GmbH”, Germany.
- 40. Unitsky, A.E.** Patent of the Russian Federation under application No. 94026782/11 (026280) dd 26/09/1994. IPC B61B 5/02, B61B 13/00, E01B 25/22. Patent holder “NTL Neue Transportlinien GmbH”, Germany.
- 41. Unitsky, A.E.** Analysis of fluctuations of span structures in a string transportation system / A.E. Unitsky [et al.] // Theses of the reports at Byelorussian Congress on Theoretic and Applied Mechanics “Mechanics-95”. – Minsk, 1995. – P. 253–254.

- 42. Unitsky, A.E.** On the Dynamics of a String Transportation System / A.E. Unitsky [et al.] // Theses of the reports at Byelorussian Congress on theoretic and applied mechanics “Mechanics-95”. – Minsk, 1995. – P. 254–255.
- 43. Unitsky, A.E.** High-Speed Road Transport NTL / A.E. Unitsky // Theses of the reports at the International scientific and practical conference. Resource and energy saving technologies in a transport and construction complex. – Gomel, 1995. – P. 69–70.
- 44. Bolton, A.** Wind excitation of steel chimneys / A. Bolton. – Struct. Eng. – 1994. – No. 5 (72). – P. 75–80.
- 45. Cai Chuh Sheng.** Rehabilitation of Deer Isle bridge: aerodynamic behavior // 10 Annu. Int. Bridge Conf., Pittsburgh, Pa, 1993. – P. 9–16.
- 46. Kalker, J.J.** A strip theory for rolling with slip and spin / J.J. Kalker. – Proc. Kon. Ned. Acad. van Wetenschappen, 1967. – B. 70. – P. 10.
- 47. Forward, R.L.** The cable catapult: putting it there and keeping it there / R.L. Forward // AIAA Papers. – 1992. – No. 3077. – P. 1–11.
- 48. Shil'ko, S.V.** Boundary element method in modelling failure of compressed metal-polymeric adhesive joints / S.V. Shil'ko, S.V. Sherbakov // Proc. of Europ. Mech. Colloquim “Euromech 227”. France, Saint-Etienn. – 1987. – P. 339–351.
- 49. Vldic, J.** Tribološke karakteristike prenosna snade putem trenja kod specifičnih transportnih masina / J. Vldic, B. Sovily // Tribology in Industry. – 1994. – No. (16). – P. 85–93.
- 50. Yip, F.C.** Surface topography effects in the estimation of thermal and electrical contact resistance / F.C. Yip, I.E.S. Venart // Metrology and properties of surfaces / Proc. Inst. Mech. Eng. 182, 1967–1968. – P. 81–93.

History of United Planetary Transport in pictures

312





First visualizations of United Planetary Transport (UPT).
UPT overpass passing through mountains and sea shelf. 1973



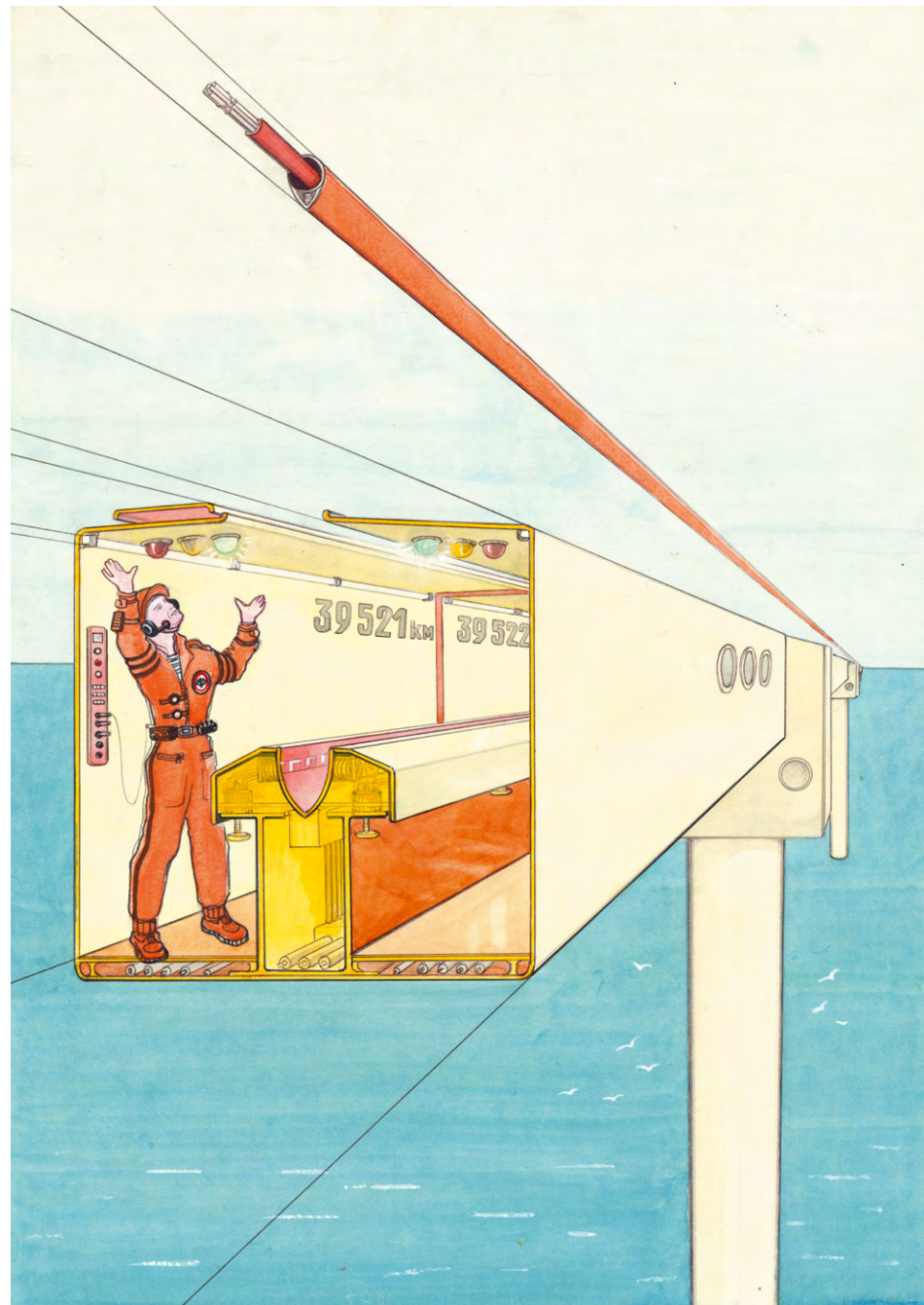
Stages of ascent of UPT rotor to outer space. 1974



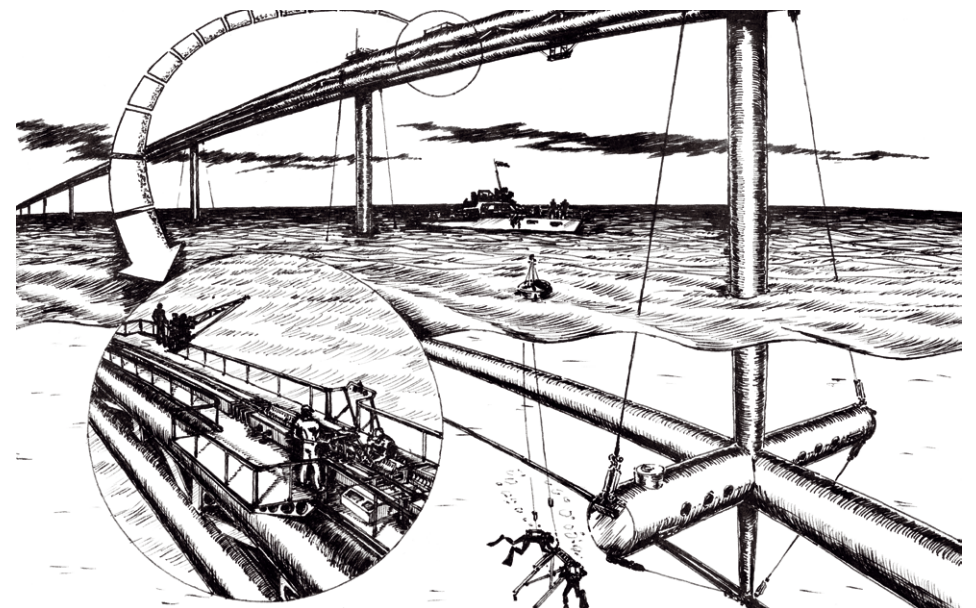
The rotor design and cargo-passenger UPT. 1974



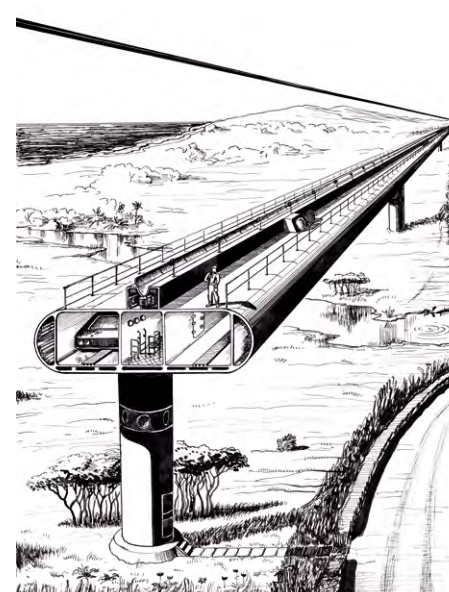
UPT with ablative protection of the rotor and UPT with vacuum protective shell. 1974



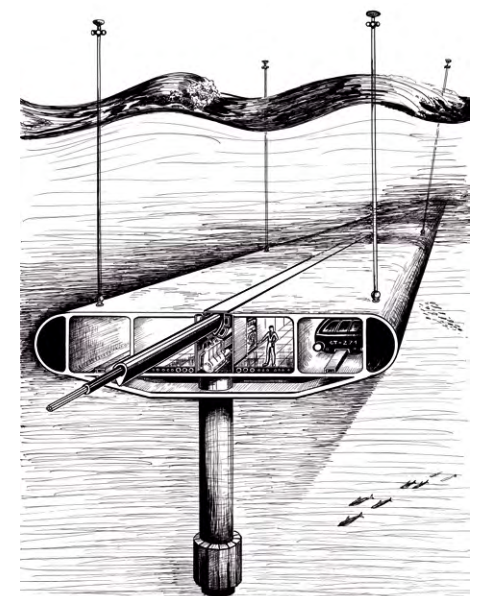
The simplest variant of UPT. 1975



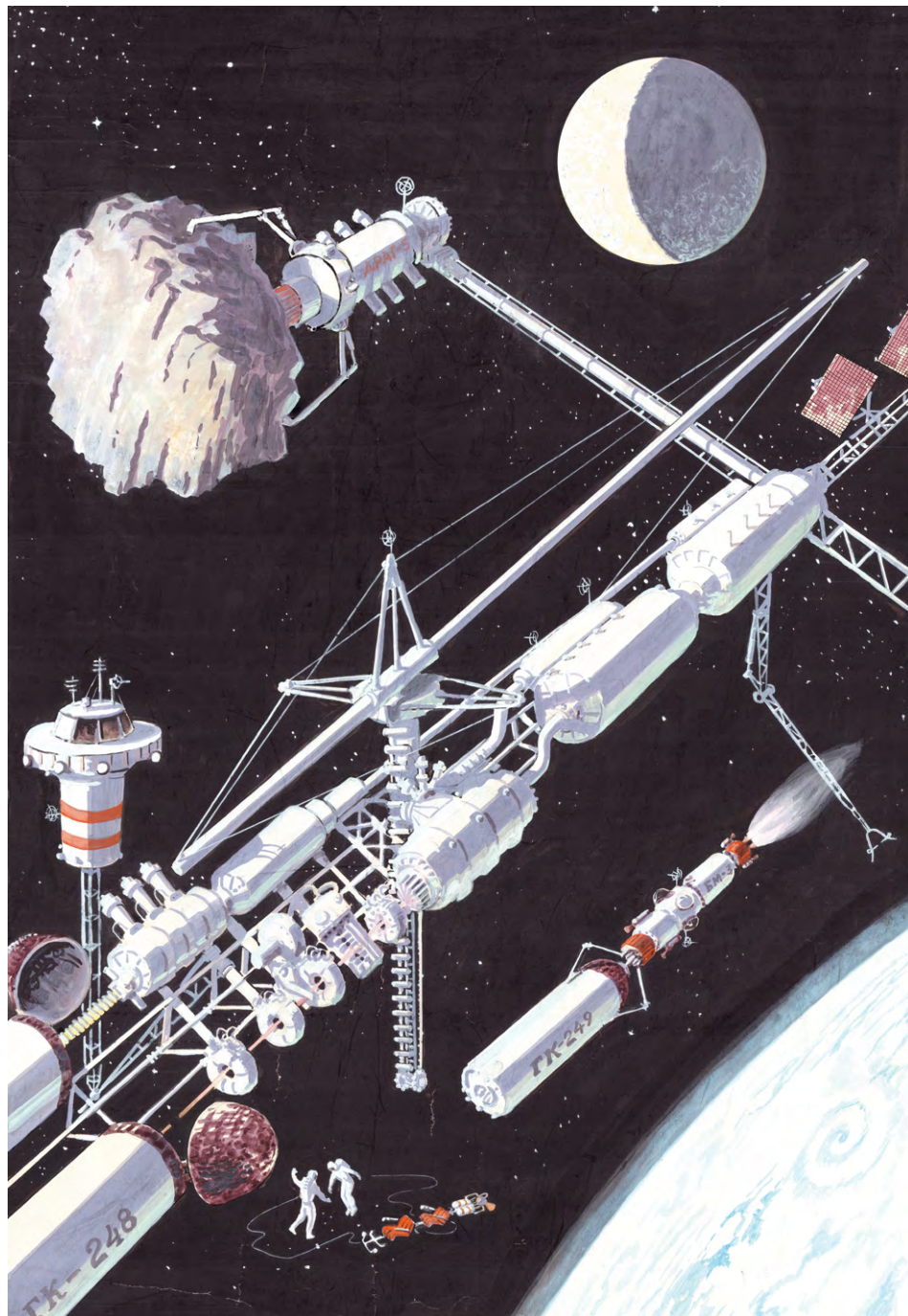
UPT offshore section with linear floats. 1976



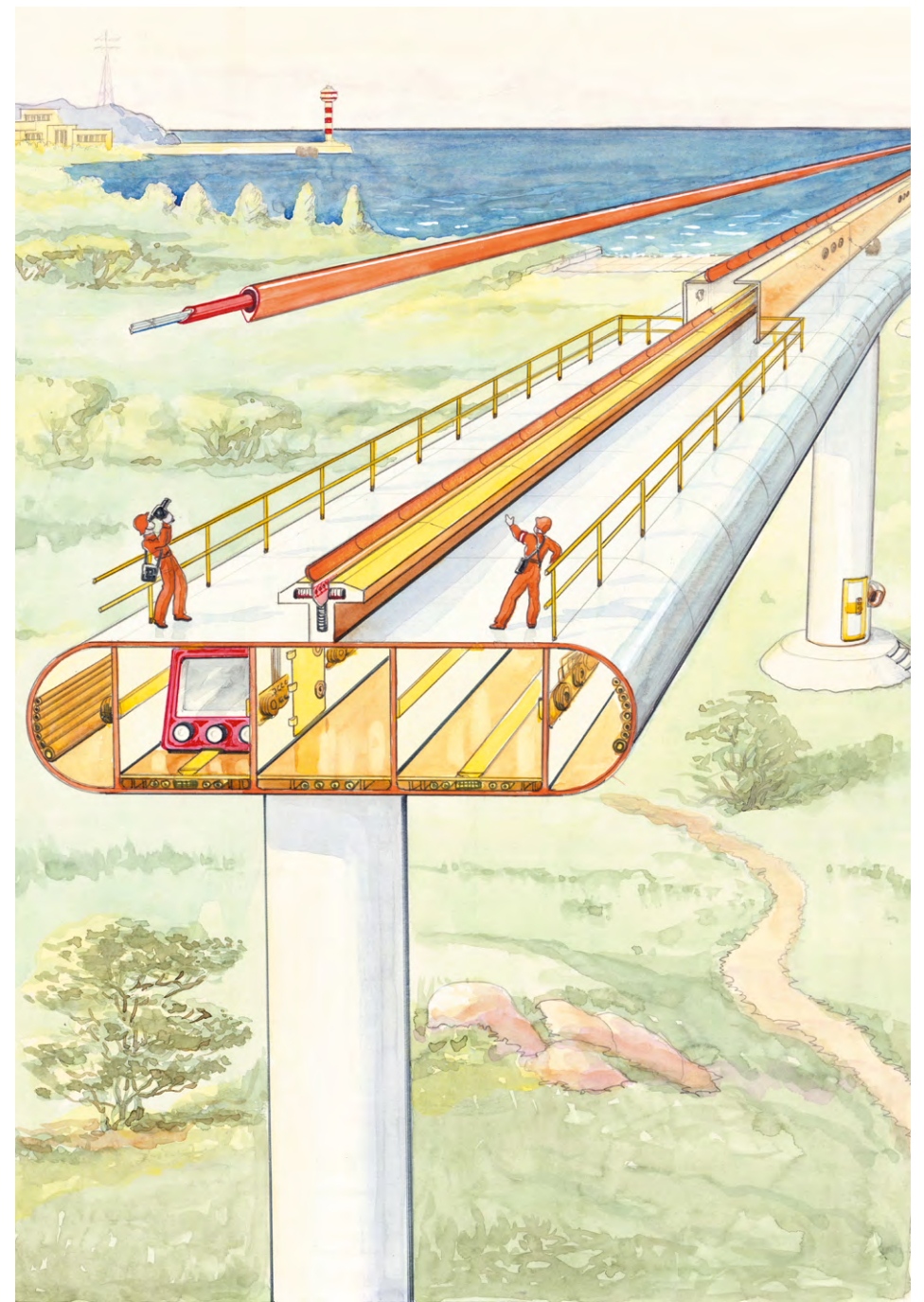
UPT overpass on land with vacuum transport tunnels. 1976



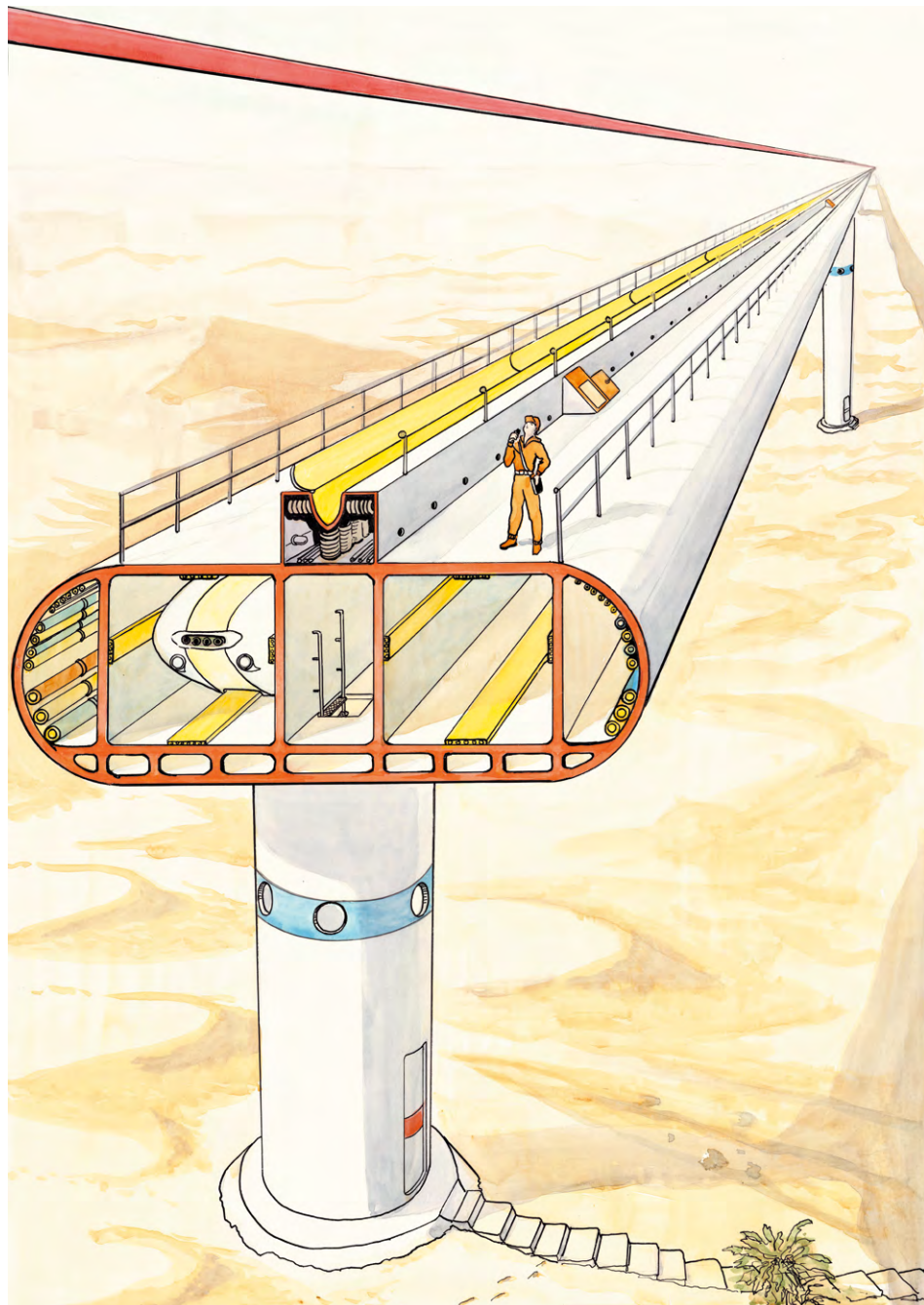
Underwater installation of UPT overpass. 1977



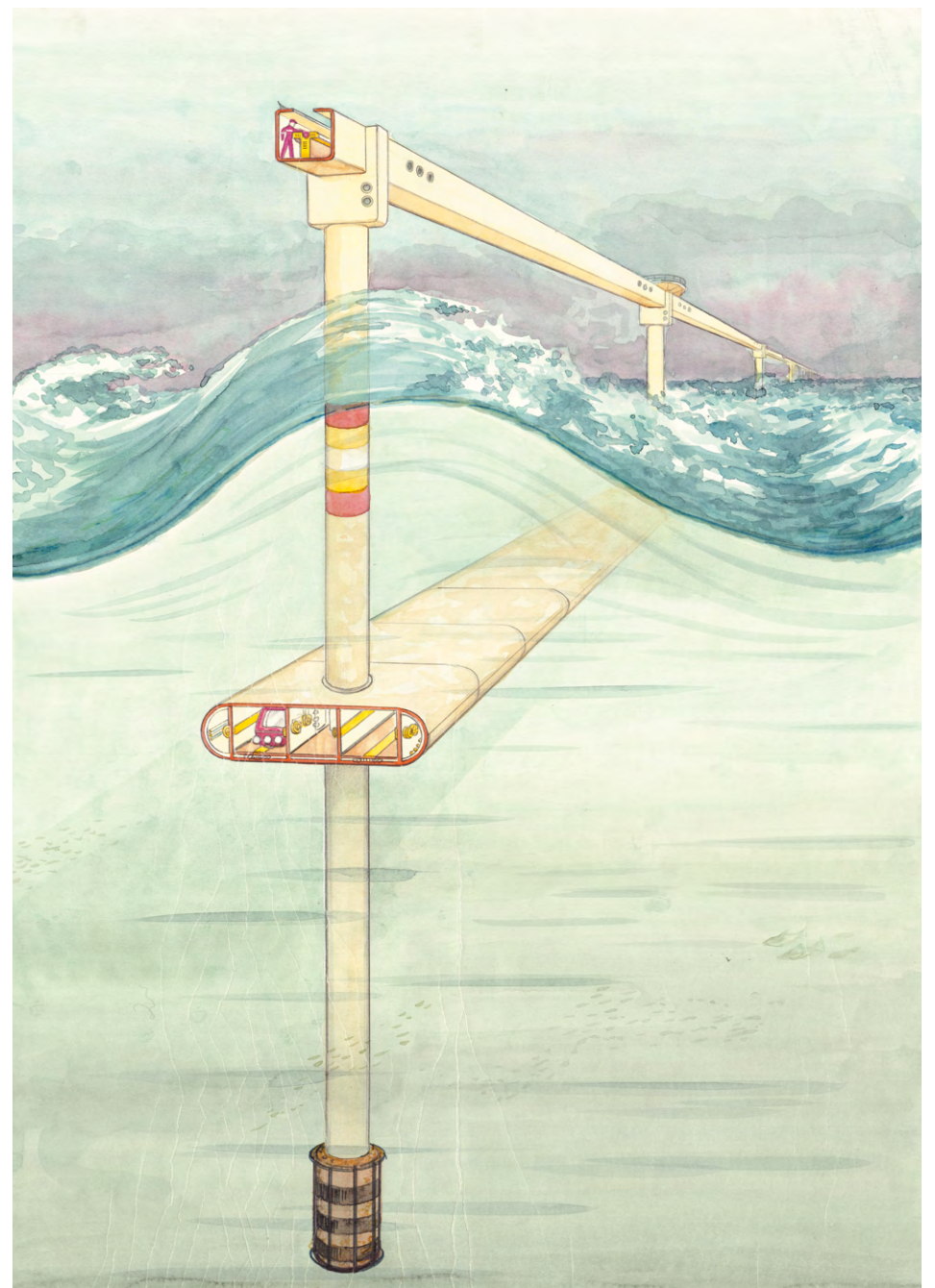
Orbital industry built using UPT. 1978



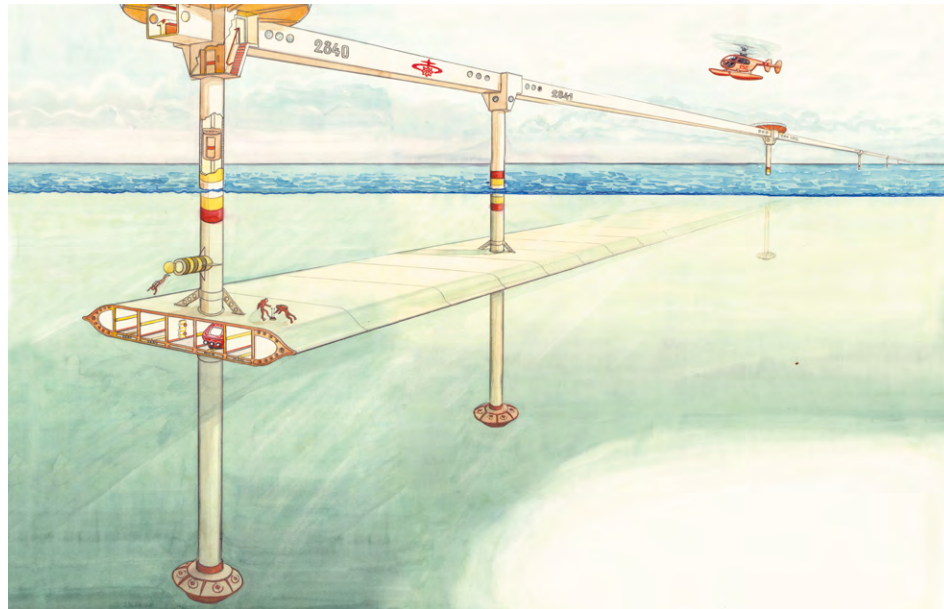
Launch of the simplest variant of cargo UPT. 1978



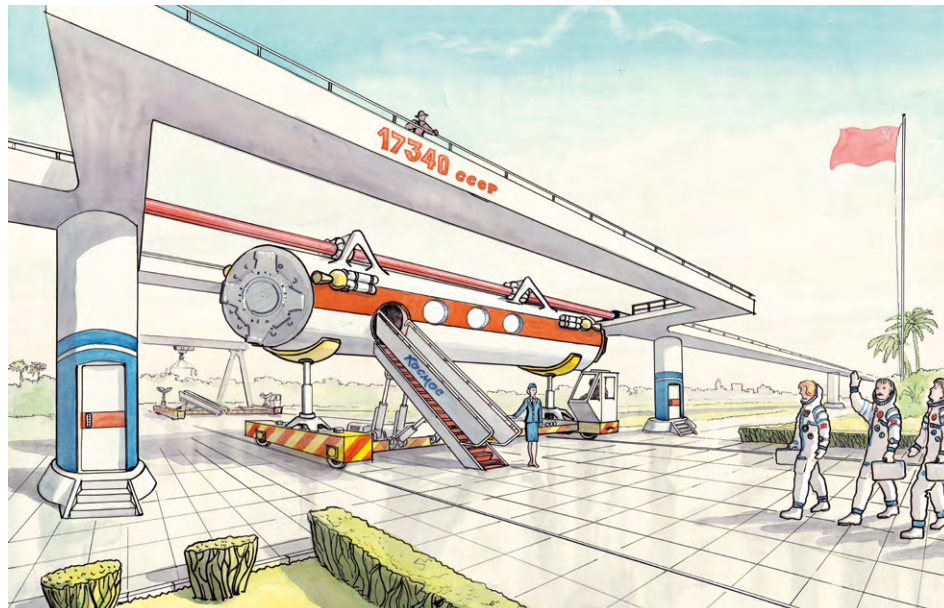
Magnetic cushion train in UPT vacuum tunnel. 1979



Variant of UPT overpass, equipped with floats,
which are combined with vacuum transport tunnels. 1979



Offshore UPT overpass. 1979

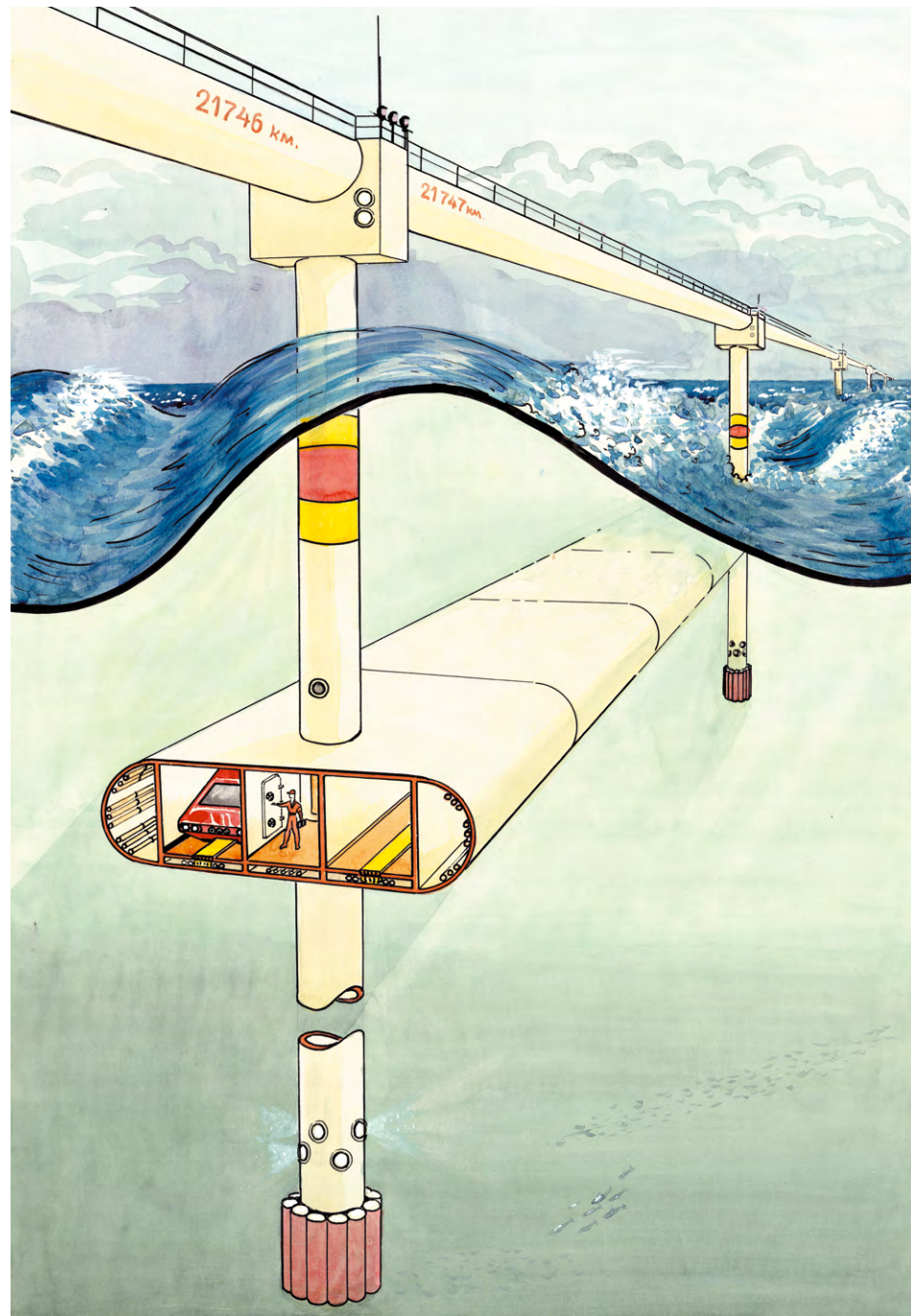


Passengers boarding UPT. 1980

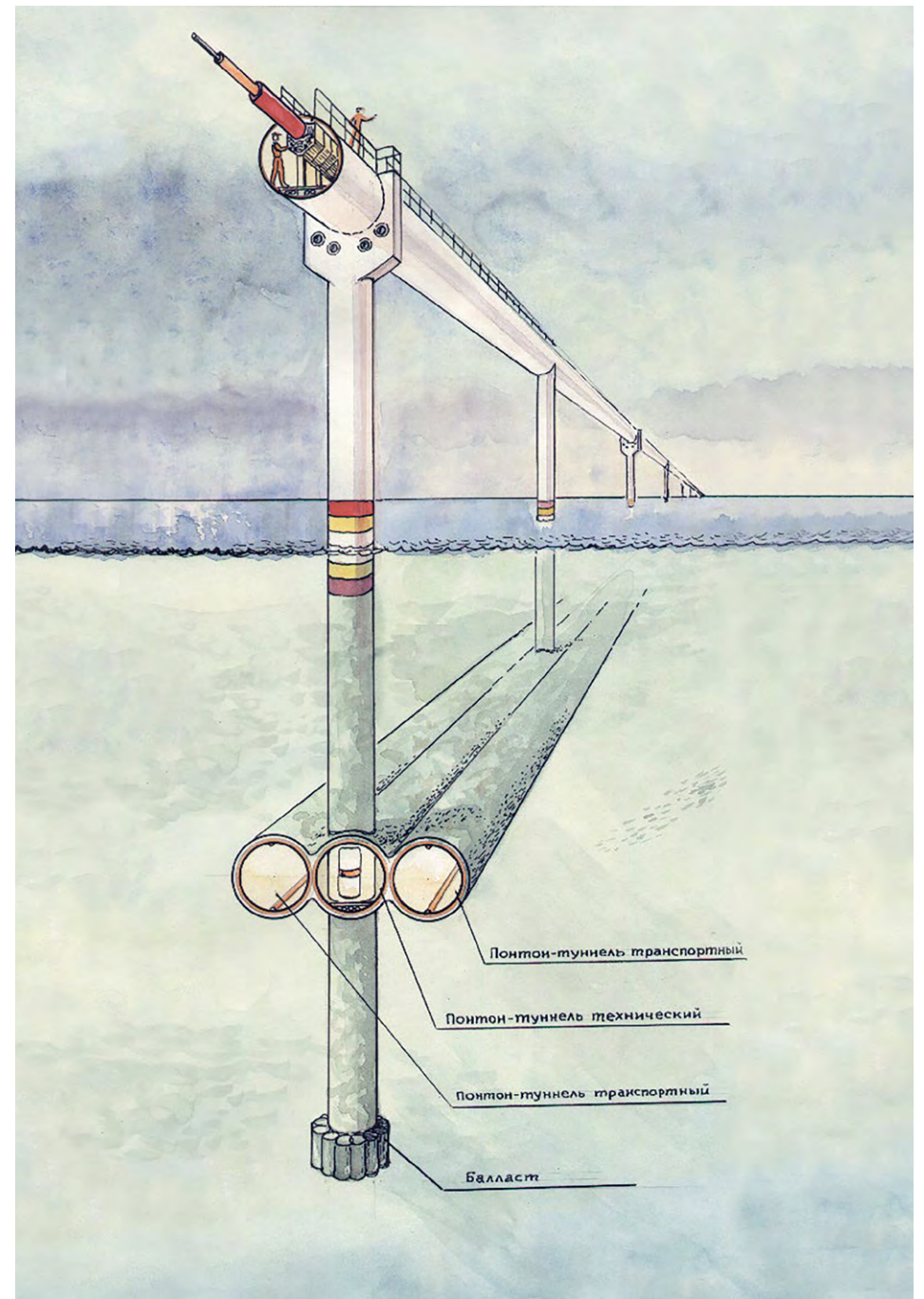
ТЕХНИКО-ЭКОНОМИЧЕСКИЕ ПОКАЗАТЕЛИ

Показатель	ПАРАМЕТР В ЗАВИСИМОСТИ ОТ КПД ОТС						
	ОТС с абляционной защитой			ОТС с защитной оболочкой			
	КПД 10%	КПД 50%	КПД 90%	КПД 10%	КПД 50%	КПД 90%	
Потребляемая мощность в процессе разгона ротора в зависимости от грузопотока (в числителе - всего, в знаменателе - на 1 км длины), кВт:	- 100 тыс. т/год	2,7 млн.	550 тыс.	300 тыс.	1,6 млн.	320 тыс.	180 тыс.
	- 1 млн. т/год	27 млн.	5,5 млн.	3 млн.	16 млн.	3,2 млн.	1,8 млн.
	- 10 млн. т/год	270 млн.	55 млн.	30 млн.	160 млн.	32 млн.	18 млн.
	- 100 млн. т/год	2700 млрд.	550 млн.	300 млн.	1600 млрд.	320 млн.	180 млн.
Затраты энергии на выведение в космос 1кг грузов:	- кВт·час	240	48	27	140	28	16
	- кг условного топлива	30	6	3,3	17	3,5	2
Себестоимость в долл./кг доставки грузов на орбиту в зависимости от грузопотока:	- 100 тыс. т/год	84	82	82	82	80	80
	- 1 млн. т/год	12	10	10	9,6	8,5	8,4
	- 10 млн. т/год	5,2	3,3	3,1	2,4	1,3	1,2
	- 100 млн. т/год	4,5	2,6	2,4	1,7	0,56	0,44

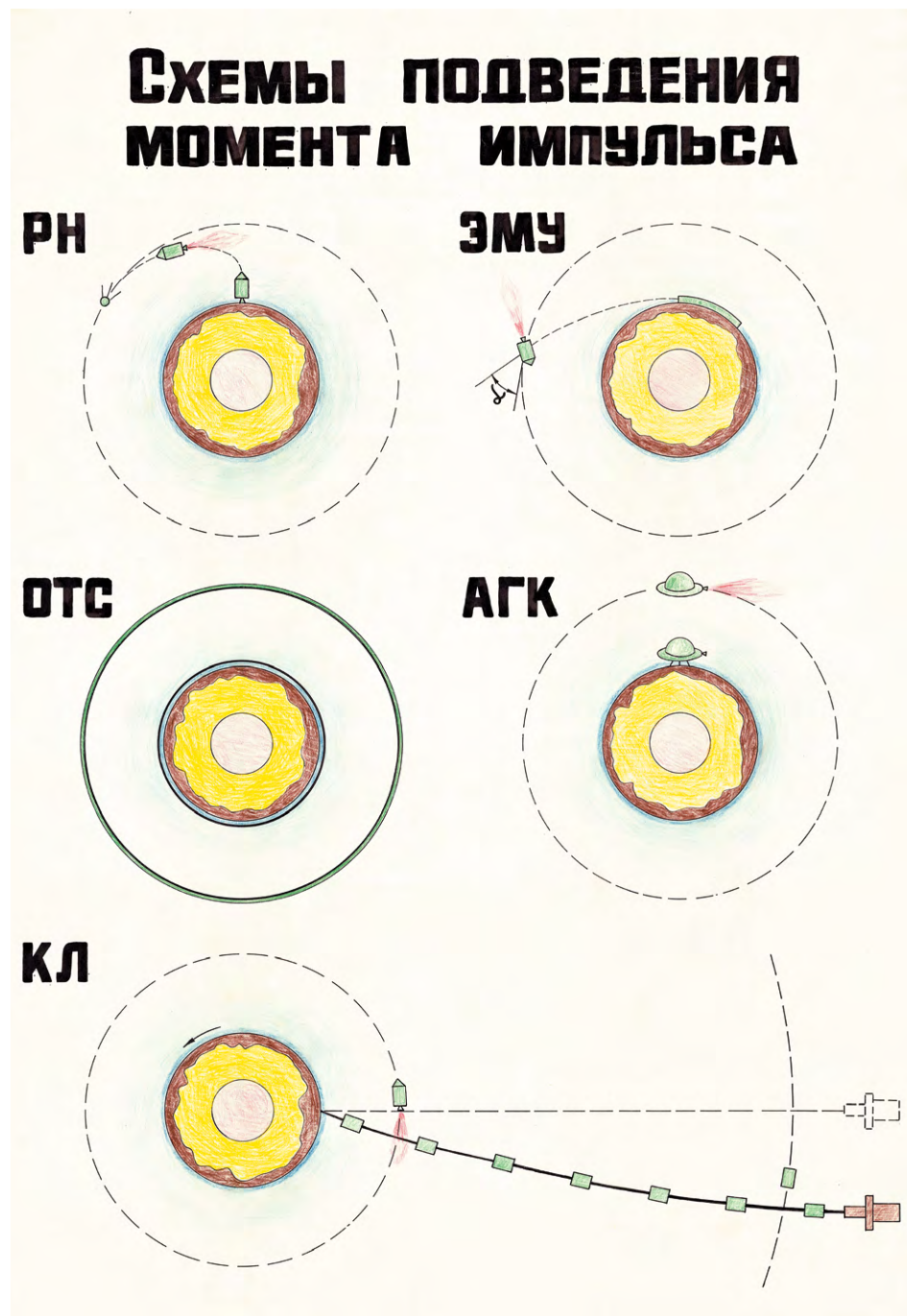
Technical and economic parameters of UPT. 1980



UPT overpass with underwater transport tunnels. 1981



Lightweight variant of UPT. 1981

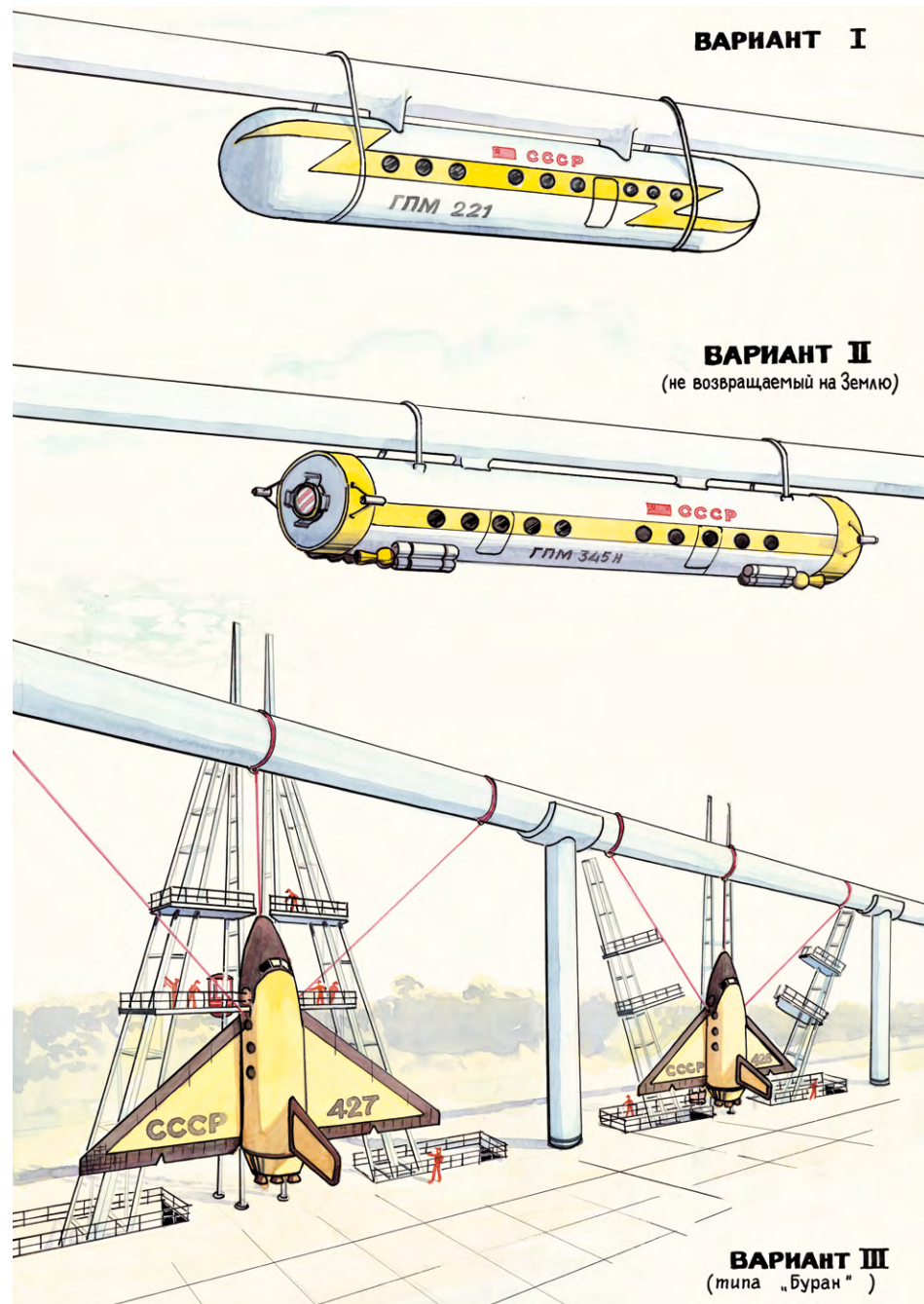


Angular momentum schemes. 1982

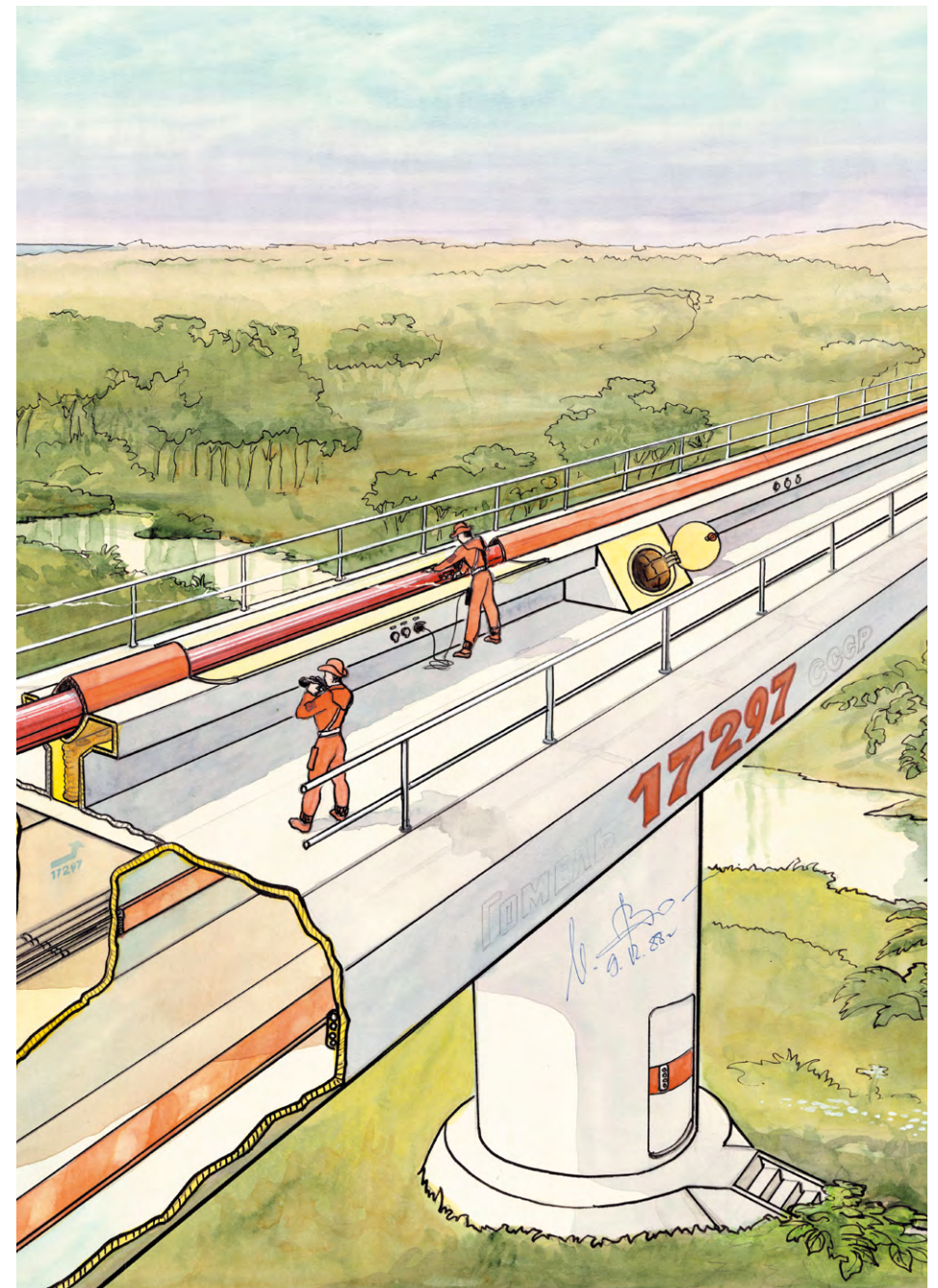


Отводной канал

Geocosmic circular transport – energy storage. 1985



UPT with various load suspension options. 1986



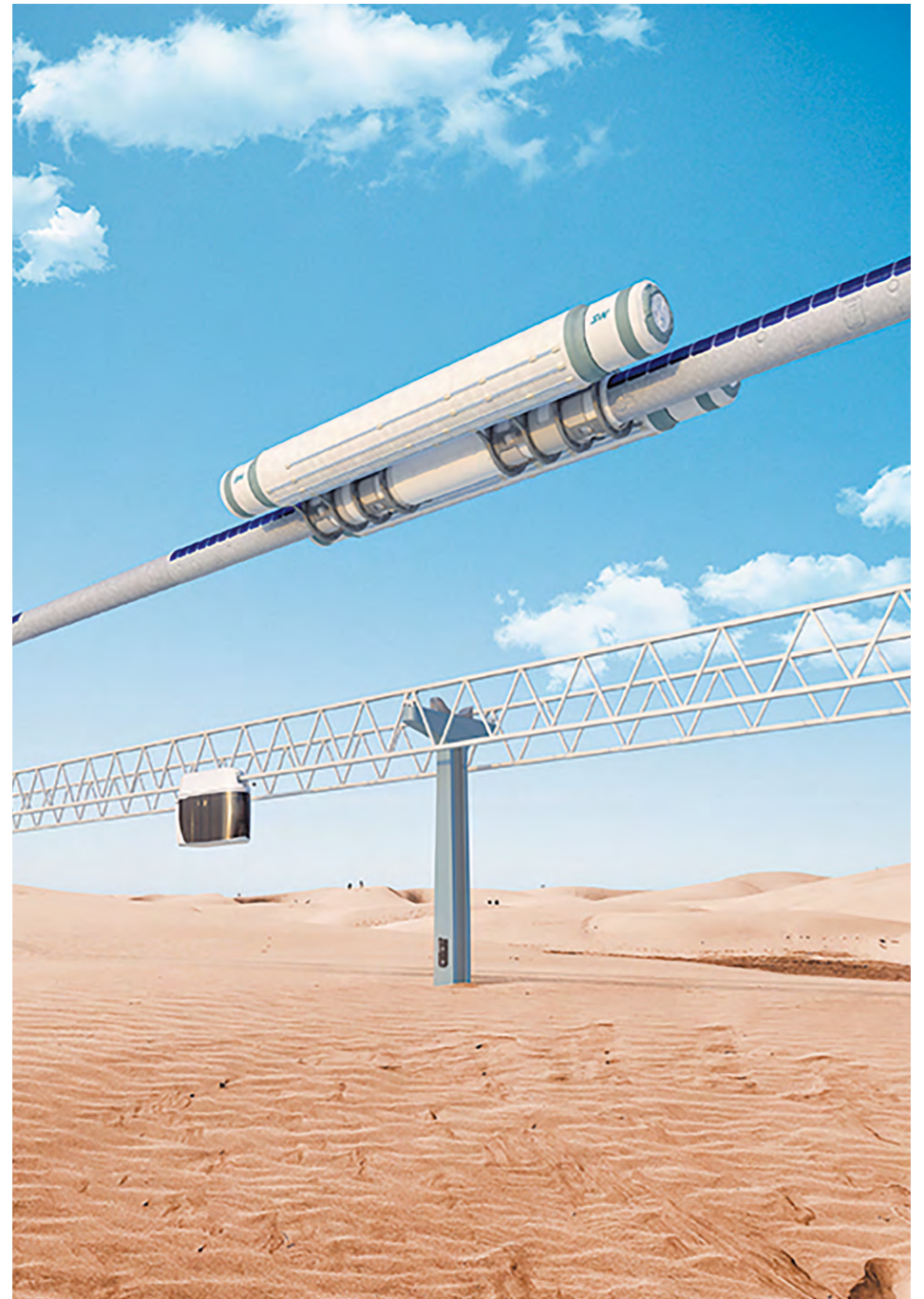
UPT poster signed by the USSR pilot-cosmonaut,
Hero of the Soviet Union Igor Volk. 1988



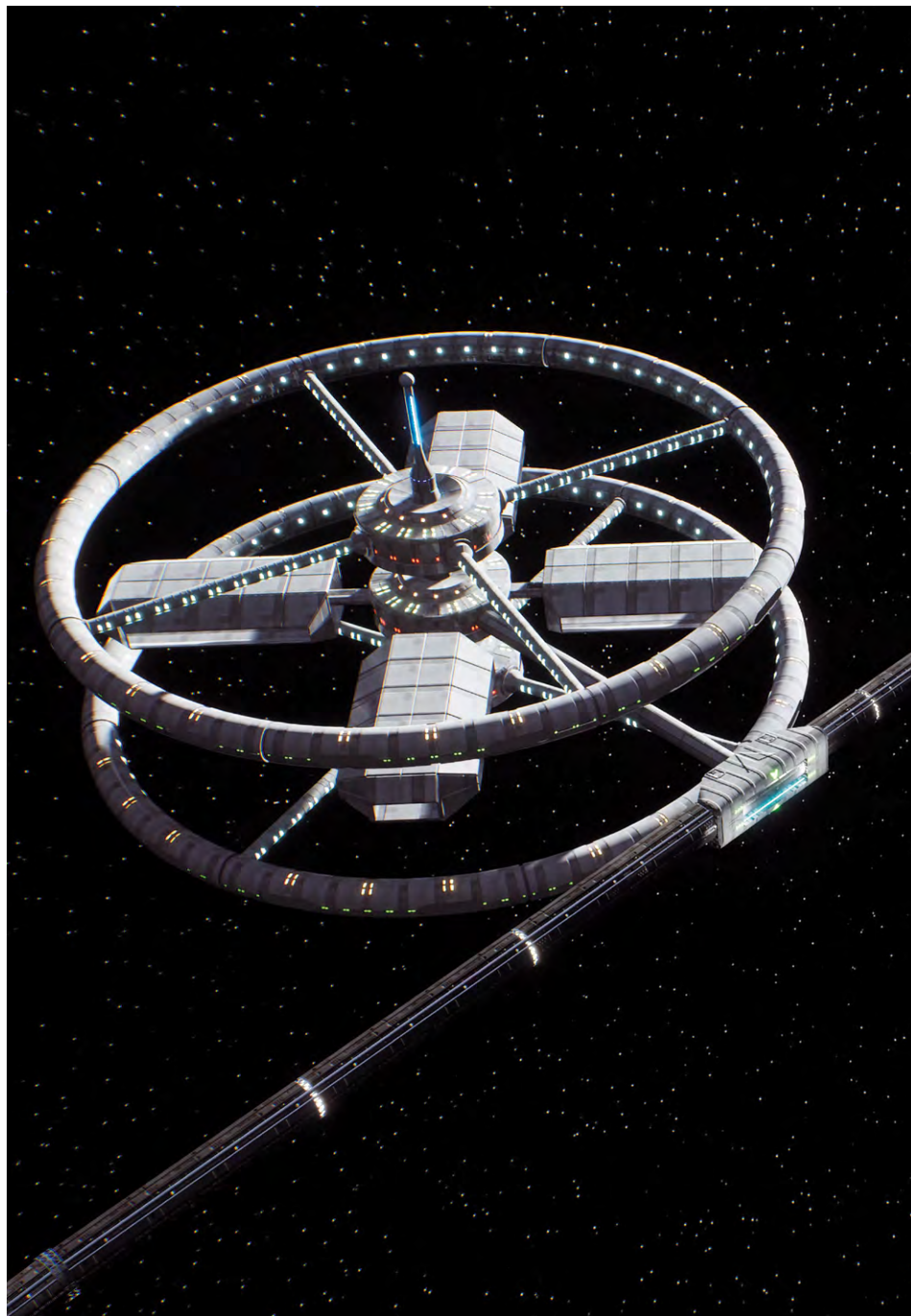
UPT (visualization). 2018



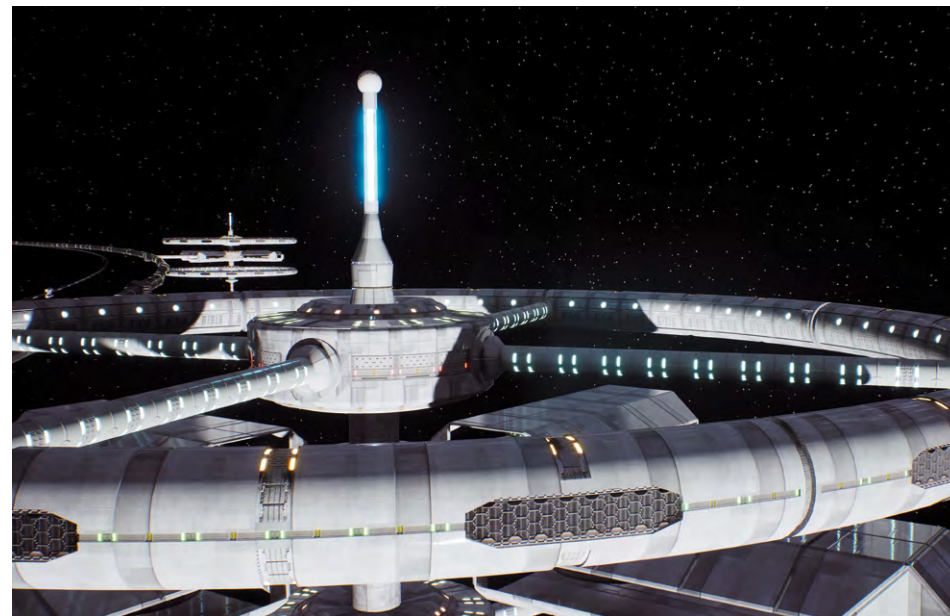
UPT (visualization). 2018



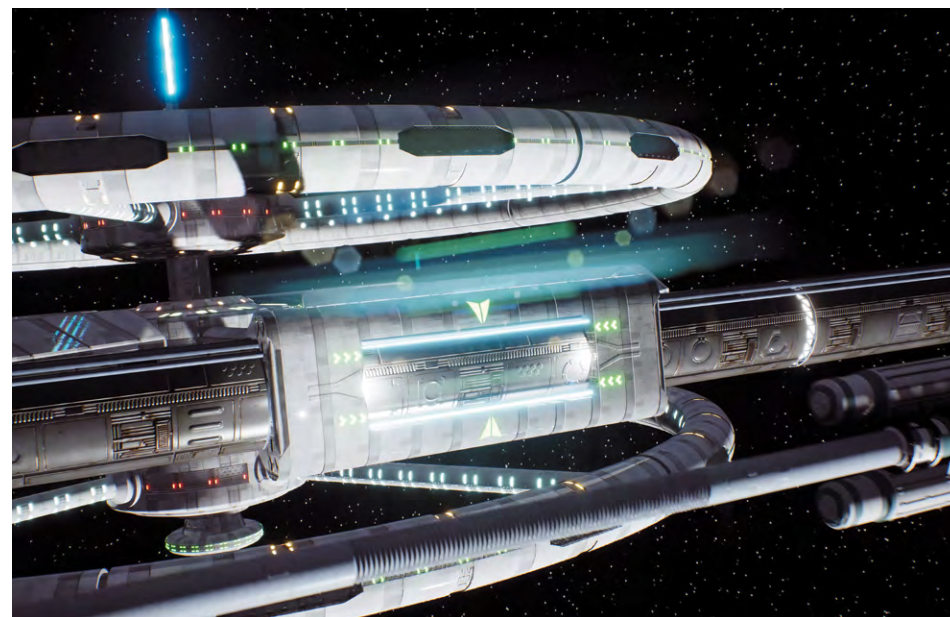
UPT (visualization). 2018



UPT (visualization). 2018



UPT (visualization). 2018



UPT (visualization). 2018

Intellectual Property Rights to geocosmic transport and infrastructure complex “United Planetary Transport”

- | | |
|---|-----|
| 1. Essence of valuation object | 338 |
| 2. Prerequisites for creating a valuation object | 339 |
| 3. Planet – for life, space – for industrial technologies | 339 |
| 4. Quantitative and qualitative characteristics of the valuation object | 342 |
| 5. Information about the author of the appraised intellectual property | 366 |

336



Intellectual Property Rights to geocosmic transport and infrastructure complex “United Planetary Transport”*

1. Essence of valuation object

The valuation object is the exclusive rights to intellectual property – the know-how “Unitsky’s United Planetary Transport” (Unitsky’s UPT) / “General Planetary Vehicle”.

The know-how “Unitsky’s United Planetary Transport” is a reusable geocosmic transport and infrastructure complex for non-rocket exploration of near-space with the purpose to create and operate near-Earth space industry in the future.

The valuation object is complex, including thousands of items, components, parts, modules, assemblies, equipment, technologies and tools, both basic and auxiliary – engineering, industrial, related to construction, infrastructure (including the creation of linear cities on the planet for billions of people to live in conditions more comfortable than on Earth), and communications (including the creation of communicational Transnet network “transport + power industry + communications” based on the breakthrough SkyWay technology, agricultural (including creation of fertile soils and humus for space settlements), power industry (including the creation of a new type of power station, both terrestrial and space), information, social, financial, terrestrial and space, and others, as well as their constructive, technological and operational characteristics and know-how, which absorbed the results of more than 40 years of intellectual, creative, scientific, experimental and production activities of Anatoli Unitsky, engineer, scientist and entrepreneur, author and owner of this intellectual property, confirmed by numerous patents of invention (more than 150), numerous scientific works (more than 100) and monographs (more than 20), scientific-popular articles (more than 200), technical, technological, constructive and engineering know-hows (more than 100) and other results.

* Extract from Report No. 1709-131 “On assessment of the market value of exclusive rights to intellectual property – the know-how “Unitsky’s United Planetary Transport”. Contractor: Limited Liability Company “Center of Business Consulting”, Moscow. Date of assessment: 01.01.2018. Date of report: 01.03.2018.

From a legal point of view, the valuation object is the intellectual rights to the results of intellectual activity and the equivalent means of individualization including the exclusive right, which is a property right.

2. Prerequisites for creating a valuation object

UPT project was developed by Anatoli Unitsky (the author) more than 40 years ago and during this time has been repeatedly investigated and proven by calculation methods, which are detailed in his popular scientific publications (“Interchange, outer space, circular” in the popular science magazine “Inventor and rationalizer”, No. 4, 1982; “To space... by wheel” in the popular scientific journal “Technology for the Youth” No. 6, 1982, “The Planet’s ring buoy” in the socio-political bulletin “XX Century and the Peace”, No. 5, 1987, etc.) and in scientific monographs (“String Transport Systems: on Earth and in Space” – Gomel: Infotribo, 1995. – 337 pages: illustrated; “String Transport Systems: on Earth and in Space” – Minsk: Belaruskaya Navuka, 2017. – 379 pages. – ISBN 978-985-08-2162-1; and others), including the most costly part of the UPT project – the transport and communication overpass, covering the planet in a plane parallel to the equator, which the author is currently developing as a self-sufficient product, spun from UPT under the SkyWay brand – ground transport and infrastructure cargo, urban and intercity high-speed complexes. Demonstration and certification center for innovative SkyWay technology was established in 2015–2018 in the town of Maryina Gorka, Republic of Belarus.

3. Planet – for life, space – for industrial technologies

Mankind does not have any experience of industrial development of near-Earth space. What should be the space industry of the future? What are its functions, what are the volumes and types of products derived? Where will this product be generally consumed – in space or on Earth? There can be many questions asked, but it is impossible to answer them straightly. Everything will depend on those specific ways of development that our earthly civilization will choose, after it has settled down to a technocratic course of development tens of thousands of years ago. At the same time, no one who is living now did ever choose this course of intellectual development of our civilization, and we cannot change this vector in the future.

Primitive technologists, who shaved hides in preparing leather and cooked meal on the fire in their house, died of lung cancer at the age of 20 until they figured it out to use these technologies in caves outside their houses.

Tens of thousands of years have passed. Modern technologists are involved now in violent disputes about which corner of the room of our common house that does not even have partitions and is called “Biosphere” shall be used to build a nuclear power plant, and which of them shall be used to bury its radioactive waste for thousands of years? Where to melt billions of tons of steel and produce even more coal, oil and natural gas, and where and how to burn them thereafter? Where to throw away carbon dioxide and what is the “safe” way to destroy the roof of our house, i.e., the ozone layer, and even get Nobel Prizes for it? Indeed, what is the “environmentally friendly” way to cause maximum damage not only in the corners, but also in the very heart of this large biosphere room, without consulting most residents of the common house, who are not only the “third world” countries, but the dumb animals called “flora” and “fauna” as well.

There is only one way out. It is necessary to be creative and brave as a primitive man and to take environmentally hazardous industries outside our home, or beyond the Earth’s biosphere, into the near space, in this case. It is necessary to share the biosphere created by God and the technosphere created by Homo sapiens in the space, since there are no other places on the planet.

In space – the ideal conditions for the most modern technologies: weightlessness and a deep vacuum. There, all-the-year-round, day and night, the natural ecologically clean thermonuclear reactor called “Sun” has been operating for 5 bln years, which, without any side effects like “Chernobyl”, will provide the extraterrestrial industry with energy for millions of years of subsequent development. There are endless raw materials, energy, technological and spatial resources.

There will be no ecological problems from the biosphere area in the space, since dead industrial waste cannot change the ecology of a dead environment. Even explosions of supernovae that sweep away neighboring stellar systems is hard to imagine, but is common there, similar to supermassive black holes that can absorb the galaxy. What can change the plant, which is placed in the space and constructed to make about billion tons of steel foam a year that will be lighter than water, but will be stronger than common steel and will serve humanity on Earth without signs of corrosion for hundreds of years? Or a plant that produces several thousand tons of unique medicines that can be obtained only in zero-gravity state?

In the future, the sphere of terrestrial material production should be moved almost entirely into the space. At the same time, humanity, as biological species of living beings on our planet, is the result of several billion years of evolution on Earth. We are perfectly tailored to the Earth’s gravity, its atmosphere, the magnetic and electric field of the Earth, its water and foodstuffs, and many other things we are not thinking of, but without which we cannot exist not only today, but in the foreseeable future. There can be no more suitable conditions



Figure 1 – United Planetary Transport during the rise into space (*visualization*)

for us, the people of Earth, anywhere in our vast universe than on our beautiful blue planet*. Therefore, the main consumer of the products of the space industry, and this is billions of people, will be on Earth. It is for this reason that the cargo flow on the highway Earth – Orbit – Earth shall make millions, and over time – billions tons of cargo per year, if in space there will be annually produced at least 100 kg of industrial output per capita of the Earth’s population.

For the entire history of rocket space exploration, no more than 400–500 tons of cargos were delivered to the orbit annually, while this is an average altitude of 300–400 km. The same transportation work (up to 500 tons per year at a distance of 300 km) will be made by one Earth horse, harnessed in a good wagon. For today, a single wagon will not be enough to serve the transport needs of more than 7 bln people (to do that, we are trying to mentally remove all transport from the planet except one wagon). Similarly, a single “space wagon” will not be able to serve the needs of the space industry tailored to the needs of billions of people of Earth. It would be extremely expensive, taking into account total costs, which exceeded 2 tln USD for 60 years of the space

* Undoubtedly, after become familiar with the outer space as new environment which conditions are fundamentally different from the Earth’s ones, those humans who wished to live in space will eventually tailor themselves to these conditions. However, the space man will evolve consciously unlike fish, which came to dry land in prehistoric times, which eventually led to the appearance of a human being on the planet. But this is a too distant prospect, which is beyond reasonable consideration.

age (a wagon made in the form of a diamond would be much cheaper), the delivery of a ton of cargo to orbit by missile carriers is about 10 mln USD. Moreover, it is already estimated that about 100 launches per year of heavy launch vehicles such as the US Space Shuttle (and this is not more than 2,000 tons of cargo per year) will lead to irreversible negative environmental changes, including in the ozone layer of the planet. The Russian launch vehicle Proton-M is not doing better, filled with hundreds of tons of highly toxic fuel (heptyl), more poisonous substance than, for example, potassium cyanide.

The “space elevator” being developed by NASA space agency specialists (the idea of the elevator belongs to the Russian scientist K. Tsiolkovsky and the Russian engineers Yu. Artsutanov and G. Polyakov) will not save the situation either. Self-supporting elevator-wrap more than 40 thous. km long weighing not less than 1 mln tons of superhard material (hundreds of times stronger than steel), fixed at the equator of the planet with its one end, could annually deliver to orbit no more than 2,500 tons of various cargoes. That is, there will be only five “space wagons,” and fabulously expensive, “diamond”.

We do not know the way the technology will develop in the future, including the space technology, as well as the future discoveries. The idea of such predictions is improper, and, in general, senseless. In order to be convinced of that, it is enough to recall naive 50 or 100 years old scientific forecasts. The only thing that can be said with full confidence is that no matter what technique is it, it will obey the fundamental laws of physics of our real world (rather than virtual Hollywood one). Such laws of nature, repeatedly tested in practice, will remain fair in the future. Applicable to mechanics, these include four conservation laws that govern all other partial conservation laws, namely, energy, momentum, angular momentum and the motion of the system’s center of mass. All modern transport, such as carts, bicycles, cars, trains, ships, airplanes, helicopters, missiles, is designed under these laws. The future space transport will prove to be no exception.

4. Quantitative and qualitative characteristics of the valuation object

4.1. General characteristics of UPT

Optimization of the space transport system based on the fundamental laws of physics has resulted in the creation of the ideal solution, namely, the United Planetary Transport (UPT), by the engineer Anatoli Unitsky in 1977.

The know-how “Unitsky’s United Planetary Transport” is reusable geospatial transport infrastructure for the near space exploration without rockets with the purpose of creation and functioning of the near-Earth space industry in the future.



Figure 2 – United Planetary Transport on Earth (*visualization*)

The engineer Anatoli Unitsky has developed a fundamentally new:

- United Planetary Transport, including the principle of operation, based on the implementation of the basic conservation laws (energy, impulse, momentum, torque of momentum, etc.), the layout structure and connections between the nodes and components; the dynamics of the UPT space launch in the equatorial plane of the Earth and the possibility of its maneuvering relative to the equatorial plane;
- device and operating principle of the accelerator for accelerating the UPT rotor in the vacuum channel;
- linear electric motor for accelerating the rotor up to space velocities;
- launching overpass around the planet for passage over land and sea, combined with high-speed ground transportation, including in a specially made fore-vacuum pipe;
- social, economic, financial, resource, geopolitical and philosophical aspects to justify the inevitability of taking an ecologically dangerous component of the earth industry out to a near-Earth orbit and the transition of the terrestrial technocratic civilization to a new stage of post-industrial development – the space stage – with the large-scale use of space technological capabilities (weightlessness, deep vacuum, etc.), as well as spatial, energy, raw materials and other resources;

- necessary resources for the realization of this most ambitious project in the whole history of mankind (namely, finances, technology, materials, structures, units and equipment, power capacities, etc.), but there is no will and understanding of the necessity and inevitability of this step to save civilization from the technosphere, occupying the same niche on the planet as the biosphere, so the degradation of the latter, up to complete destruction, including its human (biological) component is inevitable;

- justification of the fact that two-three generations remain up to the point of no return for the terrestrial technocratic civilization, after which its degradation and extinction will be impossible to stop;

- other.

One single self-supporting aircraft*, made in the form of a torus with a cross section of several meters, embracing the planet in a plane parallel to the equator, will be able to bring about 10 mln tons of cargo and up to 10 mln passengers to the orbit**. It should be noted that the cost of delivery to orbit is 1,000 USD per ton. Which means, the cost of a passenger ticket to orbit will be within 100 USD, while the comfort of travel will be higher than that in modern trains.

United Planetary Transport is the only technical solution while using which the transport system is able to transport cargo to various circular equatorial orbits without the use of jet engines***. And it's the only way to use the most environmentally friendly "Baron Munchausen principle" to enter space, since, in the process of functioning of UPT, its center-of-gravity position does not change in space. Therefore, it may spacewalk using only the system's internal forces, without any energy, mechanical, chemical or other interaction with the environment, which means this device will be extremely environmentally friendly. Moreover, if the cargo flow "Space – Earth" exceeds the return freight traffic "Earth – Space", UPT can function in the "perpetual-motion machine" mode. The excess kinetic and potential energy of the space cargo delivered to the planet will be sufficient for the subsequent launch of UPT from the planet into orbit****.

Only a stretched thread having infinitely small transverse dimensions with respect to length (ratio of about 1 : 10,000,000) can be a stable self-supporting

* See, for example, the scientific monograph of A. Unitsky "String Transport Systems: on Earth and in Space" at: http://www.yunitskiy.com/author/2017/2017_56.pdf.

** To carry out the same amount of transportation work that will be performed in just one UPT flight, modern cosmonautics would need about 100 thous. years – that is, launches of the first American space shuttles were to begin in prehistoric times, approximately when the Neanderthals learned how to obtain fire.

*** See, for example, the article by A. Unitsky "Planet's lifebuoy" in the socio-political bulletin "XX Century and Peace", No. 5, 1987, at: <http://www.yunitskiy.com/news/1987/news19870512.htm>.

**** Each "extra" ton of cargo derived from the orbit to the surface of the Earth in an environmentally friendly way, is equivalent to burning about 2 tons of oil in terms of production of energy.

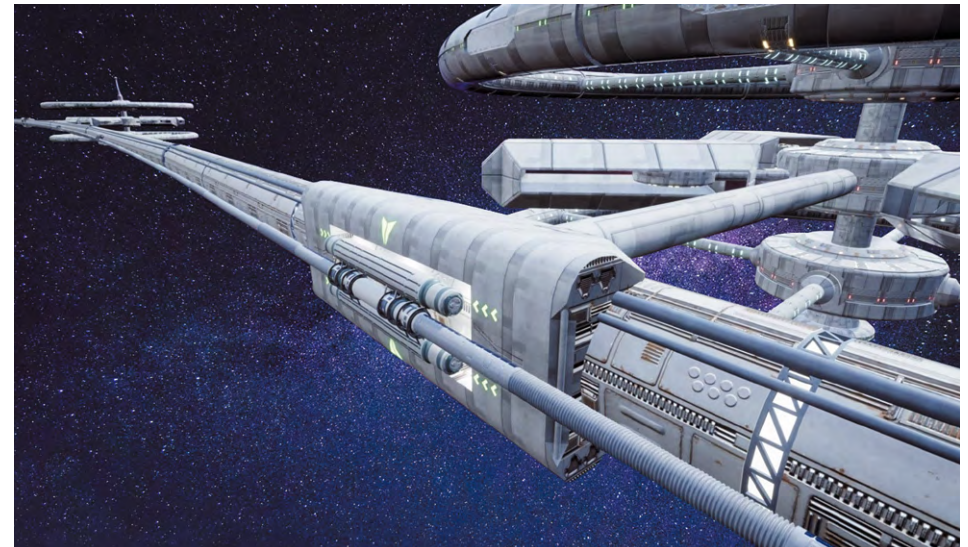


Figure 3 – United Planetary Transport docking the orbital industrial ring (visualization)

structure. Therefore, UPT is a kind of a string transport technology – otherwise this "wheel" with a diameter of more than 12 thous. km, having a diameter of only a few meters in diameter, would lose its stability in orbit. SkyWay – Unitsky's land string transport was derived from this very project in 1977. In the process of optimization, the author needed to simplify and reduce the cost of the overpasses to be used to launch UPT into outer space. The optimization has led to a pre-stressed (stretched) structure of the overpass, which only had to put the rail car (unibus) and provide it with the appropriate string rails.

4.2. Construction of UPT

The creation of United Planetary Transport includes three main directions (stages) carried out in parallel.

1. Research and development works on:

- launching equatorial overpass "5-in-1", combined with the SkyWay transport system;
- infrastructure – transport, logistics, industrial, residential, energy and informational;
- United Planetary Transport;
- transport-infrastructure and industrial complex in orbit, including new space industries: industrial, residential, energy and informational.

2. Preparation and establishment (construction) of the “5-in-1” equatorial launch overpass, combined with the SkyWay transport system, as well as buildings, structures, infrastructure (industrial and residential complexes, power plants, power lines, control and communication systems, etc.).

3. Manufacturing and installation of United Planetary Transport (length 40,076 km, total weight, without payload, – 30 mln tons), commissioning.

The entire set of works related to the UPT establishment is planned to be completed in 20 years – by 2038.

The cost of the UPT establishment and accompanying works up to the year 2037 inclusive is presented in the table 1. It should be noted that the maximum of future annual costs, equal to 260 bln USD, falling for the period 2032–2037, for example, about 2 times less than the current annual military budget of the United States. This also indicates that the UPT program can be implemented alone by such countries as the US, China, Russia, India and even Brazil, based on their budgets in these years.

The total cost of the UPT construction is comparable to the possible world costs for conventional space programs using rocket carriers in 2030.

4.3. Conditions for UPT to enter into the near-Earth orbit

Background

An artificial Earth satellite located in orbit at the altitude of h_0 has the first cosmic velocity for a given altitude, and all its elements are in a state of zero gravity.

UPT that has entered the orbit at the altitude of h_0 shall be in a state of equilibrium (not to rise or fall), therefore, in general, it should also be in a state of zero gravity or weightless.

The best option possible for the UPT operation will involve all its linear elements (covering the planet) that are in a state of zero gravity*. Thus, each UPT element must have the first cosmic velocity V_1 in orbit.

When lifting UPT into space, it is necessary not only to raise it to the altitude of h_0 , but to accelerate its body around the planet to the first cosmic velocity**. This will become possible only when pushing away the flywheel from the belts, according to the law of angular momentum conservation of the closed system***.

* An option is possible, when the elements have oppositely directed weights. For example, one flywheel moves at a velocity higher than the first cosmic, and the second flywheel – at a velocity lower than the first cosmic, and they balance each other vertically.

** Given that during the launch, UPT, lying on the overpass, is motionless relative to the surface of the Earth, that is, its body has a speed of movement (rotation) of the equatorial points of the planet – 465.1 m/s.

*** The use of external pulse sources to obtain the orbital velocity of the body, for example, jet engines, is unacceptable from an environmental point of view.

Table 1 – The cost of the UPT establishment and related work

Year	Costs by years, USD bln			Total, USD bln
	R&D on “5-in-1” equatorial overpass, infrastructure, UPT, other	Establishment of the “5-in-1” SkyWay launching equatorial overpass and ground residential and industrial infrastructure (buildings, structures, power plants, power lines, communication lines, other)	Establishment (construction) of UPT	
2018	0.1	–	–	0.1
2019	0.2	–	–	0.2
2020	0.3	–	–	0.3
2021	0.4	–	–	0.4
2022	1	–	–	1
2023	2	1	–	3
2024	3	2	–	5
2025	4	3	–	7
2026	5	4	2	11
2027	6	10	3	19
2028	7	50	5	62
2029	8	80	15	103
2030	9	150	50	209
2031	10	150	75	235
2032	10	150	100	260
2033	10	150	100	260
2034	10	150	100	260
2035	10	150	100	260
2036	10	150	100	260
2037	10	150	100	260
Total	116	1,350	750	2,216



Figure 4 – United Planetary Transport combined with SkyWay transport system (visualization)

UPT pre-launch procedure

Before start of UPT, the linear flywheels 1.1 and 1.2 (figure 5) must have a sufficient supply of kinetic energy to lift the whole system with a mass of tens of millions of tons per given orbit, taking into account all subsequent energy losses:

- aerodynamic resistance in the atmospheric section;
- losses in magnetic cushion and linear electric motors;
- energy consumption for stretching (increasing) the length of the UPT ring as the altitude is increased and its diameter increases;
- energy consumption for the system (UPT) gaining the altitude of h_0 ;
- energy loss during the returning descent to the planet (if there is no refueling with energy on the orbit and at the stage of descent);
- other.

Further, the flywheels magnetic levitation system is turned on, and the UPT linear electric motors (drive) are connected to external sources of electrical energy. The flywheel belts that do not experience resistance (they are in a vacuum), move along the vacuum channel, and, accordingly, along the body, and rotate around the planet with the axis of rotation passing through the geocenter. The faster the flywheels, the better they accumulate the amount of kinetic

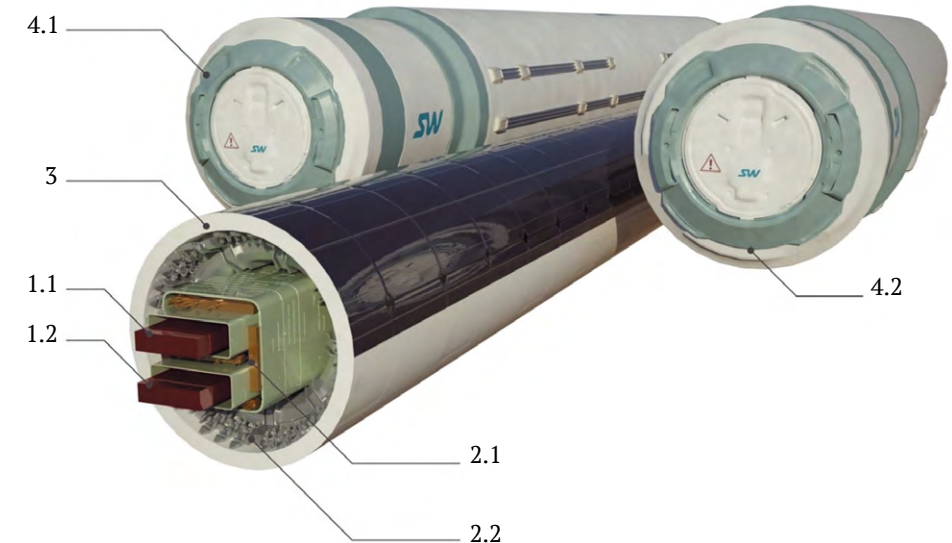


Figure 5 – UPT design (variant):
belt flywheels – 1.1 and 1.2; drive systems – 2.1 and 2.2 located inside body – 3;
external compartments (capsules) – 4: passenger – 4.1 and cargo – 4.2 (visualization)

energy and the amount of motion (the angular momentum) required UPT to get to a given orbit with a given orbital speed*.

One of the main advantages of UPT is seen here, being made in the form of a ring embracing the planet, and this is an infinite way to disperse flywheels, that is, an infinite time for charging UPT with the necessary energy. For example, a rocket has a finite starting distance (several hundred kilometers) in a finite time (several minutes), so the power of a heavy carrier rocket (that is, the total power of all its jet engines) is about 100 mln horsepower**, although the rocket puts into orbit not more than a few tens of tons of payload per flight, accelerating it to the first cosmic velocity. Now imagine that the time of energy consumption will be not several minutes, but several days, that is, thousands of times more. At the same time, the efficiency of the UPT drive will not be less than 95 %, that is, a hundred times higher than that of the rocket***.

* For example, at an altitude of 300 km in the plane of the equator, the first cosmic velocity is 7,728 m/s, at an altitude of 500 km – 7,615 m/s.

** It is difficult to imagine a herd of 100 mln horses.

*** Taking into account all energy losses for fuel preparation (for example, liquid oxygen and liquid hydrogen, their cooling and maintenance of cryogenic temperatures), fuel combustion in the jet engine, aerodynamics, etc., including loss of the first stages of the carrier rocket, which production took a lot of energy, the overall energy efficiency of the missile carrier is less than 1 %.



Figure 6 – United Planetary Transport during the landing on the overpass (visualization)

Therefore, it would be possible to transfer in space not one tons per flight, but millions tons of cargo with the same drive power as the rocket has (about 100 mln kW), that is, a million times more*.

There are various possible design and performance characteristics of UPT with flywheels of different masses (with equal masses, or one flywheel is heavier and the other is lighter), with different modes of launching acceleration of the flywheels (both flywheels are accelerated on the planet either in one direction or one of them – in one direction, and another one – in the other direction), etc.

In any case, when the speed of the flywheel belt embracing the planet reaches the first cosmic velocity in the vacuum channel**, it will become weightless. When there is an increase in flywheel speed, the vertically guided centrifugal force (that is, from the center of the Earth along its radius) will exceed

* Thus, one UPT flight will replace a million launches of heavy rockets such as the US Space Shuttles, although it has long been estimated that 60 to 80 shuttle launches a year will completely destroy the ozone layer of our planet. In other words, the rocket technology will need at least 100 thous. years for what it is capable of doing in one UPT flight. And since in one year UPT is able to perform at least 10 flights onto orbit and back, the UPT transportation work, at the same energy capacities, is equivalent to one million years of operation of the traditional transport and space complex of the whole mankind. That is, to take the earth industry out to the space in the 20th century, and this is hundreds of millions of tons of cargo, the Space Shuttles had to start launching several million years ago, even before the Neanderthal era.

** The first cosmic velocity at an altitude of 0 km in the equatorial plane amounts to 7,908 m/s; 7,671 m/s at an altitude of 400 km.

its weight, that is, it will try to take it away from the planet. When the belt fly wheels' centrifugal forces exceed the UPT weight (for example, equal to 1,000 kgf/m), the whole system will become conditionally weightless* (the UPT weight will be zero, that is, it will not press the overpass). If the flywheels are accelerated to a higher speed, then there will be an excess lifting force sufficient impacting vertically upwards on each linear meter of the vehicle to lift the whole UPT complex to the given orbit along with the payload.

To transport everything to a given orbit, for example, to an altitude of 500 km, two flywheels of UPT having an general unladen weight of 20 mln tons (500 kg/m) must generally keep the kinetic energy of 1.25×10^{18} J (about 3.5×10^{11} kWh).

Taking into account the losses and energy costs when entering the orbit (in particular, due to the efficiency of linear electric motors of about 95 %), the initial energy reserves should be 15–20 % more, that is, they will be about 1.5×10^{18} J (4.2×10^{11} kWh). Then, if the power of connecting UPT to the external power system (the planet's energy system) equal to 100 mln kW** (or 2.5 kW per a meter of the system length), the initial charging time of the geocosmic transport complex – the acceleration of the flywheels to the calculated speed – is 420 hours (17.5 days).

After the belt flywheels gain the design speed, UPT with a total mass of 40 mln tons, of which 20 mln tons fall on flywheels, is ready for take-off. But it is kept from lifting along its entire length with the help of special locks installed on the supports of the overpass. Upon loading the cargo and placing passengers in the hanging nacelles, the locks release the body along its entire length, and nothing keeps UPT on the planet anymore.

Since the flywheels are accelerated to speeds that ensure the centrifugal force exceeding the weight of each linear meter of UPT, each linear meter of the self-supporting vehicle embracing the planet starts to move from the center of rotation of the flywheels, that is, to rise vertically upwards in the equatorial plane passing through the geocenter. In this case, the UPT ring will increase in diameter symmetrically in all directions relative to the center, and its body will lengthen, stretch, without any displacement of the center of mass of this giant ring, which, according to the law of conservation, will always coincide with the center of mass of the planet.

The acceleration of a vertical rise into space depends on the excess of centrifugal forces. For example, if the lifting force acting on each linear meter is greater

* If both flywheels with a linear mass of 250 kg/m each (only 500 kg/m) are accelerated to a speed of 11,184 m/s, then UPT weighing 1,000 kg/m (the whole mass of the "wheel" will be 40.075 mln tons, of which 10 mln tons is the weight of cargo and passengers) will become weightless.

** 100 mln kW are less than 2 % of the world's net power plants today. At the same time, UPT can be fed mainly at night, when the cost of electricity is significantly reduced.

than the weight of each linear meter of UPT by 5 %, then its body will start to rise with a comfortable for passengers' acceleration of 0.5 m/s^2 , or equal to 5 % of the gravity acceleration. When driving with such acceleration, UPT will rise (expand in the equatorial plane) to a height of 100 km in 5 min 16 s and will have a vertical lift speed at this altitude equal to 570 km/h.

When lifting every 100 km above the ground, the UPT body should be extended by 1.57 %*, which is easily achievable with the use of the constructive and technological solutions, for example, telescopic connections along the length between short sections of the body, or spring (expansion) joints and other techniques known and approved.

After leaving the dense layers of the atmosphere (at altitudes of more than 10 km), the linear electric drive of the flywheel belt, which is accelerated on the earth to the cosmic speed in the direction of rotation of the planet, is switched on to the braking (generator) mode. The electric energy generated in this case is not wasted, but commuted to accelerate the second belt flywheel in the opposite direction. As a result, the UPT body receives a double pulse and starts rotating in the direction of the planet's rotation. If the acceleration of rotation is still comfortable and is 0.5 m/s^2 , then the body and all the cargo attached thereto (including the passengers placed in the nacelles) will generate a calculated orbital, that is circular, speed, for example, equal to 7,671 m/s (for an altitude of 400 km) exactly in 4 h.

The climbing and orbital speed modes are selected so that UPT could have an orbital speed (that is, 7,671 m/s) and was at equilibrium – its vertical speed would be zero – at a given altitude, for example, 400 km. To do that, when walking into space, a special ballast system is used, if necessary. Environmentally friendly substances, for example, water and oxygen (compressed or liquefied) is used as ballast. If such ballast is sprayed in a predetermined amount in the ozone layer of the planet and higher (at a height of 10 to 60 km), it will be possible to regulate the oxygen and ozone content in the upper atmosphere layers and to heal ozone holes, as well as to control weather and climate on the planet in an environmentally friendly way**.

Upon pursuing the given orbit and stabilizing UPT along its entire length (absence of local oscillations with respect to the ideal orbit), the cargoes and passengers are unloaded into the orbital ring complex (embracing the planet).

* Accordingly, the UPT diameter will also increase by 1.57 %.

** The ozone layer delays up to 4 % of solar radiation, including harmful ultraviolet rays, and up to 20 % of the reverse radiation of the Earth, warming the atmosphere and being a kind of blanket – a thermal reservoir for thermal energy in the atmosphere. At that, the content of ozone in the atmosphere is extremely low: for example, if the ozone contained in the atmosphere were at atmospheric pressure, the thickness of its layer (the reduced thickness) would not exceed 3 mm.

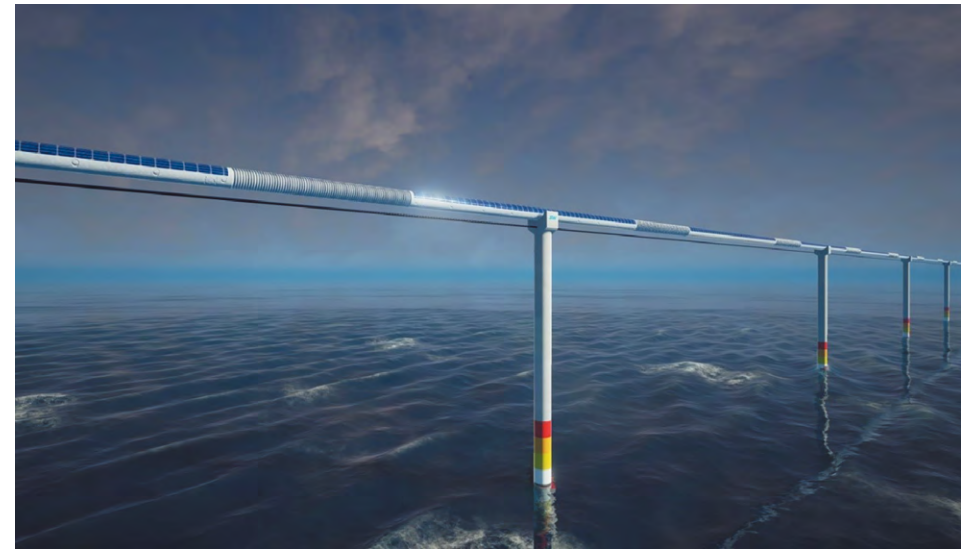


Figure 7 – The beginning of the UPT rise into space on the offshore area (visualization)

Load capacity of UPT is 250 kg/m, or 10 mln tons. This is enough to start creating the space industrial torque “Orbita” (SIT “Orbita”) around the planet Earth at the first start of UPT.

4.4. Conditions necessary for the creation of SIT “Orbita”

The space industrial torque “Orbita” is an orbital transport and infrastructure, as well as industrial-residential complex covering the planet in the equatorial plane at a given altitude (for example, at an altitude of 400 km) and having an appropriate length of 42,567 km (for a height of 400 km). The construction of SIT Orbita will start upon the very first launch of UPT.

The very first launch of UPT into space will create the basic transport and infrastructure, as well as energy information complex SpaceTransNet (STN), as the foundation for creating the space industrial torque “Orbita” at the given altitude. “Orbita” will look like a torque covering the planet in the equatorial plane, in which “small beads” are paired cargo and passenger nacelles delivered to the orbit in a distance of about 500 m (about 160 thous. pieces in total, or 10 mln tons together with cargo and passengers), connected together by a “thread” – string orbital roads and other energy and information communications. Since there is no weight of the terrestrial transport in the orbit, the string roads make pre-stressed strings made of, for example, reinforced aluminum

(for transmission of electric energy along the orbit between plants and workshops).

Over time, crystals will grow around the nacelles and around the catalyst to be the plants, factories, workshops, power stations and other industrial facilities, as well as residential space settlements – EcoSpaceHouse, in which the operating personnel of SIT Orbita will live and work. The transverse size of these structures is up to 500 m, so as not to increase their sail spread, which will impede the entire industrial complex due to the presence of a gas medium at this altitude, albeit very rare*.

SIT “Orbita” includes the following main components

1. Industry

As compared with the earth industry located on the surface of the planet, space and near-Earth space have several advantages.

Firstly, there is, contrary to the planet, zero gravity in orbit. This makes it possible to produce unique assemblies, mechanisms, equipment. For example, making steel foam, which will be stronger than common steel, but it will not sink in water and will not suffer corrosion.

Secondly, there is a deep vacuum in the orbit, which is harder to obtain on Earth than to extract oil – a cubic meter of high vacuum costs more than a ton of oil. Vacuum coupled with zero gravity will allow, for example, mastering the production of unique ultra-pure and super-strong substances and materials, including nanomaterials and biological products.

Thirdly, the space has unlimited spatial, raw, energy, and other resources. For example, it is easy to deliver powerful energy in the orbit, which is principally necessary for orbital industrial needs – after all, about 1 kW of power taken from a natural thermonuclear reactor (the Sun) can be taken from one square meter of the sunlit surface. This reactor burns smoothly for 5 bln years, and will still burn during the same period without any stopping, repairs or accidents.

With sufficient level of technology development, which will ensure the commissioning of UPT and SIT “Orbita”, extraction of such elements as platinum, cobalt and other rare minerals at asteroids with their subsequent delivery to Earth’s orbit can bring a very large profit. For example, in the prices of 1997, a relatively small metal asteroid with a diameter of 1.5 km contained a variety of metals, including precious metals, worth 20 tln USD**. In fact, all gold, cobalt, iron, manganese, molybdenum, nickel, osmium, palladium, platinum, rhenium, rhodium

* At an altitude of 400 km, we can speak of the atmosphere only conditionally, since its density is very low: $3 \times 10^{-12} \text{ kg/m}^3$.

** <https://books.google.com/?id=k9hwi3ktye8C&dq=isbn=0201328194>.

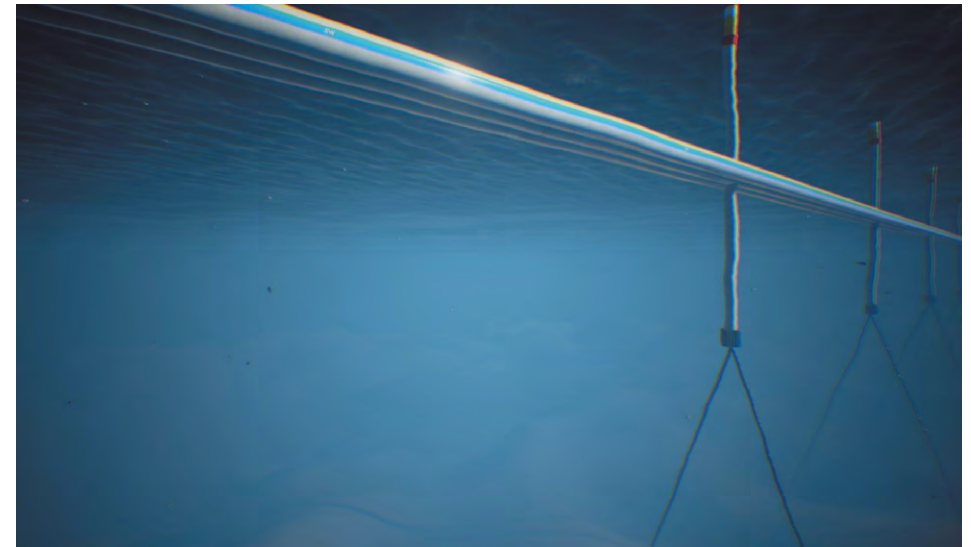


Figure 8 – The offshore area of the UPT launching overpass: the supports do not reach the seabed, being kept afloat by a system of underwater floating tunnels and anchors (*visualization*)

and ruthenium, which are now extracted from the upper layers of the Earth’s crust, are the remains of asteroids that fell to Earth during the early meteoric bombardment, when after the cooling of the crust on the planet, a huge amount of asteroid material collapsed. Because of the large mass of the planet more than 4 bln years ago, the Earth began to differentiate the depths, as a result of which most of the heavy elements gravitated to the core of the planet, so the crust was depleted of heavy elements. And on most asteroids because of the insignificant mass, there has never been a differentiation of the interior and all the chemical elements are distributed more evenly in them.

In 2004, world production of iron ore exceeded 1 bln tons. For comparison, one small asteroid of class M with a diameter of 1 km can contain up to 2 bln tons of iron-nickel ore, which is 2 times higher than ore extraction on our planet in 2004. The largest known metal asteroid (16) Psyche contains 1.7×10^{16} tons of iron-nickel ore, which is 100 thous. times greater than the reserves of this ore in the earth’s crust. This amount would be enough to meet the needs of the world’s population for several million years, even taking into account the further increase in demand. A small part of the extracted material can also contain precious metals.

People will gradually move in orbit from Earth, or rather, industrial manufactures, scientific laboratories, plant, factories, workshops will be created, first of all – in power engineering, machine building, metallurgy and chemistry.

2. Residential area

The residential sector “Orbita” will be based on multifunctional clusters of EcoSpaceHouse, each of them can host up to 10 thous. people for living and working.

To make the people’s stay in space comfortable, it is essential that the conditions will be equivalent and even superior in quality to the Earth’s ones.

- **Comfortable gravity**

Gravity in orbit can be modeled using the centrifugal forces. It may happen that the most comfortable gravity will be reduced one, similar to that on the Moon or Mars, for example, with the gravity acceleration of about 2 m/s^2 , that is 5 times lower than on Earth. Then an adult would weigh about 15 kg, could easily jump on the roof of the house and fly like a bird, if he/she had wings.

- **Comfortable atmosphere both by pressure, composition, humidity and temperature**

1. *Pressure in the atmosphere of the space house.* It is possible that the pressure will be as comfortable in orbit, as in the mountains on Earth, for example, half the atmospheric pressure, that is, 0.5 kgf/cm^2 , or 5 t/m^2 . Reducing the pressure twice will reduce the load on the body of the space house, due to the pressure of the atmosphere inside.

2. *Atmospheric composition.* In order to avoid oxygen starvation, the oxygen content can be doubled, for example, up to 40 %*, if the atmospheric pressure is reduced by half compared to the Earth’s one. The content of other gases (nitrogen, argon, neon, carbon dioxide, etc.) can also be optimized.

3. *Air humidity.* Since the human body, as well as animals and plants, gets moisture not only from food, but from the air as well, the humidity of the atmosphere in a space house must be optimal for a day and the whole year**, for example, equal to 55 %, although it can be adjusted during a day or a year.

4. *Air temperature.* Air in a space house can have an optimum temperature adjustable throughout a day or a year, for example, equal to $+21 \text{ }^\circ\text{C}$.

- **Comfortable living space (environment) for a human**

In the space house, there shall be biosphere of the planet must be fully modeled as the cradle of a man with a history of evolution numbering billions

* The oxygen content should be limited to the upper value, at which self-ignition of various combustible substances (for example, wood) can occur, which will be used in EcoSpaceHouse.

** The concept of the year in orbit loses its meaning, like the concept of the day. Therefore, a day and a year in EcoSpaceHouse can be of an optimal duration, which differ, respectively, from 24 hours and 365 days, respectively. For example, 24-hour biorhythm is imposed and violent for most modern urban residents, as evidenced by the regular use of the alarm clock.

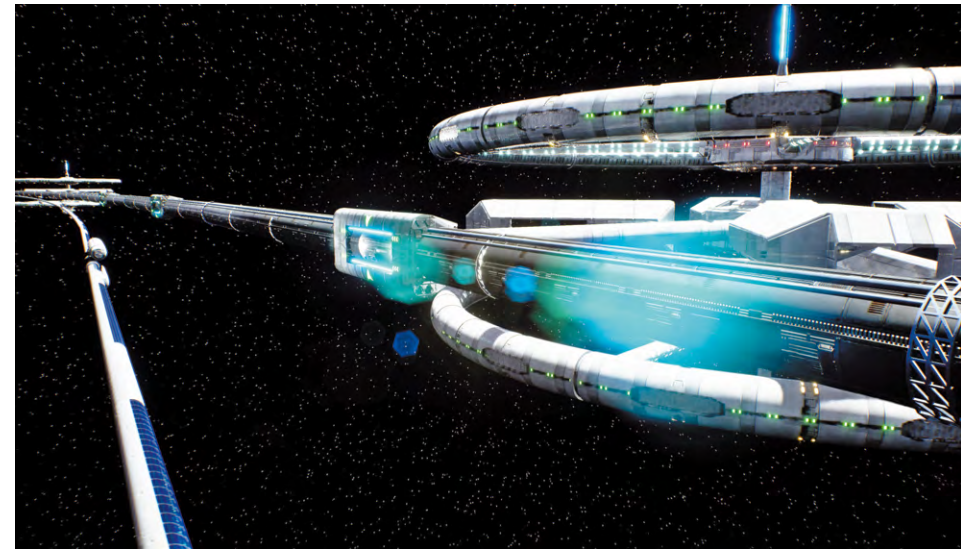


Figure 9 – The design of the space industrial torque “Orbita” fragment (variant), to which the expanding UPT fragment arrives (*visualization*)

of years, including the preceding one. The flora and fauna of our cradle should be represented here in all their diversity*, since we are rooted to it, including the microflora and the microfauna – the soil biogeocenosis with thousands of microorganisms**. Lacking a healthy (living) fertile soil in EcoSpaceHouse, it will be impossible to make living comfortable for a man who imagines himself to be the king of nature, but in fact is only a small component*** of the biosphere of the planet Earth. Even less significant for it than mold.

The biosphere of a space house must constantly produce the oxygen necessary for people and animals living there to breathe, to produce healthy food

* For example, in our blood there is the ancient ocean – its mineral composition completely corresponds to the composition of its water.

** A kilogram of healthy fertile soil contains about a trillion soil microorganisms of several thousand species – they are all necessary for the existence of flora and fauna in the terrestrial biosphere, including humans. Therefore, fertile soil on the planet is the immune system of the biosphere and the guarantee of its health. When the living fertile soil will be killed on the planet and replaced by dead soil impregnated with herbicides and pesticides and richly fertilized with mineral fertilizers, this will be the beginning of the end of the terrestrial biosphere – the one we all know and of which we are a part. Then, for example, a pandemic can easily occur, capable of killing all people within just a few days – no two-hundred-meter yacht, Boeing with missile defense, or own island in the ocean will not help anyone to survive.

*** The human immune system is the microflora and microfauna of its intestine, which, in general, is a soil. There live trillions of microorganisms of thousands of species. They work day and night, feed and drink us and even... treat. No wonder many experts consider the contents of the intestine by our second brain. But why are they of soil type? We forgot that we are all from the soil, and we will be buried there.

and to utilize all wastes of vital activity of living organisms, including humans, in humus* (living fertile soil).

- **Protection against meteorites and radiation**

The existing orbital stations do not fully protect from meteor and radiation hazard that exists in space, and in the near-Earth orbit. For example, a drop of water at a speed of 20 km/s can penetrate tank armor, and cosmic radiation can kill a person in a few days, since its level is much higher than at the emergency Chernobyl nuclear power plant. Not heavy-duty thin-walled screens, but thick multi-layered barriers can be most effective from both of these dangers. They may include foams, and a many meters layer of fertile soil inside the space ecohouse, as well as water and air.

- **Composite elements of EcoSpaceHouse**

The most optimal option of the structural part of the space-housing cluster is a hollow sphere (or cylinder or torus (figure 10) with a diameter of 200–500 m) spun around its axis. Bearing body of the sphere is made of high-strength materials and is the most non-material-consuming part of such a house. For example, if it is made of composite materials produced by industry today, the thickness of the bearing wall of such a huge structure will be just... 3 mm. The most material-intensive part of the spherical house will be anti-meteoritic and anti-radiation protection, as well as a layer of fertile soil – their total thickness will be up to several meters.

The inner surface of the sphere will be layered with the living fertile soil and forests, gardens, meadows planted with their biogeocenoses. There are ponds with fresh and seawater including their ecosystems. Part of the sphere approaching the axis of rotation of the sphere contains mountain landscapes, with streams and waterfalls and its submontane ecosystems. The air in the space house is filled with the smell of flowers and useful phytoncides, which favorable action on the human body cannot be compared with any medicines. There is no noise except for the singing of birds and the whisper of the leaves of trees.

The approximate number of materials needed to build a space house in orbit for 5,000 people will be approximately 400 thous. tons, including:

* The basis of soil fertility, including the most fertile soil on the planet (Black Earth) is humus, insoluble salts of organic humic acids of thousands of varieties, the structure of which includes 80 chemical elements of Mendeleev's table. This is a kind of canned food for plants (if humus was soluble, it would be washed with the first rain out of the soil), which reveals a kind of can opener – microorganisms living in the soil, each species of which has a narrow specialization. They translate the humus into a soluble form, and then they feed and water the plants, joining with them in a kind of the symbiosis. No plants can exist without such a symbiosis (with mushrooms), since mushrooms not only live in the plants themselves, but also form a mushroom root with their roots, which feeds and water their host.



Figure 10 – The design of the space industrial torque “Orbita” with torus-shaped EcoSpaceHouses on it (visualization)

- structural shell – 1,000 tons;
- anti-radiation and anti-meteorite protection – 90 thous. tons;
- fertile living soil (eco-black earth) – 160 thous. tons;
- water (fresh and sea) – 70 thous. tons;
- air – 5,000 tons;
- building materials and structures, including for housing inside the space house – 15 thous. tons;
- other – 59 thous. tons.

The delivery of all materials into orbit for one EcoSpaceHouse with the help of UPT will cost about 500 mln USD, the cost of materials and substances for it will cost approximately the same amount – 500 mln USD, installation work in orbit will cost about 1 bln USD. Thus, space settlements to host up to 5,000 people for living and working will cost about 2 bln USD, which is almost two times cheaper than the International Space Station*. That is, the money the humanity has spent today for up to a dozen astronauts to have the possibility of being in orbit (in very uncomfortable and life-threatening conditions)

* The International Space Station (ISS) is an undeniable leader by cost (but far from ambiguous in significance and result). According to the experts, the price of establishing and maintaining the station is already approaching or has even exceeded 150 bln USD. Read more: <http://www.rbc.ru/society/06/04/2011/5703e5c19a79473c0df1c7e6>.

will help (using UPT) to build 75 space settlements for 375 thous. inhabitants who will live and work in much more comfortable conditions than on Earth.

4.5. UPT geocosmic carrier cost

Geocosmic carrier cost using United Planetary Transport on the Earth – Orbit and Orbit – Earth route consists of three main components.

1. The cost of electrical energy for the operation of all onboard UPT systems, primarily linear electric motors and linear flywheels (rotors) magnetic levitation systems, which consumes more than 95 % of the energy.

2. Salary of maintenance staff including taxes and deductions.

3. Depreciation charges not only for UPT, but also for the ground-based transport, infrastructure and SkyWay energy-information complex that serves it.

1. Costs of electric power

The initial reserves of energy needed to raise UPT with a gross mass of 40 mln tons to space and return to land without any payload, with a gross mass of 10 mln tons left in orbit, is 4.2×10^{11} kWh.

For the operation of UPT, own power plants with a total capacity of about 100 mln kW would be better, then electric energy can be distributed within the system at a cost of about 5 cents/(kWh). Moreover, additional energy can be taken from the network of the countries on the territory of which the UPT overpass runs. It is more profitable to use it at nights only since night tariffs are 2–2.5 times lower than daily ones, despite the fact that the average weighted cost of electricity sales in the world today is 8.2 cents/(kWh)*.

The unit cost E_0 of power for the first** launch of UPT will make:

$$420,000,000,000 \text{ kWh} \times 0.05 \text{ USD/(kWh)} = 21,000,000,000 \text{ USD, or:}$$

$$E_0 = 2,100 \text{ USD/t (with total payload of 10 mln tons).}$$

During several first launches of UPT, when the one-way cargo transportation “Earth – Space” will prevail (since the space industry will only be originated, and the finished products that will need to be delivered back to Earth will be practically absent), energy costs will be needed only for the difference of cargo flows into orbit and back to Earth. Therefore, for one-way flights during the first year of operation, when the space industry will only be originated, it will

* Comparison of electric power cost by countries: <http://www.vrx.ru/treasury/346.html>.

** The first launch of UPT will require the initial spinning of flywheels to cosmic speeds in their vacuum channels, that is, the initial “filling” with kinetic energy, which, in the future, should never decrease, but only will be replenished.

be necessary to compensate for only the energy costs per flight for the cargo delivered to space, the mass of which (revenue load factor*) is 25 % of the gross mass of UPT: $k_{crg} = 10,000,000 \text{ t}/40,000,000 \text{ t} = 0.25$. Thus, during this period of operation of UPT (the first year), the delivery of one ton of cargo to the orbit will require energy costs of:

$$E_1 = 2,100 \text{ USD/t} \times 0.25 = 525 \text{ USD/t.}$$

In that, once accelerated flywheels can rotate inside the vacuum channels for years, since a permanent magnet magnetic cushion and vacuum will not create resistance to their movement with cosmic speeds.

For equal cargo flows “Earth – Orbit” and “Orbit – Earth”, which will be established approximately after 7–8 years of the UPT operation, additional energy will only be needed to compensate for losses in linear flywheel motors**. If the total energy losses within the UPT system are 10 %, then the cost of energy to deliver a ton of cargo to orbit in this case (and, correspondingly, to lower a ton of cargo to the surface of the planet) is:

$$E_2 = 2,100 \text{ USD/t} \times 0.1 = 210 \text{ USD/t.}$$

After the space industry has worked at full capacity and the development of asteroids and the Moon, sources of raw materials will begin, the need to deliver raw materials from the Earth will significantly decrease. In this case, the reverse cargo flow from orbit to the planet will be much higher than the direct one, since the bulk of industrial products for the people of Earth will be delivered from space. If the space industry products of higher quality than the current one will be produced in the future even less than today on the planet per capita, then the annual volume of transportation along the route Orbit – Earth will reach 500 mln tons over 10 years of the UPT operation, which will require 50 flights to orbit (approximately once a week). At the same time, UPT will have less time to deduce the payload into orbit (in this case, the flight will be about 20 % loaded only), basically it will go into space behind the products produced there to deliver it to the planet to consumers, who will amount about 10 bln people of Earth by that time. This will allow converting the potential and kinetic energy of the space cargo

* For carrier rockets, this figure is less than 5 %.

** If there are no losses (with the efficiency of linear electric motors and magnetic flywheels equal to 100 %) and with equal cargo flows to the space and to the Earth, UPT can operate in the “perpetual motion” mode: it can fly into space and land back on the ground without supply of energy from the outside. And if the cargo flow from the space exceeds the cargo flow from the Earth, UPT can work as a giant power plant, in which the delivery of one excess ton of cargo to the Earth is equivalent in energy efficiency to 2 tons of oil.

delivered to Earth into electricity and give energy annually equivalent to 1 bln tons of oil to the energy system of the planet. At this and subsequent phases, the energy costs will be negative, and UPT will operate in a power plant mode that generates a profit of: $500,000,000 \text{ t/year} \times 8,000 \text{ kWh/t} \times 0.05 \text{ USD/(kWh)} = 200,000,000,000 \text{ USD/year}$, or, 400 USD per each excess ton of cargo delivered from orbit to Earth as is.

At that, part of the energy will be spent on the UPT own needs (about half), so every ton of excess cargo delivered to the planet from space will give a net energy profit of $E_3 = 200 \text{ USD/t}$.

2. Salary of maintenance staff

Although UPT and the equatorial launch platform with the SkyWay system will operate in automatic mode, they will require maintenance staff of about 200 thous. people (or 5 people per 1 km of length). With an average salary of one employee, together with taxes equal to 5,000 USD/year, the annual salary costs will be 10,000,000,000 USD.

3. Depreciation costs

Depreciation costs in the project are made up of the costs of rebuilding UPT and restoring the equatorial launch platform of UPT, combined with the SkyWay routes:

$$C_{depr} = C_{UPT} + C_{SW} = 7.5 \text{ USD/t} + 13.2 \text{ USD/t} = 20.7 \text{ USD/t}.$$

The rationale for these costs is given below.

- *Depreciation costs for UPT*

The capital costs for the UPT creation (design and construction) can be estimated by analogy with modern and perspective electric vehicles, in which the bulk of the cost falls on electrical equipment. The complexity of equipment and the composition of the components of UPT is approximately equivalent to an electric vehicle (even it will be somewhat simpler) and will cost about the same, in terms of the cost for one ton of construction, no more than 25,000 USD/t*. Since the mass of the equipped UPT (without payload) is 30 mln tons, its cost will be: $30,000,000 \text{ t} \times 25,000 \text{ USD/t} = 750,000,000,000 \text{ USD}$.

UPT is designed for approximately 10 thous. launches** into space and landings back to the planet. During this time, it will transport 100 bln tons of cargo.

* See "4 best electric cars of Chinese manufacture" at: <http://www.chinamodern.ru/?p=18182>.

** Approximately the same number of take-offs and landings the modern airliner performs during its service life.

Then the depreciation costs per 1 ton of cargo from capital investments to UPT will make:

$$C_{UPT} = 750,000,000,000 \text{ USD} / 100,000,000,000 \text{ t} = 7.5 \text{ USD/t}.$$

- *Depreciation costs for the UPT equatorial launch overpass, combined with the SkyWay routes*

The length of the UPT equatorial overpass will be 40,076 km, of which about 20 % will be located onshore and 80 % – offshore.

Since UPT shall not only go out to space but, first of all, take onto orbit a payload – passengers and various cargoes – then, along it, on the planet and in the space, the transport and infrastructure complexes shall be placed with their own high-speed transport logistics*, as well as industrial, energy, information and residential infrastructure.

Therefore, the UPT launching overpass, located at the equator, will be the SkyWay transport-infrastructure communicator**, including:

1) high-speed track (at the third level, speed up to 600 km/h);

2) urban track (at the second level, speed up to 200 km/h);

3) hyper-speed track in the fore-vacuum channel (under water or underground, speed up to 1,250 km/h).

SkyWay overpass will also integrate power lines (the 4th component of the communicator) and communication lines (the 5th component). Own power plants, industrial and residential complexes will be built. Moreover, along the overpass a linear pedestrian city of cluster type will be built, with millions of people living and working.

The cost of the transport and communication part of the equatorial SkyWay, built on the "5-in-1"*** principle, can be estimated at 1,320 bln USD, based on the fact that, on average, it will cost 25 mln USD/km onshore and 35 mln USD/km offshore.

As it was mentioned earlier, UPT is designed for approximately 10 thous. launches into space and landings back to the planet. During this time, it will transport 100 bln tons of cargo. Then the depreciation costs per 1 ton of cargo from capital investments to the equatorial SkyWay transport-communication part will make:

* Basically, to move passengers and cargo along UPT, including in the sea areas, which take about 80 % of the overpass length.

** More information about SkyWay is available on the website of engineer Anatoli Unitsky at: <http://www.yunitskiy.com/>.

*** It means: 1) high-speed track; 2) urban track; 3) hyper-speed track; 4) power lines; 5) communication lines.

$$C_{sw} = 1,320,000,000,000 \text{ USD} / 100,000,000,000 \text{ t} = 13.2 \text{ USD/t.}$$

The analysis of the data given in table 2 allows drawing the following conclusions.

1. The highest prime cost of geocosmic transport – 700 USD/t – in the first year of operation, is due to the need for initial spinning of flywheels and significant energy costs for this, as well as – a relatively small amount of annual traffic.

2. Over the years, as the volume of traffic, both direct and reverse, increases, their cost is significantly reduced.

3. At the 9th year of operation, when the reverse cargo flow (from orbit to the planet) will significantly exceed the direct cargo flow (from planet to orbit), the cost of transportation will become negative. This means that the geocosmic complex will make a profit not as a transport, but as a giant power station with a length of more than 40 thous. km, having belt flywheels with a total mass of 20 mln tons, which will be able to recover the potential and kinetic energy of space cargo into electrical energy.

4.6. The economic effect of using UPT

The economic effect of using UPT or geocosmic transport on the route Earth – Orbit – Earth is determined by the difference in the cost of transportation by the existing carrier rockets and UPT. This difference, according to the author, is about 10 mln USD/t, as noted above – at the lowest weighted average prices of delivery of cargoes into orbit by rockets.

Thus, in the first year of the UPT operation, when about 100 mln tons of cargo will be brought into orbit, the economic effect will amount to 1,000 tln USD (with economy of 10 mln USD, as explained above) for the delivery of each ton of cargo to orbit. With the years, this effect will only grow. These calculations take into account only the material component of production and delivery of products.

If we reduce the economic effect obtained in 20 years to the current value of money in time with an annual discount of 25 %, then the effect will be reduced by 86.7 times, that is, the economic effect of 1,000 tln USD will “weigh” only 11.5 tln USD.

And the effect of improving the quality of life on the Earth, improving the ecological situation in the terrestrial biosphere as a whole, creating conditions for unlimited development of mankind in the future with the transition to the cosmic stage of development cannot be estimated from a financial point of view.

Table 2 – Prime cost of geocosmic transportation by years of the UPT operation

Year (since the beginning of the UPT operation)	Annual volume of transportation, mln t		Cost components for geocosmic transportation per ton of cargo, USD/t				Prime cost of transportation, USD/t (-) – profit
	To orbit	To Earth	Energy	Salary	Depreciation	Other	
1	100	10	525	90.9	20.7	63.4	700
2	200	50	450	40.0	20.7	39.3	550
3	300	100	300	25.0	20.7	24.3	370
4	400	150	200	18.2	20.7	21.1	260
5	500	200	150	14.3	20.7	15.0	200
6	500	250	100	13.3	20.7	11.0	145
7	400	300	50	14.3	20.7	10.0	95
8	300	350	0	15.4	20.7	8.9	45
9	200	400	-100	16.7	20.7	7.6	-55
10	100	500	-200	16,7	20.7	7.6	-155
11	100	500	-200	16.7	20.7	7.6	-155
12	100	500	-200	16.7	20.7	7.6	-155
13	100	500	-200	16.7	20.7	7.6	-155
14	100	500	-200	16.7	20.7	7.6	-155
15	100	500	-200	16.7	20.7	7.6	-155
16	100	500	-200	16.7	20.7	7.6	-155
17	100	500	-200	16.7	20.7	7.6	-155
18	100	500	-200	16.7	20.7	7.6	-155
19	100	500	-200	16.7	20.7	7.6	-155
20	100	500	-200	16.7	20.7	7.6	-155
Total	4,000	7,310					

5. Information about the author of the appraised intellectual property

ANATOLI UNITSKY:

- author and general designer of Unitsky's string transport (UST). Today the transport of the new generation, also known as STL (string transport lines), NTL (new transport lines), STS (string transport system) is developed under the SkyWay brand;
- the Head of two projects of the United Nations;
- member of the USSR Cosmonautics Federation;
- author of more than 150 inventions;
- author of 20 monographs and more than 200 scientific papers;
- education: 1) railway engineer; 2) patent law and invention; 3) design of high-rise buildings and infrastructure facilities;
- Chairman of the Board of Directors, General Designer of SkyWay Technologies Co. (Minsk, Republic of Belarus) and the international SkyWay Group of Companies.

Awards:

- two gold medals of the All-Russian Exhibition Center;
- three "Golden Chariots" (National public award of Russia) in the nomination "The project of the year of the transport industry";
- three Golden Quality Marks "Russian Brand";
- honorary title "Knight of Science and Arts";
- more than 40 diplomas of international exhibitions.



MONOGRAPH

PART 2

United Planetary Transport

INTRODUCTION	370
CHAPTER 1 Dynamics of the UPT exit into space in Earth's equatorial plane	395
CHAPTER 2 Dynamics of the UPT placement into orbit with energy dissipation by means of capsule ejection	426
CHAPTER 3 Rotor maneuvering in order to avoid objects moving in equatorial plane	457
CHAPTER 4 Problems of creating an accelerator for the UPT rotor	483
CHAPTER 5 Parameter estimation of the aerodynamic heating process for the UPT rotor in the absence of protective capsule	505
SUMMARY 1995	525
Conventional symbols	532
Bibliography	536
Scientific and technical reports	539

368



MONOGRAPH

PART 2

United Planetary Transport

Introduction

1. Need for space industrialization

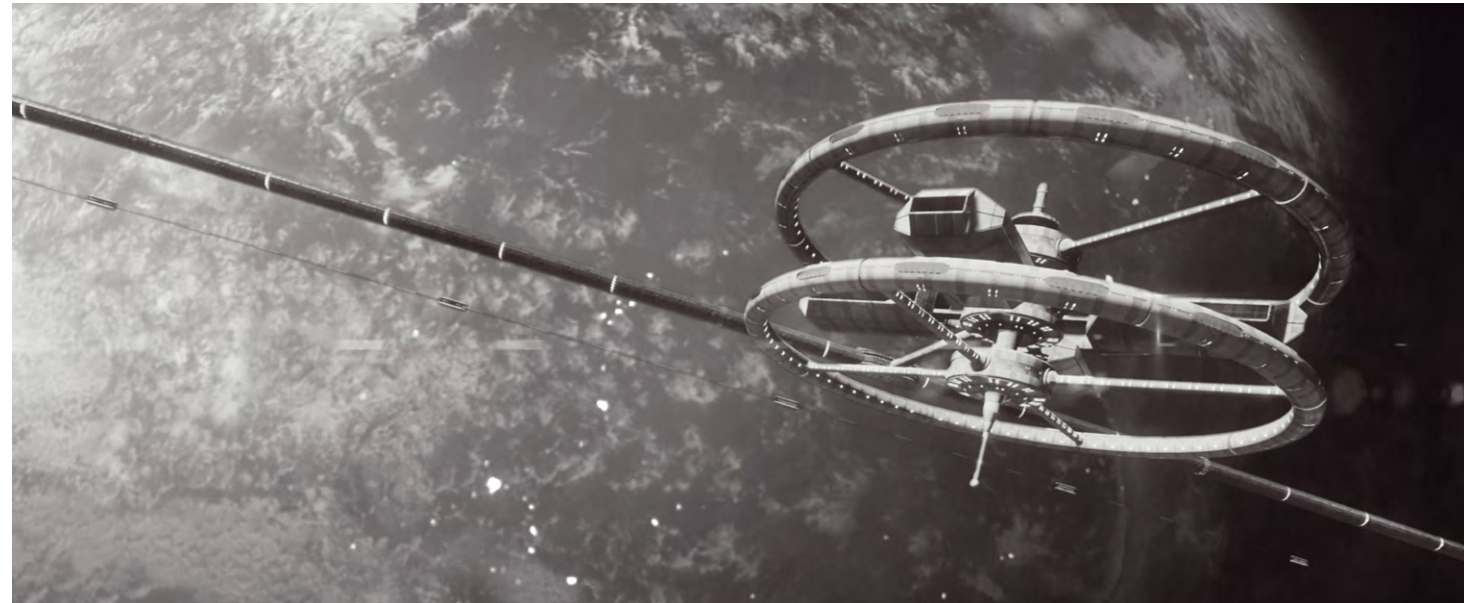
At present, several species of living organisms are disappearing daily, and this number is predicted to increase to 100 in just 20 years. They are disappearing and will soon become extinct forever, irretrievably. However, nature created these forms of life not for us to kill them.

The rate of medical conditions, such as cancer, allergy, pulmonary and cardiovascular diseases, as well as genetic disorders and hereditary diseases is rapidly growing due to contamination of water, air and soil.

Irreversible landscape changes, soil erosion, deforestation, pollution of seas and oceans are taking place, as well as an intensive destruction of the ozone layer of the planet that protects every living thing from a detrimental hard radiation of the Sun.

There are numerous reasons for the ongoing negative changes in the Earth's biosphere. But what is the root cause of these processes? It is only by understanding it that we will be able to avoid degradation of the biosphere and humanity as one of the biological species and to determine the path of harmonious development of civilization in the future.

According to modern concepts, life on the Earth originated about 4 bln years ago. Evolving, adapting to the conditions existing on the planet at that time, living organisms began to transform the environment. These transformations were not less than those that were happening with living organisms in the course of their development and improvement. Thus, oxygen-bearing



atmosphere, soil, coral reefs, ozone layer, modern landscape with its swamps, tundra, taiga and jungles appeared on the initially dead and deserted planet. In this way a biosphere was created, where millions of species of living organisms and the planet transformed with their help matched perfectly to each other. There is nothing superfluous here.

But here appeared a man who, thanks to mind, began to increase the power of muscles, senses, intellect, to create technology to master industrial processes. It happened a long time ago, hundred thousands years ago when primitive people started to make the first primitive tools, then began to cook on an open fire and tan animal skin. It was then that humanity entered the path of technological development, and it is not for us



It is only by understanding the reasons we will be able to avoid degradation of the biosphere and humanity as one of the biological species and to determine the path of harmonious development of civilization in the future.

to change that today. The modern industrial power of the earth civilization is just a logical development of technocratic direction.

Factories, power plants, machines, vehicles, etc. – these are the analogues of living organisms in the biosphere. Similar to living organisms, they exchange energy and materials with the environment; therefore, similar to organisms, they inevitably transform the Nature. In fact, from a biological point of view, it causes environmental pollution. However, from a technical point of view, factories and power plants do not pollute anything. They have raw materials at the input, and at the output – finished products and converted raw material (excluding finished products), which of course get into the same area where it was taken from – the environment. It is impossible to avoid it in principle. The creation of closed-loop technological cycles to solve environmental problems in this way is fundamentally impossible, either. It is about the same if we let us say, try to look for a way to prohibit a cow to produce milk, along with urine, manure, methane and CO₂.

Even the biosphere as a whole is not a closed system. In fact, it transformed the Earth, which was earlier dead. Only an “Earth – Biosphere” system is a closed one.

Even the entire technosphere, let alone an individual plant or factory, cannot be a closed system in terms of a specific planet. The technosphere will be inevitably transforming the Earth. But in what direction?

The technosphere* does not need oxygen-containing atmosphere. That is why the US industry, for example, even today consumes more oxygen than is produced by trees and plants in America. The Americans live in debt. They consume the oxygen generated by the Russian taiga and the Amazon rainforest. What if all countries achieve that level of industrial development?

The technosphere does not need soil. Therefore, increasingly less fertile soil is left on the planet, however more and more dross, ash and slag heaps.

Acid rains, smog, a high level of radiation, destruction of the ozone layer, etc. – all this is inevitable. It is only possible to slow down the process of transforming the earth nature, the biosphere,

There is only one drastic way out of the current situation: it is necessary to provide the technosphere with an ecological niche beyond the biosphere.

* Oxygen for technical needs is mainly irretrievably removed from the atmosphere only in the process of fuel combustion in a car engine. This is only because it is the cheapest (and not the only possible) method. In the absence of oxygen in the atmosphere, the same vehicles would operate perfectly well if they had an oxidant tank in addition to a fuel tank.

but there is no way to stop it. The technosphere occupies the same ecological niche as the biosphere on the whole: machinery, mechanisms, technological devices are located in the depth of the earth, water, air and are actively exchanging energy and materials with them. Ecological problems rose sharply in the last quarter of the twentieth century for the reason that the technosphere approached the biosphere in terms of its power supply capacity, i.e., by its ability to transform the environment. The biosphere now generates 232.5 bln tons of dry organic substance* per year, which in terms of fuel is by only ten times more than the annual power consumption of all the machinery available for the use of the terrestrial civilization. Meanwhile, the volume of soil, ore and raw material transported and processed by machinery has closely approached the volume of organic substance produced by the biosphere.

There is only one drastic way out of the current situation: it is necessary to provide the technosphere with an ecological niche beyond the biosphere. This will ensure preservation and development of the biosphere in accordance with the laws and directions that have been formed during billions of years of evolution, as well as a harmonious interaction of a people's community as biological objects with the biosphere.

There is no such an ecological niche for the technosphere on the Earth. However, it is found in space, where the majority of technological processes can have ideal conditions: zero gravity, vacuum, ultra-high and cryogenic temperatures, indefinite raw, energy and spatial resources, etc.

Thus, we have come to the conclusion on the need for space industrialization if the terrestrial civilization continues the path of technological development in the future**. Humanity does not have much time for a large-scale space exploration since its irreversible degradation along with the degradation of the human race will start, according to a number of forecasts, in two-three generations due to a technocratic oppression on the biosphere.

* Alekseev, G.N. Energy and Entropy / G.N. Alekseev. – M.: Znaniye, 1983. – P. 74.

** Apparently, humanity will not have another way – the path of technological development that has raised living standards of people and has provided the existence of about 6 bln people on the Earth to date has gone too far. The rejection of the industrial power of civilization would pose a threat of death (from hunger, diseases, cold, etc.) to billions of people (the besieged Leningrad during the Great Patriotic War can serve as an analogue of a similar situation).

We have come to the conclusion on the need for space industrialization if the terrestrial civilization continues the path of technological development in the future.

2. Selection of criteria for space industrialization

Mankind does not have any experience of industrial development of near-Earth space. What should be the space industry of the future? What are its functions, what are the volumes and types of products derived? Where will these products be mainly consumed: in space or on the Earth? A lot of questions can be posed; and hardly any definite answers can be given to any of them today. Any answer can be right and wrong at the same time – everything will depend on the specific development paths chosen by the earth civilization in the future for a large-scale space exploration.

Space industrialization implies the creation of conditions suitable for the production of various materials, power, machinery, receiving new information, carrying out technological processes and scientific experiments on orbit. Therefore, a significant traffic becomes inevitable between a consumer of material products – mankind living on the Earth, and the production located in space.

In fact, the objective reasons specified earlier (environmental restrictions, exhaustibility of earth, raw, energy, spatial and other resources, danger of atmospheric overheating and global negative climate changes, etc.) will contribute to the future almost entire relocation of the material production sphere to space. Meanwhile, humanity as a biological species similar to any other kind of living organisms on our planet is a product of a 4 bln year evolution in terrestrial conditions. We are perfectly matched to the terrestrial gravity force, terrestrial atmosphere, Earth's magnetic and electric field, earth food products and many other earth things we do not even suspect of but without which we cannot exist today or in the foreseeable future. Nowhere in the immense Universe can we, earth dwellers, have the more suitable conditions than on our beautiful blue planet. Therefore, the main consumer of products of the space industry, i.e., billions of people, will be located on the Earth*.

At the same time, the civilization will strive to increase the living standards of every individual, whose number in its turn will be growing. This means that the volume of geocosmic transportation in the future will inevitably have approximately the same scope as the modern ground transport. About 20 years ago, this volume exceeded 100 bln tons of cargo per year**. When analyzing the questions of space industrialization in the future, it is necessary to assume the volume

* It is obvious that the conditions of outer space as a new environment are fundamentally different from the earthly ones. That is why having mastered it, a part of humanity that wishes to live in space will over time transform itself under these conditions (in contrast to fish that reached the land in prehistoric times, which ultimately led to the emergence of man on the planet, the space man will be evolving consciously). However, it is too distant a prospect, which is not considered in this work.

** Compare: the amount of only slightly more than 10 thous. tons of payload, or on average about 300 tons annually had been delivered to the orbit by 1990 using carrier rockets with the efforts of entire humanity.

of geocosmic cargo traffic of millions and billions of tons per year.

The location area of the extra-terrestrial industry will be significant, as well. It should be as near as possible to the consumer, i.e., to the planetary surface with billions of people living there. Since the industry will include a great number of components (factories, technological platforms, power plants, accommodation modules, etc.), the orbits of their motion must not intercross. Otherwise, a chain reaction of the entire system breakdown (“domino principle”) can happen taking into consideration an extremely high motion speed, which will cause the death of thousands of people working in the space industry. The probability of such a catastrophe is nonzero even with the availability of the most advanced control system. There is only way to avoid it – to locate the extraterrestrial industry in the equatorial plane of the planet (sort of the Saturn, Jupiter, Uranus rings). Having this type of location of circular orbits, the velocity vectors of space bodies that can be at the same vertical at an arbitrary point of time are parallel to each other regardless of the altitude of orbit location.

In this case, the closer the neighboring orbits are to each other, the less the difference in their absolute speed is. Therefore, it is possible to speak here not about a possibility of space vehicles collision, for example as a result of some emergency situation, but about their contact with each other. This will also allow us to quite easily go from one orbit to another and exchange raw materials, energy and products made in space between the neighboring orbits.

Thus, the principle of the circumterrestrial space exploration in the future (figure 1) differs significantly from the modern space colonization (figure 2), where the orbits of artificial Earth satellites and orbital stations are arbitrary and intercross* with each other.

Humanity has explored practically the entire planet by now, having located factories, power plants and buildings not only on land but also beneath

* Only an extremely low population density of the orbits saves from devastating collisions of space vehicles at the circumterrestrial orbits at the present stage of space science development. When transferring to the industrial space exploration, these orbits must be cleared from space vehicles and garbage since they will pose a threat for the equatorial industrial zone, which in the course of its development will be converted into a disk encircling the planet.

Space industrialization implies the creation of conditions suitable for the production of various materials, power, machinery, receiving new information, carrying out technological processes and scientific experiments on orbit.

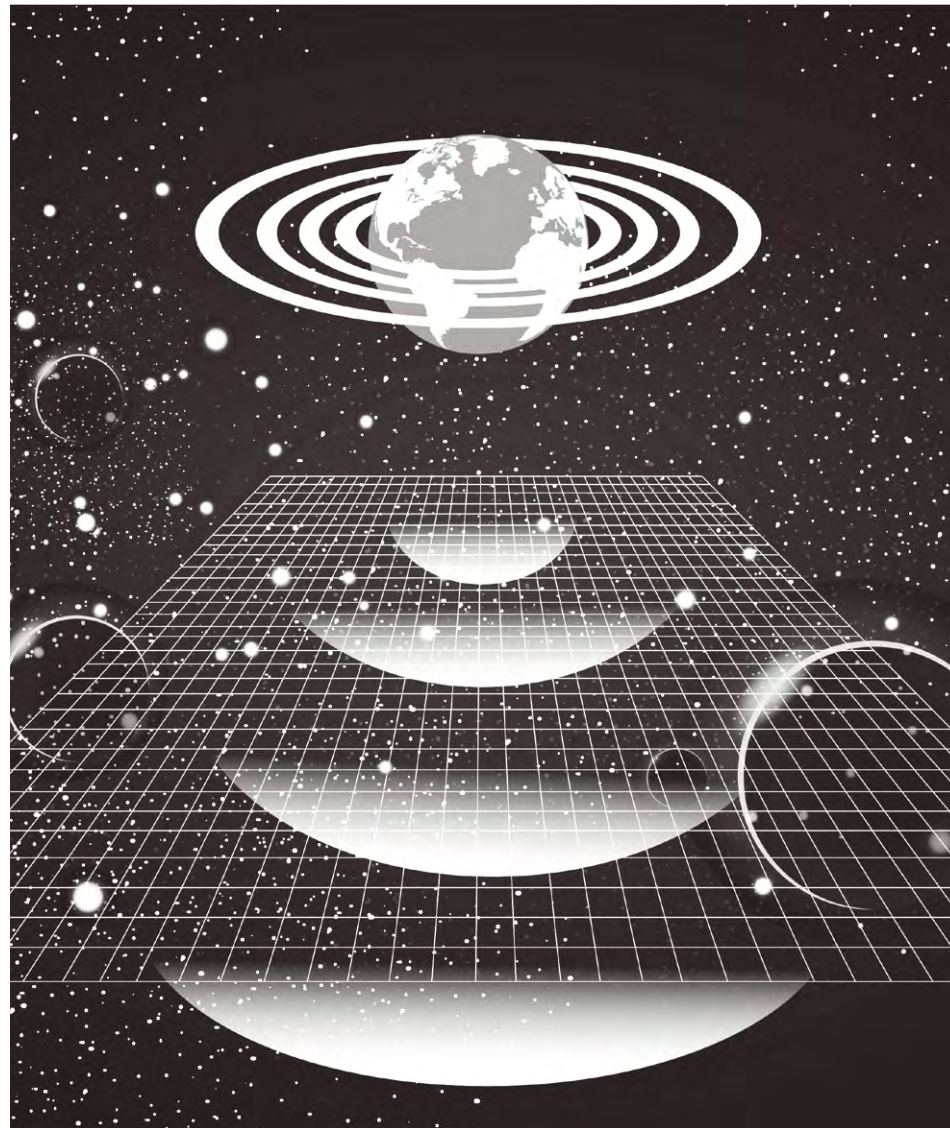


Figure 1 – Scenario for developing circumterrestrial space in the future

the ocean, in Antarctica, in the mountains and other hard-to-reach places by stretching various communications for thousands of kilometers. These communications are used to transfer raw materials, energy, finished products and information, as well as to transport people. They provided the creation, development and maintenance of the powerful modern technological civilization.

For this purpose, a powerful and extensive communication network was created on the Earth. It includes wheeled transport (automobile and railway), aviation (planes, helicopters, airships), sea and river transport (sea and river vessels, submarines), pipeline transport (oil and gas pipelines, etc.), power transmission lines, etc. However, thousand-year experience on the creation of transport network on the Earth cannot be used for space exploration, since none of the specified kinds of transport is able to go into space.

A fundamentally different approach is required in order to create geocosmic transport (GCT) capable of providing industrial space exploration and transition of the earth civilization to the space one.

Extremely high energy costs for space industrialization impose a range of serious restrictions on GCT. Its efficiency factor must be close to 100 % since even a relatively small energy outbreak into the environment at GCT operation can

A significant traffic becomes inevitable between a consumer of material products – mankind living on the Earth, and the production located in space.

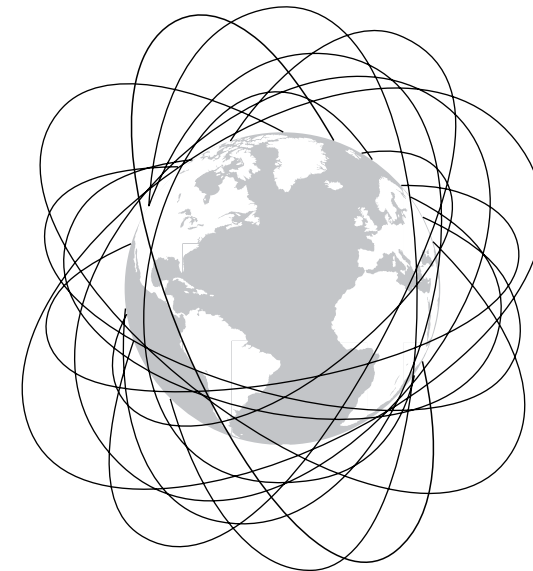


Figure 2 – Scenario for developing circumterrestrial space at present

**Nowhere
in the immense Universe
can we, earth dwellers,
have the more
suitable conditions
than on our beautiful
blue planet.**

Any kind of ground transport rests on something on the Earth: a car rests on the road, a plane – on the air, a sea vessel – on water, etc. A fundamental difference of GCT from ground transport is that it should be self-supported since there is nothing to rest on in space. Apart from that, ground transport can operate with minimal energy losses since it moves practically on a horizontal surface whereas in order to go into space, an ascent for the altitude of hundreds of kilometers is required. Ground transport can operate no matter how low the speed is, whereas in order to explore space, cosmic speed is required. The following example illustrates how large this difference is. Every kilogram of cargo taken to the low orbit has the same energy as a suburban electric train having the speed of 50 km/h*.

We do not know in what way the technology, including space technology, will be developing in the future, nor do we know what future discoveries will be made. Making such predictions is an unplausible and generally senseless idea. In order to make sure of the said, it suffices to recall naive scientific forecasts of 50 or 100 years long. The only thing that can be stated with full confidence is that no matter what kind of technology it could be, it will be subject to the fundamental laws of Nature. Such laws repeatedly proven in practice will remain to be true in the future. In the area of mechanics** they include four conservation laws, to which all other particular cases of conservation laws can be reduced, namely: energy, impulse, angular momentum and motion of mass center of the system.

* A carrier rocket spends on this by about a hundred times more energy than required, since its total energy efficiency is about one per cent taking into consideration preflight energy losses (receipt of fuel component, cooling down to cryogenic temperatures, etc.) and inflight energy losses (aerodynamic resistance, low efficiency factor of jet engine operation, loss of lower stages, whose production requires a large amount of energy, etc.).

** Factories, power plants, residential modules, communications and other components of space industry located on the orbit are mechanical systems with the total mass of millions tons; therefore, the principles of their creation and operation should be primarily considered from the perspective of mechanics.

cause considerable ecological problems, which are already becoming a major challenge on the Earth. Moreover, it is required to use the cleanest energy (which is electric energy as is known for today) as reference energy for it. In addition to solving ecological issues, a GCT increased efficiency factor will reduce the net cost of cargo delivery to the orbit. In this case, the net cost is inversely proportional to the transport system efficiency factor similar to any kind of ground transport.

Thus, the basic conditions of space industrialization:

- 1) location of space industry on the low orbits in the equatorial plane;
- 2) compliance with the conservation laws when creating the extra-terrestrial industry;
- 3) possibility of creating GCT meeting the requirements:
 - theoretical efficiency close to 100 percent;
 - provision of cargo traffic of millions and in prospect billions of tons of cargo per year;
 - use of ecologically clean electric energy for exit into space;
 - GCT must be self-supported.

3. Conservation laws in relation to geocosmic transport

3.1. Energy conservation law

The total work A_t that should be done to deliver cargo with mass m_c from R distance of the Earth's center to r distance (to the circular orbit) is as follows*

$$A_t = \frac{\mu_e m_c}{R} \left(1 - \frac{R}{2r} \right), \quad (1)$$

where μ_e – gravity parameter of the Earth.

For this purpose, the cargo should have a characteristic velocity V_{ch} (near the Earth's surface):

$$V_{ch}^2 = \frac{2\mu_e}{R} \left(1 - \frac{R}{2r} \right) = V_2^2 \left(1 - \frac{R}{2r} \right), \quad (2)$$

where V_2 – the second cosmic velocity.

The transport system has the following energy parameters.

1. Total energy losses E_t for taking cargo into space:

$$E_t = \frac{A_t}{\eta_e} = \frac{K_c}{\eta_e} = \frac{m_c V_{ch}^2}{2\eta_e} = \frac{m_c \mu_e}{\eta_e R} \left(1 - \frac{R}{2r} \right), \quad (3)$$

* Fertregt, M. Bases of cosmonautics / M. Fertregt. – M.: Prosveschenie, 1969. – P. 114.

where η_e – the GCT energy efficiency (taking into consideration all preflight and inflight energy losses); K_c – kinetic energy of cargo having the speed V_{ch} .

2. Total capacity N_t developed by GCT when taking cargo to the orbit:

$$N_t = \frac{E_t}{t} = \frac{m_c \mu_e}{\eta R t} \left(1 - \frac{R}{2r}\right) = \frac{m_c V_{ch}^2}{\eta t} \left(1 - \frac{R}{2r}\right), \quad (4)$$

where t – the GCT operating time (time required to supply energy to cargo).

3. Amount of energy E_{en} released to the environment:

$$E_{en} = E_t - A_t = \frac{m_c V_{ch}^2 (1 - \eta)}{2\eta} = \frac{m_c \mu_e (1 - \eta)}{\eta R} \left(1 - \frac{R}{2r}\right). \quad (5)$$

4. Intensity N_{en} of energy outbreak into the environment:

$$N_{en} = \frac{E_{en}}{t} = \frac{m_c V_{ch}^2 (1 - \eta)}{2\eta t} = \frac{m_c \mu_e (1 - \eta)}{\eta R t} \left(1 - \frac{R}{2r}\right). \quad (6)$$

3.2. Laws of impulse conservation and conservation of angular momentum

Industrial rings located on circular equatorial orbits at the altitude of $H = r - R$ and rotating with an orbital velocity V_{or} only have an angular momentum K_c of cargo delivered to the orbit; their momentum in relation to the planet is zero, since the radial speed (in relation to the planet) is zero. Since orbital rings should be built from the Earth (space industrialization will be carried out using production, raw, energy and labor resources of the planet – as space will not have any of these at that time*), the following condition should be met:

$$J_r \omega_r - J_c \omega_e = \Delta K_e, \quad (7)$$

where J_r and ω_r – correspondingly, inertia moment and angular velocity of the orbital ring rotation; J_c and ω_e – the same, when the original cargo used for the orbital ring construction is on the Earth's surface; ΔK_e – variation of the Earth's angular momentum.

* The expansion can take place only from inside, not from outside. The latter can happen if extra-terrestrial civilizations begin to explore near-earth space; however, this exploration would be happening for them from inside, as well.

Taking into consideration that $V_{or}^2 = \frac{\mu_e}{r}$, $J_r = m_c r^2$ and $J_c = m_c R^2$, the expression (7) can be written as follows:

$$\Delta K_e = m_c \left(\sqrt{\mu_e r} - R^2 \omega_e \right). \quad (8)$$

It follows from formula (8) that the value ΔK_e does not depend on the method of taking cargo to the orbit, but only on the cargo mass and orbit altitude. Since the Earth's angular momentum K_e (in relation to its rotation axis) is to change in any case, it must be transmitted to the planet from the GCT. In general terms, the efficiency coefficient λ of impulse supply may not be equal to one, and the following angular momentum can be discharged into the environment

$$K_{en} = \frac{m_c (1 - \lambda)}{\lambda} \left(\sqrt{\mu_e r} - R^2 \omega_e \right). \quad (9)$$

Then, the total angular impulse created by the transport system will be as follows:

$$K = \frac{m_c}{\lambda} \left(\sqrt{\mu_e r} - R^2 \omega_e \right). \quad (10)$$

3.3. Conservation law of center-of-mass motion

The mass center of industrial rings coincides with the Earth's mass center; therefore, even a large-scale space exploration does not have any impact on the planetary motion in outer space. Thanks to the fact that the position of the mass center of the "Earth – industrial rings" system is not changed in space, space industrialization can be carried out using GCT inner mechanical forces without interaction with the environment, i.e., self-supported GCT is possible. Thus, conservation laws do not impose a ban on the use of the "principle of Baron Munchausen"* when building orbital rings.

3.4. Analysis of conservation laws in relation to GCT

Energy can be supplied to cargo even at its complete immobility – for example, by means of heating it or "switching off" the force of gravity in a hypothetical antigravity ship. It should be mentioned that not only energy but also

* The principle used by Baron Munchausen, who pulled himself and the horse out of a swamp by his own hair; however, Baron tried to break the conservation law of center-of-mass motion – due to inner forces of the system, the position of the mass center cannot be changed in space.

impulse must be supplied to cargo. In this regard, the cargo will inevitably start moving in the course of energy supply; hence, the longer the energy is supplied, the bigger distance the cargo covers. This distance can be determined based on the condition that the incoming power $N(t) = \text{const}$ in the course of cargo acceleration.

Then, based on the energy conservation law

$$Nt = \frac{m_c V_{ch}^2}{2} \tag{11}$$

we derive an expression for the distance covered S :

$$S = \frac{4}{3\sqrt{3}} V_{ch} t. \tag{12}$$

The analysis of the graphs built according to the correlations (3), (4), (6), (8) and (12) for $V_{ch} = 10^4$ m/s (figures 3–8) shows that the core requirement the GCT must comply with in the course of space industrialization is ecological safety. The ecological safety is characterized by a minimal degree of chemical, energy and other impact on the environment – and more importantly, by the impact intensity rather than by an absolute value.

For example, humanity could take 300 mln tons of cargo into space annually even today at $\eta_e = 0.5$ spending only 10 % of the modern energy consumption,

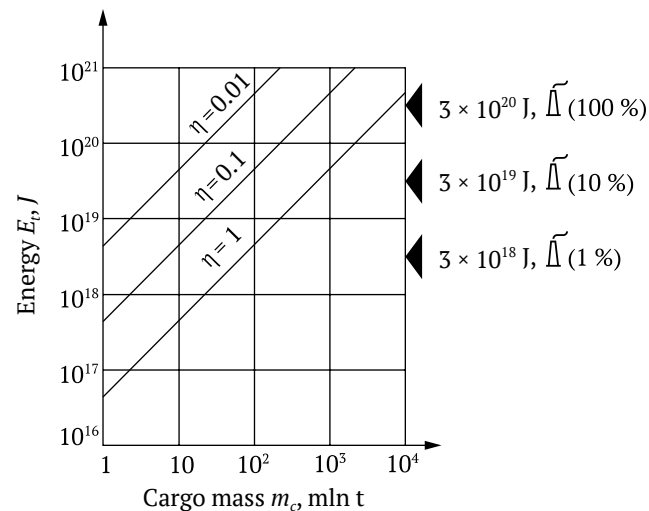


Figure 3 – Energy consumption required to take cargo to the orbit (for $V_{ch} = 10^4$ m/s)

which is roughly 3×10^{20} J (figure 3); whereas the transport system would discharge into the environment only 5 % of the amount of energy consumed by our civilization at present. Therefore, from an energy point of view, humanity is able to take hundreds of millions of tons of cargo into space per year even today.

Nevertheless, the picture is changing dramatically if we consider not the amount of energy consumption but the intensity of its consumption (figure 4) or outbreak into the environment (figures 5 and 6). The following reference figures of power (kW) are given on the ordinate axis of the graphs for comparison: 1.2×10^{14} – solar emission absorbed by the Earth; 2.4×10^{12} – all atmospheric currents of the planet; 5×10^{10} – all sea currents of the planet; 10^{10} – modern energy consumption by humanity; 10^9 – ecologically safe limit of power consumption.

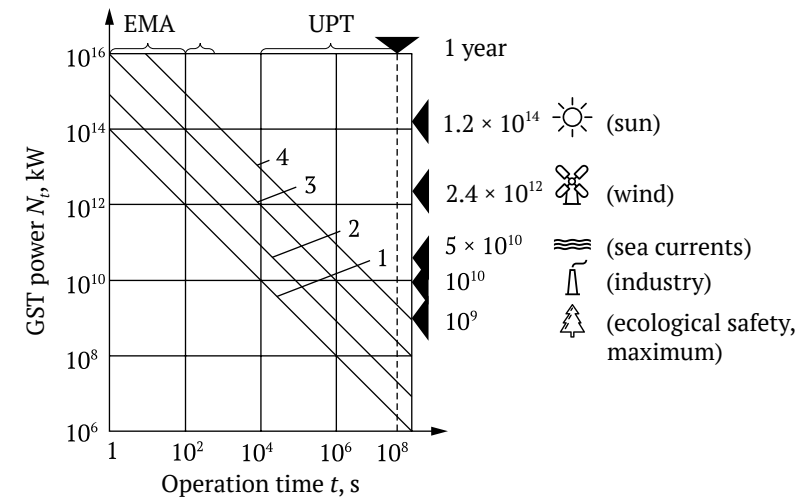


Figure 4 – GCT generated power when taking cargo to the orbit at $V_{ch} = 10^4$ m/s, $\eta = 0.5$ and m_c equal as follows: 1 – 1 mln t; 2 – 10 mln t; 3 – 100 mln t; 4 – 1 bln t

For example, for a characteristic time of an electromagnetic accelerator (EMA, or a catapult) of 1–100 s (length of the acceleration path, correspondingly, 5–500 km), its total capacity should be commensurable with the total intensity of solar emission discharged to the Earth even at $m_c = 1$ mln tons (figure 4). In this case, the intensity of energy outbreak into the atmosphere will be commensurable with the total power of atmospheric and sea currents on the planet (figures 5 and 6). The carrier rocket (CR) performance is not much better. A short duration of action of rocket or catapult engines (not only electromagnetic) – their

inherent fatal defect. In the first instance, it is due to the fact that the traction of jet engines cannot be arbitrary small (to increase the operation time) – it must exceed the rocket weight. Otherwise a rocket will not be able to get off the launch pad* even having used up all fuel. This determines the necessity of a rather fast fuel combustion, as well as a short duration of engine operation, which actually does not prevent a carrier rocket from travelling over a distance of hundreds and even thousands of kilometers (figure 8) at a powered flight. In the second case, due to the limited length of a catapult, either a missile velocity must grow during its acceleration more intensively than that of a rocket, or the length of an electromagnetic accelerator must exceed the distance of the missile ship powered flight, i.e., it must be thousands of kilometers long, which is unreal.

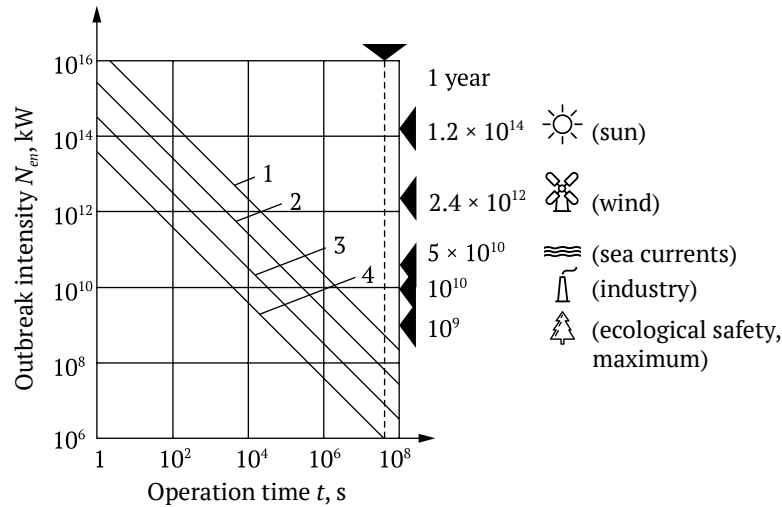


Figure 5 – Intensity of energy outbreak into the environment at $m_c = 100$ mln t, $V_{ch} = 10^4$ m/s and η equal as follows: 1 – 0.1; 2 – 0.5; 3 – 0.9; 4 – 0.99

Transport capacity is not just a figure. Scientific, design and engineering challenges of creating and operating the system, the cost of unique materials and labor required for the program implementation and, finally, the cost of materialized labor are hidden behind it. This figure also characterizes the intensity of environmental impact (figures 5 and 6), which can have disastrous

* The CR performance will be deteriorating from the given positions when the gravity force is increased – for example, when starting from the surface of the Saturn or the Jupiter – a typical rocket would not be able to enter the space from these planets.

consequences for the planet biosphere. Reusable rockets or EMA will not better the situation. Having the multiple use of 10 or 10 thous. times per year, correspondingly (reusability increases time t) and a real efficiency coefficient of such systems, which will not exceed 0.1 taking into account all associated expenses and energy losses, their total capacity, for example, at $m_c = 100$ mln tons, will amount to about $N_t = 10^{15}$ kW. It surpasses the generating capacity of the modern civilization by thirty times, whose energy consumption has come into serious collisions with the environment even now.

The consumed power decreases as the operation time of the transport system engines increases. The adequate power is reached only at $t > 10^6$ s. For example, at $t = 3.2 \times 10^7$ s (1 year), $\eta = 0.5$ and $m_c = 100$ mln tons, capacity N_t will be 3.2×10^8 kW, which is significantly less than the total capacity of the existing power plants of the world. However, it follows from figure 8 that at $t > 10^6$ s, the distance $S > 7.7 \times 10^6$ km, which is by thirty times more than the Earth's radius and dozens of times exceeds the distance to the Moon. In order to provide such a long acceleration path for cargo on the planet having limited sizes, there is only one solution – to make a circular track.

It is proposed to realize this variant in GCT known under the name of United Planetary Transport (UPT)*. It is important that motion is supplied as an angular impulse in the equatorial plane; therefore, the specified circular track

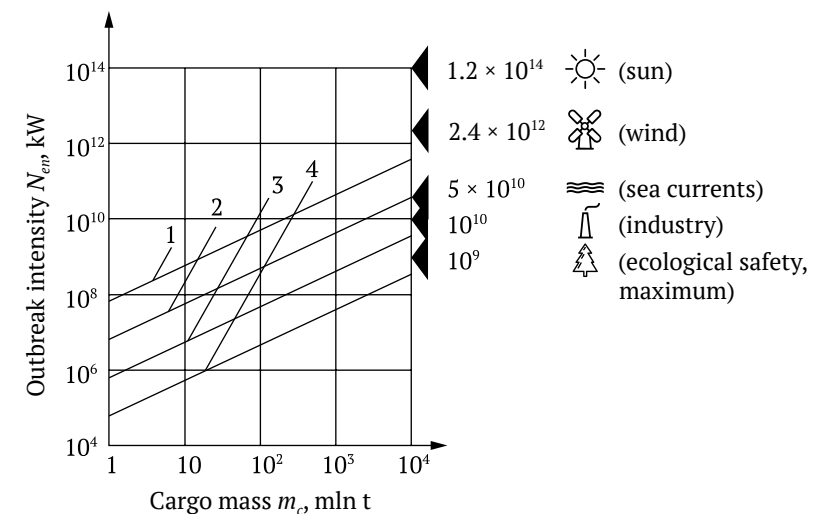


Figure 6 – Intensity of energy outbreak into the environment at $V_{ch} = 10^4$ m/s, $t = 10^7$ s and η equal as follows: 1 – 0.1; 2 – 0.5; 3 – 0.9; 4 – 0.99

* Unitsky, A. Into space without a rocket / A. Unitsky // Technology and science. – 1987. – No. 4. – P. 40–43.

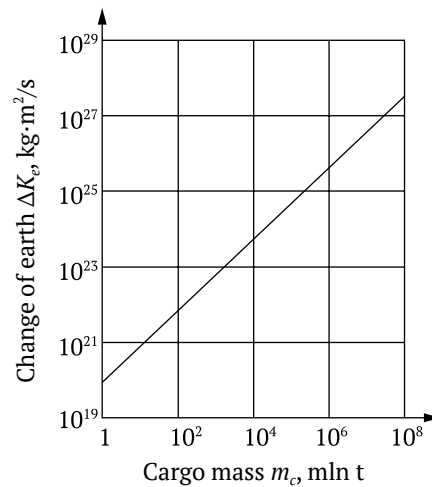


Figure 7 – Variation of the Earth’s angular momentum when taking cargo to the orbit (for $r = 10,000$ km)

must encircle the planet around its rotation axis in parallel to the equator*. It is the intensity of angular impulse supply to the cargo and not energy parameters that is going to be a bottleneck of the upcoming space industrialization. This feature determines the basic GCT parameters.

The more difficult the path of angular impulse supply from the planet to the cargo is, the more intermediate links there are here and the more ecologically dangerous the transport system is. A carrier rocket is most dangerous, since the angular impulse is transmitted to the planet (figure 7) as a result of emission of jet engines combustion products into the atmosphere, their braking in the atmosphere and further angular impulse supply due to the atmosphere friction on the Earth’s crust. In this case, powerful heat, chemical, acoustic and other types of environmental contamination take place, especially detrimental in the upper layers of the atmosphere due to its excessive rarity and necessity to involve atmospheric air in momentum transfer to the planet at vast distances.

The specified drawback can get worse as the exit velocity of jet engines combustion products increases (this direction is considered to be most

* From the perspective of theoretical mechanics, an equatorial variant of UPT is preferable since its operation will be optimal in this case. However, a latitudinal variant of UPT (up to the latitude of the North or South polar circle) is preferable based on other considerations such as the specific geography of Earth’s regions, political situation in the world, availability of industrial countries in the zone of UPT location, etc. Although, this variant would significantly complicate the UPT placement into the equatorial orbit and exclude the possibility of reverse landing on the overpass.

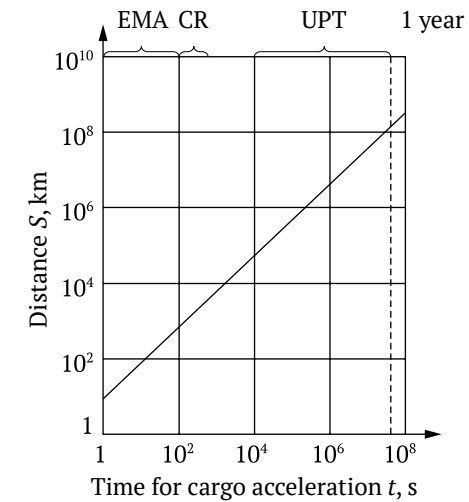


Figure 8 – Distance covered by cargo in the process of its acceleration ($V_{ch} = 10^4$ m/s)

promising in the rocket technology development: jet engines with laser energy supply, nuclear jet engines, etc.) since the impulse will be growing proportionally to the exit velocity, whereas the energy and, consequently, its outbreak into the environment – proportionally to the squared velocity. Therefore, when taking the same amount of cargo to the orbit, advanced carrier rockets will have a stronger impact on the environment compared to conventional ones, adding electromagnetic, radiation and other interference.

An electromagnetic accelerator is environmentally safer than a carrier rocket at a payload acceleration phase, since intermediate links are not required to accelerate the cargo – the impulse is transferred directly to the Earth’s crust. However, a missile at the ascent to the orbit phase gets into the atmosphere, where it is intensively braked at cosmic velocity losing a considerable part of impulse. In this case, a powerful impact on the environment takes place: formation of destructive shock waves in the atmosphere and its intensive chemical and heat contamination due to the combustion of missile materials, although they will be made from heat-resistant materials. In addition, missiles, even those discharged horizontally, have a velocity vector, which does not coincide with the line tangent to the circular orbit, when reaching a design altitude. Therefore, a significant adjustment of the missile flight direction will be required and such GCT will ultimately be a missile cannon hybrid with all the inherent defects.

A hypothetical antigravity ship will be environmentally hazardous, as well. Firstly, it must be able to switch off gravity, albeit locally. We do not know

the ecological consequences of this, although it is possible to assume that this is unlikely to be useful since the existing planetary ecology will be disturbed. Two options are possible here: 1) gravity field is fully shielded; 2) gravity field is weakened for the set value. In the first case, gravity will be switched off not only from the Earth's side, but also from the side of the Universe, which is located opposite the shield and has the escape speed (second cosmic velocity) of thousands of kilometers per second. That is why, according to the energy conservation law, the shield must be fed with energy, which is thousands or even millions of times greater than that shown on the graphs under consideration for $V_{ch} = 10^4$ m/s – it is inadmissible for the purposes of near space industrialization. In the second case, energy parameters of an antigravity ship will comply with other types of GCT, including with its generating capacity, which will depend not only on m_c but also on the time t of gravity switch off (energy supply to make the ship get out of the gravitational potential well).

Secondly, it is possible to supply energy not the impulse by switching off gravity. When falling under the action of gravity force, the normal mass moves along the gravity field force lines (to the center of the attracting body). An antigravity ship will move along the same force lines although in the opposite direction, acquiring with time a greater impulse supplied to it by the planet pushing it away with the gravity (more correctly, antigravity) field. Therefore, if special measures are not taken, such a ship can with time just fly into infinity, if the corresponding energy is supplied to its shield, but it will not be able to go into the circumterrestrial circular orbit. It can also get hung up at the altitude H but it will not be considered an exit into space since, if the payload is separated, it will fall back to the Earth. In fact, a gravitolyot will be a variety of an airship, when the gravity field itself is a buoyant force and, similar to an airship, it must have an additional drive for a horizontal movement. Therefore, the same jet engine will be required to transfer the angular impulse (to go into the circular orbit). As a result, we will get a carrier rocket hybrid, where the major work related to taking cargo to the orbit will be carried out using a jet engine with all its inherent drawbacks. As the gravitolyot circular velocity grows, the antigravity created by the same should be gradually decreased to zero (when the orbital speed of the Earth's artificial satellite is reached). Otherwise, an additional and constant force directed to the attracting center will be required to keep it on the orbit.

A space elevator* possesses more satisfactory characteristics and essentially only one operational shortage: if no additional adjustment is made, it will be able to take cargo to only one circular orbit – a geosynchronous one (35,800 km) –

* A space elevator is a ship launched to the geosynchronous orbit in the equatorial plane, equipped with a high-strength cable released in the Earth's direction up to its surface, and a cable with a counterbalance released in the opposite direction.

for example, by means of jet engines. However, design drawbacks of the lift will be fundamental; particularly the circumstance that it is stationary and self-supported. This will require a great amount of materials with unique strength properties – the lift mass can reach millions of tons; in some cases, it can surpass the mass of cargo delivered into space by the same for the entire operating period. This will create difficulties when constructing the lift since it can only be made from out in space, i.e., from outside in relation to the earth civilization. In this regard, it would be required to use other, less practical variants of GCT within quite a long time in order to construct it.

The angular momentum is transmitted from the cargo taken to the orbit to the Earth's crust as the Coriolis force directed to the normal axis of the lift representing a flexible link over 40 thous. km long. It will cause an extremely disadvantageous stress strain behavior in the structure, similar to that of a clothesline, just dozens of thousands of kilometers long. Therefore, the space elevator carrying capacity cannot be high since the Coriolis force is proportional to the cargo traffic to the orbit.

The United Planetary Transport* is free from all the drawbacks listed above. It is the only technical solution by means of which the transport system can take cargo to different equatorial orbits not using jet engines; it is the only solution where the principle of Baron Munchausen is used to go out into space. It is explained by the fact that in the process of UPT operation, the position of mass center is not changed over a distance. Therefore, it can go out into space using only the inner forces of the system, without any energy, mechanical, chemical or other types of interaction with the environment, which means it will be ecologically clean.

4. United Planetary Transport

A simple cargo variant of UPT can be arranged in the following way.

Imagine an elegant overpass located, for example, along the parallel 55 degrees north latitude (approximate Moscow latitude, central part of Great Britain, south of Canada) and thus encircling the planet as a ring in parallel to the equatorial plane. Its length in this case – 23 thous. km**. The overpass can run at other latitudes, as well. The overpass is fixed to the continents by means of ordinary

* Unitsky, A. Interchange, space, ring / A. Unitsky // Inventor and rationalizer. – 1982. – No. 4. – P. 28–29.

** Humanity today implements more ambitious programs than the UPT overpass construction. For example, if all cars existing in the world at present, which is almost 500 mln, are used as bricks to build a wall around the Earth at the specified latitude, the height of this solid wall will exceed 100 m. Moreover, the amount of concrete used for a dam of Sayano-Shushenskaya hydroelectric power station alone, and this is almost 10 mln cu. meters, would be enough to build all supports of the UPT overpass.

supports (figure 9), in the oceans – on pontoons installed below the water surface (figure 10). A track structure is laid on the overpass at the height of 10–50 m (figure 11). It comprises a linear electric motor mounted along a vacuum tube, which is put along the entire overpass. Inside the tube, there is a linear (stretched in line) rotor also encircling the planet – the same payload subjected to the exit into outer space. It includes raw materials, as well as semi-manufactured goods, components, instruments, etc. required for space construction.

So, how does such a simplest UPT operate? Prefabricated rotor parts are connected with each other and successively mounted on a tube, which is laid along the overpass, via special fill ports. Then, the air from the tube is pumped out and a giant ring is ready for operation.

A system of electromagnets used for rotor suspension and stabilization in the tube center is switched on. Then, the rotor is driven by a linear electric motor along the tube and, consequently, around the Earth. The rotor mass is substantial – its cross-sectional dimension is about 10 cm, and every running meter weighs 10–50 kg; the total rotor weight is hundreds of thousands tons; the tube diameter – 20–30 cm. Therefore, many days and even weeks pass before it reaches the first cosmic velocity and gets weightlessness due to balancing the terrestrial gravity force with centrifugal force*. Then, the velocity reaches 10 km per second. A linear electric motor system and magnetic levitation are switched off. Nothing can keep a vacuum capsule with a rushing ring rotor inside on the overpass. A special stand-alone system of magnetic levitation located inside the capsule tube continues to keep the rotor exactly in the tube center. A ring of planetary dimensions breaks away from the Earth's surface under the action of centrifugal forces that exceed the terrestrial gravity. It stretches similar to a rubber bicycle tube** and leaves the gas shell of the planet in some dozen minutes completely going into the circular orbit in the equatorial plane (figure 12).

* The said is true only for the equatorial plane. The rotor of a latitudinal UPT will not get weightlessness since the gravity force and the centrifugal force lie in different planes.

** At first, for example, up to 1–2 % – a rotor and a capsule get stretched due to elasticity of construction materials (this ensures an ascent to the altitude of about 100 km), then – due to special telescopic joints that provide double extension. The capsule can be brought into space or after breaking apart returned to the Earth via parachutes for repeated use.

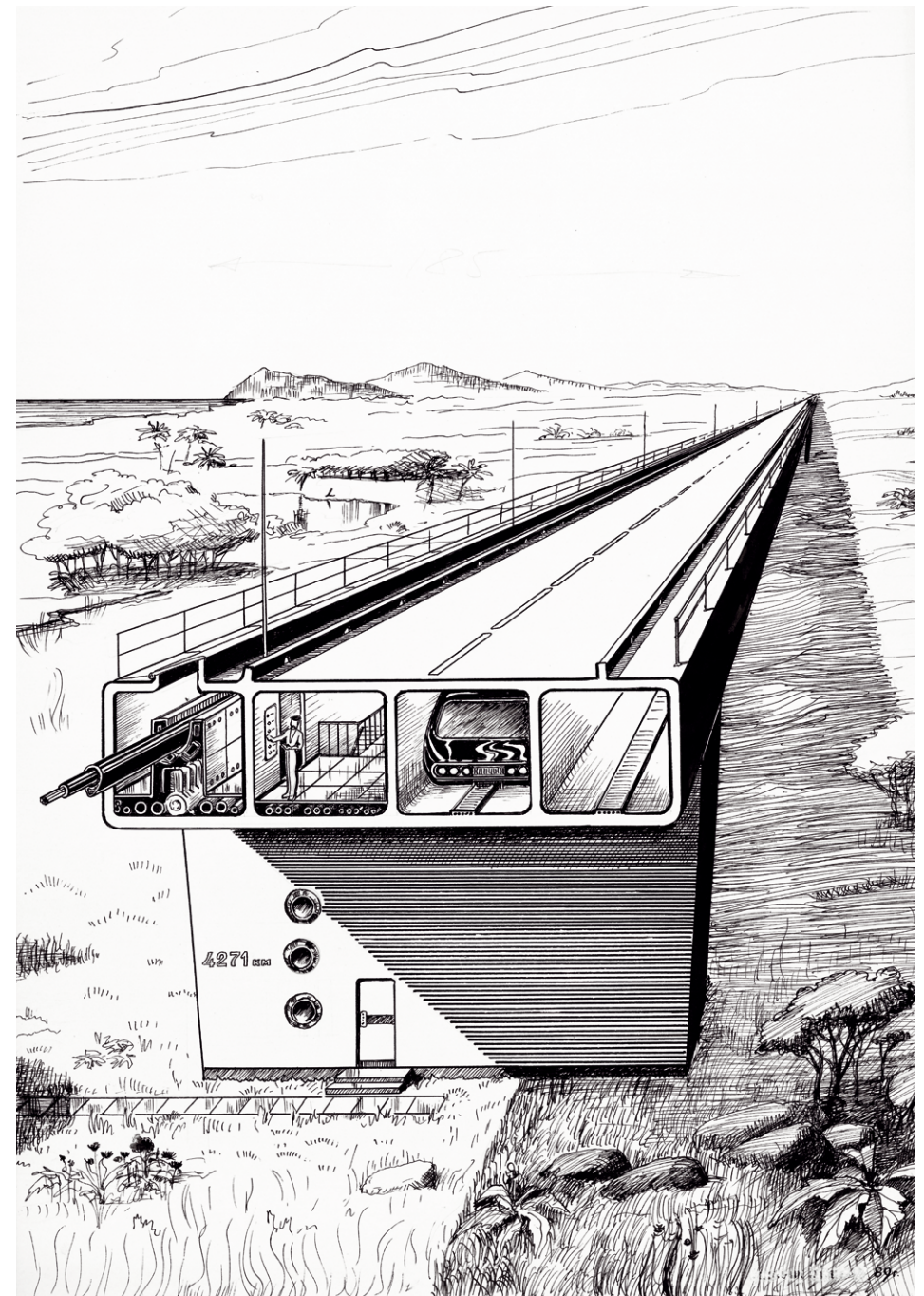


Figure 9 – Onshore section of UPT cargo variant

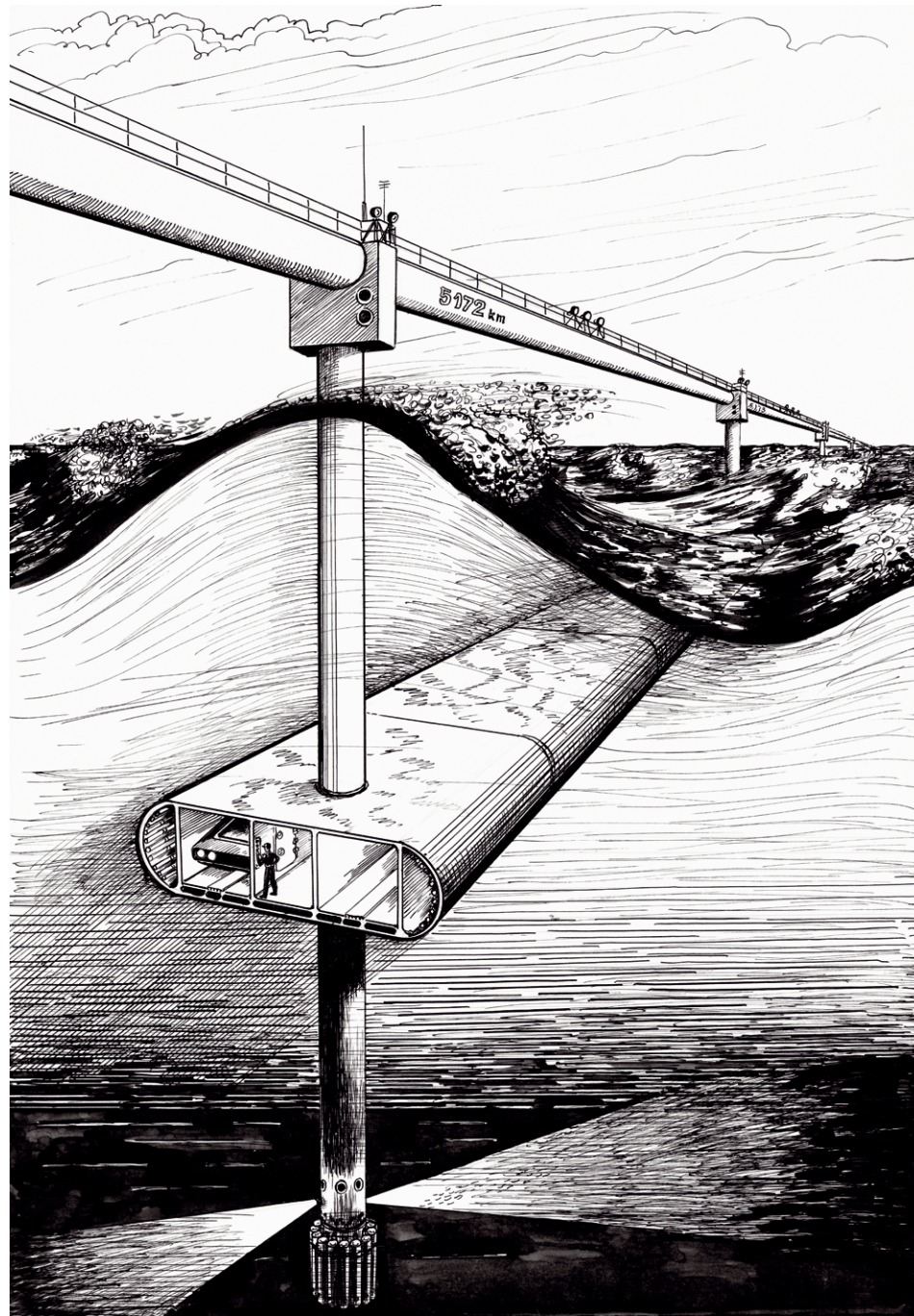


Figure 10 – Sea section of UPT cargo variant

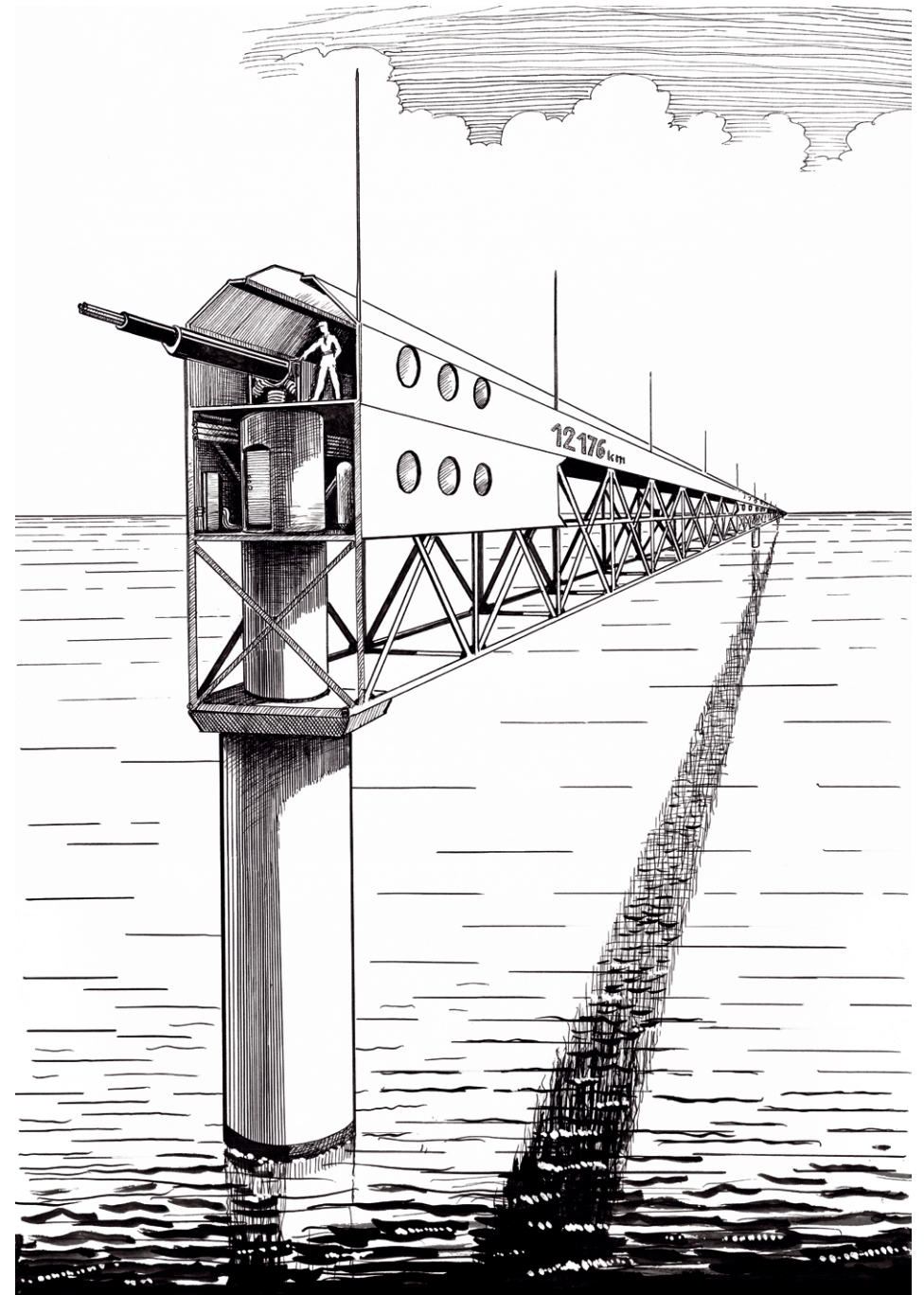


Figure 11 – Design of UPT offshore track structure

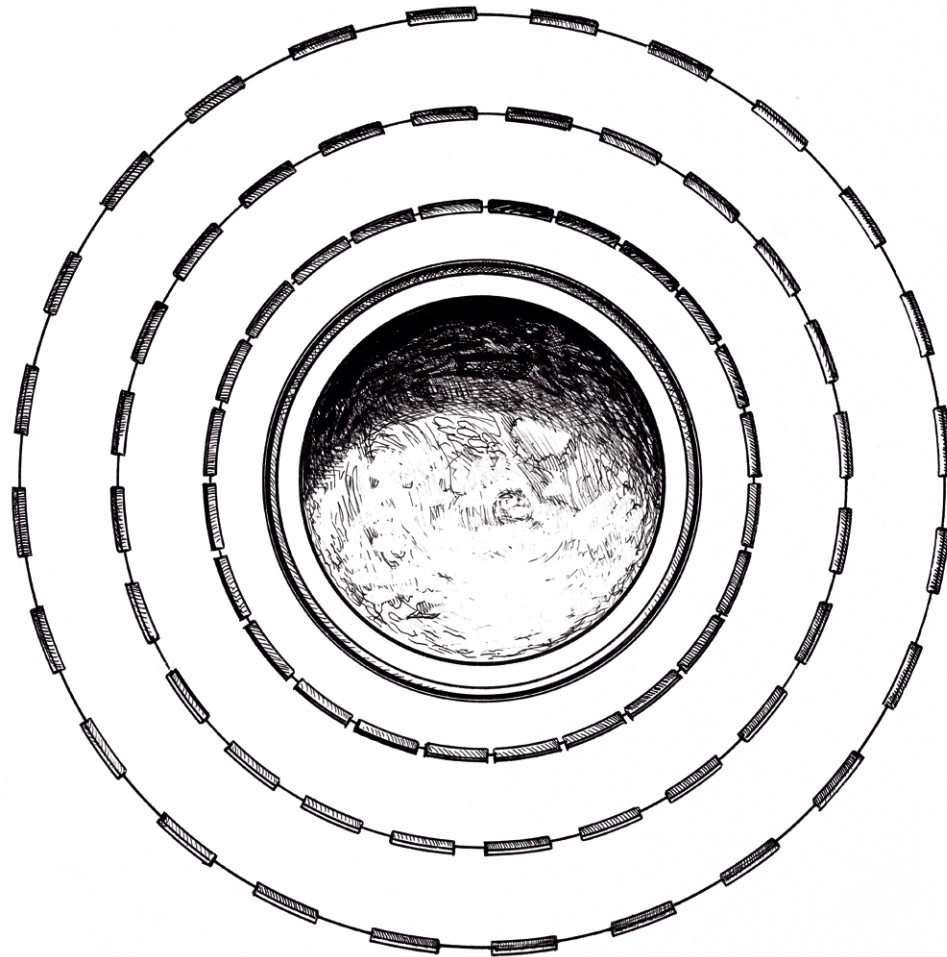


Figure 12 – Stages of rotor exit into space (planet view – from the pole)

Chapter 1

Dynamics of the UPT exit into space in Earth's equatorial plane

Let us consider a problem of UPT rotor movement in the atmosphere and outer space in case of equatorial location of a launch overpass. Let us determine the basic patterns of the ascent to the orbit process when making the most common assumptions in relation to rotor properties and conditions of its movement [1].

Let us assume a thin elastic ring with homogeneous mechanical characteristics as a rotor model, with a finite number of fragmentation and further stages of elastic or friction extension. The rotor movement through the atmosphere takes place inside the vacuum capsule, which is necessary in order to isolate a fast-moving rotor from the air environment. The capsule participates only in the radial movement; the air environment is modeled by the standard atmosphere.

The analysis of solutions to the differential equations of motion allows studying a stage-by-stage rotor movement – its position determined by the polar coordinates, the corresponding velocity and acceleration, movement time, acting forces, degree of impact on dynamic characteristics of different rotor and capsule parameters, etc. As will be shown, the rotor radial movement at arbitrary chosen parameters is oscillatory in relation to the orbit position. It is possible to use friction forces between the rotor fragments in their telescopic joints to control the rotor movement for the purpose of oscillation suppression and placement to the intended orbit. The relation between the initial rotor and capsule parameters at the beginning of radial movement has been determined; the dependence between the rotor starting velocity and the orbit position has been established.

There has been studied the dynamics of the rotor oscillatory movement in the case of free extension of fragments; determined the critical motion modes when the rotor extends infinitely moving away at infinity. Such a mode can be used to arrange transportation of payload within the Earth's space industrial zone, or to the Solar System objects and back.

1.1. Problem setting

Let us study the UPT rotor movement when launched to the orbit in the equatorial plane. The rotor moves inside a vacuum capsule when in the dense atmosphere. The initial state of the rotor – capsule system is determined by the rotor rotating along the equator at speed V and the motionless capsule. The rotor radial movement starts after being released from magnetic levitation and is communicated to the capsule. Due to electromagnetic interaction with the rotor, the capsule gets rotational movement in addition to the rotation together with the Earth. By the time of capsule separation, its total angular velocity has a small value of the Earth's angular velocity due to weak interaction and minor travel time. Therefore, the capsule rotational movement can be neglected. The capsule rotation does not change the general pattern of motion, as will be shown further, but only contributes to minor quantitative changes in the dynamic characteristics of the system.

The movement of the rotor – capsule system and then the rotor movement after the capsule ejection is determined in relation to the moving reference system with the beginning in the Earth's center.

The Z axis is directed along the rotation axis of the Earth and the rotor; the X and Y axes – in the equatorial plane. The influence of the Sun, the Moon and other bodies of the Solar System is disregarded due to their low impact.

The rotor dynamic model is assumed as a thin ring with homogeneous mechanical characteristics and the initial radius r_0 equal to the Earth's equatorial radius. An elastic extension of the ring is taken into consideration in the early stage of radial movement; after reaching the specific value of relative deformation, the rotor is divided into fragments with telescopic joints. Further relative movement of the fragments – the stage of friction extension – is studied with regard to dry friction.

The fragments relative movement stops after the connecting elements approach the dog-shores; thus, a new stage of elastic extension begins. Then, fragmentation takes place again, the stage of friction extension, etc. There can be several alternating stages of elastic and friction rotor extension. Weight values of the rotor length unit, elastic coefficient, friction forces and other characteristics averaged by the rotor length are considered at every stage.

A relative movement of fragments is possible at the rotor oscillatory movement, if there are no friction forces in telescopic joints. We assume that such movements of the fragments also take place at the rotor movement along the orbit.

The capsule is assumed as a closed thin-walled tore capable of withstanding static and dynamic atmospheric pressure and stretching elastically until it escapes from the dense atmosphere and separates from the rotor. The capsule shape in cross-section can vary from being circular to well streamlined drop-shaped.

Within the assumed rotor model and the capsule, as well as other restrictions and properties stipulated above, let us determine as follows:

1. General conditions required to launch the rotor to the intended circular orbit of R_c radius: the value of the rotor starting velocity V_{r0} , the relation between the initial parameters at the beginning of radial movement, the moments of fragmentation, the lengths of sections for elastic and friction extension, etc.

2. Parameters of control action – in this case, friction forces – to suppress the rotor energy in the radial movement with the purpose of non-oscillatory launch to the orbit.

3. Parameters of radial and rotational movement of the rotor – the position, speed, acceleration at different stages, travel time at aperiodic modes of motion and natural oscillations, etc.

4. Conditions at the final stage that provide the simultaneous vanishing of radial speed, radial acceleration and deformation of rotor fragments in the position determining the intended orbit, which are the essential conditions for further rotor movement on this orbit.

1.2. Differential equations of motion for the component of the rotor – capsule system in the atmosphere

Let us investigate the impact of elastic forces that are represented by inner forces of the system on its movement. Let us consider the component, which consists of a rotor arc and the capsule around it with the initial length l and masses m_r and m_{caps} (figure 13). Let us assume the turning angle φ and the current radius r_r of the rotor orbit as generalized coordinates of the system. The kinetic energy of the system component

$$K = \frac{1}{2}(m_r r_r^2 \dot{\varphi}^2 + m \dot{r}_r^2),$$

where $m = m_{caps} + m_r$; $\dot{\varphi} = \frac{d\varphi}{dt}$ – rotor angular velocity; $\dot{r}_r = \frac{dr_r}{dt}$ – rotor and capsule radial speed.

The forces acting on the selected component of the system:

1. Gravity force to the Earth's center

$$G = mg \frac{R^2}{r_r^2}, \quad (1.1)$$

where g – gravity acceleration at the equator [4]; R – equator radius.

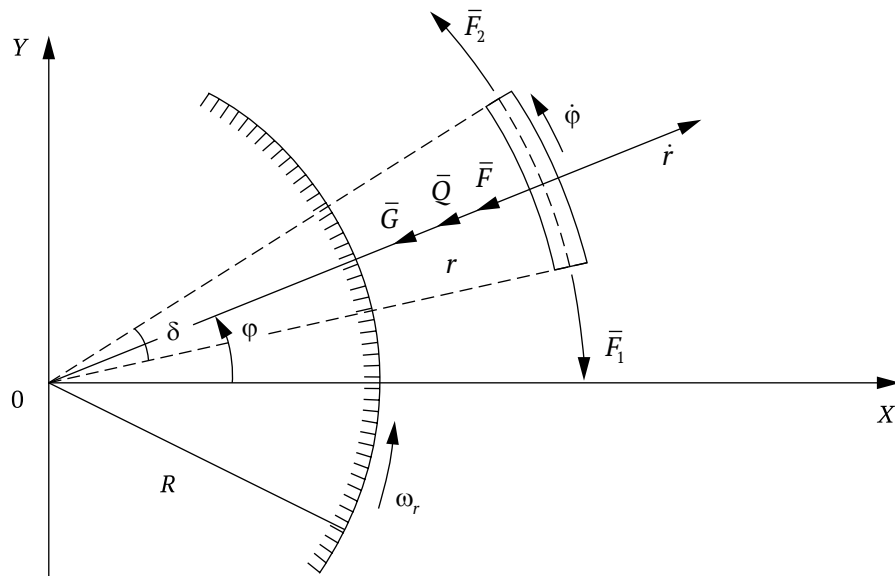


Figure 13 – Motion pattern for component of rotor – capsule system

2. Elastic forces F_1, F_2 , acting on the component ends from the rest of the rotor – capsule system; in this case, $F_1 = F_2 = F$, $F = C\Delta L$, where $C = C_{caps} + C_r$ – the total rigidity of rotor – capsule; $\Delta L = 2\pi(r_r - R)$ – extension of the rotor –capsule system. The resultant F of forces \bar{F}_1 and \bar{F}_2 exerts in the component center and directed to the Earth's center; its module $F = 2F_1 \sin \frac{\delta}{2}$, where $\delta = l/R$ – central arc angle l . Due to minor δ , let us write down $F = \delta F_1$; then,

$$F = 2\pi Cl \left(\frac{r_r}{R} - 1 \right).$$

3. Force \bar{Q} of atmospheric drag that is in contact with the capsule participates in radial movement. Taking into consideration the decrease in atmospheric density

$$Q = k_{sh} \rho_0 r_r^2 \exp \left[-\alpha_d \left(\frac{r}{R} - 1 \right) \right],$$

where k_{sh} – coefficient that depends on capsule shape; ρ_{a0} – initial atmospheric density, α_d – value where the Q impact at the height of $H_a \geq 100$ km can be neglected.

Using the Lagrange formalism and omitting the index r denoting the current rotor radius, let us write down as follows:

$$\frac{d}{dt} \frac{\partial K}{\partial \dot{\phi}} - \frac{\partial K}{\partial \phi} = 0;$$

$$\frac{d}{dt} \frac{\partial K}{\partial \dot{r}} - \frac{\partial K}{\partial r} = -G - F - Q.$$

Having made differentiation, we derive differential equations of motion for the rotor and capsule component at the initial stage after certain transformations and reductions – from the launch from the equatorial overpass to the exit from the dense atmosphere:

$$\ddot{\phi} r + 2\dot{\phi} \dot{r} = 0; \tag{1.2}$$

$$\ddot{r} = \frac{m_r}{m} r \dot{\phi}^2 - g \frac{R^2}{r^2} - \frac{2\pi Cl}{m} \left(\frac{r}{R} - 1 \right) - \frac{k_{sh} \rho_{a0}}{m} r^2 \exp \left[-\alpha_d \left(\frac{r}{R} - 1 \right) \right]. \tag{1.3}$$

The first term in equation (1.3) is acceleration caused by the centrifugal force of the rotor component inertia, the others – acceleration caused by the action of the forces specified above.

The initial conditions of the problem

$$\phi_0 = 0; \quad \dot{\phi}_0 = \frac{V_0}{R} = \omega_{r0}; \tag{1.4}$$

$$r_{r0} = R; \quad \dot{r}_{r0} = 0, \tag{1.5}$$

where ω_{r0} – initial rotor angular velocity; V_0 – rotor starting velocity.

1.3. Analysis of motion equations of the system in the atmosphere

The coordinate ϕ is cyclic. The integration of (1.2) leads to the correlation, which reflects the conservation law of the system kinetic momentum in relation to the rotor spinning axis Z . With regard to the initial conditions (1.4) we will get:

$$\dot{\phi} = \omega_0 \frac{R^2}{r^2} = \frac{V_0 R}{r^2}. \tag{1.6}$$

Thus, the rotor angular velocity decreases at its ascent inversely proportional to the squared distance of the components to the Earth's center similar to the decrease in the gravity force of the component to the Earth's center, which is determined by the formula (1.1).

The angular acceleration changes inversely proportional to the cubic distance to the Earth's center. In fact, based on (1.2) with regard to (1.6), we will derive:

$$\ddot{\phi} = -2V_{r0}R \frac{\dot{r}}{r^3}.$$

Based on the equation of radial movement (1.3) by means of conditions (1.4), (1.5), it is possible to determine radial acceleration at the beginning of the rotor ascent:

$$\ddot{r}_0 = \frac{m_r}{m} \frac{V_0^2}{R} - g.$$

Introducing dimensionless values

$$\beta = \frac{V_0^2}{gR} = \left(\frac{V_0}{V_1} \right)^2; \quad \mu_1 = \frac{m_0}{m_r},$$

where $V_1 = (gR)^{1/2}$ – the first cosmic velocity, we get $\ddot{r}_0 = \left(\frac{\beta}{1 + \mu_1} - 1 \right) g$, wherefrom follows the condition of the start of radial movement in the rotor – capsule system

$$\beta > 1 + \mu_1,$$

or

$$V_0 > \left(1 + \frac{m_0}{m_r} \right)^{1/2} V_1.$$

Let us assume, for example, that $\mu_1 = 0.3$; with the values $R = 6.37 \times 10^6$ m, $g = 9.814$ m/s² we get as follows: $V_0 = \sqrt{1.3} V_1 = 9 \times 10^5$ m/s = 9 km/s. In case $m_0 = 0.3m_r$, it is required to accelerate the rotor in relation to the overpass to reach the following relative speed in order to initiate the ascent of the rotor – capsule system

$$V_r = V_0 - V_e > 8.54 \text{ km/s},$$

where V_0 – absolute velocity; $V_e = \Omega R = 0.46$ km/s – transportation velocity; Ω – the Earth's angular velocity.

The radial acceleration in this case is not great; let us assume that $V_r = 9.54$ km/s, $V_{r0} = 10$ km/s, $\beta = 1.6$, $\mu_1 = 0.3$, then $\ddot{r}_0 = 0.233g = 2.28$ m/s². In the future, this acceleration decreases when the rotor and the capsule expand; therefore, the radial speed when moving in the atmosphere will not be great and the atmospheric resistance will be insignificant.

1.4. Dynamics of the rotor – capsule system when moving in the atmosphere

Replacing $\dot{\phi}$ in the equation (1.3) using the integral (1.6) and passing to the non-dimensional radius $x = r/R \geq 1$, let us write down a differential equation for radial movement of the system in the atmosphere:

$$\ddot{x} = F(x) - K_0(x - 1) - px^2 \exp[\alpha_d(x - 1)], \quad (1.7)$$

where

$$F(x, \mu_1) = \frac{q}{x^2} \left(\frac{\beta}{1 + \mu_1} \frac{1}{x} - 1 \right); \quad (1.8)$$

$$q = \frac{g}{R}; \quad K_0 = \frac{2\pi Cl}{mR}; \quad p = \frac{k_{sh} \rho_0 R}{m}.$$

The radial acceleration \ddot{x} decreases from the initial value

$$\ddot{x}_0 = F(1, \mu_1) = q \left(\frac{\beta}{1 + \mu_1} - 1 \right)$$

to the value $\ddot{x}_1 = F(x_1, \mu_1) - K_0(x_1 - 1)$ in the position $x_1 = 1 + H/R$, where the atmospheric effect disappears and capsule ejection takes place. Here, the following cases are possible: $\ddot{x}_1 \geq 0$ and $\ddot{x}_1 < 0$. In the first case, the restriction is obvious

$$K_0 \leq \frac{F(x_1, \mu_1)}{x_1 - 1}.$$

Using the correlation (1.8), this restriction can be expressed through the initial parameters of the system.

In the second case, it is required to provide a non-negativity constraint for a radial speed \dot{x} , which will be considered below.

Let us multiply both parts of the equation (1.7) by dx ; the left part will be transformed to have the viewy $\ddot{x}dx = d\left(\frac{\dot{x}^2}{2}\right)$. Let us integrate the derived correlation with the limits $x_0 = 1$ and x , $\dot{x}_0 = 0$ and \dot{x} ; as a result, we will find the expression for the radial speed at the stage of the system movement in the atmosphere:

$$\dot{x}^2 = (x - x_0) \left[\frac{q}{x} \left(\frac{\beta}{1 + \mu_1} \frac{x + x_0}{x} - 2 \right) \right] - 2a(x, x_0), \quad (1.9)$$

where $a(x, x_0) = p \int \dot{x}^2 \exp[-\alpha_d(x-1)] dx$ – a part of work of atmospheric drag forces per rotor – capsule mass unit.

Defining x out of (1.9) and multiplying by R , let us find the dimensional radial speed $V_{rad} = R\dot{x}(x)$.

The radial speed \dot{x} increases at the stage of movement in the atmosphere $[x_0, x_1]$ from the value $\dot{x}_0 = 0$ to some maximal value. If $\ddot{x}_1 \geq 0$, the maximal value is reached in the position x_1 . If $\ddot{x}_1 < 0$, the acceleration \ddot{x}' goes to zero in the position x' , $x_0 < x' < x_1$ and then becomes negative.

The equation (1.7) assumes an accurate solution. After simple transformations and the introduction of symbols

$$u(x) = \dot{x}^2; \quad f_1(x) = p \exp[-\alpha_d(x-1)];$$

$$f_2(x) = F(x, \mu_1) - K_0(x-1)$$

we derive a first-order equation with variable coefficients:

$$u' + 2f_1(x)u - 2f_2(x) = 0, \quad (1.10)$$

the general solution is as follows

$$u(x) = 2 \exp[-F_1(x)] \int_{x_0}^x f_2(x) \exp[-F_1(x)] dx,$$

where

$$F_1(x) = 2 \int_{x_0}^x f_1 dx = -\frac{2p}{\alpha_d} \left\{ \exp[-\alpha_d(x-1)] - 1 \right\}.$$

The integrals of equations (1.6) and (1.10) allow us to derive the solution to the problem of the motion law of the system in the atmosphere in quadratures.

We have $\dot{x} = [u(x)]^{1/2}$:

$$dt = \frac{dx}{[u(x)]^{1/2}}, \quad (1.11)$$

wherefrom we can determine the time interval when the rotor reaches the position x :

$$t = \int_{x_0}^x \frac{dx}{[u(x)]^{1/2}} = P(x). \quad (1.12)$$

Solving (1.12) in relation to x , we get the dependence:

$$x = x(t). \quad (1.13)$$

According to (1.6) $d\varphi = \omega_0 \frac{dt}{x^2}$. Using (1.11), we get $d\varphi = \frac{\omega_0 dx}{x^2 [u(x)]^{1/2}}$,

wherefrom

$$\varphi = \omega_0 \int_{x_0}^x \frac{dx}{x^2 [u(x)]^{1/2}} = \omega_0 \Phi(x). \quad (1.14)$$

Here, φ – the rotor turning angle in relation to the inertial reference system $OXYZ$. The angular position φ' in relation to the reference system $OX'Y'Z'$ connected with the Earth and initially coinciding with $OXYZ$ is defined through the correlation below

$$\varphi' = \varphi - \omega_e t = \omega_0 \Phi(x) - \omega_e P(x). \quad (1.15)$$

Using the dependence (1.13), let us express φ and φ' in the functions t

$$\varphi = \varphi(t); \quad \varphi' = \varphi'(t). \quad (1.16)$$

Thus, there have been obtained the correlations fully determining the dynamics of the rotor – capsule system at the stage of movement in the atmosphere.

1.5. Rotor dynamics at the elastic extension section in outer space

After leaving the dense atmosphere, i.e., in the position $x_1 = 1 + \frac{H_a}{R}$, there takes place an ejection of the capsule, which did not participate in the rotational movement; therefore, the equation (1.2) and its integral (1.6) also describe the further rotor motion.

The equation of radial speed is simplified since the atmospheric drag is neglected, and the value $\mu_1 = 0$:

$$\ddot{x} - F(x, 0) + K_1(x - x_0) = 0, \quad x \geq x_1. \quad (1.17)$$

The K_0 coefficient is replaced with K_1 in this case:

$$K_1 = \frac{2\pi C_1 l}{m_1 R},$$

where C_1 and m_1 – rotor rigidity and the mass of its element.

Thus, radial acceleration increases abruptly in point x_1 since $\beta > \frac{\beta}{1 + \mu_1}$ and $K_1 < K_0$; with further rotor expansion, radial acceleration monotonely decreases. As before, two cases are possible.

1. If the acceleration at the end of previous stage satisfies the condition $\ddot{x}_1 \geq 0$, it takes on the value $\ddot{x}_{10} > \ddot{x}_1$, after capsule ejection, and the radial movement accelerates.

2. If $\ddot{x}_1 < 0$, further rotor movement without delay requires fulfillment of the condition

$$\ddot{x}_{10} = F(x_1, 0) - K_1(x_1 - x_0) > 0.$$

In this case, in the position $x = x_1$ the speed \dot{x} takes on a minimal value, which corresponds to a corner point in graph $\dot{x}(t)$ shown in figure 21.

We assume in the future that the values \ddot{x}_{10} and $\dot{x}_{10} = \dot{x}_1$, initial for the section of elastic extension $x > x_1$ satisfy the conditions $\ddot{x}_{10} > 0$, $\dot{x}_{10} > 0$.

Integrating the equation (1.17) same as previous within x_1 and x , \dot{x}_{10} and \dot{x} , we derive the expression, which defines the speed \dot{x} at the first stage of rotor elastic extension in space as follows:

$$\dot{x}^2 = \dot{x}_1^2 + (x - x_1) \left[\frac{q}{xx_1} \left(\beta \frac{x + x_1}{xx_1} - 2 \right) - K_1(x + x_1 - 2) \right], \quad x \geq x_1. \quad (1.18)$$

The equations (1.17) and (1.18) determine the rotor acceleration and speed \ddot{x} and \dot{x} depending on its position x , which allows solving the problem of the rotor motion control during its ascent to the orbit. Indeed, it is possible to affect the rotor radial movement by changing parameters β and K_1 and the related parameters V_0 , m_r , C_r . The analysis of the conditions for the rotor ascent to the intended orbit and the impact of β parameter on this process will be provided below.

The control via elastic forces, which corresponds to the choice of coefficient K_1 or rotor rigidity C_r , is not effective. In fact, radial acceleration and speed in the orbit point $x = x_k$ must vanish together:

$$\ddot{x}_k = \dot{x}_k = 0. \quad (1.19)$$

It is impossible to meet these conditions simultaneously in the case under consideration, which follows from the equations (1.17) and (1.18). Indeed, acceleration $\ddot{x}(x)$ varies monotonically, therefore, it can vanish at the section $[x_1, x_k]$ only once; let it happen in point x' , $x_1 < x' < x_k$. The negative acceleration at the second part of the section $[x', x_k]$ can transform speed \dot{x}_k to zero; however, the negative acceleration itself will be different from zero, and the rotor in the future will move in the reversed direction. After passing the position x' , the acceleration will become positive and the speed will be decreasing to zero, after which the motion cycle will repeat itself. The rotor oscillatory motion arises in relation to the position x_k .

If the point x' , where $\ddot{x} = 0$, coincides with the point x_k , the speed \dot{x}_k reaches here the maximal value and the rotor will pass this position by inertia. Its further motion will be slowed till it stops in some position x_{2k} ; in this case, acceleration $\ddot{x}_{2k} < 0$, consequently the rotor will start moving in the reversed direction.

Thus, the combined action of centrifugal force, gravity force and elastic force causes the rotor oscillatory motion. The rotor motion control via elastic forces is hindered by the circumstance that rotor deformations are admissible only within a relatively small range, which is due to the real values of elastic strength and other characteristics of the rotor, whereas the amplitudes of oscillation reach great values comparable to those of the Earth's radius.

An oscillatory nature of the rotor radial movement necessitates the use of dissipative forces, particularly, dry friction forces. The author of the UPT project proposes the following options to implement the rotor motion control with the purpose of elimination of oscillations.

1. Rotor fragmentation with a telescopic joint, which prevents the emergence of large deformations. The number of fragments depends on the radius of the intended orbit, the size of fragments and their general parts, as well as on other technical features of rotor design.

2. Partial braking of a relative fragment displacement after every separation by means of dry friction forces. Let us call the stages of rotor motion having the action of friction forces as stages of friction extension. The values of friction forces are mainly chosen based on the condition of speed bleed-off of the rotor radial movement and, consequently, the energy of such movement.

3. Alternation of friction extension stages with stages of rotor elastic extension within tolerable limits of its deformations.

As shown below, the last method of energy dissipation allows controlling the rotor radial movement in a more efficient way giving it a non-oscillatory nature. In addition, the conditions (1.9) for the ascent to the permanent orbit, as well as other conditions required for the motion on the orbit are fulfilled.

1.6. Dynamics of rotor oscillatory motion

The specific features of rotor dynamics are determined when studying its oscillatory motion in case of free extension, when fragments move apart or come together in telescopic joints without friction forces. In the course of investigation, let us ignore the atmospheric effect both on the radial and rotational rotor movement. Such a situation is possible, for example, when a rotor starts from the surface of the Moon, Mars or satellites of big planets. Then the capsule aimed to protect the rotor from the atmospheric effect is not necessary, and the rotor is fragmented at the moment it starts its radial movement.

The equation of the rotor radial movement has in this case the following view:

$$\ddot{x} - F(x, 0) = 0, \quad x \geq x_0 \quad (1.20)$$

with the initial conditions

$$x_0 = 1; \quad \dot{x}_0 = 0. \quad (1.21)$$

Integrating the equation (1.20) under the conditions (1.21), we get as follows:

$$\dot{x}^2 = \frac{q}{x}(x-1) \left(\beta \frac{x+1}{x} - 2 \right), \quad x \geq 1, \quad \beta > 1,$$

or

$$\dot{x}(x) = \frac{1}{x} \left\{ q(x-1) [(\beta-2)x + \beta] \right\}^{1/2}, \quad x \geq 1. \quad (1.22)$$

After separation of variables and integration, let us determine the movement time:

$$t = \frac{1}{\sqrt{q}} \int_1^x \frac{x dx}{[(\beta-2)x^2 + 2x - \beta]^{1/2}}. \quad (1.23)$$

The integral in (1.23) according to [3] is calculated depending on the value β . If $\beta < 2$, then

$$t = \frac{1}{\sqrt{q}(2-\beta)} \left\{ \frac{1}{(2-\beta)^{1/2}} \left[\frac{\pi}{2} - \arcsin \frac{1-(2-\beta)x}{\beta-1} \right] - \left[2x - \beta - (2-\beta)x^2 \right]^{1/2} \right\}. \quad (1.24)$$

If $\beta > 2$, then

$$t = \frac{1}{\sqrt{q}(\beta-2)} \left\{ \left[(\beta-2)x^2 + 2x - \beta \right]^{1/2} - \frac{1}{\beta-2} \times \ln \frac{\left\{ (\beta-2) [(\beta-2)x^2 + 2x - \beta] \right\}^{1/2} + (\beta-2)x + 1}{\beta-1} \right\}. \quad (1.25)$$

Finally, if $\beta = 2$:

$$t = \frac{1}{3} \left(\frac{2}{q} \right)^{1/2} (x+2)(x-1)^{1/2}. \quad (1.26)$$

The analysis of the found dependencies results in the following.

1. Acceleration of radial movement \ddot{x} according to (1.20) goes to zero in the only point $x = \beta$. If $x < \beta$, then $\ddot{x} > 0$ and the rotor gets expanded; if $x > \beta$, then $\ddot{x} < 0$ and the rotor slows down its movement; and with $\dot{x} > 0$, it gets narrow. Consequently, the orbit can be stable, where there is no rotor radial movement, only in the position $x_k = \beta$.

Using expression β , let us find:

$$V_0 = (x_k g R)^{1/2} = (x_k)^{1/2} V_1, \quad (1.28)$$

the rotor starting velocity required to reach the relative orbit $x_k = r_k/R$. Here, g , R , V_1 – correspondingly, free fall acceleration, radius and the first cosmic velocity of a celestial object, wherefrom the rotor starts (the Moon, the Mars, etc. including the Earth, with neglect of the atmospheric effect).

2. The speed of radial movement \dot{x} , determined by the correlation (1.22) has a more complicated dependence on the coordinate x . This speed is absent at the permanent orbit, therefore let us consider the condition $x = 0$. This condition is fulfilled in the point $x = 1 = x_0$, i.e., at the beginning of radial movement, which fits the initial conditions (1.21).

Vanishing of the radical expression (1.22) in the point $x_k = \beta$ results in $\beta = 1$, or $x_k = x_0$; consequently, the orbit coincides in this case with the initial rotor position. The value $V_0 = V_1$, as is known, is enough only to balance gravity force with centrifugal force on the planetary surface.

If $\beta > 1$, the radial speed of the free rotor extension in the position $x_k = \beta$ differs from zero:

$$\dot{x}(x_k) = \left(\frac{q}{\beta}\right)^{1/2} (\beta - 1) = \frac{x_k - 1}{(x_k)^{1/2}} \frac{V_1}{R}.$$

The dimensional value of radial speed is written as

$$V_{rad} = \dot{x}(x_k)R = \frac{x_k - 1}{(x_k)^{1/2}} V_1. \quad (1.29)$$

This speed and the corresponding kinetic rotor energy in radial movement $\Delta K = MV_{rad}^2/2$ must be damped in order to add non-oscillatory nature to the movement. Using the expressions (1.28) and (1.29), let us find the system efficiency coefficient at the stage of rotor ascent to the orbit:

$$K_2 = \frac{K_0 - \Delta K}{K_0} = 1 - \left(\frac{V_{rad}}{V_0}\right)^2 = \frac{2x_k - 1}{x_k^2}.$$

For the case under consideration $x_k = 1.5$, we get the following in the Earth's conditions: $V_{rad} = 0.408V_1 = 3.23$ km/s, $K_2 = 0.889$.

Thus, the rotor at free extension passes the position of the permanent orbit $x_k = \beta > 1$ at the radial speed different from zero. The motion mode depends on the correlation of value β to value $\beta_{cr} = 2$, hereinafter called a critical parameter β .

If $1 < \beta < \beta_{cr}$, the radial speed is zero in the position x_{2k} determined by vanishing the second multiplier of the radical expression (1.22):

$$x_{2k} = \frac{\beta}{2 - \beta} = \frac{x_k}{2 - x_k}. \quad (1.30)$$

In the point x_{2k} the rotor has the zero radial speed and the negative radial acceleration, and moves in the future in the reversed direction passing the position x_k at the radial speed different from zero. Then, the sign of radial acceleration changes, the motion slows down and the rotor stops in the position x_0 (no energy dissipation); after that, the direct motion happens again, etc. Thus, the rotor radial movement at its free extension is oscillatory in the interval $[x_0, x_{2k}]$ in relation to the position $x = x_k$.

A relative orbit x_{2k} is at the following distance from x_k : $\Delta = x_{2k} - x_k = \frac{\beta - 1}{2 - \beta} x_k$,

If $x_k = \beta = 1.5$, then $x_{2k} = 3$, $\Delta = 1.5$ or in dimensional values: the orbit height above the equator $H_k = (x_k - 1)R = 0.5R$, the height of upper position where the rotor stops $H_{2k} = 2R$. Thus, the amplitude of oscillations is as follows: by $0.5R$ down from the orbit position; by $1.5R$ up from this position, i.e., by three times more.

The movement time depending on the rotor position is determined by the formula (1.24). The semi-oscillation, i.e., the movement time to the orbit $x = x_{2k}$:

$$\frac{\tau}{2} = \frac{\pi}{\left[q(2 - \beta)^3\right]^{1/2}}.$$

In the case $x_k = \beta = 1.5$ the period is approximately 239 min.

If $\beta = \beta_{cr}$, then according to (1.22) there is no final value $x > 1$, where radial speed becomes zero. Consequently, the rotor in this case moves off to an infinitely large distance if we stand clear of technical questions of the feasibility of such movement. This result also follows from the formula (1.30). The movement time depending on the position x is determined by the formula (1.26).

The starting velocity required for this variant of movement and having the meaning of the second cosmic velocity for the rotor is determined according to (1.28), for the orbit $x_k = \beta = 2$:

$$V_0 = (2gR)^{1/2} = \sqrt{2}V_1 = V_2.$$

For the Earth V_2 , which coincides with the known value of the second cosmic velocity, where any discrete object moves off from the Earth at infinity.

Thus, at free extension in the case $\beta = \beta_{cr}$, the rotor does not stop anywhere more and moves off at infinity after passing the position $x_k = \beta_{cr}$ (where $\ddot{x} = 0$, after which the acceleration changes the sign). In this case, the speed of radial movement according to (1.22) decreases, taking on a zero value at the limit.

The derived results have crucial significance since they impose meaningful restrictions on the choice of the UPT rotor orbits.

If $\beta > \beta_{cr}$, then $V_0 > V_2$; here, the rotor at free extension moves off at infinity as well as at $\beta = \beta_{cr}$. However, in this case, the radial speed at infinity has a value, which differs from zero: $\dot{x}_\infty = [q(\beta - 2)]^{1/2}$. The dependence of movement time on the position is determined by the formula (1.25).

Let us point out in the conclusion.

1. The action of centrifugal and gravity forces, as well as elastic forces under elastic extension cause an oscillatory radial movement of the rotor in relation to the orbit position. Depending on the parameter value β (or a starting rotor velocity V_0), it is possible that the rotor expands indefinitely moving off at infinity.

2. Friction forces between the fragments or any other dissipative forces, as shown below, change the picture of rotor movement: an oscillatory motion can become fading or non-oscillatory at all. The critical value of β_{cr} parameter can increase in this case taking on any values, which results in the increased radii of rotor permanent orbits and lifting the restrictions specified above.

3. The use of the radial movement energy dissipation is possible only partially, up to some rotor position $x' < x_k$. If the radial speed vanishes in this position and the rotor then expands freely without any impact of dissipative forces, it will oscillate at some interval $[x', x'']$ in relation to the orbit x_k . Such a rotor can serve as a vehicle for communication with concentric industrial complexes moving along the orbits x' and x'' .

4. The options described above, when the rotor moves off at infinity at radial movement, can be used to transport payload (raw materials, energy, finished products, etc.) from the Moon, the Mars and other celestial objects with a weak atmosphere or without it at all. After a start from the surface of such objects, rotor fragments completely separate from each other and move on unwinding spirals at some rotational and radial speed. It is possible to provide fragment movement towards the space industrial zone of the Earth by communicating additional impulses to fragments, for example, by means of jet engines or solar sails.

1.7. Rotor motion equations at the friction extension section

As shown above, it is required to use dissipative forces during the ascent to the intended orbit in order to damp the rotor oscillatory radial movement. These can include dry friction forces between the fragments in telescopic joints;

electromagnetic forces under a transformation of mechanical energy into electric energy in the mode of its generation in the same joints; reaction forces of fluid jets taken as ballast directed against the rotor movement; as well as various combinations of these forces. In order to damp oscillations, it is also possible to use gradual ejection of capsule parts. The most feasible method of the radial motion energy dissipation must meet all the technical and design requirements.

Let us study only two methods of dissipation – by means of using friction forces and raising capsule parts, as well as some their combinations.

As pointed out in clause 1.1, the stage of elastic extension finishes with rotor fragmentation; in order to prevent an abrupt contraction of extended fragments, friction braking is introduced in their telescopic joints. Apart from energy dissipation of the elastic rotor extension, friction forces are used for the radial motion energy dissipation, adding an aperiodic mode of motion to it.

Let us assume that the rotor is divided into fragments in the position $x_2 > x_1$. There can be several separations like that, let us assume n , then every separation is partial: only the n th part of the amount of the rotor connection joints intended for its separation into fragments is separated. Other separation techniques are possible, as well – let us assume that in all connection joints at a time; we will limit ourselves to the consideration of the specified method only.

The amount of joints and fragments, the size of fragments and their general parts in telescopic joints must be determined based on the condition of a possibility to exit into the orbit of radius $r_k = x_k R$. In this case, the following conditions must be met.

1. The rotor retains its integrity, i.e., the fragments are not completely separated.

2. When moving along the orbit, the fragments can make free movements in relation to each other, which eliminates the emergence of deformations and stresses in them.

The rotor after fragmentation looks like a system of inseparable and spreading fragments, whose relative displacement is braked by friction forces. Friction forces can vary under some program depending on the rotor position x , which is achieved by the change of normal pressure between friction elements or friction coefficient at different sections.

The damped energy of the radial rotor motion passes to the heat energy and is then dissipated in the rotor mass and in outer space. In this case, friction elements wear out under heat and power load. Therefore, the method of partial and successive rotor fragmentation appears to be feasible: their friction elements are not used in the future, having served at some section of radial motion

and possibly having lost the required operating features, and are replaced with other elements at further fragments.

We have a system of inseparable and non-spreading fragments at the section of friction extension, with various elastic, strength and other properties, different unit weight, etc. Apart from centrifugal and gravity forces proportional to elements masses, these fragments are affected by friction and elastic forces that arise under the elements tension. Relative displacements for various pairs of fragments connected to each other can be different.

When calculating the movement of the specific rotor with the given mechanical properties, the specific arrangement of system fragmentation, with the known properties of friction elements, etc., it is required to build the complete motion scheme, derive the corresponding differential equations, make their analysis and find the solution.

When studying the dynamics of rotor movement during its ascent to the orbit, let us consider a rotor model with averaged features: an average value of unit weight, average values of friction forces, etc. The tension of rotor components with friction forces results in their deformation – however, a significantly lower one compared to the deformation at the stage of elastic extension, when a relative displacement of fragments is possible.

The rigidity of unfragmented rotor components and its separated fragments differ enormously. For the entire rotor:

$$C_r = \frac{ES_r}{L},$$

where E – an elasticity modulus of rotor material; S_r – the area of its cross-section, L – the rotor length.

For the fragmented rotor components

$$C_{ij} = \frac{E_i S_i}{L_{ij}},$$

where E_i , S_i – an elasticity modulus and the cross-section area of individual fragments; L_{ij} – the distance between friction elements with numbers j and $j + 1$ at the i^{th} fragment.

If the values E_i , S_i are comparable to E and S_r , distance L_{ij} is much less than the total length of rotor L . Therefore, rigidity C_{ij} exceeds manifold C_r , and the rotor can be considered inextensible at individual sections between friction elements of the fragments.

Let us consider, as before, the rotor element with the element length l and mass $m = m_r/x_2$ after separation in point x_2 . Apart from centrifugal and gravity forces, tension force \bar{F}' and \bar{F}'' exert at the element ends, tangentially

directed and numerically equal to the total of friction forces acting on friction devices of the fragment containing this element: $F' = F'' = F_{2fr}$. The action of forces \bar{F}' and \bar{F}'' is the same as shown in figure 13 for elastic forces \bar{F}_1 and \bar{F}_2 ; their resultant.

$$F = F_{2fr} l/r_2 = \frac{F_{2fr} l}{x_2 R}$$

exerts in the center of the element and is directed radially opposite the movement.

The first stage of friction extension takes place from the position x_2 to the position x_3 , where the separated fragments move to the dog-shores in telescopic joints, and then the second stage of elastic extension begins.

Friction forces are inner rotor forces; therefore, the equation of rotational movement (1.2) and the integral (1.6) are not subject to change at the stage $[x_2, x_3]$. The equation of radial motion is subject to change: in the first part, instead of elastic forces and their resultant, friction forces and their resultant \bar{F}_2 appear. The differential equation of radial motion at the stage of friction extension is written as follows:

$$\ddot{x} - F(x, 0) + f_2 = 0, \quad x_2 \leq x < x_3; \quad (1.31)$$

$$f_2 = \frac{F_{2fr} l}{m_r R^2}.$$

It was assumed earlier that friction force F_{2fr} changes depending on the radial position of rotor x . This feature will be required at the final section before the ascent to the orbit. Let us assume that F_{2fr} and f_2 are constant at the first section of friction extension. In order for the acceleration \ddot{x} to become negative, and consequently the radial motion decelerated, the following condition must be met

$$f_2 \geq F(x_2, 0).$$

If it is required to vanish the acceleration \ddot{x} at some point $x' > x_2$ of the friction extension section, then

$$f_2 \geq F(x', 0) = f_2', \quad x_2 < x' \leq x_3.$$

For $x > x'$ the acceleration is negative and decreases in the future.

Based on the condition of non-destruction of friction elements, it follows that $F_{fr} \leq F_{\max}$; therefore, the value f_2 must be limited from above:

$$f'_2 \leq f_2 \leq f_{\max} = \frac{F_{\max} l}{m_r R^2}. \quad (1.32)$$

The case $f'_2 > f_{\max}$ implies that radial acceleration does not vanish at the section $[x_2, x_3]$.

Integrating (1.31), we find the dependence of radial speed on the rotor position:

$$\dot{x}^2 = \dot{x}_2^2 + (x - x_2) \left[\frac{q}{xx_2} \left(\beta \frac{x + x_2}{xx_2} - 2 \right) - 2f_2 \right], \quad x_2 \leq x \leq x_3, \quad (1.33)$$

where \dot{x}_2^2 is determined at the end of the elastic extension section according to (1.18). The elastic extension energy of the rotor element accumulated at the section $[x_0, x_2]$ can be damped by the work of friction forces at some section $[x_2, x'']$, where friction partial braking takes place. This can be expressed by the equal work of elastic and friction forces:

$$K_1 (x_2 - x_0)^2 / 2 = f_2 (x'' - x_2), \quad x_2 < x'' < x_3,$$

where f_2 complies with the restrictions (1.32). The friction work at the section $[x'', x_3]$ goes to energy dissipation of the rotor radial motion.

Friction extension takes place at the section, whose start and final points are chosen by certain rule; below is proposed one of the possible techniques to choose such points.

1.8. Choice of sections

of elastic and friction extension.

Dynamics of the controlled radial rotor motion

Let us choose alternating sections of the elastic and friction rotor extension in respect to the task of launching the rotor into the orbit to the position $x_k = 1.5$, i.e., at the height $H_k = 0.5R = 3,185$ km. Assuming an ascent of 1 km as a typical size, which corresponds to the span $\Delta x = 1.57 \times 10^{-4}$, we will get the following value for the non-dimensional height $h_k = 3,185\Delta x$.

A possible diagram of the sections of elastic and friction rotor extension is given in figure 14 along the X axis, where a non-dimensional rotor radius is plotted; the sections are highlighted. The whole numbers below the sections – 300, 500, etc. – imply the height in kilometers (if in dimensional values); the number of spans Δx (if in non-dimensional value).

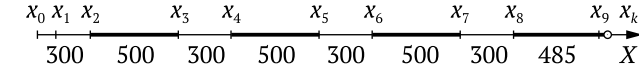


Figure 14 – Diagram of the sections of elastic and friction rotor extension

The numbers of points dividing the sections are subject to a specific rule. Odd-numbered points x_1, x_3, x_5, x_7 are the points of the rotor ascent to the sections of elastic extension, which are further designated by the same numbers. The point x_1 corresponds to the beginning of the rotor without a capsule ascent to the section of elastic extension in space. A non-dimensional rotor deformation $\Delta x'_1 = x_1 - x_0$ in point x_1 differs from zero; deformation is equal to zero in points x_3, x_5, x_7 , which are the ends of previous sections of friction extension. The point x_0 – a critical point of the last friction extension section (see clause 1.9).

Even-numbered points x_2, x_4, x_6, x_8 are the points of rotor fragmentation and the beginning of friction extension sections; the last ones will also have even numbers. The point $x_0 = 1$ can be included into even-numbered points, taking into consideration that it is the start point at the section $[x_0, x_1]$, where external forces act – aerodynamic drag forces and capsule gravity force to the Earth – instead of internal dissipative (friction) forces.

Let us point out three criteria for choosing points $x_2, x_3, x_4, \dots, x_8$ and thus the values of the sections of elastic and friction extension.

The first criterion follows from the boundedness condition of the rotor relative deformations at the sections of its elastic extension. Let us assume that the permissible value of relative deformation $\Delta x_{\max} = 0.05$, then the value of the elastic extension sections is determined by the following condition

$$\Delta x_i = \frac{L_{i+1} - L_i}{L_i} = \frac{x_{i+1} - x_i}{x_i} \leq \Delta x_{\max}, \quad i = 3, 5, 7, \quad (1.34)$$

where $L_i = 2\pi x_i R$ – the rotor length in positions x_i .

At the first elastic extension section

$$\Delta x_1 = \frac{x_2 - x_0}{x_0} = 300 \Delta x = 0.0471 < 0.05,$$

i. e., Δx_1 also meets the restriction (1.34). It is easy to make sure that this condition is also satisfied at other elastic extension sections having the values shown in figure 14).

The second criterion is related to the limitation of the friction force value. In order to damp the radial motion kinetic energy, it is necessary that the total of friction work at all friction extension sections is approximately equal to the energy

$$\Delta K_2 = \frac{(x_k - 1)^2}{x_k} \frac{mV_1^2}{2},$$

where x_k is put instead of x . The longer the friction sections are, the less their friction force value can be, and the easier it is to comply with the restrictions above (1.26) and thus ensure a reliable operation of friction elements. Consequently, the friction extension sections should be possibly longer.

The dependence of radial speed on rotor position x facilitates the determination of friction forces. Let us assume that radial speed in point x_2 has the value \dot{x}^2 ; let us necessitate that the speed decreases, for example, by $\frac{1}{4}$: $\dot{x}_3 = \frac{3}{4}\dot{x}_2$ at the end x_3 of the friction extension section. Substituting this value in (1.33) at $x = x_3$, let us find the corresponding value f_2 . The values f_4 and f_6 at the 4th and 6th sections of friction extension are calculated based on the conditions

$$\dot{x}_5 = \frac{1}{2}\dot{x}_4; \quad \dot{x}_7 = \frac{1}{4}\dot{x}_6.$$

The general rule can be written as follows:

$$\dot{x}_{i+1} = \lambda_i \dot{x}_i, \quad i = 2, 4, 6, \quad (1.35)$$

where $0 \leq \lambda_i \leq 1$. If the speed at the end of the friction extension stage decreases by λ_i times, the radial motion kinetic energy at the end of this stage decreases by λ_i^2 times. The values derived from (1.33) are checked for compliance with the restrictions (1.32). If the peak limiting is violated, there should be reviewed the lengths of friction destruction sections, numbers of fragmentation, etc. After the rotor ascent into space, it is possible not to introduce the sections of elastic extension and only use friction extension at the section $[x_1, x_k]$ with the preset modification program for the coefficient $\lambda(x)$ of radial speed decrease and thus the energy of the rotor radial motion. The dependence $\lambda(x)$ through which the value $f(x)$ is expressed must in this case comply with the restrictions (1.32).

The third criterion is related to the preset orbit height, which affects the rotor extension, the number and length of fragments, their general parts, numbers of fragmentation and other technical requirements. For example, it was assumed for the chosen motion pattern in figure 14 that the total length of general fragment parts during the first rotor fragmentation provides an increase in its length by

$$\Delta L = L_3 - L_0 = 1,600\pi = 5,024 \text{ km.}$$

In this case, the condition is met, where the rotor deformation is equal to zero at the end of the first stage $[x_0, x_3]$ including the sections of elastic and friction extension. The same changes in rotor length are at the second and third stages, a little less – at the fourth.

The dynamics of the rotor radial movement at the sections $[x_i, x_{i+1}]$, $i = 1, 2, 3, 4, 5, 6, 7$ is described by equations similar to (1.17), (1.18) at the sections of elastic extension (odd-numbered values i) and (1.31), (1.33) at the sections of friction extension (even values i).

At the sections of elastic extension ($i = 1, 3, 5, 7$):

$$\ddot{x} = F(x, 0) - K_i(x - x_i), \quad x_i \leq x \leq x_{i+1}; \quad (1.36)$$

$$\dot{x}^2 = \dot{x}_i^2 + (x - x_i) \left[\frac{q}{xx_i} \left(\beta \frac{x + x_i}{xx_i} \right) - K_i(x - x_i) \right],$$

where $K_i = \frac{2\pi C_i l}{m_r R}$, C_i – rotor rigidity at the i^{th} section. For $i = 1$ the equations

slightly differ having the view (1.17) and (1.27).

At the sections of friction extension ($i = 2, 4, 6$):

$$\ddot{x} = F(x, 0) - f_i, \quad x_i \leq x \leq x_{i+1};$$

$$\dot{x}^2 = \dot{x}_i^2 + (x - x_i) \left[\frac{q}{xx_i} \left(\beta \frac{x + x_i}{xx_i} - 2 \right) - 2f_i \right],$$

where $f_i = \frac{F_{ifr} l}{m_r R^2}$, F_{ifr} – the total of friction force acting on the fragments at the i^{th} section of friction extension. The values f_i are determined based on the conditions (1.35):

$$f_i = \frac{\dot{x}_i^2}{2} \frac{1 - \lambda_i^2}{x_{i+1} - x_i} + \frac{q}{2x_{i+1}x_i} \left(\beta \frac{x_{i+1} + x_i}{x_{i+1}x_i} - 2 \right). \quad (1.37)$$

Other dynamic rotor characteristics – movement time $t(x)$, turning angle $\varphi(x)$, etc. are determined similarly to the correlations (1.11)–(1.16), where $u(x) = \dot{x}^2$ is determined according to (1.36), (1.37) at every section $i = 1, 3, \dots, 7$.

1.9. Rotor motion at the final stage

The final stage of the rotor radial movement before the ascent to the orbit cannot take place in the mode of elastic or, even more so, free extension: the rotor in both cases will oscillate (see clauses 1.5 and 1.6).

Indeed, at the positive radial speed and positive acceleration in point x_8 , the rotor in the general case passes the position x_k at radial speed different from zero, which causes oscillations. Consequently, in order to complete the process of energy dissipation and fully reduce the radial speed, it is required that the radial acceleration at this stage is negative, which is only possible in the mode of friction extension within the assumed motion pattern. For a more effective rotor motion control and compliance with some additional conditions, let us consider the total friction force F_{8fr} as a variable, which depends on the rotor position x . A differential equation of the rotor radial movement is written as:

$$\ddot{x} = F(x, 0) - f_8(x), \quad x \geq x_8. \quad (1.38)$$

Integrating this equation, we will get as follows:

$$\dot{x}^2 = \dot{x}_8^2 + \frac{q}{xx_8} (x - x_i) \left(\beta \frac{x + x_8}{xx_8} - 2 \right) - 2 \int_0^x f_8(x) dx. \quad (1.39)$$

The condition (1.19) must be met in order to take the rotor to the orbit x_k

$$\ddot{x}_k = \ddot{x}(x_k) = 0; \quad \dot{x}_k = \dot{x}(x_k) = 0. \quad (1.40)$$

Two more conditions must be complied with when exiting the orbit and moving along it further.

1. Free, without restrictions, relative displacement of fragments (moving apart and coming together) in their telescopic joints. The rotor is affected at large time intervals by the disturbing action of the Moon and the Sun, which causes periodic variation of the shape and length of individual rotor sections. In order to counteract these adverse consequences, it is required to let the specified variations happen without significant opposition and, consequently, without energy dissipation, the loss of orbital velocity and early descent from the orbit. This is an approximate mechanism providing a long-term existence of the rings of Saturn, Uranus and other large planets.

2. Elimination of deformations and stresses in rotor fragments at the moment of exiting the orbit.

Both these conditions are provided if we necessitate vanishing of friction force in the position x_k and at further rotor movement in orbit:

$$f_8(x_k) = 0. \quad (1.41)$$

The violation of this condition will result in fragments jamming and, consequently, in the emergence of stresses in them. Their abrupt (shock) unloading is possible at rotor disassembly, for example, to carry out construction works.

The condition $\ddot{x}_k = 0$ with regard to (1.38) and (1.41) results in

$$\beta = x_k, \quad (1.42)$$

which states that the rotor permanent orbit is only possible in the position x_k , where the resultant of centrifugal and gravity forces goes to zero. If the resultant is not equal to zero, there is a corresponding radial acceleration, radial speed arises; consequently, the rotor will make radial motion.

The equality (1.42) is an indispensable prerequisite for the rotor ascent to the orbit in the position x_k . Taking into consideration that $\beta = V_0^2/gR$, the starting circular velocity

$$V_0 = (x_k gR)^{1/2} = (x_k)^{1/2} V_1. \quad (1.43)$$

For $x_k = 1.5$ we will $V_0 = 9.68$ km/s, the value $\mu = m_0/m_r$ in this case must be less than 0.5.

Let us determine the rotor orbital velocity using the integral (1.6):

$$V_{orb} = r_k \dot{\phi}_k = \frac{V_0}{x_k} = \frac{V_1}{(x_k)^{1/2}}. \quad (1.44)$$

The derived V_{orb} can be checked by means of a known condition for a free discrete object of mass m – the equality of gravity and centrifugal forces at the circular orbit of radius r_k :

$$mg \frac{R^2}{r_k^2} = m \frac{V_{orb}^2}{r_k},$$

wherefrom

$$V_{orb} = \left(\frac{gR^2}{r_k} \right)^{1/2} = \left(\frac{gR}{x_k} \right)^{1/2},$$

which coincides with (1.44). If $x_k = 1.5$, then $V_{orb} = 6.45$ km/s.

Let us consider the second condition (1.40) and determine the dependence $f_8(x)$ upon condition (1.41). Let us divide the section $[x_8, x_k]$ in half by the point x_9 ; let us assume that in the first half $f_8 = \text{const}$, whereas in the second half $f_8(x)$ decreases from f_8 up to zero in linear fashion:

$$f_8(x) = \begin{cases} f_8 = \text{const}, & x_8 \leq x \leq x_9; \\ f_8 = \frac{x_k - x}{x_k - x_9}, & x_9 \leq x \leq x_k. \end{cases} \quad (1.45)$$

In this case, the integral in (1.39) takes on the following values:

$$I(x) = \int_{x_8}^x f_8(x) dx = \begin{cases} f_8(x - x_8), & x_8 \leq x \leq x_9; \\ f_8(x_9 - x_8) + f_8 \frac{x - x_9}{x_k - x_9} \left[x_k - \frac{1}{2}(x + x_9) \right], & x_9 \leq x \leq x_k. \end{cases}$$

In the point $x = x_k$ we will get as follows: $I(x_k) = \frac{1}{2} f_8 (x_9 + x_k - 2x_8)$. Let us assume that $x_9 = x_8 + 400\Delta x$. For x_k , let us find $x_k = x_8 + 485\Delta x$; then,

$$I(x_k) = \frac{1}{2} f_8 885\Delta x.$$

Let us determine the value f_8 based on the condition that the radial speed drops to zero in the point x_k . According to (1.39),

$$\dot{x}_8^2 + \frac{q}{x_k x_8} (x_k - x_8) \left(\beta \frac{x_k + x_8}{x_k x_8} - 2 \right) - 885 f_8 \Delta x = 0. \quad (1.46)$$

Based on this, the value f_8 and the dependence (1.45) meeting the conditions (1.40) and (1.41) of the rotor placement into orbit x_k are determined.

Thus, the conditions of the UPT rotor ascent to the orbit in the preset position x_k have the view (1.42), (1.43). The rotor dynamics at the final stage is determined by the equations (1.38), (1.39) and the correlations (1.45), (1.46); the rotor movement on the orbit is subject to the conditions (1.40), (1.41), (1.44).

The critical value of parameter β can be increased by means of selecting the values f_8 in compliance with the condition (1.45) at $\beta \geq 2$ and final values x_k .

1.10. Problem of the UPT rotor placement into orbit. Example

Let us set the values for three groups of the problem parameters.

1. Constant parameters: the Earth's radius R , gravity acceleration g at the equator, the initial atmospheric density ρ_0 , etc. Let us assume that for a model of standard atmosphere, $H_a = 6,665$ m – a piezometric height of average atmosphere with constant temperature, $\alpha_d = \frac{R}{H_a} = 995.736$ – an exponential index of power in Halley's formula determining the density decrease with the height [5,18].

2. Parameters determining the orbit position, the value of the corresponding starting velocity of the rotor, its mechanical properties, aerodynamic characteristics of the capsule, etc.:

$$x_k = 1.5; \quad V_0 = \sqrt{x_k} V_1 = 9.68 \times 10^5 \text{ m/s}; \quad m_r = 25 \text{ kg/m};$$

$$m_0 = 0.2m_r = 5 \text{ kg}; \quad C_1 = ES/L = 42.39 \text{ N/m},$$

where $E = 2.16 \times 10^{11}$ N/m² – steel elasticity modulus; $S = \pi d^2/4$ – rotor cross-section area; $d = 0.1$ m; $L = 2\pi R = 4 \times 10^7$ m; $\lambda = C_x S_0/2 = 0.1365$ m², where $C_x = 0.9$ – the coefficient of capsule aerodynamic drag, $S_{caps} = d_{caps} l$ – capsule element cross-section area; $d_{caps} = 0.3$ m – capsule diameter; l – element length.

3. Parameters determining the position of the sections of rotor elastic and friction extension, the points of fragmentation (figure 14), etc.; let us also set an iteration step at every section, the coefficients of radial speed decrease at the end of friction sections according to the rule (1.35). Let us assume that coefficients $\lambda_2 = 1$; $\lambda_4 = 0.5$; $\lambda_6 = 0.25$, etc.

Let us solve the problem without regard to the restrictions on friction force of type (1.32).

The graphs show the change in the characteristics of radial rotor movement depending on its position and the preset motion modes at individual sections of X axis, along which the values of non-dimensional radius are plotted.

Figure 15 shows the variation in the radial acceleration $w = \ddot{x}R$ m/s². The acceleration at the section $[x_0, x_1]$ of motion in the atmosphere is the result of a complex interaction of nonlinear forces; the greatest excitation is caused by aerodynamic resistance to the capsule radial movement. In the exit point x_1 from the atmosphere, there takes place capsule ejection and a jump-like increase in acceleration.

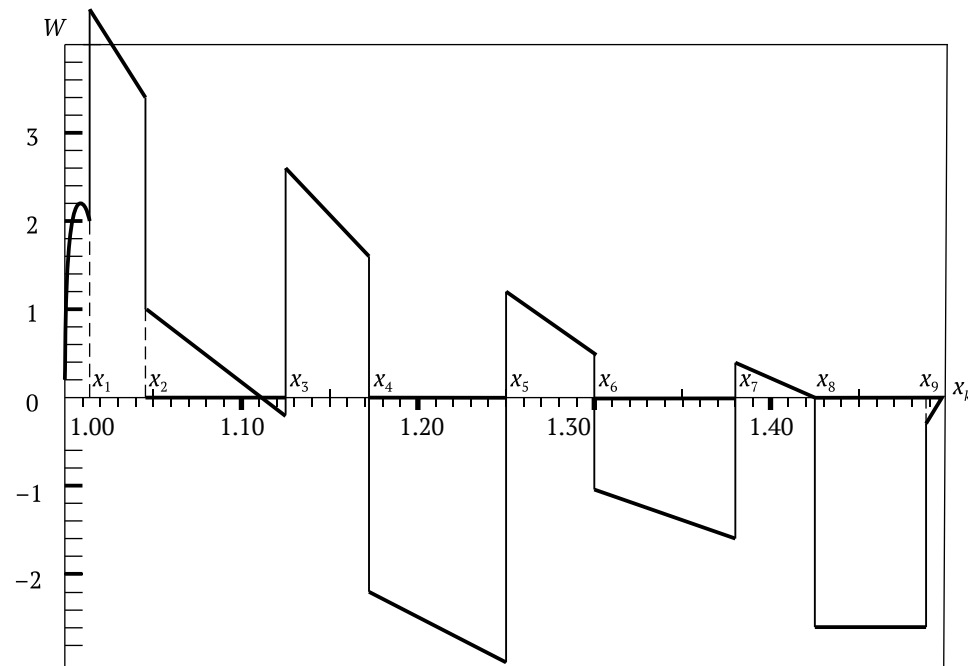


Figure 15 – Radial rotor acceleration

The acceleration at the first section of elastic extension $[x_1, x_2]$ decreases monotonely up to the point x_2 , where fragmentation happens and a friction extension section begins, with the decelerating friction force constant in magnitude. This causes a jump-like change in acceleration again; the acceleration at the section $[x_2, x_3]$ becomes negative changing the sign for the first time.

The variation w at other sections takes place in a similar way. As for the last section $[x_8, x_k]$ – the process takes place as described in clause 1.9. Due to minor effect on the acceleration of centrifugal and gravity forces, the acceleration is constant at the section $[x_8, x_9]$ within the accuracy of the drawing. The acceleration changes linearly at the section $[x_9, x_k]$ vanishing in the final point x_k .

Based on acceleration curves, it is possible to determine friction force at friction sections. The highest value is reached in point x_4 ; according to the correlations $\Delta w_4 = f_4 R = 3.8 \text{ m/s}^2$ and $f_4 = F_{4fr} / m_1 R^2$, we will get as follows: $F_{4fr} = m_1 R \Delta w_4 / l = 6.08 \times 10^5 \text{ kN}$.

Friction force at other sections of friction extension decreases. An average value of friction force can be determined based on the condition of equality of its work at displacement equal to the sum of increments of the rotor length at friction sections:

$$F_{fr} \Delta L = M_1 V_{rad}^2 / 2,$$

where $\Delta L = 2\pi \times 1,985 \times 10^3 \text{ m}$; $V_{rad}^2 = (x_k - 1)^2 V_1^2 / x_k$; M_r – rotor mass, wherefrom $F_{fr} = 4.19 \times 10^5 \text{ kN}$.

If the elastic extension sections are replaced with friction ones, in other words to have one friction extension section $[x_1, x_k]$, the average value of friction force will decrease: $F_{fr} = 2.6 \times 10^5 \text{ kN}$.

Figure 16 shows the graph of change in radial speed $V = \dot{x}R \text{ m/s}$. An increase in speed takes place at the sections of elastic extension where the acceleration is positive; the speed is almost 600 m/s at the end of the motion in the atmosphere stage, whereas the highest value is achieved at the end of the elastic extension second stage – 1,880 m/s.

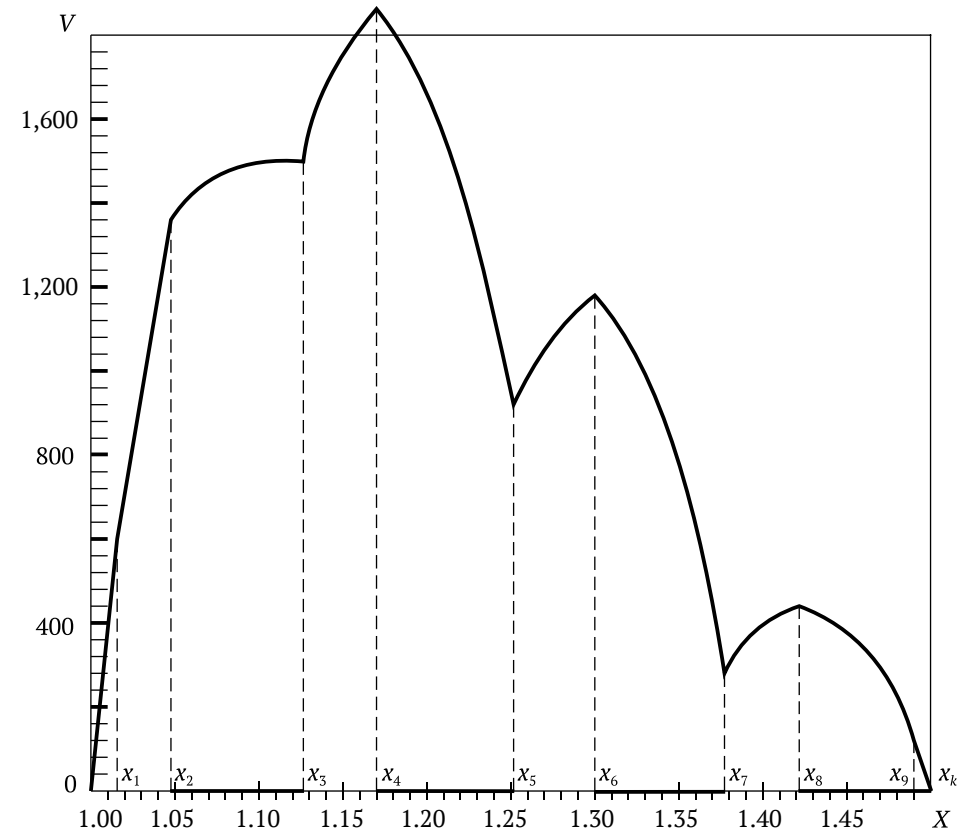


Figure 16 – Radial rotor speed

The speed can decrease in compliance with the preset program at the sections of friction extension. The velocity curve has corner points in the points of the motion mode change, where the acceleration changes in a jump-like manner; the speed varies monotonely in between.

The radial speed decreases at the final section of motion reaching a zero value in the orbit point x_k , which together with the condition $w(x_k) = 0$ denotes damping of radial motion and rotor placement into the intended orbit.

Figure 17 shows the time $t(x)$ (in minutes) of rotor displacement from the initial position to the current position. Also, this graph allows determining the travel time from one intermediate position to another.

At the beginning of movement, when the radial speed is insignificant, the time grows quickly, then, an increase in time slows down at the sections with the highest speed. The time grows most intensively at the final stage, when the radial speed decreases tending to zero. This testifies a very smooth rotor

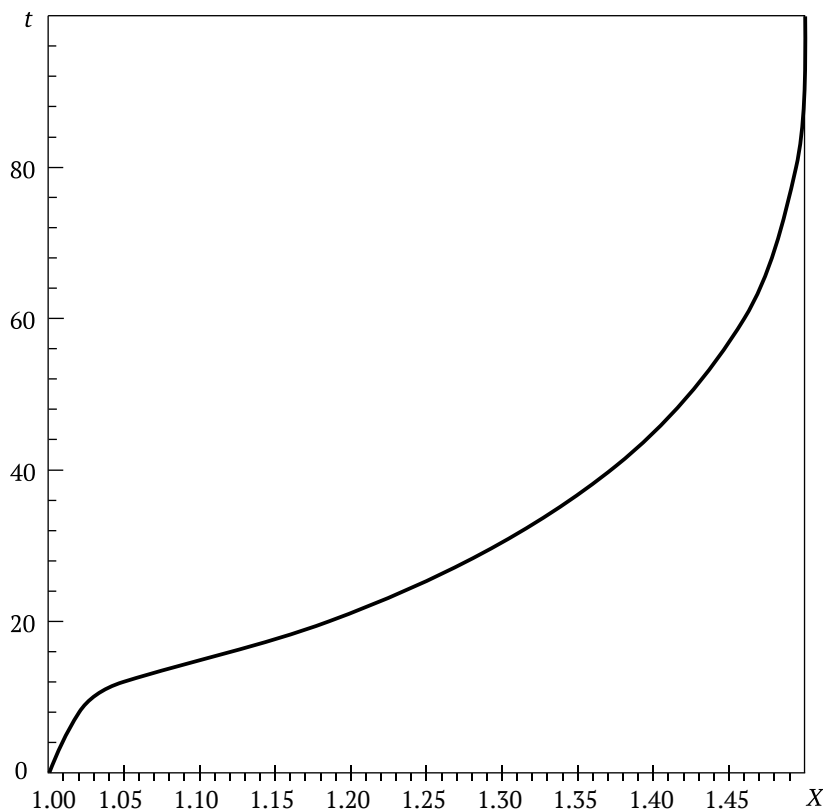


Figure 17 – Time of rotor movement depending on its position

approach to its orbit. The total travel time of the rotor to the orbit $x_k = 1.5$ – about 100 min.

The graph transaction allows us to find the law of the rotor radial movement, i.e., the dependence $x = x(t)$.

The analysis of the problem on the UPT rotor ascent to the orbit enables the following conclusions.

1. The initial kinetic rotor energy required for the ascent to the intended orbit is excessive, which results in rotor oscillations in relation to the orbit position. The redundancy arises due to a different type of dependence of the rotor energy kinetic momentum on the initial speed – the linear one in the first case and the quadratic one in the second case; in addition, there must be met the condition of the kinetic momentum conservation in any rotor position, including in the initial and final positions. The factor of excessive kinetic energy is a consequence of the general laws of nature and cannot be eliminated, at least at the beginning of motion.

2. It is possible to control the radial rotor movement with the help of forces conserving its kinetic momentum and causing the dissipation of excessive energy in the process of movement. A principal possibility of the rotor motion control with the help of forces changing its kinetic momentum is of interest; for example, using interaction forces with the Earth's magnetic field, sunlight pressure, etc.

3. The rotor radial motion control only with the help of friction forces is unfeasible due to extremely large forces, which can result in irreversible deformations of rotor fragments or even their breakage.

Further studies are required as to the choice of the most feasible method of energy dissipation and kinetic momentum change. The dissipation process by means of the uplift and gradual ejection of capsule parts has good prospects.

4. In order to solve the problem on the launch of a real rotor to the orbit, it is required to develop its more comprehensive model, which would take into consideration the whole range of its physical, mechanical and other features, including the rotor and capsule electromagnetic interaction, different mechanical properties of various rotor parts, etc. The process of concretization and clarification of the rotor model is obviously possible in the course of elaborating design of the rotor and its components.

The development of the physical rotor model requires further development of mathematical models of its motion, methods of their analysis, synthesis of motion control systems, etc. The results obtained in this chapter can serve as a basis for building more comprehensive mathematical models of rotor movement and as an initial approximation when solving more complicated problems of rotor dynamics.

Chapter 2

Dynamics of the UPT placement into orbit with energy dissipation by means of capsule ejection

The UPT rotor radial movement in space in the general case is oscillatory in relation to its orbit position. The use of energy dissipation to add an aperiodic or, at least, quick fading nature to the radial motion is a relevant problem at this stage of motion.

In the previous chapter, friction forces between fragments in their telescopic joints were used for dissipation. Specific calculations have shown that the total friction forces acting on one fragment reach 4×10^5 kN. This value can be decreased by approximately twofold if only one – friction stage – is used instead of alternating stages of friction and free rotor extension. However, in this case, the use of friction forces is impractical due to a number of reasons: it is required to provide operating properties of friction elements and strength of rotor fragments, to withdraw huge amounts of heat under vacuum conditions, etc.

Let us further consider another method of dissipation by means of the uplift and gradual discharge of inert cargo, when a part of kinetic energy of the rotor radial movement goes to potential energy of the cargo lifted in the Earth's gravity field and is then lost during its discharge. It is possible to use a vacuum capsule as such cargo, where the rotor is accelerated and moves in the dense atmosphere; without rotational movement, it slows down radial movement. Instead of its entire ejection when leaving the atmosphere, it is possible to eject it by parts, similar to how cargo is released when a hot-air balloon is being raised. In this case, a challenging problem of heat rejection does not arise since it is absent. The necessity for friction devices is eliminated, as well.

In order to determine the mass of the capsule ejectable parts, let us use the conditions of rotor stop in its radial movement at the moment of ejecting these parts. The vanishing conditions in the specified positions of radial speed enable the determination of the required capsule masses at motion stages preceding the stops, as well as the masses of the parts required to be ejected so as to resume radial speed at the next stage.

It is possible to take capsule parts in the form of its discrete fragments to the orbit as additional payload. The fragments can be used to raise out-of-gauge

payload – passenger modules, scientific and industrial equipment, building structures, etc.

After leading the rotor with additional cargo in the form of capsule parts to the position of the intermediate orbit, where the radial speed and acceleration vanish simultaneously their circular velocity should be adjusted. The considered system is represented as a rotating rotor and almost motionless capsule fragments held on the rotor by means of TLS remainders (traction levitation system) and capable of autonomous operation. The rotor angular velocity exceeds the velocity designed for the reached orbit, which is required to carry inert cargo.

It is possible to adjust their circular velocity by including the TLS into the mode of rotor braking and motion acceleration of capsule fragments. In this case, the entire system switches to a new constant operation due to the speed change. Using speed adjustment it is possible to control the system movement towards the permanent orbit, which is essential in the case when there is another rotor on this orbit, and the led rotor serves to deliver cargo.

Thus, energy dissipation of the rotor radial movement when raising the capsule allows us to avoid problems of friction braking, take additional payload to the orbit, including out-of-gauge cargo, and finally control the process of the system transfer to the intended orbit.

2.1. Motion control of the rotor – capsule element in the atmosphere with regard to capsule rotation

The rotor and vacuum capsule movement is considered in relation to the inertial reference system OXYZ with the beginning in the Earth's center; the OZ axis – rotational axis of the Earth, rotor and capsule, the OX and OY axes are located in the equatorial plane.

Let us assume a thin solid homogeneous ring as a rotor model at the stage of movement in the atmosphere; the ring can expand due to elastic extension. At the initial moment, the rotor has a radius $r_{r0} = R$, where R – the Earth's equatorial radius, and absolute velocity $\omega_0 = V_0$, where V_0 – starting circular velocity determined based on the condition of exit to the intended orbit. It is believed that a thin solid homogeneous capsule (tore) encircling the rotor in a non-contact manner and expanding together with it due to elastic extension does not lose leak-tightness. The initial capsule radius $r_{c0} = R$; the starting angular velocity is equal to the angular velocity ω of the Earth's daily rotation; the starting radial velocity of the rotor and capsule $V_{r0} = 0$; the system movement takes place in the equatorial plane. The forces holding the rotor along the axial line of the ascent are taken into consideration at all stages of the ascent, whereas tangential components are disregarded due to their small values.

When moving in outer space, the rotor and capsule are gradually fragmented. In this case, rotor fragments, having telescopic joints and expanding freely or under the action of friction forces, retain the shape of the ring. Capsule fragments get completely separated from each other, possibly except for the initial stage, and then gradually ejected to the Earth.

Let us solve the problem of the aperiodic motion synthesis of the rotor – capsule system in dense atmosphere and outer space with the exit to the intended intermediate orbit under the conditions: a vacuum capsule is released by parts after leaving the atmosphere; some parts are delivered to the orbit; the system radial speed is zero at the moments of ejecting capsule parts.

Let us consider the rotor element movement having the initial length l and mass m_r , and the capsule element of the same length and mass m_0 . The selected element of the system has three degrees of freedom; its position is determined by three generalized coordinates: r – distance to the Earth's centre equal to the rotor and capsule radius; φ – rotor turning angle around the OZ axis; ψ – capsule turning angle around the OZ axis in rotational movement arising due to daily motion together with the Earth in the initial position.

The kinetic energy of the system component in this case

$$K = \frac{m_r + m_0}{2} \dot{r}^2 + \frac{m_r}{2} r^2 \dot{\varphi}^2 + \frac{m_0}{2} r^2 \dot{\psi}^2,$$

where $\dot{r} = \frac{dr}{dt} = V_r$ – radial speed of the component; $\dot{\varphi} = \frac{d\varphi}{dt}$, $\dot{\psi} = \frac{d\psi}{dt}$ – rotor and capsule corner velocities.

The forces acting on the system element at the stage of motion in the atmosphere are determined similar to those considered in Chapter 1. Let us ignore the tangential viscous resistance force caused by a difference of rotational movements between the capsule and the atmosphere due to its small value.

Using the Lagrange formalism, we will get a system of differential equations for the system element motion in the dense atmosphere at the section $[r_0, r']$:

$$(m_r - m_0)\ddot{r} = m_r r \dot{\varphi}^2 + m_0 r \dot{\psi}^2 - (m_r + m_0) \frac{gR^2}{r^2} - 2\pi l (C + C_0) \left(\frac{r}{R} - 1 \right) - \lambda \rho_0 r^2 \exp \left[-\alpha_d \left(\frac{r}{R} - 1 \right) \right]; \quad (2.1)$$

$$m_r (r\ddot{\varphi} + 2\dot{r}\dot{\varphi}) = 0; \quad (2.2)$$

$$m_0 (r\ddot{\psi} + 2\dot{r}\dot{\psi}) = 0. \quad (2.3)$$

The initial motion conditions

$$r_{r_0} = R_e; \quad \dot{r}_0 = 0; \quad \varphi_0 = 0; \quad \dot{\varphi}_0 = \omega_0; \quad \dot{\psi}_0 = \omega_e.$$

The equations (2.2) and (2.3) have the first integrals, which are the conservation laws of the rotor and capsule kinetic momentum:

$$r^2 \dot{\varphi} = r_0^2 \omega_{r_0} = V_0 R;$$

$$r^2 \dot{\psi} = r_0^2 \omega_e = V_e R,$$

where $V_e = \omega_e R$ – linear speed of equator points rotational movement. From here it follows that

$$\dot{\varphi} = \omega_0 \frac{R^2}{r^2} = \frac{\omega_0}{x^2}; \quad \dot{\psi} = \Omega \frac{R_e^2}{r^2} = \frac{\omega_e}{x^2}. \quad (2.4)$$

Substituting (2.4) in (2.1), we will get the following equation of the system radial motion:

$$\ddot{x} = \frac{q}{x^2} \left(\frac{\beta_0}{x} - 1 \right) - K_0 (x - 1) - p_0 x^2 \exp \left[-\alpha_d (x - 1) \right], \quad (2.5)$$

where $\dot{x} = \frac{r}{R}$; $\ddot{x} = \frac{\ddot{r}}{R}$; $x' = x_0 + \Delta x$; $\Delta x = \frac{H}{R}$; $x_0 \leq x \leq x'$; H_a – the height of dense atmosphere;

$$q = \frac{g}{R}; \quad K_0 = \frac{2\pi l (C + C_0)}{mR(1 + \mu_0)} = \frac{K}{1 + \mu_0}; \quad \mu_0 = \frac{m_0}{m}; \quad (2.6)$$

$$p_0 = \frac{\lambda_1 \rho_0 R_3}{m(1 + \mu_0)} = \frac{p}{1 + \mu_0}; \quad \beta_0 = \frac{V_0^2 + \mu_0 V_e^2}{V_1^2 (1 + \mu_0)} = \frac{\beta + \mu_0 \beta_e}{1 + \mu_0};$$

$$\beta = V_0^2/V_1^2; \quad \beta_e = V_e^2/V_1^2; \quad V_1^2 = gR.$$

Here V_1 – the first cosmic velocity. The initial conditions of the system radial movement

$$x_0 = 1; \quad \dot{x}_0 = 0. \quad (2.7)$$

The obvious condition of the system radial movement $\ddot{x}(x_0) > 0$ with regard to (2.5), (2.6) and (2.7) leads to the correlation $\beta_0 > x_0$ or

$$V_0 > V_1 \left[(1 + \mu_0)x_0 - \mu_0\beta_e \right]^{1/2}. \quad (2.8)$$

Let us solve inequality (2.8) in relation to the parameter μ_0 :

$$\mu_0 < \frac{\beta - x_0}{x_0 - \beta_e} = \frac{V_0^2 - V_1^2}{V_1^2 - V_e^2}.$$

From here follows the restriction to the choice of the initial mass of capsule element

$$m_0 < m \frac{V_0^2 - V_1^2}{V_1^2 - V_e^2}. \quad (2.9)$$

If the inequality sign in (2.9) is replaced with the equality sign, we will get the critical mass value of the capsule element $m_0 = m_{cr}$, when the system cannot start radial motion at any starting velocity V_0 . For example, for $V_0 = 10$ km/s, $V_1 = 7.8$ km/s, $V_e = 0.46$ km/s we will get $m_{cr} = 0.59m$.

2.2. Dynamics of the system radial motion in atmosphere

The equation of the radial motion for the rotor – capsule element (2.5) does not contain variables ϕ and ψ . This allows integrating it in quadratures despite the equation nonlinearity and studying the system dynamics in dense atmosphere and then in outer space. After determining the dependence of radial speed \dot{x} , radial acceleration \ddot{x} , motion time t as well as corner velocities $\dot{\phi}$, $\dot{\psi}$ according to (2.4), and angles ϕ , ψ on rotor position x , it is possible to control the motion of the rotor – capsule system, to set system parameters and motion characteristics, and to identify the conditions of its realization.

Depicting the left side of equation (2.5) as follows

$$\ddot{x} = \frac{d\dot{x}}{dx} \frac{dx}{dt} = \frac{d}{dx} \left(\frac{\dot{x}^2}{2} \right) = \frac{1}{2} \frac{du}{dx} = \frac{1}{2} u',$$

we will get a differential first-order equation with variable coefficients in relation to $u(x) = \dot{x}^2$:

$$u' + f_1(x)u = f_2(x), \quad f_1(x) = 2p_0 \exp[-\alpha_d(x-1)]; \quad (2.10)$$

$$f_2 = 2 \left[\frac{q}{x^2} \left(\frac{\beta_0}{x} - 1 \right) - K_0(x-1) \right].$$

Taking into consideration that $u_0 = \dot{x}^2 = 0$, the solution to the equation (2.10) is written as [9]:

$$u(x) = \exp \left[\frac{2p_0}{\alpha_d} \exp\{-\alpha_d(x-1)\} \right] \int_{x_0}^x f_2(x) \exp \left[\frac{2p_0}{\alpha_d} \exp\{-\alpha_d(x-1)\} \right] dx.$$

Substituting here the expression $f_2(x)$ and integrating term by term, let us find:

$$u(x) = \dot{x}^2 = 2 \exp \left[\frac{2p_0}{\alpha_d} \exp\{-\alpha_d(x-1)\} \right] \left[q\beta_0 J_1(x) - qJ_2(x) - K_0 J_3(x) \right];$$

$$J_1(x) = \int_{x_0}^x \exp \left[-\frac{2p_0}{\alpha_d} \exp\{-\alpha_d(x-1)\} \right] \frac{dx}{x^5};$$

$$J_2(x) = \int_{x_0}^x \exp \left[-\frac{2p_0}{\alpha_d} \exp\{-\alpha_d(x-1)\} \right] \frac{dx}{x^2};$$

$$J_3(x) = \int_{x_0}^x (x-1) \exp \left[-\frac{2p_0}{\alpha_d} \exp\{-\alpha_d(x-1)\} \right] dx,$$

$$x_0 \leq x \leq x'.$$

Kinematic characteristics of the rotor – capsule system motion in the atmosphere are described by the following correlations

$$\dot{x} = \sqrt{u(x)}; \quad dt = \frac{dx}{\dot{x}}; \quad t(x) = \int_{x_0}^x \frac{dx}{\dot{x}}. \quad (2.11)$$

According to the equations (2.4)

$$\phi(x) = \omega_0 \int_{x_0}^x \frac{dx}{\dot{x}x^2}; \quad \psi(x) = \omega_e \int_{x_0}^x \frac{dx}{\dot{x}x^2}.$$

At the final point of the motion stage in the atmosphere $x' = x_0 + \Delta x = 1 + \Delta x$, when the atmospheric density is ignored:

$$\exp[-\alpha_d(x' - 1)] = \exp(-\alpha_d \Delta x) \rightarrow 0;$$

$$\exp\left[\frac{2p_0}{\alpha_d} \exp\{-\alpha_d \Delta x\}\right] = 1,$$

wherefrom follows

$$\dot{x}(x') = \left\{2\left[q\beta_0 J_1(x') - qJ_2(x') - K_0 J_3(x')\right]\right\}^{1/2}. \quad (2.12)$$

Let us determine the elastic forces acting in point x' at the ends of the element:

$$F_{el}(x') = 2\pi R(C + C_0)(x' - 1) = 2\pi R(C + C_0)\Delta x \quad (2.13)$$

and the resultant of these forces

$$F(x') = \frac{l}{R} F_{el}(x') = 2\pi l(C + C_0)\Delta x,$$

or

$$f(x') = \frac{F(x')}{(m + m_0)R} = \frac{2\pi l(C + C_0)}{mR(1 + \mu_0)} = \frac{K}{1 + \mu_0} \Delta x = K_0 \Delta x. \quad (2.14)$$

2.3. Radial system motion with stop in position $x = x'$

In the position $x = x' = x_0 + \Delta x$, where $\Delta x = H_a/R$, H_a – the height of dense atmosphere, the rotor and capsule are fragmented with telescopic joints; in this case, capsule depressurization is possible. The system makes radial motion at the speed determined by the formula (2.12); fragments of the system at the moment of separation are elastically stretched by forces (2.13) and have the relative deformation Δx .

In order to prevent sharp compression of stretched fragments, there is required a compensation of elastic forces by, for example, friction forces between the rotor and capsule fragments. Let us determine parameter μ_0 , the related initial mass m_0 of capsule element and parameters of friction forces so that

the rotor and the capsule could stop at radial motion in the preset position $x_1 > x'$ having zero deformation.

Let us determine the law of variation for friction forces F_{fr} , necessitating the equality of their elastic forces at the moment of fragmentation and vanishing in point x_1 together with elastic forces and deformations. Based on this, let us prescribe the law of variation for F_{fr} at the section $[x', x_1]$ with a linear function:

$$F_{fr}(x) = F_{el}(x') \frac{x_1 - x}{x_1 - x'}, \quad x' \leq x \leq x_1.$$

With F_{fr} decreased, the resultant elastic strain force of rotor and capsule fragments equal to it will decrease, as well as their elastic deformation, vanishing in point x_1 . The radial speed and radial acceleration are equal to zero in this point. Further movement of the system takes place in the opposite direction from the position x_1 towards x_0 , and then backwards. A part of energy at this oscillatory movement is spent to overcome atmospheric drag forces and friction work; in this case, the amplitude of oscillation is decreased.

In order to prevent backward movement at the moment the system stops in point x_1 and to make radial acceleration change the sign and the system resume the radial motion away from the Earth, it is envisaged to eject individual fragments of the capsule.

In this case, neither the rotor nor the remaining capsule fragments supported by electromagnetic forces change their size and shape due to the absence of deformations and strain.

There is a possibility to make a multilayer vacuum capsule and eject either entire layers or individual parts of these layers. Here, many difficult questions as to the functioning of the rotor – capsule system are eliminated; for example, the question on local sags or the change in the rotor curve radius in the places of passing through the remaining capsule fragments, or the interaction of the rotor and capsule fragments in the points of entry and exit from the fragment, etc.

Let us assume for simplicity that the section $[x', x]$ is equal to $\Delta x = x_1 - x'$. The resultant of the element tension forces directed radially to the Earth's center is determined similarly to (2.14):

$$f(x) = \frac{F_{fr}(x)}{R(m + m_0)} = \frac{K}{1 + \mu_0} (x_1 - x) = K_0 (x_1 - x).$$

The differential equation of the system element radial movement at the section $[x', x]$ is written as (2.5), but the atmospheric drag forces are ignored:

$$\ddot{x} = \frac{q}{x^2} \left(\frac{\beta_0}{x} - 1 \right) - K_0 (x_1 - x), \quad x' \leq x \leq x_1.$$

The designations (2.6) are used here. The integral is written as follows:

$$\dot{x}^2(x) = \dot{x}^2(x_1) + (x - x_1) \left\{ \frac{q}{xx'} \left(\beta_0 \frac{x + x'}{xx'} - 2 \right) - K_0 [2x_1 - (x + x')] \right\}, \quad (2.15)$$

where $\dot{x}(x')$ is determined by the formula (2.12).

If $\dot{x}(x_1) = 0$, then the right part of the expression (2.15) vanishes in point x_1 . Substituting here $\dot{x}(x')$ determined by the formula (2.12), we will get after the transformations

$$\mu_0 = \frac{\beta A_1 - A_2 - \frac{K}{q} A_3}{A_2 - \beta_e A_1}; \quad (2.16)$$

$$A_1 = J_1(x') + \frac{(x_1 + x') \Delta x}{2x_1^2 (x')^2}; \quad A_2 = J_2(x') + \frac{\Delta x}{x_1 x'};$$

$$A_3 = J_3(x') + \frac{\Delta x^2}{2}.$$

The correlation (2.16) is a non-linear equation to determine μ_0 since μ_0 is included into the right part through the value $p_0 = \frac{p}{1 + \mu_0}$ in the indices of subintegral exponents in the expressions for $J_1(x')$, $J_2(x')$, $J_3(x')$.

A further iteration procedure for solving the equation (2.16) is possible. The value μ_0 is close to the critical value $\mu_{cr} = m_{cr}/m$, when the system cannot start radial motion in the initial position. Substituting $\mu_0 \approx \mu_{cr}$ in the right part (2.16), we will get a revised value μ_{0i} , which is substituted in the right part again, etc. The process goes on until the module of difference μ_{0i} and μ_{0i-1} becomes less than some preset small positive value ε :

$$|\mu_{0i} - \mu_{0i-1}| \leq \varepsilon.$$

The value ε is determined based on the permissible tolerance of definition m_0 and consequently M_0 – mass of the entire capsule – in relation to the rotor element mass m and the entire rotor mass M_r : $\mu_0 = m_0/m = M_0/M_r$. For example: determining M_0 to the accuracy up to 1 ton at $M = 10^6$ tons, we will get $\varepsilon = 10^{-6}$.

Computer calculation of μ_0 showed a very fast iteration process convergence. Table 2.1 shows as an example the calculations for $V_0 = 10.612$ km/s, $m = 25$ kg, $\mu_{cr} = 0.8052$. The initial value $\mu_0 = 0.8037$, the 4th iteration provides the solution with the required accuracy: $\mu_0 = 0.7656$, $m_0 = 19.1398$ kg.

Table 2.1 – Iteration procedure to determine parameter μ_0

i	μ_{0i}
1	0.80370496
2	0.76561654
3	0.76559303
4	0.76559301

The initial stage $[x_0, x_1]$ of the system radial motion is divided into two sections by physical conditions. The capsule at the section $[x_0, x']$ where there is dense atmosphere must be leak-tight; apart from gravity forces, the rotor – capsule elastic tension and atmospheric drag are taken into consideration; the initial kinetic energy of the system is consumed to overcome these forces. The atmospheric action at the second section $[x', x_1]$ is ignored; the rotor and capsule fragmentation takes place in point x' . In this case, friction forces are introduced between the moving apart fragments in order to prevent sharp compression of the elastically stretched rotor and capsule; the system kinetic energy is mainly spent to overcome gravity forces.

Thus, a part of the initial kinetic energy is lost at the stage $[x_0, x_1]$ to overcome atmospheric drag as well as elastic and friction forces, and to raise the system itself. It is possible to determine the initial mass m_0 of the capsule element to make the radial motion decelerate till the stop in point x_1 . In order to resume further motion, a part Δm_1 of the capsule element mass must be released; the value Δm_1 is determined by motion conditions at the next stage.

2.4. Rotor and capsule movement at later stages

The next stage of the system radial motion in outer space takes place at the section $[x_1, x_2]$, where $x_2 > x_1$ – some preset value. If the initial stage is called a zero stage, then this stage is the first one.

Let us determine mass Δm_{caps} of a part of the capsule element ejected in point x_1 so that the rotor with the capsule could stop in the position x_2 after resuming radial motion and raising the remaining capsule mass $m_{caps}^{(1)} = m_0 - \Delta m_{caps}$.

Note 1. The uniform ejection of capsule parts along the entire length is most efficient. This method is used if the capsule is multilayer and either the entire layer of mass Δm_{caps} or a part of the layer, assuming the lower one, with the same mass is ejected. In case of ejecting individual capsule fragments, the value of mass Δm_{caps} of the released parts corresponding to the selected element, average along the capsule length, is taken into consideration.

Note 2. At this and further stages of system motion in outer space, it is possible to introduce friction forces between rotor fragments as well as between capsule fragments if it is multilayer and the rotor shape integrity is not disturbed. However, this complicates the system structure and decreases the proportion of payload. In addition, there arises a problem of rejecting a large amount of heat. Therefore, let us limit ourselves to the consideration of the dissipation case only due to the capsule uplift.

The system of differential equations for the system motion at the 1st stage is written as follows:

$$\begin{aligned} (m + m_{caps}^{(1)})\ddot{r} &= mr\dot{\varphi}^2 + m_{caps}^{(1)}r\dot{\psi}^2 - (m + m_{caps}^{(1)})\frac{qR^2}{r^2}; \\ \frac{d}{dt}(mr^2\dot{\varphi}) &= 0; \quad \frac{d}{dt}(m_{caps}^{(1)}r^2\dot{\psi}) = 0. \end{aligned} \quad (2.17)$$

The initial conditions at the 1st stage correspond to the final conditions at the zero stage: let us write down the first derivatives of motion coordinates in point x_1 :

$$\dot{r}_1 = 0; \quad \dot{\varphi}_1 = \frac{\omega_0}{x_1^2}; \quad \dot{\psi}_1 = \frac{\omega_e}{x_1^2}, \quad (2.18)$$

where $\dot{\varphi}_1$ and $\dot{\psi}_1$ are similar to (2.4).

The laws of conservation of the rotor and capsule kinetic momentum with regard to (2.18) have the following form:

$$\dot{\varphi} = \dot{\varphi}_1 \frac{r_1^2}{r^2} = \frac{\omega_0}{x^2}; \quad \dot{\psi} = \dot{\psi}_1 \frac{r_1^2}{r^2} = \frac{\omega_e}{x^2},$$

i.e., the same form (2.4) as at the zero stage. Leaving out $\dot{\varphi}$ and $\dot{\psi}$ and passing to non-dimensional (except for time) values, we derive the first equation (2.17) as follows:

$$\ddot{x} = \frac{q}{x^2} \left(\frac{\beta_1}{x} - 1 \right), \quad x_1 \leq x \leq x_2, \quad (2.19)$$

where parameter β is replaced with β_1 :

$$\beta_1 = \frac{\beta + \mu_1 \beta_e}{1 + \mu_1}; \quad \mu_1 = \frac{m_{caps}^{(1)}}{m}, \quad (2.20)$$

and q , β , β_e are determined by formulae (2.6).

Integrating (2.19), we will get the expression of speed \dot{x} of the system radial motion at the 1st stage:

$$\dot{x}^2 = \frac{q}{xx_1} (x - x_1) \left(\beta_1 \frac{x_1 + x}{x_1 x} - 2 \right), \quad x_1 \leq x \leq x_2.$$

It follows herefrom that the radial speed \dot{x} is equal to zero at the beginning and end of the 1st stage as the multipliers in round brackets vanish. Setting the expression in the second bracket to zero and taking into consideration (2.20), we will get as follows:

$$\mu_1 = \frac{\beta(x_1 + x_2) - 2x_1 x_2}{2x_1 x_2 - \beta_e(x_1 + x_2)}. \quad (2.21)$$

Let us find mass $m_{caps}^{(1)}$ of the remaining part of the capsule and mass Δm_{caps} of the ejected parts at the beginning of the 1st stage:

$$m_1 = \mu_1 m; \quad \Delta m_{caps} = m_0 - m_{caps}^{(1)} = (\mu_0 - \mu_1)m.$$

Substituting (2.21) in formula (2.20), let us find:

$$\beta_1 = \frac{2x_1 x_2}{x_1 + x_2}.$$

The changes of the system radial acceleration at the 1st stage have the following consistencies.

1. After releasing mass Δm_{caps} of the capsule in the position x_1 , acceleration abruptly acquires a positive value:

$$\ddot{x}(x_1) = q \frac{x_2 - x_1}{x_1^2 (x_1 + x_2)}. \quad (2.22)$$

2. Acceleration is then decreased and goes to zero in point $x = x'_1 = \beta_1$, which follows directly from (2.19).

3. Acceleration is negative at the end of the first stage in point $x = x_2$

$$\ddot{x}(x_2) = -q \frac{x_2 - x_1}{x_2^2(x_1 + x_2)}. \quad (2.23)$$

Based on (2.22) and (2.23) it follows that accelerations at the beginning and end of the first stage are inversely proportional to the squares of coordinates of these points:

$$\frac{\ddot{x}(x_1)}{\ddot{x}(x_2)} = -\frac{x_2^2}{x_1^2}.$$

The system radial speed equal to zero in the extreme points of the stage reaches the maximal value in point x'_1 :

$$x(x'_1) = (x_2 - x_1) \left[\frac{q}{2x_1x_2(x_1 + x_2)} \right]^{1/2}. \quad (2.24)$$

The system motion time $t(x)$ and turning angles $\varphi(x)$, $\psi(x)$ are determined similarly to (2.11).

Let us split the radial motion interval of the rotor – capsule system into n stages $[x_i, x_{i+1}]$, $i = 0, 1, 2, \dots, n - 1$, up to the intermediate orbit, where the radial speed and acceleration vanish at the same time. The motion at the first two stages has been considered. At later stages, except for the last one, it is similar to the motion at the first stage: some mass $\Delta m_{caps}^{(i)}$ of the capsule is ejected at the initial points x_i , so that after resuming the motion, the system could stop at final points x_{i+1} with the remaining part of the capsule having mass $m_{caps}^{(i)} = m_{caps}^{(i-1)} - \Delta m_{caps}^{(i)}$.

Kinematic and other parameters of the system at the i^{th} stage, $i = 1, 2, 3, \dots, n - 1$ are determined similarly to the parameters of the first stage; the main of them are written as follows:

$$\ddot{x} = \frac{q}{x^2} \left(\frac{\beta_i}{x} - 1 \right); \quad \dot{x}^2 = \frac{q(x - x_i)}{xx_i} \left(\beta_i \frac{x + x_i}{xx_i} - 2 \right);$$

$$\beta_i = \frac{\beta + \mu_i \beta_e}{1 + \mu_i} = \frac{2x_i x_{i+1}}{x_i + x_{i+1}}; \quad (2.25)$$

$$\mu_i = \frac{m_{caps}^{(i)}}{m} = \frac{\beta(x_i + x_{i+1}) - 2x_i x_{i+1}}{2x_i x_{i+1} - \beta_e(x_i + x_{i+1})}, \quad x_i \leq x \leq x_{i+1}.$$

Radial acceleration differs from zero and speed goes to zero at the final points of stages. It follows from here that adjusting the masses of the released and remaining on the rotor capsule parts, simultaneous vanishing of radial acceleration and radial speed required for the system placement into the intermediate orbit is impossible. However, it is possible to achieve arbitrarily small values of the system radial speed. Indeed, the maximal value of speed in intermediate points $x'_i = \beta_i$, where acceleration changes the sign, is determined by formula (2.24) where indices 1 and 2 are replaced with indices x_i and x_{i+1} . It follows that the speed decreases when approaching to the final point due to the increase in x_i and x_{i+1} ; it can be decreased to an even greater degree by means of reducing the length of stages $x_{i+1} - x_i$. If the ejection process of capsule parts is interrupted in some point x_i , then with the zero radial speed and negative acceleration, the system will start movement in this position in the opposite direction and then will start oscillating slowly in relation to the position where $\dot{x} = 0$, with deviations to the extreme points x_i and x_{i+1} of the corresponding stage. The smaller the length of the stage is, the higher the probability is to launch the system to the intermediate orbit to the position x'_i . The permanent orbit is then obtained by means of aligning circular velocities of the rotor and the remaining capsule parts, as will be shown in clause 2.7.

An aperiodic process of the system ascent to the intermediate orbit is provided by the action of another type of dissipation to be considered in the next paragraph.

In conclusion, let us point out that it is possible to set a task on a continuous change of capsule mass and identification of the corresponding pattern of the system radial motion, i.e., to consider a problem on the motion of a system with a variable mass. Special ballast released at an active motion section will provide a change of the UPT mass under the desired law. Water, compressed or liquid air, oxygen or nitrogen and other substances and materials safe for the environment, and first and foremost for the planet's atmosphere, will be used as ballast.

2.5. System motion at the last stage

It is required to provide simultaneous vanishing of the system radial acceleration and radial speed at the end of the final motion stage $[x_{n-1}, x_n]$.

In this case, acceleration must be positive in the beginning so that the system could start the movement at a zero starting velocity and after changing the sign become negative in order to decelerate the developed speed and become zero along with the speed in point x_n .

It is possible to achieve positive acceleration in point x_{n-1} by the last ejection of the capsule part. Here, the ejected and remaining masses must provide vanishing of the acceleration component due to the actions of centrifugal and gravity forces. Let us designate the mass of the remaining part of capsule element $m_{caps}^{(n-1)}$ and introduce the parameter $\mu_{(n-1)} = m_{caps}^{(n-1)}/m$, then this condition takes on the following form:

$$\frac{\beta_{n-1}}{x^n} - 1 = 0, \quad (2.26)$$

where $\beta_{n-1} = \frac{\beta + \mu_{n-1}\beta_e}{1 + \mu_{n-1}}$. Let us point out that $m_{caps}^{(n-1)}$ – a value (average along along the rotor length) of the remaining capsule mass per rotor element of the initial length m , i.e., $m_{n-1} = M_{caps}^{(n-1)}l_{n-1}/L_{n-1}$, where $M_{caps}^{(n-1)}$ – capsule remaining mass, $l_{n-1} = x_{n-1}l$, $L_{n-1} = x_{n-1}L$ – length of the corresponding element and the entire rotor in position x_{n-1} .

Solving (2.26) in relation to $\beta = V_0^2/V_1^2$, we will get as follows:

$$\beta = (1 + \mu_{n-1})x_n - \mu_{n-1}\beta_e. \quad (2.27)$$

Let us find herefrom the reference circular rotor velocity V_0 necessary to provide the system ascent to the position x_n with the uplift of the remaining mass of capsule elements m_{n-1} :

$$V_0 = V_1 \left[(1 + \mu_{n-1})x_n - \mu_{n-1}\beta_e \right]^{1/2}. \quad (2.28)$$

Formulae (2.27) and (2.28) represent a generalization of formulae (1.42) and (1.43) from Chapter 1 in case of an ascent of capsule inertial mass $m_{n-1} = \mu_{n-1}m$, coinciding with them at $\mu_{n-1} = 0$.

The radial speed at the last stage is damped by an acceleration component caused by friction forces between rotor fragments in their telescopic joints. Let us assume that the tension of rotor element caused by friction forces exerted at the element ends are equal to $F_{fr}(x)$, dependent on the element position. The resultant of these forces exerted in the centre of the element and directed radially towards the Earth's center is determined in the same way as in Chapter 1:

$$F(x) = F_{fr}(x) \frac{l_{n-1}}{r_{n-1}} = F_{fr}(x) \frac{l}{R},$$

or

$$f(x) = F_{fr}(x) \frac{l}{mR^2(1 + \mu_{n-1})}. \quad (2.29)$$

The differential equation of the system element radial motion at the last stage is written as follows:

$$\ddot{x} = \frac{q}{x^2} \left(\frac{\beta_{n-1}}{x} - 1 \right) - f(x), \quad x_{n-1} \leq x \leq x_n.$$

Let us use linear dependence $F_{fr}(x)$ and $f(x)$ on coordinate x in order to make the radial speed vanish. Let us assume that some internal point x_* of stage $[x_{n-1}, x_n]$, that can be set arbitrarily divides this stage into parts $\Delta x_1 = x_* - x_{n-1}$ and $\Delta x_2 = x_n - x_*$. Then, let us submit $f(x)$ as follows:

$$f(x) = \begin{cases} f_* \frac{x - x_{n-1}}{\Delta x_1}, & x_{n-1} \leq x \leq x_*; \\ f_* \frac{x_n - x}{\Delta x_2}, & x_* \leq x \leq x_n, \end{cases}$$

where constant f_* – the highest value $f(x)$ in point x_* . In this case, $f(x)$ becomes zero at the end of the stage, whereas complex radial acceleration x_n is equal to zero in the position \ddot{x} .

The system radial speed is determined based on the correlation

$$\dot{x}^2 = \frac{q}{xx_{n-1}} (x - x_{n-1}) \left(\beta_{n-1} \frac{x + x_{n-1}}{xx_{n-1}} - 2 \right) - a(x); \quad (2.30)$$

$$a(x) = \begin{cases} \frac{f_*}{2\Delta x_1} (x - x_{n-1})^2, & x_{n-1} \leq x \leq x_*; \\ \frac{f_*}{2} \left[\Delta x_1 + \frac{(x - x_*)(2x_n - x - x_*)}{\Delta x_2} \right], & x_* \leq x \leq x_n. \end{cases} \quad (2.31)$$

Radial speed \dot{x} is equal to zero in the final position x_n ; taking into consideration (2.26), (2.30) and (2.31) let us find from here

$$f_* = 2q \frac{x_n - x_{n-1}}{x_{n-1}^2 x_n},$$

after which the dynamics of the system radial motion is completely determined at the last stage.

Taking into consideration (2.29), the maximal value of element tension caused by friction forces between rotor fragments

$$F_* = \frac{2mg(1 + \mu_{n-1})R}{lx_{n-1}^2 x_n} (x_n - x_{n-1}).$$

This value can be adjusted: the less the difference $x_n - x_{n-1}$ is, the less F_* is, reaching the values close to the weight of the system element $mg(1 + m_{n-1})$ upon condition $R(x_n - x_{n-1})/lx_{n-1}^2 x_n \rightarrow 1$.

The mass coefficient of the system efficiency is determined as a relation of the uplifted mass to the initial mass:

$$\eta = \frac{m_r + m_{caps}^{(n-1)}}{m_r + m_{caps}} = \frac{1 + \mu_{n-1}}{1 + \mu_0}. \quad (2.32)$$

The value η is close to one for low orbits and is decreased for higher orbits, which is similar to the energy efficiency behavior. In any case, it is vastly superior to the corresponding value for rocket systems.

2.6. Dependence between system parameters at the initial and final motion stages

Fulfillment of the condition (2.8) is required to start the system radial motion; fulfillment of the condition (2.28) is required to launch the system with the parameter of the remaining capsule mass $\mu_{n-1} = m_{caps}^{(n-1)}/m$ (in this case $\mu_{n-1} < \mu_0 = m_{caps}/m$) to the position of the intermediate orbit x_n . The collation of the rights parts (2.28) and (2.8) results in the following:

$$(1 + \mu_{n-1})x_n - (1 + \mu_0)x_0 > -(\mu_0 - \mu_{n-1})\beta_e.$$

The right part is negative, therefore the derived inequality is particularly fulfilled if the left part is equal to zero:

$$(1 + \mu_n)x_n = (1 + \mu_0)x_0. \quad (2.33)$$

It is taken into consideration here that the mass $m_{caps}^{(n-1)}$ at the stage $[x_{n-1}, x_n]$ is not changed, i.e., $m_{caps}^{(n-1)} = m_{caps}^{(n)}$, $\mu_{n-1} = \mu_n$.

Based on (2.33) follows inverse proportionality of the masses and distances. Multiplying both parts (2.33) by the rotor element mass m , we will get as follows:

$$(m + m_{caps}^{(n)})x_n = (m + m_0)x_0. \quad (2.34)$$

This correlation has a simple mechanical interpretation. Multiplication of the element mass by the distance to some center is a static inertia moment, whereas dependence (2.34) is a condition of equality of the system elements inertia moments in the final x_n and initial x_0 positions relative to the Earth's center (figure 18).

The ordinate $m + m_0$ in point x_0 is equal to the sum of the initial mass of rotor and capsule elements, whereas the ordinate $m_0 + m_{cr}$, where $m_{cr} = \mu_{cr}m$ – to the sum of the initial and critical capsule masses.

The ordinate in point x_n is equal to the sum of final masses $m + m_{caps}^{(n)}$. The correlation (2.34) or (2.33) can be interpreted as a rule of conservation of weight moments concentrated in points x_0 and x_n similar to the rule of lever balance supported in the Earth's centre. Archimedes must have dreamt of having a lever of such dimension back in his times.

Points x_n and x_0 can be chosen arbitrarily, which follows from the rule of celestial mechanics [23]. Therefore, all points of the straight line passing through

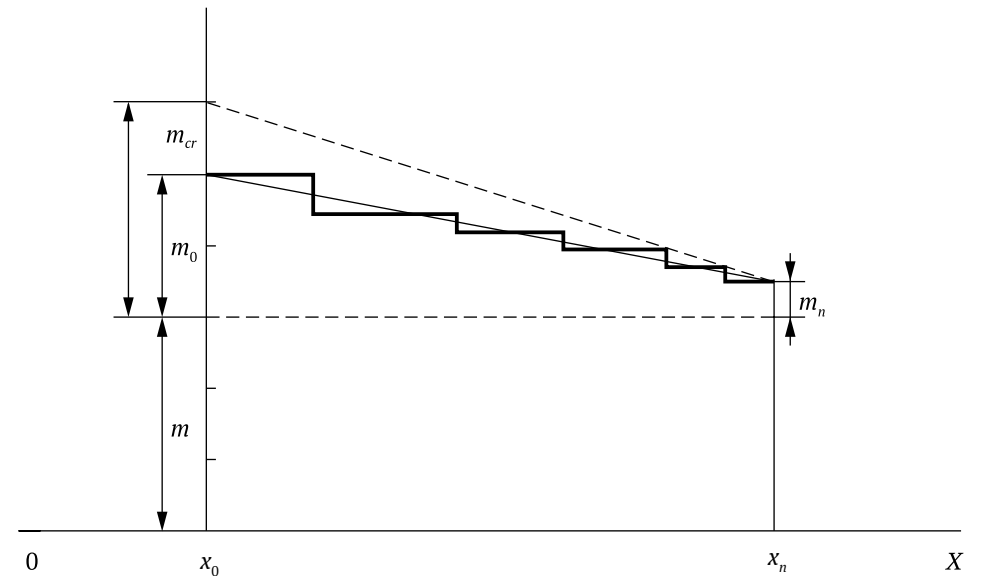


Figure 18 – Conservation law of weight moments

the ends of the marked vertical sections must comply with the rule of conservation of weight moments (2.34). The equation of this straight line is written as follows

$$m(x) = m + m_0 - \left(m_0 - m_{caps}^{(n)}\right) \frac{x - x_0}{x_n - x_0} \quad (2.35)$$

and represents a law of capsule mass linear variation at continuous ejection of its parts. This line approximates a stepped graphic of capsule mass variation at discrete ejection of its parts and characterizes the variation of capsule mass depending on the system position. The correlations (2.28), (2.32) and (2.33) are used when making table 2.2, which shows the dependence of the initial and final system parameters. For the preset position of the intermediate orbit $x_n = 1.5$ and six coefficient values μ_n of the remaining capsule mass specified in the table, there have been determined the following parameters: μ_0 – coefficient of initial capsule mass; μ_{cr} – coefficient of capsule critical mass; $\Delta\mu = \mu_0 - \mu_n$ – coefficient of capsule mass variation; $\eta_1 = \Delta\mu/\mu_n$ – relation of the released mass to the remaining one; $\eta_2 = \Delta\mu/\mu_0$ – relation of the released mass to the initial one; V_0 – the required initial rotor speed; $\beta = V_0^2/V_1^2$ – orbit coefficient. The material efficiency factor of the system in all six cases is the same:

$$\eta = \frac{1 + \mu_n}{1 + \mu_0} = \frac{x_0}{x_n} = \frac{2}{3}.$$

Table 2.2 – Dependence of initial and final system parameters

μ_n	0.1	0.5	1.0	1.5	2.0	3.0
μ_0	0.65	1.25	2.0	2.75	3.5	5.0
μ_{cr}	0.693	1.309	2.074	2.852	3.609	5.147
$\Delta\mu$	0.55	0.75	1.0	1.25	1.5	2.0
η_1	5.5	1.5	1.0	0.83	0.75	0.67
η_2	0.846	0.6	0.5	0.455	0.429	0.4
$V_0, \text{ km/s}$	10.15	11.85	13.675	15.288	16.746	19.335
$\gamma, \text{ kWh/kg}$	13.008	13.002	12.987	12.985	12.983	12.981
β	1.6497	2.2483	2.9966	3.7449	4.4932	5.99

Energy consumption per one lift of 1 kg of payload mass (without regard to losses in TLS) appears to be the same as well:

$$\gamma = \frac{K_*}{m + m_{caps}^{(n)}} = \frac{V_0^2}{2(1 + \mu_n)} \approx \frac{V_1^2}{2} x_n,$$

where K_* – kinetic energy of the system element; V_0 – approximate value (2.28), where $\beta_e \approx 0$. In case of orbit variation, the specific energy consumption changes proportionally to coordinate x_n .

It follows from table 2.2 that some values increase, albeit slowly, as the remaining mass grows; they include the initial and critical mass, the coefficient of mass variation, the initial rotor speed V_0 and orbit coefficient. The relation of the released mass to the remaining and initial capsule masses decreases; in this case, the first value decreases significantly. Thus, mass characteristics improve as the remaining capsule mass increases and the specific energy consumption calculated by formula $e = \frac{V_0^2}{2(1 + \mu_n)}$ remains almost constant.

When exiting the intermediate orbit x_n , the rotor and the capsule have angular velocity of rotational motion :

$$\dot{\phi}_n = \frac{\omega_e}{x_n^2}; \quad \dot{\psi}^2 = \frac{\omega_e}{x_n^2}. \quad (2.36)$$

The corresponding linear speed:

$$V_n = \dot{\phi}_n x_n R = \frac{V_0}{x_n}; \quad V_{en} = \dot{\psi}_n x_n R = \frac{V_e}{x_n}. \quad (2.37)$$

Taking into consideration formula (2.28) for V_0 , we will get as follows:

$$V_n = \frac{V_1}{x_n} \left[(1 + \mu_n) x_n - \mu_n \beta_e \right]^{1/2},$$

or, if ignoring the small value β_e :

$$V_n \approx V_1 \left(\frac{1 + \mu_n}{x_n} \right)^{1/2}. \quad (2.38)$$

Thus, the rotor speed when moving on the intermediate orbit depends both on the orbit position and on the value of the remaining capsule mass. Based

on the collation (2.38) and formula (1.44) for the case considered in Chapter 1, when the capsule is entirely released, it follows that the value V_n is larger than V_{orb} by $(1 + \mu_n)^{1/2}$ times and coincides with it if $\mu_n = 0$. This is due to the fact that the rotor in this case is required not only for the uplift being a load-bearing member, but also for supporting the capsule inertia mass on the orbit.

Let us find the system kinetic momentum and kinetic energy at the intermediate orbit:

$$L_n = mr_n^2 \dot{\phi}_n + m_{caps}^{(n)} r_n^2 \dot{\psi}_n = (mV_0 + m_{caps}^{(n)} V_e) R;$$

$$K_n = \frac{mV_n^2}{2} + \frac{m_{caps}^{(n)} V_{en}^2}{2} = \frac{mV_0^2 + m_{caps}^{(n)} V_e^2}{2x_n^2}.$$

The same values at the moment of system start:

$$L_0 = (mV_0 + m_0 V_e) R; \quad K_{sys}^0 = \frac{1}{2} (mV_0^2 + m_0 V_e^2).$$

The losses when exiting the intermediate orbit amount to:

$$\Delta L = L_0 - L_n = (m_0 - m_n) V_e R;$$

$$\Delta K = K_{sys}^0 - T_n = \frac{mV_1^2}{2} \left[\beta \left(1 - \frac{1}{x_n^2} \right) + \beta_e \left(\mu_0 - \frac{\mu_n}{x_n^2} \right) \right].$$

The decrease in kinetic momentum takes place only due to the ejection of part $m_{caps} - m_{caps}^{(n)}$ of capsule mass. The reasons for decreasing kinetic energy are various and mainly result from uplifting the mass of rotor and capsule part to the orbit, a stepped release of capsule parts as well as overcoming the atmospheric drag, friction and elastic forces.

Taking into consideration formula (2.27) for β , let us find:

$$\Delta K = \frac{mV_1^2}{2} \left[(1 + \mu_n) \left(x_n - \frac{1}{x_n} \right) + \beta_e (\mu_0 - \mu_n) \right].$$

If the second summand is ignored here, then

$$\Delta K \approx \frac{mV_1^2}{2} (1 + \mu_n) \left(x_n - \frac{1}{x_n} \right).$$

Let us calculate the work by the rotor and capsule uplift to the orbit x_n ; in this case, let us assume the average value $\frac{1}{2}(m_{caps} + m_{caps}^{(n)})$ for the capsule mass:

$$A(G) = \left[m + \frac{1}{2} (m_{caps} + m_{caps}^{(n)}) \right] g R^2 \int_{r_0}^{r_n} \frac{dr}{r^2} = \frac{mV_1^2}{2} (2 + \mu_0 + \mu_n) \left(\frac{1}{x_0} - \frac{1}{x_n} \right).$$

According to the law of energy conservation, we get $\Delta K = A(G)$, disregarding small values of other work; after certain transformations and ignoring β_e , we derive herefrom the correlation (2.33) found earlier in another way.

The derived correlations allow us to:

- visually and easily find the dependence of the initial and final (remaining) capsule masses with regard to the intermediate orbit position;
- get confirmation of the fundamental possibility on energy dissipation of the radial rotor motion due to the uplift of capsule parts, based on the general law of energy conservation;
- set a problem on radial motion energy dissipation at continuous capsule mass variation using the law of linear capsule mass variation (2.35). In this case, it is expected to achieve the best characteristics of system motion; particularly, it is possible to curtail drastically the overall motion time by eliminating intermediate stops.

2.7. System dynamics when entering the permanent orbit

As it follows from (2.36) and (2.37), angular and linear velocities of the rotor and the remaining capsule part differ enormously after the system enters the intermediate orbit to the position x_n . It is required to preliminarily align the rotor and capsule rotational speeds in order to perform assembly work, industrial production, cargo exchange with other systems, etc.

Let us consider electromagnetic forces that may arise in TLS remains at relative motion of the rotor and capsule parts. It is assumed that these interaction forces depend linearly on speed differential

$$F_{elm} = \sigma r (\dot{\phi} - \dot{\psi}), \quad (2.39)$$

decelerate the rotor element speed and increase the capsule element speed. According to the theorem on kinetic momentum variation, let us write down the equations for the rotor and capsule elements

$$\frac{d}{dt}(mr^2\dot{\phi}) = -\sigma r^2(\dot{\phi} - \dot{\psi}); \quad \frac{d}{dt}(m_{caps}^{(n)}r^2\dot{\psi}) = \sigma r^2(\dot{\phi} - \dot{\psi}). \quad (2.40)$$

The initial motion conditions at this stage are determined according to (2.36).

The equations of type (2.40) result in the integral, which represents a law of conservation of kinetic momentum of the system. With regard to (2.36), after certain reductions, let us find:

$$\dot{\phi} + \mu_n \dot{\psi} = \frac{r_n^2}{r^2}(\dot{\phi}_n + \mu_n \dot{\psi}_n). \quad (2.41)$$

Dividing equation (2.40) written for the rotor element into m , and a similar equation written for the capsule element into $m_{caps}^{(n)}$ subtracting from the first one, we will get an equation with separable variables:

$$\frac{d}{dt}[(\dot{\phi} - \dot{\psi})r^2] = -\delta(\dot{\phi} - \dot{\psi})r^2,$$

where $\delta = \sigma \left(\frac{1}{m} + \frac{1}{m_{caps}^{(n)}} \right)$. Its solution takes on the form:

$$\dot{\phi} - \dot{\psi} = \frac{r_n^2}{r_k^2} \frac{\dot{\phi}_n + \mu_n \dot{\psi}_n}{1 + \mu_n}. \quad (2.42)$$

It follows from here that equal values of corner velocities are achieved over an infinite time interval, which is typical at linear dependence of interaction forces of type (2.39). However, the process of exiting the permanent orbit is completed over a finite time interval, when velocities of the rotor and capsule parts differ slightly and it is possible to engage brake mechanisms of another type, for example, mechanical brakes.

Based on the correlation (2.41), we will get as follows:

$$\dot{\phi}_k = \dot{\psi}_k = \frac{r_n^2}{r^2} \frac{\dot{\phi}_n + \mu_n \dot{\psi}_n}{1 + \mu_n}, \quad (2.43)$$

where index k denotes the final values of variables.

On the other hand, based on the condition of equality of centrifugal and gravity forces at the final orbit, let us find:

$$\dot{\phi}_k = \dot{\psi}_k = \frac{R}{r_k} \left(\frac{g}{r_k} \right)^{1/2}. \quad (2.44)$$

Solving equations (2.43) and (2.44) using in this case the designations (2.6) and correlations (2.28), (2.36), let us finally determine the system parameters during its motion at the permanent orbit:

$$r_k = \frac{(V_0 + \mu_n V_e)^2}{V_1^2 (1 + \mu_n)^2} R = \left(\frac{\beta^{1/2} + \mu_n \beta_e^{1/2}}{1 + \mu_n} \right)^2 R; \quad (2.45)$$

$$\dot{\phi}_k = \dot{\psi}_k = g V_1^2 \left(\frac{1 + \mu_n}{V_0 + \mu_n V_e} \right)^3 = \frac{g}{V_1} \left(\frac{1 + \mu_n}{\beta^{1/2} + \mu_n \beta_e^{1/2}} \right)^3; \quad (2.46)$$

$$V_k = \dot{\phi}_k r_k = \frac{g V_1^2}{V_1} \frac{1 + \mu_n}{\beta^{1/2} + \mu_n \beta_e^{1/2}} = V_1 \frac{1 + \mu_n}{\beta^{1/2} + \mu_n \beta_e^{1/2}}, \quad (2.47)$$

where $\beta = \frac{V_0^2}{V_1^2} (1 + \mu_n) x_n - \mu_n \beta_e$; $\beta_e = \frac{V_e^2}{V_1^2}$; $V_1^2 = gR$.

Ignoring the small value β_e , let us derive the approximate values:

$$r_k = \frac{x_n R}{1 + \mu_n}; \quad (2.48)$$

$$\dot{\phi}_k = \dot{\psi}_k = \frac{g}{V_1} \left(\frac{1 + \mu_n}{x_n} \right)^{3/2} = \sqrt{gR} \left(\frac{1 + \mu_n}{r_n} \right)^{3/2}; \quad (2.49)$$

$$V_k = V_1 \left(\frac{1 + \mu_n}{x_n} \right)^{1/2} = V_1 \left[(1 + \mu_n) \frac{R}{r_n} \right]^{1/2}. \quad (2.50)$$

Let us determine the system radial movement at the stage of speed alignment using the approximate value r_k :

$$\Delta r = r_n - r_k = \frac{\mu_n}{1 + \mu_n} r_n.$$

This value is non-negative; therefore, the radius of permanent orbit r_k in the general case is less than the radius of intermediate radius r_n , and the system moves backwards in the process of speed alignment, towards the Earth.

If $\mu_n = 0$, the entire capsule mass is released, then $\Delta r = 0$ and the orbits coincide. At large values μ_n the displacement of orbits Δr reaches the values close to r_n .

Let us use formulae (2.37) and (2.47) in order to determine the variation of the rotor linear speed:

$$\Delta V = V_n - V_k = V_1 \frac{\mu_n \beta_e^{1/2} (\beta^{1/2} - \beta_e^{1/2})}{x_n \beta^{1/2} + \mu_n \beta_e^{1/2}}.$$

The difference ΔV is also negative in the general case since $\beta > \beta_e$. This result, strange as it may seem at first glance, has the following explanation. At the intermediate orbit, which is higher than the final one, the rotor must support the inertial mass of capsule remains due to centrifugal force; therefore, its speed is higher than it is necessary for self-contained movement. The rotor speed at the permanent orbit decreases due to the fact that the capsule received a part of kinetic momentum from the rotor and is now self-supporting; after that, the speed is increased due to the orbit lowering. The first variation is however more visible than the second one.

If $\mu_n = 0$, then $\Delta V = 0$ similar to the first case. If the small value β_e is ignored, we will get $\Delta V \approx 0$ or $V_k \approx V_n$, although the orbit can change for the final value. It is obvious that variations of the rotor speed caused by two oppositely acting factors take place almost in equal measure.

Solving (2.45) in relation to V_0 , let us find the correlation between the position of the final orbit $r_k = x_k R$, the remaining capsule mass $m_{caps}^{(n)} = \mu_n m$ and the initial rotor speed V_0 :

$$V_0 = V_1 \left[(1 + \mu_n) x_k^{1/2} - \mu_n \beta_e^{1/2} \right].$$

The system motion at the stage of speed alignment is described by the first-order differential equations in relation to parameters ϕ and ψ obtained when dividing the equations (2.41) and (2.42) using the initial conditions (2.36)

$$\begin{aligned} \dot{\phi} &= \frac{V_0 + \mu_n V_e + \mu_n (V_0 - V_e) \exp(-\delta t)}{(1 + \mu_n) R} \frac{1}{x^2}, \\ \dot{\psi} &= \frac{V_0 + \mu_n V_e - (V_0 - V_e) \exp(-\delta t)}{(1 + \mu_n) R} \frac{1}{x^2} \end{aligned} \quad (2.51)$$

and the second-order equation in relation to the radial coordinate

$$\ddot{x} = \frac{1}{x^2} \left[\frac{(V_0 + \mu_n V_e)^2 + \mu_n (V_0 - V_e)^2 \exp(-\delta t)}{(1 + \mu_n)^2 R^2} \frac{1}{x} - q \right], \quad (2.52)$$

derived after eliminating $\dot{\phi}$ and $\dot{\psi}$ by means of correlations (2.51) from the radial motion equation:

$$(m + m_{caps}^{(n)}) \ddot{r} = m r \dot{\phi}^2 + m_{caps}^{(n)} r \dot{\psi}^2 - (m + m_{caps}^{(n)}) g \frac{R^2}{r^2}.$$

Using the designations (2.6), the equation (2.52) can be made to take on the form similar to the radial motion equation (2.25) at the intermediate stage:

$$\ddot{x} = \frac{q}{x^2} \left(\frac{\beta_k(t)}{x} - 1 \right), \quad (2.53)$$

where the variable parameter $\beta_k(t)$ is written as follows:

$$\beta_k(t) = \frac{(\beta^{1/2} + \mu_n \beta_e^{1/2})^2 + \mu_n (\beta^{1/2} - \beta_e^{1/2})^2 \exp(-2\delta t)}{(1 + \mu_n)^2}.$$

The integration of the equation system (2.51)–(2.52) is possible by a numerical method. If the current and final values of radial acceleration \ddot{x} are known, it is possible to evaluate the timespan t_k from the beginning of the stage under consideration when the acceleration differs from the zero value by the preset small value $\varepsilon > 0$:

$$\frac{q}{x_k^2} \left(\frac{\beta_k(t_k)}{x_k} - 1 \right) \leq \varepsilon.$$

In this case, it is assumed that the orbit position $x(t_k)$ practically does not differ from the final position x_k . After the transformations, we will get time evaluation of the system motion:

$$t_k \geq -\frac{1}{2\delta} \ln \frac{\varepsilon (\beta^{1/2} + \mu_n \beta_e^{1/2})^6}{q (1 + \mu_n)^4 (\beta^{1/2} - \beta_e^{1/2})^2}.$$

Ignoring value β_e compared to β , let us find a more simple evaluation:

$$t_k \geq -\frac{1}{2\delta} \ln \frac{\varepsilon\beta^2}{q(1 + \mu_n)^4}.$$

Using the correlation (2.27), we will get in the same approximation as follows:

$$t_k \geq -\frac{1}{2\delta} \ln \frac{gR}{\varepsilon r_k^2} = \frac{1}{2\delta} \ln \frac{V_1^2}{\varepsilon r_k^2}.$$

Thus, time evaluation of speed alignment for the rotor and capsule parts depends on values r_k – position of the final orbit, and ε – accuracy of approximation of the radial acceleration to the zero one.

2.8. Problem of system placement into the intermediate orbit

There has been developed a program and estimated an example of system placement into the intermediate orbit 3,200 km high above the equator, in order to study the considered method of the radial motion energy dissipation due to the uplift of capsule parts. Similar to the example in clause 1.10, let us set three groups of parameters.

1. Constant parameters whose values are identical with those in clause 1.10.
2. Parameters of the intermediate orbit: $x_n = 1.502655$, $\mu_n = 0.2$. The corresponding value of the initial rotor speed $V_0 = 10.612$ km/s; other parameters have the values identical with those in clause 1.10.
3. Parameters that depend on the coordinates of intermediate stages: the height of dense atmosphere $H = 100$ km ($x' = 1.0154$); the height where the first system stop and ejection of capsule part take place $H_1 = 200$ km ($x_1 = 1.0354$). The rest 3,000 km is divided into five stages by 600 km each. At the beginning and end of these stages, except for the fifth one, the next stop and then an ejection of capsule part take place. The stage is then again divided into five stages by 120 km and the procedure of stops and ejections of capsule parts is repeated. The splitting of the last stage is repeated five times, whereas the length of the final stage is 0.96 km. Friction force between rotor fragments steps in at this stage, and the system is placed in the position of the intermediate orbit. The total amount of stages $n = 21$. As clarified in clause 2.5, the splitting of the last stages is required to decrease friction force used at the system deceleration.

The computational results are shown in figures 19–23.

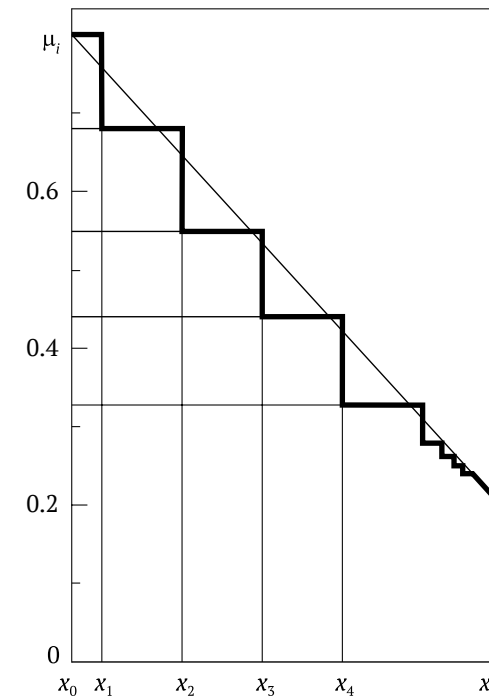


Figure 19 – Stepped variation of capsule mass coefficient

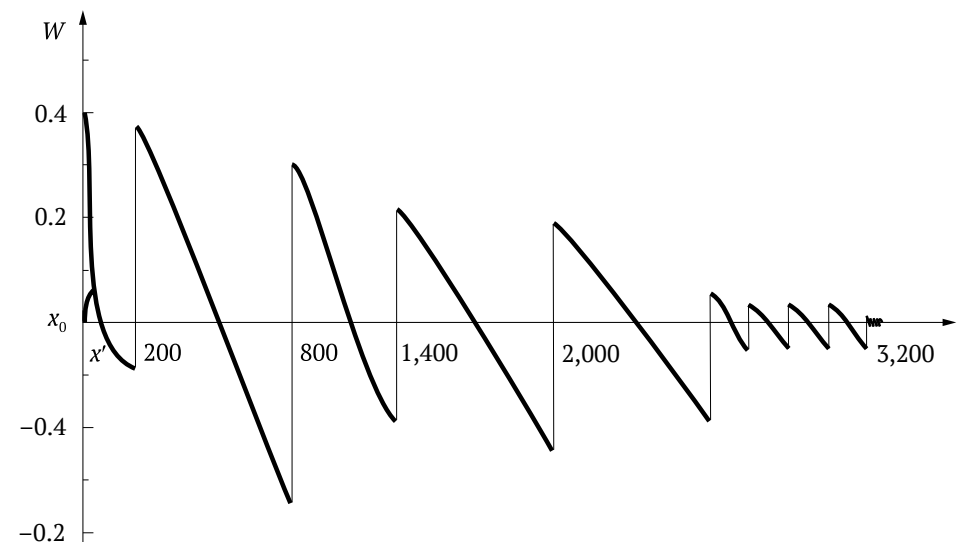


Figure 20 – Variation of radial system acceleration

Figure 19 shows a stepped variation of the capsule mass coefficient $\mu_i = m_{caps}^{(i)}/m$ where m_i – the capsule mass at the next i^{th} stage of system motion. A non-dimensional radius of the system with the denotation of the first splitting out of five at the last stage is plotted along the axis of abscissas. The coefficient μ , including the initial μ_0 and critical μ_{cr} values is plotted along the axis of ordinates. A solid straight line is a graph of the capsule mass continuous variation pursuant to the law of conservation of inertia moment (2.35). This straight line approximates a stepped graphic.

Figure 20 shows the variation of radial acceleration $W = \ddot{x}R$ (m/s²) of the system. The graph has a sawtooth view with jumps in the points of stops and further ejections of capsule parts. The change of the acceleration sign takes place in points of ejection, as well as in intermediate points of continuous variation, which provides initial acceleration at each stage, and then deceleration until the stop at the end of the stage. The splitting of the last stage leads to the decrement of acceleration by approximately five times; the graph of further stages is not provided.

2.9. Variation of radial system acceleration

The comparison with figure 15 shows that there exists a significant difference on retention of the radial acceleration characteristic features – a stepped variation and change of signs: in the second case, acceleration is by ten times less compared to that in the first case, although it is included in the free fall acceleration. Overloads and problems related to the same do not exist here.

Figure 21 shows variation of radial speed $V_r = \dot{x}R$ (m/s), where the graph looks like a blunt saw with a different height of teeth. The speed is decreased

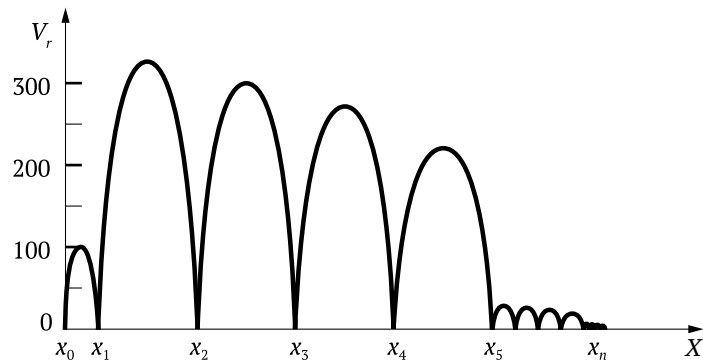


Figure 21 – Variation of radial system speed

by approximately five times at the stage of splitting. Based on the comparison with figure 16, it is seen that the maximal speeds in the considered examples differ by ten times, as well.

Figures 22 and 23 show the system speed and acceleration at the final stage in other scales, with placement into the intermediate orbit x_n . The accelerations are almost linear, whereas the speed graph normally looks like a blunt tooth with an almost linear slope to the point x_n , where the system radial acceleration and radial speed vanish simultaneously. This is in fact a feature of non-oscillatory placement to the position of the intermediate orbit. The maximal value of the total friction force between fragments achieved in this case $F_* = 83.32$ kN.

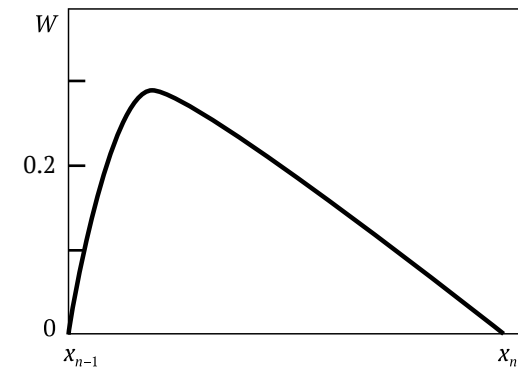


Figure 22 – Radial speed at the final motion stage

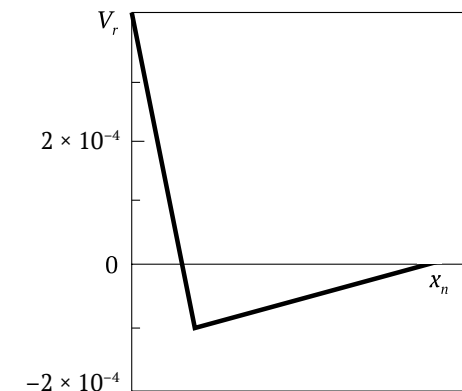


Figure 23 – Radial acceleration at the final motion stage

Due to a small value of radial acceleration and speed, the time for ascent to orbit t_n in the considered example is significant; it can be calculated by steps using the integrals of type (2.11). A discrete procedure was used in calculations instead of quadratures, as follows: $t_i = t_{i-1} + \Delta x / \dot{x}_i$, where t_{i-1} – motion time to this section; $\Delta x / \dot{x}_i$ – time step-out at this section. Due to the finite movement Δx_i and acceleration \dot{x} closeness to zero at the ends of stages, this method appeared to be crude significantly misrepresenting the system time motion. The value t_n can be evaluated using the average value of the radial system speed $V_{av} \approx 157$ m/s. Then, motion time $t_n \approx (r_n - R) / V_{av} = 2.04 \times 10^4$ s ≈ 340 min; in Chapter 1, there was required about 100 min in order to reach the same orbit.

The position of the final orbit and the final circular velocity of the system after speed alignment of the rotor and the remaining capsule part are determined by formulae (2.48) and (2.50):

$$r_k \approx \frac{r_n}{1 + \mu_n} = 7,978.3 \text{ km}; \quad x_k \approx 1.2522; \quad V_k = \frac{V_1}{x_k^{1/2}} = 7.064 \text{ km/s}.$$

The difference of positions of the intermediate and final orbits reaches $\Delta x = 0.2504$ or $\Delta r = 1,607.7$ km, i.e., about one fourth of the Earth's radius; the final orbit is twice lower than the intermediate one in terms of its height above the equator.

Theoretical calculations and the provided example justify the conclusion on the crucial possibility of radial motion energy dissipation due to the uplift and the stepped and continuous ejection of capsule parts. Friction forces in relation to the small value are used here only in two cases: to compensate forces of the rotor and capsule elastic extension after leaving the dense atmosphere and at the final stage before the placement into the intermediate orbit. The combination of both factors of dissipation throughout the stage of the system placement into orbit is also possible.

It is fundamental that, apart from a difference in physical nature of these factors, external forces of gravitational attraction to the Earth relative to the rotor – capsule system are used in one case; whereas in the other case – internal forces that require creation of friction elements and provision of their operating conditions.

It is possible to affect the process of aligning rotational speed of the rotor and capsule remains by means of further ejection of its parts. In this case, parameters of the final orbit will be obviously different. There exists a possibility of using other kinds of force interaction, internal or external in relation to the system, which may be dissipation factors.

Chapter 3

Rotor maneuvering in order to avoid objects moving in equatorial plane

The optimal variant for the UPT construction and operation is the availability of two overpasses – equatorial and latitudinal. Successive launches of UPT rotors enable choosing the best starting points in terms of weather conditions, seismic activity, etc. no reducing their overall rate. There can arise situations in the already functioning system that could require adding of a new rotor, replacement of the old one, cargo delivery to some rotor or removal of rotor with cargo outside the terrestrial gravity. All this is impossible when launching from the equatorial overpass, since the orbits of operating rotors are located in the equatorial plane and their collision with a new one is inevitable, unless special measures are taken*. In contrast, the rotor movement from a latitudinal overpass allows performing a maneuver to avoid obstacles or a part of them, placing the rotor to the preset position in clear space, as well as to approaching any object of the system.

High mountain groups, the vast of ocean, deep waters, powerful currents can cause delays in the construction of an equatorial overpass, and the high-priority construction of a more simple latitudinal overpass along one of the parallels where the same difficulties may be encountered, just at a smaller scale. This enables choosing the most optimal variant in terms of cost effectiveness, reliability, manufacturability, etc. The experience in the construction and operation of such an overpass can be then used when building an equatorial overpass.

Another variant, although seemingly unusual at first glance, envisages the extraction and processing of raw materials at other bodies of the Solar System, as well as product delivery to the Earth by means of rotors launched from latitudinal overpasses erected at those bodies. In this case, the rotors must have a wide variety of trajectories and other motion characteristics, which will allow reaching the Earth with minimal correcting pulses.

Under the conditions of giant planets, there arise problems related to over-coming of natural rings and satellite systems, as well as those related to the

* Maneuvering is also possible when launching the UPT from the equatorial overpass, for example, using aerodynamic forces when the rotor at the atmospheric motion section is withdrawn from the equatorial plane to another one parallel to it.

construction in rarefied atmosphere and in the absence of a solid basis. However, it is possible to freeze an overpass and other structures, rather durable and light at the same time, that would float in the upper atmosphere. Other possible variants include pneumatic tents, similar to bicycle tubes, etc., overpasses and other structures or their parts designed with an artificially created human environment. The crucial thing is that the planets have raw material required for the earth civilization, since human inventiveness and persistence know no limits.

Apart from ecological woes caused by uncontrolled human activity, an external threat related to the possibility of collision between the Earth and large asteroids poses a major hazard for humanity; in fact, this has happened more than once throughout the geological history of the Earth. The Moon's surface is almost entirely covered in numerous impact craters. The same picture can be observed at other bodies of the Solar System where the surface is hard and the atmosphere is weak or is not available at all. However, the atmosphere is not an obstacle for large asteroids; it can only mitigate their impact.

A probability of collision with an asteroid in the near future is rather high, and possible consequences can be immense – climate change, extinction of many terrestrial species, heavy losses for humanity. Therefore, this problem cannot be disregarded any longer. Coming to a global activity level, a person must take on the functions on Earth's protection from external dangers, as well. As is known, there have been created international and national organizations to study the asteroidal danger. However, only the first steps have been made in this direction.

The UPT project represents interesting opportunities here, as well.

Firstly, the use of the rotor system creates much better conditions of observation for the movement of the Solar System small bodies, regardless of the weather, atmospheric disturbances, with a substantial base for observations means. In case observation stations are located at the rotor moving along the geostationary orbit, the distances between the stations can reach 80,000 km, which significantly enhances observation accuracy and prediction of asteroids trajectory, their sizes, weight, structure and other parameters. The monitoring service efficiency and the decision window in case an asteroid endangers the Earth are increased.

Secondly, rotors can serve as a base for locating destruction means or other weapon to affect an approaching asteroid: atomic rockets, lasers, etc. with autonomous energy provision due to solar irradiation, and the control system for these means. The factor of ecological cleanliness of these means is of no small importance, either. In case of their action on the earth surface, the environment can suffer severe damage as a result of a large number of missile launches, huge laser powers, etc.

A specially designed UPT rotor equipped with the tools known at present and developed in the future can produce the most effective impact on the dangerously approaching asteroid. It is possible to calculate the controlled motion of the rotor taken outside the Earth's attraction zone and fragmented so that individual groups of fragments could approach an asteroid simultaneously. A close-range laser action, simultaneous shots of a large amount of nuclear charges or other concentrated impacts can destroy an asteroid, crush it or deviate its trajectory.

In this case, an asteroid or its fragments are subject to a multiple coordinated action: first, from the side of several groups of fragments of a special rotor, then from the means of tackling an asteroid hazard for the industrial ring and finally, from the means concentrated on the earth surface. In accordance with the laws of a large-scale war, only a deeply echeloned defense can be successful.

When considering these and other challenges, there arises a problem of studying the rotor launched from a latitudinal overpass in case there exist any obstacles like rotors, rings or discrete space objects, whose orbits are in the equatorial plane.

3.1. Setting a problem on the UPT rotor maneuvering

Let us study the UPT rotor motion at its placement into the orbit from a latitudinal overpass located in plane P_0 parallel to plane P_1 of the planet equator. Let us assume that there are in plane P_1 natural obstacles in the form of rings, satellites similar to those at giant planets Jupiter, Saturn, Uranus, or artificial ones – other rotors placed into the orbit earlier, space stations, etc., which possibly form some ring-shaped structures. The location and size of obstacles in the general case are arbitrary; however it is believed that their cross sectional dimensions perpendicular to plane P_1 are small compared to the planet size, and there are free gaps between the obstacles orbits. As for large natural satellites, they are usually significantly remote, to the distance that exceeds the planet radius by ten times or more. It is also believed that the orbits of all artificial objects within the planet vicinity are inside the orbits of large natural satellites. In case the UPT rotor goes beyond the planet attraction, it is necessary to take into consideration the size of large satellites and provide the conditions for rotor motion not in contact with the same.

The rotor orbit can be located only in the equatorial plane; it is set with regard to the rotor placement in one of the free gaps between the orbits of the existing obstacles. The rotor motion in equatorial plane P_1 is impermissible due to inevitability of colliding with obstacles. The motion outside this plane is

achieved by means of an aeromaneuver in the atmosphere, for example using a wing-shaped capsule or at the start from a latitudinal overpass. The second variant is considered below.

As is shown further, the rotor makes oscillations in relation to a characteristic point, which determines the position of the rotor plane P relative to plane P_1 . The rotor proper rotation angle being a cyclic coordinate is excluded from further review.

Let us formulate the problem on rotor maneuvering as a choice of control for the two specified rotor motions so that the rotor starting in plane P_0 and not colliding with any of obstacles could reach the intended orbit in plane P_1 damping radial and rotational oscillations. The second part of the problem: take the rotor outside the planet attraction under the same conditions.

The factors of control and dissipation can include external actions, for example magnetic field of the planet and internal friction forces between the sliding apart rotor fragments. In this case, it is assumed to have a possibility to adjust dissipative forces from zero to maximum values. Let us consider three modes of rotor motion at sliding apart fragments.

1. There are no dissipative forces; let us call this mode as free motion or free rotor expansion.
2. Only external dissipative force act.
3. Only internal (friction) dissipative forces act.

For brevity sake, let us use the following names: the first (I), the second (II) and the third (III) modes of rotor motion. The fourth (IV) mode is also possible, when both types of dissipative forces or all forces possible in this case are used in order to accelerate the energy dissipation process of the rotor radial motion.

Let us point out some features of further research.

1. Questions on technical feasibility of the UPT project in specific conditions of this or that planet are not discussed: creation of an overpass, rotor assembly and launch, rotor design and its features.

2. The stage of rotor motion in the capsule in dense atmosphere is not considered so as not to complicate the problem on maneuvering to be solved. The research starts from the moment of the rotor exit from the atmosphere and ejection of the entire capsule; it is assumed in this case that the rotor radial speed at this time is zero and the rotor does not have elastic tensile deformations.

3. The examples of solving the problem on maneuvering on Uranus and Saturn are for illustrative purposes; physical properties of the planets and their atmosphere are not considered. Only the systems of rings and satellites are considered to be obstacles that the rotor has to overcome when going into the intended orbit.

3.2. Differential equations of the UPT rotor motion outside the equatorial plane

The rotor motion is determined relative to the inertial reference system with the beginning in the planet center; in this case, Z axis is directed along the planet and rotor rotation axis, X and Y axes – in the equatorial plane P_1 . The influence of the Sun, other planets, large satellites, as well as obstacles near which the rotor passes by is ignored.

The rotor in the initial state rotates at an angular speed ω_0 around the Z axis in plane P_0 parallel to P_1 at the distance $z_0 = R \sin \psi_0$ from it, where R – radius of the sphere limiting the dense atmosphere; ψ_0 – initial angle value ψ determining the motion of rotor plane P relative to the equator plane P_1 (figure 24). The initial radius of rotor orbit $r_{r0} = R \cos \psi_0$, the initial linear speed of rotational movement $V_0 = \omega_0 r_{r0} = \omega_0 R \cos \psi_0$.

As it was mentioned, the initial rotor state and values R , ω_0 and V_0 correspond to the moment of its exit from the atmosphere and ejection of the entire capsule. If the planet does not have an atmosphere, the starting state (also without a capsule) corresponds to the position at a latitudinal overpass.

Let us assume a thin ring with homogeneous mechanical properties as a rotor model that is divided into fragments with telescopic joints at the launch time.

The scheme of the third (friction) mode of rotor motion, some acting forces and obstacles is shown in figures 24 and 25. Figure 24 shows two components of motion of intersection point M for the rotor and XOZ plane: radial motion and plane P motion in relation to plane P_1 . Let us further call the M point as a characteristic point of rotor motion.

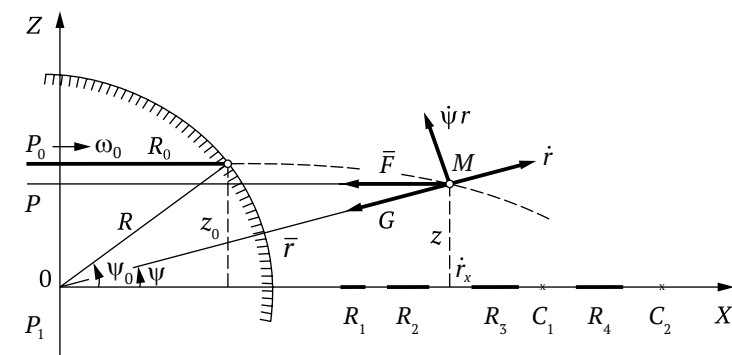


Figure 24 – Motion scheme of intersection point M for the rotor motion trajectory and plane XOZ ; P_0 and P – starting and current planes of rotor motion

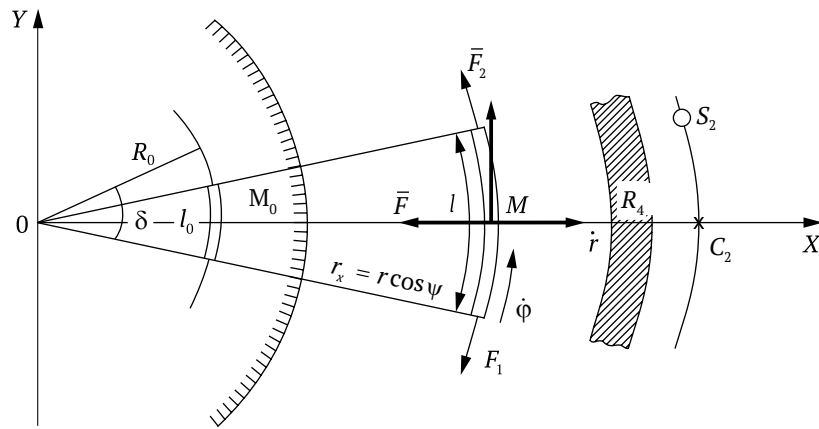


Figure 25 – Motion scheme of rotor element in plane P ; ring R_4 and satellite S_2 – in equatorial plane P_1

Let us assume that the sections R_1, R_2, \dots, R_n – traces (in bold) of intersection of XOZ plane with obstacles in the form of rings or rotors launched earlier; the length of the sections considers possible eccentricities of the obstacles or bits. Starts C_1, C_2, \dots, C_n – intersection points of satellite orbits or artificial discrete objects with the same plane; taking into consideration the eccentricities of these orbits, the traces of intersection can have some length along the OX axis.

Figure 25 shows the movement of element l in rotor plane P . In order not to overload the figure, a fragment of one ring R_4 and the orbit of one satellite S_2 located in equatorial plane P_1 are specified as obstacles, with traces R_4 and C_2 of their intersection with XOZ plane.

Let us consider the motion of the rotor element with mass m and initial length l_0 . At rotor motion, the length of the selected element is increased due to the fragments moving apart proportionally to the rotor radius, whereas the mass remains constant:

$$l = l_0 \frac{r \cos \psi}{R \cos \psi_0}, \quad m = \text{const.}$$

The generalized coordinates of the element include:

- 1) turning angle φ in plane P , where it is located at the moment;
- 2) the element distance r to the planet center; let us further consider r as a radius vector module \bar{r} specifying the center-of-gravity position of the element relative to the $OXYZ$ inertial reference system;

3) the angle ψ of deflection \bar{r} from equatorial plane P_1 . The initial values of these parameters and their derivatives

$$\varphi_0 = 0; \quad \dot{\varphi}_0 = \omega_0; \quad r_{r0} = R \cos \psi_0; \quad \dot{r}_{r0} = \omega_0; \quad \psi_0 \neq 0; \quad \dot{\psi}_0 = 0. \quad (3.1)$$

Kinetic energy of the element

$$K = \frac{m}{2} (\dot{\varphi}^2 r^2 \cos^2 \psi + \dot{r}^2 + \dot{\psi}^2 r^2).$$

The forces acting on the selected element depend on the mode of rotor motion. The element gravity force to the planet center acts in all three modes:

$$\bar{G} = mg \frac{R^2}{r^2},$$

where g – gravity acceleration in the rotor launch position.

In the second mode, the element is additionally under the action of external dissipative force \bar{P} , which we assume to exert in the element centre and directed perpendicular to radius vector \bar{r} towards speed $\dot{\psi}r$ (figure 24). Force \bar{P} is also a control one and is subject to the determination based on the maneuver conditions to bypass obstacles.

In the third mode, tension forces \bar{F}_1 and \bar{F}_2 , arising as a result of friction between fragments in the course of their frictional separation, act on the element additionally to \bar{G} . These forces exert at the element ends tangentially to the rotor and have equal values: $F_1 = F_2 = F_{fr}$ (figure 25). Their resultant \bar{F} exerts in the element centre in rotor plane P and is directed to the OZ axis along its radius; its module equals to $F = 2F_{fr} \sin \frac{\delta}{2}$, where $\delta = l_0 / r_{r0} \frac{1}{r} \cos \psi$. Taking into consideration small value δ and dependence $r_{r0} = R \cos \psi_0$, it is possible to write down as follows

$$F = F_{fr} \delta = F_{fr} \frac{l_0}{R \cos \psi_0}.$$

The generalized forces take on the following values depending on modes I, II and III of rotor motion:

$$Q_\varphi = 0; \quad Q_r = \begin{cases} -G; \\ -G; \\ -(G + F \cos \psi); \end{cases} \quad Q_\psi = \begin{cases} 0; & \text{I} \\ Pr; & \text{II} \\ Fr \sin \psi. & \text{III} \end{cases} \quad (3.2)$$

The system of differential equations of the rotor element motion is written as:

$$\ddot{\phi}r \cos \psi + 2\dot{\phi}r \dot{\psi} \cos \psi - 2\dot{\phi}\dot{\psi}r \sin \psi = 0; \quad (3.3)$$

$$\ddot{r} - \dot{\phi}^2 r \cos^2 \psi - \dot{\psi}^2 r = \frac{1}{m} Q_r; \quad (3.4)$$

$$\ddot{\psi} + 2\dot{\psi} \frac{\dot{r}}{r} + \dot{\phi}^2 \sin \psi \cos \psi = \frac{1}{mr^2} Q_\psi. \quad (3.5)$$

The coordinate ψ is cyclic; the corresponding integral has the meaning of the law of conservation of kinetic momentum of the rotor relative to the OZ axis:

$$\dot{\phi} = \dot{\phi}_0 \frac{R^2 \cos^2 \psi_0}{r^2 \cos^2 \psi} = V_0 \frac{R \cos \psi_0}{r^2 \cos^2 \psi}. \quad (3.6)$$

Going to the non-dimensional coordinate $x = r/R$ and using the designations

$$q = \frac{g}{R}; \quad \beta = \frac{V_0^2 \cos^2 \psi_0}{gR} = \frac{V_0^2}{V_1^2} \cos^2 \psi_0; \quad f = \frac{F}{mR}; \quad p = \frac{P}{mR},$$

taking into consideration integral (3.6), expressions (3.2), after certain rearrangement of equations (3.4) and (3.5) we get as follows:

$$\dot{\phi} = \frac{(q\beta)^{1/2}}{x^2 \cos^2 \psi};$$

$$\ddot{x} = \frac{q}{x^2} \left(\frac{\beta}{x} \frac{1}{\cos^2 \psi} - 1 \right) + \dot{\psi}^2 x - \begin{cases} 0; \\ 0; \\ f \cos \psi; \end{cases} \quad (3.7)$$

$$\ddot{\psi} + 2\dot{\psi} \frac{\dot{x}}{x} + q\beta \frac{\sin \psi}{x^4 \cos^3 \psi} = \begin{cases} 0; \\ \frac{p}{x}; \\ \frac{f}{x} \sin \psi. \end{cases}$$

As it was mentioned earlier, forces P and F are not only dissipative, but also control the rotor motion: let us assume them and their dependent values P and f as functions of coordinate x :

$$P = P(x); \quad p = p(x); \quad F_1 = F_1(x); \quad f = f(x).$$

Let us reduce the problem on rotor maneuvering to the determination of starting velocity V_0 and functions $P(x)$, $F_1(x)$ under conditions: the rotor must, not colliding with any of the obstacles, go in plane P_1 into the orbit determined by the preset coordinate x_* , in whose collar neighborhood there are no obstacles; the angular and radial motion must be reduced at a specified position x_* :

$$\psi(x_*) = \dot{\psi}(x_*) = \ddot{\psi}(x_*) = 0; \quad \dot{x}(x_*) = \ddot{x}(x_*) = 0. \quad (3.8)$$

The second problem on rotor removal from the planet attraction zone can be formulated as the determination of such value V_0 to make the rotor leave the planet attraction zone passing the area of obstacles without colliding with any of them. It is not necessary to introduce dissipative forces in this case; moreover, they are undesirable here since they lead to energy losses by braking the rotor motion.

3.3. Method of problem solving

The system of two nonlinear differential equations (3.7) relative to coordinates X and Y contains control functions not known yet $p = p(x)$ and $f = f(x)$. Apart from initial conditions (3.1), there are final conditions (3.8).

Let us outline the method of problem solving.

1. Let us linearize the equation of system (3.7) limiting ourselves to the case of small values of ψ angle and its first derivative $\dot{\psi}$.

2. Let us pass on to a new independent variable – non-dimensional radial coordinate x .

3. Let us determine the scheme of rotor motion when bypassing obstacles and going into the collar neighborhood of the intended orbit. In this case, the division of stages of dampening two rotor motions is possible: at first, motion at ψ angle is damped, then – radial motion at coordinate x .

The two last equations of system (3.7) linearized at ψ and $\dot{\psi}$ take on the view:

$$\ddot{x} = F(x, 0) = \begin{cases} 0; \\ 0; \\ f; \end{cases} \quad (3.9)$$

$$\ddot{\psi} + 2\dot{\psi} \frac{\dot{x}}{x} + q\beta \frac{\psi}{x^4} = \begin{cases} 0; \\ p/x; \\ f\psi/x. \end{cases} \quad (3.10)$$

The first equation contains only variable x and its second derivative, and in mode III – control function $f(x)$.

Integrating this equation with the limits from $x_0 = 1$ to x , we will get as follows:

$$\dot{x}^2 = \frac{q}{x}(x-1) \left[\beta \left(1 + \frac{1}{x} \right) - 2 \right] - 2 \int_{x_0}^x f(x) dx, \quad (3.11)$$

where the summand with an integral is added only at the third friction mode of rotor motion.

Equations (3.9) and (3.11) determine radial acceleration \ddot{x} and radial speed \dot{x} depending on the rotor position x (and control function $f(x)$ in mode III).

Let us assume ψ as a composite time function t ; i.e., $\psi = \psi(x(t))$. Then,

$$\dot{\psi} = \frac{d\psi}{dt} = \psi' \dot{x}; \quad (3.12)$$

$$\ddot{\psi} = \frac{d^2\psi}{dt^2} = \frac{d}{dt}(\psi' \dot{x}) = \psi'' \dot{x}^2 + \psi' \ddot{x}^2, \quad (3.13)$$

where the derivatives of x are marked with a prime, and derivatives of t – with dots.

Substituting (3.12), (3.13) into equation (3.10) we will get as follows:

$$\psi'' \dot{x}^2 + \psi' \left(\ddot{x} + 2 \frac{\dot{x}^2}{x} \right) + \psi \frac{q\beta}{x^4} = \begin{cases} 0; \\ p/x; \\ f\psi/x, \end{cases} \quad (3.14)$$

where \ddot{x} and \dot{x}^2 look like (3.9) and (3.11).

Equation (3.14) is a linear differential second-order equation relative to $\psi(x)$ with variable right parts, which have control parameters $p(x)$ and $f(x)$ at rotor motion modes II and III.

3.4. Dynamics of rotor free motion. Problem solution on rotor removal from the planet attraction zone

The first mode of rotor motion is free, without dissipative expansion forces for telescopically connected fragments. In this case, equations (3.9), (3.11) take on the form:

$$\ddot{x} = \frac{q}{x^3}(\beta - x); \quad \dot{x}^2 = q \frac{x-1}{x^2} [(\beta - 2)x + \beta]; \quad (3.15)$$

$$x^2 \psi'' [(\beta - 2)x^2 + 2x - \beta] + x \psi' [2(\beta - 2)x^2 + 3x - \beta] + \psi \beta = 0. \quad (3.16)$$

In order to determine function $\psi = \psi(x)$, there was obtained a linear differential second-order equation with polynomial coefficients. Let us find a particular solution $\psi_1(x)$ also as a polynomial [9]:

$$\psi_1(x) = x^n + a_1 x^{n-1} + \dots + a_n, \quad (3.17)$$

whose exponent n is determined when substituting (3.17) in (3.16) and equating the higher coefficient to zero. Let us find $n = -1$, then

$$\psi_1 = \frac{1}{x} + a, \quad (3.18)$$

where constant $a = -1/\beta$ is determined by substituting (3.18) in equation (3.16).

The second particular solution is written as:

$$\psi_2 = \psi_1 - \int \frac{\exp[-\int h(x) dx]}{\psi_1^2(x)} dx, \quad (3.19)$$

where

$$h(x) dx = \frac{2(\beta - 2)x^3 + 3x^2 - \beta x}{(\beta - 2)x^4 + 2x^3 - \beta x^2} dx = \frac{1}{2} \frac{du}{u},$$

if the term of fraction is marked as $u(x)$. Then

$$\int h(x) dx = \frac{1}{2} \ln u;$$

$$\psi_2(x) = \beta^2 \psi_1(x) \int \frac{x dx}{(\beta - x)^2 [(\beta - 2)x^2 + 2x - \beta]^{1/2}}. \quad (3.20)$$

Making sequential replacements:

$$\frac{1}{\beta - x} = z; \quad \beta z - 1 = y; \quad y^2 = S,$$

let us reduce the integral in (3.20) to get a standard one

$$\psi_2(x) = \frac{K}{2} \psi_1(x) \int \frac{ds}{(S - b)^{1/2}} = K \psi_1(x) (S - b)^{1/2},$$

where

$$K = \beta^{3/2} (\beta - 1); \quad b = \frac{1}{(\beta - 1)^2}.$$

After making the replacements in reverse order, let us find the second particular solution:

$$\psi_2(x) = \frac{1}{(\beta - 1)^2} \frac{\beta}{x} \left\{ (x - 1) [(\beta - 2)x + \beta] \right\}^{1/2}.$$

The general solution to equation (3.16) equals to the linear combination of particular solutions:

$$\psi(x) = C_1 \psi_1(x) + C_2 \psi_2(x),$$

where constant C_1, C_2 are determined based on the initial conditions (3.1):

$$C_1 = \frac{\psi_0 \beta}{\beta - 1}; \quad C_2 = 0.$$

Finally

$$\psi(x) = \frac{\psi_0}{\beta - 1} \left(\frac{\beta}{x} - 1 \right), \quad x \geq x_0 = 1. \quad (3.21)$$

Thus, ψ angle determining in the first mode the rotor plane P motion in relation to equatorial plane P_1 changes under a simple law (3.21).

Let us determine the time of rotor motion. The correlation (3.15) allows us to find an explicit dependence of motion time t on rotor position x :

$$t = \int_{x_0}^x \frac{dx}{\dot{x}} = \frac{1}{q^{1/2}} \int_{x_0}^x \frac{x dx}{[(\beta - 2)x^2 + 2x - \beta]^{1/2}}.$$

The results of integration depending on value β in relation to critical value $\beta_{cr} = 2$ coincide with the expressions found in Chapter 1 and are not given here. The analysis of rotor motion made in clause 1.6 is true here too, with some correction taking into consideration the availability of another coordinate – ψ angle. Let us only point out the following.

1. The constant rotor orbit x_* is achieved in the position, where $\ddot{x} = 0$:

$$\dot{x} = \beta.$$

2. The required rotor starting velocity is determined by the formula

$$V_0 = V_1 \frac{\beta^{1/2}}{\cos \psi_0}.$$

This value exceeds the one found earlier for the equatorial variant of rotor motion and increases with an increase in latitudinal angle ψ_0 of the rotor launch position.

3. If $\beta < \beta_{cr}$, the rotor makes oscillations relative to the position x_* , with the maximal distance from the planet center:

$$x_{**} = \frac{\beta}{2 - \beta} = \frac{x_*}{2 - x_*}. \quad (3.22)$$

4. If $\beta = \beta_{cr} = 2$, the rotor goes into infinity, and the starting velocity depends on the first and second cosmic velocity:

$$V_0 = V_1 \frac{\sqrt{2}}{\cos \psi_0} = \frac{V_2}{\cos \psi_0}. \quad (3.23)$$

The final radial speed in this case vanishes: $V_{r\infty} = \dot{x}_\infty R = 0$.

5. If $\beta > \beta_{cr}$, the rotor also goes into infinity, with a finite value of radial speed:

$$V_{r\infty} = \dot{x}_\infty R = R[q(\beta - 2)]^{1/2} = V_1(\beta - 2).$$

In the last two cases, the rotor is removed from the planet attraction zone, and formula (3.23) determines the minimal value of the required starting velocity.

Let us study the rotor motion at ψ angle described by correlations (3.21), (3.12) and (3.13).

In case of oscillatory motion at $\beta < \beta_{cr}$ within $x_0 = 1$ to $x_{**} = \frac{2}{2 - \beta}$, the ψ angle changes according to (3.21) within ψ_0 to $\psi_{**} = -\psi_0$. Angular velocity $\dot{\psi} = \psi' \dot{x}$ in the extreme points vanishes, which results from $\dot{x}(x_0) = \dot{x}(x_{**}) = 0$; the largest value in module is achieved in the position $x_* = \beta$:

$$\dot{\psi}(x_*) = -\frac{\psi_0}{\beta} \left(\frac{q}{\beta}\right)^{1/2}.$$

Angular acceleration $\ddot{\psi} = \psi'' \dot{x}^2 + \psi' \ddot{x}$ after substituting derivatives $\psi''(x)$ and $\psi'(x)$ is written as follows:

$$\ddot{\psi}(x) = \frac{\psi_0 \beta}{\beta - 1} \frac{2\dot{x}^2 - \ddot{x}x}{x^3}.$$

In points $x_0 = 1$, $x_* = \beta$, $x_{**} = \frac{\beta}{2 - \beta}$ it has the following values, correspondingly:

$$-\psi_0 \beta q; \quad 2\psi_0 q(\beta - 1)^2 / \beta^4; \quad \psi_0 q(2 - \beta)^4 / \beta^3.$$

In cases $\beta = \beta_{cr}$ and $\beta > \beta_{cr}$ when the rotor goes into infinity, the ψ angle has ultimate values:

$$\psi_1(\infty) = -\frac{\psi_0}{\beta_{cr} - 1} = -\psi_0; \quad \psi_2(\infty) = -\psi_0 \frac{1}{1 - \beta},$$

in this case, angular velocity and angular acceleration vanish.

Let us introduce a variable

$$z = R x \sin \psi, \tag{3.24}$$

which is a natural value of rotor height above the equatorial plane. Limiting ourselves to small values ψ and linearizing (3.24) at ψ , with regard to (3.21) we will get as follows:

$$z = \frac{\psi_0 R}{\beta - 1} (\beta - x). \tag{3.25}$$

Value z is also an applicate of point intersection M for rotor and XOZ plane (figures 24 and 26), and dependence (3.25) is a trajectory equation of this point. Taking into consideration the small value of ψ angle, this trajectory is a straight line with the beginning in M_0 point, crossing the equatorial plane in the only point $x_* = \beta$, where the permanent rotor orbit goes through (figure 26). At rotor free motion, the values $\dot{x}, \dot{\psi}, \ddot{\psi}$ in point x_* are not zero; consequently, the M point goes through the position x_* without a stop. In case of an oscillatory motion, the M point moves along the straight line to the position M_{**} with a coordinate x_{**} determined according to (3.22), after which a reverse motion towards the initial point M_0 starts.

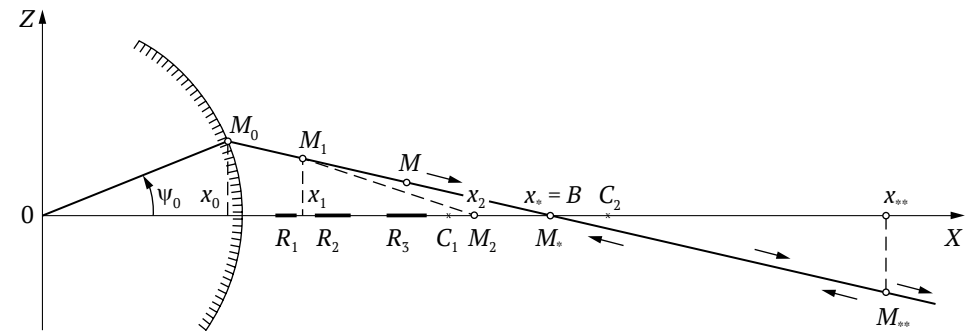


Figure 26 – Motion scheme of characteristic point M . In mode I – solid line $M_0M_1M_2M_{**}$; in mode II – dotted line M_1M_2 ; in mode III – section M_2M_* .

When moving in critical cases $\beta \geq \beta_{cr}$, the M point goes at infinity along the straight line M_0M_{**} .

The rotor movement is represented in the form of oscillations that take place on the cone surface with generating $M_0M_1M_2M_{**}$, when the rotor sinks down and goes up in turns. In this case, the rotor rotates at angular velocity ϕ around the OZ cone axis, decreasing and increasing its value in turns. In critical cases, oscillatory motion degenerates into unlimited sliding down along the cone.

In case the rotor launch position is located in the southern hemisphere of the planet, sliding is replaced with an ascent along the cone to the northern semi-space relative to the equatorial plane.

In all cases, the position of point x_* must be chosen on the condition of absence of any obstacles in its vicinity, more exactly – in the corresponding circular part of plane P_1 . The choice $x_* = \beta$ also determines the direction of further rotor motion from the launch position M_0 through M_* relative to the equatorial plane. This trajectory affects the condition of non-contact movement past large natural satellites located in this plane, as well as the minimality condition for correcting pulses when rotor fragments move to the intended target.

3.5. Rotor dynamics at the stage of angular motion damping

Let us consider a problem on rotor maneuvering with the purpose of bypassing obstacles and reaching the permanent orbit damping oscillations. The trajectory of characteristic point M crosses the equatorial plane in the only point $x_* = \beta$, which has a crucial importance for problem solving on fulfillment of conditions (3.8). The location diagram for obstacles in the equatorial plane allows providing their bypassing moving the rotor above this plane by means of setting the position x_* in a free zone. The second part of the problem – oscillation damping – can be solved by introducing dissipative forces.

1. External dissipative forces, affecting the rotor center-of-mass motion, can be used to damp oscillations in the rotor plane relative to the equatorial plane, i.e., movement at ψ angle.

2. Internal dissipative forces – the friction ones in this case – affecting reciprocal displacements of parts of the system, can be used to damp radial motion of rotor fragments, i.e., movement at x parameter.

3. Introduction of friction forces, as will be shown further, allows increasing value β_{cr} , when the range of precritical modes of rotor motion expands beyond $\beta = 2$. This circumstance extends an opportunity of choosing the orbit $x_* = \beta$, providing a manoeuvre to bypass any obstacles.

Processes on oscillation damping at parameters ψ and x can be carried out regardless of each other, in turns or simultaneously. Let us assume further the sequence of three stages of rotor exit to the orbit, which differ in motion modes; in this case, the rotor position is determined by parameters ψ and x , whereas x is an independent argument, as before. Due to the small value of ψ angle, let us assume that a radial coordinate $x = r/R$ coincides with abscissa $x = \frac{r}{R} \cos \psi \approx r/R$ of characteristic point M .

The free rotor motion without dissipative forces, i.e., mode I, takes place at the first stage from the initial position M_0 with coordinate x_0 (figure 26) to some position M_1 with coordinate x_1 . The rotor here gains radial speed moving at the blunted cone with a rectilinear generator M_0M_1 . The characteristic point M moves along the straight-line section M_0M_1 ; let us determine the position x_1 below.

The rotor motion mode II, with the involvement of external dissipative forces, takes place at the second stage – from position M_1 to position M_2 . Position M_2 is determined at X axis at the same section free from obstacles that the orbit point M_* ; in this case, $x_2 < x_*$. In figure 26, points M_2 and M_* are chosen at the section between orbits C_1 and C_2 of two satellites. The coordinate of M_1 point is chosen within $[x_0, x_2]$. The trajectory of characteristic point M is a curve line M_1M_2 marked in dots.

The purpose of motion at stage II is motion damping at ψ angle, with the fulfillment of conditions at the end of the stage

$$\psi(x_2) = \dot{\psi}(x_2) = \ddot{\psi}(x_2) = 0.$$

The rotor motion mode III, with the involvement of friction forces, takes place in the equatorial plane from position M_2 to the final position. The purpose of this motion is damping of radial motion at x coordinate, with the fulfillment of conditions at the end of the stage

$$\dot{x}(x_*) = \ddot{x}(x_*) = 0.$$

The radial motion at stage I is described by correlations (3.15); angular motion at ψ – with correlations (3.12), (3.13) and (3.21). At the end of the first and beginning of the second stages, values ψ and ψ' take on in point x_1 the following values

$$\psi(x_1) = \frac{\psi_0}{\beta - 1} \left(\frac{\beta}{x_1} - 1 \right); \quad \psi'(x_1) = -\frac{\psi_0}{\beta - 1} \frac{\beta}{x_1^2}. \quad (3.26)$$

Let us consider the rotor dynamics at the second stage $[x_1, x_2]$. The differential motion equations in this case are written as the second correlations (3.9) and (3.10).

$$\ddot{x} = \frac{q}{x^2} \left(\frac{\beta}{x_1} - 1 \right); \quad \ddot{\psi} + 2\dot{\psi} \frac{\dot{x}}{x} + \psi \frac{q\beta}{x^4} = \frac{p(x)}{x}.$$

The first equation has an integral

$$\dot{x}^2 = \dot{x}_1^2 + \frac{q}{xx_1}(x - x_1) \left(\beta \frac{x + x_1}{xx_1} - 2 \right), \quad (3.27)$$

where \dot{x}_1 – rotor radial speed in position x_1 , which is determined according to (3.15).

The second equation is used to determine the control parameter $p(x)$ by setting the dependence $\psi = \psi(x)$, which complies with the following boundary conditions.

1. ψ and ψ' coincidence with the values (3.26) in the point, which provides smooth conjunction of ψ angle at the first and second stages.

2. ψ , $\dot{\psi}$ and $\ddot{\psi}$ vanishing in point x_2 , i.e., fulfillment of conditions of angular motion damping at ψ .

These conditions can be met if we set ψ angle at the section $[x_1, x_2]$ in the following way:

$$\psi(x) = (x_2 - x)^3(ax + b), \quad x_1 \leq x \leq x_2. \quad (3.28)$$

The derivatives of this function are written as:

$$\begin{aligned} \psi' &= -(x_2 - x)^2(4ax - ax_2 + 3b); \\ \psi'' &= 2(x_2 - x)(6ax - 3ax_2 + 3b). \end{aligned} \quad (3.29)$$

The first multipliers in the right parts (3.28) and (3.29) with regard to (3.12), (3.13) provide the fulfillment of conditions of motion damping at ψ angle. The second multipliers with indefinite coefficients a and b are used to meet the matching conditions in point x_1 . Equating ψ in (3.28) and ψ' in (3.29) to values in (3.26), let us find:

$$\begin{aligned} a &= \frac{\psi_0}{\beta - 1} \frac{\beta(4x_1 - x_2) - 3x_1^2}{x_1^2(x_2 - x_1)^4}; \\ b &= -\frac{\psi_0}{\beta - 1} \frac{(5\beta + x_2)x_1 - 2\beta x_2 - 4x_1^2}{x_1(x_2 - x_1)^4}. \end{aligned}$$

It is easy to make sure that function $p(x)$ has the structure $p(x) = q(x_2 - x)p_1(x)$, which provides its vanishing in point $x = x_2$ together with ψ angle and its derivatives. The external force required for the damping process at ψ angle:

$$P(x) = mRp(x).$$

Choosing the end points M_1 and M_2 of the stage under study, it is possible to determine the trajectory of characteristic point M depending on the number type, location and size of obstacles, the size of free zone, etc. The M_1 point with coordinates x_1, z_1 can be chosen arbitrarily; however, the closer it is to the initial point M_0 , the less the required external dissipative force $P(x)$ is. In principle, M_1 point can coincide with M_0 point. The point $M_2(x_2, z_2 = 0)$ is chosen in the same free zone as the orbit point M_* ($x_*, z_* = 0$) so that the distance from M point to the nearest obstacle could be sufficiently large, surpassing possible obstacle sizes.

In case of availability of discrete obstacles in the form of satellites or stations, whose orbital planes differ from equatorial, a further method of their overcoming with the rotor is possible. At the moment the rotor crosses the orbit of some object, the object itself must be located in another place of the orbit, on the one or another side from the rotor plane. In order to overcome a system of such objects, it is required to calculate the optimal rotor starting moment, with regard to their position and motion, to enable the rotor to successively cross the orbits of these objects whilst fulfilling the same condition.

3.6. Rotor motion at the stage of radial motion damping

The rotor motion at the final stage $[x_2, x_*]$, where the radial motion is damped, takes place in mode III, where friction forces are used as dissipative forces. The motion equation and its integral are written as follows:

$$\ddot{x} = q \frac{\beta - x}{x^5} - f(x), \quad x_2 \leq x \leq x_*; \quad (3.30)$$

$$\dot{x}^2 = \dot{x}_2^2 + \frac{q}{xx_2}(x - x_2) \left(\beta \frac{x + x_2}{xx_2} - 2 \right) - 2 \int_{x_2}^x f(x) dx, \quad (3.31)$$

where $f(x)$ – control parameter; \dot{x}^2 – radial speed at the end of the previous section determined according to (3.27) at $x = x_2$.

Let us find the control parameter based on the conditions of radial motion damping in the position $x_* = \beta$:

$$\ddot{x}(x_*) = 0; \quad \dot{x}(x_*) = 0. \quad (3.32)$$

From (3.30) and the first condition (3.32) it follows that parameter $f(x)$ also vanishes in point x_* : $f(x_*) = 0$. Let us find $f(x)$ in the form of a linear function:

$$f(x) = (x_* - x)f_* = (\beta - x)f_*. \quad (3.33)$$

Substituting this expression in (3.30) and (3.31), we will get equations for the rotor motion at the final stage:

$$x = (\beta - x) \left(\frac{q}{x^3} - f_* \right); \quad (3.34)$$

$$\dot{x}^2 = \dot{x}_2^2 + (x - x_2) \left[\frac{q}{xx_2} \left(\beta \frac{x + x_2}{xx_2} - 2 \right) - f_* (2\beta - x_2 - x_*) \right]. \quad (3.35)$$

The multiplier f_* is determined with the help of the second condition (3.32):

$$f_* = \frac{\dot{x}_2^2}{(\beta - x_2)^2} + \frac{q}{\beta x_2^2}. \quad (3.36)$$

The first summand depends here on radial speed \dot{x}_2 in point x_2 and on the distance of point x_2 to the orbit point $x_* = \beta$: the less x_2 is, the less \dot{x}_2 and the bigger the difference $\beta - x_2$ are, with the fixed β , and the less the first summand is. In contrast, the second summand increases with x_2 decreased.

The function f_* has a minimum, which depends on the choice of point x_2 . Taking into consideration the dependence \dot{x}_2^2 in (3.27) on x_2 , we will get, by means of equating the derivative $\frac{df_*}{dx_2}$ to zero, a cubic equation to determine x_2 , which in its turn depends on the choice of point x_1 :

$$x_2^3 \dot{x}_1^2 + q \left[\beta x_2 \left(\frac{x_2^2}{x_1^2} - 1 \right) - 2x_2^2 \left(\frac{x_2}{x_1} - 1 \right) + (\beta - x_2)^2 + \frac{2x_2}{\beta} - 1 \right] = 0.$$

Here, x_1 and \dot{x}_1 are assumed to be fixed; for the case $x_1 = x_0 = 1$, $\dot{x}_1 = \dot{x}_0 = 0$, the equation is simplified:

$$(\beta - 2)x_2^5 + 3x_2^3 + \left(\frac{2}{\beta} - 3\beta \right)x_2 + \beta^2 - 1 = 0.$$

The analysis of these equations is not provided.

Let us substitute function f_* derived according to (3.36) in dependence (3.33) for the control parameter $f(x)$, which provides the fulfillment of conditions (3.32) of radial motion damping at the end of the studied stage. The rotor dynamics at this stage is determined by correlations (3.34) and (3.35). The value of friction force $F_{fr}(x)$ required to enable the process:

$$F_{fr}(x) = mR^2 f(x) \cos \psi_0 / l_0.$$

Thus, there has been obtained a solution to the problem on rotor maneuver when bypassing a group of obstacles and at its ascent to the intended permanent orbit in the equatorial plane with oscillation damping.

3.7. Problems on rotor maneuvering in Uranus and Saturn conditions

Let us consider problems on maneuver in Uranus and Saturn conditions as examples for rotor overcoming an arbitrary system of obstacles.

1. The Planet Uranus has ten rings located as a compact group. Eight of them including the last one have a noticeable eccentricity, i.e., the ellipse form. Seven rings have a slight deviation from the equatorial plane.

Table 3.1 shows the values of ring radii R_i , i – number of the ring, their relative values $x_i = R_i/R$, where $R = 26,200$ km – the Uranus radius, and relative distances between the rings $\Delta x = x_i - x_{i-1}$. As it follows from the table, the whole group of rings lies within [1.58; 1.98] of the inertial reference system plotted along the X axis. The distance between the rings does not exceed 0.084, which corresponds to 200 km. Taking into consideration ellipticity of the rings, this span is small to enable the safe rotor removal to the orbit in the zone of rings.

Apart from rings, there was discovered a group of ten small Uranus satellites in 1986. The orbit of one of them is located between the eighth and ninth rings; the rest move above the ring zone, within the relative radii 2.05; 3.28 (table 3.2). The last satellite is the largest, its diameter is 165 km. The rest – from 25 to 100 km; the distances between them range between 10,800–50,000 km.

The first of the earlier known satellites – Miranda – has a diameter of 483 km and orbital radius of 129,000 km (table 3.2, No. 11, $x_{11} = 4.92$).

Between it and the tenth small satellite, there is a big ring-shaped span of width $\Delta x = 1.64$, or 43,000 km, which is supposed to be free from rings and satellites.

Let us set an orbit in this span in the position $x_* = \beta = 4.6$; i.e., at approximately 2/3 of the distance between the tenth and eleventh satellites.

Table 3.1 – Radii and relative position of Uranus rings

Ser. No.	Radius R_i , km	Relative radius x_i	Height difference $\Delta x = x_i - x_{i-1}$
1	41,600	1.58777	0.58777
2	42,000	1.60306	0.01529
3	42,400	1.61831	0.01525
4	44,600	1.70227	0.08396
5	45,600	1.74044	0.03817
6	47,200	1.80151	0.06107
7	47,600	1.81678	0.01527
8	48,400	1.84731	0.03053
9	50,200	1.91601	0.06870
10	51,800	1.97708	0.06107

Table 3.2 – Orbital radii and relative position of the first 11 Uranus satellites

Ser. No.	Radius R_i , km	Relative radius x_i	Height difference $\Delta x = x_i - x_{i-1}$	Selected values x_2, x_*
1	49,750	1.89846	0.05115	
2	53,770	2.05187	0.07479	
3	59,160	2.25755	0.20568	
4	61,770	2.35714	0.09959	
5	62,650	2.39072	0.03358	
6	64,630	2.46628	0.07656	
7	66,100	2.52238	0.05610	
8	69,930	2.66853	0.14615	
9	75,200	2.86963	0.20110	
10	86,000	3.28176	0.41213	$x_2 = 4.0$
11	129,000	4.92367	1.64191	$x_* = 4.6$

Notes to tables 3.1 and 3.2.

1. The difference $\Delta x = x_1 - x_0 = 0.58777$ is a relative distance between the first ring and the planet surface.

2. The first satellite is between the 8th and 9th rings, the second one – above the 10th, the value Δx for them is a height difference between the 8th ring and the 1st satellite, the 10th ring and the 2nd satellite.

The starting rotor speed required to reach the intended orbit:

$$V_0 = V_1 \sqrt{\beta} / \cos \psi_0 = 25.58 \times 10^3 \text{ m/s} = 35.58 \text{ km/s},$$

where $\psi_0 = 0.1$ – the angle value determining the position of the rotor launching plane P_0 in relation to the equator; $V_1 = (qR)^{1/2} = 16.5 \text{ km/s}$, $V_2 = V_1 \sqrt{2} = 23 \text{ km/s}$ – the first and the second cosmic velocities at Uranus, correspondingly; $g = 10.4 \text{ m/s}^2$ – gravity acceleration at the surface of Uranus; $R = 2.62 \times 10^7 \text{ m}$ – equator's radius.

Let us assume $x_2 = 4.0$ for the M_2 point, where the rotor must go out to the equatorial plane damping the angular motion at ψ , i.e., beyond a group of ten rings and ten small satellites. Then, let us assume $x_1 = 1.9$ for the M_1 point, where the second motion stage starts with the involvement of dissipative forces, i.e., at the section between rings 8 and 9 (table 3.1).

Thus, the prescribed scheme of rotor motion is as follows. Starting the motion from the position M_0 at the surface of Uranus, which is determined by the width $\psi_0 = 0.1$, the rotor at the section $[x_0, x_1]$ makes free motion. At the section $[x_1, x_2]$, controlled motion in the second mode takes place with the purpose of damping angular motion at ψ . The rotor passes above the equator plane at these two sections, at the height of $z = R\psi x$, overcoming the systems of all ten rings and ten small Uranus satellites.

The rotor at the last section $[x_2, x_*]$ moves in the equatorial plane; here, damping of radial motion and ascent to the permanent orbit $x_* = \beta = 4.6$ take place, with the help of friction forces.

The bench-mark data of the problem, some results, graphs and their analysis are given below, see clause 3.

2. Out of the Solar System giant planets, the Saturn has the most massive and complicated system of rings and satellites. The system of main rings D , C , B , A , F , G , E actually consists of a large number of individual, narrower rings, as well as a variety of intermediate rings invisible from the Earth, and makes almost a solid ring, which spreads nearly from the planet atmosphere to the distance $8R$, where $R = 6.01 \times 10^7 \text{ m}$ – the Saturn radius. In relative values R_i/R , this corresponds to the interval [1; 8].

12 small Saturn satellites move in the spans between individual rings, which make up external systems of rings G and E . The first large satellite Rhea located outside the rings has a relative orbital radius of $x = 8.5$; then follows a large free ring-shaped span, width of $\Delta x = 11.5$, to the largest satellite Titan with a relative orbital radius of $x = 20$.

Let us set a problem on the UPT rotor ascent to the large span between the Rhea and Titan satellites specified above, ignoring individual rings of the system, their radii, the intervals between them, as well as small satellites moving between them. Let us assume for this as follows: $x_i = 3.0$; $x_2 = 9.0$; $x_* = \beta = 15.0$.

The corresponding starting velocity of the rotor $V_0 = 83$ km/s, although $\psi_0 = 0.1$ as before. Gravity acceleration on Saturn $g = 9.54$ m/s², the first and second cosmic velocities $V_1 = 24$ km/s, $V_2 = 34$ km/s. All these values are calculated as a sum of transfer velocity from the Saturn rotational motion and relative speed (in relation to the points of launch position): $V_a = V_e + V_r$, where $V_e = R\Omega \cos\psi_0 \approx 10$ km/s, $\Omega = 1.68 \times 10^{-4}$ s⁻¹ – the Saturn angular velocity. The components of the speeds given above, achieved at rotor acceleration, equal to 73 km/s, 14 km/s and 24 km/s, correspondingly.

3. The results of computer-aided problem solution. Table 3.3 shows constant values in problem setting; here, m and Δx – mass of the rotor length unit and step of calculation; other values are clarified in clauses 1 and 2.

Table 3.3 – Constants in the problem of rotor maneuvering in Uranus and Saturn conditions

Planet	R, km	g, m/s ²	m, kg	x ₁	x ₂	x _*	Δx
Uranus	26,200	10.4	100	1.9	3.6	4.6	0.1
Saturn	60,100	9.54	100	3.0	9.0	15.0	0.25

Figure 27 shows the dependence of rotor dynamic characteristics at its motion in Uranus conditions on a non-dimensional radial coordinate x . The position of rings and ten small satellites are designated on the X axis in heavy points (traces of intersection of rings and XOY vertical plane) and in stars (traces of intersection of the same plane and satellite orbits).

The values having a different order are shown in the graphs in a non-dimensional form and special scales, which reduce non-dimensional analogues to the same order. The connection of non-dimensional analogues with true values is clarified in the text under the figures.

Radial acceleration W at the sections $[x_0, x_1]$ and $[x_1, x_2]$ changes under the action of centrifugal and gravity forces, tending to zero in the orbital point x_* ; at the final section $[x_2, x_*]$, it changes the sign under the action of friction force F_{fr} , damping radial speed V and vanishing together with the same in point x_* .

Radial speed V changes intensively only at the initial and final sections; it is almost constant at the central section; its highest value is about 27 km/s.

The rotor height z changes linearly above the equator at the section $[x_0, x_1]$. According to (3.25), the dashed line continues through the orbital point $x_* = \beta$. The angle ψ (figure 27) along with height z decrease quickly to zero values in point x_2 under the action of external dissipative force P introduced at the section $[x_1, x_2]$.

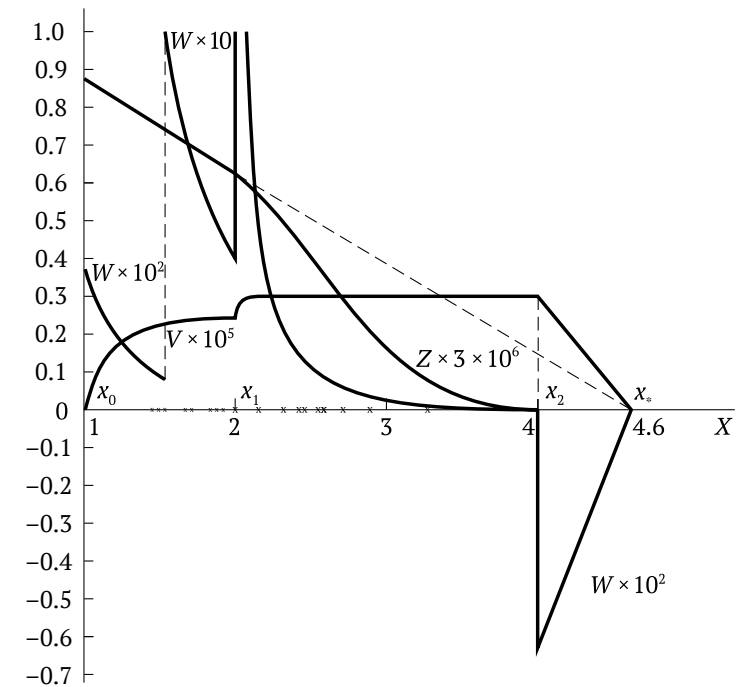


Figure 27 – Diagrams of radial speed V , radial acceleration W and rotor height Z in Uranus conditions

The rotor goes at a sufficiently large height above the location area of rings and small satellites, with the exception of the tenth satellite, whose rotor height above the orbit is about 40 km.

This height is obviously insufficient taking into consideration the satellite size ($d = 165$ km) and possible deviation of its orbit from the equatorial plane. It is possible to improve the position in three ways:

- transfer point x_1 to the right, where force P acts;
- transfer point x_2 to the right, where the rotor lowers to the equatorial plane;
- choose another law of controlled variation for angle ψ and height z instead of (3.28).

Dissipative force $P(x)$ controlling the movement at angle ψ and height z per rotor length unit has the highest values of about 300 N and changes the sign in the position $x = 2.5$. This is obviously a consequence of the desired law (3.28) for angle ψ variation. It is possible that force $P(x)$ will have a constant sign under a different law, monotonously decreasing its values.

Friction dissipative force $F_{fr}(x)$, which is a sum of friction forces equal to the fragment tension force, changes linearly, according to (3.33), taking on large values, in the general case. The reason for it is a very small curvature of rotor elements. Therefore, tension forces directed tangentially in final points of the element have a rather small value of the resultant, which is directed radially and must brake radial motion. In order to decrease value F_{fr} , it is possible to introduce this force from the moment of rotor start in the position x_0 , as well as to use gravity braking (ascent and stepped ejection of capsule parts) and other dissipative forces, including the external ones.

Angular acceleration $\ddot{\psi}$ changes at the section of free rotor expansion $[x_0, x_1]$ from the initial negative value $-1.83 \times 10^{-7} \text{ s}^{-2}$ to the maximal positive value $0.37 \times 10^{-7} \text{ s}^{-2}$ and then starts decreasing. Acceleration $\ddot{\psi}$ jumps taking on negative values and accelerating the rotor plane motion to the equator under the action of dissipative force $P(x)$ in point x_1 . After the change of acceleration sign in point $x = 2.2$, the motion is braked and damped in point x_1 .

The motion time t has intervals, where the speed significantly increases at the beginning of motion and at the end of motion, when it starts decreasing. The time t changes linearly between these intervals depending on radial distance x , which results from almost constant radial speed. The total motion time to reach the orbit in the position $x_* = 4.6$, which corresponds to the radial displacement of 94,000 km, makes 111 min at an average motion speed of 14 km/s.

The rotor motion scheme in Saturn condition is similar, varying by only numerical values of characteristics. For example, the total motion time is 430 min, which exceeds the value specified above by nearly four times, whereas the radial displacement is 840,000 km at an average speed of 32 km/s.

Chapter 4

Problems of creating an accelerator for the UPT rotor

This chapter contains a problem setting on the creation of a combined traction and levitation system (TLS) of UPT enabling the rotor suspension inside the vacuum capsule and its non-contact acceleration up to the cosmic velocity. A more detailed study of these questions is given in the reports [III, IV].

There has been studied a dynamics of rotor acceleration assumed at the first stage as a rigid thin ring, taking into consideration the action of traction forces, which change inversely proportional to the rotor speed. There has been studied a problem setting on rotor motion under the action of a specific type of perturbing factors [VI].

4.1. System of rotor lift to the capsule center

The rotor acceleration relative to the overpass is preceded by the rotor lift or levitation up to the position of a vacuum capsule central line. If we stick to the case of an equatorial UPT location, the lift system must comply with the following main requirements.

1. Rotor levitation must be non-contact, which can be achieved by means of interaction between magnetic fields and electric currents.
2. Levitation must be non-oscillatory, in extreme case – have rapidly damping oscillations. The final position – coaxially in the capsule center, with a gap between a rotor and capsule of about 0.1 m.
3. Force and other parameters of magnetic levitation per 1 m of rotor length must enable overcoming and further balancing of the rotor element weight of the same length. The elastic tension force is eliminated by creating plays in telescopic joints of fragments.
4. In the process of rotor acceleration, the weight of its elements decrease – as a resultant of gravity force and centrifugal force oppositely directed along the radius. Consequently, the magnetic pressure force acting on the rotor must decrease; consequently, a feedback between the rotor linear speed and magnetic pressure force, or between the gap variation and magnetic force is compulsory.

5. At the moment of reaching the first cosmic velocity V_1 , the resultant of traction force and centrifugal force of every rotor element vanishes (zero gravity state), and then, with the speed increase, changes the direction. Similarly, the magnetic pressure force must change its direction, retaining the rotor from expansion. When reaching the design speed $V_0 > V_1$, this force has the value as follows:

$$N = \frac{m_r V_0^2}{R} - m_r g = \frac{m_r}{R} (V_0^2 - V_1^2),$$

where m_r – rotor element mass; R – equator radius; g – gravity acceleration at the equator; $V_1 = (gR)^{1/2}$.

6. After the radial motion start (second stage), the suspension system must support the capsule at the expanding rotor, retaining the gap between them without power supply from external sources.

There are known three types of magnetic levitation system:

- 1) suspension by permanent magnets;
- 2) electromagnetic suspension;
- 3) electrodynamic levitation.

Also, different combinations of these three main types are possible.

Suspension by permanent magnets uses the repulsive force of the magnet like poles. For this purpose, four magnet pairs are installed on the exterior rotor surface and internal capsule surface: two – for vertical levitation and two – for horizontal stabilization.

Characteristics of the existing magnets are insufficient to obtain the parameters required for rotor suspension, taking into consideration their size in respect to the capsule and rotor cross sectional dimensions; particularly, pressure force per rotor mass unit. This drawback is eliminated by the fact that all load of the rotor weight at the motion stage at a speed $V < V_1$ is transferred only to lower magnets; magnetic pressure force from upper magnets is added to gravity force. After reaching speed V_1 , the situation is changed – the main load is transferred to upper magnets. In both cases, the load is taken by a vacuum capsule, whose strength assurance causes a significant increase in its mass. Substantial difficulties are also created by a high specific density of the permanent magnet material and, consequently, their big relative mass.

The use of attractive forces of unlike poles is impossible at all since such a system is fundamentally unstable: the attractive force decreases with the gap increased, and grows with the gap decreased. Either way, this can result in the interruption of a noncontact state. In order to prevent such a situation, it is required to control the magnet force; however, it is impossible for permanent magnets.

Thus, permanent magnets do not always meet the requirements necessary to provide a noncontact rotor suspension inside the capsule at all stages of acceleration and ascent in dense atmosphere.

The developers of high-speed ground magnetic cushion transport have also come to the conclusion on non-feasibility of permanent magnets application, i.e., when solving a more simple technical problem, with a much smaller motion speed and mass parameters. But this does not completely exclude the possibility of using permanent magnets in UPT in the future, since such a suspension is the least energy-consuming.

Electromagnetic suspension is based on the application of attractive forces of electromagnets with ferromagnets. For this purpose, the UPT rotor must contain elements of ferromagnetic material, whereas electromagnets are located on the capsule. It is not feasible to locate electromagnets on the rotor since this causes a problem of power supply to them.

When displacing a ferromagnet in relation to electromagnets, eddy currents arise in it and create a magnetic flow produced by electromagnets. The force arising in this case can be decomposed as a brake force directed against the direction of rotor motion, and a repulsive force directed against the levitating suspension force. The impact of eddy currents can be more significant with the rotor motion speed increased; therefore, the measures to compensate for the specified forces are required. The repulsive force can be compensated by the control system through a significant current increase in electromagnet winding, whereas the brake force can be compensated by an increase in the linear motor traction force.

The use of electromagnetic suspension for the UPT rotor levitation is hindered due to a small gap width and unstable suspension. The magnetic force is increased with the gap decrease, and it is decreased with the gap increase. Thus, as pointed out earlier, the system with attractive forces is unstable; it has a negative elastic coefficient, and it is required to apply a feedback mechanism for its stabilization, which controls the magnet current consuming a significant amount of energy.

Electrodynamic levitation is based on the application of Lenz's rule. According to it, the current induced in the conducting loop by a magnetic field is directed so as to keep a constant magnet flow. The induced current magnetic field is opposite in direction to the external variable magnetic field, thus repulsive forces arise between a magnet and a loop. The system with repulsive forces is resistant to a relative shift since repulsive forces increase with the gap decrease between the system elements.

At a constant magnetic field, the induced current is increased with an increase of the field alternating frequency asymptotically saturated at high frequencies. The saturation is reached, when the magnetic field stops penetrating

into a conductor, whereas the repulsive force also increases with a frequency reaching then a limiting value.

When developing a system with repulsive forces, there arises a problem of energy dissipation as a result of a loop conductor finite conductivity. Similar to inductive heating, this dissipation depends on the field alternating frequency, reaching the maximum at a certain frequency and dropping to zero at high frequencies.

The system with repulsive forces is feasible to be applied in the UPT since it enables the use of superconductive magnets to generate the required magnetic field. A strong magnetic field in great volume is created with the help of such magnets, which has a crucial impact on the entire system structure.

The electrodynamic levitation system in the UPT has a simple scheme. Superconductive magnets are linearly arranged on the rotor moving relative to the capsule, whereas loops of diamagnetic material are placed on the capsule. The created magnetic field is constant relative to the rotor, but variable relative to the capsule and loops. As a result, there arises a repulsive force, which retains the rotor relative to the capsule. However, if the rotor is motionless, the lifting force is zero; therefore, another, steady-state levitation system must act at the beginning of motion.

Electrodynamic levitation has two benefits compared to the levitation with permanent magnets and electromagnetic suspension:

- 1) the gap between magnets and loops can be ten times larger, which is fundamental at high speed;
- 2) a strong magnetic field created in great volume can be used not only for suspension, but also to set the UPT rotor in motion, i.e., combine the mechanisms of suspension and rotor speed-up.

The last fact is especially essential since it dramatically simplifies the whole TLS of the UPT accelerator, reduces the consumption of current-conducting material, energy, etc.

However, there are two problems associated with electrodynamic levitation: the need to provide an additional type of suspension at small speed and cryoprotection of superconducting magnets. The second problem can be solved using high temperature superconductivity.

4.2. Problems of creating a linear electric motor for rotor acceleration to cosmic velocity

An electric motor to set the rotor in motion relative to the overpass must comply with the following major requirements [III].

1. Electric motor power supply is carried out from some power stations connected in parallel, with the same current frequency and the preset total capacity.

2. Electric energy transfer to the rotor is inadmissible during its acceleration.

3. An electric motor must provide an adequate amount of starting force and the required efforts to reach the desired speed of the rotor rotational motion within a reasonable timespan – several days.

4. An electric motor structural scheme provides its multifunctionality.

- 4.1. An electric motor serves as a UPT rotor accelerator.

- 4.2. An electric motor is a part of the rotor electrodynamic levitation system enabling, together with other types of suspension, its noncontact levitation relative to the capsule, including the stage of rotor and capsule motion in dense atmosphere.

- 4.3. After the rotor ascent to orbit, the TLS elements must be used to create energy and, particularly, transport systems within the given industrial ring based on the rotor and between the given and other rings of the space industrial zone.

- 4.4. A TLS must be optimal in terms of energy losses and material consumption.

These diverse requirements can be met by means of rational compromises when solving a multicriteria optimization problem.

Below are briefly considered the peculiarities and possibilities of meeting the specified requirements to the three main types of motor: asynchronous, synchronous and a direct current commutator.

According to the asynchronous motor scheme, a stator, including a core with a polyphase winding, is fixed on the capsule to start the UPT rotor.

Secondary winding, made as a tire of metal with high electrical conductivity or as closed-loop conductors at butt ends, is installed on the rotor.

The force acting on the rotor winding can be generated only in case its motion speed is less than the speed of a magnetic driving force wave. Thus, with the rotor speed increase, the wave speed must increase as well, which can be achieved by increasing the frequency of supply voltage. For this purpose, the synchronization of a large number of frequency convertors working in parallel is rather complicated.

The power of a UPT asynchronous motor is extremely high; a starting current will evoke an unacceptable voltage drop in the network at direct start. In addition, heat energy, equal to the kinetic energy of the driven rotor, is released in the rotor winding at start. Energy release in the primary circuit is normally somewhat greater than in the second one, which can provoke engine overheating. Therefore, a direct start is impossible and a reduced voltage start should be used. The overall engine efficiency is not high, reaching 0.2–0.25.

Requirements 2 and 3 are inaccessible when using an asynchronous motor. There is expressly met only requirement 2 about the elimination of the electric energy transmission to the rotor in a galvanic way.

Thus, the features of the asynchronous motor scheme and operation hardly allow it to be used as a motor for the UPT rotor.

According to the synchronous motor scheme, a polyphase winding is fixed on the capsule for rotor acceleration, and the inductor excitation winding – on the rotor. In this case, the excitation winding is superconductive, operating in the frozen flow mode; therefore, there is no need to transmit electric energy to the rotor after the winding power supply and short-circuiting.

The synchronous motor startability requires frequency adjustment of the current fed to the armature winding from zero to nominal values. However, the adjustment problem, especially in the range of low frequencies, is not solved at present.

On the other hand, the use of a superconductive inductor excitation winding allows abandoning a ferromagnetic core for the armature. Therefore, the windings and conducting elements located on the capsule can be combined so that they could provide, in addition to traction, the functions of an electrodynamic levitation system. In this case, the synchronous motor efficiency is significantly higher. Thus, an essential hindrance when using a synchronous motor for the UPT rotor acceleration is only a problem of starting and adjustment of supply frequency.

The commutator motor scheme is similar to that of a synchronous motor: a superconductive winding of the inductor operating in the frozen flow mode is fixed on the rotor, and the armature winding is fixed on the capsule. The sections of armature winding are fed from the alternating-current mains operating for rectifiers, through a thyristor switch. Its purpose is to switch the sections of armature winding by the signals of special sensors depending on the arrangement of inductor poles. As a result, there arises a traction force of constant direction, which depends on the voltage supplied to the armature winding; this significantly simplifies the problems of rotor starting and speed adjustment. The efficiency of this motor is higher than that of a synchronous one; clauses 1 and 2 on the multifunctionality requirement are also met. It means that, apart from acceleration, it can perform the function of rotor levitation.

The report [IV] gives preference to an asynchronous motor without using superconductivity; however, only as a rotor accelerator in this case. The efficiency of this motor can be made to reach 0.9.

Thus, an electrodynamic levitation system is preferable for the UPT rotor acceleration out of the three magnetic levitation systems and three types of electric motor, with regard to the given above requirements to such systems; and a direct current motor with thyristor switches combining both functions – as

an accelerator. In this case, an efficient operation of levitation and acceleration systems can be possible only if superconductive excitation windings not requiring electric energy supply to the rotor in the course of its motion are used as a source of permanent magnetic field.

The elements of the considered systems designed to lift and accelerate the rotor with the mass of 1–4 mln tons are located on the rotor itself and the vacuum capsule, which is also lifted at the stage of motion in the atmosphere, being a significant drawback of these systems. Such an arrangement of the elements substantially reduces the share of payload lifted by the rotor and increases the capsule mass. Moreover, immense energy consumption is required for the TLS levitation, acceleration and ascent, which will result in the reduction of the overall system efficiency.

This drawback may be eliminated by creating a combined levitation system of the rotor using all three main types specified in clause 4.1. In this case, the basic part of the system must be stationary, i.e., located on the overpass outside the vacuum capsule.

Combining the last requirement and the requirement on the elimination of the possibility for heat losses in the rotor, as well as the requirements to the suspension system in clause 4.1 and the acceleration system in this clause, we will get an ideal rotor TLS. The solution to the arising problems will also find application when creating future advanced systems of the ground superspeed transport.

4.3. Project of the combined rotor acceleration and levitation system

Taking into consideration the peculiarities of rotor motion and TLS operation, the working cycle of rotor acceleration and ascent in the atmosphere together with the capsule is divided into 4 periods [IV].

The first period (starting) is characterized by the rotor speed variation from zero to V' , which is 100–200 m/s. The electrodynamic lifting force is insignificant here, whereas the braking force in the electrodynamic lift system reaches a peak value. Therefore, rotor levitation in the first period must be carried out by means of a traction motor or an auxiliary stationary system, which is preferable. When moving within the specified speed range, the commutator motor control does not present much difficulty.

The second period includes the range of the rotor speed variation from V' to V_1 – the first cosmic velocity, when the rotor becomes weightless. In this case, there takes place gradual shifting from the stationary to the electrodynamic levitation system, which is best subject to adjustment and self-regulation.

The suspension force changes depending on the gap width, disappearing when the rotor reaches the position along the central capsule axis. Considering weight variability of rotor elements as a resultant of centrifugal and gravity forces, the system can be adjusted so that the suspension force will equal to the weight of the elements, disappearing by the end of the period. The engine power output goes mainly to create traction force.

The rotor speed variation in the third period – from speed V_1 to design speed V_0 , which is final for the acceleration stage and initial for the lifting stage. In this case, there takes place a direction change of the resultant of centrifugal and gravity forces: it is now directed upwards on a local vertical for every rotor element. The electrodynamic levitation force must also change the direction to the opposite. The maximal value of this force per rotor length unit is $\frac{V_0^2 - V_1^2}{V_1^2}$

of the weight of the corresponding element of a motionless rotor.

The fourth period is intermediate between the stages of rotor acceleration and motion in outer space. Its main feature is rotor motion in a vacuum capsule through the atmosphere in the mode of elastic expansion. From the moment of separation from the overpass and until the exit from the dense atmosphere at the height of approximately 100 km, the gap between the rotor and the capsule is sustained with the help of a self-sufficient electrodynamic levitation system, without power supply from external sources. The levitation force must be sufficient to overcome capsule inertance at its radial motion, as well as gravity force, atmospheric drag and elastic forces at capsule extension.

The beginning of radial motion depends on the correlation of capsule and rotor masses: the bigger it is, the bigger initial kinetic energy of the rotor for this period must be.

A large capsule mass results in additional power consumption, but allows energy dissipation of the rotor radial motion at the ascent and stepped ejection of its parts.

The choice of a TLS diagram, power, mass and other characteristics must be subject to the accepted laws of rotor motion at the stage of ascent to orbit.

When developing a linear electric motor for the UPT, there was found an ingenious TLS diagram [III], which can be a part of a more comprehensive system providing rotor suspension and acceleration at the acceleration stage, as well as a noncontact accelerated rotor and capsule radial motion in the atmosphere. The main thing in the proposed diagram (figure 28) is the use of superconductive excitation windings (SCEW) 4 installed vertically on rotor 5 in its longitudinal central plane, and discrete coils of electrodynamic levitation 6 on the internal capsule surface 7. Superconductive excitation windings have an elongated shape close to rectangular, and are located along the rotor length in a chain – one by one. Discrete short-circuited levitation coils form two rows

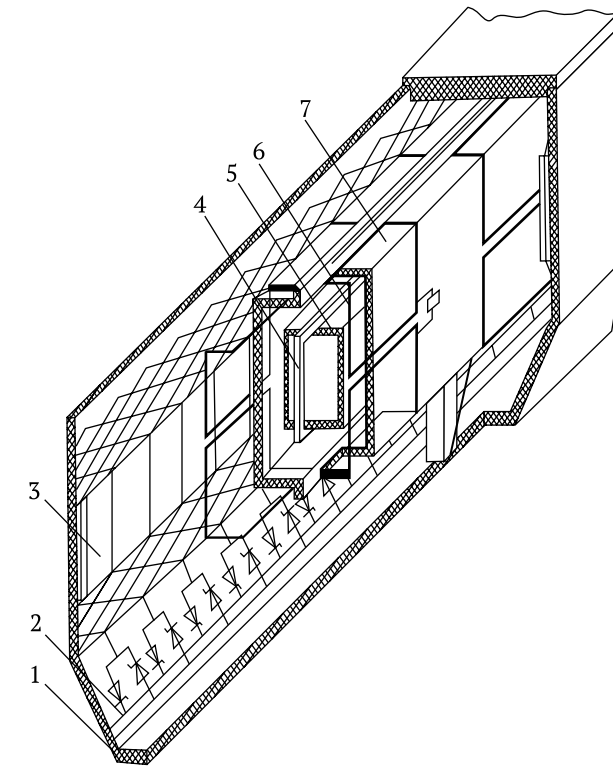


Figure 28 – UPT layout diagram with proposed TLS:
1 – overpass; 2 – feeder line with a commutator; 3 – linear electric motor armature winding;
4 – superconducting excitation winding; 5 – rotor;
6 – short-circuited coils of electrodynamic levitation system; 7 – vacuum capsule

shifted relative to each other in the direction of rotor motion by half of coil wrap pitch. Every coil, in its turn, consists of two loops of an angle section located in a vertical plane one above the other. Upper and lower longitudinal conductors of each coil are bent towards the rotor and located in the plane of superconductive excitation windings.

Stator windings of a double-sided linear direct current electric motor 3 are located on both vertical walls of overpass 1. The winding has a coil structure; the connection of its sections to feeder line 2 is carried out by means of a solid-state switch, whose key elements are uniformly distributed along overpass 1. Thus, the majority of the linear electric motor elements meets the requirement on a stationary state being located on the overpass, which gives a possibility of its multiple use.

The TLS works in the following way. Before the engine start, preparatory operations are made:

- in order to reduce losses at rotor acceleration in a range of small speeds, when braking force in the electrodynamic levitation system reaches its peak, levitation coils are opened;

- superconductive rotor excitation windings are fed with direct current, in which case it is assumed to use high-temperature, within 20–30 °C, superconductive materials in order to eliminate cryostatting of windings;

- including an additional (stationary) levitation system for the noncontact rotor suspension inside the capsule.

The engine is started by means of voltage supply to stator windings. The rotor comes into motion under the action of the emerging electromagnetic traction force. When reaching force V' , the coils of electrodynamic levitation short circuit. Under the impact of a variable magnetic field of moving SCEW, there arise eddy currents, whose value is sufficient to provide further rotor levitation relative to the vacuum capsule. The steady-state suspension system is disconnected.

The feature of the proposed TLS is the creation of the required traction force value and provision of noncontact rotor and capsule interaction at the last three periods of the acceleration and motion in the atmosphere process, in a self-regulation mode:

- the interaction between SCEW and short-circuited coils within a speed range from V' to V_1 , when the rotor has a positive weight, is characterized by repulsion from lower coil loops and attraction to upper ones;

- the rotor moves closer to upper coil loops within a speed range from V_1 to V_0 . In this case, SCEW push away from upper coil loops and are attracted to lower coil loops;

- the grippers keeping the capsule from displacement are released, when the design speed V_0 is reached; when expanding, the rotor makes the capsule move radially, as well. In this case, the suspension system provides a noncontact capsule suspension relative to the rotor.

This multifunctionality of the suspension system is achieved due to the special arrangement of short-circuited coils. The necessary electrical calculations, energy, power, mass and other system parameters are given in [III]. Particularly, it is shown that the electrodynamic levitation force of the proposed structure is zero and the suspension system operates without energy losses, when the circular rotor velocity equals to the first cosmic velocity V_1 , with the rotor being weightless. If the engine and the suspension system get disconnected, the rotor will move for an indefinitely long time, in the absence

of aerodynamic and other losses. The rotor can be used as an effective energy storage unit, for which speed V_1 is required in its stationary position.

4.4. Problem on the UPT rotor acceleration

Let us study the rotor motion at the acceleration stage under very general assumptions concerning its properties, the engine traction force, etc. Let us assume a ring-shaped rod located coaxially inside the vacuum capsule and uniformly loaded with longitudinal traction forces from a linear electric motor section as a physical rotor model. The rotor mass M_r , its radius R – the Earth's equatorial radius, the inertia moment relative to the rotor rotation axis $J_z = M_r R^2$. The principal moment of traction forces relative Z axis:

$$M_z = \Sigma qR = QR,$$

where q – traction force from one engine section; $Q = \Sigma q$ – gross tractive effort.

The rotor motion is considered in relation to two reference systems with the general beginning in the geocenter O . Let us ignore the action of the surrounding celestial bodies – the Sun, the Moon, etc. The point O displacement does not affect the process of rotor acceleration; therefore, let us assume point O to be motionless.

The axes in the $OXYZ$ system are motionless; the Z axis is directed along the Earth's and rotor's rotational axis; the X and Y axes are located in the equatorial plane. The rotor motion relative to this system is absolute.

The X_1, Y_1 axes in the $OX_1Y_1Z_1$ system are also located in the equatorial plane and rotate around the coincident axes Z and Z_1 at an angular velocity ω_e of the Earth. The rotor motion together with this system is transportation, and with regard to it – relative.

Let us consider during the acceleration period the rotor motion in relation to the overpass, stationary with regard to the $OX_1Y_1Z_1$ system, i.e., a relative part of motion. Let us also consider absolute motion at the moment of acceleration end, the beginning of rotor radial motion and its further motion. There exists the following correlation between the speeds of rotor points

$$V_a = V_e + V_r,$$

where V_a – absolute motion; $V_e = \omega_e R = 0.46$ km/s – transfer velocity, and V_r – relative velocity of rotor points. At the moment of acceleration end $V_a = V_0$, where V_0 – initial absolute speed at the stage of rotor ascent to orbit.

Let us assume the electric motor power output W constant at the stage of rotor acceleration; the consumed power $W' = W/K_1$, where K_1 – engine efficiency.

In the general case, only the transmitted power W' is constant, whereas K_1 and W depend on speed V_r of the rotor relative motion. In this case, the functional dependence is determined by the realized engine diagram, levitation system, etc. When studying the rotor dynamics in the acceleration period, let us assume averaged values K_1 and W . The averaged value of gross tractive effort is connected with the rotor speed by the correlation $Q = W/V_r$. At the initial time, when $V_r = 0$ and at some small span $[0, t']$, this formula is inapplicable and is replaced with another one, which has no exceptions. The launch time is eliminated from consideration due to its smallness and, consequently, insignificant variation in rotor speed and displacement.

Let us write down the differential equation of the rotor rotational movement as follows:

$$J_z \frac{d\omega_r}{dt} = M_z,$$

where $\omega_r = V_r/R$ – relative rotor angular velocity. After simplifications, we will get:

$$M_r = \frac{dV_r}{dt} = Q = \frac{W}{V_r}. \quad (4.1)$$

As a result of integration, let us find the dependence of the relative rotor speed on movement time:

$$V_r = \left(\frac{2Wt}{M_r} \right)^{1/2}. \quad (4.2)$$

Let us assume that acceleration time $t = 5$ days, final absolute speed $V_a = 10$ km/s, consequently, $V_r = V_a - V_e = 9.54$ km/s, rotor mass $M_r = 2 \times 10^9$ kg at mass per unit length of 50 kg/m. Based on (4.2), let us find the required power output $W = M_r V_r^2 / 2t = 211$ mln kW.

Let us take $K_1 = 0.5$ as efficiency, whereas total power $W' = 422$ mln kW, exceeding the power of the Energia carrier rocket by just 3.5 times. However, the specific power per ton of payload to be lifted is 211 kW/t, whereas the same parameter for the Energia is 1.2×10^6 kW/t, i.e., by approximately 6,000 times more. None of the cargo lifting systems in space that are used or developed at present do not have such a low value of specific power as the UPT system.

Representing V_r as a ds/dt derivative, where s – an arc coordinate of some characteristic rotor point, and integrating (4.2), let us find the law of rotor motion along the overpass at the acceleration stage:

$$s = \frac{2}{3} \left(\frac{2W}{M_r} \right)^{1/2} t^{3/2}. \quad (4.3)$$

The tangential acceleration of rotor points:

$$w_\tau = \frac{dV_r}{dt} = \frac{1}{2} \left(\frac{2W}{M_r} \right)^{1/2} t^{-1/2}, \quad (4.4)$$

except for t values belonging to a small span $[0, t']$ of electric motor start.

In the normal projection, the correlation for the rotor element with unit length and the corresponding mass m is written as follows:

$$\frac{mV_a^2}{\rho} = mg - N,$$

where ρ – the trajectory curve radius; N – the suspension system magnetic pressure. For undisturbed motion, $\rho = R$, then

$$N = m \left(g - \frac{V_a^2}{R} \right).$$

This is magnetic levitation force per 1 m of rotor length. It changes to zero depending on the element weight mg_1 at the beginning of acceleration ($g_1 = g - \frac{V_e^2}{R}$ – free fall acceleration at the equator), when $V_a = V_1 = (gR)^{1/2}$, then it changes the sign and reaches the value $m \left(\frac{V_0^2}{R} - g \right)$ at the end of the ac-

celeration stage. This value is less than the rotor element weight at the interval of its absolute speed variation $[V_1, V_2]$, where $V_2 = (2gR)^{1/2}$ – the second cosmic velocity. At the time of reaching V_2 , the N effort takes on the value equal to the element gravity force, directed downwards though. The N value can exceed the rotor element weight by several times at the overpass sections, where $R_{cr} < R$ under conditions of local terrain.

4.5. Dynamics of rotor disturbed motion upon violations of the acceleration system operation

At an immense overpass length and during a long period of acceleration – several days – there can arise various emergency situations in the acceleration

system, deflecting the process of rotor acceleration from the nominal mode. These include the following: failure of one or several units at one of power stations supplying energy to some section of the acceleration system; failure of the entire power station or its power supply system; operational disorders of the acceleration system leading to power loss at some section, etc. Such failures may not cause serious disturbances, changing only general characteristics of rotor motion – acceleration, velocity, speedup time. However, irreversible consequences can be caused at higher-level violations. The most serious of them include the rotor touching of the capsule, a dangerous level of rotor longitudinal oscillations, occurrence of resonance, etc. and can result in the UPT system destruction.

There arises a problem of identification of all potential deviations from the normal mode, a variety of their combinations, detection of the level of exposure on the rotor acceleration process, determination of the limits of permissible variations not causing serious implications, as well as the measures aimed at the elimination of deviations outside such limits.

A large group of violations results in power change at some section ΔL of a linear electric motor and, consequently, change in traction effort at this section. Non-uniformity of power action will primarily have an impact on local (in terms of location and time) variations of acceleration and speed of rotor parts passing section ΔL . The consequence of these variations will be longitudinal oscillations in rotor design.

In order to study such oscillations, let us use a discrete rotor model in the form of system n of material points with equal mass m closed in a ring shape and connected with viscoelastic bonds. Let us introduce potential energy of elastic bonds:

$$P(u_i) = \frac{C}{2} \sum_{i=1}^n (u_i - u_{i+1})^2, \quad (4.5)$$

where C – rigidity of bonds; $u_i(t)$ – deviation of the i^{th} point from its position in the rotor taken as a rigid ring, at its nominal acceleration mode described by equation (4.1) and dependences (4.2)–(4.4) correspondingly for the rotor speed, displacement and acceleration. In this case, the condition of ring closure is fulfilled $u_{n+1} = u_1$.

When determining the equivalent rigidity of each coupling spring, let us use correlation [15]:

$$C = \frac{nEF}{L},$$

where E – the average elasticity modulus of rotor material; F – its cross section area; L/n – length of the section between two neighbouring points; L – rotor length.

Elastic force acting on the i^{th} point:

$$F_i = -\frac{\partial P}{\partial u_i} = -C(2u_i - u_{i-1} - u_{i+1}). \quad (4.6)$$

Similar to (4.5), a Rayleigh dissipative function [2] is introduced:

$$R(\dot{u}_i) = \frac{\lambda}{2} \sum_{i=1}^n (\dot{u}_i - \dot{u}_{i+1})^2,$$

where λ – viscosity coefficient of rotor material; $\dot{u}_i = \frac{du_i}{dt}$ – speed of the i^{th} point disturbed motion. The dissipative force

$$R_i = -\frac{\partial R(\dot{u}_i)}{\partial \dot{u}_i} = -\lambda(2\dot{u}_i - \dot{u}_{i-1} - \dot{u}_{i+1}).$$

Let us assume that $\pm \Delta W_1$ – deviation of linear electric motor power at the section ΔL_1 (figure 29). Index 1 is introduced as there can be several sections of this type arising successively with the course of time, ΔL_1 being the first of them. The location of this section is determined by an arc coordinate S , counted along the overpass from some characteristic point O' taken as a reference point, suppose a point of intersection between an overpass and a zero meridian, to the beginning of section ΔL_1 . Let us assume that t_1 – moment of time counted from the beginning of rotor motion when the mode was disturbed;

$V_{r1} = \left(\frac{2W}{M_r} t_1 \right)^{1/2}$ – average speed of rotor points at this moment. If the i^{th} rotor point is above section ΔL_1 at the moment t_1 , then the time $\Delta t_{1,i}$ of its motion above the section is determined with the help of dependence (4.3):

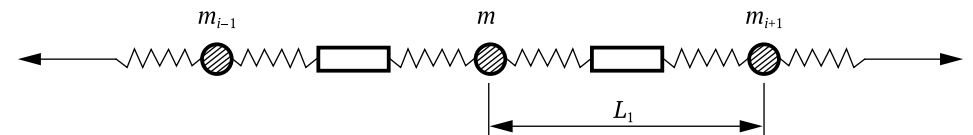


Figure 29 – Discrete viscoelastic rotor model

$$\Delta t_{1,i} = \left[t_1^{3/2} + \frac{3}{2} \left(\frac{M_r}{2P} \right)^{1/2} \Delta L_1 \right]^{2/3} - t_1. \quad (4.7)$$

The disturbance force at this time span

$$\Delta Q_{1,i} = \pm \frac{\Delta W_1}{V_{r1}}$$

acts on the i^{th} point. For greater accuracy, it is possible to substitute an average value of rotor speed during this period in the denominator:

$$V'_{r1} = [V_r(t_1) + V_r(t_1 + \Delta t_{1,i})].$$

The following moments of time when the i^{th} point approaches section ΔL_1 are determined based on the condition: $S(t_{k,i}) - S(t_1) = (k-1)L$, $k = 2, 3, \dots$. Herefrom we will get an expression for the k^{th} moment of contact between the i^{th} point and section ΔL_1 :

$$t_{k,i} = \left[t_1^{3/2} + \frac{3}{2} \left(\frac{M_r}{2W} \right)^{1/2} (k-1)L \right]^{2/3}, \quad k = 1, 2, 3, \dots \quad (4.8)$$

The length of such contact

$$\Delta t_{k,i} = \left[t_{k,i}^{3/2} + \frac{3}{2} \left(\frac{M_r}{2W} \right)^{1/2} \Delta L_1 \right]^{2/3} - t_{k,i}, \quad k = 1, 2, 3, \dots \quad (4.9)$$

Due to the fact that the rotor speed grows, the values $\Delta t_{k,i}$ decrease; the module of disturbing action $|\Delta Q_{k,i}| = \frac{\Delta W_1}{V_r(t_{k,i})}$ decreases, as well. It follows therefrom that the disturbing action of local power deviation ΔW_1 on the rotor decreases with the course of time; the graph of disturbing action is shown in figure 30.

The first contact of the $i+1^{\text{th}}$ point with section ΔL_1 takes place with a shift in time determined by the distance L/n between the points:

$$t_{1,i+1} = \left[t_1^{3/2} + \frac{3}{2} \left(\frac{M_r}{2W} \right)^{1/2} \frac{L}{n} \right]^{2/3}. \quad (4.10)$$

Taking into consideration (4.10), the following moments of the $i+1^{\text{th}}$ point approach to section ΔL_1 and length of the contact are determined similarly to (4.8) and (4.9), where $t_{1,i+1}$ and $t_{k,i+1}$ should be substituted instead of t_1 and $t_{k,i}$.

The formulae (4.7)–(4.10) used the initial, unperturbed value of actual output W , with regard to the smallness of value ΔW_1 compared to W . A more accurate value of actual output $W_1 \pm \Delta W_1$.

A picture of disturbances abruptly gets more complicated if several violations of the acceleration mode take place: $\pm \Delta W_j$ at sections ΔL_j , at the moments of time t_j , $j = 1, 2, \dots$. Disregarding a similar situation, let us write out an equation of disturbed motion of a discrete viscoelastic rotor model in case of one disturbance $\pm \Delta W_1$. Taking into consideration the expression (4.6) for elastic and dissipative forces, we will derive after some transformations as follows:

$$m\ddot{u}_i + \lambda(2\dot{u}_i - \dot{u}_{i-1} - \dot{u}_{i+1}) + C(2u_i - u_{i-1} - u_{i+1}) = \pm \Delta Q_{k,i};$$

$$\Delta Q_{k,i} = \frac{\Delta W_1 M_r^{1/2}}{(2W_1)^{1/2} \left[t_1^{3/2} + \frac{3}{2} \left(\frac{M_r}{2W_1} \right)^{1/2} (k-1)L \right]^{3/2}} \quad (4.11)$$

at the time interval of another k^{th} contact between the i^{th} point and section ΔL_1 : $[t_{k,i}, t_{k,i} + \Delta t_{k,i}]$ and $\Delta Q_{k,i} \equiv 0$ at the rest of the time interval till the moment $t_{k+1,i}$ of the next approach of the i^{th} point to the disturbance section.

The initial conditions of the problem

$$u_i(t_1) = \dot{u}_i(t_1) = 0, \quad i = 1, 2, 3, \dots$$

The integration of equations (4.11) is carried out till the moment t , when the value of relative speed $V_r = V_0 - V_e$ is reached. These equations are represented as a rather lengthy system of linear nonhomogeneous differential equations with constant coefficients and almost periodic right parts of impulse character with a decreasing intensity and duration of action. The solution to these equations is not given here.

A scheme of disturbed motion of a discrete viscoelastic rotor model is represented as follows. In the rotor part, which passes above the disturbance section ΔL_1 , there arise forced longitudinal damped oscillations of points relative to the rigid rotor basis moving under the laws (4.2)–(4.3) of undisturbed motion. In a particular case, it can also be an aperiodic damped motion of points relative to the basis. The rotor parts neighboring to the disturbance section are under

its disturbing action. Disturbances in more remote parts damp to their total disappearance. The intensity of disturbances decreases as the rotor speed increases, since the disturbing action and the duration of its exposure on separate rotor parts decrease.

In this case, some analogy with tsunami waves is possible, when a wave of greatest intensity moves along an undisturbed surface; it is followed by waves of decreasing intensity until their total attenuation. There can also be drawn an analogy with a single soliton wave.

The cases, when a value of local deviations exceeds a critical value, where irreversible phenomena take place – yielding of rotor material or its destruction – pose a threat. It is required to study the cases, when the rate of rise in deviations exceeds the sonic speed of rotor material and the interaction has a shock character.

Given there are several disturbance sections $\Delta L_1, \Delta L_2, \dots$ a resonance effect is also possible, when the frequency of separately safe disturbances coincides with the rotor natural vibration frequencies, as a result of which the amplitude of oscillation increases. It is also necessary to take into account that such parameters as the mass of separate parts, their rigidity, viscosity coefficients, strength properties, etc. in a real rotor are different in the general case.

The main research objective for the equation system (4.11) is to determine the character of disturbed motion, maximum deviations, deviation rates, permissible values of disturbing actions, conditions for changing the motion mode, conditions for resonance occurrence, etc. In the presence of several disturbances, the task becomes much more complicated.

Preventive actions or measures aimed at reliable liquidation of any type of deviations from the TLS nominal operation conditions are of crucial significance.

4.6. Other possible disturbances of rotor motion when accelerating

Apart from the analyzed disturbances related to the operation of technical and energetic parts of the UPT system, disturbances of natural origin are also possible – large-scale changes of surface relief – mountain groups, plateau, etc., as well as earthquakes, storms, tsunami, whose nature is impossible to change, much less to prevent.

When the overpass is located on the sections with significant changes of surface relief, the major disturbing factor is the modification of the track curve radius. The most adverse cases include those, where the curvature sign is changed or the curve radius is decreased, with the curvature sign being constant. The first

case must be excluded, since the centrifugal force of rotor elements acts in the same direction as the attractive force. Therefore, it does not tear away these elements but presses them to the overpass. In the second case, there must be no corner points in junction places of sections and various curve radii.

In case the track runs through a mountain range or a plateau, this can be achieved according to the scheme shown in figure 30. Here, AB is a track section along the equator with a curve radius R ; BC is a section with a variable curve radius ρ_k from R to $\rho_1 < R$, smoothly mating with sections AB and CD ; CD is a section with a constant curve radius ρ_1 ; further follows section DE with a variable radius $\rho_1 \leq \rho_k \leq R$ and the equatorial section EF with smooth junctions in points D and E .

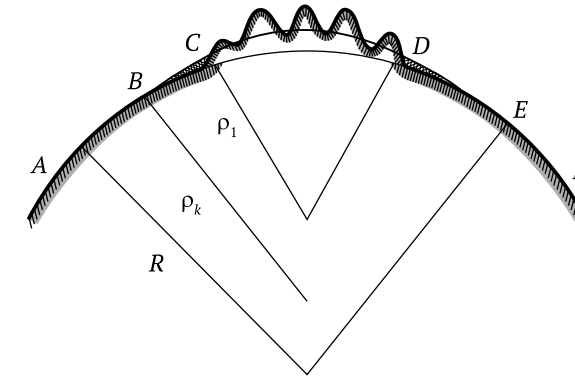


Figure 30 – UPT overpass track in a mountain area.
Original relief – dashes; embankments – double dashes.
Smooth junction of sections and curve radii R, ρ (variable) and ρ_1 , in points B, C, D, E

The track in a mountain area CD runs along the canyon lying through the ridges. The extracted earth's formations are used to build embankments through the gorges at sections BC and DE . This track is more economical compared to the one that would have a constant curve radius R everywhere, since the canyon depth is less in the first case than in the second case.

Let us consider a rotor element moving at the section $BCDE$ with a curve radius different from R . Let us assume that m is a mass of this element; mg is attractive force directed to the Earth's center along the local equator radius R ; q_{el} – electric motor traction force acting on this element; N – levitation force from the suspension system.

In the absence of corner points, the differential motion equation of the considered element in the projection on the tangent to the trajectory looks as follows:

$$m \frac{dV_r}{dt} = q \pm mg \sin \alpha, \quad (4.12)$$

where α – an angle between a tangent to the trajectory and the corresponding tangent to the equator line, equal to the angle between a local curve radius ρ_k and equator radius R . This angle is very small, therefore it can be written as $\sin \alpha = \alpha$; a negative sign is assumed at section BC_1 ; a positive sign – at section C_1E , where C_1 – an average point of section CD . The rotor element here rides in a slightly sloping hill, then rides down.

If equation (4.12) is summed up over all rotor elements, we will get an undisturbed rotor motion equation (4.1), where $M_r = \sum m$, $Q = \sum q$.

A disturbed motion equation for a viscoelastic discrete rotor model looks as (4.11). The disturbance force $\pm mq \sin \alpha$ changing the sign in point C_1 should be put in the right part here. The disturbed motion, as in the previous case, represents longitudinal damped oscillations or an aperiodic mode of motion sort of a solitary wave.

In the normal projection to the trajectory coinciding with the direction of a local curve radius, we will get a formula of levitation force N :

$$N = m \left(g \cos \alpha - \frac{V_a^2}{\rho} \right), \quad V_a \leq V^* < V_1,$$

where $V^* = (g\rho_k \cos \alpha)^{1/2}$ – absolute speed, where N goes to zero. In the interval of speed variation $V^* \leq V_a \leq V_0$ force N changes the direction and is determined by the formula below:

$$N = m \left(\frac{V_a^2}{\rho_k} - q \cos \alpha \right).$$

In this interval, force N can take the values exceeding the element weight. Let us assume that the maximal permissible value N at section BE exceeds gravity force by five times, whereas the obtained correlation for the smallest curve radius at section BE is as follows:

$$\rho_1 \geq \frac{V_0^2}{g(5 + \cos \alpha)}.$$

If $V_0 = 10$ km/s and $\cos \alpha = 1$, then $\rho_1 \geq 1,610$ km. The suspension system at section BE with a variable curve radius must provide levitation force at all stages of rotor acceleration.

In the general case, the distortion of an overpass shape relative to the equatorial plane is possible: the overpass can go beyond this plane at separate sections, going round especially large obstacles (mountains, plateau, major cities, etc.) and coming then back to this plane again. In the absence of corner points, the right part of equation (4.12) contains only accelerating force q_{el} of a linear electric motor, that is, there is no rotational rotor disturbance.

The side pressure of magnetic levitation, which should be provided in this case:

$$N_{side} = mV_r^2 / \rho_2,$$

where ρ_2 – overpass curve radius in the plan. If $\max N_{\text{бок}} = 5mg$, then $\rho_2 \geq 2,100$.

Similar overpass distortions are possible at sea sections in case of a storm. The overpass fixed with flexible links can distort in the plan under the action of lateral wind of constant direction and waves. If this is the case, the accelerating rotor plays a stabilizing role: similar to a water flow in a rubber hose, it rectifies the distorted overpass sections. This process must take place without any contact between the rotor and the capsule; therefore, it is required to envisage a mechanism of creating noncontact side pressure on the rotor from the overpass, or to take measures preventing an overpass distortion at sea sections under the action of natural factors.

Constant distorted overpass sections both in the equatorial plane (vertical distortions) and outside it (horizontal distortions) create disturbances not only rotor acceleration, but also at the ascent to the orbit. The rotor will behave as a stretched string having at the initial moment local deviations from the shape, where the string energy is minimal. As is known, such a string makes oscillations.

In addition to the rotational and radial movement (undisturbed motion), the rotor in this case makes complicated longitudinal and transverse vibrations (disturbed motion). Oscillation damping is encouraged by the growing rotor and capsule tensioning at their expansion, atmospheric drag, and after the capsule ejection – rotor fragmentation and the action of dissipative forces. There arises a problem related to the creation of the system capable of providing a noncontact rotor and capsule interaction without an outside power supply at their spatial vibrations.

The problem is simpler, when there exist only vertical track distortions; then transverse vibrations of the system are also made in the equatorial and rotor plane, and the noncontact interaction is provided by the levitation system at the acceleration stage.

The sections with vertical distortion, where the rotor lifting force is greater than on the equator line, can be used to lift into space out-of-gauge cargo

suspended on the capsule – passenger modules, individual units, assemblies, installations for space industry and power industry, scientific equipment.

Seismic impact is highly dangerous in the period of rotor acceleration, as it can cause overpass distortions and breakage; therefore, the development of an overpass design with a high level of seismic resistance gains in importance. In order to prevent time coincidence between the UPT rotor acceleration process and the Earth's seismic activity in the regions adjacent to the track, reliable methods of earthquake prediction will be instrumental.

The TLS power and energy characteristics for the UPT with a superconductive excitation winding with the rotor speed changing to the values $V_0 > V_1$, the mass per unit length 100 kg/m, the cross-section dimension 0.3 m and the consumed power 10 kW/m, calculated in [III] suggest the feasibility of such a technical solution. It can become a reality however only on the condition of creating superconductors, which would be at the level of modern low-temperature superconductors in terms of electrophysical, weight and cost parameters.

Nevertheless, there still arise many issues on the TLS implementation in this case – increasing engine efficiency, UPT reliable and sustainable energy supply when accelerating the rotor, resistance of the system infrastructure to natural factors, environmentally safe return of TLS parts to establish energy and transport structures, etc. in space.

The work on the UPT project issues is relevant from the earth's perspective, too. Apart from achieving the main objective – creation of the means of non-rocket space exploration – in the course of technical implementation of the idea of noncontact suspension and rotor traction, there can be obtained fundamentally new, highly economical, ecologically clean technologies raising power energy and high-speed ground transport to a qualitatively new level.

The issues related to the UPT rotor motion at the acceleration and ascent stages together with the capsule in the atmosphere, are not the easy ones. The key difficulties consist in detecting potential disturbing actions, their thorough classification, studying their sources and nature, identifying the level of impact on rotor motion and control measures to fight it.

Chapter 5

Parameter estimation of the aerodynamic heating process for the UPT rotor in the absence of protective capsule

To this point, there has been considered a case, when the rotor at the stages of acceleration and ascent in the dense atmosphere was in the vacuum inside the protective capsule, which is a complex engineering structure, providing:

- reliable tightness of the internal capsule space on the condition of its constant deformation – extension, bending, torsion;
- high strength at minimal mass;
- noncontact rotor position relative to the internal capsule surface and magnetic levitation components installed on it;
- location of compact power supply and control systems.

The complexity of the comprehensive solution to all these issues makes look for another option for the UPT project, when the rotor ascent from the planet surface through the dense atmosphere is carried out without a protective capsule. In this case, however, new challenges arise; one of them is aerodynamic heating of the rotor moving in the atmosphere at a speed of about 10 km/s.

5.1. Investigation results on aerodynamic machinery heating. Review

The UPT rotor Mach number at a speed of about 10^4 m/s at the starting moment is about thirty, this value being rather high. The known currently operating aviation equipment and rocketry, artillery shells, etc. have the speed in the dense atmosphere limited by the Mach number from above, equal to several units. A characteristic feature of the system operation in such conditions is a sharp rise in aerodynamic drag and significant aerodynamic heating. These factors increase manifold at cosmic travel speed, for example for re-entering bodies, which requires taking actions on their preservation.

Overcoming an aerodynamic drag is not an issue for the UPT rotor since there is no face part in fact. However, possible technological projections protruding beyond the boundary layer can be a source of significant aerodynamic resistance up to 10^7 – 10^8 Pa and result in shock waves of high intensity. For this reason, technological projections on the installation surface must be minimal.

For the considered UPT system option without a protective vacuum capsule, the more important is an issue of the surface aerodynamic heating [1, 12], which is caused by the surface viscous friction on the air and its compression on face parts; and in the UPT case – on technological projections. Here, the air temperature can reach the values close to the braking temperature:

$$T_{brak} = T_{\infty} \left(1 + \frac{\gamma - 1}{2} M^2 \right), \quad (5.1)$$

where T_{∞} – free-stream temperature; M – Mach number; γ – specific air heat ratio at constant pressure and volume.

In terms of the UPT, in compliance with (5.1), the braking temperature is about 27,500 °K. The temperature of the projected part is somewhat lower due to the heat exchange with the environment and neighboring structure elements.

When considering questions of the structural aerodynamic heating in the literature, the availability of the installation face part is generally envisaged. The density of the supplied heat flow q_h is estimated by formula [16]:

$$q_h = C_* \rho_a^n V^m,$$

where ρ_a – air density; V – free-stream velocity; n , m – indices of power; C_* – the coefficient, which depends on many factors, including on the local angle of attack of the selected point on the streamlined surface.

In terms of the calculation of aerodynamic heating parameters for the UPT rotor having no face part, it is problematic to directly use the known results. This is also related to the fact that aerodynamic machinery normally has the maximal speed in less dense atmosphere, whereas the UPT rotor, in contrast, reaches the maximal speed in more dense atmosphere.

Transatmospheric vehicles (TAV) [16, 17] are a close analogue. The maximal steady-state temperature in the critical point and at the wing leading edge can reach 3,000–4,000 °K at the ascent of this vehicle. These parts of the vehicle probably need an active thermal protection, for example, by means of sublimated covers. The expected temperature at the vehicle descent is approximately 1,500 °K lower.

The maximal temperature on the center line of this vehicle from upwind is 1,300–1,500 °K, when both lifting and lowering; therefore, a greater part of the TAV surface can efficiently cool down by means of radiation.

The aerodynamic drag at the speed of 7.2 km/s at the height of 75 km will make about $10^4 \div 10^5$ Pa, whereas a thermal flow supplied to the TAV surface is $10^3 \div 10^4$ kW/m². Please note that the thermal flow supplied to the surface of reusable space vehicles (RSV) has a value of the same order of magnitude [13].

Obviously, the represented data cannot be directly transferred to the UPT rotor case, however give an idea of the expected values of temperatures and thermal flows on the rotor surface and allow us to estimate the results obtained in the following sections specifically for the UPT.

Let us point out two possible directions of the aerospace machinery thermal protection. The first one is the use of heat-resistant coatings [17]; in this case, a mechanism of radiation heat exchange with the environment is implemented. The second direction is based on the use of sublimated, melting and other special coatings, whose protective effect is related to their mass removal [1, 12, 20]. It appears that a combined use of sublimated coatings formed on the capsules of heat-resistant materials is permissible.

With the space vehicle moving in the atmosphere, there also arises a problem of protecting its surfaces at a high temperature against the interaction with atomic oxygen. Perfluoro polymers of a teflon type and siloxane polymers are least active at their interaction with atomic oxygen [7]. Teflon can be used as material for sublimated coating.

5.2. Problem setting

Let us consider a non-stationary problem on air heating due to viscous friction in order to make a quantitative estimation of the temperature field in the UPT rotor vicinity at the initial launch stage, which is most unfavorable from the perspective of structural heating. A precise problem statement and its solving are problematic; however, in order to obtain simplest estimations, let us assume an approximate approach based on a range of simplifying assumptions.

1. At the launch time, the rotor having as a result of acceleration the maximal speed in the vacuum inside the protective capsule, instantly contacts with the static air.

2. Let us neglect aerodynamic and other effects related to the practically instant capsule depressurization.

3. Let us neglect the impact of the rotor speed radial component on aerodynamic and thermophysical processes occurring in its vicinity.

4. The value of the tangent to the rotor velocity component practically does not change at the studied time intervals.

5. The air flow in the rotor vicinity is laminar and one-dimensional; here, only the air particle velocity component directed along the rotor central line distincts from zero.

6. Let us neglect the curvature of the rotor central line compared to the curvature of its cross-section area. Thus, aerodynamic and thermophysical processes in the vicinity of the rotor surface are similar to the processes in the vicinity of the surface of the infinitely long cylinder when it moves along its axis.

7. Slipping of air particles on the rotor surface is ignored.

8. Aerodynamic and thermophysical air characteristics are constant. Their numerical values correspond to some average temperature.

9. Let us neglect heat transfer inside the rotor from its surface.

10. The heated air does not radiate energy and does not absorb radiation coming from the rotor surface.

11. Considering air heating in the vicinity of the rotor surface, let us neglect the process of air ionization and chemical reactions proceeding in this case.

12. The process of possible sublimation of the protective cover has little effect on hydrodynamic processes nearby the rotor surface.

13. The temperature on the rotor surface, in case of a sublimated coating, is assumed to be constant and equal to the temperature of the phase transition.

Further simplifying assumptions are introduced as may be necessary.

The proposed system of assumptions allows us to build a rather simplified model of the expected hydrodynamic and thermophysical processes; therefore, the results obtained below should be considered as evaluative only.

Let us introduce a cylindrical coordinate system shown in figure 31, directing the Z axis along the rotor axis. Taking into consideration the assumptions above, the distribution of air velocity v_{air} and its temperature T in the vicinity of the rotor surface is described by a system of equations following from the general provisions of hydrodynamics and the convective heat transfer theory [8, 22] (from now on, the index *air* with air velocity is omitted):

$$\rho \frac{\partial v}{\partial t} = \frac{1}{r} \frac{\partial}{\partial r} \left(\mu r \frac{\partial v}{\partial r} \right); \quad (5.2)$$

$$\rho C_t \frac{\partial T}{\partial t} = \frac{1}{r} \frac{\partial}{\partial r} \left(\lambda r \frac{\partial T}{\partial r} \right) + \mu \left(\frac{\partial v}{\partial r} \right)^2, \quad (5.3)$$

where ρ – density; μ – coefficient of dynamic viscosity; C_t – specific heat capacity; λ – air thermal conductivity; t – time; r – radial coordinate. The given equations are written under an additional assumption on axial symmetry of the velocity field and temperature, as well as the assumption on the independence of the basic features of the process on Z coordinate. It is also assumed that the air pressure is constant. Thus, variables v and T are the functions of time t and radial coordinate r . The equation (5.3) describes a convective non-stationary heat transfer with regard to the mechanical energy dissipation.

The boundary and initial conditions of the considered problem take the form as follows:

$$r = R; \quad v = V; \quad T = T_w = T_s; \quad (5.4)$$

$$\lambda \frac{\partial T}{\partial r} = \varepsilon \sigma (T_w^4 - T_\infty^4) + JL; \quad (5.5)$$

$$r \rightarrow \infty; \quad v = 0; \quad T = T_\infty; \quad (5.6)$$

$$t = 0; \quad v = 0; \quad T = T_\infty; \quad (5.7)$$

$$R_r = R_{r0}. \quad (5.8)$$

Here R_{r0} , R_r – the initial and current radius of the rotor cross-section area; T_w – the temperature of rotor surface; T_∞ – ambient temperature in unperturbed state; L – specific heat of a phase transition (for example, sublimation) on the rotor surface; J – density of mass flow discharged from the rotor surface;

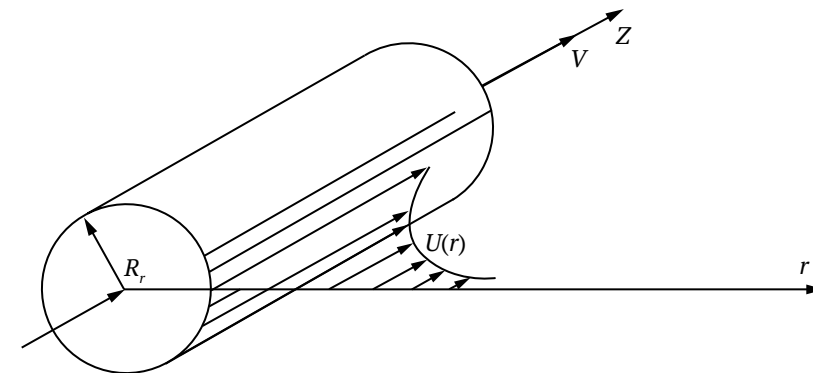


Figure 31 – Rotor design diagram

ε – total emissivity of the rotor surface; $\sigma = 5,67 \times 10^{-8} \text{ W}/(\text{m}^2\text{K}^4)$ – Stefan – Boltzmann constant; T_s – phase transition temperature; V_z – axial component of rotor speed.

Let us introduce another equation for the protective cover evaporation dynamics, within a quasi-stationary approximation:

$$\frac{dR_r}{dt} = -\frac{J}{\rho_w},$$

where ρ_w – density of coating material.

5.3. Approximate calculation of air flow parameters in the rotor surface vicinity

The equation (5.2) describing the distribution of air velocity in the rotor surface vicinity can be considered independent of (5.3).

If we apply the Laplace transformation to (5.2), we will get a differential Bessel's equation relative to the image $\tilde{v}(s, r)$ of the required function $v(t, r)$. The solution to this equation under the boundary conditions (5.4), (5.6) after their transition to the image area looks as follows:

$$\tilde{v}(s, r) = \frac{V}{s} \frac{K_0(r\beta)}{K_0(R\beta)}, \quad (5.9)$$

where $K_0(\xi)$ – Macdonald function; $\beta = \left(\frac{\rho s}{\mu}\right)^{1/2}$.

Let us use a famous Macdonald function behavior estimation, according to which under large values of the argument $\xi \gg 1$, it decreases by the exponential rule [30]. In this case, the solution (5.9) in the first approximation can be presented as follows:

$$\tilde{v}(s, r) = \frac{V}{s} \left(\frac{R_r}{r}\right)^{1/2} \exp[-(r - R_r)\beta]. \quad (5.10)$$

If we apply the inverse Laplace transformation to (5.10), we will get:

$$v(t, r) = V \left(\frac{R_r}{r}\right)^{1/2} \operatorname{erfc}\left[\frac{-(r - R_r)}{2} \left(\frac{\rho}{\mu t}\right)^{1/2}\right], \quad (5.11)$$

where

$$\operatorname{erfc}(\xi) = 1 - \frac{2}{\sqrt{\pi}} \int_0^{\xi} \exp(-\eta^2) d\eta$$

complementary Gauss error function [30].

Based on the derived solution it follows that the air is captured by the rotor and is propelled in the entire external environment up until the infinity. Here, the air velocity decreases quickly as it moves away from the rotor central line; therefore, it is permissible to be restricted to the final area of radius $r_{0\infty}$ when carrying out specific calculations. We assume that $r_{0\infty}$ is a radius of capture, where the air velocity $v(t, r_{0\infty})$ makes the given in advance part ε_1 of the axial component of rotor speed V_z .

Under this approach, the radius of the preferential air flow area represents a solution to the equation

$$\varepsilon_1 = \left(\frac{R_r}{r_{0\infty}}\right)^{1/2} \operatorname{erfc}\left[\frac{r_{0\infty} - R_r}{2} \left(\frac{\rho}{\mu t}\right)^{1/2}\right],$$

where the radius $r_{0\infty}$ changes with the course of time and characterizes a conventional border of the non-stationary boundary layer formed on the external rotor surface.

Let us the following value as the upper estimate for $r_{0\infty}$

$$r_{\infty}(t) = R_r + 2\varepsilon_2 \left(\frac{\mu t}{\rho}\right)^{1/2},$$

where ε_2 – argument of Gauss error function, where it takes on value ε_1 .

It should be considered here that for any arbitrary time with other parameters being equal

$$r_{0\infty}(t) < r_{\infty}(t).$$

Table 5.1 gives an idea on the radius of the air flow area r_{∞} and its time variation. The table shows two predetermined values of sound speed $v(t, r_{\infty})$: 340.3 m/s ($\varepsilon_1 = 0.034$, $\varepsilon_2 = 1.49$) and a practically zero one in terms of aerospace speed scale 2.36 m/s ($\varepsilon_1 = 0.000236$, $\varepsilon_2 = 2.6$). The calculations were carried out at $R_r = 0.05$ m and air parameters $\mu = 13.9 \times 10^{-9}$ Pa·s and $\rho = 0.08$ kg/m³ corresponding to the temperature 4,273 °K.

Table 5.1 – Time variation of the air flow area radius

$v(t, r_\infty)$, m/s	r_∞ , m		
	$t = 0.1$ s	$t = 1$ s	$t = 10$ s
340.3	0.089	0.175	0.444
2.36	0.119	0.267	0.736

Let us assume that $R_r \approx r$, then the correlation (5.11) can be presented as follows:

$$v(t, r) = \text{Verfc} \left[\frac{r - R_r}{2} \left(\frac{\rho}{\mu t} \right)^{1/2} \right]. \quad (5.12)$$

Air friction forces of the rotor surface per 1 m of its length are easily calculated by the formula below:

$$F_{fr} = -2\pi R_r \mu \left. \frac{\partial v}{\partial r} \right|_{r=R_r}.$$

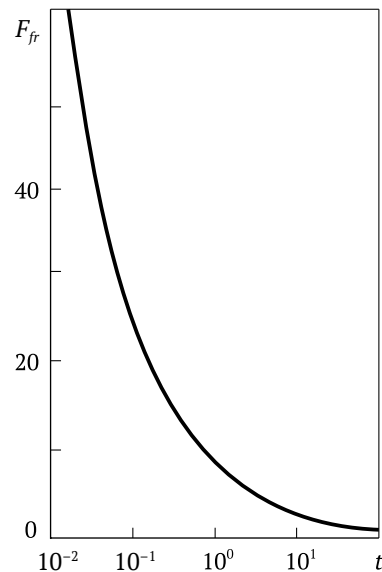


Figure 32 – Specific air friction force of rotor surface-time dependence

Substituting (5.12) here, we will get as follows:

$$F_{fr} = 2R_r \left(\frac{\pi \mu \rho}{t} \right)^{1/2}.$$

As an example, figure 32 shows the F_{fr} -time dependence, built under $R_r = 0.05$ m for $\mu = 1.819 \times 10^{-5}$ Pa·s, $\rho = 1.166$ kg/m³ corresponding to the air temperature 293 °K. As shown by calculations, the choice of another, larger value of air temperature results in the decrease in the design value F_{fr} ; therefore, the dependence in figure 32 represents the upper estimate F_{fr} .

5.4. Approximate calculation of temperature field in the rotor surface vicinity in the absence of the protective cover sublimation process

The temperature field in the vicinity of the rotor surface, in the absence of sublimation process, can be determined by means of equation (5.3). With regard to (5.12), this equation, after certain transformations, will be written as follows:

$$C\rho \frac{\partial T}{\partial t} = \frac{1}{r} \frac{\partial}{\partial r} \left(\lambda r \frac{\partial T}{\partial r} \right) + \frac{V_z^2 \rho}{\pi t} \exp \left[-\frac{\rho(r - R_r)^2}{2\mu t} \right]. \quad (5.13)$$

Let us introduce non-dimensional variables

$$T' = \frac{T - T_\infty}{T_* - T_\infty}; \quad t' = \frac{t}{t_*}; \quad r' = \frac{r}{R_r}, \quad (5.14)$$

where T_* , t_* – typical values of air temperature and time.

Using designations (5.14), let us transform the equation (5.13) to get the view as follows:

$$\frac{\partial T'}{\partial t'} = \frac{A_1}{r'} \frac{\partial}{\partial r'} \left(r' \frac{\partial T'}{\partial r'} \right) + \frac{A_3}{t'} \exp \left[-\frac{(r' - 1)^2}{A_2 t'} \right]; \quad (5.15)$$

$$A_1 = \frac{\lambda t_*}{C\rho R_r^2}; \quad A_2 = \frac{2\mu t_*}{\rho R_r^2}; \quad A_3 = \frac{V^2}{\pi C(T_* - T_\infty)} \quad (5.16)$$

non-dimensional parameters.

Boundary conditions (5.5), (5.8) and the initial condition (5.7) in a non-dimensional form are written as follows:

$$r' = 1; \quad \frac{\partial T'}{\partial r'} = A_4 \left[(T' + A_5)^4 - A_5^4 \right]; \quad (5.17)$$

$$r' = r'_\infty = 1 + \varepsilon_2 (2A_2 t')^{1/2}; \quad T' = 0; \quad (5.18)$$

$$t' = 0; \quad T' = 0, \quad (5.19)$$

where

$$A_4 = \frac{\varepsilon \sigma (T_* - T_\infty)^3 R_r}{\lambda}; \quad A_5 = \frac{T_\infty}{T_* - T_\infty}. \quad (5.20)$$

Comparing the boundary condition (5.18) with (5.6), we can observe that a point at a conventional border of the air flow area $r' \rightarrow \infty$ is assumed as an infinitely remote point $r' \rightarrow r_\infty$. In this case, it is assumed that the air temperature beyond this area is T_∞ .

The equation (5.15) with boundary and initial conditions (5.17)–(5.19) was solved using a numerical method under the following parameter values: $V = 10^4$ m/s; $T_\infty = 300$ °K; $\varepsilon = 0.5$; $R_r = 0.05$ m; $\varepsilon_2 = 2.6$. Hydrodynamic and thermophysical air properties ρ, μ, λ, C were assumed constant and corresponding to some average temperature T_0 . The research results on the impact of choosing temperature T_0 on the rotor surface temperature T_w at different moments of time are summarized in table 5.2.

It follows from the values T_w presented in the table and calculated for the same moment of time but for different values of temperature T_0 that the simplifying assumption 8 in (5.2) is quite permissible for making evaluative calculations. Temperature T_w , with T_0 increased from 293 °K to 2,273 °K, decreases by not more than 10–15 %; therefore, the calculated rotor surface

Table 5.2 – Impact of air temperature on rotor surface temperature

$T_0, \text{°K}$	Rotor surface temperature T_w (°K) at the moment of time		
	$t = 0.0006 \text{ s}$	$t = 0.003 \text{ s}$	$t = 0.06 \text{ s}$
293	3,110	2,120	2,010
873	3,110	2,050	1,940
2,273	3,000	1,970	1,870

temperature under hydrodynamic and thermophysical air parameters ρ, μ, λ, C , corresponding to the value $T_0 = 293$ °K, gives the upper estimate for T_w . Further, the calculations are made for temperature $T_0 = 293$ °K.

When discussing the UPT rotor option without a protective vacuum capsule, it is of interest to see the dependence of the rotor surface temperature T_w on time, shown in figure 33. Within the considered mathematical model, the highest temperatures are expected at the launch time ($t = 0$). Based on the heat transfer equation it follows that a sudden impulsive contact between a fast-moving surface with the air results in the infinite large surface temperature at the initial time. In reality, the upper estimate of air temperature at the rotor surface corresponds to the full braking temperature at the launch time. Further, the temperature falls quickly and makes about 2,000 °K in as little as 0.05.

Heating to this temperature will cause an intensive heat radiation from the rotor surface. For the considered example, figure 34 shows the dependence of radiation power W_{rad} per 1 m of rotor length, and figure 35 – the dependence of radiant flux density q_{rad} at the rotor surface on time. With regard to the results of equation (5.15), W_{rad} and q_{rad} were calculated by the formulae below

$$q_{rad} = \varepsilon \sigma (T_w^4 - T_\infty^4); \quad W_{rad} = 2\pi R_r q_{rad}.$$

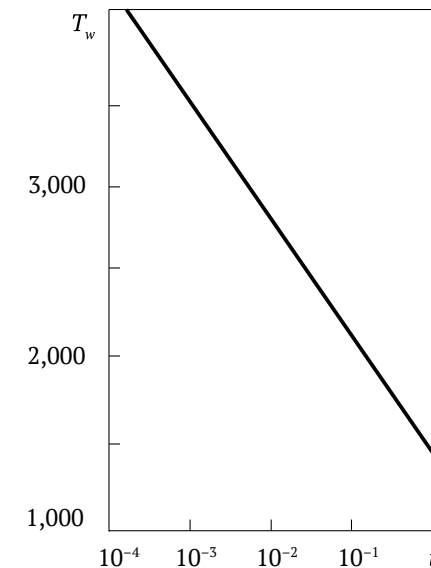


Figure 33 – Dependence of rotor surface temperature on time

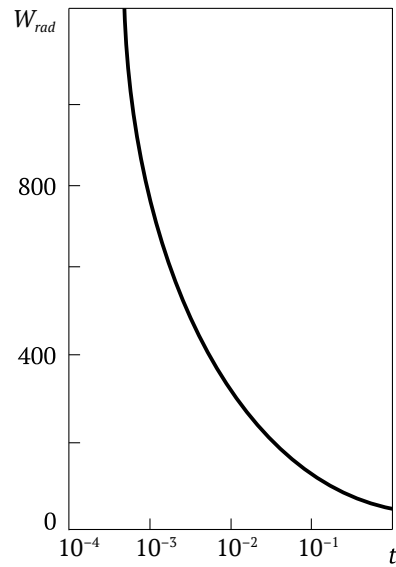


Figure 34 – Dependence of specific rotor radiation power on time

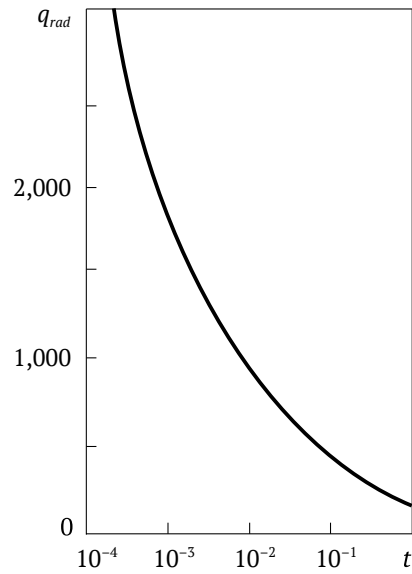


Figure 35 – Dependence of radiant flux density at rotor surface on time

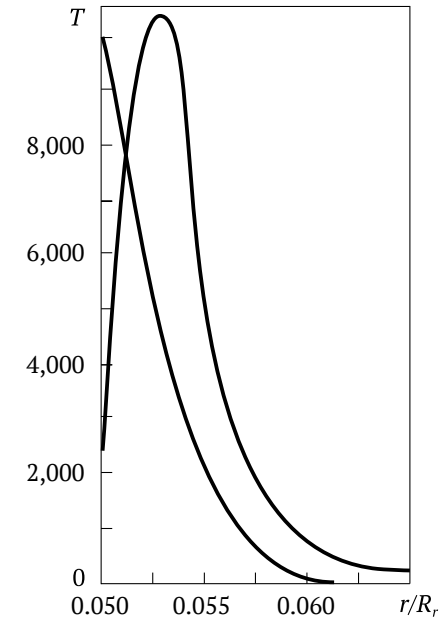


Figure 36 – Dependence of air velocity and its temperature on the radial coordinate at time $t = 0.481$ s

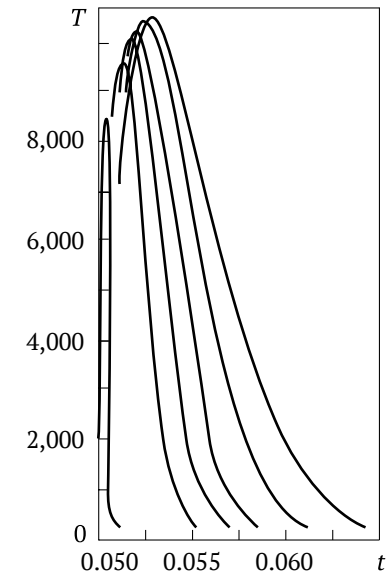


Figure 37 – Air temperature profile-time dependence

In addition, a sharp decrease in these values is observed here with the course of time.

The nature of radial distribution of air velocity and its temperature in the rotor vicinity at the definite time $t = 0.48$ s is shown in figure 36. The temperature curve has a strongly marked maximum; the peak air temperature exceeds 10^4 °K.

The time change of temperature profile is shown in figure 37. It follows from the comparison of the curves built for various time moments that the growth of peak temperature is retarded with the course of time. At the same time, a heat wave of the heated air is formed and moves over a distance from the rotor surface to the flow range periphery.

5.5. Quasi-stationary calculation of rotor surface temperature in the absence of sublimation process

The solution to equation (5.15) requires numerical methods. Let us use a quasi-stationary approach in order to obtain approximated evaluative results, for which we will ignore the partial derivative $\partial T'/\partial t'$ in (5.15). In this case, the impact of time on temperature is considered in the time dependence (5.18) of the flow range conventional border. The equation (5.15) takes on the view:

$$\frac{\partial}{\partial r'} \left(r' \frac{\partial T'}{\partial r'} \right) = - \frac{A_3}{A_1} \frac{r'}{t'} \exp \left[- \frac{(r' - 1)^2}{A_2 t'} \right]. \quad (5.21)$$

Integrating (5.21) over r' within 1 to ∞ with regard to the boundary condition (5.17), we will get, after certain transformations, the expression for a non-dimensional temperature on the rotor surface:

$$T'_w = \left\{ A_3^4 + \frac{A_2 A_3}{2 A_1 A_4} \left[1 + \left(\frac{\pi}{A_2 t'} \right)^{1/2} \right] \right\}^{1/4} - A_5. \quad (5.22)$$

When deriving, it was assumed that

$$\lim_{r' \rightarrow \infty} \left(r' \frac{\partial T'}{\partial r'} \right) = 0. \quad (5.23)$$

Using (5.14), (5.16), (5.20), we will get a dimensional form of temperature expression on the rotor surface:

$$T_w = \left\{ T_\infty^4 + \frac{\mu V_z^2}{\pi \varepsilon \sigma R_r} \left[1 + \left(\frac{\pi \rho R_r^2}{2 \mu t} \right)^{1/2} \right] \right\}^{1/4}. \quad (5.24)$$

The T_w determination by formula (5.24) is less accurate compared to the direct solution of equation (5.13); this formula however is convenient for evaluative calculations.

Table 5.3 shows as an example T_w values calculated by (5.24) for the same time moments t and temperature T_0 as in table 5.2 built based on the solution of equation (5.13).

Table 5.3 – Changes of rotor surface temperature depending on time and air temperature

$T_0, \text{°K}$	Rotor surface value T_w (°K) at the moment of time		
	$t = 0.0006$ s	$t = 0.03$ s	$t = 0.06$ s
293	4,030	2,470	2,270
873	3,870	2,380	2,200
2,273	3,800	2,360	2,180

As follows from the comparison of tables 5.2 and 5.3, formula (5.24) provides conservative values for T_w compared to the more accurate results obtained when solving equation (5.13). The biggest difference, as could be expected, is registered at the time moments close to the initial one. These differences are smoothed further and in as little as 0.06 s, the results obtained by the formula (5.24) and with the correct solution of equation (5.13) differ by 10–15 %. The formula (5.24) gives the upper estimate T_w .

The lower estimate T_w can be derived from (5.24) by passing to the limit at $t \rightarrow \infty$:

$$T_{w, \min} = \left(T_\infty^4 + \frac{\mu V_z^2}{\pi \varepsilon \sigma R_r} \right)^{1/4}. \quad (5.25)$$

Such a temperature must become established on the rotor surface at its unlimited in time rotation in the atmospheric layer. If the air viscosity is taken for the corresponding temperature $T_0 = 293$ °K, then we will find $T_{w, \min} = 803$ °K from (5.25). If $T_0 = 3,000 \div 5,000$ °K, then the lower estimate of the rotor surface temperature $T_{w, \min} = 1,180 \div 1,300$ °K. With $T_0 = 10^4$ °K corresponding to the peak air temperature (figure 37), we will find based on (5.25) $T_{w, \min} = 1,490$ °K.

5.6. Quasi-stationary calculation of evaporation dynamics of sublimated coating for the rotor thermal protection

The rotor surface temperature, as follows from the results obtained above, for $t \geq 0.05$ s reaches 1,500–2,000 °K. For the majority of materials, such temperatures, especially those arising at the initial time moment, are rather high.

Therefore, the consideration of an active rotor thermal protection by means of sublimated coatings is of interest.

In this case, the rotor cross section radius R_r is not a constant value, since it will be decreasing as the protective cover evaporates. Let us assume that $R_r = R_{r0}$ – the initial radius value.

In a quasi-stationary case, the heat transfer equation (5.13) in a non-dimensional form looks as follows:

$$\frac{\partial}{\partial r'} \left(r' \frac{\partial T'}{\partial r'} \right) = -\frac{A_6 r'}{t} \exp \left[-\frac{(r' - R'_r)^2}{A_2 t} \right]. \quad (5.26)$$

The agreed notations are as follows

$$T' = \frac{T - T_\infty}{T_s - T_\infty}; \quad r' = \frac{r}{R_{r0}}; \quad R'_r = \frac{R_r}{R_{r0}};$$

$$t' = \frac{t}{t_*}; \quad A_6 = \frac{\rho V^2 R_{r0}^2}{\pi t_* \lambda (T_s - T_\infty)},$$

where T_s – the rotor surface temperature assumed to be constant, equal to the sublimating temperature of the protective cover material.

The boundary conditions for (5.26) with regard to (5.4), (5.5), (5.23) are written as follows:

$$r' = R'_r; \quad T' = 1; \quad \frac{\partial T'}{\partial r'} = A_4 \left[(1 + A_5)^4 + A_5^4 \right] + J'; \quad (5.27)$$

$$r' \rightarrow \infty; \quad r' \frac{\partial T'}{\partial r'} \rightarrow 0; \quad J' = \frac{JLR_{r0}}{\lambda(T_s - T_\infty)}. \quad (5.28)$$

Here, A_2 and A_4 are determined by formulae (5.16), (5.20) replacing R_r and T_s with R_{r0} and T_s .

The equations (5.8) of the protective cover evaporation dynamics in a non-dimensional form:

$$\frac{dR'_r}{dt'} = -A_7 J', \quad (5.29)$$

where

$$A_7 = \frac{\lambda(T_s - T_\infty)t_*}{L\rho_w R_{r0}^2}.$$

Integrating (5.26) over r' within R'_r to ∞ engaging boundary conditions (5.27), (5.28), we will get, after certain transformations, a formula of non-dimensional mass flow:

$$J' = -A_4 \left[(1 + A_5)^4 - A_5^4 \right] + \frac{A_2 A_6}{2R'_r} + \frac{A_6}{2} \left(\frac{\pi A_2}{t'} \right). \quad (5.30)$$

Substituting (5.30) into (5.29), we will get a differential equation:

$$\frac{dR'_r}{dt'} = B_1 - \frac{B_2}{R'_r} - \frac{B_3}{(t')^{1/2}}, \quad (5.31)$$

describing the R'_r change with the course of time. The agreed notations are as follows:

$$B_1 = A_4 A_7 \left[(1 + A_5)^4 - A_5^4 \right]; \quad B_2 = \frac{A_2 A_6 A_7}{2}; \quad B_3 = \frac{A_6 A_7}{2} (\pi A_2)^{1/2}.$$

As an initial condition for (5.31), let us assume as follows

$$t' = 0; \quad R'_r = 1.$$

Figure 38 shows the dependence of the rotor cross section radius on time, obtained using the numerical solution to equation (5.31). When calculating, let us adopt that $R_{r0} = 0.05$ m and $V = 10^4$ m/s and assume that the protective cover is made of the material with the parameters close to teflon parameters ($T_s = 445$ °K; $L = 1.743 \times 10^6$ J/kg; $\rho_w = 1,500$ kg/m³). Curves 1 and 2 correspond to air parameters at the temperature 293 °K and 2,273 °K.

The rotor mass loss as a result of sublimation expressed in the percentage of the initial mass is characterized by curves 1 and 2 in figure 39. When calculating,

it was assumed that the average rotor density is equal to the density of its protective cover.

As is seen in the figures, approximately in one minute of motion after the starting moment, the density of protective cover made of the material close to teflon in its parameters will decrease by 1.3–2.1 mm, which makes the rotor mass loss 5.2–8.1 % of its initial mass. The air temperature near the rotor surface can decrease to 1,000–1,500 °K by that time, which corresponds to the working temperatures of modern heat-resistant coatings. The conservative density of the protective sublimated layer can be assumed 2.3–4.2 mm. After evaporation of the sublimated layer in 1–2 min after the start, the rotor thermal protection can be provided by a heat-resistant capsule.

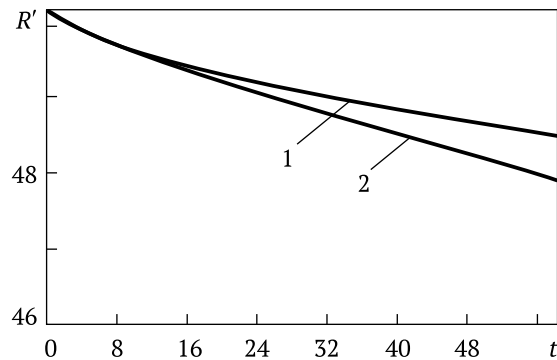


Figure 38 – Dependence of rotor cross section radius with sublimated coating on time

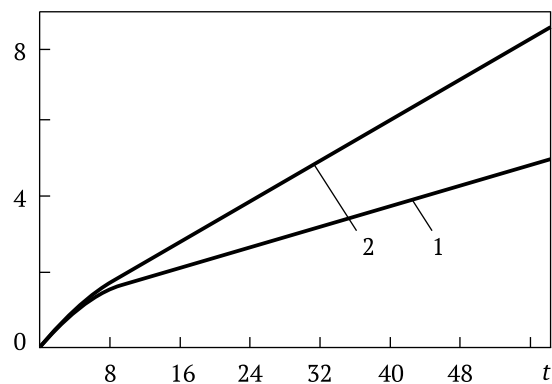


Figure 39 – Dependence of rotor mass loss percentage on time

5.7. Certain conclusions

As noted previously, the models considered above are significantly simplified. In reality, there can be expected a more complex picture of air flow in the vicinity of the rotor surface and heat transfer process. The obtained results therefore represent the first approximation to real parameters of the process, although they allow formulating certain conclusions.

The rotor variant without a protective vacuum capsule is apparently feasible in principle; however, serious issues may arise in the course of its engineering study. Let us point out some of them, the most obvious ones.

1. The discussed mathematical model assumes that the rotor is a smooth cylinder; the rotor curvature compared to the curvature of its cross section can be neglected, therefore the real structure of such a long mileage will not be perfectly smooth prone to various surface irregularities – projections, dimples, for example in the joints of fragment elements. Such projections will be sources of substantial drag up to 10^7 – 10^8 Pa. The mechanism of heating such projections is somewhat different; therefore their temperature can materially exceed the temperature on the rotor surface.

2. The launch installations and equipment must envisage protection against heat radiation and shock waves formed as a result of technological projections on the rotor surface. The need for the launching equipment thermal protection stems from the fact that the air temperature near the rotor surface can reach 10^4 °K, whereas the density of radiation flow at the initial time – 5×10^3 – 10^4 kW/m². Air velocity in the rotor vicinity is comparable to that of its surface.

3. Rotor heating will cause its thermal distortions. Weather conditions in different parts of the Earth – precipitations, cloudiness, ambient temperature, wind force and direction, etc. – will affect the distortion of separate rotor sections in different ways.

4. The air temperature near the rotor can reach 10^4 °K. The air temperature close to the rotor surface, in the absence of a protective cover, for example a sublimated one, takes on a maximal value at the initial time moment; then it falls so rapidly that it makes around 2,000 °K in 0.05 s. It is difficult to determine the maximal temperature of the rotor surface at the initial time moment within the considered model. It can be assumed, however, that this temperature is below the temperature at full braking.

5. The use of protective sublimated coatings will enable heat load reduction on the rotor starting section. The calculations have shown that the use of such a coating 2.3–4.2 mm thick made of the material close to teflon in parameters, provides reliable rotor thermal protection during the first minute of motion after

the start, when the air temperature near the rotor surface decreases to 1,000–1,500 °K. The further rotor thermal protection after evaporation of the sublimated coating can be carried out using a heat-resistant capsule.

6. Air heating in the rotor surface vicinity up to 10^4 °K will result in air ionization and will activate chemical reactions sort of molecular dissociation to form active atomic oxygen. The consequences of these processes have to be especially studied.

7. The considered model assumes that the rotor surface at the starting moment immediately contacts with static air, which brings about a sharp increase in thermal performance of the process. It is expected that when removing a protective cover, the rotor will contact with the environment, whose parameters vary quickly, but not instantly, from the values corresponding to the vacuum to the values of atmospheric air. Allowing for this circumstance, the initial temperature of the surface, density of the thermal radiation flow and radiation intensity decrease.

8. The calculated surface temperature and thermal flows density are in line with the results related to the TAV [16, 17] and RSV [13].

9. The used model does not allow studying the initial period of motion lasting about 0.05 s. This period requires building of a more accurate mathematical model.

Summary 1995

In case of geocosmic freight traffic of 10–100 mln tons per year to the stratosphere by means of the UPT, it is possible to deliver on its way 1–20 mln tons of ballast (water, as an example), sufficient to stabilize the ozone level and control the ozonosphere state of the entire planet*.

The process of water vapor separation constantly takes place in the upper atmosphere under the impact of solar UV emission; however, it is underactive due to a small content of water vapor in the stratosphere. A part of water vapor not separated into hydrogen and oxygen will serve as an original filter to bind and return to the Earth's surface the ozone layer impurities that deplete it but in such quantities do not pose any danger for the near the ground atmosphere, wherefrom the majority of them go to higher altitude.

By regulating the total ozone content as well as its concentration at separate sections, it is possible to control the weather and climate both on the entire planet and locally in an ecologically clean way; for example, suppress the formation of destructive storms, typhoons and cyclones. It can be easily implemented: although the ozone takes only the one ten-millionth part of the entire atmosphere, it consumes about four percent of solar energy falling on the Earth, which by hundreds of times exceeds the amount of heat emitted to the environment by the existing industry. Therefore the impact of the ozone layer state on the weather and climate at the planet is much stronger than the man-made impact on the near the ground air layers, as well as the greenhouse effect. Isn't it the reason why the weather and climate have been changing drastically recently, with the global warming taking place? The answer may well be related to the fact that as a result of the ozone layer depletion in the stratosphere, more solar energy and heat go to the lower atmosphere.

It will be possible to control the weather in the Southern hemisphere as well since the UPT at the closing stage of ascent into space will make oscillations relative to the equatorial plane. It is crucial that such an interference with

* Unitsky, A.E. Ozone layer: shield – today, shroud – tomorrow? / A.E. Unitsky // News of Science and Technology. Supplement to the APN Bulletin Sovetskaya Panorama/Soviet Panorama. – 1988. – No. 13 (156).

It is not inconceivable that a system of Saturn's rings is of technocratic origin since the rocket way of space exploration from this giant planet is not feasible for a number of technical reasons.

carrying out the earth industry and power engineering to space, will largely surpass the costs associated with the implementation of the UPT freight version (approximately a trillion USD). Thus, taking into consideration the existing growth trend in ozone deficiency in the stratosphere, there can be expected a drop in the annual biomass buildup on the planet by at least 10 % as early as in the coming decades. In that case, there will be produced by 20 bln tons of dry organic substance less on the Earth annually. If this underproduced organic matter is evaluated in terms of fuel at the price of 50 USD per 1 ton of fuel equivalent, and considering that a part of it is agricultural products that cost significantly more expensive, the damage caused to the biosphere will make over a trillion USD per year.

What about evaluating the annual undersupply of 10 bln tons of oxygen generated by green plants? Thus, in order to generate the same amount of oxygen by means of water decomposition to compensate its deficiency in the atmosphere, the annual costs will also make not less than a trillion dollars. However, the terrestrial civilization intends to exist for many a year; therefore, in order to live in the future in a decent way, humanity will have to spend such hefty bills over the course of decades. Furthermore, what about evaluating in monetary terms the damage due to the depletion of the ozone layer, which is expressed in the progressing health deterioration, the growth of skin cancer incidence rate, disorders in people's immune system and DNA?

* It is not inconceivable that a system of Saturn's rings is of technocratic origin since the rocket way of space exploration from this giant planet is not feasible for a number of technical reasons. It is feasible however with the use of the system similar to the UPT.

the nature of the weather will be ecologically safe, as ozone will not be foreign to the ozone layer.

With time, the UPT will provide the creation of space industry being similar to Saturn's rings* in its structure. There must even be the gaps between the rings, similar to the Saturn's Cassini divisions, in order to let the UPT go into high orbits without contacting with industrial rings.

The benefit from the prevention of the emerging decrease in photosynthesis in plants on our planet as a result of the destruction of the ozone layer, let alone the economic effect from the weather and climate control,

There can be placed vacuumed tunnels in the overpass for high-speed magnetic levitation trains (motion speed – 1,000 m/s). Then, it will be possible to get to America or Japan from Europe in 2–3 h. The overpass can be built gradually – at first, for example, on the territory of Russia. Every built kilometer will be paid off since the high-speed transport will enable the development and settlement of Siberia and the Far East connecting them with the European part of the country, where it will be possible to arrive in 1–2 h.

In fact, people living along the overpass will be able to reach any meridian of the Russian Federation in several hours; such notions as “the outskirts” or “a province” will start disappearing. This will make the settlement along the overpass in underdeveloped however ecologically clean regions with picturesque nature and favorable climate attractive for millions of people. In this way, almost half of the UPT overpass length will be built and the creation of a linear city based on the principles of harmony between man and nature will be under way. Further, the overpass will be extended through Europe up to Great Britain, and in the east through the Bering Sea – to the USA (Aleutian Islands) and Canada. Then, the overpass will be erected through Canada, and from England – it will be thrown over the Atlantic Ocean encircling the planet. Simultaneously with the overpass construction, there will be put up well-developed infrastructure and a planetary linear city Ecopolice, where billions of people will be able to live after the UPT commissioning.

The overpass can be constructed by 2025 in case of starting the design and survey work in the closest time, whereas the simple UPT freight version can be commissioned by the year 2050. Immediately after this, a large-scale industrialization of near-Earth space will be launched, where, first and foremost, powerful energy engineering (about a billion kW power) will be created within the first ten years. This will enable the conservation of most ecologically dangerous power stations on the Earth (nuclear power plants, heat and hydroelectric power stations) as well as fuel processing industry polluting the environment.

The availability of powerful energy engineering on orbit will allow transferring almost the entire resource extraction industry into space by the end of the next century (to the asteroid zone and to the Moon). The same relates to metallurgy, chemical and other types of ecologically hazardous industry, as well as the production, which requires weightlessness, vacuum, radiation and cryogenic and ultra-high

There can be placed vacuumed tunnels in the overpass for high-speed magnetic levitation trains (motion speed – 1,000 m/s).

EE
Having learnt through its bitter experience, people will start exploring and settling Space guided by the principle of eternal beauty and harmony of Nature.

temperatures. In this case, the ecology of space environment will not be disturbed since the notion “ecology” in space conditions loses its meaning due to the absence of life there. As an example, the Chernobyl disaster at a nuclear power plant resulted in the emergence of serious environmental problems on vast areas. At the same time, the fact that at the distance of some hundred or thousand kilometers above, there are Van Allen radiation belts, where the level of radiation is by thousands of times higher, is considered normal and causes no fear.

This is not to say that Space must be domesticated randomly and thoughtlessly like the Earth. Having learnt through its bitter experience, people will start exploring and settling Space guided by the principle of eternal beauty and harmony of Nature.

Based on the conducted analysis, even in the worst scenario, as with the freight traffic of 10 mln tons per year and efficiency factor 50 %*, the cost of cargo delivery to orbit using the UPT will be less than 10 USD per 1 kg, which is by thousands of times less compared to current prices. In addition, every 100 mln kW of UPT power supply in the global energy system (or depending on the width of its location only 2.5–5 kW per meter run) will secure the delivery of about 20 mln tons of cargo into space per year**.

After the latitudinal freight UPT comes into commission and the industrialization of outer space begins, the need for geocosmic transportation will be growing drastically. At first, this need can be satisfied by increasing the launch rate.

At the same time, there will be an increased demand for passenger transportation, which will be impossible to meet by means of rocket and space transport or suspended modules attached to the freight UPT capsule and placed into orbit. Therefore, there will be created a powerful industry in space, which will enable the construction of the freight and passenger UPT (figure 40) on orbit, in the equatorial plane, with two stationary flywheel rotors. Such a UPT built of space raw materials under space technologies and fed by orbital power stations will be reusable – it can sit on the planet and go into space.

* By order of the “Zvyosdny Mir/Star World” Centre (Gomel), there was developed a linear electric motor diagram for the UPT, with the expected efficiency factor 92 percent and the use of conventional conductors (Report on Contract 16/UPT “Analysis of technical means providing acceleration of an object of indefinite length in a vacuum channel to the speed up to 10 km/s.” – Moscow, 1989).

** Compare: the power of the largest Energia carrier rocket (Russia) capable of taking a total of 10 tons of cargo into orbit also makes about 100 mln kW.

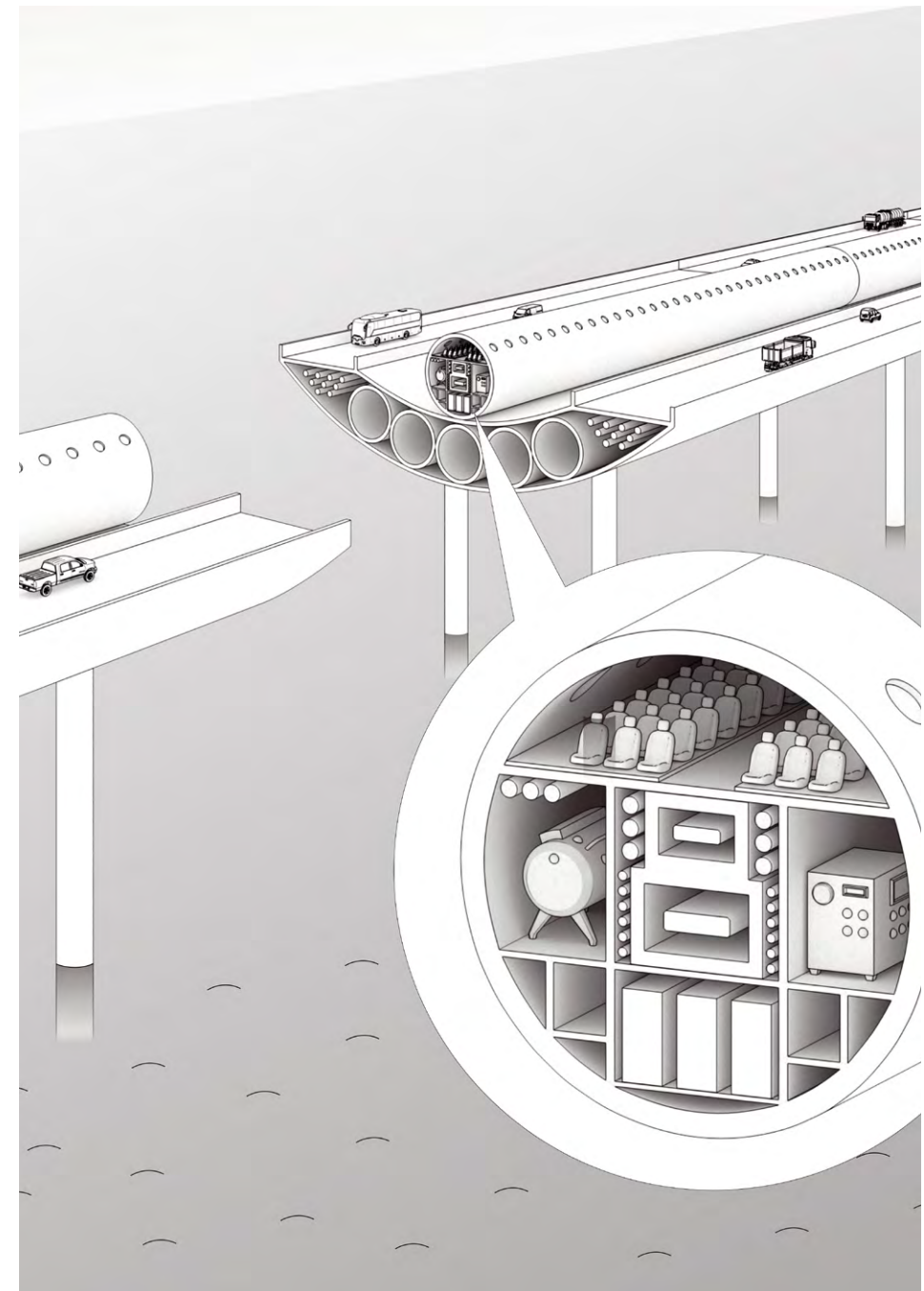


Figure 40 – Freight and passenger UPT

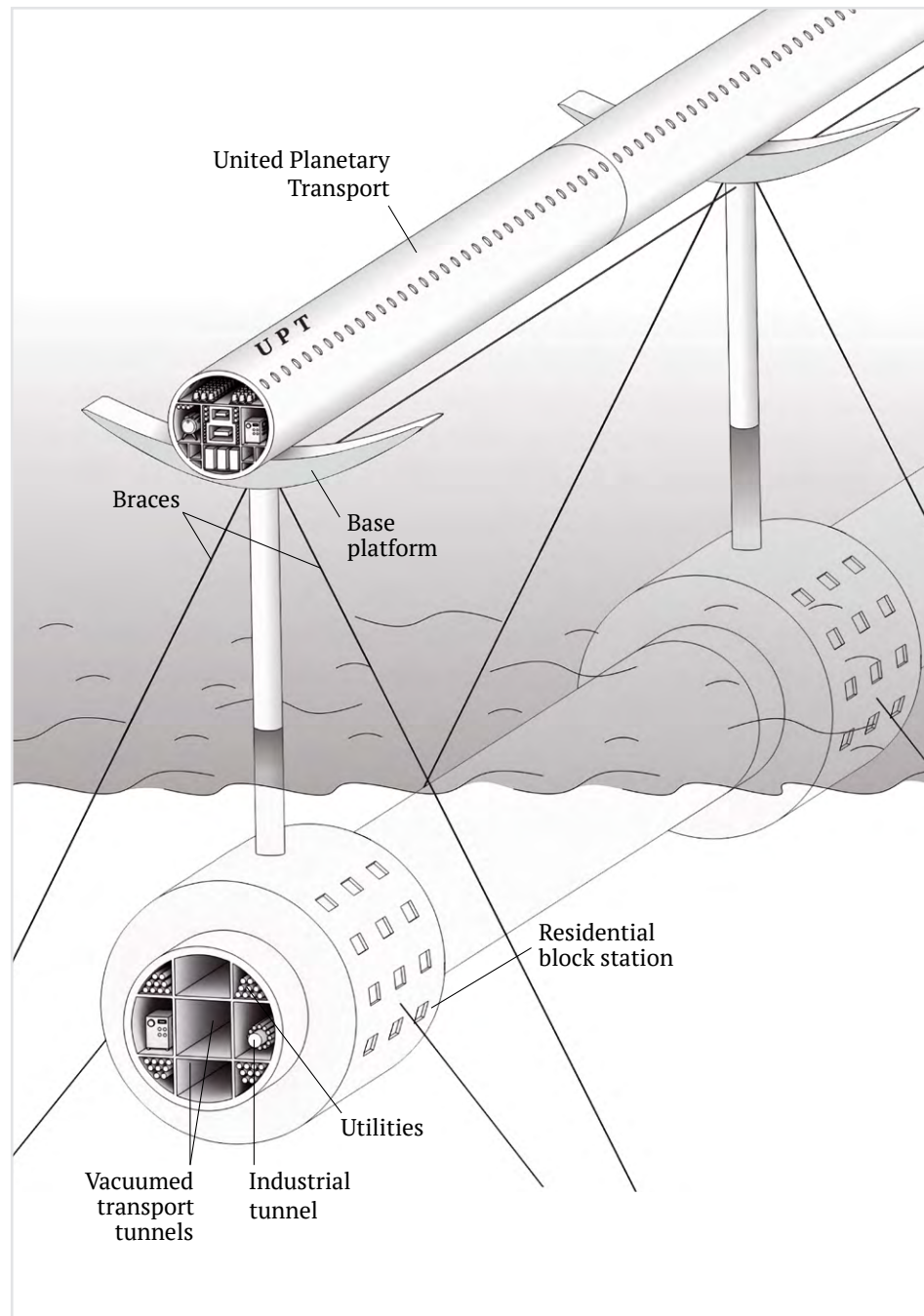


Figure 41 – Sea section of freight and passenger UPT

Thanks to three ring elements encircling the planet (the body and two flywheel rotors), the UPT recuperates kinetic energy and angular momentum, completely eliminating the necessity for interaction with the environment*. By that time humanity, having the experience in the construction of a simple UPT version and possessing a powerful space industry and energy engineering, will be able to build a second, more powerful equatorial overpass (figure 41). This can happen at the end of the next century.

The described program might seem a pie in the sky since it requires significant intellectual, financial and material expenses, whereas a vast number of issues on the Earth today still remain unsolved. However, the means and resources contributed in the future will be meant to preserve the civilization and not to be spent on weapons or an armaments race as this is the case at present.

According to a number of estimates, over 20 tln USD will be spent on the arms in the last quarter of the 20th century worldwide. In case of implementing the program of the UPT construction, it would be possible to steer this money not to destruction but to creation. In this case, due to its exceptional scientific content and the coverage of nearly all areas of knowledge and branches of industry, the proposed program will ensure the conversion of military industrial facilities and will prove to be a guarantor of peace on the Earth.

* Theoretically, with the engine efficiency factor 100 %, which is viable when using superconductors, the UPT will be able to sit on the Earth and go back into space without extra power costs, that is in the mode of “eternal engine”. This does not contradict the physical laws, since, with the established and equal freight traffic to the Earth and in space, the total mechanical work is equal to zero. In case the amount of cargo delivered to the Earth exceeds the return freight traffic, not only the UPT does not consume energy but, vice versa, operates as a superpower station, whose capacity will reach 1 bln kW and higher, if the return freight traffic exceeds 100 mln tons per year.



***The means and resources
contributed in the future
will be meant to preserve
the civilization
and not to be spent
on weapons
or an armaments race
as this is the case
at present.***

Conventional symbols

A_t – total work;
 C – total rigidity of capsule and rotor;
 C_{caps} – rigidity of capsule element;
 C_r – rigidity of rotor element;
 C_d – capsule drag coefficient;
 C_t – specific heat capacity;
 d – diameter;
 E – elasticity modulus of rotor material;
 $\text{erfc}(\xi)$ – Gauss error function;
 e – specific energy consumption to lift 1 kg of payload;
 F – elastic force;
 F_{fr} – friction force;
 F_* – maximal value of friction force;
 f_i – superficial friction factor;
 G – attractive force to the planet center;
 g – gravity acceleration;
 H – orbital height above the equator;
 H_a – height of dense atmosphere;
 $h_k = H/R$ – non-dimensional orbital height;
 J – density of mass flow discharged from the rotor surface;
 K – kinetic energy;
 K_* – kinetic energy at the stage of rotor placement into orbit;
 K_0 – system parameter;
 L – rotor length;
 L_s – specific heat of phase transition;
 l – length of rotor element;
 M – Mach number;
 M_r – mass of entire rotor;
 M_{caps} – mass of entire capsule surrounding the rotor;
 M_z – principal moment of traction forces relative to Z axis;

m – total mass of rotor elements and capsule;
 m_{caps} – mass of capsule element surrounding the rotor;
 m_r – mass of rotor element;
 m_{cr} – critical mass of rotor element;
 m_c – cargo mass;
 N – suspension system magnetic pressure (levitation force);
 $P(x)$ – dissipative force;
 p – parameter of system motion;
 Q – atmospheric drag force;
 Q_r, Q_φ, Q_ψ – generalized forces;
 Q_* – gross tractive effort;
 q – traction force from one electric motor section;
 $q_* = g/R$ – gravity parameter of system motion;
 q_h – density of supplied heat flow;
 q_{el} – traction force from electric motor;
 R – Earth's equatorial radius;
 R_a – radius of the sphere limiting dense atmosphere;
 R_c – radius of rotor circular orbit;
 R_{cur} – curve radius of rotor motion trajectory;
 R_r – current radius of rotor cross section;
 R_{r0} – initial radius of rotor cross section;
 R_* – current radius of rotor cross section;
 r_{r0} – initial radius of rotor orbit;
 r_r – current radius of rotor orbit;
 r_∞ – radius of ambient air capture area for rotor;
 S – route length;
 S_r – rotor cross section area;
 s – arc coordinate;
 T – temperature;
 T_0 – ambient temperature in unperturbed state;
 T_s – phase transition temperature;
 T_w – temperature of rotor surface;
 T_∞ – free-stream temperature;

t – time;
 t_n – time for rotor ascent to the intended orbit;
 $u(x) = \dot{x}^2$ – speed parameter;
 V – rotor speed;
 V_1, V_2 – first and second cosmic velocity;
 V_e – transfer velocity;
 V_0 – starting rotor circular velocity;
 V_r – relative speed;
 V_{r0} – initial radial rotor and capsule speed;
 V_z – axial component of rotor speed;
 v_r – linear speed of equator points rotational movement;
 v_{air} – air velocity;
 W – radial acceleration;
 W_{el} – electric motor power output;
 $x = r/R$ – non-dimensional radius;
 x_0, x_n – initial and final position of the system relative to the Earth center;
 x_k – orbital point, where radial speed and rotor acceleration vanish at the same time;
 X, Y, Z – coordinates;
 α – angle between tangents to the motion trajectory and equator;
 α_d – value that depends on the height of atmospheric layer;
 $\beta = (V_0/V_1)^2$ – non-dimensional parameter depending on rotor speed;
 γ – relation of air specific heat under constant pressure and constant volume;
 δ – central arc angle;
 ε – preset small positive value;
 ε_* – total emissivity of rotor surface;
 η – mass system efficiency factor (relation of the uplifted mass to the initial one);
 η_{el} – energy efficiency factor of the system;
 η_{en} – engine efficiency factor;
 k_{sh} – coefficient that depends on capsule shape;

λ – air thermal conductivity;
 μ – coefficient of dynamic viscosity;
 $\mu_0 = m_{caps}/m_r$ – relation of capsule and rotor element masses;
 $\mu_1 = m_{caps}/m$ – relation of capsule element mass to the total capsule and rotor element mass;
 $\mu_1 = m_r/m_1$ – relation of remaining capsule element mass (after partial ejection) to rotor mass;
 μ_e – Earth's gravity coefficient;
 ρ – material density;
 ρ_w – density of rotor coating material;
 ρ_a – atmospheric density;
 ρ_{a0} – initial atmospheric density;
 σ – Stefan – Boltzmann constant;
 τ – oscillation period;
 φ – rotor turning angle;
 ψ – capsule turning angle;
 ψ_0 – initial angle value ψ ;
 ω_e – Earth angular velocity;
 ω_r – angular rate of rotor rotation;
 ω_{r0} – initial angular rate of rotor rotation.

Bibliography

1. **Avduevsky, V.S.** Fundamentals of heat transfer in aviation and rocket-space technologies / V.S. Avduevsky, B.M. Galitseyskiy, G.A. Glebov [et al.]. – M.: Mashinostroenie [Machine-building], 1975. – 624 p.
2. **Gantmacher, F.R.** Lectures in Analytical Mechanics / F.R. Gantmacher. – M.: Fizmatgiz, 1960. – 296 p.
3. **Gradshteyn, I.S.** Table of Integrals, Sums, Series and Products / I.S. Gradshteyn, I.M. Ryzhik. – 5th Edition. – M.: Nauka, 1971.
4. **Grushinskiy, N.P.** In the World of Gravity Forces / N.P. Grushinskiy, A.N. Grushinskiy. – M.: Nedra, 1978. – 175 p.
5. **Clark, R.K.** Pyrolytic coatings on heat-resistant thermal-protection shields increasing the emissivity factor and reducing catalytic activity of the surface / R.K. Clark, G.R. Cunningham, G.K. Robinson // *Aerokosmicheskaya tekhnika* [Aerospace technology]. – 1987. – No. 11. – P. 60–67.
6. **Krasnov, N.F.** Aerodynamics of Bodies of Revolution / N.F. Krasnov. – M.: Mashinostroenie [Machine-building], 1964.
7. **Lezhe, L.Zh.** Protection of spacecraft from the impact of atomic oxygen / L.Zh. Lezhe, G.T. Veisentein // *Aerokosmicheskaya tekhnika* [Aerospace technology]. – 1987. – No. 2. – P. 7–11.
8. **Loitsyanskii, L.G.** Mechanics of Liquids and Gases / L.G. Loitsyanskii. – M.: Nauka, 1973. – 848 p.
9. **Matveev, N.M.** The collection of problems and exercises on ordinary differential equations / N.M. Matveev. – M.: Rosvuzizdat, 1962. – 291 p.
10. **Narimanov, E.A.** Space solar power plants / E.A. Narimanov. – M.: Znanie, 1991. – No. 3. – 54 p.
11. **Osadin, V.A.** Will the Unitsky's Wheel Fly? / V.A. Osadin // *Energiya*. – 1989. – No. 8. – P. 50–54.
12. **Polezhaev, Yu.V.** Thermal Protection / Yu.V. Polezhaev, F.E. Yurevich. – M.: Energiya, 1976. – 392 p.

13. **Prabhu, D.K.** Numerical analysis of RSV streamlining with regard to real gas effects / D.K. Prabhu, G.K. Taniehill // *Aerokosmicheskaya tekhnika* [Aerospace technology]. – 1987. – No. 11. – P. 60–67.
14. **Sullivan, W.** We Are Not Alone / W. Sullivan. – M.: Mir, 1967. – 383 p.
15. **Mechanical Engineering Handbook**; Edited by A.N. Dinnik. – M. – L.: Gostekhizdat, 1949.
16. **Tauber, M.E.** Aerothermodynamics of Transatmospheric Vehicles / M.E. Tauber, H.G. Adelman // *Aerokosmicheskaya tekhnika* [Aerospace technology]. – 1989. – No. 3. – P. 109–120.
17. **Tauber, M.E.** Characteristics of Aerothermodynamics of Transatmospheric Vehicles / M.E. Tauber, G.P. Menees, H.G. Adelman // *Aerokosmicheskaya tekhnika* [Aerospace technology]. – 1988. – No. 6. – P. 41–51.
18. **Fabrikant, N.Ya.** Aerodynamics / N.Ya. Fabrikant. – M.: Nauka, 1964.
19. **Fertregt, M.** Basic space science / M. Fertregt. – M.: Prosveschenie, 1969. – 114 p.
20. **Hunter, L.V.** Technology of ablation analysis of graphite coating for return vehicle at supersonic and subsonic flying speed / L.V. Hunter, L.L. Pirini, D.V. Konn, P.T. Brenza // *Aerokosmicheskaya tekhnika* [Aerospace technology]. – 1987. – No. 8. – P. 31–37.
21. **Chekalin, S.V.** Influence of transport space systems launches on Earth's atmosphere. Space and Ecology / S.V. Chekalin, Ya.T. Shatrov. – M.: Znanie, 1991. – No. 7.
22. **Schlichting, H.** Boundary-Layer Theory / H. Schlichting. – M.: Nauka, 1974. – 712 p.
23. **Elyasberg, P.E.** Introduction to the flight theory of artificial Earth satellites. – M.: Nauka, 1965. – 540 p.
24. **Unitsky, A.E.** Interchange, outer space, circular / A.E. Unitsky // *Inventor and Rationalizer*. – 1982. – No. 4. – P. 28–29.
25. **Unitsky, A.E.** To Space... by Wheel / A.E. Unitsky // *Technology for the Youth*. – 1982. – No. 6. – P. 34–36.

26. Unitsky, A.E. Into Space Without a Rocket / A.E. Unitsky // Technology and Science. – 1987. – No. 4. – P. 40–43.

27. Unitsky, A.E. The Planet's Ring Buoy / A.E. Unitsky // Bulletin "XX Century and Peace". – 1987. – No. 5. – P. 14–19.

28. Unitsky, A.E. Ozone layer: shield – today, shroud – tomorrow? / A.E. Unitsky // News of Science and Technology. Supplement to the APN Bulletin Sovetskaya Panorama/Soviet Panorama. – 1988. – No. 13 (156).

29. Unitsky, A.E. Geocosmic Transport Alternatives. Program of the Star World Center. Project Globe of the Future / A.E. Unitsky. – Exhibition Catalogue. – M.: 1990. – P. 33–35.

30. Yanke, E. Special Functions / E. Yanke, F. Emde, F. Lesh. – M.: Nauka, 1977. – 344 p.

31. Bakhvalov, Yu.A. Transport with Magnet Suspension / Yu.A. Bakhvalov, V.I. Bocharov, V.A. Vinokurov, V.D. Nagorskiy; Edited by V.I. Bocharov and V.D. Nagorskiy. – M.: Mashinostroenie [Machine-building], 1991. – 320 p.

Scientific and technical reports

I. Kazban, A.M., Kolodyozhnov, V.N., Unitsky, A.E. Problems of UPT rotor ascent to orbit. – Voronezh – Gomel, 1989. – 187 p.

II. Krivko, O.P., Logvinov, G.F., Unitsky, A.E. Analysis of UPT overpass design variants and its optimization. – Gomel, 1989. – 109 p.

III. Omelyanenko, V.I., Goncharenko, L.V., Kudina, N.V., Sergeev, S.A. Analysis of possibility of superconductivity use to create UPT rotor traction and electrodynamic suspension. – Kharkov, 1989. – 164 p.

IV. Polyashov, L.I., Efimov, V.G., Malkov, V.F., Nikitin, A.N., Podguzova, E.V., Rodionov, N.I., Sokolov, Yu.D., Unitsky, A.E. Analysis of technical means providing acceleration of an object of indefinite length in a vacuum channel to the speed up to 10 km/s. – M., 1989. – 159 p.

V. Khozin, G.S., Chapis, A.A., Unitsky, A.E. Scientific Basis for Non-Rocket Space Industrialization. – Gomel – M., 1989. – 109 p.

VI. Shishakov, M.L., Shilko, S.V., Unitsky, A.E., Trokhova, T.A. The creation of mathematical models of UPT rotor motion at stages of acceleration and exit into the atmosphere. – Gomel, 1989. – 180 p.

VII. Unitsky, A.E. EcoWorld Programme. – M.: Academy of New Thinking, Institute of Social and Scientific Technical Innovations, 1990. – 82 p.

Summary 2019

**Optimal
transport systems
as a platform
for the transition
to a new stage
of civilization**

540



Summary 2019

Optimal transport systems as a platform for the transition to a new stage of civilization*

I will tell you about the transportation systems of the future. Everything that you will learn is based on the laws of physics – the basic science that describes motion. I devoted 50 years of my life to create the theory of transport and infrastructure complexes that are optimal from the point of view of this science and the world around it. The team I assembled in the Republic of Belarus today implements this transport. In the near future, the technologies developed by us will ensure the transition of humanity to a fundamentally new stage of civilization. As a result, our technocratic civilization will be able to:

- solve global environmental problems and challenges;
- relocate harmful industrial production facilities from the surface of the planet beyond its biosphere – to near-Earth orbits;
- live on the Earth comfortably and safely in harmony with Nature.

The foundation of such a program is SkyWay.



* Planar report of Eng. Anatoli Unitsky at the solemn award ceremony “Golden Chariot” for achievements in the field of transport. The forum for advanced technologies, innovative solutions and new projects, was to be held in the capital of Brazil in November 2018, but was postponed by the organizers to 2019.



The laws of physics are the basis for optimal transport

SkyWay SkyWay is the transport and infrastructure complexes in which passengers and cargo are moved at speeds of up to 500 km/h (and in future, up to 1,200 km/h in a forevacuum tube) along string rails forming light and strong transport overpasses.

Over time, cargo, urban and long-distance high-speed SkyWay lines will create a transport and infrastructure network of dozens of millions of kilometers – TransNet, which will become the basis for creating a global system of geocosmic transportation, thousands of times more efficient throughout modern cosmonautics.

How have I been creating the optimal transport? My reasoning was very simple. What will happen from the point of view of physics if I travel from point A to point B (for example, from Belarus to Brazil) using any type of transport: railway, ship, by plane, car or rocket? At the beginning and at the end of the journey, I am at about the same height above sea level, which means that as a result of the movement, my potential energy has not changed. At both points, I remained motionless relative to the surface of the Earth, which means that my kinetic energy also has not changed. Therefore, if the energy state has not changed, the useful transportation will be null, and the efficiency of such transport will also be null. There is nothing to change and improve. How can the null be improved?

Where does all the energy go then? It turns out that all 100 % of the energy in any type of land transport goes not to move, but to fight against the environment and to destroy it. I concluded that in order to improve the transport, it is necessary to minimize these energy costs. At the same time, it is necessary to understand that for high-speed transport with speeds above 350 km/h (which SkyWay applies to) more than 90 % of the energy expenditure during its movement goes to aerodynamic resistance.

In the mathematical formula that determines the aerodynamic drag power, there is only one indicator – the speed of movement – raised to the third power. A fivefold increase in speed (from 100 to 500 km/h) will require an increase in engine power

From virtually every known area of technology, we take the best process and embed it into the string transport to make it even more efficient.

of $5 \times 5 \times 5 = 125$ times, for example, from 20 to 2,500 kW (like in six Soviet T-34 tanks). This is the problem: in aerodynamics, even a small increase in speed entails a significant increase in energy consumption. For this reason, one of the fastest cars, Bugatti Veyron, with an engine power of 1,500 HP will not be able to move at a speed of 500 km/h. For this, it has not enough power.

I realized that the most important thing in high-speed land transportation is the aerodynamics; therefore, it is necessary to improve it in the first place. Here SkyWay achieved great success: the drag coefficient of our rail car, called “unibus”, is seven times lower than that of the Bugatti. It is 0.06. The optimal aerodynamic shape of the unibus is determined on the basis of dozens of tests in a wind tunnel, since 1995. Such high values have been achieved by eliminating the screen effect.

It is known that air is unevenly, above and below, flows through a vehicle moving along roadway. There are air seals (under the bottom) and turbulence (behind). And if you just take and lift the vehicle high above the roadway, as it is done in the string transport, the aerodynamics improves immediately by 2.5 times.

Our rolling stock moves along the string rails that do not create a screen effect, in fact they are strung through the air.

SkyWay overpass consists of:

- anchor supports that bear horizontal tension load and are installed every 5 km or less;
- intermediate supports installed 50–2,000 m from each other;
- thin composite string rails.

We make the track structure uncut and pre-stressed by stretching special strings, thanks to which our tracks:

- have no expansion joints;
- have low material consumption and high durability;
- provide high evenness;
- are much cheaper than other elevated transport systems.

In addition, our vehicle shows excellent ride comfort thanks to a comprehensive solution:

- the best model of a wheel bearing on the rail according to the “cylinder-on-the-plane” scheme (increases the service life of a rail and the rolling efficiency of a steel wheel);
- the second most important issue (after the aerodynamics) in energy costs (for the suspension of a vehicle to the track structure) is effectively solved;
- materials in a “steel wheel – steel rail” pair are optimized.



Of all the known vehicle suspension options to the track structure – an air cushion, magnetic levitation and even anti-gravity – the “steel wheel on a steel rail” scheme has the highest efficiency, equal to 99.8 %, since a force of 2 kg can move a 1-ton trolley horizontally on a rail track.

Our vehicles are driven by artificial intelligence; motor wheels (high-performance electric motors fitted into steel wheels) move them. Confidential information flows within the transport complex are protected using Blockchain technology. From virtually every known area of technology, we take the best, process and embed it into the string transport to make it even more efficient. But the main thing that allows us to come closer to perfection is the maximum attention to the laws of physics. The science of Nature, broadly speaking.

Humanity owes the nature

Today, everyone talks about environmental problems: the greenhouse effect, the ozone depletion and the global warming, as well as many other hazards associated with the industrial impact on the nature. All this, despite its objective significance, will have disastrous consequences only in the long term. Almost nothing is said about the real damage that the industrial technosphere is causing to people today, in those very minutes. While these words were spoken,

the machinery killed more than ten people and crippled hundreds. Think about it: there are 9 mln deaths annually caused only by water and air pollution. The main source of pollution in industrialized countries is road transport. In addition, it causes another 1.5 mln annual road deaths and 10 mln cases of disability. This is a very high price. How are we going to pay it?

The myth sounds like this: the technology has freed the man, so we may not care about heat and water in houses, spend less effort on the production of food, clothing and other everyday stuff, move with greater speed at any distance, see distant countries and be a part of exciting adventures without getting up from a couch. Such freedom of a modern man turns out to be an illusion. Heating for our homes pollutes the air; the production of commodities poisons water, soil, and food; traveling for most people is too expensive, and easily accessible entertainment is just a way to distract and forget about the meaninglessness of your life in the short intervals between shifts at unloved job in service, factory or office. The world in which we live reflects the best intentions with which it was born, but it is wrong in most of its manifestations, because the mirror is false.

The modern ecological crisis is a natural result of the experience accumulated by the mankind in the process of interaction with the nature. The population is increasing, and the level of its consumption is growing: in the modern world for 15 years, so much natural resources have been consumed, as much as has been used by the mankind for all the previous time of its existence.

The diversity of flora and fauna is diminishing, and this threatens the Earth's layer – the biosphere. Since the early 80s of the past century, on average, one species of animals disappeared daily, and one of plants – weekly. Every year, more than 10 bln tons of fuel are burned – coal, oil, gas, firewood, tens of billions of tons of harmful substances, ash, and dust are released into the biosphere. The steppes completely disappeared as a type of ecosystems and landscapes; the forest areas sharply decreased (before the man, they occupied approximately 70 % of the land, and now they are less than 20 %). There is a further, unprecedented destruction of forest ecosystems, especially the most valuable and complex – tropical, straightening of river beds, creation of industrial areas.

Only two-three generations remain up to the point of no return, when the detrimental impact of a technogenic civilization on the biosphere becomes irreversible and makes the Earth unsuitable for living.

Scientists have introduced the concept of the Earth Overshoot Day. This is the day in the year before which the mankind has time to consume the amount of resources generated by the planet for the year. In 1986, such a day was at the end of the year – December 31, and in 2018 it was August 1. This trend will lead us to that in 2049 the Earth Overshoot Day will be on February 1. We live in debt and deplete the planet, consuming more than the Earth can give us. Only two-three generations remain up to the point of no return, when the detrimental impact of a technogenic civilization on the biosphere becomes irreversible and makes the Earth unsuitable for living. This is the time we have to take a decisive action.

There is only one essential way out of this situation: it is necessary to provide the Earth's technosphere with an ecological niche outside its biosphere. This step will ensure the preservation and development of the biosphere according to the laws formed over billions of years of evolution, as well as the harmonious interaction of people with the biosphere. There is no such ecological niche on the Earth, but there is in space, very close – at a distance of some 100 km and more from the surface of the planet, where ideal conditions exist for most technological processes: weightlessness, vacuum, high and cryogenic temperatures, unlimited raw materials, energy and spatial resources. To accomplish such a qualitative transition, the mankind already today has all the necessary resources. The SkyWay transport system I described is the first step in the implementation of the program for relocating the industry into space.

SkyWay: In harmony with nature

Due to the design features and high efficiency of SkyWay, the level of harmful environmental effects will be significantly lower than that of all existing and prospective types of transport. SkyWay unibus, including the family type, which any family can buy, is distinguished by unique aerodynamic parameters.

For example, an improvement of this indicator compared to a high-speed car, Bugatti Veyron, if it was moving at 500 km/h, gives a decrease in drive power by more than 1,000 kW. With its operation only 2 hours per day (average of a regular passenger car), this will save 180 tons of fuel per year with an average world cost of more than 200 thous. USD. If there are only 100 mln SkyWay vehicles on the entire planet with such indicators that there are not so many (today there are more than 1 bln cars in the world), this will save about 18 bln tons of fuel worth over 20 tln USD a year. It is easy to calculate what environmental improvement will occur: for every billion tons burned on the Earth, more than 3 bln tons of oxygen is burned out of the atmosphere, or almost 15 tln m³ of air, which gives more than 4 bln tons of environmentally harmful combustion products.



Such an advanced country as Germany set an ambitious goal: in the period from 2007 to 2020 to reduce CO₂ emissions by 40 %. As a result, 580 bln USD was spent, but the designated bar was not reached.

Maybe it was worth taking a different approach? For example, the string transport would provide:

- reducing the harmful emissions into the atmosphere, soil and water;
- reducing fuel costs and reducing consumption of natural resources;
- shifting the Earth Overshoot Day by the end of the year, gaining time for future generations.

Along with these environmental benefits, SkyWay transport systems have a number of others:

- electrically operated – allows integrating solar panels and wind power stations into the overpasses, which is especially important for cities;
- safety – due to the fact that the tracks are located above the ground and the system is controlled automatically, we avoid the collision of vehicles or other objects on the way.

The widespread replacement of road transport for SkyWay annually could save 1.5 mln lives and prevent more than 10 mln disabilities, which would have an annual economic and socio-political effect of 3 tln USD.

ff
The creation of TransNet global transport network based on SkyWay string transport will now be able to give our planet its original appearance and provide the best conditions for life and travel, leisure and work.

In addition, the land under the SkyWay tracks remains untouched due to the small land acquisition and the minimum amount of excavation work: forests, farming, natural soil hydrology and migration of animals will emerge.

Modern roads and railways cannot provide all of the above: today the area equal to five Great Britains are “rolled up” and “buried” under railways and asphalt. Along the roads the soils are degraded and contaminated by carcinogens. These lands, and first of all fertile soil, should be returned to the former land users – the Nature, living creatures inhabiting the biosphere. After all, it is living fertile soil – the basis of the health of the biosphere, in essence, its immune system.

Thus, the creation of TransNet global transport network based on SkyWay string transport will now be able to give our planet its original appearance and provide the best conditions for life and travel, leisure and work. The next step in the development of the network will be a decisive breakthrough in the future, the transition of humanity into the space era.

The need for the relocation of industry into outer space is dictated by the same logic and physics. They also determine what technical means will allow humanity to make such a breakthrough – probably one of the most important breakthroughs in the entire history of our technocratic civilization.

Of course, we do not know how the technology will develop in the future, including space technology, and we do not know about future discoveries. Such predictions are unseemly, and, in general, meaningless undertaking. In order to be convinced of what has been said, it suffices to recall the naive scientific forecasts of past 50 or 100 years. The only thing that can be stated with complete confidence, whatever this technology may be, it will obey the fundamental laws of the Nature. Such laws, repeatedly tested by practice, will remain fair in the future. In the field of mechanics, they include four conservation laws, namely: energy, momentum, angular momentum, and center-of-mass motion.

Based on these laws, the basic conditions for the space industrialization are as follows:



- relocation of the space industry in orbits in the equatorial plane;
- compliance with the physical laws of conservation when creating an extra-terrestrial industry;
- creating geocosmic transport:
 - with efficiency close to 100 %;
 - running on clean energy (electrical);
 - providing turnovers in millions and in the future billions of tons per year;
 - being a self-supporting structure that does not interact with the environment.

Rocket way is a dead end

If you do not comply with these conditions, the technologies for moving large volumes of cargo into space will either be inoperative or pose a significant danger to the biosphere, as well as modern rocket carriers considered as the main transport for large-scale space exploration and popularized, for example, by American billionaires Elon Musk and Jeff Bezos. Speaking about saving the Earth, such businessmen either simply use it to attract additional investments and increase their huge bankroll, or they do not understand that

EE
In addition to extinguishing the ozone, rocket carriers also change the physical chemistry of the upper atmosphere, cause turbulence in the ionosphere, and even affect the geomagnetic field.

the measures they are proposing can destroy our planet.

The rocket way of space exploration, applied by the mankind today, is a dead end. The main goal, which is pursued in the rocket and space industry, is to reduce the launch cost due to the creation of reusable carriers. However, even if it is possible to reduce the cost of delivering goods to orbit by 100 times, for example, to 100 thous. USD per ton of cargo, large-scale space exploration will still be expensive. As an illustrative example, one can draw parallels with earthly reality: it is senseless to build a plant

at the price of one brick commensurate with the price of a car.

The other circumstance that makes senseless attempts to industrialize space with rockets is their extremely low efficiency — less than 1 %. It sounds like a paradox, but the transport performance of the entire modern world rocket and space industry is comparable to one horse cart, which I said for the first time 36 years ago and that KGB of the USSR did not like. Such a cart, which has continuously transported 1 ton of cargo over a distance of a rocket into orbit (approximately 300 km) since 1957, would have transported as many goods as all the rockets delivered it into space.

Moreover, inefficient rocket astronautics creates global environmental problems. The speed of jet flow during a rocket flight is 4 km/s, which is five times higher than the speed of a sniper rifle bullet. The temperature of the jet reaches 4,000 °C, which is almost three times higher than the melting temperature of steel. All this power is released in an extremely vulnerable ozone layer in the form of a chemically active flame. Each launch of a heavy carrier makes a hole in the ozone layer of the size of an average European country such as France.

Back in the 1980s, Americans who were inclined to underestimate the environmental impact of rockets on the environment estimated that a shuttle could destroy up to 40 mln tons of ozone in one start, because it uses ozone-reducing substances as fuel components, chlorine and other chemical elements. Given that there are only about 4 bln tons of this gas in the Earth's atmosphere, it is easy to calculate that to completely destroy the ozone layer, it is enough to simultaneously launch only about 100 carriers of this type. In addition to extinguishing the ozone, rocket carriers also change the physical chemistry

of the upper atmosphere, cause turbulence in the ionosphere, and even affect the geomagnetic field. Reusable rockets and the transition to new types of rocket fuel will not be able to solve this problem, since the industrialization of space will require a number of launches thousands of times more than it is today. It will simply kill the planet.

Just like reusable rockets, other projects promoted at the state level are also meaningless because of their inefficiency.

For example, the "Space Elevator", which can carry 2,500 tons of cargo per year, which, of course, is several times more successful than the rockets, but not enough for the industrialization of space, is only five "space carts". Or 0.3 g of cargo per year per person on the planet, that is, just one milligram per day (!). It is not even a grain of sand, but, so one speck of dust for each inhabitant of the planet under the motto: "Let there be space industrial happiness!"

Another famous project StarTram can be compared with the old Soviet bus for 20 people, which can carry 400 thous. people a year, or about 1,000 passengers a day. Imagine an industry which interested about 10 bln people, and whose maintenance staff will consist of only 1,000 employees — one for every 10 mln people on the planet. No need to prove that this is not just nonsense. It is absurd.

UPT – United Planetary Transport

The solution proposed and implemented today in the framework of the SkyWay project was first announced by me in the early 80s and became widely known in the USSR. Since then, a lot of work has been done, an own scientific and design institute has been created, on the basis of which this solution was studied and verified. This project, called "United Planetary Transport" (UPT), can be implemented in the foreseeable future with the political will and business consolidation.

UPT is a reusable geocosmic transport system for rocket-free exploration of near space. UPT will allow putting into orbit about 10 mln tons of cargo and 1 mln people for one flight who will be involved in the creation and operation of the near-earth space industry. In one year, UPT will be able to go into space up to 100 times. What UPT can do in one year, a modern world rocket and space industry, in which trillions of dollars have already been invested, will take about a million years. At the same time, the cost of delivering each ton of payload to orbit will be tens of thousands of times lower than that of modern carriers.

Environmentally friendly UPT, operating exclusively on electric energy, will allow industrializing the near space. To do this, it will be necessary to close all the industrial production facilities that are harmful to the Earth's biosphere,

creating them again in near-Earth orbit on new principles that are environmentally friendly for space. This step will open access to fundamentally new industrial technologies through the use of unique space capabilities not available on the Earth: weightlessness, deep vacuum, ultra-low and ultra-high temperatures, inexhaustible sources of energy and resources, including mineral and spatial. Amazing opportunities are opening up in the field of information and energy communications. Bringing industry out of the planet will radically improve our common habitat, our common home – the Earth's biosphere, especially in industrialized regions, without any restrictions on production growth.

Almost all engineering solutions used in the project are widely known, tested in practice and are currently implemented in industry. The project budget will be about 2 tln USD. This is not so much if we consider that the annual military budget of the United States is almost 700 bln. At the same time, SkyWay systems will be the technological basis for the construction of the launch overpass, which will make it possible to profit from the project at the initial stages of its implementation by transporting passengers and cargo on land.

SkyWay: the present and the future full of confidence

String tracks will raise funds, people will be able to build housing and develop business around them. It is a new environmentally friendly transport which will make life even more attractive in the area of transport accessibility. String transport and infrastructure complexes will give impetus to the exploration of previously undeveloped lands. Thanks to SkyWay overpasses, the lines of modern information communications, power, water and fertile soil will come to the most remote corners of the planet. Life will appear around them, deserts will disappear from the planet, housing in the mountains and on the sea shelf will be more prestigious than, for example, in New York or Paris. The Man and the Nature will finally be in harmony with each other.

At the same time, UPT will be studied and developed, which will require about 5 % of the total investment. In total, the solution of all engineering problems will require at least a couple of decades. In spite of the fact that the work is already underway, the implementation of the project is hardly possible by the efforts of the team I created.

It is hoped that such a global geocosmic program with common goals and objectives will unite all the developed countries of the world, will attract them to finance this super-ambitious project, designed to save humanity. Due to its technical features, the project will directly affect the territory of dozens of countries (mainly located along the equator), and for political and economic reasons – the whole world. UPT will also become an indispensable platform for the future development of deep space with reusable spacecraft, such



as those developed by companies such as SpaceX and Blue Origin. The project implementation period will be about 20 years, taking into account sociopolitical, research, development, design, survey, construction and installation.

The world around us was created by engineers. Not bankers, not politicians, not artists, but engineers! However, this world is often ruled by others – those for whom personal enrichment is at the forefront; those who naively believe that in a situation where the planet will be on the verge of death, money can save them. They are confident that, together with their families, they will be able to hide on personal islands, in underground bunkers, on submarines and Boeing with antimissile defense. But they are wrong. Planet is a big room, devoid of partitions. Once, primitive people, along with their leaders, burned fires in their caves and died of lung cancer at the age of 20. They were able to survive only due to the fact that they had guessed to move the fire outside their home. So now we, the terrestrial civilization, must move the technosphere beyond the limits of the biosphere.

SkyWay systems will be the technological basis for the construction of the launch overpass.

“It is hoped that such a global geocosmic program with common goals and objectives will unite all the developed countries of the world, will attract them to finance this super-ambitious project, designed to save humanity.”

Transport project it will be necessary to cope with even more difficulties, both technically and socially. However, they are insignificant compared to the problems that the civilization has to solve if it wants to survive and develop.

Ideas that have changed the world in the past have always seemed fantastic and unreal to contemporaries, but with the efforts of engineers they became real. Science has given us the tools to make the world a better place, but we don't want to use it because of our inertia and conservatism. Are we ready to put up with the fact that we have to move to Mars, at the price of a one-way ticket in a billion dollars, and die there, continuing to build millions of kilometers of roads and considering the rocket the only “key” to the Space? I do not want to believe it. If this is not the case and we want to live, then for this we need to find the courage to change. Each of us! We did not inherit the Earth from our ancestors, we borrowed it from our descendants. We are obliged to work out this debt, otherwise we will not have the future for everyone – the earthly technocratic civilization will disappear as a failed experiment of the Universe.

All engineering solutions for this step, ensuring the transition of humanity to a new stage of civilization, have already been created.

If once I could have been considered a dreamer and even a madman, the SkyWay string transport project I implemented is a weighty argument against the votes of skeptics. Everything works exactly as it was calculated by me as an engineer decades ago. The demand for the technology is a confirmation of its economic efficiency. On the way to proving this, I had to overcome a lot. There is no doubt that in the course of the implementation of the United Planetary



UDC [629.3 + 629.78].01

Unitsky A. String Transport Systems: on Earth and in Space / A. Unitsky. – Silakrogs: «PNB Print», 2019. – 560 p. – ISBN 978-985-90498-2-8.

This edition is based on the monograph “String Transport Systems: on Earth and in Space” by Anatoli Unitsky, first published in 1995. The fundamental scientific paper sets out the theory, state of development, prospects and main results of the studies of high-speed land transportation, which moves along a string track structure, and non-rocket space transport in the form of a circular string system, covering the planet parallel to the equator.

In 2017, the scientific publication, supplemented by the author’s preface and new illustrations, was published for the second time.

The Edition 2019 is supplemented with a new author’s preface, new illustrations, as well as other materials that reveal the string transport system, telling about the history of the development of the innovative transport and infrastructure technologies – SkyWay. In addition, this edition includes Section “Intellectual property rights to geocosmic transport and infrastructure complex “United Planetary Transport”, which displays the results of more than 40 years of intellectual, creative, scientific, experimental and production activities of Engineer, Scientist and Businessman Anatoli Unitsky.



Signed for printing on 25/01/2019
Format 170×240
Total circulation 2500 copies
Order № 120269

Printed by «PNB Print». «Jansili», Silakrogs, Ropazu nov., LV-2133

ISBN 978-985-90498-2-8

© Unitsky A., 2019

Scientific publication

Anatoli Unitsky

**String Transport Systems:
on Earth and in Space**

Publishing Group – SkyWay Technologies Co.